Nanopartículas lipídicas de Apigenina y Melatonina en farmacoterapia oncológica y ocular

Lorena Bonilla Vidal

UNIVERSITAT DE BARCELONA

Facultad de Farmacia y Ciencias de la Alimentación

Nanopartículas lipídicas de Apigenina y Melatonina en farmacoterapia oncológica y ocular

Lorena Bonilla Vidal

2024

UNIVERSITAT DE BARCELONA

PROGRAMA DE DOCTORADO

Investigación, Desarrollo y Control de Medicamentos

Nanopartículas lipídicas de Apigenina y Melatonina en farmacoterapia oncológica y ocular

Memoria presentada por **Lorena Bonilla Vidal** para optar al título de doctora por la Universidad de Barcelona

Directoras

Dra. Elena Sánchez López **Dra. Marta Espina García** **Dra. Anna Gliszczyńska**

Doctoranda

Lorena Bonilla Vidal

Tutora

Dra. María Luisa García López

“It’s not about winning, but it’s about not giving up. It’s not about how many times you get rejected, or you fall down, or you’re beaten up. It’s about how many times you stand up, and are brave, and you keep on going.

If you have a dream, fight for it.”

Stefani Joanne Angelina Germanotta

Agradecimientos

Agradecimientos

Si me preguntaran si volvería a escoger este camino, la respuesta sería que sí, volvería a hacer todo exactamente tal y como ha sido. Todos los hechos y decisiones tomadas me han llevado a donde estoy, con experiencias que jamás olvidaré, conocimiento que me ha hecho ver el mundo de una manera diferente, y lo más importante, rodeada de gente maravillosa que han hecho que todo este camino haya valido la pena. Cuando me preguntaba a mí misma si tenía que seguir, la respuesta siempre ha sido que sí, cada experimento, cada día madrugando, cada día llegando tarde a casa, cada lágrima y cada sonrisa, cada experiencia... Sí, valió la pena.

Quiero agradecer a mi familia, quienes han estado siempre conmigo y me han apoyado en todo. Mis padres, mis hermanos, mis sobrinas, mis abuelos, mi tío, mis perros, mis loros y mis otras mascotas, os quiero con todo mi corazón (¡aunque no suela decirlo!). En especial, quería agradecerle a mi abuelo, quien me inspiró a estudiar ciencias de la salud, para así poder dedicar mi vida a mejorar la de los demás. También quiero agradecerle especialmente a mi madre y a mi padre, quienes me han brindado su apoyo incondicional, siempre han intentado entender toda mi investigación para aconsejarme lo mejor posible, y quienes han compartido mis alegrías y mis tristezas desde que nací. Sois un ejemplo a seguir, gracias por todo, ¡os quiero!

Víctor, mi compañero de vida, simplemente gracias por todo.

Me gustaría dar las gracias a las científicas que me han acompañado durante todos estos años, mis directoras y mi tutora Elena, Marta y Marisa. Gracias por haberme guiado, aconsejado, ayudado y enseñado tanto durante este tiempo. Soy muy afortunada de haber podido compartir este camino con vosotras, y haber formado esta pequeña familia en el laboratorio. Also, I would like to acknowledge my supervisor Anna, thank you for all your help and hospitality, dziękuję!

A mis compañeros de laboratorio, tanto los actuales como los que pasaron por él, Gerard, Jordi, Xavi y Xavi, Cinzia, Nerea, Francesca, Rubén, Eva, María, Eva, Víctor, Thiru, Lena, Mayra, Magda... Muchas gracias por todo, desde desgracias como tener que ordenar apresuradamente el laboratorio hasta logros como conseguir arreglar un equipo o que un experimento salga a la primera, ha sido

increíble por haberlo compartido con vosotros. Pero especialmente quiero agradecer a Gerard, el compañero de doctorado con el cual empezó todo. A pesar de que cuando nos conocimos antes del doctorado nos odiáramos al instante (sin razón ninguna), ahora eres un gran amigo. Todas las experiencias inolvidables en el laboratorio han sido contigo, espero que podamos seguir compartiendo recuerdos, ¡pero ya como doctores!

Mil gracias a mis compañeros de carrera, los pivones farmacéuticos Aitor, Marina, Noel y Sofia. Hicisteis que los años de carrera fueran inolvidables, las prácticas en el laboratorio muy divertidas, y seguir con vosotros, aunque hayamos tomado caminos tan diferentes, es todo un regalo. En particular, quiero agradecer a Aitor, que además de ser uno de mis mejores amigos desde que éramos jóvenes y atléticos, es un ejemplo a seguir, una persona que siempre perseguirá sus sueños sin importar cuan adversa sea la situación. Eres increíble y un gran profesional, gracias por tu amistad todos estos años (¡y los que quedan!).

Quiero agradecer a la Farmacia Olímpic, tanto a mis jefes como a mis queridos compañeros de finde. Moltes gràcies Lluc i Moni per tots aquests anys, sempre portaré la farmàcia en el meu cor. Moltes gràcies Lluc, que més que un jefe, ets un amic, moltes gràcies per tot. A los compis de finde que aún estáis a pie de cañón, y a los que ya huyeron a una vida mejor, Tania, Lluís, Laura, Sandra, Guillem, Joaquim, Edu, Estel, Mar, Andrea y Lilian, muchas gracias por todos esos sábados, domingos, Navidades, San Juanes, Años nuevos, etc. vividos con vosotros. Os aseguro que, sin personas tan increíbles y profesionales como vosotros, no habría podido estar tanto tiempo soportando el estrés de trabajar de cara al público. Especialmente quiero agradecer a Tania, que en tan poco tiempo has pasado de compañera a mi mejor amiga, eres una persona maravillosa, así que no cambies nunca. Y a Lluís y Joaquim, con quienes empecé a trabajar e iniciamos esta gran familia de findes, guardo muchísimos recuerdos junto a vosotros. ¡Gracias a todos!

Me gustaría agradecer a todas las personas del departamento de Fisicoquímica, quienes me acogieron rápidamente y su amabilidad hizo que me sintiera como en casa. Vull fer una especial menció a la Josefina, les Montses i l'Alba, que m'han donat suport dia a dia i sempre s'han ofert a ajudar-me en tot

moment amb un somriure. També volia agrair a la Pepita i la Laura del departament de Bioquímica, per haver-me deixat un lloc en el seu laboratori i ser una més del grup, y a Sergio, Yeni y Ceci por toda la ayuda y la simpatía que tuvieron desde que pisé el laboratorio.

También quiero agradecer a las compañeras que fueron del Lab2 que, aunque no coincidí o estuve poco tiempo con ellas en el laboratorio, aprendí muchísimo y me inspiraron a seguir. Ana, Paulina, Amanda y Fani, ¡sois increíbles!

Quiero agradecer a mi familia política, quienes siempre me han brindado su apoyo, su cariño y sus consejos. Gracias por dejarme ser una más en vuestra familia.

Finalmente, no quería acabar sin dar las gracias a muchas otras personas que me han ayudado a ser como soy. A todos los profesores que me han guiado en el ámbito académico, comenzando en Badalona por mi colegio Ítaca, seguido de mi instituto Barres i Ones, como los años en la Facultad. Quería agradecer a ciertas personas que me enseñaron cómo ser profesores que te marcan de por vida, Gemma, Carles i Àlex, moltíssimes gràcies per haver sigut uns excel·lentíssims professors i persones, us estic molt agraïda per haver guiat a una Lorena jove pel camí acadèmic fins arribar a la universitat. También quiero agradecer a antiguas amistades que aún perduran, en especial a Anabel, una gran amiga que me acompañó durante toda mi adolescencia hasta la adultez.

Muchas gracias a todos, gracias de corazón.

Índice

Abreviaturas

AINE	Antiinflamatorios no esteroideos
AMD	Degeneración macular relacionada con la edad
APC	Células presentadoras de antígeno
APG	Apigenina
APG-MEL-NLC	Sistemas lipídicos nanostructurados duales encapsulando Apigenina y Melatonina
APG-MEL-NLC+	Sistemas lipídicos nanostructurados encapsulando Apigenina y Melatonina, con carga superficial positiva
APG-NLC	Sistemas lipídicos nanostructurados encapsulando Apigenina
bFGF	Factor de crecimiento fibroblástico básico
CAM	Membrana corioalantoidea
COX	Ciclooxigenasa
DDAB	Bromuro de dimetildioctadecilamonio
DED	Síndrome del ojo seco
DLS	Dispersión dinámica de la luz
DoE	Diseño de experimentos
DSC	Calorimetría diferencial de barrido
EE	Eficiencia de encapsulación
EMA	Agencia europea de medicamentos
EPR	Efecto de permeabilidad y retención mejorada
FDA	Administración de alimentos y medicamentos
FTIR	Espectroscopia de infrarrojo con transformada de Fourier
GRAS	Generalmente reconocido como seguro
HA	Ácido hialurónico
HA-APG-NLC	Sistemas lipídicos nanostructurados encapsulando Apigenina, recubiertos con ácido hialurónico y con carga superficial positiva
HCE-2	Línea celular corneal humana
HET-CAM	Prueba de la membrana corioalantoidea del huevo de gallina

IL	Interleucina
IOP	Presión intraocular
MCP	Proteína quimiotáctica de monocitos
MDR	Multiresistencia a los fármacos
MEL	Melatonina
MEL-NLC	Sistemas lipídicos nanostructurados encapsulando Melatonina
MEL-NLC+	Sistemas lipídicos nanostructurados encapsulando Melatonina, con carga superficial positiva
MTT	Bromuro de 3-(4,5-dimetiltiazol-2-il)-2,5-difeniltetrazolio
NLC	Sistemas lipídicos nanostructurados
LPS	Lipopolisacárido
NF-κB	Factor de transcripción nuclear-κB
NPs	Nanopartículas
PDI	Índice de polidispersión
PEG	Polietilenglicol
RHO	Aceite de rosa mosqueta
ROS	Especies reactivas de oxígeno
SLN	Nanopartículas de lípidos solidos
SOD	Superóxido dismutasa
TEM	Microscopia electrónica de trasmisión
T_m	Temperatura de fusión
TNF	Factor de necrosis tumoral
UM	Melanoma de úvea
XRD	Difracción de rayos X
Z_{av}	Tamaño promedio de partícula
ZP	Potencial zeta
ΔH	Entalpía de fusión

Resumen-Abstract

RESUMEN

Los sistemas nanoestructurados lipídicos (NLC) han surgido como una herramienta prometedora en la nanomedicina, ofreciendo una gran versatilidad para la administración dirigida de fármacos. Su biocompatibilidad, capacidad de carga y liberación prolongada los hacen ideales para aplicaciones terapéuticas.

En el tratamiento del cáncer, los NLC pueden encapsular múltiples fármacos, mejorando su eficacia y reduciendo sus efectos secundarios. Compuestos como la Apigenina (APG) y la Melatonina (MEL) han demostrado propiedades anticancerígenas y pueden beneficiarse de la protección y liberación controlada que ofrecen los NLC. La APG, un flavonoide con propiedades antioxidantes y antiinflamatorias ha mostrado potencial en la prevención y tratamiento de diversos tipos de cáncer. La MEL, una neurohormona con propiedades antioxidantes y antitumorales, además de demostrar su potencial en diferentes estudios clínicos, también puede complementar la acción de la APG.

En el campo de la oftalmología, los NLC también ofrecen grandes ventajas. Su capacidad para penetrar barreras oculares, prolongar el tiempo de residencia de los fármacos y de hidratar epitelios, los convierte en sistemas de liberación potenciales para el tratamiento de enfermedades como el síndrome del ojo seco, enfermedades inflamatorias y el cáncer ocular. Tanto la APG como la MEL han mostrado propiedades beneficiosas para la salud ocular, como la reducción de la inflamación y la protección contra el daño oxidativo.

El objetivo de esta investigación es optimizar y evaluar seis sistemas de liberación de fármacos basados en NLC, encapsulando APG y MEL, donde tres formulaciones presentaron carga superficial negativa para el tratamiento de enfermedades proliferativas y tres se formularon con carga superficial positiva para su uso en oftalmología. Todas las formulaciones evaluadas exhibieron propiedades fisicoquímicas adecuadas y un perfil de liberación sostenido de APG y MEL. En los ensayos *in vitro* para explorar el potencial antitumoral de las formulaciones, mostraron una citotoxicidad elevada en todas las líneas celulares tumorales, siendo capaces de internalizarse en solo 5 minutos,

manteniéndose en su interior hasta 4 horas. Por otra parte, los sistemas oftálmicos evaluados demostraron una excelente biocompatibilidad, según los ensayos de MTT y HET-CAM, y no indujeron irritación ocular en el test de Draize. Además, los ensayos de eficacia, que incluyeron modelos celulares y animales, confirmaron su potencial terapéutico en los tratamientos del ojo seco, del melanoma uveal y de la inflamación ocular del segmento anterior. Los resultados presentados en este estudio respaldan la hipótesis de que los sistemas nanoestructurados a base de APG y MEL constituyen una alternativa terapéutica segura y eficaz para el tratamiento de las enfermedades oncológicas y oftálmicas.

ABSTRACT

Nanostructured lipid carriers (NLC) have emerged as a promising tool in nanomedicine, offering a versatile platform for drug target delivery. Their biocompatibility, high loading capacity, and prolonged release makes them an excellent potential therapeutic tool.

In cancer treatment, NLC can encapsulate multiple drugs, improving their efficacy and reducing side effects. Compounds such as Apigenin (APG) and Melatonin (MEL) have demonstrated antitumoral properties, and they can be protected and released in a sustained manner due to NLC loading capacity. APG, a flavonoid with antioxidant and anti-inflammatory properties, has shown potential in the prevention and treatment of various types of cancer. MEL, a neurohormone with antioxidant and antitumor properties, in addition to demonstrating its potential in different clinical trials, can also complement the action of APG.

In the field of ophthalmology, NLC also offer great advantages. Their ability to penetrate ocular barriers, prolong the residence time of drugs, as well as their ability to hydrate epithelia, turns them into potential delivery systems for the treatment of diseases such as dry eye syndrome, inflammatory pathologies, and ocular cancer. Both APG and MEL, have shown beneficial properties for ocular health, such as reducing inflammation and protecting against oxidative damage.

The objective of this research is to optimize and evaluate six drug delivery systems based on NLC, encapsulating APG and MEL, in which three formulations presented a negative surface charge for the treatment of proliferative diseases and three were formulated with a positive surface charge to be used in ophthalmology. All formulations evaluated exhibited adequate physicochemical properties and a sustained release profile of APG and MEL. *In vitro* assays were performed to explore the antitumoral potential of NLC, showing enhanced cytotoxicity in all tumoral cell lines and also, being able to be internalize after 5 minutes and remaining inside the cells up to 4 hours after administration. On the other hand, the evaluated ophthalmic systems demonstrated excellent biocompatibility, according to MTT and HET-CAM assays, and did not induce ocular irritation *in vivo*. Additionally, efficacy assays performed in cellular and animal models, confirmed their therapeutic potential in the treatment of dry eye, uveal melanoma and anterior segment inflammation. The results presented in this study support the hypothesis that APG and MEL-based nanostructured systems constitute a safe and effective therapeutic alternative for the treatment of oncological and ophthalmic diseases.

1

Introducción

1. Introducción

La nanomedicina es una disciplina relativamente reciente que surge como una necesidad para los pacientes, con el objetivo de mejorar y revolucionar los tratamientos farmacológicos. Ésta se basa en la capacidad de modificar diferentes materiales a escala nanométrica para crear nanomateriales, dispositivos y sistemas de liberación de fármacos. Esto ha supuesto un gran avance para la farmacología, gracias a su capacidad de mejorar propiedades de los fármacos encapsulados en estos sistemas, como la difusión, el tiempo de semivida, la liberación de fármacos y los perfiles de distribución [1]. Estas propiedades, como el elevado ratio superficie/volumen, la capacidad de transportar fármacos y la capacidad de interactuar con las biomoléculas, permiten a los nanomateriales realizar funciones que no son posibles con las tecnologías tradicionales [2].

Históricamente su progreso puede dividirse en tres etapas. En su inicio, aproximadamente en los años 60, se descubrieron los liposomas, que no fueron aprobados hasta el 1995 como sistemas de liberación de fármacos, siendo los liposomas encapsulando doxorrubicina el primer sistema liposomal en el mercado. En una segunda etapa comenzaron a validarse clínicamente y comercializarse diferentes nanotratamientos, y simultáneamente, surgieron nuevos sistemas de liberación como el DepoDur® (morfina liposomal) o el Onyvide® (irinotecan liposomal) [3]. Finalmente, en la etapa actual, la nanofarmacoterapia ha experimentado una gran expansión para la prevención y tratamiento de diferentes patologías [4], existiendo más de 50 formulaciones aprobadas para uso clínico [5].

El interés de la nanotecnología en la comunidad científica ha ido aumentando desde su descubrimiento gracias a sus múltiples características, tales como la mejora en la liberación de fármacos con baja solubilidad en agua, su capacidad de dirigir fármacos a células o tejidos de manera específica, la liberación de combinaciones de agentes terapéuticos, la posible visualización del vehículo *in vivo*, y la capacidad de proteger principios activos [6]. Con el objetivo de cumplir todas las características mencionadas, durante las últimas décadas se

han desarrollado una gran variedad de nanosistemas orgánicos e inorgánicos. Los nanosistemas inorgánicos, tales como las nanopartículas (NPs) metálicas o los *quantum dots*, se consideran generalmente más tóxicos que los orgánicos debido a que éstos últimos pueden ser mayoritariamente digeridos por el tracto gastrointestinal humano y no se acumulan en el organismo [7,8]. Por otro lado, los nanosistemas orgánicos, formados por proteínas, carbohidratos, lípidos o polímeros, se caracterizan generalmente, por tener una baja toxicidad y ser biodegradables. Además, normalmente su matriz se genera por interacciones intermoleculares no covalentes, de manera que suelen ser más lábiles *in vivo* y tienen rutas de eliminación establecidas en el cuerpo [9].

En el año 1990, M.R. Gasco y R.H. Müller desarrollaron las NPs lipídicas como alternativa a los diferentes nanosistemas orgánicos ya conocidos, tales como las NPs poliméricas, cuya producción a gran escala era más costosa [10,11]. La idea del desarrollo de estos nuevos sistemas surgió debido a que el uso de los lípidos para liberación de fármacos era conocido, ya que existían en el mercado diferentes medicamentos a base de estos, como los liposomas [11]. Asimismo, los lípidos son muy bien tolerados por el cuerpo como por ejemplo, los glicéridos que se encuentran en soluciones para la nutrición parenteral o las cremas a base de ácidos grasos que se usan para hidratar la piel [11]. Las primeras NPs lipídicas que se desarrollaron fueron las NPs de lípidos sólidos o *solid lipid nanoparticles* (SLN) y posteriormente en el año 1999 se introdujo una segunda generación de éstas primeras, los sistemas lipídicos nanoestructurados o *nanostructured lipid carriers* (NLC) [12]. Sin embargo, no fue hasta unos 20 años después (2018) cuando se aprobó el primer medicamento, Onpattro®, conteniendo el fármaco patisiran para el tratamiento de la amiloidosis hereditaria por transtiretina, y ganaron visibilidad en el 2020, con la llegada de las vacunas contra la COVID-19, cuando fueron utilizadas las NPs lipídicas como vectores no víricos para administrar cadenas de ARNm al organismo [13].

1.1. Nanopartículas lipídicas: SLN y NLC

La primera generación de NPs lipídicas desarrolladas, las SLN, fueron ideadas para combinar las ventajas generales de las NPs con las de las emulsiones a base de lípidos, creando un sistema de liberación de fármacos natural y biocompatible [14]. Las SLN son partículas de tamaño submicrónico, constituidas por lípidos biocompatibles y biodegradables sólidos a temperatura ambiente y a temperatura corporal [15]. Las ventajas de las SLN son diversas, como su capacidad de liberar de manera controlada los fármacos encapsulados, tanto hidrofílicos como hidrofóbicos, la posibilidad de dirigirlas de manera activa o pasiva a diferentes dianas, la protección ante la degradación del fármaco incorporado, el incremento en la biodisponibilidad del activo, su baja toxicidad junto a su elevada afinidad por las barreras biológicas aumentando así su penetración en tejidos más internos, su capacidad de modificar los parámetros farmacocinéticos y de distribución del fármaco encapsulado y la facilidad de su producción a gran escala [15,16]. A pesar de todas sus ventajas como sistema de liberación de fármacos, las SLN presentan algunos inconvenientes. Debido a su matriz formada únicamente a base de lípidos sólidos y tensioactivos, éstas poseen una estructura que cristaliza rápidamente, de manera que tienen una baja capacidad de cargar fármacos ya que estos pueden ser expulsados de la matriz durante su almacenamiento y tienen problemas de estabilidad a largo plazo, como la agregación y degradación de los componentes (Figura 1) [15,17].

Con el objetivo de mejorar los inconvenientes de las SLN, casi 10 años después, Müller desarrolló la segunda generación de NPs lipídicas, los NLC, en las cuales se incorporó un lípido líquido, es decir un aceite, modificando así la estructura cristalina de las SLN. La incorporación de un aceite en su estructura condujo a una disminución de la cristalinidad de la muestra, volviéndola más amorfa. Este cambio mejoró las características de las NPs lipídicas, aumentando la capacidad de carga de fármaco en el interior de la matriz, previniendo y modulando la liberación del activo y aumentando su estabilidad [18].

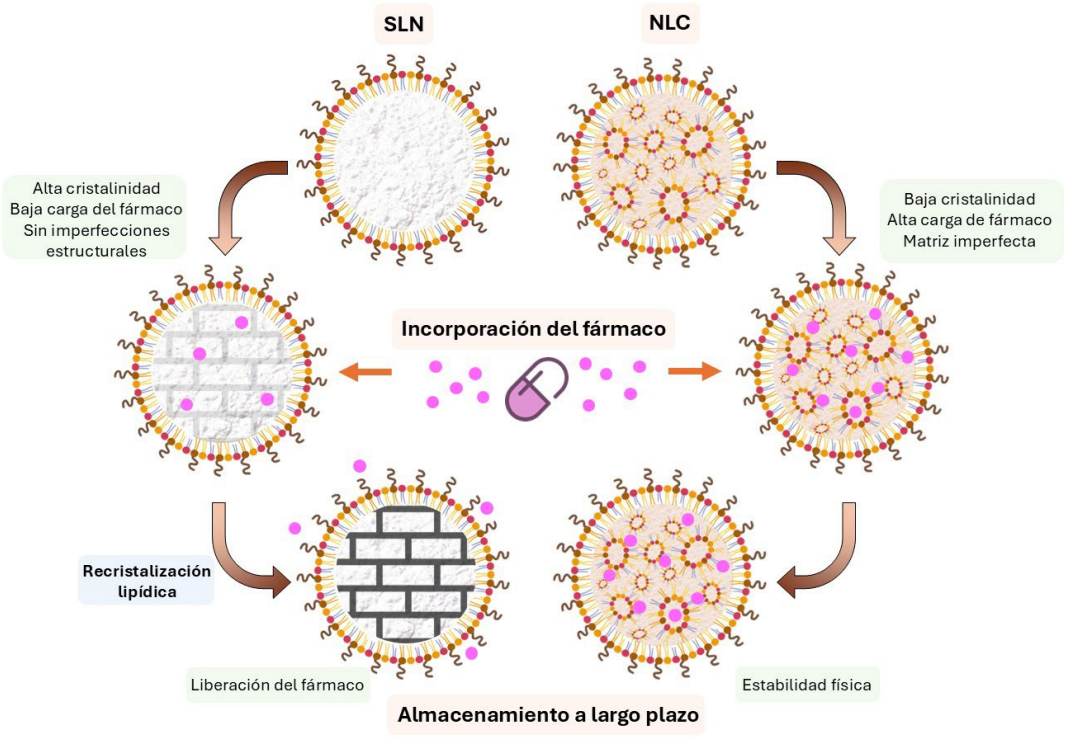

Figura 1. Diferencias estructurales y capacidad de carga de fármaco entre las matrices de SLN y NLC almacenados a largo plazo. Basado en [19].

La variación del contenido de lípidos y los diferentes parámetros de la formulación provocan un cambio en la matriz lipídica y en la disposición de los lípidos sólidos y líquidos dentro de los NLC. Müller *et al.* clasificaron los NLC en tres tipos según estas posibles variaciones [12,20]:

- **Tipo 1 (Cristal imperfecto):** se forman con un contenido bajo de lípido líquido que deforma la estructura cristalina del lípido sólido. Dado que los fármacos lipofílicos son más solubles en los lípidos líquidos, un aumento en la concentración lipídica total se traduce en una mayor incorporación del fármaco [12,20].
- **Tipo 2 (Múltiples tipos):** contienen una alta cantidad de aceite, lo que da lugar a la formación de compartimentos nanométricos de aceite dentro de la nanopartícula, donde se acumula el fármaco solubilizado.

La elevada liposolubilidad conduce a una baja expulsión del activo y una liberación lenta del mismo [12,20].

- **Tipo 3 (Amorfo):** se forma mediante la mezcla de lípidos sólidos y líquidos de manera específica para evitar la cristalización del núcleo. Este enfoque da como resultado una menor expulsión del fármaco debido a la cristalización del núcleo sólido [12,20].

Por otro lado, la estabilidad estructural de los NLC está asociada principalmente a su composición y la concentración de tensioactivo. Por lo tanto, estos parámetros deben tenerse en cuenta para garantizar su estabilidad y almacenamiento. Durante la preparación y almacenamiento, los triglicéridos sufren modificaciones cristalinas α, β y β' (Figura 2) [21].

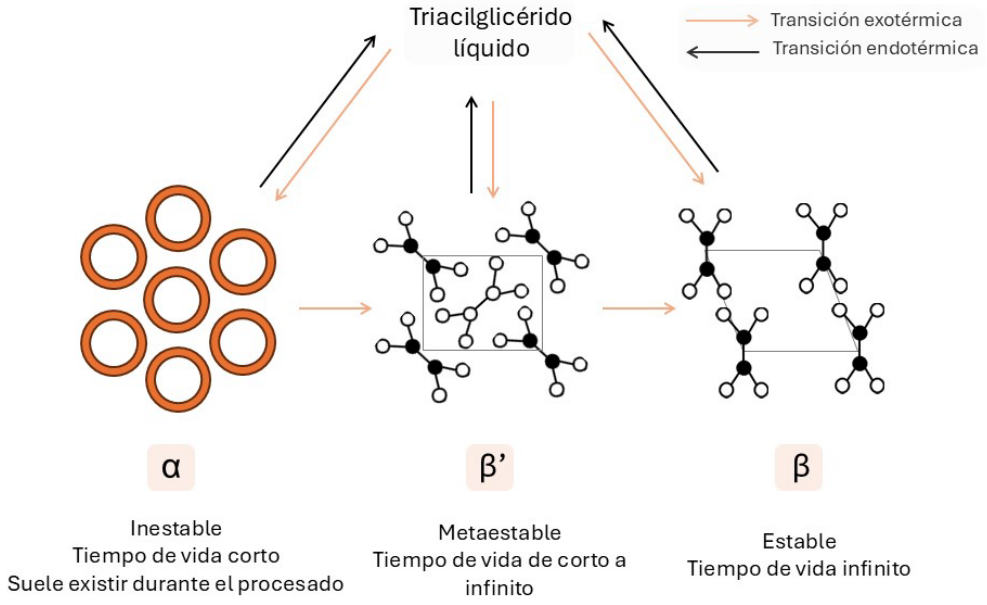

Figura 2. Formas polimórficas de cristales de triacilglicéridos, donde aparecen representadas las posibles transiciones polimórficas, las estructuras de empaquetamiento de subceldas y las características de estabilidad. Basado en [22].

La forma α (hexagonal) de los triglicéridos es la menos estable con un punto de fusión y calor latente más bajos. En contraposición, la forma β (triclínica) es la

más estable con un punto de fusión y calor latente más elevados [23]. Estas formas polimórficas pueden estudiarse a través de estudios de interacción tales como la difracción de rayos X (*X-ray diffraction* o XRD) y calorimetría diferencial de barrido (*differential scanning calorimetry* o DSC), con el objetivo de entender y predecir el estado cristalino de la muestra y con ello su estabilidad [24].

Por lo tanto, la composición de los NLC es un parámetro importante en su fabricación puesto que tanto los lípidos que la componen como sus proporciones afectan a los parámetros fisicoquímicos de la formulación final [25].

1.1.1. Composición de los sistemas lipídicos nanoestructurados

Los NLC están formados por lípidos sólidos y líquidos en una proporción que varía de 70:30 a 99,9:0,1. Esta mezcla provoca una estructura amorfa, creando espacios adicionales donde pueden incorporarse fármacos. Como las moléculas lipofílicas suelen ser más solubles en lípidos líquidos, esta "imperfección" favorece la carga de fármacos en los NLC [26].

Además, los materiales utilizados en la formulación de NLC deben ser biocompatibles y no presentar toxicidad, ya que actuarían como excipientes en la formulación final. La Administración de Alimentos y Medicamentos de los Estados Unidos (FDA) clasifica estos materiales como generalmente reconocidos como seguros (*Generally Recognized as Safe*, GRAS) y la Agencia Europea del Medicamento (EMA) les da una numeración según cómo se clasifican [27,28]. La elección de los excipientes juega un papel crucial en la determinación del tamaño de partícula y las propiedades fisicoquímicas de los NLC [29].

Los lípidos son el componente principal de los NLC y juegan un papel clave en la capacidad de carga de fármacos, en la acción prolongada y en la estabilidad de las formulaciones. Se han utilizado diferentes tipos de lípidos sólidos para

la fabricación de NLC, como ácidos grasos, triglicéridos, diglicéridos, monoglicéridos y ceras [30]. Entre los diferentes lípidos sólidos, las mezclas de éstos son los más interesantes para la fabricación de NLC, debido a que la mezcla de diferentes tipos puede crear una matriz lipídica más imperfecta [24]. Por ejemplo, el behenato de glicerilo, más conocido como Compritol® 888 ATO, es una mezcla de glicéridos de ácidos grasos, predominantemente el ácido behénico. Éste es un excipiente lipídico que se utiliza generalmente en industria cosmética como tensioactivo, agente emulsionante y agente inductor de viscosidad en emulsiones o en cremas. Este lípido es muy utilizado en la fabricación tanto de SLN como de NLC, debido a sus características favorables, como su apolaridad, menor citotoxicidad que otros lípidos, su elevada capacidad de disolver fármacos gracias a la presencia de mono-, di- y triglicéridos y los espacios adicionales que se crean por su mezcla de acilgliceroles [31].

En cuanto a los lípidos líquidos, también juegan un papel importante en las propiedades fisicoquímicas de las NPs, como el tamaño, la viscosidad y la distribución del fármaco. Se han usado diferentes lípidos líquidos para la preparación de NLC, principalmente aceites que contienen diferentes ácidos grasos, como el ácido oleico [12]. Una estrategia muy interesante es el uso de aceites naturales que además de ayudar a crear una matriz más amorfa aportan características farmacológicas a ésta [32]. Un claro ejemplo es el aceite de rosa mosqueta (RHO), que destaca por su alto contenido en compuestos bioactivos, lo que le confiere interesantes propiedades funcionales y cosméticas [33]. El RHO se extrae de las semillas del fruto de la rosa silvestre (*Rosa canina*) [34] y contiene una gran concentración de ácidos grasos poliinsaturados como el ácido linoleico, el ácido alfa-linolénico y el ácido oleico [35], que participan en la estructura de las membranas celulares y desempeñan un papel fundamental en la respuesta inflamatoria [36]. Además, contiene otros compuestos bioactivos como los tocoferoles, los carotenoides (precursores de la vitamina A que actúan como antioxidantes y estimulan la regeneración celular), los fitoesteroles, que poseen propiedades antiinflamatorias [37,38], y el ácido trans-retinoico, un derivado de la vitamina A responsable de promover la renovación celular epitelial, siendo uno de los

componentes al que se le atribuye sus propiedades cicatrizantes, además de tener propiedades antiproliferativas [39–41]. Debido a su composición con gran potencial farmacéutico, el RHO se ha utilizado durante décadas en el campo médico para tratar heridas y cicatrices. Además de su uso tradicional, tiene un gran potencial para tratar otras afecciones, como las enfermedades proliferativas u oculares [35,42].

Finalmente, el tipo y número de tensioactivos también es un parámetro de formulación importante. Se emplean uno o una combinación de tensioactivos (entre el 1,5 y el 5 % p/v) para estabilizar el nanosistema, formando una capa a su alrededor. Utilizar más de un tensioactivo puede conducir a un menor tamaño de partícula y menor cristalinidad que un sistema con un solo tensioactivo [29]. Durante la formulación de los NLC, la cristalización de las partículas coloidales y su solidificación, son procesos que se producen simultáneamente, y a su vez, el área superficial de éstas aumenta, de modo que todo el sistema se vuelve inestable. Por tanto, el uso de uno o más tensioactivos es un requisito para mejorar la estabilidad de los NLC, dado que éstos se adsorben en la interfaz entre las fases lipídica y acuosa, reduciendo la tensión superficial gracias a su naturaleza anfipática [30,43]. Los polisorbatos, concretamente el polisorbato 80 (Tween® 80), son tensioactivos no iónicos conocidos por su capacidad de aumentar la penetración de las NPs en tejidos muy restrictivos, como la barrera hematoencefálica o la barrera hematorretiniana [44]. Por lo tanto, su uso en NPs para que puedan acceder a tejidos diana muy protegidos puede suponer una estrategia para aumentar la biodisponibilidad del fármaco en estos tejidos. Por otro lado, la adición de un co-tensioactivo a la formulación de otra naturaleza al usado, por ejemplo, uno de naturaleza catiónica e hidrófoba si se usa el polisorbato 80, el cual es no iónico e hidrofílico, puede aumentar la estabilidad de los NLC y aportar alguna característica adicional, como carga positiva [45]. La carga positiva de las NPs puede suponer una ventaja para aumentar su tiempo de residencia en un tejido específico que posea carga negativa, como el cartílago, el menisco, los tendones y ligamentos, el núcleo pulposo, el epitelio ocular, el vítreo y la piel [46,47].

En conclusión, la elección de la composición de los NLC no tan solo afecta a sus propiedades fisicoquímicas, sino que también es relevante para su efecto terapéutico.

1.1.2. Características fisicoquímicas de los NLC

Las características fisicoquímicas de los NLC son parámetros clave que determinarán diferentes aspectos de las mismas [48]. Los cambios que sufren las NPs tras la exposición a los fluidos biológicos pueden ser tanto ventajosos como altamente perjudiciales para su funcionalidad esperada en el sitio diana, lo que debe tenerse en cuenta durante su diseño (Tabla 1). Las NPs pueden penetrar las membranas de los sistemas celulares (orgánulos o núcleos) e interactuar con dianas naturales debido a sus características fisicoquímicas. Por otra parte, los métodos de fabricación de los NLC pueden modificar estas características. Los diferentes procedimientos de formulación incluyen métodos de alta (homogeneización de alta presión y ultrasonidos) o baja energía (emulsificación/evaporación de solventes o microemulsión). Las características más importantes que influyen en la interacción de las NPs con los sistemas biológicos incluyen su tamaño y carga, sus propiedades hidrófilas/hidrófobas, y la composición del recubrimiento superficial o su funcionalización [49].

El tamaño reducido de las NPs constituye una de sus principales características, permitiéndoles atravesar barreras biológicas, penetrar fácilmente en células y desplazarse a través de ellas, llegando a los tejidos y órganos diana. Esto influye significativamente en su valor terapéutico y diagnóstico. Diversos factores, como la captación celular y la eliminación, el tráfico intracelular, la citotoxicidad, la penetración tumoral y el tiempo de circulación en sangre se ven afectados por el tamaño de las NPs [49,50].

La carga superficial de las NPs, determinada en base al potencial zeta (ZP), también tiene un impacto significativo en sus interacciones con las células. El ZP puede afectar el grado de captación celular y la interacción de las partículas con las biomoléculas. Además, la carga superficial está relacionada con la estabilidad de las NPs, ya que ejerce una repulsión electrostática entre ellas,

lo que impide la agregación. Generalmente, las NPs con un valor de ZP superior a ± 20 mV se consideran estables y tienen menos tendencia a agregarse [51].

Las propiedades hidrófilas/hidrófobas de las NPs es otro de los factores clave que juega un papel importante en su capacidad para interactuar con biomoléculas y células. Generalmente, las NPs de carácter hidrófobo como los NLC, por su naturaleza lipídica, tienden a ser captadas por las membranas biológicas, penetrando directamente en la membrana celular [52].

Tabla 1. Relación entre las características fisicoquímicas de las NPs y su toxicidad. Adaptado de [53,54].

Características fisicoquímicas	Efecto en la toxicidad
Tamaño y área superficial	Las NPs más pequeñas (<100 nm) son más tóxicas debido a su capacidad para penetrar en el núcleo celular. A mayor disminución del tamaño, mayor aumento del área superficial y mayor reactividad. Influye en la distribución y eliminación del material en el sistema biológico.
Forma y morfología	Las nanopartículas no esféricas pueden fluir a través de los capilares y causar consecuencias biológicas. Las formas alargadas bloquean canales iónicos y son más tóxicas que las esféricas.
Carga superficial	Las partículas cargadas positivamente suelen ser más tóxicas, debido a la mayor captación celular y/o su efecto dañino sobre las membranas celulares y lisosomales.
Composición y estructura cristalina	La composición química y la estructura cristalina influyen en la liberación de iones tóxicos y en la formación de radicales libres.
Recubrimiento superficial y rugosidad	El recubrimiento puede reducir la toxicidad estabilizando las nanopartículas y evitando la liberación de iones tóxicos. La rugosidad afecta la interacción célula-NP.

El recubrimiento de las NPs es una estrategia que puede proporcionar estabilidad, proteger contra la degradación y optimizar la interacción con tejidos específicos [55]. Los recubrimientos más utilizados para las NPs son poliméricos, como el polietilenglicol (PEG), el chitosano o el ácido hialurónico (HA) entre otros [56]. Concretamente, el HA posee aplicaciones muy prometedoras en la administración tópica debido a que se encuentra en la matriz intercelular de la mayoría de los tejidos conectivos, especialmente en la piel, donde tiene una función protectora y estabilizadora de la estructura [57]. A nivel ocular se ha demostrado que el HA aumenta la estabilidad de la película lagrimal, reduce la tensión superficial, mejora la sensibilidad al contraste y la calidad óptica de la superficie. El HA demuestra propiedades viscoelásticas que pueden lubricar la superficie ocular, reduciendo la fricción durante el parpadeo y los movimientos oculares [58]. Por otra parte, aunque las NPs se dirigen a ciertas dianas terapéuticas de manera pasiva, la liberación dirigida es una estrategia prometedora para mejorar la afinidad de unión y la especificidad de las células diana [59]. Esta liberación se basa en la unión covalente de ligandos moleculares pequeños como carbohidratos, péptidos, anticuerpos o aptámeros, a la superficie de las NPs que pueden interactuar específicamente con los receptores de las células diana [60].

1.1.3. Acción terapéutica dual de los sistemas lipídicos nanoestructurados

Los NLC son sistemas nanoestructurados muy versátiles que surgieron de la unión de dos estrategias diferentes: las ventajas terapéuticas que aportan las NPs para alcanzar órganos diana y transportar así fármacos, y las características más dermocosméticas de las emulsiones, aportando lípidos capaces de hidratar, lubricar y ejercer una acción oclusiva a nivel tópico [61,62].

Estos sistemas han demostrado un potencial creciente como vehículos para transportar fármacos, particularmente al mejorar significativamente la eficiencia de encapsulación para fármacos lábiles, tanto hidrófilos como hidrófobos, protegiéndolos de la degradación en el organismo y evitando la

degradación química, mejorando su biodisponibilidad y modulando su liberación. Los NLC se pueden utilizar para administrar fármacos por diversas vías, como la parenteral, tópica, oral, oftálmica y pulmonar, para el tratamiento de enfermedades del sistema nervioso central, enfermedades inflamatorias, tumores, afecciones de la piel, infecciones bacterianas, fúngicas y víricas, así como para la administración de anestésicos locales [63]:

- **Administración tópica:** es un área de gran potencial para los NLC. Las ventajas distintivas de los NLC en la administración tópica de fármacos son la capacidad de proteger ingredientes químicamente lábiles frente a la descomposición, la posibilidad de modular la liberación del fármaco y la propiedad de formar películas lipídicas adhesivas sobre la piel que pueden tener un efecto oclusivo [64].
- **Administración parenteral:** los NLC se pueden utilizar para todas las aplicaciones parenterales, desde intraarticulares e intramusculares hasta subcutáneas e intravenosas, dependiendo de su tamaño de partícula, y el objetivo terapéutico, ya que pueden dirigir fármacos a órganos específicos. Las NPs, al igual que todas las partículas coloidales inyectadas por vía intravenosa, suelen eliminarse de la circulación por el hígado y el bazo [65].
- **Administración oral:** su administración es posible como una dispersión acuosa o como una forma farmacéutica tradicional, es decir, comprimidos, pellets, cápsulas o polvos en cápsulas. El efecto protector de las NPs, junto con sus propiedades de liberación sostenida y controlada, previenen la degradación prematura de los fármacos y mejoran su estabilidad en el tracto gastrointestinal. La reducción de efectos secundarios y el enmascaramiento del sabor también son dos objetivos relevantes para su administración oral [66].
- **Administración pulmonar:** los NLC protegen a los fármacos encapsulados de las enzimas presentes en el epitelio bronquial y alveolos, además de aumentar su biodisponibilidad y disminuir los efectos sistémicos de éstos. Su composición reduce la probabilidad de inducir una respuesta inmune, ya que los lípidos administrados son biocompatibles y biosimilares [67].

- **Administración ocular:** los NLC tienen un gran potencial para tratar enfermedades oftálmicas ya que pueden mejorar la bioadhesión corneal y la permeación del fármaco, para tratar los tejidos más internos del ojo, como la retina y el nervio óptico [12].
- **Administración nasal:** los NLC tienen un gran potencial para mejorar la administración de fármacos al cerebro después de su administración intranasal, principalmente debido a su capacidad para penetrar membranas biológicas y promover la partición de gotas de tamaño nanométrico en la mucosa nasal, lo que resulta en un mayor tiempo de residencia [68].

Por otro lado, los NLC poseen este perfil dual de acción, debido a que a nivel tópico presentan diferentes características como su capacidad para mejorar la estabilidad química de los activos, protegiendo los ingredientes de la degradación por factores ambientales como la luz y el oxígeno. Asimismo, mejoran la biodisponibilidad de los activos en la piel, facilitando su penetración y absorción en las capas cutáneas, y aumentan la estabilidad física de las formulaciones tópicas, evitando la agregación de partículas y manteniendo la uniformidad del producto [69]. Además, son capaces de proporcionar un efecto oclusivo en la superficie de la piel, creando una película protectora que reduce la pérdida de agua transepidérmica y aumenta la hidratación de la piel. Los NLC proporcionan una mejor hidratación y oclusión de la piel en comparación con los sistemas de administración tradicionales (por ejemplo, las emulsiones) debido a su tamaño pequeño. El grado de oclusión depende del tamaño de las partículas, donde las partículas más pequeñas permiten una menor evaporación de agua [69,70].

Debido a esta capacidad dual de los NLC, tanto como sistema de liberación de fármacos como de acción local hidratante, los NLC pueden aplicarse a una gran variedad de patologías con diferentes fines terapéuticos, desde tratar enfermedades como las enfermedades proliferativas que requieren un uso dirigido de fármacos a los tejidos internos, hasta su aplicación tópica con el fin de mejorar superficies como la piel o el ojo.

1.2. NLC para el tratamiento de enfermedades proliferativas

El cáncer es una enfermedad con una gran morbididad y mortalidad a nivel mundial. Esta patología se puede considerar como un conjunto de enfermedades caracterizadas por el crecimiento descontrolado y la proliferación de células anormales en el cuerpo [71]. Estas células, denominadas células cancerosas o tumorales, pueden invadir y destruir tejidos sanos y pueden diseminarse a otras partes del cuerpo a través del sistema sanguíneo o linfático, un proceso conocido como metástasis [72]. Anualmente, decenas de millones de personas son diagnosticadas con cáncer en todo el mundo y más de la mitad de los pacientes fallecen. En muchos países europeos el cáncer ocupa el segundo lugar como causa de muerte, solo superado por las enfermedades cardiovasculares [73]. Según el último análisis a nivel mundial (Figura 3), en el año 2022 hubo una incidencia de alrededor de 20 millones de casos, con una mortalidad de 10 millones de personas aproximadamente [74]. Debido a las mejoras significativas en el tratamiento y la prevención de las enfermedades cardiovasculares, el cáncer se convertirá próximamente en la principal causa de muerte en varias regiones del mundo. Dado que la población adulta de edad avanzada es la más susceptible al cáncer y el envejecimiento poblacional continúa aumentando en muchos países, el cáncer seguirá siendo un importante problema de salud global [75,76].

Los tratamientos terapéuticos convencionales utilizados para el tratamiento del cáncer son la cirugía, la quimioterapia, la radioterapia, la inmunoterapia y la terapia hormonal. Aunque la quimioterapia y la radioterapia pueden ser citostáticas y citotóxicas, estos métodos a menudo se asocian con efectos secundarios agudos y un alto riesgo de recidivas. Los efectos secundarios más comunes inducidos por estos tratamientos incluyen neuropatías, supresión de la médula ósea, trastornos gastrointestinales y cutáneos, pérdida de cabello y fatiga [77].

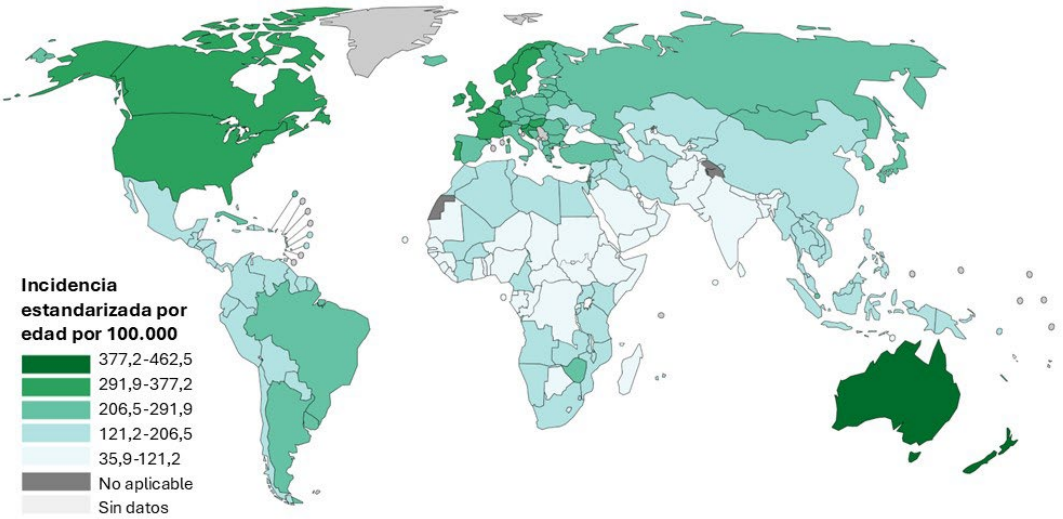

Figura 3. Incidencia estandarizada por edad de cáncer en el 2022 según la agencia internacional de investigación contra el cáncer "*Global Cancer Observatory*" [74].

Además, los fármacos utilizados en la quimioterapia pueden acabar presentando multiresistencia a fármacos (*multidrug resistance* o MDR), que limitan su eficacia. Por otra parte, los agentes inmunoterapéuticos han mostrado resultados prometedores no solo en el tratamiento del cáncer primario, sino también en la prevención de las metástasis y la reducción de la tasa de recurrencia. Sin embargo, la inmunoterapia puede acabar provocando, como principal efecto secundario, una enfermedad autoinmunitaria. Además, diferentes estudios sugieren que la inmunoterapia es menos efectiva frente a tumores sólidos que linfomas [78]. Estos cánceres generan una matriz extracelular inusual que dificulta la infiltración de las células inmunitarias. Estas terapias e inmunoterapias interfieren con las vías de señalización cruciales para los comportamientos malignos y las funciones homeostáticas normales de la epidermis y la dermis, causando efectos adversos dermatológicos [79]. Otra estrategia novedosa es la medicina personalizada o medicina de precisión en oncología, que es un enfoque emergente para el tratamiento y la prevención de tumores que tiene en cuenta la variabilidad inter e intratumoral en los genes, el entorno inmunológico tumoral y el estilo de vida y las morbilidades de cada persona diagnosticada con cáncer [80]. Sin

embargo, su implementación llevará tiempo y requerirá inversiones sustanciales en infraestructura. Se requieren modificaciones fundamentales en la infraestructura y los métodos de recopilación, intercambio y almacenamiento de datos para lograr un tratamiento personalizado [81].

La demanda de desarrollar nuevas estrategias para buscar terapias precisas contra el cáncer sigue ganando impulso en estos últimos años. En las últimas décadas, las NPs están ganando interés para abordar las limitaciones de los enfoques terapéuticos actuales. Los sistemas de administración de fármacos basados en NPs han demostrado beneficios en el tratamiento y control del cáncer al ofrecer una buena farmacocinética, una diana precisa, menos efectos secundarios y menor efecto MDR [82].

Siguiendo los avances de la nanotecnología, desde el año 2010 se han comercializado varios fármacos nanoterapéuticos y muchos otros han entrado en la fase clínica. Estos fármacos han progresado en el campo de los sistemas de administración de fármacos y la MDR a fármacos antitumorales al brindar la oportunidad de terapias combinadas y la inhibición de los mecanismos de resistencia a los fármacos [83]. Concretamente, las NPs han demostrado ser capaces de penetrar profundamente en los tejidos, lo que potencia el efecto de permeabilidad y retención mejorada (EPR) (Figura 4). Además, las características de su superficie influyen en la biodisponibilidad y la vida media al atravesar eficazmente las fenestraciones epiteliales. El EPR se considera una razón importante para la focalización pasiva de tumores por partículas submicrónicas, como las NPs menores de 400 nm [84].

La ventaja más importante de los NLC en la administración de fármacos quimioterapéuticos es la capacidad de este sistema nanoestructurado de encapsular más de un fármaco con diferentes propiedades fisicoquímicas debido a la presencia de dos lípidos distintos [84,85]. Durante la preparación de los NLC, se puede controlar con precisión la proporción de dos antineoplásicos diferentes con propiedades fisicoquímicas distintas para su administración conjunta a las células tumorales. Además, materiales genéticos como ARN, ADN, etc., también pueden administrarse conjuntamente con fármacos quimioterapéuticos lipofílicos. Los NLC poseen

una mayor capacidad de carga de fármacos lipofílicos debido a su composición de lípidos líquidos y proporcionan una mayor estabilidad de almacenamiento, una expulsión de fármaco insignificante y una liberación controlada del fármaco en comparación con otros sistemas nanoparticulados [84,86].

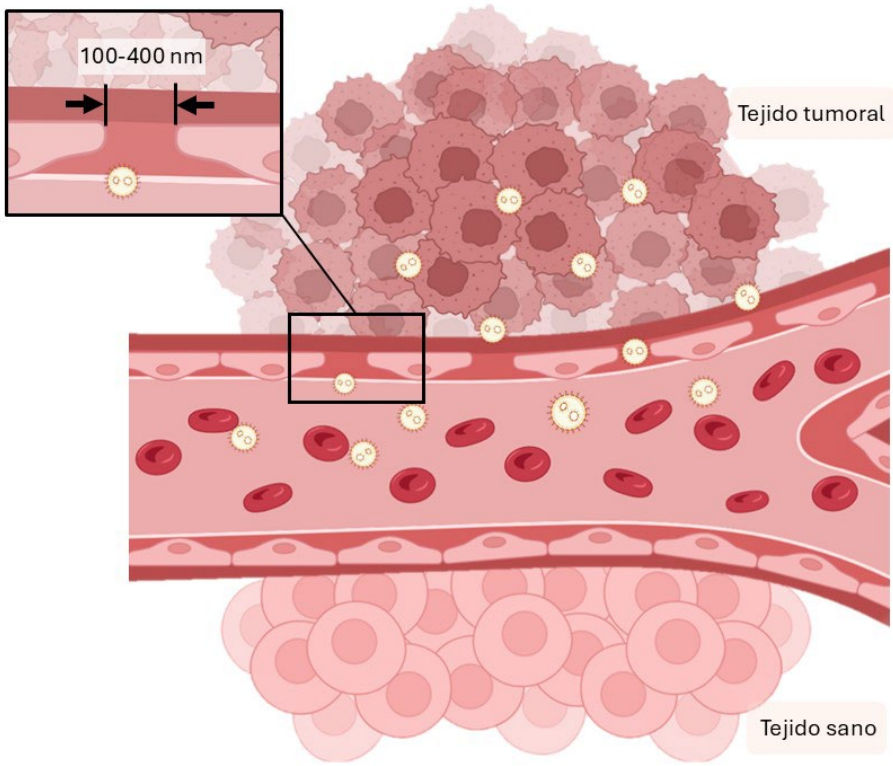

Figura 4. Los tejidos normales carecen de espacios entre las células endoteliales adyacentes, lo que permite que las NPs se extravasen de la vasculatura. Los tejidos tumorales presentan espacios grandes (100-400 nm) entre las células endoteliales de la vasculatura tumoral. El EPR permite que las nanopartículas no dirigidas de tamaño adecuado se unan, internalicen y liberen fármacos en el tumor. Basado en [87].

En la actualidad, los productos naturales juegan un papel crucial en la terapia del cáncer. Un número considerable de agentes anticancerígenos utilizados en la clínica son naturales o derivados de fuentes naturales como plantas, animales y microorganismos (incluidos los de origen marino). Ejemplos clásicos de compuestos derivados de plantas son la vincristina, la irinotecan,

el etopósido y el paclitaxel, los cuales son ampliamente utilizados en el tratamiento del cáncer [88,89]. Por este motivo la comunidad científica ha buscado nuevos tratamientos contra los diferentes procesos tumorales, con principios activos como la Apigenina (APG) y la Melatonina (MEL).

Además, se podría utilizar matrices activas como el RHO para potenciar la actividad terapéutica de éstos. El RHO ha demostrado en un estudio en el cual usaron un sistema de liberación nanométrico (nanocápculas) conteniendo el RHO como excipiente, incrementaba dos veces el efecto antitumoral en una línea celular de cáncer de mama (MCF-7) y una de glioma, sin afectar a la viabilidad de los astrocitos [90]. Por otro lado, el extracto del fruto y las semillas de *Rosa canina*, que comparte cierta similitud con la composición del RHO, ha sido objeto de varias investigaciones que demuestran su eficacia en este ámbito (Tabla 4).

Tabla 2. Resumen de los estudios de la actividad antiproliferativa del rosa de mosqueta.

Extracto	Línea celular	Resultados	Ref.
Extracto etanólico	Cáncer de mama MCF-7 y MDA-MB-468	Inducción de apoptosis tardía en MCF-7 y apoptosis temprana en MDA-MB-468.	[91]
Extracto del fruto	Cáncer colorrectal Caco-2	Alteraciones en el ciclo celular (muerte celular por una vía apoptótica).	[92]
Extracto acuoso	Cáncer colorrectal HT-29	Disminución de la motilidad celular dosis-dependiente.	[93]
Extracto crudo	Glioblastoma A-172, U-251 MG y U-1242 MG	Inhibición de la proliferación celular al disminuir la fosforilación de AKT, MAPK y p70S6K.	[94]
Polifenoles acídicos	Cáncer colorrectal Caco-2	Disminución de la viabilidad celular.	[95]
Tres fracciones del té	Cáncer cervical HeLa, de mama MCF-7 y cáncer colorrectal HT-29	Los flavonoides mostraron la actividad antirradical y mayor inhibición del crecimiento celular en comparación a las otras dos fracciones (vitamina C y fenoles).	[96]

A pesar de que los mecanismos exactos por los cuales el extracto de *Rosa canina* ejerce su efecto antiproliferativo no están completamente dilucidados, se ha propuesto que la reducción de las especies reactivas de oxígeno (ROS), la modulación del ciclo celular y la inducción de apoptosis podrían estar involucrados [97]. Concretamente se ha descrito que el extracto regula el ciclo celular, ralentizando el crecimiento de las células cancerosas en la fase G_0/G_1 o induciendo su apoptosis [91,94].

1.3. NLC para el tratamiento de enfermedades oculares

El ojo humano es un órgano complejo con intrincadas barreras anatómicas y fisiológicas. Éste tiene una estructura esférica de tres capas: la capa externa y fibrosa es la esclerótica; la capa media y vascular se llama úvea; y la capa más interna, formada por tejido nervioso, la retina. Además, el ojo se divide en el segmento anterior y el segmento posterior. El segmento anterior contiene la córnea, la conjuntiva, el iris, los procesos ciliares, el cristalino, el aparato lagrimal, los párpados y las cámaras anterior y posterior. El segmento posterior, que se encuentra fisiológicamente muy protegido por diferentes barreras, está detrás del cristalino y contiene la esclerótica, la coroides, la retina, el humor vítreo y el nervio óptico (Figura 5) [12].

Las enfermedades más comunes que afectan el segmento anterior del ojo son el síndrome del ojo seco (*dry eye disease* o DED), el glaucoma, la conjuntivitis alérgica, la uveítis anterior y las cataratas [99]. Las enfermedades prominentes que afectan el segmento posterior del ojo incluyen la degeneración macular relacionada con la edad (*age-related macular degeneration* o AMD), el edema macular diabético, la vitreoretinopatía proliferativa, la uveítis posterior y el citomegalovirus [100]. A nivel global, la discapacidad visual es un problema de salud pública significativo. Según datos recientes, aproximadamente 258 millones de personas en el mundo presentan alguna discapacidad visual, y de ellas, 39 millones son completamente ciegas [101]. Estos datos resaltan la necesidad de intensificar la investigación en el desarrollo de nuevas estrategias terapéuticas para el tratamiento de las enfermedades oculares, con el objetivo

de mejorar significativamente la calidad de vida y la función visual de los pacientes.

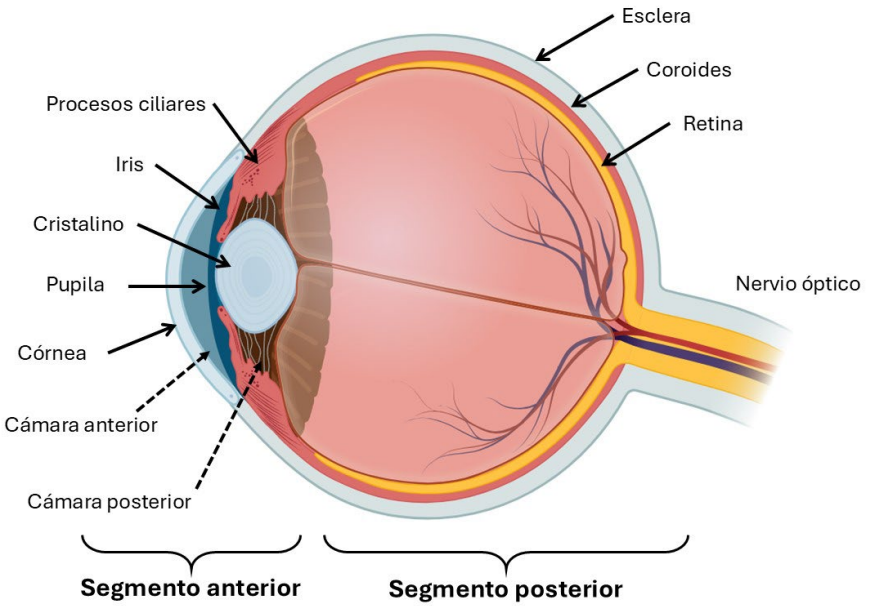

Figura 5. Anatomía del ojo humano. Basado en [98].

La administración tópica de medicamentos oftálmicos a través de gotas o pomadas es el método más común para tratar afecciones oculares. Sin embargo, la biodisponibilidad de estos fármacos en el ojo es limitada debido a diversos factores fisiológicos y anatómicos [102]. La producción constante de lágrimas por las glándulas lacrimales diluye los medicamentos, reduce su tiempo de contacto con la superficie ocular y dificulta su penetración a través del epitelio corneal. Además, el volumen administrado de las formulaciones oftálmicas puede ser drenado rápidamente a través del conducto nasolacrimal hacia la circulación general, disminuyendo aún más la cantidad de fármaco que alcanza los tejidos oculares. Por último, la circulación sanguínea en la conjuntiva también puede influir en la absorción de los medicamentos tópicos [103].

En conjunto, estas barreras fisiológicas y anatómicas resultan en una pérdida significativa de fármaco durante la administración tópica, estimada en

alrededor del 95 % [101]. Esto plantea un desafío para el desarrollo de formulaciones oftálmicas más efectivas que puedan superar estas limitaciones y mejorar la eficacia terapéutica.

Debido a la complejidad anatómica del ojo, las NPs son un sistema de liberación de fármacos capaces de penetrar estas barreras para llegar a cualquier tejido ocular [104]. En particular, los NLC poseen propiedades que las hacen únicas respecto al resto de sistemas nanoscópicos, posicionándolas como un tratamiento prometedor para diferentes patologías oculares debido a su potencial como sistemas de liberación, pero también sus mecanismos con los cuales hidratan la superficie ocular (Figura 6) [105]. La biocompatibilidad y las propiedades mucoadhesivas de los NLC mejoran su interacción con la mucosa ocular, lo que contribuye a prolongar el tiempo de residencia corneal del fármaco cargado, aumentando su biodisponibilidad ocular y reduciendo tanto los efectos secundarios locales como sistémicos. Los NLC podrían diseñarse para tratar los trastornos oculares más importantes, como la inflamación, el DED, procesos tumorales o incluso enfermedades que afectan a estructuras del segmento posterior del ojo [106].

Los productos naturales se han utilizado en la medicina tradicional durante siglos y siguen desempeñando un papel importante en el desarrollo de tratamientos modernos y en la terapéutica clínica. Recientemente, ha habido un aumento en la investigación que explora la eficacia de los productos naturales en el tratamiento de los trastornos oculares y sus mecanismos fisiológicos subyacentes [108]. La suplementación con productos naturales ha demostrado efectos preventivos y terapéuticos en personas con riesgo de padecer o con enfermedades oculares relacionadas con la edad debido a su capacidad para eliminar radicales libres, disminuir las moléculas inflamatorias, neutralizar la reacción de oxidación que ocurre en las células fotorreceptoras, disminuir el factor de crecimiento endotelial vascular y aumentar el sistema de defensa antioxidante [109]. Por este motivo la comunidad científica ha buscado nuevos tratamientos a base de productos naturales, como la APG y la MEL.

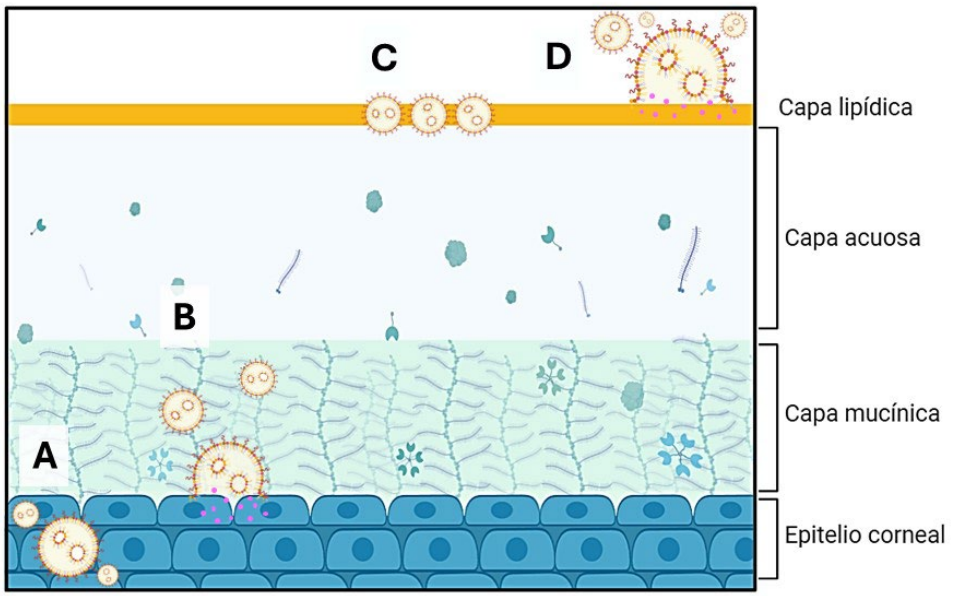

Figura 6. Mecanismos de acción propuestos de las NPs lipídicas cuando son administradas en forma de colirio. (A) Internalización en el epitelio corneal. (B) Unión a la glicocálix del epitelio y liberación sostenida del fármaco encapsulado en el epitelio corneal. (C) Unión a la capa lipídica de la película lagrimal. (D) Fusión de los NLC con la capa lipídica, mejorando la estabilidad de la película lagrimal. Basado en [107].

Además, podría utilizarse un excipiente natural como el RHO para potenciar el efecto de la APG y la MEL, debido a que es ampliamente conocido por sus propiedades hidratantes y cicatrizantes a nivel tópico. Sin embargo, el uso del aceite como excipiente activo en afecciones oculares no ha sido investigado. Por un lado, el efecto directo que podría aportar el RHO aplicado tópicamente en la superficie ocular es su capacidad regeneradora, necesario en enfermedades como el DED. En piel se ha descrito que las lesiones cutáneas tratadas con RHO exhiben una mejor reconstrucción y mayor formación de colágeno, un incremento en la proliferación de fibroblastos y menor infiltración de células inflamatorias [110]. Uno de los mecanismos que se han descrito para su capacidad regenerativa es la modulación de los macrófagos, que adoptan dos fenotipos principales: M1 (proinflamatorio) y M2 (antiinflamatorio). La transición efectiva de M1 a M2 es esencial para una cicatrización adecuada, donde el RHO promueve este cambio, favoreciendo la

cicatrización [110]. Por otra parte, debido a sus propiedades antioxidantes y antiinflamatorias, tendría potencial en muchas enfermedades oculares, como el DED o cualquier otra afección que curse con inflamación, como la uveítis o el glaucoma. Se han realizado diferentes estudios en distintos tejidos utilizando el extracto de rosa mosqueta, que han puesto en relieve una gran capacidad de reducir la inflamación a través de diversos mecanismos [111], como la inhibición del proceso de señalización factor nuclear κB (NF-κB), reduciendo la producción de enzimas (MMP, COX-2) y citoquinas proinflamatorias (TNFα, IL-1β, IL-6, CCL5) [112,113]. Además, los galactolípidos juegan un papel importante en sus efectos antiinflamatorios ya que son capaces de inhibir específicamente la producción de moléculas inflamatorias como las prostaglandinas y el óxido nítrico. Esto, a su vez, reduce la secreción de diversas citoquinas que alimentan la inflamación [34].

1.3.1. Inflamación ocular

La inflamación ocular se ha convertido en un tema clave en oftalmología. Existen numerosas enfermedades inflamatorias oculares que pueden afectar distintas localizaciones, incluyendo la órbita, los anexos oculares, la superficie ocular, la conjuntiva, la córnea, la esclerótica, la úvea, los vasos retinianos y el nervio óptico. El abordaje de la inflamación ocular presenta desafíos diagnósticos y terapéuticos, considerando la etiología y el pronóstico individual. Recientemente se ha evidenciado que algunas patologías previamente consideradas no inflamatorias, como la AMD, el edema macular, el glaucoma, los procesos tumorales y el síndrome del ojo seco dependen en cierto grado de mediadores inflamatorios, por lo que su tratamiento debería abordarse, al menos parcialmente, como una condición inflamatoria [114]. Para el tratamiento de la inflamación ocular, existen dos principales grupos de fármacos con propiedades antiinflamatorias: los antiinflamatorios no esteroideos (AINE) y los corticosteroides [115]. Sin embargo, los tratamientos a largo plazo con éstos pueden inducir efectos adversos locales. En el caso de los AINE, pueden provocar úlceras y perforaciones en la córnea [116], y los corticoides pueden producir muchas complicaciones, tales como la toxicidad epitelial, hipertensión ocular o cataratas [117].

Los NLC constituyen un sistema prometedor para tratar la inflamación ocular, debido a que pueden aumentar la biodisponibilidad de fármacos con acción antiinflamatoria y además, su matriz lipídica puede aportar propiedades adicionales al fármaco encapsulado, ya que muchos lípidos tienen propiedades antiinflamatorias y antioxidantes [118].

1.3.2. Síndrome del ojo seco (DED)

El DED es una patología multifactorial que afecta la película lagrimal y la superficie ocular provocando síntomas de incomodidad, alteraciones visuales y potencialmente daño en la superficie del ojo, pudiendo producir úlceras corneales en los casos más graves. Se caracteriza por una desestabilización de la película lagrimal, donde se produce un aumento de la osmolaridad del film lagrimal, irritando la superficie ocular y provocando inflamación [119]. Además, el estrés desecante, el oxidativo y el de hiperosmolaridad activan las vías de señalización celular en la superficie ocular, lo que conduce a la producción de citocinas proinflamatorias (TNF-α, IL-1β e IL-6) y metaloproteinasa de matriz (principalmente MMP9). Estos factores promueven la maduración de las células presentadoras de antígenos y permiten que las células presentadoras de antígenos maduras migren a los ganglios linfáticos a través de los vasos linfáticos aferentes. En los ganglios linfáticos, las células presentadoras de antígeno (APC) inducen a las células T efectoras (Th1 y Th17) y las reclutan para migrar a la superficie ocular. Mientras tanto, las APC activan el inflamasoma NLRP3, promoviendo la secreción de IL-1β e IL-18 y agravando aún más la inflamación de la superficie ocular (Figura 7) [120].

La primera línea de tratamiento consiste en aplicar lágrimas artificiales en forma de colirio, gel o pomada para lubricar el ojo, manteniendo así la humedad de la superficie ocular. Estas lágrimas artificiales actúan aliviando instantáneamente los síntomas al disminuir la osmolaridad de la lágrima y diluir los marcadores inflamatorios. Sin embargo, las lágrimas artificiales carecen de propiedades antiinflamatorias y no abordan la patogenia fundamental de la enfermedad. Por otro lado, los tratamientos habituales para la inflamación ocular incluyen corticosteroides y AINE, pero su uso prolongado

conlleva efectos secundarios severos [121,122]. En estos últimos años la nanotecnología ha ido ganando espacio en el mercado de DED. En particular, los NLC debido a su composición lipídica, pueden mejorar y contribuir a formar un recubrimiento lipídico sobre la superficie ocular, evitando así la evaporación de los componentes acuosos de la lágrima. Además, cuando se combinan con excipientes acuosos como el HA o el PEG, los NLC mejoran las deficiencias tanto acuosas como lipídicas de la película lagrimal, contribuyendo a una reducción de las molestias oculares que experimentan los pacientes que sufren esta enfermedad ocular [123].

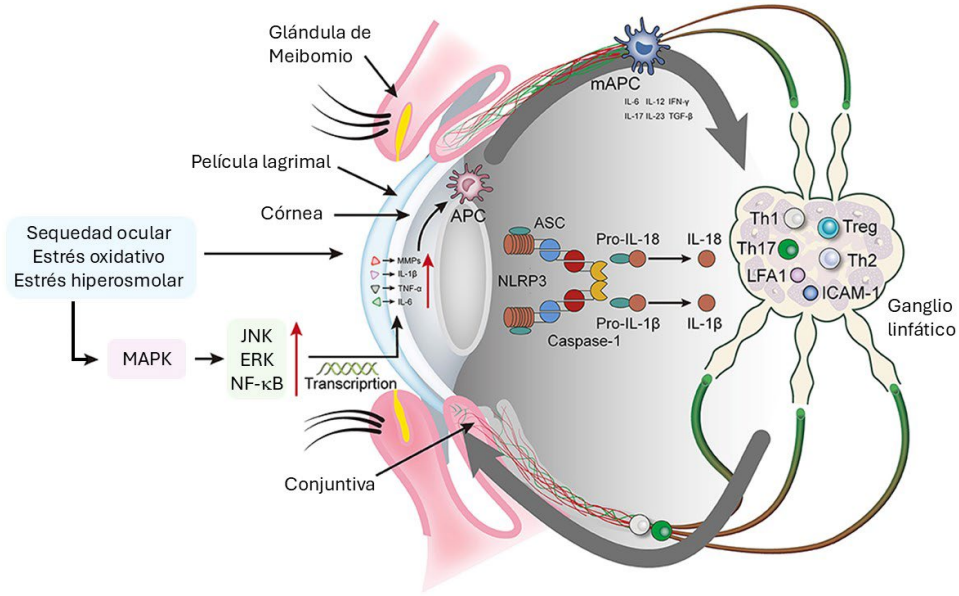

Figura 7. Respuesta inflamatoria de la superficie ocular en el ojo seco. Adaptado de [120].

1.3.3. Melanoma ocular

El cáncer ocular es una enfermedad que se caracteriza por el crecimiento descontrolado de células anormales en el ojo, que puede afectar a cualquier parte del ojo, incluyendo la retina, la úvea (principalmente iris y coroides) y el párpado. Estudios epidemiológicos previos en poblaciones occidentales sugieren que los tumores oculares representan alrededor del 0,2 % de los

diagnósticos de cáncer y menos del 0,1 % de las muertes por cáncer. Sin embargo, a pesar de su baja incidencia, estos cánceres disminuyen significativamente la calidad de vida y son mortales si no se tratan. El melanoma uveal (*uveal melanoma* o UM) es el cáncer intraocular más frecuente en adultos y también el más letal, con una tasa de supervivencia del 50 % a 10 años. En niños, el cáncer intraocular más común es el retinoblastoma cuyo tratamiento de primera línea es la enucleación, lo que conlleva a una ceguera irreversible [124]. El uso de NPs se ha investigado ampliamente en el diagnóstico y tratamiento de procesos tumorales oculares, dado que facilitan una administración de fármacos sostenida y dirigida con efectos secundarios mínimos. Su tamaño nanométrico, morfología y características superficiales facilitan su entrada en el tejido ocular, superando las barreras oculares, mejorando así su biodisponibilidad y eficacia terapéutica. Son lo suficientemente grandes para no filtrarse a través de la vasculatura y lo suficientemente pequeñas para ser eliminadas de la circulación por fagocitosis [125].

1.4. Apigenina

La APG, también conocida como 4',5,7-trihidroxiflavona (Figura 8), es uno de los flavonoides más abundantes y estudiados. Se encuentra en cantidades significativas en plantas como el tomillo y otras especies, pero principalmente se encuentra en la manzanilla (*Matricaria chamomilla*). Es un metabolito secundario vegetal, que suele encontrarse en la naturaleza en forma glicosilada, siendo más soluble que su forma pura, la cual es inestable y poco soluble en agua [126]. Por esta razón, una estrategia para proteger y solubilizar a la APG sería su encapsulación en NLC.

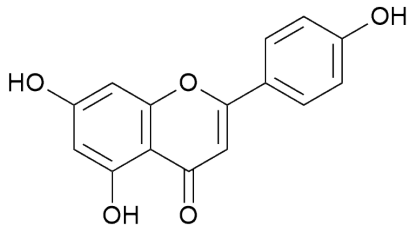

Figura 8. Estructura química de la APG.

1.4.1. Apigenina como tratamiento antiproliferativo

La primera referencia científica de la APG se remonta a la década de 1950, pero fue en los años 80 cuando se estableció su conexión con los procesos tumorales. Estudios pioneros revelaron sus propiedades terapéuticas, destacando su capacidad para inhibir la mutagénesis y la promoción tumoral. Desde entonces la APG ha sido objeto de una intensa investigación, posicionándose como un prometedor agente quimiopreventivo del cáncer en una amplia gama de tumores [127,128]. Su mecanismo de acción es complejo y multifactorial. La APG interactúa con diversas vías moleculares, modulando la expresión de genes supresores de tumores y alterando procesos clave como la angiogénesis, la inflamación (a través de la inhibición del NF-κB) y la muerte celular programada. Además, se ha observado que induce la autofagia, un proceso celular fundamental en la eliminación de componentes dañados, lo que contribuye a su efecto antitumoral [129]. Estos hallazgos sugieren que la

APG podría actuar en múltiples frentes, lo que la convierte en una molécula con un gran potencial terapéutico en estos procesos [130].

1.4.2. Apigenina en patologías oculares

La manzanilla ha sido tradicionalmente una de las plantas más usadas a nivel ocular para tratar conjuntivitis y limpiar la zona ocular [131]. Uno de los principales componentes de ésta es la APG, que además de sus prometedoras propiedades antioxidantes, antinflamatorias y antibacterianas posee ciertas propiedades protectoras a nivel ocular (Tabla 2) [132].

Por un lado, la APG destaca como antiinflamatorio debido a que ha demostrado ser capaz de reducir citoquinas proinflamatorias, como las interleucinas 6 (IL-6), IL- 1β y el TNF-α y aumentar las interleucinas antiinflamatorias como la IL-10 [133]. Esto hace que la APG pueda resultar un fármaco muy útil en enfermedades que cursan con inflamación ocular, como podría ser el DED. Por otro lado en las capas más internas del ojo, es decir retina y nervio óptico, la APG ha demostrado tener capacidad neuroprotectora principalmente gracias a su poder antioxidante, protegiendo estos tejidos del daño oxidativo [134]. Debido a todas estas propiedades prometedoras, la APG es un activo con un elevado potencial a nivel ocular, tanto para tratar afecciones que afectan a las capas más externas del ojo, como el DED, como para las que afectan a los tejidos más internos, como el glaucoma, la retinopatía diabética, o la AMD.

Tabla 3. Evidencias científicas de la APG para su uso oftálmico en diferentes modelos *in vitro* e *in vivo*.

Modelo	Resultados	Ref.
Ratas Sprague–Dawley, administración por sonda gástrica.	- Recuperación de la función de la superficie ocular. - Disminución de los niveles de factor de TNF-α, IL-1β e IL-6.	[133]
Ratones C57BL/6 KO Nrf2, administración intragástrica.	- Promoción de la translocación nuclear de Nrf2. - Incremento de los niveles de expresión de Nrf2. - Aumento de las actividades del superóxido dismutasa y GSH-Px. - Disminución de los niveles de ROS y malondialdehido.	[134]
Cultivo primario de células de ganglionares de retina de rata.	- Disminución de la viabilidad de las células ganglionares de la retina (RGC) inducida por el TNF-α. - Inhibición de la apoptosis inducida por TNF-α. - Aumento de la producción de ATP y la captación de oxígeno. - Reducción de la actividad de la caspasa-3. - Disminución de la activación del NF-κB.	[135]
Células humanas endoteliales microvasculares de la retina. Ratones C57BL/6, administración intravítrea.	- Bloqueo de múltiples citoquinas que inducen hiperpermeabilidad. - Estabilización de tres tipos de monocapas de células endoteliales vasculares primarias. - Mejora de la función de la barrera vascular retiniana *in vivo*.	[136]
Línea celular de retina de rata (R28). Ratas Wistar, administración intravítrea.	- Protección de la capa plexiforme interna de la retina y el complejo de células ganglionares. - Reducción de la apoptosis de las RGC y la liberación de lactato deshidrogenasa. - Aumento del potencial de membrana mitocondrial. - Disminución de la producción de las ROS extracelulares.	[137]

Línea celular de microglía de ratón (BV2). Ratones rd1, administración intravítrea.	- Supresión de la producción de quimiocinas inducida por lipopolisacárido (LPS). - Inhibición de la activación M1 inducida por LPS. - Reducción de las quimiocinas inflamatorias en la retina. - Supresión de la activación de microglía y glía de Müller. - Aumento del grosor de la capa nuclear externa de la retina de los ratones.	[138]
Línea celular de microglía humana (HMC3). Ratones C57BL/6J.	- Disminución de la producción de factores inflamatorios inducidos por LPS e IFN-γ en la microglía *in vitro*. - Reducción de los puntajes clínicos y patológicos de la uveítis autoinmune. - Reducción de los niveles de las citoquinas inflamatorias en la retina. - Inhibición de la transición de microglía M1 en la retina.	[139]
Ratones C57BL/6J, administración intravítrea o intraperitoneal.	- Supresión de la neovascularización. - Efectos antiapoptóticos y antioxidantes en la retinopatía inducida por oxígeno.	[140]
Células humanas endoteliales de la vena umbilical. Ratas pardas de Noruega.	- Inhibición del desarrollo de la neovascularización coroidea. - Modulación de la proliferación y migración de las células endoteliales.	[141]
Línea celular del epitelio pigmentario de la retina humana (ARPE-19).	- Aumento de la supervivencia de las células tratadas con peróxido. - Protección de las células ante la apoptosis inducida por peróxido. - Aumento de la expresión de ARNm, de la proteína de Nrf2 y estimulación de su translocación nuclear. - Incremento de la expresión y actividad de enzimas antioxidantes. - Disminución de los niveles de ROS y MDA.	[142]

1.5. Melatonina

La MEL es una neurohormona producida principalmente por la glándula pineal que regula el ritmo circadiano y los ciclos de sueño (Figura 9). La MEL se ha identificado en todos los grupos principales de seres vivos, incluyendo bacterias y otros microorganismos unicelulares, plantas y animales, así como en humanos [143]. En la actualidad, la MEL se prescribe para ayudar a conciliar el sueño, aunque presenta muchos otros efectos beneficiosos. Por esta razón, actualmente se acepta que la MEL no solo es una hormona, sino también un protector celular, involucrado en la inmunomodulación, los procesos antioxidantes y la hematopoyesis. Además, numerosos estudios han demostrado que posee importantes propiedades oncoestáticas, tanto a través de mecanismos dependientes como independientes de receptores [144].

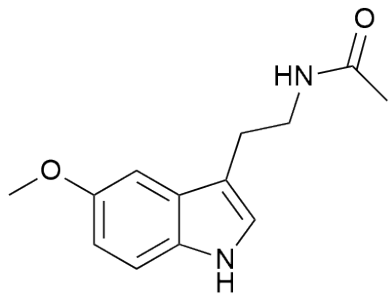

Figura 9. Estructura química de la MEL.

Sin embargo, la MEL tanto a nivel fisiológico como químico, se degrada principalmente por la luz, aunque también le afecta la temperatura y se desestabiliza en solución acuosa [145]. Por esta razón, su encapsulación en NLC la protegería de esta degradación por factores externos, permitiendo ejercer su acción.

1.5.1. Melatonina como tratamiento antiproliferativo

En la actualidad, muchas de las propiedades antitumorales de la MEL están bastante bien descritas y la evidencia de diferentes estudios clínicos (Tabla 3) indican una relación entre la MEL y la supresión tumoral. Los estudios *in vitro* sugieren que tanto dosis farmacológicas como fisiológicas son capaces de

reducir el crecimiento de células malignas de mama y otras células tumorales. En modelos de roedores, la pinealectomía (extirpación de la glándula pineal) estimula el crecimiento tumoral, mientras que la administración exógena de MEL ejerce actividad anti-iniciadora y oncoestática en diversos cánceres inducidos químicamente [146].

Tabla 4. Evidencia clínica de los efectos anticancerígenos de la MEL. Adaptado de [147].

Tipo de estudio	Tipo de cáncer	Conclusión
Ensayo prospectivo de fase II	Mama	La MEL mejoró el sueño y la calidad de vida en pacientes con cáncer.
Ensayo clínico aleatorizado de fase II	Cabeza y cuello	La MEL redujo la mucositis y mejoró el dolor en pacientes tratados con radiación concurrente.
Ensayo clínico aleatorizado	Pulmón metastásico	La administración concomitante de la MEL puede reducir la anemia inducida por cisplatino en pacientes con cáncer.
Estudio piloto aleatorizado	Gastrointestinal	La MEL puede producir un efecto estabilizador del peso.
Estudio aleatorizado	Colorrectal	La IL-2 subcutánea en dosis bajas y la MEL se pueden utilizar como terapia de segunda línea para el tratamiento.
Estudio piloto de fase II	Mama metastásico	La MEL indujo regresiones tumorales objetivas en pacientes con cáncer de mama metastásico refractario al tamoxifeno.

Los mecanismos más destacados propuestos para explicar la acción antitumoral de la MEL incluyen su actividad antimitótica y antioxidante, y su potencial modulación de la duración del ciclo celular a través del control de la vía p53-p21. Se cree que la MEL tiene actividad antimitótica por su efecto directo sobre la proliferación dependiente de hormonas a través de la interacción con receptores nucleares. Otra explicación es que esta hormona aumenta la expresión del gen supresor tumoral p53. Se ha demostrado que las células que carecen de p53 son genéticamente inestables y por lo tanto, más propensas a desarrollar tumores [148,149].

1.5.2. Melatonina en patologías oculares

Fisiológicamente, la MEL se encuentra en los tejidos oculares, ya que tiene diferentes receptores específicos en retina, córnea, cuerpo ciliar, cristalino, coroides y esclera [150]. Aunque no se conoce exactamente el rol de la MEL en el ojo, se le han atribuido diferentes propiedades. La acción más reconocida es su relación rítmica con la presión intraocular (*intraocular pressure* o IOP), reduciéndola cuando la MEL se encuentra en su pico máximo del día [151]. Otra propiedad atribuida a la MEL debido a sus receptores en la córnea, es su capacidad de acelerar la epitelización de la córnea y regular su hidratación [150]. Sus receptores en el cristalino parecen estar relacionados con su posible acción protectora frente a las cataratas [152]. A nivel de retina, se ha sugerido que los receptores de la MEL participan en los cambios relacionados con el envejecimiento. La disminución fisiológica de los niveles de MEL en las personas mayores se ha relacionado con el inicio de la AMD, lo que sugiere la participación de estos receptores en la protección contra dicha degeneración [153].

Se ha demostrado que la MEL actúa directamente como un captador de radicales libres y además, estimula diversas enzimas antioxidantes, incluyendo la superóxido dismutasa, la glutatión peroxidasa y la glutatión reductasa. Mediante estas acciones combinadas, esta hormona podría ser un agente protector contra diversas enfermedades oculares en las que la generación de radicales libres y el estrés oxidativo se consideran factores causales, como la AMD, las cataratas y el glaucoma [154]. Más allá de su acción antioxidante, se están acumulando evidencias que sugieren que los eventos mediados por los receptores de la MEL son cruciales para el mantenimiento de los ritmos oculares normales y que la alteración de estos ritmos podría conducir a una variedad de trastornos oculares, como el UM. Los primeros estudios realizados en 1997 y 1998 demostraron que la MEL puede inhibir el crecimiento de células de UM. Los precursores de la MEL, el triptófano y la serotonina no mostraron este efecto. Además, el UM podría expresar receptores transmembrana para la MEL, haciendo que esta neurohormona pueda ser un potencial tratamiento para este tipo de cáncer [155].

2

Hipótesis y objetivos

2. Hypothesis and objectives

The doctoral thesis hypothesis is the development of novel controlled drug delivery systems containing APG, MEL, or both encapsulated in biocompatible lipid NPs, which can provide an effective treatment to deliver these active compounds either to tumors, or to act topically to improve the functionality of the ocular surface. Therefore, our main hypothesis is that by incorporating APG and MEL into NLC, it may improve both drugs delivery, enhance their therapeutic efficacy, and potentially offer a new treatment for these pathologies.

The main objective of this doctoral thesis is the development and evaluation of a novel controlled drug delivery system based on NLC encapsulating APG and MEL, either individually or in combination. This system aims to address the limitations associated with the current therapies for ocular and proliferative diseases, including poor solubility, bioavailability, and chemical instability.

Therefore, the specific objectives of this research are the following ones:

- To develop and optimize nanostructured lipid systems containing APG, MEL and/or both drugs manufactured by using the hot high pressure homogenization method.
- To characterize the physicochemical properties of the formulations in terms of morphometry (average size and polydispersity index), surface charge (zeta potential) and encapsulation efficiency.
- To study the interactions between the components and their crystallinity, evaluate the stability, and demonstrate that NLC possess a controlled drug release profile.
- To evaluate the anti-proliferative activity of negatively charged formulations in different cancer cell lines, as well as their accumulation into a selected cancer cell line.

- To corroborate that the positively charged formulations are suitable for ocular administration using *in vitro* and *in vivo* models.
- To determine the *in vivo* effectiveness of the positively charged APG-NLC in a rabbit model of DED and its side effects such as inflammation.
- To investigate the potential of the positively charged MEL-NLC to treat uveal melanoma by using uveal melanoma cell line and to assess its ocular biodistribution in a rabbit model.

3

Resultados

3. Resultados

El desarrollo de la presente investigación dio lugar a seis publicaciones en forma de artículos científicos y una patente.

3.1. Dually active Apigenin-loaded nanostructured lipid carriers for cancer treatment.

3.2. Antitumoral Melatonin-loaded nanostructured lipid carriers.

3.3. Novel nanostructured lipid carriers loading Apigenin for anterior segment ocular pathologies

3.4. Melatonin loaded nanostructured lipid carriers for the treatment of uveal melanoma

3.5. Nanostructured lipid carriers co-encapsulating Apigenin and Melatonin: an innovative strategy against cancer

3.6. Combination of Apigenin and Melatonin loaded nanostructured lipid carriers as a natural ocular inflammation treatment

ANEXO. Patent: Lipid nanoparticles for the treatment of ocular diseases.

3.1. Dually active Apigenin-loaded nanostructured lipid carriers for cancer treatment

Lorena Bonilla Vidal, Marta Świtalska, Marta Espina, Joanna Wietrzyk, Maria Luisa García, Eliana B Souto, Anna Gliszczyńska, Elena Sánchez López.

International Journal of Nanomedicine

FI (JCR 2023): 6.6, Pharmacology & Pharmacy 20/354 (Q1)

2023

10.2147/IJN.S429565

International Journal of Nanomedicine

Dovepress
open access to scientific and medical research

Open Access Full Text Article

ORIGINAL RESEARCH

Dually Active Apigenin-Loaded Nanostructured Lipid Carriers for Cancer Treatment

Lorena Bonilla-Vidal[1,2], Marta Świtalska[3], Marta Espina[1,2], Joanna Wietrzyk[3], Maria Luisa García[1,2], Eliana B Souto[4,5], Anna Gliszczyńska[6,*], Elena Sánchez López[1,2,7,*]

[1]Department of Pharmacy, Pharmaceutical Technology and Physical Chemistry, University of Barcelona, Barcelona, Spain; [2]Institute of Nanoscience and Nanotechnology (IN^{2}UB), University of Barcelona, Barcelona, Spain; [3]Department of Experimental Oncology, Ludwik Hirszfeld Institute of Immunology and Experimental Therapy, Polish Academy of Sciences, Wrocław, Poland; [4]Laboratory of Pharmaceutical Technology, Department of Drug Sciences, Faculty of Pharmacy, University of Porto, Porto, Portugal; [5]Associate Laboratory i4HB—Institute for Health and Bioeconomy, Faculty of Pharmacy, University of Porto, Porto, Portugal; [6]Department of Food Chemistry and Biocatalysis, Wrocław University of Environmental and Life Sciences, Wrocław, Poland; [7]Unit of Synthesis and Biomedical Applications of Peptides, IQAC-CSIC, Barcelona, Spain

*These authors contributed equally to this work

Correspondence: Elena Sánchez López; Anna Gliszczyńska, Email esanchezlopez@ub.edu; anna.gliszczynska@upwr.edu.pl

Purpose: Cancer is one of the major causes of death worldwide affecting more than 19 million people. Traditional cancer therapies have many adverse effects and often result in unsatisfactory outcomes. Natural flavones, such as apigenin (APG), have demonstrated excellent antitumoral properties. However, they have a low aqueous solubility. To overcome this drawback, APG can be encapsulated in nanostructured lipid carriers (NLC). Therefore, we developed dual NLC encapsulating APG (APG-NLC) with a lipid matrix containing rosehip oil, which is known for its anti-inflammatory and antioxidant properties.

Methods: Optimisation, physicochemical characterisation, biopharmaceutical behaviour, and therapeutic efficacy of this novel nanostructured system were assessed.

Results: APG-NLC were optimized obtaining an average particle size below 200 nm, a surface charge of −20 mV, and an encapsulation efficiency over 99%. The APG-NLC released APG in a sustained manner, and the results showed that the formulation was stable for more than 10 months. In vitro studies showed that APG-NLC possess significant antiangiogenic activity in ovo and selective antiproliferative activity in several cancer cell lines without exhibiting toxicity in healthy cells.

Conclusion: APG-NLC containing rosehip oil were optimised. They exhibit suitable physicochemical parameters, storage stability for more than 10 months, and prolonged APG release. Moreover, APG-NLC were internalised inside tumour cells, showing the capacity to cause cytotoxicity in cancer cells without damaging healthy cells.

Keywords: antitumoral, lipid nanoparticles, apigenin, rosehip oil

Introduction

Cancer is one of the leading causes of death worldwide. In 2020, there were almost 19 million patients, and almost 10 million deaths were attributed to cancer.[1,2] Traditional therapies such as chemotherapy and radiotherapy have many adverse effects and unsatisfactory treatment outcomes.[3,4] Particularly, it has been estimated that over 50% of cancer patients usually receive chemotherapy at some stage of their disease.[5] However, most existing cancer therapies simultaneously affect healthy and tumour cells, resulting in significant adverse effects.[6–8] In addition, these therapies can lead to chemoresistance. Therefore, the development of novel therapeutic strategies is an unmet medical need.[9–11]

In recent years, herbal medicines have gained wide attention owing to their beneficial effects against various diseases such as cancer.[12,13] Apigenin (APG) is a plant-derived flavone that possesses interesting properties, particularly potent antitumour activity. It has been reported that APG possesses antitumour activity against different types of cancer by triggering apoptosis, inducing autophagy, modulating the cell cycle, decreasing cell motility, inhibiting cancer cell migration and evasion, and stimulating the immune response.[14–16] Despite being a highly effective molecule that acts

Received: 5 August 2023
Accepted: 24 October 2023
Published: 23 November 2023

on many mechanisms inside the cell, its main problem is low bioavailability because of its poor water solubility and metabolization in the intestine and liver.[5,17]

In recent years, pharmaceutical research has focused on the development of nanotechnological systems applied in different fields, with special relevance to drug delivery.[18] Nanocarriers can be designed to deliver drugs into specific tissues. These nanocarriers can overcome the limitations of conventional treatments by enhancing drug solubility, improving pharmacokinetics, increasing efficacy, and reducing adverse effects. In particular, nanoparticles for cancer therapy constitute a highly interesting alternative because of the possibility of establishing passive targeting, since tumoural cell properties allow them to selectively accumulate in these cells due to their enhanced permeability and retention.[19,20] Among several nanocarriers, lipid nanoparticles and nanostructured lipid carriers (NLC) have gained attention because of their ability to encapsulate both lipophilic and hydrophilic drugs, employment of biocompatible lipids, prolonged drug release, and easy scale-up.[21–23]

To increase the solubility of APG promoting an improvement of its bioavailability, in the present work we developed APG-loaded NLC for the treatment of different types of tumors. Moreover, rosehip oil, a natural compound extracted from the seeds of wild roses, was chosen as the liquid lipid owing to its pharmaceutical properties. Rosehip oil has traditionally been used for dermal applications as a skin regenerator and possesses anti-inflammatory and antioxidant effects. Furthermore, recent studies indicate that rosehips contain active compounds with antitumoral activity.[24,25] These properties might result in a synergic way between the anticarcinogenic activity of APG and the promising activity of this active liquid lipid.[26,27]

A dual formulation of last-generation lipid nanoparticles was developed and optimised for administration of APG and rosehip oil. Physicochemical and morphological characterisation, compound interactions, and in vitro release profiles were studied. Moreover, their antiangiogenic properties and cellular internalisation were evaluated. Furthermore, the antiproliferative activity in different tumour cell lines was assesed.

Materials and Methods

Materials

APG was obtained from Apollo Scientific (Cheshire, UK). Compritol® 888 ATO was kindly gifted by Gattefossé (Madrid, Spain). Tween® 80 (polysorbate 80) and Nile Red (NR) were purchased from Sigma–Aldrich (Madrid, Spain). Rosehip oil was purchased from Acofarma Fórmulas Magistrales (Barcelona, Spain). All the other reagents were of analytical grade. A Millipore Milli-Q Plus system was used to obtain purified water.

Preparation of APG-NLC

The production of APG-NLC was carried out using the hot high-pressure homogenisation method (Homogeniser FPG 12800, Stansted, United Kingdom). Firstly, a primary emulsion with a mixture of an aqueous phase containing the surfactant, and a lipid phase containing the lipids and the drug, was prepared using an Ultraturrax® T10 basic (IKA, Germany) at 8.000 rpm for 30 s. The production conditions were 85°C, three homogenisation cycles, and 900 bar of pressure.[28]

The production of APG-NLC labelled with NR (APG-NLC-NR) was carried out following the same procedure as APG-NLC, but with the addition of a 0.0375 % of NR to the formulation.[29]

Optimization of APG-NLC

Design of Experiments (DoE) was used to optimise the formulation parameters because of its ability to acquire information by decreasing the number of experiments.[30,31] A central composite factorial design (which contained 2 replicated centre points, 16 factorial points, and 8 axial points) was prepared using Statgraphics Centurion® 18 version 18.1.12 software (Virginia, USA). Four independent variables, APG concentration, surfactant concentration, lipid phase concentration, and solid lipid concentration (LS/lipid phase), were analyzed to determine their effect on NLC physico-chemical properties. The dependent variables studied were the mean particle size (Z_{av}), polydispersity index (PDI), zeta potential (ZP), and encapsulation efficiency (EE).

Physicochemical Characterization of APG-NLC

Z_{av} and PDI were evaluated by dynamic light scattering by using a ZetaSizer Nano ZS (Malvern Instruments, Malvern, UK). Electrophoretic mobility was used to assess the ZP. For Z_{av} and PDI, the formulations were diluted 1:10 with Milli-Q water. For ZP measurements, the nanoparticles were diluted 1:20. The entrapment efficiency (EE) was indirectly measured by quantifying the non-encapsulated APG in the APG-NLC. Prior to analysis, the non-encapsulated APG was separated from NLC by filtration/centrifugation at 14,000 rpm (Mikro 22 Microliter Centrifuge, Germany) using an Amicon® Ultra-0.5 centrifugal filter device (Amicon Millipore Corporation, Ireland). The non-encapsulated APG passed through the filter, which was analysed by HPLC. EE was determined using Eq. 1:[32]

$$EE\ (\%) = \frac{Total\ initial\ amount\ of\ APG - non - encapsulated\ APG}{Total\ initial\ amount\ of\ APG} \cdot 100 \quad (1)$$

APG quantification was performed using reverse-phase high-performance liquid chromatography (RP-HPLC). In brief, samples were quantified using HPLC Waters 2695 (Waters, Massachusetts, USA) separation module, and a Kromasil® C18 column (5 µm, 150 × 4.6 mm) with a mobile phase formed by a water phase containing 2 % acetic acid, and an organic phase constituted by methanol. A gradient was applied (from 40 % to 60 % of water phase in 5 min and back in next 5 min) at 0.9 mL/min. To quantify APG, a diode array detector Waters® 2996 at 300 nm was used, and data were evaluated using Empower® 3 Software.[33,34]

Interaction Studies

Interaction Studies

Differential scanning calorimetry (DSC) was performed on a DSC 823e system (Mettler-Toledo, Barcelona, Spain). Thermograms of APG-NLC and their components were obtained in a nitrogen atmosphere by using a heating ramp from 25 to 105 °C at 10 °C/min. The data acquired was evaluated with the software Mettler STARe V 9.01 dB (Mettler-Toledo, Barcelona, Spain).[28,32]

Fourier transform infrared (FTIR) spectra of APG-NLC and their components were determined using a Thermo Scientific Nicolet iZ10 spectrometer coupled to a diamond ATR crystal and a DTGS detector (Barcelona, Spain).[35]

X-ray diffraction (XRD) profile of APG-NLC and their components was also assessed placing the samples between two polyester layers of 3.6 µm and exposing them to CuKα radiation (45 kV, 40 mA, λ = 1.5418 Å), in a working range (2θ) of 2–60°, and using a step size of 0.026°, during 200 s per step.[28]

Morphological Studies

Transmission electron microscopy (TEM) was employed to determine the morphology of the APG-NLC using a Jeol 1010 (Jeol USA, Massachusetts, USA). Firstly, copper grids were activated by UV light, and the APG-NLC (previously diluted 1:10) were stained negatively with 2% of uranyl acetate.[32]

Stability Studies

APG-NLC were stored at 3 different temperatures (4, 25, and 37°C) for several months. The study was performed by analysing light backscattering (BS) profiles using Turbiscan® Lab equipment (Formulation Inc, Worthington, USA). For this purpose, 10 mL of the sample was placed into a glass measurement cell, and BS data were acquired every 15–30 days. At the same timepoints, the values of Z_{av}, PDI, ZP, and EE were measured at 15 days or once a month until destabilization.[31]

Biopharmaceutical Behaviour

The in vitro APG release study was carried out by using Franz-type diffusion cells (Permegear, Germany) with a diffusion area of 0.20 cm^2 and cellulose dialysis membrane (MWCO 12 kDa). A receptor medium accomplishing sink conditions was used, which was constituted by a solution of PBS with 5% Tween® 80 and 20% ethanol at pH 7.4.[36] The formulations were compared to free APG. The assay was carried out at 37 ± 0.5 °C for 48 h. 300 µL of each formulation were placed on the donor compartment, and at certain time intervals, 150 µL of the sample was collected

using a syringe, and the withdrawn volume was replaced with the receptor solution. APG content of the receptor medium was analysed using HPLC. Each sample was performed in triplicate, and the cumulative amount of APG was calculated.[28]

Antiangiogenic Capacity

To determine the antiangiogenic effects of APG-NLC, a modified chorioallantoic membrane (CAM) test was used.[37] It was carried out using fertilised chicken eggs incubated at 37 °C and 85 % humidity. A lateral window was opened on the eggshell on the third day of incubation, and after 24 h of stabilization, 40 µL of the sample were inoculated to the CAM. Afterwards, the membrane was sealed and incubated for 48 h. The controls of the experiments were NaCl as a normal angiogenic development and basic fibroblast growth factor (bFGF) as a pro-angiogenic control (20 µL at 10 ng/mL). Once CAM was evaluated, membranes were fixed by adding 4 % paraformaldehyde overnight at 4 °C. Next, membranes were extracted and observed using a binocular loupe. Afterwards, the obtained images were processed, and the density of the vessels in the CAM was automatically measured using ImageJ vessel analysis plugin.

Biological Studies

Cell Lines

Human biphenotypic B myelomonocytic leukaemia MV4-11 and normal breast epithelial MCF-10A cells were acquired from American Type Culture Collection (USA). Human lung carcinoma A549 and breast cancer MCF-7 cells were from the European Collection of Authenticated Cell Cultures (UK). Human breast cancer MDA-MB-468 cells were acquired from the Leibniz Institute, DSMZ-German Collection of Microorganisms and Cell Cultures (Germany). Cells were grown at 37 °C with 5 % CO_2 humidified atmosphere, and media were supplemented with 2 mM l-glutamine (Merck, Germany), 100 units/mL penicillin (Polfa Tarchomin S.A., Poland), and 100 µg/mL streptomycin (Merck, Germany).

MV4-11 and MDA-MB-468 cells were cultured in RPMI 1640 medium (IIET PAS, Poland) with 1.0 mM sodium pyruvate (only MV4-11), 10% (MV4-11), or 20% (MDA-MB-468) fetal bovine serum (FBS) (all from Merck, Germany). A549 cells were cultured in RPMI 1640+Opti-MEM (1:1) (IIET PAS, Poland and Gibco, UK) supplemented with 5% foetal bovine serum (Merck, Germany). The MCF-7 cells were cultured in Eagle's medium and supplemented with insulin and 1% of MEM non-essential amino acids (Merck, Germany). Normal breast epithelial MCF-10A cells were cultured in the HAM'S F-12 medium (Corning), supplemented with 10 % Horse Serum (Gibco), 0.5 µg/mL Hydrocortisone, 20 ng/mL EGFh, 10 µg/mL insulin, and 0.05 mg/mL Cholera Toxin from *Vibrio cholerae* (all from Merck, Germany).

Determination of Antiproliferative Activity

The solutions of APG (1 mg/mL), APG-NLC (1 mg APG/mL) and empty NLC were prepared by APG and NLC in DMSO and water, respectively. Twenty-four hours prior the addition of the tested compounds, the cells were seeded in 96-well plates (Sarstedt, Germany) at a density of 1×10^4 or 0.5×10^4 (A549) cells/well. Antiproliferative capacity was studied after 24 and 72 h of cells exposure to four different concentrations. Cytotoxic effects were examined using MTT (MV4-11) or SRB assays, previously described.[38] The IC_{50} (inhibitory concentration 50 %), which is cytotoxic to 50 % of the cells, was calculated. IC_{50} values were evaluated for each experiment separately using the Prolab-3 system based on Cheburator 0.4 software,[39] and the mean values ± SD are presented in Table 1. Both APG and APG-NLC were assessed in triplicate, and the experiments were repeated up to 5 times.

Determination of Compounds Accumulation in Cells by Flow Cytometry

The APG-NLC were fluorescently labelled with NR to determine their accumulation in cells. Leukemia MV4-11 cells were incubated for 5, 15, and 30 min and 60, 120, and 240 min with APG-NLC-NR (1.675 and 0.335 µg/mL). After incubation, cells were collected and washed with PBS. The mean fluorescence of cells incubated with the tested compounds labelled with NR was analyzed by flow cytometry using a BD LSRFortessa cytometer (BD Bioscience, San Jose, USA). Untreated cells were used as unlabeled controls. The results were analysed using the Flowing software 2 (Cell Imaging Core, Turku Centre for Biotechnology, University of Turku Åbo Akademi University).

Table 1 Design of experiments and characterization of the different formulations developed

Independent Variables								Dependent Variables			
Coded Level	cApig (%)	Coded Level	cLipid (%)	Coded Level	cLS (%)	Coded Level	cTw (%)	Z_{av} ± SD (nm)	PDI ± SD	ZP ± SD (mV)	EE ± SD (%)
Factorial points											
-1	0.1	-1	5	1	85	-1	2	176.1 ± 2.3	0.278 ± 0.009	-21.7 ± 0.7	99.9 ± 0.1
1	0.2	-1	5	-1	65	1	4	221.5 ± 2.5	0.313 ± 0.012	-21.4 ± 0.5	96.7 ± 0.1
1	0.2	1	10	-1	65	-1	2	253.9 ± 4.4	0.246 ± 0.012	-22.6 ± 0.3	99.9 ± 0.1
-1	0.1	1	10	1	85	-1	2	271.4 ± 5.5	0.273 ± 0.008	-23.0 ± 0.8	99.9 ± 0.1
-1	0.1	1	10	-1	65	-1	2	243.7 ± 0.7	0.236 ± 0.014	-24.6 ± 0.5	99.7 ± 0.3
-1	0.1	-1	10	-1	65	1	4	214.7 ± 1.6	0.181 ± 0.010	-18.2 ± 0.9	99.9 ± 0.1
-1	0.1	-1	5	1	85	1	4	165.9 ± 1.2	0.265 ± 0.012	-17.6 ± 0.2	99.9 ± 0.1
-1	0.1	-1	5	-1	65	-1	2	161.2 ± 2.3	0.255 ± 0.023	-22.3 ± 0.4	95.1 ± 0.2
1	0.2	1	10	-1	65	1	4	212.2 ± 1.8	0.217 ± 0.019	-19.6 ± 0.2	99.9 ± 0.1
-1	0.1	1	10	1	85	1	4	236.8 ± 2.0	0.244 ± 0.017	-18.4 ± 0.5	99.9 ± 0.1
1	0.2	-1	5	1	85	1	4	191.9 ± 2.7	0.318 ± 0.058	-19.2 ± 0.6	99.9 ± 0.1
-1	0.1	-1	5	-1	65	1	4	202.7 ± 2.4	0.203 ± 0.002	-18.7 ± 0.2	97.7 ± 0.1
1	0.2	1	10	1	85	-1	2	304.6 ± 5.7	0.276 ± 0.007	-20.1 ± 0.4	99.1 ± 0.1
1	0.2	-1	5	-1	65	-1	2	188.7 ± 2.3	0.374 ± 0.008	-22.2 ± 0.4	99.9 ± 0.1
1	0.2	1	10	1	85	1	4	240.5 ± 2.5	0.277 ± 0.015	-18.0 ± 0.4	99.6 ± 0.1
1	0.2	-1	5	1	85	-1	2	200.5 ± 2.8	0.425 ± 0.015	-22.4 ± 0.6	99.9 ± 0.1
Axial points											
-2	0.05	0	7.5	0	75	0	3	181.2 ± 1.4	0.221 ± 0.029	-19.5 ± 0.3	99.9 ± 0.1
2	0.25	0	7.5	0	75	0	3	230.3 ± 2.7	0.327 ± 0.007	-20.2 ± 0.2	99.9 ± 0.1
0	0.15	-2	2.5	0	75	0	3	202.0 ± 3.9	0.556 ± 0.015	-22.3 ± 0.3	99.9 ± 0.1
0	0.15	2	12.5	0	75	0	3	280.9 ± 5.7	0.259 ± 0.009	-20.7 ± 0.4	99.9 ± 0.1
0	0.15	0	10	-2	55	0	3	187.3 ± 1.3	0.195 ± 0.012	-20.4 ± 0.5	99.9 ± 0.1
0	0.15	0	10	2	95	0	3	202.5 ± 3.3	0.331 ± 0.026	-20.7 ± 0.2	99.9 ± 0.1
0	0.15	0	10	0	75	-2	1	271.0 ± 4.3	0.231 ± 0.020	-24.1 ± 0.7	99.9 ± 0.1
0	0.15	0	10	0	75	2	5	239.1 ± 1.6	0.182 ± 0.027	-17.2 ± 0.8	98.1 ± 0.3
Central points											
0	0.15	0	7.5	0	75	0	3	202.0 ± 0.8	0.267 ± 0.012	-20.3 ± 0.4	99.9 ± 0.1
0	0.15	0	7.5	0	75	0	3	199.3 ± 0.7	0.292 ± 0.038	-19.6 ± 0.1	99.9 ± 0.1

Results

APG-NLC Characterization and Optimization

The homogenisation parameters in order to produce NLC by high-pressure homogenization were previously optimised using a composite factorial design with three levels and two factors. The independent variables were pressure, number of homogenisation cycles, and primary emulsion time, and the dependent variables were Z_{av} and PDI (Figure 1). The results showed that with an increase in the number of homogenisation cycles up to two and pressures up to 800 bar, it was possible to produce nanocarriers with lower Z_{av} and PDI. However, it was established that the primary emulsion time using Ultraturrax® did not affect the studied parameters; therefore, the method was set up in three homogenisation cycles at 900 bar with a primary emulsion time of 30 s.

An optimised formulation was obtained by means of the DoE approach. The independent variables studied were the amount of APG, the lipid phase (solid lipid and liquid lipid mixture), the percentage of solid lipids in the lipid phase, and the amount of surfactant.

Table 1 shows the effect of the independent variables on the dependent variables analysed and the values obtained. As can be observed, the Z_{av} of the formulations was 200 nm in most cases, as well as PDI values around 0.2, thus indicating a homogeneous distribution of nanoparticles.[40] The developed APG-NLC exhibited a negative surface charge of ZP < −20 mV. This negative charge may be due to the ionisation of glyceryl behenate (a fatty acid in Compritol® 888 ATO).[41] Since the surface charge values are associated with the stability of colloidal dispersions, the developed formulations with values of −20 mV were considered the most stable.[42] In all cases EE was higher than 95%, thus meaning that APG was completely encapsulated.

As shown in Figure 2, the four variables studied had a significant effect on the formulation of NLC. The Z_{av} and PDI of APG-NLC were significantly influenced by the concentration of the lipid phase but followed an opposite trend because more solid lipids increased size ($p < 0.05$) but decreased NLC PDI ($p < 0.01$). Moreover, the surface charge was significantly influenced by the surfactant ($p < 0.001$), and the EE % was significantly influenced by both liquid and solid lipids.

As shown in Figure 3, higher concentrations of the lipid phase provided larger APG-NLC but with less size dispersion (Figure 3A and B). According to the surface response, in order to obtain APG-NLC below 200 nm, less than 9 % of lipid

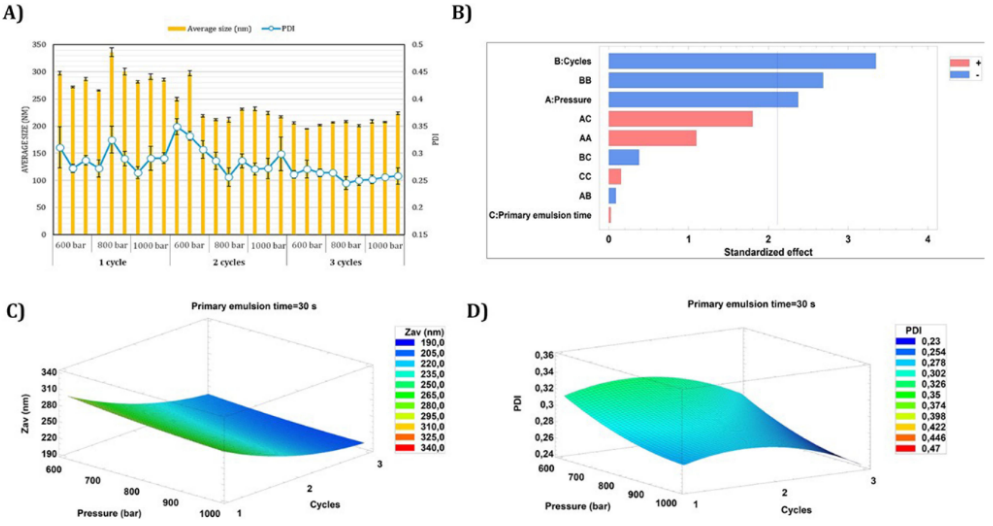

Figure 1 Initial screening for APG-NLC development. (**A**) Representation of the values obtained of Z_{av} and PDI against the homogenization cycles and homogenization pressure; (**B**) Pareto's chart of the homogenization parameters; (**C**) Surface response of the influence of the pressure and cycles on the Zav; (**D**) Surface response of the influence of the pressure and cycles on the PDI.

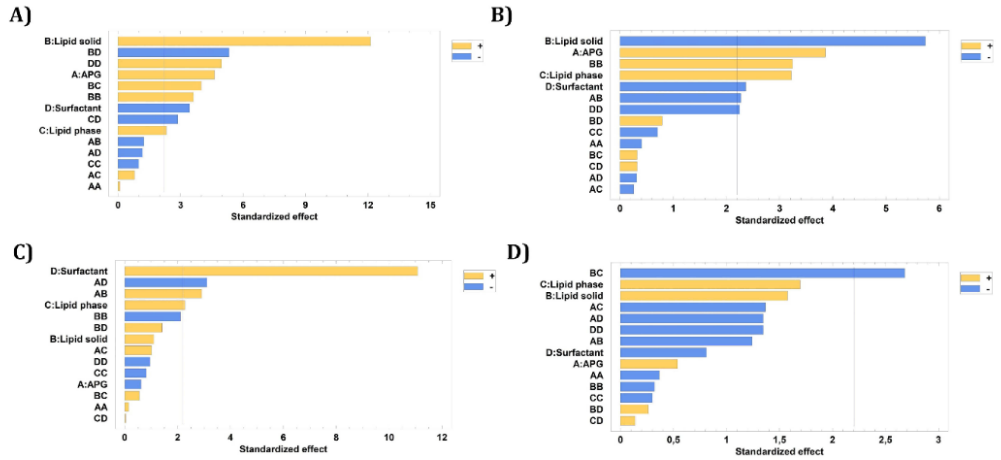

Figure 2 Pareto's chart of the influence of the independent variables for each dependent variable. (**A**) Z_{av}; (**B**) PDI; (**C**) ZP; (**D**) EE.

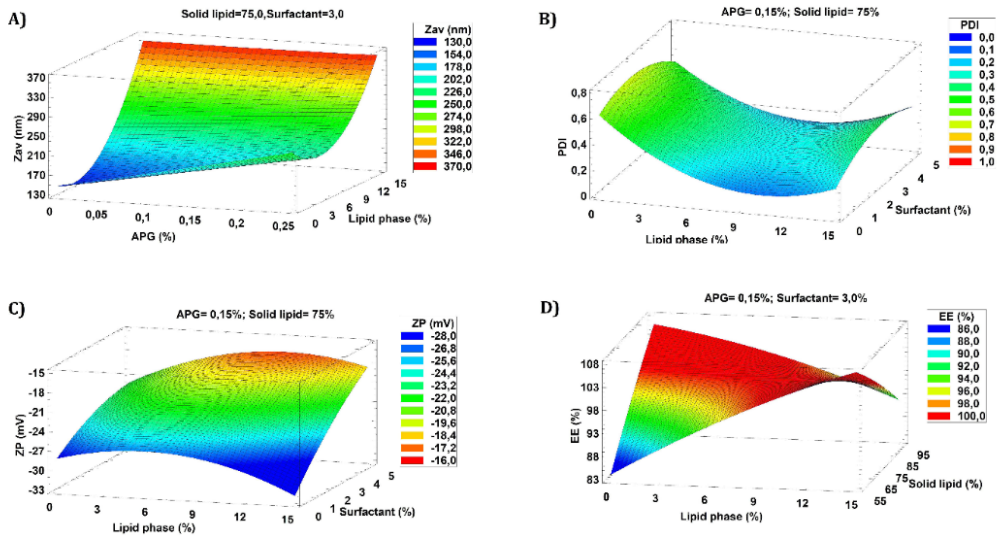

Figure 3 DoE surface response of APG-NLC. (**A**) Concentration of Solid lipid regarding to the lipid phase and Surfactant influence on Z_{av}; (**B**) Concentration of APG and Solid lipid regarding to the lipid phase influence on PDI; (**C**) Concentration of Surfactant and Solid lipid regarding to the lipid phase influence on ZP; (**D**) Concentration of APG and Surfactant influence on EE.

phase and APG concentrations below 0.2 % should be used. However, to obtain a PDI of less than 0.2, higher concentrations of the lipid phase seem necessary. Moreover, with respect to ZP, a lower surface charge was obtained when a higher concentration of the surfactant was added (Figure 3C). EE was highly influenced by the amount of solid lipids with low EE as the solid lipid content increased (Figure 3D). Considering all the evaluated parameters and the trends, a formulation containing 0.1 % of APG, 7.5 % of total lipids, 65 % of solid lipids, and 3.5 % of surfactant has been optimized to carry out further experiments.

Interaction Studies of APG-NLC

The interactions between APG and the lipid matrix, carried out by DSC, FTIR, and XRD are shown in Figure 4. DSC was performed to study the variations in the crystallinity and melting point of the lipid mixtures against APG-NLC. In this sense, the melting temperature (T_m) of the lipid mixture was slightly lower than that of the lipid mixture with APG (69.50 and 70.22°C, respectively). Moreover, the T_m of the APG-NLC was slightly lower than that of the physical mixture, probably because of its small size and surfactant incorporation.[43] Enthalpy values (ΔH) were similar between the lipid mixture and lipid mixture-APG (ΔH Lipid mixture = 88.87 Jg^{-1}, ΔH Lipid mixture-APG = 97.79 Jg^{-1}). Moreover, ΔH of APG-NLC was lower being 71.10 Jg^{-1}. In addition, APG was also assessed showing a T_m of 365.5°C and ΔH = 198.5 Jg^{-1}.[44]

FTIR analysis was used to study the interactions between APG, surfactant, and the lipid matrix (Figure 4B). The FTIR spectrum of pure APG presented vibrational bands at approximately 3278 cm^{-1}, characteristic of the O-H group. Moreover, the C-H group exhibits multiple small peaks at 2800 cm^{-1}. Additional peaks at 1650 and 1605 cm^{-1} were observed for the C-O group.[45] Furthermore, there was no evidence of new strong bonds formed in the APG-NLC, and APG peaks were not observed, thus confirming APG encapsulation in the lipid matrix.

The XRD profiles in Figure 4C show the physical states of the APG, APG-NLC, and their physical mixture. Intense and sharp peaks for APG and the solid mixture of lipids are observed, indicating that these components possess a crystalline structure. Typical signals of APG such as 7.07, 10.09, 11.25, 14.12, 15.03, 15.97, and 18.18° (2θ) were found.[46] Interestingly, APG peaks were not detected in the APG-NLC, which may indicate that APG was present in a dissolved state in the NLC (molecular dispersion). Additionally, the crystallinity of the structures of all components was studied. The lipid mixture showed three peaks, the smaller one in 19.34° (2θ), ie d = 0.46 nm, indicated the most stable form of triacylglycerols, the β form, and two pronounced peaks at 21.38° (2θ) ie d=0.42 nm and 23.43° (2θ) ie d=0.38 nm, indicating the second stable form of triacylglycerols, the β' form. In contrast, the APG-NLC profile showed the most intense peak at 19.39° (2θ) and 23.62° (2θ), indicating good stability of the formulation.[44,47,48]

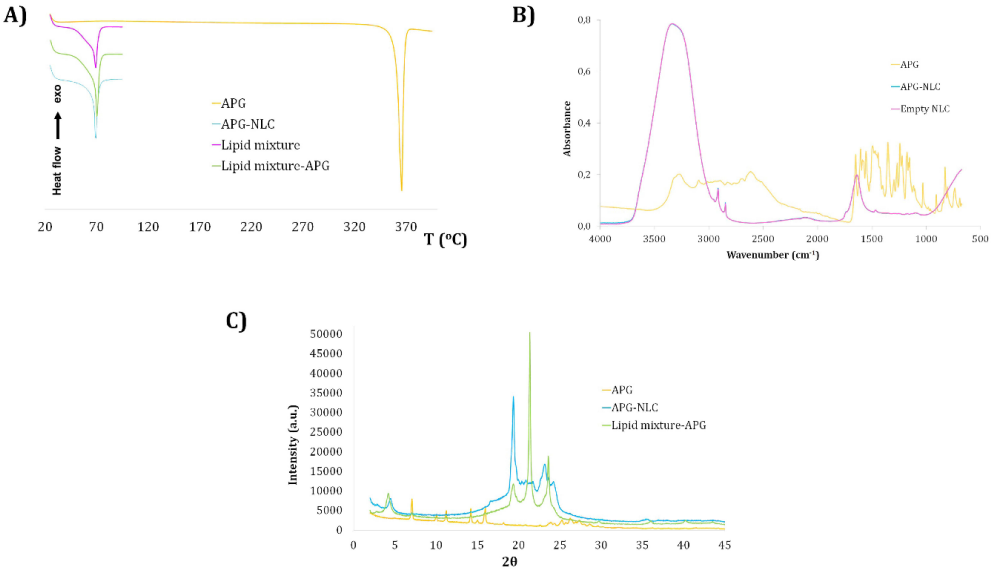

Figure 4 Interaction studies of APG-NLC and their components. (**A**) DSC curves; (**B**) FTIR analysis; (**C**) X-ray diffraction patterns.

Morphological Studies

Due to the fact that a single technique is not enough to characterise NLC, the morphology of the APG-NLC was evaluated by TEM and compared with the results obtained by dynamic light scattering (Figure 5). Using TEM, it can be observed that the APG-NLC showed almost spherical and soft round shapes with Z_{av} values below 200 nm. This was consistent with the results found by dynamic light scattering. Moreover, as predicted by the obtained ZP values (−20 mV), particle aggregation was not observed.

Stability of APG-NLC

Stability studies were performed by measuring Z_{av}, PDI, ZP, and EE as well as by analysing the BS profiles at different temperatures. Specifically, BS provides information on destabilisation mechanisms, such as sedimentation, agglomeration, or aggregation, which can be observed when differences greater than 10 % are obtained.[49] In this way, BS profiles of APG-NLC were studied at 4, 25, and 37 °C (Figure 6). The APG-NLC formulation was stable at 4 °C for a period of 11 months, maintaining constant physicochemical parameters, while at 25 °C, the stability endured 3 months, and at 37°C, it was stable for only 15 days.

Moreover, high temperatures accelerated particle destabilisation by decreasing the ZP. As it can be seen in Table 2, the formulations kept at three different temperatures maintained their physicochemical parameters until the ZP diminished (12 months at 4 °C, 4 months at 25 °C and 15 days at 37 °C). All these phenomena were in accordance with the BS results. As can be observed, at all the temperatures, the BS profile increased, probably because of decrease in ZP, promoting aggregation phenomena that, in the case of 4 °C, seem to start after 1 year of storage. Additionally, the EE was maintained at all temperatures. Considering these results into account, APG-NLC were stored at 4°C showing a good stability up to 12 months.

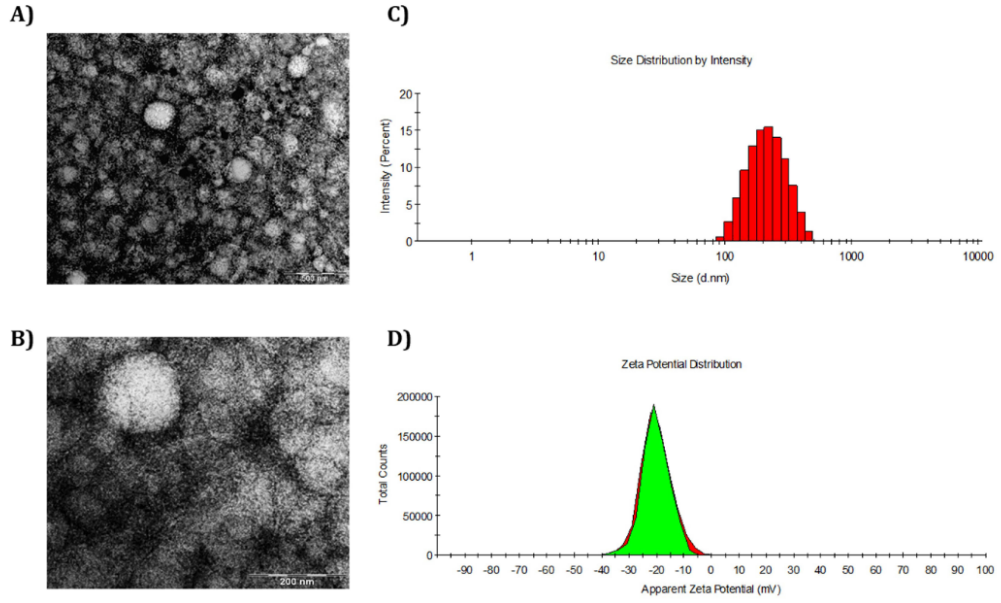

Figure 5 Physicochemical and morphological characterization. (**A**) TEM images with scale bar 500 nm; (**B**) TEM images with scale bar 200 nm; (**C**) Histogram of average size distribution measured by dynamic light scattering; (**D**) Zeta potential plot measured by laser-Doppler electrophoresis.

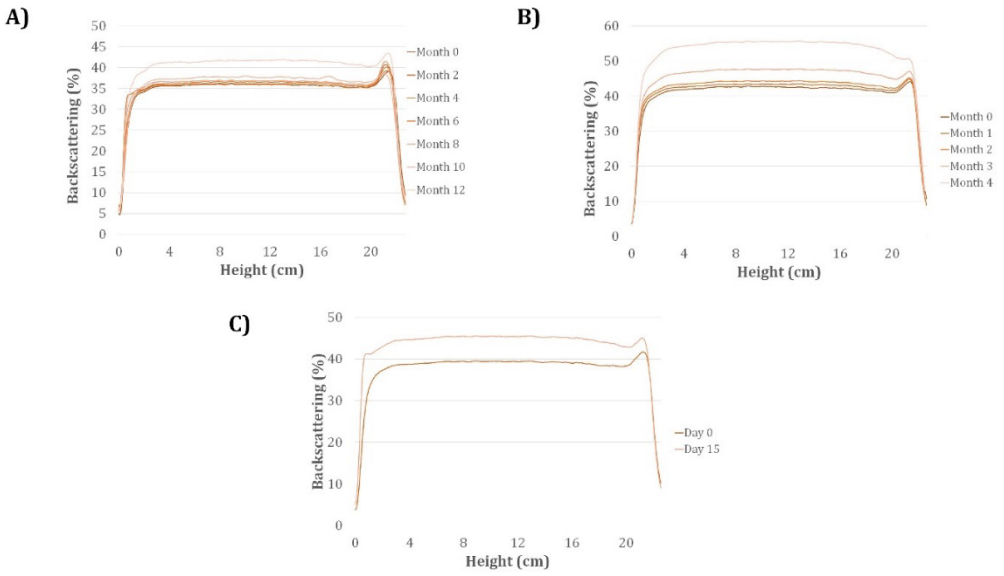

Figure 6 Backscattering profiles of APG-NLC stored at (**A**) 4 °C; (**B**) 25 °C; and (**C**) 37 °C.

Biopharmaceutical Behaviour

The in vitro release profile of APG from NLC against free APG demonstrated that the lipid formulation had a kinetic profile characteristic of prolonged drug release formulations. The APG release from NLC best fit was a two-phase association. As shown in Figure 7, an initial burst release of APG from the NLC was observed during the first 2 h. Afterwards, a slow release of APG occurs probably releasing the APG encapsulated in the inner lipid core. Moreover, free APG showed a fast release, achieving a 100 % before 24 h while the APG-NLC just released less than 30 %. The dissociation constant (K_d) of APG-NLC was higher in both the slow and fast phases than in free APG (0.07 and 0.27 vs 0.02 h), thus indicating a prolonged release.[37] Moreover, the half-life results ($t_{1/2}$) showed that there was a burst release at the beginning during the fast phase of the formulation, but during the slow phase, it had a sustained release, with a $t_{1/2}$ value of 160.5 h.[50]

Table 2 Physicochemical Parameters of APG-NLC Stored at Different Temperatures

Temperature (°C)	Month/Day	Z_{av} ± SD (nm)	PDI ± SD	ZP ± SD (mV)	EE ± SD (%)
	0	195.2 ± 0.4	0.170 ± 0.011	−19.3 ± 0.1	99.9 ± 0.1
4	2	193.2 ± 0.7	0.171 ± 0.026	−17.7 ± 0.3	99.9 ± 0.1
	4	195.4 ± 0.9	0.160 ± 0.002	−17.0 ± 0.3	99.9 ± 0.1
	6	194.9 ± 0.3	0.164 ± 0.017	−17.7 ± 0.2	99.9 ± 0.1
	8	195.0 ± 1.8	0.148 ± 0.009	−17.5 ± 0.4	99.9 ± 0.1
	10	193.0 ± 1.9	0.151 ± 0.015	−20.8 ± 0.3	99.9 ± 0.1
	12	193.5 ± 2.1	0.161 ± 0.002	−15.2 ± 0.2	99.9 ± 0.1
25	2	201.9 ± 2.9	0.123 ± 0.017	−18.3 ± 0.2	99.9 ± 0.1
	4	199.8 ± 1.7	0.125 ± 0.034	−14.8 ± 0.3	99.9 ± 0.1
37	15 days	209.2 ± 0.9	0.161 ± 0.025	−15.5 ± 0.3	99.9 ± 0.1

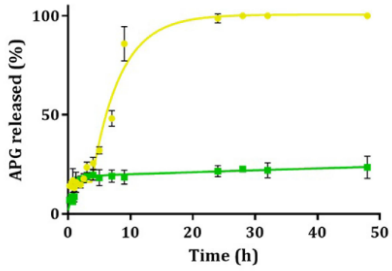

Parameter	Free APG	APG-NLC
K_d (h)	0.02298	K_{fast} = 0.2662 K_{slow} = 0.06623
$t_{1/2}$ (h)	3.18	$t_{1/2\ fast}$ = 0.7728 $t_{1/2\ slow}$ = 160.5
R^2	0.7745	0.9765

Figure 7 In vitro release profile of APG-NLC vs free APG carried out for 48 h and adjustment to a two-phase association and Plateau followed by one phase decay model respectively.

Antiangiogenic Capacity

To study the antiangiogenic capacity of free APG, APG-NLC, and empty NLC, an in vitro assessment using CAM of embryonated eggs was carried out. As shown in Figure 8, APG-NLC possessed a significantly lower ($p < 0.01$) vascular density than the negative control (NaCl). Although free APG seems to exert antiangiogenic effects, these effects are not significant. Moreover, empty NLC did not seem to have any effect on the blood vasculature.

Cytotoxicity Towards Selected Cancer Cell Lines

The antiproliferative activities of APG and APG-NLC towards leukemia (MV4-11), lung (A549), and two breast MCF-7 (ER+) and MDA-MB-468 cancer cell lines were evaluated after 24 h and 72 h. The toxicity of these compounds was tested in normal human breast epithelial MCF-10A cells. The results were obtained by assessing cellular viability using MTT (MV4-11) or SRB colorimetric assays. The data for the in vitro anticancer activity are reported in Table 3 and expressed as the IC_{50} concentration of the compound (in µg/mL) that inhibited proliferation of the cells by 50% compared to the untreated control cells.

As shown in Table 3, APG after 24 h of incubation was active only against leukaemia MV4-11 cells, and the activity was 10 times lower than that observed after 72 h. Both empty and APG-NLC had similar activity after 24 h and 72 h against MV4-11 leukemia cells, whereas in human lung cancer A549 cells, the activity was similar only after 72

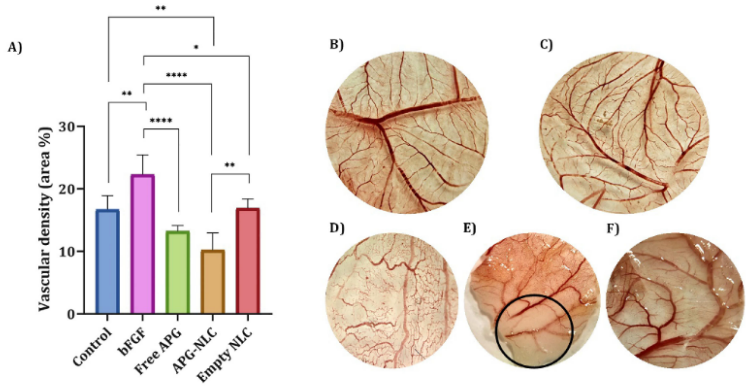

Figure 8 Anti-angiogenic capacity. (**A**) Measurement of the vascular area (%) of the extracted membranes after 48 h of stimulation with each compound. Differences between groups analysed by one-way ANOVA; (* $p < 0.05$; ** $p < 0.01$; ****$p < 0.001$); (**B–F**) Membranes after the incorporation of 48 h of product: (**B**) bFGF, (**C**) NaCl, (**D**) Free APG, (**E**) APG-NLC with a black circle highlighting its effect, (**F**) Empty NLC.

Table 3 The Half Maximal Inhibitory Concentrations (IC_{50}) of APG, Empty NLC and APG-NLC Against Selected Cancer Cell Lines and Non-Tumorigenic Human Breast Epithelial Cell Line (MCF-10A)

Compound	Cell Lines IC_{50} [μg/mL]									
	MV4-11		A549		MDA-MB-468		MCF-7		MCF-10A	
	24h	72h	24h	72h	24h	72h	24h	72h	24h	72h
APG	23.0 ± 9.8	2.5 ± 0.7	n.a.	33.5 ± 6.3	n.a.	11.3± 2.6	n.a	26.0 ± 5.9	n.a	10.1 ± 5.0
Empty NLC	0.4 ± 0.0	0.5 ± 0.2	2.3 ± 0.4	2.6 ± 0.7	2.5 ± 0.5	0.6 ± 0.2	16.4 ± 1.3	2.3 ± 0.3	n.a	20.5 ± 4.8
APG-NLC	0.3 ± 0.1	0.3 ± 0.1	7.7 ± 3.2	2.4 ± 0.3	2.9 ± 0.9	0.4 ± 0.1	16.2 ± 0.6	1.8 ± 0.6	n.a	14.9 ± 5.6

Notes: n.a. – not active, IC_{50} value higher than 33.5 μg/mL. Data are presented as mean ± standard deviation (SD) calculated using Prolab-3 system based on Cheburator 0.4 software.

h. Probably due to slow APG release, after 24 h, the activity was lower in the case of APG-NLC. Additionally, in breast cancer cells, the effect was more potent after 72 h of incubation.

Moreover, the IC_{50} of the APG-NLC was 10–27 times lower against cancer cells than that of free APG. According to the results obtained in Table 3, the most sensitive cell lines were leukemia MV4-11 and breast cancer MDA-MB-468 cells. Moreover, the comparison of APG-NLC anticancer activity against two different breast cancer models showed that APG-NLC after 24 h and 72 h was more active against triple negative breast cancer (TNBC) MDA-MB-468 cells (IC_{50} 2.9 μg/mL and 0.41 μg/mL) than ER-positive MCF-7 cells (IC_{50} 16.2 μg/mL and 1.8 μg/mL). TNBC is usually more aggressive, harder to treat, and more likely to come back (recur) than cancers that are hormone receptor- or HER2-positive. APG-NLC also showed selective efficacy against tumour cells compared with normal MCF-10A cells (SI index >1, Table 4). Importantly, this selectivity was not observed for the free APG, because it showed cytotoxicity in both, the healthy and the cancer cell line.

Accumulation of APG-NLC in Tumoral Cells

To determine whether APG nanoformulations have the ability to accumulate in leukemia cells, a cytometric method and staining of cell culture with the fluorescent dye NR was proposed. This dye binds to neutral fats and phospholipids. The amount of bound dye is directly proportional to the content of neutral fats in the cells. Leukemia cells MV4-11 were incubated with fluorescently labelled formulation APG-NLC-NR (two concentrations of APG-NLC-NR were studied, 0.335 and 1.675 μg/mL, respectively). After several time points, cell fluorescence was analysed using flow cytometry, and the results are presented in Figure 9A and B. The obtained results confirm the assumption of the conducted research that NLC formulations are an effective method of delivering biologically active substances inside the cells. The mean fluorescence intensity (MFI) of the cells after incubation with APG-NLC-NR was compared with that of the control (unlabelled cells). As shown in Figure 9A, after 5 min of incubation with labelled APG-NLC-NR, significantly higher fluorescence was observed. At all time points, a significantly higher MFI was obtained than that of the control ($p < 0.05$). Moreover, the accumulation of APG-NLC in the cells was fast and stable, and after 5 min, significant differences against the control were obtained. After 240 min of incubation, the MFI values were maintained. The confirmation of accumulation of APG-NLC-NR in the cancer cells is also the graph Figure 9B on which histogram for cells incubated

Table 4 The Selectivity Index (SI) of Tested Compounds

Compound	Cell Lines/Calculated Selectivity Index SI			
	MV4-11	A549	MDA-MB-468	MCF-7
APG	4.04	0.31	0.89	0.39
Empty NLC	41.00	7.88	34.17	8.90
APG-NLC	55.20	6.30	36.30	8.30

Notes: The SI index = IC_{50} for normal cell line (MCF-10A)/ IC_{50} for respective cancerous cell line. A beneficial SI > 1.0 indicates a drug with efficacy against tumor cells greater than toxicity against normal cells.

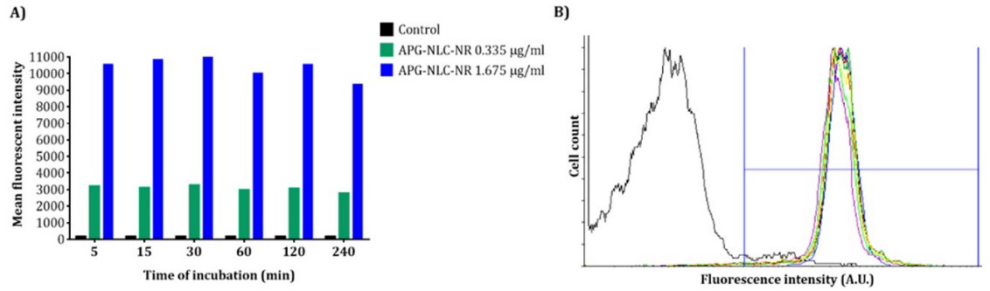

Figure 9 Accumulation of APG-NLC in MV4-11 cells. (**A**) Mean fluorescent intensity after 5, 15, 30, 60, 120, 240 min with low and high concentration of APG-NLC; (**B**) Flow cytometry histogram for higher concentration (1.675 µg/mL) of APG-NLC-NR. Black line: unlabelled control, red line: after 5 min; dark green line: after 15 min; blue line: after 30 min, light green line: after 60 min; yellow line: after 120 min and purple line: after 240 min.

with labelled formulations is shifted in higher fluorescence intensity (A.U.) in comparison to control free unlabelled leukaemia cells.

Discussion

In this study, a new formulation was developed loading of APG into a rosehip-based NLC. The fabrication method selected was hot high-pressure homogenization, due to its multiple advantages such as its ability of large-scale production, the avoidance of organic solvents, and its low cost.[51] Due to the high energy input, it allows to prepare small uniform particles, which is suitable for nanoparticulate formulations.[52]

To optimise the formulation, a design of experiments was applied. Using these studies, a full factorial design was developed, and the analysis showed that all parameters induced statistically significant differences in Z_{av}, in which the concentration of the lipid phase had the greatest influence, followed by the concentration of APG. These results are in accordance with those obtained by other authors, in which increased drug and lipid amounts led to larger nanoparticles.[53] Furthermore, the lipid phase significantly influenced the PDI, showing high values when the lipid phase decreased. Otherwise, ZP was mainly affected by the concentration of the non-ionic surfactant Tween® 80, which became more neutral with increasing surfactant amounts. This trend may be related to the absorption of the surfactant onto the NLC surface.[54] Furthermore, APG encapsulation was high in all the assessments (>95%), probably because of the lipophilic character of APG which had more affinity for the lipid-based internal structure of the NLC.[55,56] Other authors encapsulated APG into different NLC matrix by using a hot homogenizer method along with ultrasonication, obtaining smaller nanoparticles, but less stable due to its ZP closer to 0 mV.[57] Other research group prepared SLN encapsulating APG by the melt emulsification and ultra-sonication method, in which they obtained small particles around 100 nm, but with a higher PDI.[58] Moreover, Liang and colleagues also prepared NLC but encapsulating a similar molecule, quercetin, another natural flavone. In their study, they used a low energy method for the preparation of the NLC, the emulsifying technique, leading to a polydisperse formulation (PDI > 0.3).[59]

Interaction studies showed that the lipid matrix of the formulation became more amorphous in the presence of APG, indicating that APG was solubilised in lipids.[60] FTIR studies confirmed that no covalent bonds were formed between the drug and the lipid matrix, so hydrogen bonds and hydrophobic forces could be the main forces between them, facilitating the accommodation of APG inside the NLC and promoting its liberation from the particle.[61] Furthermore, the XRD results suggested that APG-NLC could possess good and long stability due to the presence of the most stable forms of triacylglycerols, the β and β' forms.[44,47,48] These results are in agreement with the stability studies, in which the formulation was stable at 4°C for 12 months. Subsequently, the electrostatic forces between the APG-NLC may begin to decrease, leading to aggregation and sedimentation (as observed in the backscattering profile).[62] Despite this, in some cases, sedimentation can be reversed by agitation, and in order to obtain stability for more than 12 months, APG-NLC

can be freeze-dried.[63] Moreover, interaction studies showed that APG was encapsulated into the NLCdue to the absence of signals of APG in the different studied techniques.

In addition, the APG-NLC showed a sustained in vitro release profile, whereas the APG solution was released rapidly. The fitted model for APG-NLC was a two-phase association, due to the formulation being able to provide a first fast release, followed by a slow and prolonged liberation of APG to the medium. This kind of model explains many chemical and biological processes, which could indicate a more complicated binding kinetics mechanism.[64–66] It was observed that the release of the APG from the NLC reached approximately 30%, showing an initial burst release of APG in the early phase, followed by a delayed release of APG (up to 24 h). Compared to other studies, these NLC showed a slower release, which might be related to the high solubility of APG in the lipid matrix.[67–69]

In in ovo angiogenesis studies, the anti-angiogenic activity of the APG-NLC was confirmed. It is well known that APG exhibits antiangiogenic activity, which is related to its antitumoral properties.[70] The controls of this study were the negative control (NaCl) and a positive growth control (bFGF), which is known to activate angiogenesis. Although bFGF is one of the most effective inducers of angiogenesis, it frequently contributes to pathological angiogenesis by stimulating vascular endothelial mitogenesis and has been frequently used as an angiogenic polypeptide.[71] In this study, a solution of APG at the same concentration as APG-NLC was used (1 mg/mL). The results showed that APG slightly decreased the number of microvessels in CAM. Other authors have reported that at higher concentrations than those assessed (from 1.35 to 5.4 mg/mL), APG was able to suppress normal angiogenesis in chick embryo.[72] In contrast, APG-NLC significantly decreased vascular density in the negative and positive controls. These results indicate that the encapsulation of APG into lipid nanoparticles increases the bioavailability and bioactivity of the flavonoid.[73] Since APG is an inhibitor of several growth factors such as vascular endothelial growth factor (VEGF) and bFGF[74] and empty NLC do not exert any angiogenesis modulation effect, the developed NLC were able to enhance APG penetration, thus enhancing APG antiangiogenic activity.[75–77] Moreover, since angiogenesis provides an expanding tumour with oxygen and nutrients, which are necessary for tumour growth, inhibition of angiogenesis could provide an effective tool for anticancer therapy.[78]

The antiproliferative activity of APG, empty NLC, and APG-NLC towards five different cell lines was evaluated after 24 and 72 h. For the leukaemia cell line (MV4-11), a solution of APG showed greater activity at 72 h than at 24 h. It has been described that APG stimulates signalling pathways that result in cell proliferation inhibition and cell-cycle arrest in fast-cycling cell. Moreover, other authors have confirmed that by increasing the incubation time of APG with leukaemia cells, cytotoxicity increased.[79] APG-NLC showed 20 times more activity than free APG at 24 and 72 h of exposure. This was probably due to the ability of NLC to penetrate into the cells, increasing the amount of drug intracellularly.[80] This was confirmed by flow cytometry, which showed high and fast NLC internalisation. Moreover, in the lung cancer cell line (A549), APG was not active at 24 h, but its activity increased at 72 h. Conversely, APG-NLC showed a greater effect against this cell line, with the highest effect observed at 72 h. The worst prognosis for survival and most treatment-related issues are associated with TNBC, which accounts for 10% to 22% of all cases of breast cancer that are diagnosed. Furthermore, the absence of response to conventional hormonal therapy or therapies directed at specific receptors makes treatment difficult.[81] In order to evaluate the potential of APG in aggressive cancer, the cell line MDA-MB-468 was used. In the first 24 h, the flavonoid solution was not cytotoxic, as reported.[82] At 72 h, it showed higher activity, which could be related to its mechanism of action, targeting different signal transduction pathways.[83] Nevertheless, APG-NLC showed great cytotoxicity against the TNBC cell line after 24 and 72 h. Another breast cancer cell line (MCF-7) showed cytotoxicity similar to that of APG. Other studies have reported that APG inhibits growth and induces apoptosis in a dose-dependent relationship.[84] Similarly, APG-NLC were more cytotoxic than APG, and their activity increased at 72 h, probably because of the sustained release of APG from the formulation. To confirm the safety and selectivity of the tested compounds, the cytotoxicity of the formulations was tested against a non-tumourigenic cell line (MCF-10A), and the SI was calculated. The SI is an important parameter for the development of novel formulations. A low selectivity of compounds means that patients are unable to receive the drug doses necessary to eradicate all cancer cells, because doing so would be fatal and eradicate all other body cells.[85] The results showed that APG was not selective for cancer lines, except for leukaemia cells, whereas APG-NLC were selective for all tumour cells.

In contrast, empty NLC showed similar antiproliferative activity against all tumour cell lines and high selectivity, demonstrating excellent safety and efficacy. Since two of the three ingredients of the empty formulation had described pharmacological interest, this led to the potent antitumour effects of the empty NLC. On the one hand, the non-ionic surfactant Tween 80® can effectively inhibit P-gp and plays an important role in mediating the opening of tight junctions, which could enhance the paracellular uptake of NLC, increasing their permeability.[86,87] On the other hand, besides the traditional medicinal of rosehip oil when applied on the skin, in the last few year researchers have been reporting novel pharmacological features. Rosehip oil is made from the seed of *Rosa canina* sp. and is rich in polyunsaturated fatty acids, linoleic acid, linolenic acid, and phytosterols such as β-sitosterol.[88] Recently, some authors assessed the extract of rosehip against different cancer cell lines, including colon, lung, prostate, cervix, liver, brain, and breast, suggesting its potential role in chemotherapy.[25,89] After treating these cancer cell lines with whole rose hip extract or purified fractions of its most important components, all studies have reported a noticeable decline in cell viability. These antioxidant properties may be responsible for their antiproliferative effect.[25] However, its activity may not only be due to its antioxidant properties but is also capable of preventing cell proliferation.[90] In another study, researchers tested the rosehip extract against TNBC, and the results showed that it was able to decrease cell migration and inhibit cell growth by reducing two enzymes (MAPK and Akt). In addition, in combination with commonly used chemotherapy, it was able to reduce cell proliferation and migration in tissue cultures, suggesting that rosehip extract might be a useful addition to the thorough treatment regime for patients with TNBC.[91] These results revealed that the proposed combination of APG loading of NLC containing rosehip oil could be a promising platform for the treatment of several cancers.

The cellular uptake of APG-NLC was studied by encapsulating the fluorescent dye NR using flow cytometry. The selected cell line was leukaemic owing to its high cytotoxic activity. APG-NLC-NR showed rapid uptake in the first 5 min, and the fluorescence intensity remained stable for all experiments (4 h). These results could explain the high activity against these cells, in which NLC were able to penetrate and remain inside. Some researchers concede that NLC represent a good delivery system owing to their composition. As liquid lipids give NLC a less ordered lipid matrix, drugs may be more effectively accommodated; in this case, the fluorescent die NR prevents premature drug release and fluorescence signal loss. The incorporation of liquid lipids promotes higher cellular uptake and permeability across the cellular membrane.[92,93]

Conclusion

APG was successfully encapsulated into NLC containing rosehip oil with a particle size below 200 nm, a monodisperse population, and high entrapment efficiency. The APG-NLC showed suitable stability for almost one year, as well as prolonged release. In ovo and in vitro assays in tumour cells confirmed that APG increased its activity when encapsulated in NLC. APG-NLC decreased the formation of new blood vessels, highlighting their antiangiogenic activity. Moreover, the antiproliferative assays confirmed APG-NLC selectivity against tumour cells and cytotoxicity in leukaemia, lung, and breast cancer cells. In addition, empty NLC did not show significant antiangiogenic properties, but in vitro antitumoral assessments showed selective cytotoxicity against cancer cells, probably owing to the pharmaceutical properties of rosehip oil.

These findings constitute a first approach for this type of nanoparticles including two natural active ingredients, such as APG and rosehip oil, in which both the encapsulated compound and the matrix contribute to the pharmacological effect, acting in a synergic way. This kind of formulation could establish a novel therapeutic approach for the treatment of cancer.

In conclusion, APG-NLC have been successfully developed and physicochemically characterised, showing prolonged release, antiangiogenic properties, and suitable activity against tumour cell lines.

Acknowledgments

This research was supported by the Spanish Ministry of Science and Innovation (PID2021-122187NB-C32) and by Wrocław University of Environmental and Life Sciences (Poland) under the Leading Research Groups support project. The APC/BPCis were financed/co-financed by Wrocław University of Environmental and Life Sciences.

EBS acknowledges FCT—Fundação para a Ciência e a Tecnologia, I.P., in the scope of the project UIDP/04378/2020 and UIDB/04378/2020 of the Research Unit on Applied Molecular Biosciences—UCIBIO and the project LA/P/0140/2020 of the Associate Laboratory Institute for Health and Bioeconomy—i4HB.

E.S.-L. acknowledges the support of Grants for the Requalification of the Spanish University System.

Disclosure

The authors report no conflicts of interest in this work.

References

1. Ferlay J, Colombet M, Soerjomataram I, et al. Cancer statistics for the year 2020: an overview. *Int J Cancer*. 2021;149(4):778–789. doi:10.1002/IJC.33588
2. Sung H, Ferlay J, Siegel RL, Laversanne M, Jemal ISA, Bray F. Global cancer statistics 2020: GLOBOCAN estimates of incidence and mortality worldwide for 36 cancers in 185 countries. *CA Cancer J Clin*. 2021;71(3):209–249. doi:10.3322/CAAC.21660
3. Gavas S, Quazi S, Karpiński TM. Nanoparticles for cancer therapy: current progress and challenges. *Nanoscale Res Lett*. 2021;16(1):1–21. doi:10.1186/S11671-021-03628-6
4. Yu Z, Gao L, Chen K, et al. Nanoparticles: a new approach to upgrade cancer diagnosis and treatment. *Nanoscale Res Lett*. 2021;16(1):1–17. doi:10.1186/S11671-021-03489-Z
5. Sharma A, Ghani A, Sak K, et al. Probing into therapeutic anti-cancer potential of apigenin: recent trends and future directions. *Recent Pat Inflamm Allergy Drug Discov*. 2019;13(2):124–133. doi:10.2174/1872213X13666190816160240
6. Allahyari M, Motavalizadeh-Kakhky AR, Mehrzad J, Zhiani R, Chamani J. Cellulose nanocrystals derived from chicory plant: an un-competitive inhibitor of aromatase in breast cancer cells via PI3K/AKT/mTOP signalling pathway. *J Biomol Struct Dyn*. 2023;20:1–15. doi:10.1080/07391102.2023.2226751
7. Taheri R, Hamzkanlu N, Rezvani Y, et al. Exploring the HSA/DNA/lung cancer cells binding behavior of p-Synephrine, a naturally occurring phenyl ethanol amine with anti-adipogenic activity: multi spectroscopic, molecular dynamic and cellular approaches. *J Mol Liq*. 2022;368:120826. doi:10.1016/J.MOLLIQ.2022.120826
8. Kalhori F, Yazdyani H, Khademorezaeian F, et al. Enzyme activity inhibition properties of new cellulose nanocrystals from Citrus medica L. pericarp: a perspective of cholesterol lowering. *Luminescence*. 2022;37(11):1836–1845. doi:10.1002/BIO.4360
9. Ahmed SA, Parama D, Daimari E, et al. Rationalizing the therapeutic potential of apigenin against cancer. *Life Sci*. 2021;267:118814. doi:10.1016/J.LFS.2020.118814
10. Malek-Esfandiari Z, Rezvani-Noghani A, Sohrabi T, Mokaberi P, Amiri-Tehranizadeh Z, Chamani J. Molecular dynamics and multi-spectroscopic of the interaction behavior between bladder cancer cells and calf thymus DNA with rebeccamycin: apoptosis through the down regulation of PI3K/AKT signaling pathway. *J Fluoresc*. 2023;33(4):1537–1557. doi:10.1007/S10895-023-03169-4/METRICS
11. Darban RA, Shareghi B, Asoodeh A, Chamani J. Multi-spectroscopic and molecular modeling studies of interaction between two different angiotensin I converting enzyme inhibitory peptides from gluten hydrolysate and human serum albumin. *J Biomol Struct Dyn*. 2016;35(16):3648–3662. doi:10.1080/07391102.2016.1264892
12. Khashkhashi-Moghadam S, Soleimani S, Bazanjani A, et al. Fabrication of versatile and sustainable cellulose nanocrystals from lettuce stalks as potential tamoxifen delivery vehicles for breast cancer treatment: biophysical, cellular and theoretical studies. *New J Chem*. 2023;47(31):14768–14791. doi:10.1039/D3NJ02388E
13. Sharifi-Rad A, Mehrzad J, Darroudi M, Saberi MR, Chamani J. Oil-in-water nanoemulsions comprising Berberine in olive oil: biological activities, binding mechanisms to human serum albumin or holo-transferrin and QMMD simulations. *J Biomol Struct Dyn*. 2020;39(3):1029–1043. doi:10.1080/07391102.2020.1724568
14. Patel D, Shukla S, Gupta S. Apigenin and cancer chemoprevention: progress, potential and promise. *Int J Oncol*. 2007;30(1):233–245. doi:10.3892/IJO.30.1.233/HTML
15. Shukla S, Gupta S. Apigenin: a promising molecule for cancer prevention. *Pharm Res*. 2010;27(6):962–978. doi:10.1007/S11095-010-0089-7
16. Yan X, Qi M, Li P, Zhan Y, Shao H. Apigenin in cancer therapy: anti-cancer effects and mechanisms of action. *Cell Biosci*. 2017;7(1):1–16. doi:10.1186/s13578-017-0179-x
17. Zhang J, Liu D, Huang Y, Gao Y, Qian S. Biopharmaceutics classification and intestinal absorption study of apigenin. *Int J Pharm*. 2012;436(1–2):311–317. doi:10.1016/J.IJPHARM.2012.07.002
18. Raj S, Khurana S, Choudhari R, et al. Specific targeting cancer cells with nanoparticles and drug delivery in cancer therapy. *Semin Cancer Biol*. 2021;69:166–177. doi:10.1016/J.SEMCANCER.2019.11.002
19. Thi TTH, Suys EJA, Lee JS, Nguyen DH, Park KD, Truong NP. Lipid-based nanoparticles in the clinic and clinical trials: from cancer nanomedicine to COVID-19 vaccines. *Vaccines*. 2021;9(4):359. doi:10.3390/VACCINES9040359
20. Dadwal A, Baldi A, Kumar Narang R. Nanoparticles as carriers for drug delivery in cancer. *Artif Cells Nanomed Biotechnol*. 2018;46:295–305. doi:10.1080/21691401.2018.1457039
21. García-Pinel B, Porras-Alcalá C, Ortega-Rodríguez A, et al. Lipid-based nanoparticles: application and recent advances in cancer treatment. *Nanomaterials*. 2019;9(4):638. doi:10.3390/NANO9040638
22. Bonilla L, Espina M, Severino P, et al. Lipid nanoparticles for the posterior eye segment. *Pharmaceutics*. 2022;14(1):90. doi:10.3390/PHARMACEUTICS14010090
23. Haider M, Abdin SM, Kamal L, Orive G. Nanostructured lipid carriers for delivery of chemotherapeutics: a review. *Pharmaceutics*. 2020;12(3):288. doi:10.3390/PHARMACEUTICS12030288
24. Bhave A, Schulzova V, Chmelarova H, Mrnka L, Hajslova J. Assessment of rosehips based on the content of their biologically active compounds. *J Food Drug Anal*. 2017;25(3):681–690. doi:10.1016/J.JFDA.2016.12.019

25. Mármol I, Sánchez-De-Diego C, Jiménez-Moreno N, Ancín-Azpilicueta C, Rodríguez-Yoldi M. Therapeutic applications of rose hips from different Rosa species. *Int J Mol Sci*. 2017;18(6):1137. doi:10.3390/IJMS18061137
26. Ayati Z, Amiri MS, Ramezani M, Delshad E, Sahebkar A, Emami SA. Phytochemistry, traditional uses and pharmacological profile of rose Hip: a review. *Curr Pharm Des*. 2018;24(35):4101–4124. doi:10.2174/1381612824666181010151849
27. Strugała P, Gładkowski W, Kucharska AZ, Sokół-letowska A, Gabrielska J. Antioxidant activity and anti-inflammatory effect of fruit extracts from blackcurrant, chokeberry, hawthorn, and rosehip, and their mixture with linseed oil on a model lipid membrane. *Eur J Lipid Sci Technol*. 2016;118 (3):461–474. doi:10.1002/EJLT.201500001
28. Carvajal-Vidal P, Fábrega MJ, Espina M, Calpena AC, García ML. Development of Halobetasol-loaded nanostructured lipid carrier for dermal administration: optimization, physicochemical and biopharmaceutical behavior, and therapeutic efficacy. *Nanomed Nanotechnol Biol Med*. 2019;20:102026. doi:10.1016/J.NANO.2019.102026
29. Teeranachaideekul V, Boonme P, Souto EB, Müller RH, Junyaprasert VB. Influence of oil content on physicochemical properties and skin distribution of Nile red-loaded NLC. *J Control Release*. 2008;128(2):134–141. doi:10.1016/J.JCONREL.2008.02.011
30. Elmsmari F, González Sánchez JA, Duran-Sindreu F, et al. Calcium hydroxide-loaded PLGA biodegradable nanoparticles as an intracanal medicament. *Int Endod J*. 2021;54(11):2086–2098. doi:10.1111/IEJ.13603
31. Sánchez-López E, Ettcheto M, Egea MA, et al. Memantine loaded PLGA PEGylated nanoparticles for Alzheimer's disease: in vitro and in vivo characterization. *J Nanobiotechnology*. 2018;16(1):1–16. doi:10.1186/S12951-018-0356-Z/FIGURES/9
32. Sánchez-López E, Esteruelas G, Ortiz A, et al. Dexibuprofen biodegradable nanoparticles: one step closer towards a better ocular interaction study. *Nanomaterials*. 2020;10(4). doi:10.3390/NANO10040720
33. Gomathy S, Narenderan ST, Meyyanathan SN, Gowramma B. Development and validation of HPLC method for the simultaneous estimation of Apigenin andLuteolin in commercial formulation. *Artic J Crit Rev*. 2020;7(19):4785. doi:10.31838/jcr.07.19.560
34. Esteruelas G, Halbaut L, García-Torra V, et al. Development and optimization of Riluzole-loaded biodegradable nanoparticles incorporated in a mucoadhesive in situ gel for the posterior eye segment. *Int J Pharm*. 2022;612:121379. doi:10.1016/j.ijpharm.2021.121379
35. Cano A, Ettcheto M, Chang JH, et al. Dual-drug loaded nanoparticles of Epigallocatechin-3-gallate (EGCG)/Ascorbic acid enhance therapeutic efficacy of EGCG in a APPswe/PS1dE9 Alzheimer's disease mice model. *J Control Release*. 2019;301:62–75. doi:10.1016/J.JCONREL.2019.03.010
36. Liu P, De Wulf O, Laru J, et al. Dissolution studies of poorly soluble drug nanosuspensions in non-sink conditions. *AAPS PharmSciTech*. 2013;14 (2):748. doi:10.1208/S12249-013-9960-2
37. Esteruelas G, Souto EB, Espina M, et al. Diclofenac loaded biodegradable nanoparticles as antitumoral and antiangiogenic therapy. *Pharmaceutics*. 2022;15(1):102. doi:10.3390/PHARMACEUTICS15010102
38. Czarnecka M, Switalska M, Wietrzyk J, Maciejewska G, Gliszczyńska A. Synthesis and biological evaluation of phosphatidylcholines with cinnamic and 3-methoxycinnamic acids with potent antiproliferative activity. *RSC Adv*. 2018;8(62):35752. doi:10.1039/C8RA07002D
39. Nevozhay D. Cheburator software for automatically calculating drug inhibitory concentrations from in vitro screening assays. *PLoS One*. 2014;9 (9):e106186. doi:10.1371/JOURNAL.PONE.0106186
40. Zeb A, Qureshi OS, Kim HS, et al. High payload itraconazole-incorporated lipid nanoparticles with modulated release property for oral and parenteral administration. *J Pharm Pharmacol*. 2017;69(8):955–966. doi:10.1111/JPHP.12727
41. Khan AA, Abdulbaqi IM, Abou Assi R, Murugaiyah V, Darwis Y. Lyophilized hybrid nanostructured lipid carriers to enhance the cellular uptake of verapamil: statistical optimization and in vitro evaluation. *Nanoscale Res Lett*. 2018;13:323. doi:10.1186/S11671-018-2744-6
42. Folle C, Marqués AM, Díaz-Garrido N, et al. Thymol-loaded PLGA nanoparticles: an efficient approach for acne treatment. *J Nanobiotechnology*. 2021;19(1):359. doi:10.1186/S12951-021-01092-Z
43. Bunjes H, Westesen K, Koch MHJ. Crystallization tendency and polymorphic transitions in triglyceride nanoparticles. *Int J Pharm*. 1996;129(1–2):159–173. doi:10.1016/0378-5173(95)04286-5
44. Souto EB, Mehnert W, Müller RH. Polymorphic behaviour of Compritol 888 ATO as bulk lipid and as SLN and NLC. *J Microencapsul*. 2006;23 (4):417–433. doi:10.1080/02652040600612439
45. Alshehri SM, Shakeel F, Ibrahim MA, et al. Dissolution and bioavailability improvement of bioactive apigenin using solid dispersions prepared by different techniques. *Saudi Pharm J*. 2019;27(2):264–273. doi:10.1016/J.JSPS.2018.11.008
46. Pápay ZE, Kósa A, Böddi B, et al. Study on the pulmonary delivery system of Apigenin-loaded albumin nanocarriers with antioxidant activity. *J Aerosol Med Pulm Drug Deliv*. 2017;30(4):274–288. doi:10.1089/JAMP.2016.1316
47. Freitas C, Müller RH. Correlation between long-term stability of solid lipid nanoparticles (SLN) and crystallinity of the lipid phase. *Eur J Pharm Biopharm*. 1999;47(2):125–132. doi:10.1016/S0939-6411(98)00074-5
48. Zimmermann E, Souto EB, Müller RH. Physicochemical investigations on the structure of drug-free and drug-loaded solid lipid nanoparticles (SLN) by means of DSC and 1H NMR. *Pharmazie*. 2005;60(7):508–513.
49. Stability of Dispersions | 3P Instruments. Available from: https://www.3p-instruments.com/measurement-methods/stability-turbiscan/. Accessed November 22, 2021.
50. Anwer MK, Mohammad M, Ezzeldin E, Fatima F, Alalaiwe A, Iqbal M. Preparation of sustained release apremilast-loaded PLGA nanoparticles: in vitro characterization and in vivo pharmacokinetic study in rats. *Int J Nanomedicine*. 2019;14:1595. doi:10.2147/IJN.S195048
51. Tapeinos C, Battaglini M, Ciofani G. Advances in the design of solid lipid nanoparticles and nanostructured lipid carriers for targeting brain diseases. *J Control Release*. 2017;264:306–332. doi:10.1016/J.JCONREL.2017.08.033
52. Amasya G, Aksu B, Badilli U, Onay-Besikci A, Tarimci N. QbD guided early pharmaceutical development study: production of lipid nanoparticles by high pressure homogenization for skin cancer treatment. *Int J Pharm*. 2019;563:110–121. doi:10.1016/J.IJPHARM.2019.03.056
53. Bahari LAS, Hamishehkar H. The impact of variables on particle size of solid lipid nanoparticles and nanostructured lipid carriers; a comparative literature review. *Adv Pharm Bull*. 2016;6(2):151. doi:10.15171/APB.2016.021
54. Oh KS, Kim RS, Lee J, Kim D, Cho SH, Yuk SH. Gold/chitosan/pluronic composite nanoparticles for drug delivery. *J Appl Polym Sci*. 2008;108 (5):3239–3244. doi:10.1002/APP.27767
55. Seo Y, Lim H, Park H, et al. Recent progress of lipid nanoparticles-based lipophilic drug delivery: focus on surface modifications. *Pharmaceutics*. 2023;15(3):772. doi:10.3390/PHARMACEUTICS15030772

56. Kazmi I, Al-Abbasi FA, Imam SS, et al. Formulation and evaluation of Apigenin-loaded hybrid nanoparticles. *Pharmaceutics*. 2022;14(4):783. doi:10.3390/PHARMACEUTICS14040783
57. Mahmoudi S, Ghorbani M, Sabzichi M, Ramezani F, Hamishehkar H, Samadi N. Targeted hyaluronic acid-based lipid nanoparticle for apigenin delivery to induce Nrf2-dependent apoptosis in lung cancer cells. *J Drug Deliv Sci Technol*. 2019;49:268–276. doi:10.1016/J.JDDST.2018.11.013
58. Gilani SJ, Bin-jumah MN, Imam SS, Alshehri S, Jahangir MA, Zafar A. Formulation and optimization of nano lipid based oral delivery systems for arthritis. *Coatings*. 2021;11(5):548. doi:10.3390/COATINGS11050548
59. Liu L, Tang Y, Gao C, et al. Characterization and biodistribution in vivo of quercetin-loaded cationic nanostructured lipid carriers. *Colloids Surfaces B Biointerfaces*. 2014;115:125–131. doi:10.1016/J.COLSURFB.2013.11.029
60. Ojo AT, Ma C, Lee PI. Elucidating the effect of crystallization on drug release from amorphous solid dispersions in soluble and insoluble carriers. *Int J Pharm*. 2020;591:120005. doi:10.1016/J.IJPHARM.2020.120005
61. Huang Z, Ma C, Wu M, et al. Exploring the drug-lipid interaction of weak-hydrophobic drug loaded solid lipid nanoparticles by isothermal titration calorimetry. *J Nanoparticle Res*. 2020;22(1):1–14. doi:10.1007/S11051-019-4671-6/METRICS
62. Pochapski DJ, Carvalho Dos Santos C, Leite GW, Pulcinelli SH, Santilli CV. Zeta Potential and colloidal stability predictions for inorganic nanoparticle dispersions: effects of experimental conditions and electrokinetic models on the interpretation of results. *Langmuir*. 2021;37(45):13379–13389. doi:10.1021/ACS.LANGMUIR.1C02056
63. Kan KHM, Li J, Wijesekera K, Cranston ED. Polymer-grafted cellulose nanocrystals as pH-responsive reversible flocculants. *Biomacromolecules*. 2013;14(9):3130–3139. doi:10.1021/BM400752K
64. Hoare SRJ. Analyzing kinetic binding data. Assay Guidance Manual; 2021. Avaiable from: https://www.ncbi.nlm.nih.gov/books/NBK569501/. Accessed September 7, 2023.
65. Chamani J, Moosavi-Movahedi AA, Hakimelahi GH. Structural changes in β-lactoglobulin by conjugation with three different kinds of carboxymethyl cyclodextrins. *Thermochim Acta*. 2005;432(1):106–111. doi:10.1016/J.TCA.2005.04.014
66. Hosseinzadeh M, Nikjoo S, Zare N, Delavar D, Beigoli S, Chamani J. Characterization of the structural changes of human serum albumin upon interaction with single-walled and multi-walled carbon nanotubes: spectroscopic and molecular modeling approaches. *Res Chem Intermed*. 2019;45(2):401–423. doi:10.1007/S11164-018-3608-5/METRICS
67. Mujtaba MA, Alotaibi NM, Alshehri SM, et al. Novel therapeutic approach in PEGylated chitosan nanoparticles of Apigenin for the treatment of cancer via oral nanomedicine. *Polymers (Basel)*. 2022;14(20):4344. doi:10.3390/POLYM14204344
68. Zoubari G, Staufenbiel S, Volz P, Alexiev U, Bodmeier R. Effect of drug solubility and lipid carrier on drug release from lipid nanoparticles for dermal delivery. *Eur J Pharm Biopharm*. 2017;110:39–46. doi:10.1016/J.EJPB.2016.10.021
69. Alfaleh MA, Hashem AM, Abujamel TS, et al. Apigenin loaded Lipoid–PLGA–TPGS nanoparticles for colon cancer therapy: characterization, sustained release, cytotoxicity, and apoptosis pathways. *Polymers (Basel)*. 2022;14(17):3577. doi:10.3390/POLYM14173577/S1
70. Imran M, Aslam Gondal T, Atif M, et al. Apigenin as an anticancer agent. *Phyther Res*. 2020;34(8):1812–1828. doi:10.1002/PTR.6647
71. Sun D, Liu Y, Yu Q, et al. The effects of luminescent ruthenium(II) polypyridyl functionalized selenium nanoparticles on bFGF-induced angiogenesis and AKT/ERK signaling. *Biomaterials*. 2013;34(1):171–180. doi:10.1016/J.BIOMATERIALS.2012.09.031
72. Fu J, Zeng W, Chen M, et al. Apigenin suppresses tumor angiogenesis and growth via inhibiting HIF-1α expression in non-small cell lung carcinoma. *Chem Biol Interact*. 2022;361:109966. doi:10.1016/J.CBI.2022.109966
73. Gunasekaran T, Haile T, Nigusse T, Dhanaraju MD. Nanotechnology: an effective tool for enhancing bioavailability and bioactivity of phytomedicine. *Asian Pac J Trop Biomed*. 2014;4(Suppl 1):S7. doi:10.12980/APJTB.4.2014C980
74. Chen L, Wang S, Feng Y, et al. Utilisation of chick embryo chorioallantoic membrane as a model platform for imaging-navigated biomedical research. *Cells*. 2021;10(2):1–41. doi:10.3390/CELLS10020463
75. Kim TJ, Zhang YH, Kim Y, et al. Effects of apigenin on the serum- and platelet derived growth factor-BB-induced proliferation of rat aortic vascular smooth muscle cells. *Planta Med*. 2002;68(7):605–609. doi:10.1055/S-2002-32901
76. Fang J, Xia C, Cao Z, Zheng JZ, Reed E, Jiang B-H. Apigenin inhibits VEGF and HIF-1 expression via PI3K/AKT/p70S6K1 and HDM2/p53 pathways. *FASEB J*. 2005;19(3):342–353. doi:10.1096/FJ.04-2175COM
77. Lee WJ, Chen WK, Wang CJ, Lin WL, Tseng TH. Apigenin inhibits HGF-promoted invasive growth and metastasis involving blocking PI3K/Akt pathway and beta 4 integrin function in MDA-MB-231 breast cancer cells. *Toxicol Appl Pharmacol*. 2008;226(2):178–191. doi:10.1016/J.TAAP.2007.09.013
78. El-Kenawi AE, El-Remessy AB. Angiogenesis inhibitors in cancer therapy: mechanistic perspective on classification and treatment rationales. *Br J Pharmacol*. 2013;170(4):729. doi:10.1111/BPH.12344
79. Ruela-De-Sousa RR, Fuhler GM, Blom N, Ferreira CV, Aoyama H, Peppelenbosch MP. Cytotoxicity of apigenin on leukemia cell lines: implications for prevention and therapy. *Cell Death Dis*. 2010;1. doi:10.1038/cddis.2009.18
80. Behzadi S, Serpooshan V, Tao W, et al. Cellular uptake of nanoparticles: journey inside the cell. *Chem Soc Rev*. 2017;46(14):4244. doi:10.1039/C6CS00636A
81. Wojtowicz W, Wróbel A, Pyziak K, et al. Evaluation of MDA-MB-468 cell culture media analysis in predicting triple-negative breast cancer patient sera metabolic profiles. *Metabolites*. 2020;10(5):173. doi:10.3390/METABO10050173
82. Bauer D, Mazzio E, Hilliard A, Oriaku ET, Soliman KFA. Effect of apigenin on whole transcriptome profile of TNFα–activated MDA–MB–468 triple negative breast cancer cells. *Oncol Lett*. 2020;19(3):2123–2132. doi:10.3892/OL.2020.11327/HTML
83. Way TD, Kao MC, Lin JK. Apigenin induces apoptosis through proteasomal degradation of HER2/neu in HER2/neu-overexpressing breast cancer cells via the phosphatidylinositol 3-kinase/Akt-dependent pathway. *J Biol Chem*. 2004;279(6):4479–4489. doi:10.1074/JBC.M305529200
84. Bai H, Jin H, Yang F, Zhu H, Cai J. Apigenin induced MCF-7 cell apoptosis-associated reactive oxygen species. *Scanning*. 2014;36(6):622–631. doi:10.1002/SCA.21170
85. Calderón-Montaño JM, Martínez-Sánchez SM, Jiménez-González V, et al. Screening for selective anticancer activity of 65 extracts of plants collected in western Andalusia, Spain. *Plants*. 2021;10(10):2193. doi:10.3390/PLANTS10102193/S1
86. Badr-Eldin SM, Aldawsari HM, Ahmed OAA, et al. Optimized semisolid self-nanoemulsifying system based on glyceryl behenate: a potential nanoplatform for enhancing antitumor activity of raloxifene hydrochloride in MCF-7 human breast cancer cells. *Int J Pharm*. 2021;600:120493. doi:10.1016/J.IJPHARM.2021.120493

87. Khuda SE, Nguyen AV, Sharma GM, Alam MS, Balan KV, Williams KM. Effects of emulsifiers on an in vitro model of intestinal epithelial tight junctions and the transport of food allergens. *Mol Nutr Food Res*. 2022;66(4):e2100576. doi:10.1002/MNFR.202100576
88. Ilyasoğlu H, Ilyaso H. Characterization of rosehip (Rosa canina L.) seed and seed oil. *Int J Food Prop*. 2014;17(7):1591–1598. doi:10.1080/10942912.2013.777075
89. Mármol I, Jiménez-Moreno N, Ancín-Azpilicueta C, Osada J, Cerrada E, Rodríguez-Yoldi MJ. A combination of Rosa Canina extracts and gold complex favors apoptosis of Caco-2 cells by increasing oxidative stress and mitochondrial dysfunction. *Antioxidants*. 2019;9(1):17. doi:10.3390/ANTIOX9010017
90. Cagle P, Idassi O, Carpenter J, Minor R, Goktepe I, Martin P. Effect of rosehip (Rosa Canina) extracts on human brain tumor cell proliferation and apoptosis. *J Cancer Ther*. 2012;2012(5):534–545. doi:10.4236/JCT.2012.35069
91. Federation of American Societies for Experimental Biology (FASEB). Natural extract shows promise for preventing breast cancer, study suggests – ScienceDaily; 2015. Avaiable from: https://www.sciencedaily.com/releases/2015/03/150329141007.htm. Accessed May 14, 2023.
92. Neves AR, Queiroz JF, Costa Lima SA, Figueiredo F, Fernandes R, Reis S. Cellular uptake and transcytosis of lipid-based nanoparticles across the intestinal barrier: relevance for oral drug delivery. *J Colloid Interface Sci*. 2016;463:258–265. doi:10.1016/J.JCIS.2015.10.057
93. Jeitler R, Glader C, Tetyczka C, et al. Investigation of cellular interactions of lipid-structured nanoparticles with oral mucosal epithelial cells. *Front Mol Biosci*. 2022;9:554. doi:10.3389/FMOLB.2022.917921/BIBTEX

3.2. Antitumoral Melatonin-loaded nanostructured lipid carriers

Lorena Bonilla Vidal, Marta Świtalska, Marta Espina, Joanna Wietrzyk, María Luisa García, Eliana B Souto, Anna Gliszczyńska, Elena Sánchez López.

Nanomedicine

2024

IF (JCR-2023) 4.7, Biotechnology & Applied Microbiology 29/174 (Q1)

10.1080/17435889.2024.2379757

NANOMEDICINE
https://doi.org/10.1080/17435889.2024.2379757

Taylor & Francis
Taylor & Francis Group

RESEARCH ARTICLE

Antitumoral melatonin-loaded nanostructured lipid carriers

Lorena Bonilla-Vidal[a,b], Marta Świtalska[c], Marta Espina[a,b], Joanna Wietrzyk[c], Maria Luisa García[a,b], Eliana B Souto[d], Anna Gliszczyńska[‡,**,e] and Elena Sánchez-López[‡,*,a,b]

[a]Department of Pharmacy, Pharmaceutical Technology & Physical Chemistry, University of Barcelona, Barcelona, 08028, Spain; [b]Institute of Nanoscience & Nanotechnology (IN^{2}UB), University of Barcelona, Barcelona, 08028, Spain; [c]Department of Experimental Oncology, Ludwik Hirszfeld Institute of Immunology & Experimental Therapy, Polish Academy of Sciences, Weigla 12, 53-114, Wrocław, Poland; [d]Laboratory of Pharmaceutical Technology, Department of Drug Sciences, Faculty of Pharmacy, University of Porto, Rua de Jorge Viterbo Ferreira, 228, Porto, 4050-313, Portugal; [e]Department of Food Chemistry & Biocatalysis, Wrocław University of Environmental & Life Sciences, Norwida 25, 50-375, Wrocław, Poland

ABSTRACT

Aim: Cancer constitutes the second leading cause of death worldwide, with conventional therapies limited by significant side effects. Melatonin (MEL), a natural compound with antitumoral properties, suffers from instability and low solubility. To overcome these issues, MEL was encapsulated into nanostructured lipid carriers (MEL-NLC) containing rosehip oil to enhance stability and boost its antitumoral activity. **Methods:** MEL-NLC were optimized by a design of experiments approach and characterized for their physicochemical properties. Stability and biopharmaceutical behavior were assessed, along with interaction studies and *in vitro* antitumoral efficacy against various cancer cell lines. **Results:** Optimized MEL-NLC exhibited desirable physicochemical characteristics, including small particle size and sustained MEL release, along with long-term stability. *In vitro* studies demonstrated that MEL-NLC selectively induced cytotoxicity in several cancer cell lines while sparing healthy cells. **Conclusion:** MEL-NLC represent a promising alternative for cancer, combining enhanced stability and targeted antitumoral activity, potentially overcoming the limitations of conventional treatments.

Plain language summary: Despite current advances, cancer is the second cause of death worldwide, but conventional therapies have side effects and limited efficacy. Natural therapies are emerging as suitable alternatives and, among them, Melatonin is a well-known compound with antitumoral properties. However, it is degraded by light, decreasing its therapeutical activity. In order to effectively deliver Melatonin into cancer cells, it has been encapsulated into biodegradable nanoparticles containing rosehip oil, which may boost the antitumoral properties. These nanoparticles have been optimized, showing a small size and a high Melatonin encapsulation, sustained drug release and good stability. Furthermore, *in vitro* studies demonstrated antitumoral activity against several cancer cell lines, also showing a high internalization inside them. Moreover, studies conducted using chicken embryonated eggs, showed that nanoparticles were non-toxic, thus confirming its promising therapeutical applications.

ARTICLE HISTORY
Received 20 April 2024
Accepted 10 July 2024

KEYWORDS
antitumoral; lipid nanoparticles; melatonin; nanostructured lipid carriers; natural compounds; rosehip oil

1. Background

Cancer represents a significant global health challenge, with predictions indicating that cancer diagnoses will rise to 24 million by 2035 [1–3]. Due to this high economical and societal burden, early detection and effective cancer treatment have been among the main goals of medical researchers [4]. Despite some success in current therapies, resistance to chemotherapeutic drugs remains one of the challenges to overcome, as it is responsible for treatment failure and tumoral relapse [4,5].

In order to search for novel and effective therapies, several compounds have been investigated [6]. Among them, natural products have gained increased interest due to their low toxicity and potent antitumoral activity [7]. One of the most well-known endogenous compounds, Melatonin (MEL), has shown relevant promising properties against cancer [8]. MEL, a derivative of tryptophan, is a neurohormone produced in the pineal gland and other organs like skin, retina, gastrointestinal tract and bone marrow [9]. MEL is widely known due to its antioxidant and anti-inflammatory activities, but it also plays a crucial role in tumoral processes [10,11]. Specifi-

CONTACT Elena Sánchez-López esanchezlopez@ub.edu; Anna Gliszczyńska anna.gliszczynska@upwr.edu.pl
‡Authors contributed equally
Supplemental data for this article can be accessed at https://doi.org/10.1080/17435889.2024.2379757

cally, MEL has shown effects on proliferation, regulation of immune responses, angiogenesis, replicative immortality, metastasis, cell death and genome instability [12,13]. Moreover, there is clinical evidence when using MEL as an adjuvant therapy in chemotherapy, showing significant improvements in tumor remission and a reduction of side effects of chemodrugs [14,15]. In particular, by influencing on mitochondrial homeostasis and functioning, and being a highly effective free radical scavenger, MEL could inhibit cancer progression and protect normal tissues [16,17]. Despite MEL promising properties, it is sensitive to both air and light, complicating its formulation and administration [18]. Furthermore, it has a short plasma half-life, variable oral absorption and a low bioavailability because of its first pass metabolism. For these reasons, currently available conventional oral dosage forms are not suitable candidates for MEL effective delivery [19].

To overcome MEL degradation and deliver it efficiently to cancer cells, nanotechnology has emerged as a suitable tool to encapsulate active compounds, protecting them from air and light and increasing their bioavailability. Particularly, nanoparticles (NPs) are able to encapsulate active compounds protecting them against degradation and providing prolonged release [20–22]. Among the different types of NPs, lipid NPs have gained special attention due to their easy scale-up and low toxicity [23]. The first generation of lipid NPs, the solid lipid nanoparticles (SLN), emerged in the early 1990s. Despite great results, they still presented some drawbacks, such as expulsion of the entrapped drug during storage and low drug loading capacity [24,25]. In order to overcome these problems, the second generation of lipid NPs, the nanostructured lipid carriers (NLC), emerged. In these systems, the addition of a liquid lipid in the formulation enhances the cargo capacity of the NPs and, at the same time, increases stability during storage [26].

In previous studies, we have demonstrated that NLC produced using natural compounds may constitute a promising system to encapsulate antitumoral drugs [27]. Therefore, in this work, we aim to encapsulate an endogenous and natural compound with potent antitumoral activity but high sensitivity to degradation into NLC (MEL-NLC). Furthermore, the liquid lipid rosehip oil has been selected to enhance MEL cytotoxic activity due to its selective apoptotic properties [28–30]. MEL antiproliferative activity has been investigated alone or in combination with conventional anticancer therapies, but a combination of MEL with rosehip oil has never been attempted. Moreover, their loading in NLC may constitute an interesting approach to obtain antitumoral effects avoiding the side effects of conventional chemodrugs [31–33]. MEL-NLC are aimed to protect MEL from oxidation processes and increase its short half-life. NLC have been developed and optimized for the encapsulation of MEL by using a Design of Experiments (DoE), studying the effect of several independent variables on their physicochemical parameters. NPs characterization by photon correlation spectroscopy, differential scanning calorimetry (DSC), X-ray diffraction (XRD), Fourier-transform infrared (FTIR) and *in vitro* release profile, has been carried out. Furthermore, antitumoral efficacy was demonstrated by cytotoxicity studies in selected tumoral cell lines (MV4-11, A549, MCF-7 and MDA-MB-468).

2. Materials & methods

2.1. Materials

MEL was purchased from Thermo Fisher Scientific (Massachusetts, USA). Compritol® 888 ATO (Glyceryl distearate) was donated by Gattefossé (Madrid, Spain). Rosehip oil was obtained from Acofarma Fórmulas Magistrales (Barcelona, Spain). Tween® 80 (Polysorbate 80) and Nile red (NR) were purchased from Sigma Aldrich (Madrid, Spain). The additional chemical reagents and components utilized were of analytical grade. Purified water was obtained using a Millipore Milli-Q Plus device.

2.2. MEL-NLC preparation & optimization

The production of MEL-NLC was performed by hot high-pressure homogenization method (FPG 12800 Homogenizer, Stansted, UK), previously optimized [27,34]. Briefly, an aqueous phase containing Tween® 80, and a lipid phase formed by the solid lipid (SL) and the liquid lipid, and MEL were mixed with an Ultraturrax® T10 basic (IKA, Staufen, Germany) at 8000 rpm for 30 s. The emulsion was homogenized with the conditions of 85 °C, three homogenization cycles and 900 bars.

In order to produce MEL-NLC labeled with NR (MEL-NLC-NR), the same procedure was performed, but with the addition of NR at 0.0375 % (w/v) to the lipid phase [35].

The optimization of the formulation was performed through a DoE due to its capacity to provide maximum information using a reduced number of experiments [36]. A central composite factorial design was implemented to analyze the effect of independent variables, namely, MEL concentration (%), Tween® 80 concentration (%), lipid phase concentration (%) and SL concentration (SL/Lipid phase, %), on the dependent variables, namely, the mean particle size (Z_{av}), polydispersity index (PI), zeta potential (ZP) and encapsulation efficiency (EE) [37].

Following the developed composite design matrix generated by Statgraphics Centurion 18® version 18.1.12 software (Virginia, USA), 26 experiments were required.

2.3. Physicochemical parameters

To measure Z_{av} and PI, MEL-NLC were placed in a disposable cell (Malvern Instruments, Malvern, UK) and diluted 1:10 with MilliQ® Water. Measurements were performed using photon correlation spectroscopy employing a Zeta-Sizer Nano ZS (Malvern Instruments, Malvern, UK) at 25 °C. Assays were carried out in triplicate. The surface charge of particles was determined using laser-Doppler electrophoresis with the same device. Samples were diluted 1:20 in MilliQ® water, and assays were also performed in triplicate [38,39].

To estimate the percentage of MEL entrapped in the NLC, EE was calculated indirectly by measuring the non-encapsulated drug in the formulation by high-performance liquid chromatography (HPLC) [40]. To separate the non-entrapped MEL from the MEL-NLC, an Amicon® Ultra-0.5 centrifugal filter device (Amicon Millipore Corporation, Ireland) was used with an ultracentrifuge (Beckman Optima®, Ultracentrifuge, California, USA) at 14100 rpm for 15 min. Then, the supernatant containing the non-encapsulated MEL was used to evaluate the EE according to the Equation (1):

$$EE\ (\%) = \frac{Total\ amount\ of\ MEL - Free\ amount\ of\ MEL}{Total\ amount\ of\ MEL} \times 100 \quad (1)$$

The measurement of the sample was carried out using HPLC with a Kromasil® C18 column (particle size: 5 μm, dimensions: 150 mm × 4.6 mm). The mobile phase consisted of an aqueous solution containing 2 % acetic acid and an organic phase composed of methanol. A gradient was implemented by increasing the water phase from 40 % to 60 % over a period of 5 min, and then reversing the gradient over the next 5 min. The flow rate used was 0.9 ml/min. MEL detection was performed using a diode array detector (Waters® 2996) with a wavelength of 300 nm. The results obtained were analyzed using Empower 3® Software [36,41].

2.4. Characterization of optimized MEL-NLC

2.4.1. Transmission electron microscopy

MEL-NLC samples were subjected to negative staining using a 2 % solution of uranyl acetate. The staining was carried out on copper grids that had been activated with UV light. The morphology of NLC was examined using transmission electron microscopy (TEM) on a JEOL 1010 microscope (Akishima, Japan) [42].

2.4.2. Interaction studies

A Mettler-Toledo DSC 823e System (Barcelona, Spain) was used to conduct a thermal profile characterization of MEL-NLC using DSC. For system calibration, we employed indium (with a purity of ≥ 99.95 %, sourced from Fluka, Switzerland) and utilized an empty pan as a reference. The samples underwent a heating ramp of 10 °C/min, ranging from 25 to 105 °C, under a nitrogen atmosphere. Data analysis was carried out using the Mettler STARe V 9.01 dB software, provided by Mettler-Toledo in Barcelona, Spain [36].

We evaluated the crystallinity of the samples through XRD analysis. The samples were placed between polyester films with a thickness of 3.6 μm and exposed to CuKα radiation with a voltage of 45 kV and a current of 40 mA, with a wavelength of 1.5418 Å. The radiation was applied throughout an angular range of 2–60°, as measured by 2θ. We utilized a step size of 0.026° and a dwell period of 200 s each step for the duration of the exposure [40].

A Thermo Scientific Nicolet iZ10 (Barcelona, Spain) equipped with an ATR diamond and DTGS detector was used to obtain FTIR spectra of MEL-NLC [42].

2.4.3. Stability studies

MEL-NLC were stored at 4, 25 and 37 °C for 17 months to assess their physical stability. Stability experiments were performed by analysing the light backscattering (BS) using a Turbiscan® Lab (Formulaction, Toulouse, France). A volume of 10 ml of sample was placed in a glass measuring cell and pulsed near infrared light-emitting diode LED (λ = 880 nm) was used as radiation source. BS profiles were acquired by a BS detector located at an angle of 45° from the incident beam [38]. The physical stability of the NLC was also evaluated by monitoring modifications of the physicochemical parameters Z_{av}, PI and ZP at the different storage temperatures. Furthermore, EE was analyzed to measure the possible drug diffusion from the NLC to the aqueous medium over time at three different storage temperatures.

2.4.4. Biopharmaceutical behavior

The *in vitro* release profile of MEL from NLC compared with free MEL was investigated using a direct dialysis method under sink conditions for 48 h (n = 3) [43]. Briefly, 9 ml of each formulation were loaded into separate dialysis bags (cellulose membrane, MWCO 12–14 kDa, diameter 3.20/32 inches, Iberlabo). The bags were then immersed in the release medium composed of 0.1 M phosphate-buffered saline (PBS) containing 0.1 % sodium dodecyl sulphate (SDS) at pH 7.4 and maintained at 37 °C. At predetermined time intervals, 0.3 ml aliquots of the release medium were withdrawn and replaced with fresh medium. MEL concentration in the collected samples was quantified, and the data were subsequently analyzed by fitting to various kinetic models [36,44].

2.5. Biological studies

2.5.1. Cell lines

For the cell viability studies, several human cell lines were used. MV4-11 (biphenotypic B myelomonocytic leukemia) and MCF-10A (normal breast epithelium) were sourced from the American Type Culture Collection (ATCC, VA, USA). A549 (lung carcinoma) cell line was obtained from the European Collection of Authenticated Cell Cultures (ECACC, Porton Down, UK), and MDA-MB-468 (breast cancer) cell line was obtained from the Leibniz Institute DSMZ-German Collection of Microorganisms and Cell Cultures (Germany). All cell lines were maintained at the Hirszfeld Institute of Immunology and Experimental Therapy (PAS, Wroclaw, Poland).

MV4-11 and MDA-MB-468 cells were grown in RPMI 1640 medium (IIET PAS, Warsaw, Poland) supplemented fetal bovine serum (FBS, Merck, Germany) at different concentrations (10 % for MV4-11, 20 % for MDA-MB-468). MV4-11 cultures additionally received sodium pyruvate 1.0 mM (all from Merck, Germany). A549 cells were maintained in an equal mixture of RPMI 1640 and Opti-MEM (Gibco®, Paisley, Scotland) supplemented with 5 % FBS (Merck, Germany). MCF-7 cells were cultured in Eagle's medium (IIET PAS, Poland) adding 8 μg/ml insulin and 1 % MEM non-essential amino acids (both from Merck, Darmstadt, Germany). Finally, MCF-10A cells were grown in HAM'S F-12 medium (Corning, Warsaw, Poland) containing Hors serum (Gibco®, Paisley, Scotland), 20 ng/ml EGF, 10 μg/ml insulin, 0.5 μg/ml hydrocortisone and 0.05 mg/ml cholera toxin from *Vibrio cholerae* (all from Merck, Darmstadt, Germany).

All cell lines were cultured under 5 % CO_2 in a humidified atmosphere, at 37 °C. and supplemented with 2 mM L-glutamine (Merck, Darmstadt, Germany), 100 μg/ml streptomycin (Merck, Darmstadt, Germany) and 100 units/ml penicillin (Polfa Tarchomin SA, Warsaw, Poland).

2.6. Determination of antiproliferative activity

For cytotoxicity evaluation, solutions of MEL (0.5 mg/ml) and MEL-NLC (equivalent to 0.5 mg/ml MEL) were prepared in DMSO and water, respectively. The samples to be tested were subsequently diluted in culture medium at different concentrations. Cells were seeded at a density of 1×10^4 cells/well (except for A549, which was seeded at 0.5×10^4 cells/well) in 96-well plates (Sarstedt, Nümbrecht, Germany) and allowed to adhere for 24 h prior to treatment. Following 24 and 72 h of exposure to four different concentrations of the samples, the *in vitro* cytotoxic effect was assessed using either the MTT assay (for MV4-11 cells) or the SRB assay, as previously described [45]. The concentration inhibiting 50 % of cell growth (IC_{50}) was calculated using the Prolab-3 system based on Cheburator 0.4 software [46]. Each treatment and concentration were tested in triplicate within a single experiment, with the entire experiment repeated three- to five-times for statistical analysis.

2.7. Determination of accumulation of MEL-NLC in cells by flow cytometry

Following incubation, cells were collected, washed with PBS and analyzed by flow cytometry. Cells treated with NR-conjugated compounds were subjected to quantification of the mean fluorescence intensity (MFI) using a BD LSRFortessa cytometer (BD Biosciences, San Jose, USA). Untreated cells served as a negative control. The acquired data were analyzed using FlowJo software version 2 (Cell Imaging Core, Turku Centre for Biotechnology, Turku Åbo Akademi University) [27].

2.8. MEL-NLC safety evaluation using the chicken choriolantoic membrane assay

In ovo biological compatibility of MEL solution and MEL-NLC was evaluated using the chick embryo choriolantoic membrane (CAM) assay [47]. Fertilized chicken eggs were incubated at 37 °C and 85 % relative humidity. On embryonic day 3, a lateral window was aseptically opened in the eggshell to access the CAM. Following a 24 h stabilization period, CAM ($n = 6$) were inoculated with 40 μl of the test sample. The window was then sealed, and the eggs were returned to the incubator for an additional 48 h. Posteriorly, CAM were evaluated though a stereomicroscope (STEMI DV4 model, from ZEISS).

2.9. Statistical analysis

Data were analyzed using two-way analysis of variance (ANOVA) followed by Tukey's post-hoc test for multiple comparisons between groups. Student's *t*-test was employed for comparisons between two groups only. All data are presented as mean $\pm$ standard deviation (SD). Statistical significance was set at $p < 0.05$ using GraphPad Prism 9 software.

3. Results

3.1. MEL-NLC preparation & optimization

The optimization process was carried out using the DoE approach by developing a full composite factorial design of four levels and four factors. Previously, the fabrication process was optimized, setting-up conditions involving three homogenization cycles at 900 bar of pressure and 30 s of pre-emulsion time [27]. Regarding the lipid NLC composition, Compritol® 888 ATO was selected due to MEL high solubility in this solid lipid, and rosehip oil

was chosen due to its antioxidant, anti-inflammatory and antiproliferative activity [29,48]. The surfactant Tween® 80 is advocated to inhibit P-gp, which is relevant in cancer drug delivery because of its overexpression in multidrug resistance (MDR) tumors [49–51]. A statistical analysis was performed in order to study the effect of the independent variables (MEL amount, concentration of lipid phase (SL and liquid lipid mixture), ratio of SL and surfactant concentration), against the dependent variables (Z_{av}, PI, ZP and EE). The independent variables were selected because of their high influence on the physicochemical parameters of the formulation [52–54].

As shown in Table 1, formulation sizes remained around 200 nm, and PI values were approximately 0.2, which indicates an homogeneous distribution of the NPs [55]. Furthermore, the formulations showed a negative ZP under -20 mV, which predicts suitable stability of the NPs [56]. MEL-NLC negative charge may be attributed to the ionization of the solid lipid composing Compritol® 888 ATO (glyceryl behenate) [57]. EE values were about 70 %, thus indicating that MEL had more affinity for the lipid matrix because of its low solubility in water [58].

As can be observed in Figure 1, the four studied variables showed a significant effect on MEL-NLC size. The range of Z_{av} was between 100 and 300 nm, which was strongly influenced by the concentration of the lipid phase ($p < 0.05$). As shown in the Pareto's diagram (Figure 1A), when the concentration of the lipid phase increased, MEL-NLC Z_{av} also increased. The same effect was also observed in the ratio of SL, the particles became bigger with the increase of the solid/liquid lipid ratio. On the other hand, the concentration of the surfactant affected inversely to Z_{av}, decreasing it when surfactant concentration increased. Regarding the PI, its values ranged from 0.1 to 0.26. It was highly influenced by the concentration of the SL, being more polydisperse as more Compritol® 888 ATO was added (Figure 1B). On the other hand, higher amounts of surfactant reduced PI. Moreover, regarding the ZP, a lower surface charge was obtained when the lowest or the highest concentration of MEL was used (Figure 1C). EE was slightly influenced by the amount of MEL, in which low MEL amounts led to higher EE (%) probably due to the fact that it is easier to accommodate less amounts of drug inside the NLC matrix (Figure 1D). Considering all the evaluated parameters, the formulation containing 0.05 % (w/v) of MEL, 7.5 % (w/v) of lipid phase, 7.125 % (w/v) of solid lipid, 0.375 % of liquid lipid and 5 % (w/v) of surfactant was chosen as optimized to carry out further experiments. With these optimal parameters, MEL-NLC of Z_{av} of 129.8 ± 1.0 nm, low PI of 0.199 ± 0.002, ZP of -20.2 ± 0.2 mV and high EE of 79.8 ± 0.3 % were obtained.

3.2. Characterization of optimized MEL-NLC

3.2.1. Transmission electron microscopy

To characterize the morphology of MEL-NLC, TEM was used and compared with the data obtained by photon correlation spectroscopy (Supplementary Figure S1A & C). The analysis confirmed that the average size of MEL-NLC was below 200 nm and that particles exhibited soft round shapes, with an amorphous lipid matrix. Particle aggregation phenomena was not observed, which is in agreement with the values of -20 mV recorded for the ZP parameter (Supplementary Figure S1B & D).

3.2.2. Interaction studies

The interactions between MEL and the lipid matrix were carried out using different techniques and are shown in Figure 2.

DSC was employed to characterize the thermal behavior of the lipid mixtures and of MEL-NLC. Thermograms (Figure 2A) showed endothermal peaks of 70.31 °C for lipid mixture, 69.74 °C for the empty NLC and 68.60 °C for MEL-NLC. The lower melting temperature of the particles in comparison to the lipid mixture was due to the lower crystallinity of the former since they contain additional ingredients, including the surfactant Tween® 80 [59,60]. The presence of drug also contributed to reduce the crystallinity of MEL-NLC in comparison to empty NLC. As the sample became more amorphous, the peak was shifted to lower melting temperatures [60]. The melting enthalpy for the lipid mixture was 106.19 Jg^{-1}, for the empty NLC was 82.96 Jg^{-1} and for the MEL-NLC 80.24 Jg^{-1}. The results of the melting enthalpy are aligned with the recorded melting points, in other words, the lower the melting point the lower the melting enthalpy and the lower crystallinity of the matrices [60]. MEL melting transition was characterized by an endothermal peak at 118.52 °C ($\Delta H = 134.70\ Jg^{-1}$) followed by decomposition.

XRD profiles in Figure 2B show the physical state of MEL incorporated in NLC. MEL and the solid mixture of lipids possess a crystalline structure confirmed by intense and sharp peaks. Some of the characteristic MEL peaks (19.13, 19.94 and 24.27°) showed a lower intensity in MEL-NLC profile, which could indicate that the drug was dispersed in the NLC matrix. The crystallinity of the other formulation compounds was also studied. The physical mixture of the lipids showed pronounced peaks at 21.28° (2θ), $d = 0.42$ nm and 23.20° (2θ), $d = 0.46$ nm. These signals were also found in the Compritol® 888 ATO XDR profile. MEL-NLC showed a very intense peak at 19.41° (2θ),

Table 1. Design of experiments and characterization of the different formulations developed.

	Independent variables								Dependent variables			
	MEL (%)		LP (%)		SL (%)		Tw (%)		Z_{av} ± SD (nm)	PI ± SD	ZP ± SD (mV)	EE ± SD (%)
Factorial points												
M1	-1	0.1	1	10	1	85	-1	2	284.7 ± 1.8	0.256 ± 0.006	-24.5 ± 0.8	71.1 ± 0.1
M2	1	0.2	-1	5	1	85	1	4	135.7 ± 0.6	0.177 ± 0.026	-20.0 ± 0.5	71.4 ± 0.1
M3	1	0.2	1	10	1	85	-1	2	284.4 ± 2.2	0.265 ± 0.022	-19.0 ± 0.3	61.0 ± 0.9
M4	-1	0.1	1	10	-1	65	-1	2	213.7 ± 2.5	0.164 ± 0.013	-19.9 ± 0.8	56.7 ± 0.2
M5	1	0.2	1	10	1	85	1	4	207.9 ± 0.7	0.229 ± 0.010	-16.8 ± 0.3	73.4 ± 0.1
M6	1	0.2	-1	5	-1	65	-1	2	142.2 ± 0.6	0.179 ± 0.010	-21.5 ± 0.3	66.4 ± 0.1
M7	-1	0.1	-1	5	-1	65	-1	2	141.6 ± 0.8	0.206 ± 0.016	-22.5 ± 1.3	62.0 ± 0.6
M8	-1	0.1	-1	5	1	85	1	4	146.5 ± 1.4	0.178 ± 0.018	-16.5 ± 0.4	70.4 ± 0.2
M9	-1	0.1	1	10	-1	65	1	4	199.3 ± 1.9	0.138 ± 0.003	-16.9 ± 0.1	71.5 ± 0.2
M10	1	0.2	-1	5	-1	65	1	4	160.7 ± 1.3	0.138 ± 1.300	-19.8 ± 1.4	71.1 ± 0.1
M11	-1	0.1	-1	5	-1	65	1	4	182.7 ± 0.7	0.147 ± 0.029	-16.9 ± 0.1	71.5 ± 0.3
M12	1	0.2	-1	5	1	85	-1	2	167.3 ± 1.9	0.239 ± 0.014	-22.3 ± 0.2	62.9 ± 0.3
M13	-1	0.1	-1	5	1	85	-1	2	155.6 ± 2.8	0.252 ± 0.008	-23.7 ± 0.4	61.4 ± 0.1
M14	1	0.2	1	10	-1	65	1	4	211.2 ± 0.9	0.106 ± 0.026	-17.3 ± 0.5	70.3 ± 0.1
M15	-1	0.1	1	10	1	85	1	4	212.6 ± 0.3	0.232 ± 0.012	-17.5 ± 0.3	73.1 ± 0.1
M16	1	0.2	1	10	-1	65	-1	2	204.0 ± 3.4	0.183 ± 0.012	-24.0 ± 0.8	63.9 ± 0.1
Axial points												
M17	-2	0.05	0	7.5	0	75	0	3	174.8 ± 1.6	0.199 ± 0.016	-19.2 ± 0.8	72.4 ± 0.1
M18	2	0.25	0	7.5	0	75	0	3	179.1 ± 1.4	0.200 ± 0.042	-20.2 ± 0.9	69.9 ± 0.1
M19	0	0.15	-2	2.5	0	75	0	3	100.1 ± 0.2	0.202 ± 0.006	-21.4 ± 0.9	66.6 ± 0.1
M20	0	0.15	2	12.5	0	75	0	3	267.7 ± 1.1	0.224 ± 0.009	-16.1 ± 0.5	68.3 ± 0.1
M21	0	0.15	0	10	-2	55	0	3	169.9 ± 2.3	0.135 ± 0.007	-17.6 ± 0.1	66.0 ± 0.1
M22	0	0.15	0	10	2	95	0	3	203.8 ± 1.7	0.263 ± 0.010	-20.5 ± 0.9	67.4 ± 0.3
M23	0	0.15	0	10	0	75	-2	1	253.7 ± 1.9	0.223 ± 0.018	-22.7 ± 0.1	48.1 ± 0.1
M24	0	0.15	0	10	0	75	2	5	204.2 ± 0.9	0.126 ± 0.009	-16.2 ± 0.4	74.7 ± 0.1
Central points												
M25	0	0.15	0	7.5	0	75	0	3	189.7 ± 1.0	0.181 ± 0.060	-20.1 ± 0.4	68.1 ± 0.2
M26	0	0.15	0	7.5	0	75	0	3	188.5 ± 0.6	0.188 ± 0.029	-19.3 ± 0.4	68.0 ± 0.1

EE: Encapsulation efficiency; LP: Lipid phase; MEL: Melatonin; PI: Polydispersity index; SL: Solid lipid; Tw: Tween® 80; Zav: Mean particle size; ZP: Zeta potential.

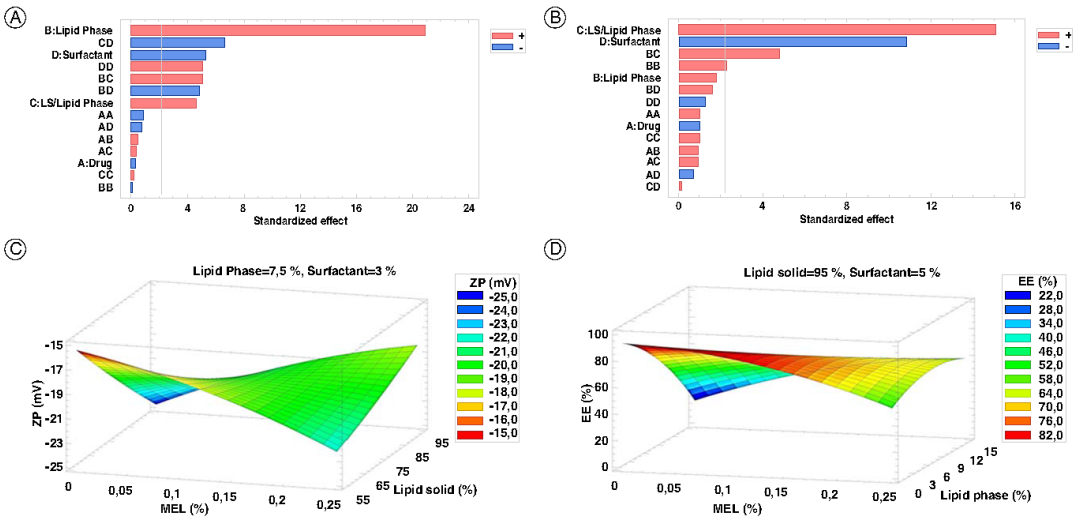

Figure 1. Design of experiments (DoE) results. **(A)** Pareto's chart of the independent variables effect for mean average size (Z_{av}). **(B)** Pareto's chart of the independent variables effect for polydispersity index (PI). **(C)** Surface response of the concentration of MEL and SL regarding to the lipid phase influence on zeta potential (ZP). **(D)** Surface response of the concentration of MEL and Lipid phase influence on encapsulation efficiency (EE).

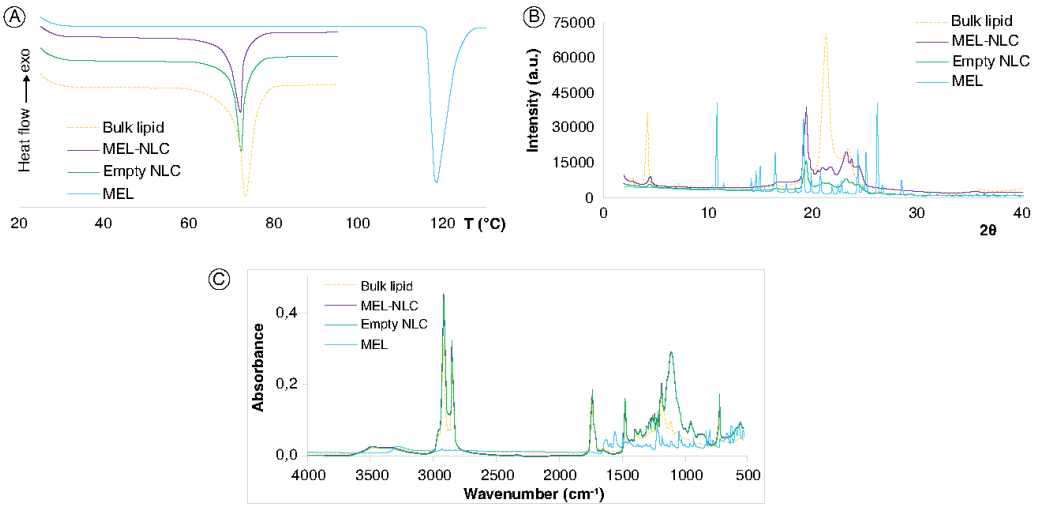

Figure 2. Characterization of optimized MEL-NLC and their components. **(A)** Differential scanning calorimetry (DSC) curves. **(B)** X-ray diffraction (XRD). **(C)** Fourier-transform infrared (FTIR).

$d = 0.46$ nm, and other one at 23.27° (2θ), $d = 0.38$ nm, indicating good stability of the formulation whereas the empty NLC only showed one of these peaks, observed at 19.41°, although it was less intense.

FTIR analysis was employed to investigate potential interactions between MEL, Tween® 80, and lipid matrix in the NLC formulation (Figure 2C). The characteristic peaks of MEL were at 3303 cm^{-1} (N-H), 1629 cm^{-1} (C=O), 1555 cm^{-1} (C-O) and 1212 cm^{-1} (C-N). The spectrum of the NLC (empty and loaded) showed a pronounced peak at 1100 cm^{-1} which corresponds to the surfactant [61]. Small peaks of MEL at 1000–1200 cm^{-1} were observed in the MEL-NLC spectrum. There was no indication of strong bonds between MEL and lipid phase and the surfactant.

3.2.3. Stability studies

The physical stability of MEL-NLC was evaluated by monitoring the changes in the physicochemical parameters Z_{av}, PI and ZP at different storage temperatures (Table 2). Furthermore, EE was analyzed to measure the possible drug diffusion from the NLC to the aqueous medium over time, at three different storage temperatures. BS profiles were also analyzed to identify potential destabilization mechanisms. A significant difference (greater than 10 %) in BS profiles compared with the initial state may indicate phenomena, such as sedimentation, aggregation or agglomeration of the NPs [62]. The physical stability revealed that MEL-NLC were not stable at 37 °C (Figure 3A). Furthermore, MEL-NLC were stable at 25 °C until day 30 (Figure 3B), when an increase in PI and a decrease in ZP occurred, which could mean that the formulation started to aggregate because of the reduction of the surface charge, becoming more neutral [63]. The physicochemical parameters remained constant at 4 °C for all the study (more than 1 year), confirming that 4 °C was a suitable storage temperature (Figure 3C).

3.3. Biopharmaceutical behavior

The *in vitro* release profile of MEL from NLC exhibited a unique kinetic profile typical of prolonged drug release formulations (Figure 4A & B). The best fit for free MEL was one-phase decay ($r^2 = 0.9873$). As shown in Figure 4A, 100 % of MEL was released during the first 7 h. MEL-NLC release was fitted to two-phase decay model ($r^2 = 0.9915$). In this case, 58 % of MEL was released from the NLC during the first 7 h, which translates a slower prolonged release. The half-life time ($t_{1/2}$, the time required for the initial concentration to decrease to one-half), and the kinetic constant (K) confirm that MEL-NLC released MEL in a slower manner in comparison to the free MEL, this latter with the $t_{1/2}$ shorter, and K lower for MEL-NLC. MEL-NLC showed a suitable *in vitro* release, in which most of the MEL was released to the receptor medium during the first 48 h (*plateau* of ~ 80 %), with an initial burst of MEL, and a second phase in which MEL was released in a sustained manner. This biphasic behavior usually occurs in NLC, attributed to the first release of the drug placed in the surface of NLC (burst release), followed by a prolonged release of the encapsulated drug [64].

Table 2. Physicochemical characterization of MEL-NLC stored at three temperatures.

Temperature (°C)	Day	Z_{av} ± SD (nm)	PI ± SD	ZP ± SD (mV)	EE ± SD (%)
	0	130.6 ± 0.9	0.198 ± 0.007	-20.6 ± 0.4	79.8 ± 0.2
37	15	230.1 ± 4.7	0.223 ± 0.025	-12.1 ± 0.7	75.1 ± 0.5
25	15	139.9 ± 0.7	0.224 ± 0.014	-15.3 ± 0.1	78.4 ± 0.1
	30	140.4 ± 0.2	0.269 ± 0.010	-9.9 ± 0.1	76.1 ± 0.2
4	60	129.0 ± 1.2	0.218 ± 0.012	-17.3 ± 0.9	77.9 ± 0.6
	120	132.2 ± 0.7	0.213 ± 0.014	-18.6 ± 0.5	78.4 ± 0.1
	240	133.9 ± 0.4	0.213 ± 0.004	-17.0 ± 0.2	76.8 ± 0.8
	280	132.2 ± 1.4	0.218 ± 0.021	-16.2 ± 0.4	78.9 ± 0.3
	300	133.3 ± 1.7	0.219 ± 0.005	-19.9 ± 0.5	77.1 ± 0.4
	360	132.4 ± 1.6	0.212 ± 0.015	-18.7 ± 0.7	77.6 ± 0.1
	420	132.9 ± 0.5	0.212 ± 0.007	-16.9 ± 0.7	78.3 ± 0.5
	480	130.5 ± 1.9	0.208 ± 0.009	-18.8 ± 0.6	79.8 ± 0.2
	510	133.5 ± 1.1	0.206 ± 0.013	-19.5 ± 0.6	75.6 ± 0.1

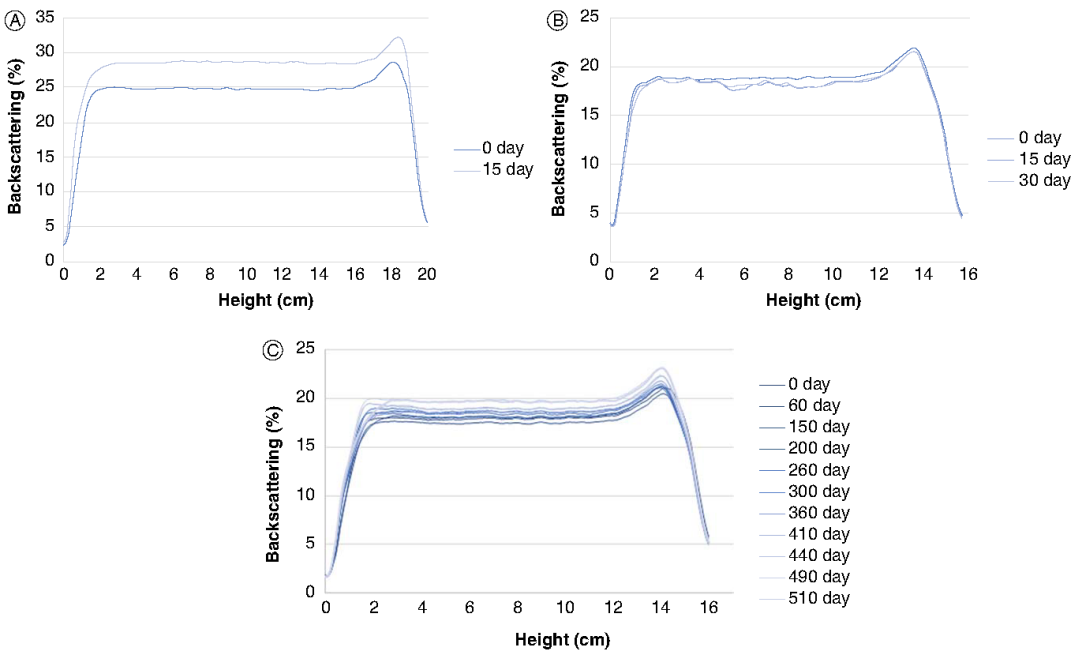

Figure 3. Backscattering profiles of MEL-NLC stored at different temperatures. **(A)** 37 °C, **(B)** 25 °C and **(C)** 4 °C.

3.4. Biological studies

3.4.1. Cytotoxicity of MEL-NLC in selected cancer & non-cancer cells

This study investigated the antiproliferative activity of MEL and MEL-NLC against various cancer cell lines: MV4-11, A549, MCF-7 (estrogen receptor (ER)-positive breast) and MDA-MB-468 (triple-negative breast cancer, TNBC). Additionally, the cytotoxicity against the non-cancerous human breast epithelial MCF-10A cells was assessed. Cell viability was evaluated after 24 and 72 h of exposure using either the MTT assay (MV4-11) or the SRB colorimetric assay. The obtained data of *in vitro* anticancer activity are presented in Table 3 and reported as IC_{50} values (μg/ml), representing the concentration of the compound required to inhibit cell proliferation by 50 % compared with untreated control cells.

Results obtained in Table 3 showed that MEL did not inhibit cell proliferation after 24 h of incubation, although some low antiproliferative activity was observed after 72 h (IC_{50} in the range 28–56 μg/ml). After 24 h of incubation, the antiproliferative activity of both empty NLC and MEL-NLC was observed against solid tumor cell lines (A549, MCF-7 and MDA-MB-468). After 72 h of incubation, both empty NLC and MEL-NLC showed 10–15-times more cytotoxicity than free MEL against cancer cells. On the MV4-11 leukemia cell line, both formulations presented low IC_{50}, showing MEL-NLC a better result due to the slow

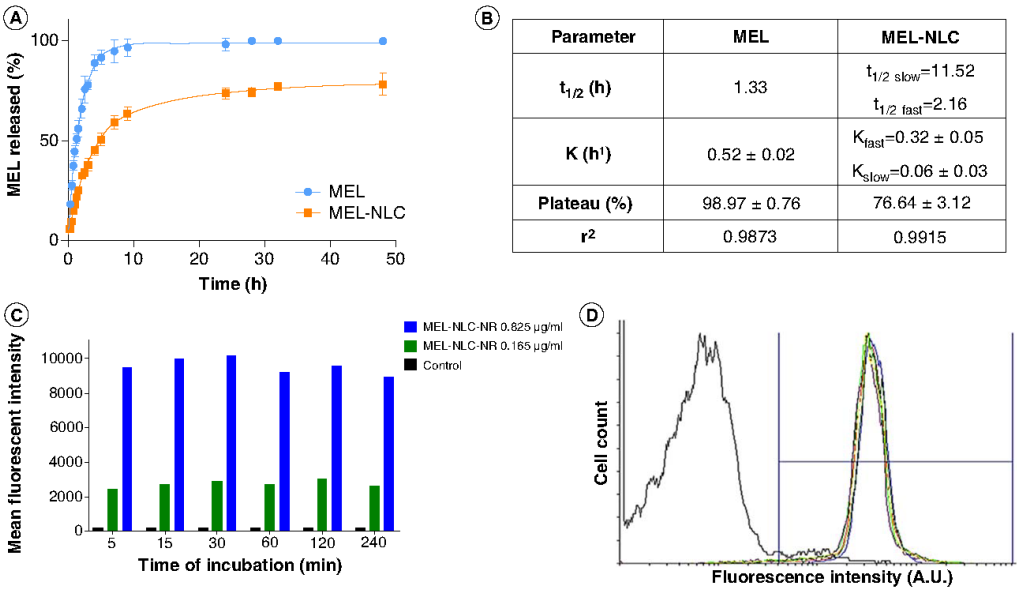

Parameter	MEL	MEL-NLC
$t_{1/2}$ (h)	1.33	$t_{1/2\ slow}$=11.52 $t_{1/2\ fast}$=2.16
K (h^{-1})	0.52 ± 0.02	K_{fast}=0.32 ± 0.05 K_{slow}=0.06 ± 0.03
Plateau (%)	98.97 ± 0.76	76.64 ± 3.12
r^2	0.9873	0.9915

Figure 4. *In vitro* studies of MEL-NLC. **(A)** *In vitro* release profile of MEL-NLC vs. free MEL carried out for 48 h. **(B)** Adjustment to a two-phase decay model and one-phase decay model respectively. **(C)** Mean fluorescent intensity after 5, 15, 30 min and 1, 2 and 4 h in low (0.165 µg /ml) and high (0.825 µg/ml) concentration of compound in MV4-11 cells. **(D)** fluorescent intensity: histogram image from flow cytometry (for high concentration of compound): black line: unlabeled control; red line: after 5 min.; green line: after 15 min.; blue line: after 30 min.; light green line: after 1 h; yellow line: after 2 h; purple line: after 4 h.

Table 3. Half maximal inhibitory concentrations (IC_{50}) of free MEL, MEL-NLC and empty NLC against chosen cancer cell lines and non-tumorigenic human cell line (MCF-10A).

Compound	Cell lines IC_{50} [µg/ml]									
	MV4-11		A549		MCF-7		MDA-MB-468		MCF-10A	
	24 h	72 h	24 h	72 h	24 h	72 h	24 h	72 h	24 h	72 h
Free MEL	n.a.	28.2 ± 8.3	n.a.	48.4 ± 4.2	n.a	36.9 ± 3.3	n.a	51.5 ± 17	n.a	56.6 ± 11.9
Empty NLC	n.a	3.5 ± 1.3	7.3 ± 1.4	3.1 ± 0.1	7.8 ± 1.1	3.2 ± 0.5	4.4 ± 0.1	3.5 ± 0.4	10.8 ± 4.3	8.0 ± 4.6
MEL-NLC	n.a	2.5 ± 0.8	13.8 ± 1.2	3.2 ± 0.2	10.6 ± 0.1	3.4 ± 0.6	4.5 ± 0.2	3.7 ± 0.5	8.6 ± 3.2	15.4 ± 1.8

Data are presented as mean ± SD calculated using Prolab-3 system based on Cheburator 0.4 software.

release of MEL from the NLC. Against lung cancer cell line A549, both formulations showed a great cytotoxicity at 72 h, with similar IC_{50} values, which could be related to rosehip oil [65]. Both breast cancer cell lines, MCF-7 and MDA-MB-468, were also sensitive to MEL and MEL-NLC. However, the effect of MEL-NLC anticancer activity on the two different breast cancer models ER+ (MCF-7) and TNBC (MDA-MB-468), a cancer that is usually more aggressive and harder to treat, did not show differences in their antiproliferative activity after 72 h of incubation, but after 24 h the activity was two-times higher against MDA-MB-468 cells.

The selectivity index (SI) was determined at 72 h as the ratio between the IC_{50} values of each tested formulation in a non-cancerous cell line (MDF-10A) and the IC_{50} in a corresponding cancerous cell line. A higher SI value indicates greater anticancer activity, and the compounds displaying SI values higher than 1 were categorized as selective to that cancer cell line, and SI values higher than 3 were categorized as a highly selective [66]. Free MEL SI calculations ranged from 1.10 to 2.00, empty NLC ranged between 2.27 and 2.60, and MEL-NLC ranged from 4.21 and 6.09, being the highest SI value for MV4-11 leukemia cell line.

3.4.2. Determination of MEL-NLC uptake in cells by flow cytometry

To determine NPs uptake, MV4-11 cells were incubated with MEL-NLC-NR. After predetermined timepoints, fluo-

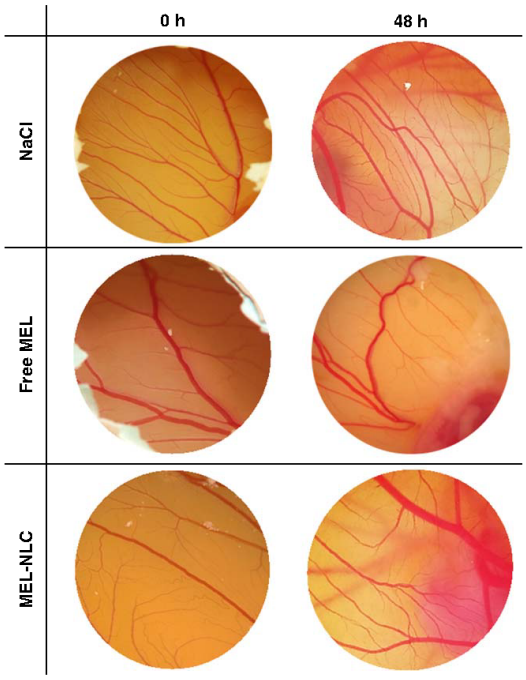

Figure 5. Toxicity studies on chick chorioallantoic membrane at time 0 h and after 48 h post-instillation of the control (NaCl), a solution of MEL (Free MEL), and the nanoformulation (MEL-NLC).

rescence was analyzed by flow cytometry and untreated cells were used as an unlabeled control (Figure 4C & D).

Cells were incubated with MEL-NLC-NR using two different concentrations: low (0.165 μg/ml) and high (0.825 μg/ml). After 5 min of incubation, cell fluorescence was observed by means of the histograms shift after incubation (color lines), in comparison to unlabeled cells (black line) and the mean intensity of fluorescence for each time of incubation in the range 5 min–4 h was similar (Figure 4C & D). The uptake of MEL-NLC in the cells was fast (after 5 min the fluorescence intensity was high) and stable (after 4 h of incubation the intensity of fluorescence was similar to the level of intensity after 5 min).

3.4.3. MEL-NLC safety using the chicken choriolantoic membrane assay

Toxicity of free-MEL solution, MEL-NLC was evaluated against a negative control (NaCl) though the application of each sample on a chicken CAM. In Figure 5, it can be observed the CAM surface at the beginning of the experiment, and after 48 h post-administration of each sample. In all cases, no lethal effects were observed on the growing embryo. Furthermore, toxic effects such as hemorrhages, neoangiogenesis or ghost vessels and embryo death were not observed, thus confirming the safety of all the tested formulations.

4. Discussion

In this work, a new formulation based on loading of MEL into rosehip-based NLC has been developed. The DoE approach was used in order to optimize the formulation, employing a full factorial design. The obtained results showed that most of the parameters induced statistically significant differences on Z_{av} ($p < 0.05$), with the lipid phase being the parameter that caused the highest variations. Other authors also reported similar results, obtaining larger NPs with increasing amounts of lipids [67]. The amount of surfactant highly affected the PI of MEL-NLC, as higher surfactant amounts led to lower PI values. This effect aligns with observations made by other authors who found that higher concentrations of surfactant in the external aqueous phase resulted in smaller particles and lower PI [68]. Moreover, MEL-NLC exhibited a negative surface charge (ZP < -20 mV). This negative value may be due to the ionization of glyceryl behenate [57]. Furthermore, it was observed that increasing the amount of Tween® 80 resulted in more neutral ZP likely due to its role as a stabilizing layer surrounding the particles [62]. Lastly, MEL encapsulation was high in most formulations (around 70 %), likely due to the lipophilic character of MEL and its higher affinity with the lipid internal structure of the NLC matrix [69,70]. This fact has been widely described highlighting that NLC could be a versatile drug delivery system, due to their capacity to encapsulate hydrophilic and lipophilic drugs [71–73]. This is particularly relevant because most of chemotherapeutic drugs have lipophilic properties [74,75]. Taking all these results into account, the optimized formulation was found to be based on the highest amount of solid lipid and the highest tested concentration of the surfactant Tween® 80.

The DSC and XRD studies showed that MEL was successfully incorporated into NLC [76]. DSC results indicated that MEL-NLC was the most amorphous sample due to the decrease in the melting point and lower melting enthalpy, in comparison to the non-loaded NLC and bulk lipid mixtures [60,64]. XRD results confirmed that in MEL-NLC spectra, in other words, the peak at 21.28° (2θ) decreased and a new peak was found at 19.34° (2θ), $d = 0.46$ nm indicating the most stable form of triacylglycerols, the β form. These results may indicate that after the NPs were formed, the crystalline structure of the NLC adopted a more stable form, improving their stability [59].

MEL-NLC showed an *in vitro* release profile prolonged compared with MEL solution, which was rapidly released. Moreover, data indicate that the half-time of MEL was faster than that of MEL-NLC. In the initial 60 min, MEL

solution reached its *plateau* rapidly, diffusing approximately 100 %, while MEL-NLC required nearly 24 h to achieve it, releasing around 80 % of MEL into the receptor medium. Compared to other studies, the optimized MEL-NLC demonstrated a much slower release; in previous studies, formulations reached maximum release of MEL from the NPs within 6 h [70,77–79]. Other authors reported this biphasic behavior in NLC, such as Marathe et at. [80], who prepared paclitaxel-loaded NLC, showing an initial burst followed by a sustained drug release over 48 h [80]. Czajkowska-Kośnik et al. [81] also reported this biphasic release in their etodolac-loaded NLC, which in the first 4 h an initial burst occurred followed by a long-term sustained release until 24 h [81].

The antiproliferative activity of MEL, empty NLC and MEL-NLC against five different cell lines was evaluated after 24 and 72 h. Cell viability studies on leukemia cell line MV4-11 showed that the formulations did not have any effect at 24 h. Otherwise, at 72 h the three samples showed antiproliferative effects, being MEL-NLC the most cytotoxic, probably related to the composition of the matrix and the prolonged release of MEL. On one hand, it is known that MEL owns positive and protective effects on several physiological responses and normal bone marrow cells, and it is known to be effective in the treatment of leukemia. In several studies, MEL showed to protect lymphocytes against DNA damage induced by reactive oxygen species (ROS). In addition, clinical studies showed a connection between MEL disruption and hematological neoplasms [82]. Some authors reported the activity of MEL against MV4-11 cell line, confirming our obtained results [83,84]. On the other hand, the lipid matrix formed by the antitumoral active rosehip oil could be related to the cytotoxicity of the empty NLC. Some authors reported that the extract of rosehip oil was active against different leukemia cell lines due to its antioxidant properties [85]. Furthermore, it has been reported that NLC toxicity could result from the oversaturation of the lipid matrix in the cellular membrane, or breakdown of the membrane lipid bilayer structure driven by the introduction of some lipids to the cellular membrane [65]. The dual activity of the lipid matrix beside the MEL antileukemia activity resulted in a high cytotoxicity against MV4-11 leukemia cell line. For the lung cancer A549 cell line, although MEL solution did not show significant therapeutic effect at 24 h, empty NLC and MEL-NLC showed cytotoxicity from this timepoint. This faster effect could be related to the high interaction that NLC may establish with the cell membrane [65]. At 72 h the cytotoxicity of the three samples increased. It has been reported that MEL possessed antitumoral activity against A549 cell line. Other authors observed that MEL was cytotoxic against this cell line, and significantly inhibited the migration of A549 cells by different mechanisms, also limiting tumoral metastasis [86–88].

Cytotoxicity was also examined in two different breast cancer cell lines, ER+ (MCF-7) and TNBC (MDA-MB-468). Breast cancer is the most common cancer in women worldwide, and its treatment depends on the stage, but in the metastatic stage there is no cure [89,90]. Specially, TNBC is a heterogeneous group of tumors characterized by the lack of estrogenic receptor, progesterone receptor and overexpression of human epidermal growth factor receptor 2 gene, which poses diagnostic challenges, limiting the therapeutic options compared with other breast cancer subtypes [91]. Over the last 80 years, the relationship between MEL and breast cancer has been reported. Clinicians observed that women affected by breast cancer had lower levels of MEL [92]. Also, it has been established that disruption of the circadian rhythm of MEL levels due to several factors such as night lights, sleep deprivation, shift work, chronic jet lag, MEL gene mutations and aging which have shown to increase the oxidative sensitivity and cytokine levels of the normal breast cells, leading to an increase of breast cancer risk [92,93]. In the present study, MEL solution had activity against MCF-7 at 72 h, while MEL-NLC and empty NLC had cytotoxic effect at 24 and 72 h (higher for MEL-NLC). Other authors reported the activity of MEL in MCF-7 cell line, observing that MEL stimulated apoptosis and autophagy [94,95]. For MEL-NLC, a high cytotoxic effect was observed at 24 and 72 h. This higher effect in comparison to MEL solution could be related to the efficient and prolonged release of MEL in the cancer cells, increasing the availability of MEL to produce its toxic effects. Regarding TNBC, a similar effect was obtained for MEL solution and MEL-NLC. MEL has been reported by other authors to be cytotoxic in the MDA-MB-468 cell line, decreasing cell invasion, migration and angiogenesis [96,97]. Empty NLC in both cases induced a high cytotoxicity, which could be related to the activity of rosehip oil. In the study by Aslan et al. [98], the authors reported that the rosehip extract was able to induce late apoptosis in MCF-7 and early apoptosis in MDA-MB-468, and also the levels of caspase-3, which played an important role in apoptotic response, were increased in the MDA-MB-468 cell line. In this way, MEL-NLC showed to be an effective and powerful tool for breast cancer treatment, as they were cytotoxic in both cancer cell lines, and the lipid matrix acted in a synergic manner with MEL to increase its therapeutic efficacy. In addition to these findings, SI was calculated at 72 h for the tested samples. It was found that MEL-NLC were more selective against cancer cell lines in comparison to MEL solution and empty NLC, highlighting that they could constitute a safe manner to treat some types of cancer with diminished side effects.

Cellular uptake studies demonstrated that MEL-NLC containing the fluorescent dye NR were able to penetrate fast, in the first 5 min incubation, into leukemia cancer cells, and the fluorescent signal was maintained during the timeframe of the study (4 h). It is well known that lipid NPs owe the ability to penetrate easily to lipid membranes due to their lipid structure [65,99]. These results may explain the superior effect against these cells, in which the NLC were able to penetrate and remain inside.

In order to confirm the safety of the developed formulation, *in ovo* studies on chicken embryo CAM were performed. The results showed that both, free MEL and MEL-NLC did not cause any lethal effects on the chicken embryo nor damaged or provoked morphological changes to the CAM, thus confirming that they were safe and biocompatible. Because of the fact that the CAM is a highly vascularized, extraembryonic membrane that lacks innervation, and it is functionally analogous to the mammalian placenta, it offers a valuable alternative to conventional rodent studies, being compliant to the principles of Reduction, Refinement and Replacement (3Rs) for animal research [100]. Other authors also used this method to analyze the toxicity of their nanoformulations [47,101]. Wierzbicki et al. [101] compared their silver NPs and silver NPs coated with graphene oxide against a control after 48 h incubation [101]. The results showed that silver NPs caused morphological changes in the CAM, decreasing the number of capillary vessels, which the authors related to the direct toxicity of silver NPs to the endothelial and mesenchyme cells. Moreover, similar to our results, silver NPs coated with graphene oxide were biocompatible.

5. Conclusion

This study successfully optimized rosehip oil-based NLC encapsulating MEL. MEL-NLC achieved an average particle size below 200 nm, with a monodispersed population and high MEL encapsulation efficiency. MEL-NLC exhibited excellent stability for over a year, and *in vitro* release confirmed prolonged release of MEL from the NLC. Furthermore, antiproliferative assays confirmed the selectivity of MEL-NLC against tumoral cells, demonstrating cytotoxic effects on leukemia, lung and breast cancer cells. Empty NLC also demonstrated *in vitro* antitumor selective cytotoxicity against cancer cells, attributed to the pharmacological properties of rosehip oil. This property could potentially synergize with MEL, enhancing the antitumoral efficacy. Furthermore, *in ovo* experiments confirmed that MEL-NLC did not exhibit any toxicity on the chicken CAM. Therefore, the development of MEL-NLC presents a significant advancement in cancer treatment by addressing current challenges, such as limited drug efficacy and high toxicity. The prolonged release profile and enhanced anti-tumor activity of MEL-NLC improve the therapeutic impact of MEL, potentially overcoming its instability drawbacks. This innovative approach may increase selectivity, offering a more effective and safer alternative to conventional cancer therapies.

Article highlights

- Melatonin-loaded NLC containing rosehip oil were optimized employing the design of experiments approach.
- Melatonin-loaded NLC showed suitable physicochemical properties (average size <200 nm, PI <0.2, ZP $\approx$ -20 mV and encapsulation efficiency $\approx$80%).
- Melatonin lipid nanoparticles interaction studies revelated the successful loading of the drug into NLC, with a more amorphous matrix.
- Melatonin-NLC showed a prolonged release over 48 h, adjusted to a two-phase decay model.
- Melatonin-loaded NLC demonstrated a long-term stability for more than 1 year.
- Melatonin-loaded NLC were cytotoxic against tumoral cell lines, being internalized in a fast and sustained manner.

Acknowledgments

This research was supported by the Spanish Ministry of Science and Innovation (PID2021-122187NB-C32) and a Llavor project from AGAUR (LLAV 0004). E Sánchez-López acknowledges the support of Grants for the Requalification of the Spanish University System.

Author contributions

L Bonilla-Vidal has contributed trough methodology and investigation as well written and edited the original manuscript draft. M Świtalska has contributed to methodology, investigation and review and editing of the manuscript. M Espina has supervised and reviewed the manuscript. J Wietrzyk has contributed to methodology and review and editing of the manuscript. ML García has funded and contributed with the methodology and investigation. EB Souto has funded and contributed with the methodology and investigation. A Gliszczyńska has contributed to methodology, investigation and review and editing of the manuscript. E Sánchez-López has funded, supervised and contributed with the methodology and investigation and reviewed and edited the manuscript.

Financial disclosure

This research was supported by the Spanish Ministry of Science and Innovation (PID2021-122187NB-C32) and a Llavor project from AGAUR (LLAV 0004). E Sánchez-López acknowledges the support of Grants for the Requalification of the Spanish University System. The authors have no other relevant affiliations or financial involvement with any organization or entity with a financial interest in or financial conflict with the subject matter or materials discussed in the manuscript apart from those disclosed.

Competing interests disclosure

The authors have no competing interests or relevant affiliations with any organization or entity with the subject matter or materials discussed in the manuscript. This includes employment, consultancies, honoraria, stock ownership or options, expert testimony, grants or patents received or pending, or royalties.

Writing disclosure

No writing assistance was utilized in the production of this manuscript.

ORCID

Lorena Bonilla-Vidal https://orcid.org/0000-0002-2043-2092
Marta Świtalska https://orcid.org/0000-0001-7920-2251
Marta Espina https://orcid.org/0000-0003-1269-3847
Joanna Wietrzyk https://orcid.org/0000-0003-4980-6606
Maria Luisa García https://orcid.org/0000-0002-4526-3344
Eliana B Souto https://orcid.org/0000-0002-9737-6017
Anna Gliszczyńska https://orcid.org/0000-0002-0218-6369
Elena Sánchez-López
https://orcid.org/0000-0003-2571-108X

References

Papers of special note have been highlighted as: • of interest; •• of considerable interest

1. Pilleron S, Sarfati D, Janssen-Heijnen M, et al. Global cancer incidence in older adults, 2012 and 2035: a population-based study. Int J Cancer. 2019;144:49–58. doi:10.1002/IJC.31664
2. Philip C, Mathew A, John MJ. Cancer care: challenges in the developing world. Cancer Res Stat Treat. 2018;1:58. doi:10.4103/Crst.Crst_1_17
3. Gaidai O, Yan P, Xing Y. Future world cancer death rate prediction. Sci Rep. 2023;13:1–9. doi:10.1038/s41598-023-27547-x
   • **Overview of world statitics regarding cancer and its impact.**
4. Wang X, Zhang H, Chen X. Drug resistance and combating drug resistance in cancer. Cancer Drug Resist. 2019;2:160. doi:10.20517/CDR.2019.10
5. Vasan N, Baselga J, Hyman DM. A view on drug resistance in cancer. Nature. 2019;575:299–309. doi:10.1038/s41586-019-1730-1
6. Huang M, Lu J-J, Ding J. Natural products in cancer therapy: past, present and future. Nat Products Bioprospect. 2021;11:5–13. doi:10.1007/S13659-020-00293-7
7. Deng S, Shanmugam MK, Kumar AP, et al. Targeting autophagy using natural compounds for cancer prevention and therapy. Cancer. 2019;125:1228–1246. doi:10.1002/CNCR.31978
8. Asghari MH, Ghobadi E, Moloudizargari M, et al. Does the use of melatonin overcome drug resistance in cancer chemotherapy? Life Sci. 2018;196:143–155. doi:10.1016/J.LFS.2018.01.024
9. Kvetnoy I, Ivanov D, Mironova E, et al. Melatonin as the cornerstone of neuroimmunoendocrinology. Int J Mol Sci. 2022;23:1835. doi:10.3390/IJMS23031835
10. Mortezaee K, Najafi M, Farhood B, et al. Modulation of apoptosis by melatonin for improving cancer treatment efficiency: an updated review. Life Sci. 2019;228:228–241. doi:10.1016/J.LFS.2019.05.009
    •• **Melatonin mechanism of action in cancer therapeutics.**
11. Talib WH. Melatonin and cancer hallmarks. Molecules. 2018;23:518. doi:10.3390/molecules23030518
12. Bonmati-Carrion MA, Tomas-Loba A. Melatonin and cancer: a polyhedral network where the source matters. Antioxidants. 2021;10:210. doi:10.3390/antiox10020210
13. Mortezaee K, Potes Y, Mirtavoos-Mahyari H, et al. Boosting immune system against cancer by melatonin: a mechanistic viewpoint. Life Sci. 2019;238:116960. doi:10.1016/J.LFS.2019.116960
14. Liu S, Madu CO, Lu Y. The role of Melatonin in cancer development. Oncomedicine. 2018;3:37–47. doi:10.7150/ONCM.25566
15. Sanchez-Barcelo EJ, Mediavilla MD, Alonso-Gonzalez C, et al. Melatonin uses in oncology: breast cancer prevention and reduction of the side effects of chemotherapy and radiation. Expert Opin Investig Drugs. 2012;21:819–831. doi:10.1517/13543784.2012.681045
16. Ma Z, Xu L, Liu D, et al. Utilizing Melatonin to alleviate side effects of chemotherapy: a potentially good partner for treating cancer with ageing. Oxid Med Cell Longev. 2020;2020:6841581. doi:10.1155/2020/6841581
17. Kvietkauskas M, Zitkute V, Leber B, et al. The role of melatonin in colorectal cancer treatment: a comprehensive review. Ther Adv Med Oncol. 2020;12:175883592093171. doi:10.1177/1758835920931714
18. Lopes Rocha Correa V, Assis Martins J, Ribeiro de Souza T, et al. Melatonin loaded lecithin-chitosan nanoparticles improved the wound healing in diabetic rats. Int J Biol Macromol. 2020;162:1465–1475. doi:10.1016/J.IJBIOMAC.2020.08.027
19. Talib WH, Alsayed AR, Abuawad A, et al. Melatonin in cancer treatment: current knowledge and future opportunities. Molecules. 2021;26:2506. doi:10.3390/molecules26092506
20. Awasthi R, Roseblade A, Hansbro PM, et al. Nanoparticles in cancer treatment: opportunities and obstacles. Curr Drug Targets. 2018;19:1696–1709. doi:10.2174/1389450119666180326122831
21. Raj S, Khurana S, Choudhari R, et al. Specific targeting cancer cells with nanoparticles and drug delivery in cancer therapy. Semin Cancer Biol. 2021;69:166–177. doi:10.1016/J.SEMCANCER.2019.11.002
22. Aghebati-Maleki A, Dolati S, Ahmadi M, et al. Nanoparticles and cancer therapy: perspectives for application of nanoparticles in the treatment of cancers. J Cell Physiol. 2020;235:1962–1972. doi:10.1002/JCP.29126
    •• **Advantages of nanoparticles for cancer treatment.**
23. Bonilla L, Espina M, Severino P, et al. Lipid nanoparticles for the posterior eye segment. Pharmaceutics. 2021;14:90. doi:10.3390/pharmaceutics14010090
24. Nasirizadeh S, Malaekeh-Nikouei B. Solid lipid nanoparticles and nanostructured lipid carriers in oral cancer drug delivery. J Drug Deliv Sci Technol. 2020;55:101458. doi:10.1016/J.JDDST.2019.101458
25. Bayón-Cordero L, Alkorta I, Arana L. Application of Solid Lipid Nanoparticles to improve the efficiency of anticancer drugs. Nanomaterials. 2019;9:474. doi:10.3390/NANO9030474

26. Haider M, Abdin SM, Kamal L, et al. Nanostructured Lipid Carriers for delivery of chemotherapeutics: a review. Pharmaceutics. 2020;12:288. doi:10.3390/pharmaceutics12030288
27. Bonilla-Vidal L, Świtalska M, Espina M, et al. Dually active apigenin-loaded nanostructured lipid carriers for cancer treatment. Int J Nanomedicine. 2023;18:6979–6997. doi:10.2147/IJN.S429565

•• Optimization of MEL-NLC fabrication methods.

28. Mármol I, Jiménez-Moreno N, Ancín-Azpilicueta C, et al. A combination of Rosa Canina extracts and gold complex favors apoptosis of Caco-2 cells by increasing oxidative stress and mitochondrial dysfunction. Antioxidants. 2019;9:17. doi:10.3390/ANTIOX9010017
29. Cagle P, Idassi O, Carpenter J, et al. Effect of rosehip (Rosa Canina) extracts on human brain tumor cell proliferation and apoptosis. J Cancer Ther. 2012;2012:534–545. doi:10.4236/JCT.2012.35069
30. Turan I, Demir S, Kilinc K, et al. Cytotoxic effect of Rosa canina extract on human colon cancer cells through repression of telomerase expression. J Pharm Anal. 2018;8:399. doi:10.1016/J.JPHA.2017.12.005
31. Seely D, Wu P, Fritz H, et al. Melatonin as adjuvant cancer care with and without chemotherapy: a systematic review and meta-analysis of randomized trials. Integr Cancer Ther. 2012;11:293–303. doi:10.1177/1534735411425484

• Clinical trials using Melatonin in cancer.

32. Radajewska A, Moreira H, Bęben D, et al. Combination of Irinotecan and Melatonin with the natural compounds Wogonin and Celastrol for colon cancer treatment. Int J Mol Sci. 2023;24:9544. doi:10.3390/IJMS24119544
33. Mafi A, Rezaee M, Hedayati N, et al. Melatonin and 5-fluorouracil combination chemotherapy: opportunities and efficacy in cancer therapy. Cell Commun Signal. 2023;21:1–17. doi:10.1186/S12964-023-01047-X
34. Carvajal-Vidal P, Fábrega MJ, Espina M, et al. Development of Halobetasol-loaded nanostructured lipid carrier for dermal administration: optimization, physicochemical and biopharmaceutical behavior, and therapeutic efficacy. Nanomedicine Nanotechnology Biol Med. 2019;20:102026. doi:10.1016/J.NANO.2019.102026

• Development and optimization of nanostructured lipid carriers.

35. Teeranachaideekul V, Boonme P, Souto EB, et al. Influence of oil content on physicochemical properties and skin distribution of Nile red-loaded NLC. J Control Rel. 2008;128:134–141. doi:10.1016/J.JCONREL.2008.02.011
36. Esteruelas G, Halbaut L, García-Torra V, et al. Development and optimization of Riluzole-loaded biodegradable nanoparticles incorporated in a mucoadhesive *in situ* gel for the posterior eye segment. Int J Pharm. 2022;612:121379. doi:10.1016/j.ijpharm.2021.121379
37. Sánchez-López E, Egea MA, Cano A, et al. PEGylated PLGA nanospheres optimized by design of experiments for ocular administration of dexibuprofen-*in vitro*, *ex vivo* and *in vivo* characterization. Colloids Surfaces B Biointerfaces. 2016;145:241–250. doi:10.1016/j.colsurfb.2016.04.054
38. López-Machado A, Díaz N, Cano A, et al. Development of topical eye-drops of lactoferrin-loaded biodegradable nanoparticles for the treatment of anterior segment inflammatory processes. Int J Pharm. 2021;609:121188. doi:10.1016/J.IJPHARM.2021.121188
39. Gonzalez-Pizarro R, Carvajal-Vidal P, Halbault Bellowa L, et al. *In-situ* forming gels containing fluorometholone-loaded polymeric nanoparticles for ocular inflammatory conditions. Colloids Surfaces B Biointerfaces. 2019;175:365–374. doi:10.1016/j.colsurfb.2018.11.065
40. Sánchez-López E, Esteruelas G, Ortiz A, et al. Dexibuprofen biodegradable nanoparticles: one step closer towards a better ocular interaction study. Nanomaterials. 2020;10(4):720. doi:10.3390/NANO10040720
41. Brugnera M, Vicario-De-la-torre M, Andrés-Guerrero V, et al. Validation of a rapid and easy-to-apply method to simultaneously quantify co-loaded Dexamethasone and Melatonin PLGA microspheres by HPLC-UV: encapsulation efficiency and *in vitro* release. Pharmaceutics. 2022;14:288. doi:10.3390/PHARMACEUTICS14020288/S1
42. Elmsmari F, González Sánchez JA, Duran-Sindreu F, et al. Calcium hydroxide-loaded PLGA biodegradable nanoparticles as an intracanal medicament. Int Endod J. 2021;54:2086–2098. doi:10.1111/IEJ.13603
43. Ma Q, Yang J, Huang X, et al. Poly(Lactide-Co-Glycolide)-Monomethoxy-Poly-(Polyethylene glycol) nanoparticles loaded with melatonin protect adipose-derived stem cells transplanted in infarcted heart tissue. Stem Cells. 2018;36:540–550. doi:10.1002/STEM.2777
44. Sánchez-López E, Ettcheto M, Egea MA, et al. Memantine loaded PLGA PEGylated nanoparticles for Alzheimer's disease: *in vitro* and *in vivo* characterization. J Nanobiotechnology. 2018;16:1–16. doi:10.1186/S12951-018-0356-Z
45. Czarnecka M, Switalska M, Wietrzyk J, et al. Synthesis and biological evaluation of phosphatidylcholines with cinnamic and 3-methoxycinnamic acids with potent antiproliferative activity. RSC Adv. 2018;8:35752. doi:10.1039/C8RA07002D

• Methodolody of biological studies.

46. Nevozhay D. Cheburator software for automatically calculating drug inhibitory concentrations from *in vitro* screening assays. PLOS ONE. 2014;9:e106186. doi:10.1371/JOURNAL.PONE.0106186
47. Ahmad KA, Mohammed AS, Abas F. Chitosan nanoparticles as carriers for the delivery of ΦKAZ14 bacteriophage for oral biological control of colibacillosis in chickens. Molecules. 2016;21:256. doi:10.3390/MOLECULES21030256
48. Bhave A, Schulzova V, Chmelarova H, et al. Assessment of rosehips based on the content of their biologically active compounds. J Food Drug Anal. 2017;25:681–690. doi:10.1016/J.JFDA.2016.12.019
49. Li Y, Wu M, Zhang N, et al. Mechanisms of enhanced antiglioma efficacy of polysorbate 80-modified paclitaxel-loaded PLGA nanoparticles by focused ultrasound. J Cell Mol Med. 2018;22:4182. doi:10.1111/JCMM.13695
50. Ravichandran V, Lee M, Cao TGN, et al. Polysorbate-based drug formulations for brain-targeted drug delivery and anticancer therapy. Appl Sci. 2021;11:9336. doi:10.3390/APP11199336
51. Schwartzberg LS, Navari RM. Safety of polysorbate 80 in the oncology setting. Adv Ther. 2018;35:767. doi:10.1007/S12325-018-0707-Z
52. Pinto F, de Barros DPC, Reis C, et al. Optimization of nanostructured lipid carriers loaded with retinoids by

central composite design. J Mol Liq. 2019;293:111468. doi:10.1016/J.MOLLIQ.2019.111468
53. Cunha S, Costa CP, Loureiro JA, et al. Double optimization of rivastigmine-loaded nanostructured lipid carriers (NLC) for nose-to-brain delivery using the quality by design (QbD) approach: formulation variables and instrumental parameters. Pharmaceutics. 2020;12:599. doi:10.3390/PHARMACEUTICS12070599
54. Kim MH, Kim KT, Sohn SY, et al. Formulation and evaluation of nanostructured lipid carriers (NLCs) of 20(S)-Protopanaxadiol (PPD) by Box-Behnken design. Int J Nanomedicine. 2019;14:8520. doi:10.2147/IJN.S215835
55. Zeb A, Qureshi OS, Kim HS, et al. High payload itraconazole-incorporated lipid nanoparticles with modulated release property for oral and parenteral administration. J Pharm Pharmacol. 2017;69:955–966. doi:10.1111/JPHP.12727
56. Folle C, Marqués AM, Díaz-Garrido N, et al. Thymol-loaded PLGA nanoparticles: an efficient approach for acne treatment. J Nanobiotechnology. 2021;19:359. doi:10.1186/S12951-021-01092-Z
57. Khan AA, Abdulbaqi IM, Abou Assi R, et al. Lyophilized hybrid nanostructured lipid carriers to enhance the cellular uptake of verapamil: statistical optimization and *in vitro* evaluation. Nanoscale Res Lett. 2018;13:323. doi:10.1186/S11671-018-2744-6
58. de Chuffa LGA, Seiva FRF, Novais AA, et al. Melatonin-loaded nanocarriers: new horizons for therapeutic applications. Mol. 2021;26:3562. doi:10.3390/MOLECULES26123562
59. Souto EB, Mehnert W, Müller RH. Polymorphic behavior of Compritol 888 ATO as bulk lipid and as SLN and NLC. J Microencapsul. 2006;23:417–433. doi:10.1080/02652040600612439
60. Bunjes H, Westesen K, Koch MHJ. Crystallization tendency and polymorphic transitions in triglyceride nanoparticles. Int J Pharm. 1996;129:159–173. doi:10.1016/0378-5173(95)04286-5
61. Fu X, Kong W, Zhang Y, et al. Novel solid-solid phase change materials with biodegradable trihydroxy surfactants for thermal energy storage. RSC Adv. 2015;5:68881–68889. doi:10.1039/C5RA11842E
62. Llorente X, Esteruelas G, Bonilla L, et al. Riluzole-loaded nanostructured lipid carriers for hyperproliferative skin diseases. Int J Mol Sci. 2023;24:8053. doi:10.3390/IJMS24098053/S1
63. Rasmussen MK, Pedersen JN, Marie R. Size and surface charge characterization of nanoparticles with a salt gradient. Nat Commun. 2020;11:1–8. doi:10.1038/s41467-020-15889-3
64. Khosa A, Reddi S, Saha RN. Nanostructured lipid carriers for site-specific drug delivery. Biomed Pharmacother. 2018;103:598–613. doi:10.1016/J.BIOPHA.2018.04.055
65. Strachan JB, Dyett BP, Nasa Z, et al. Toxicity and cellular uptake of lipid nanoparticles of different structure and composition. J Colloid Interface Sci. 2020;576:241–251. doi:10.1016/J.JCIS.2020.05.002
66. Wu XL, Liu L, Wang QC, et al. Antitumor activity and mechanism study of riluzole and its derivatives. Iran J Pharm Res. 2020;19:217–230. doi:10.22037/IJPR.2020.1101149
67. Bahari LAS, Hamishehkar H. The impact of variables on particle size of solid lipid nanoparticles and nanostructured lipid carriers; a comparative literature review. Adv Pharm Bull. 2016;6:151. doi:10.15171/APB.2016.021
68. Zambaux MF, Bonneaux F, Gref R, et al. Influence of experimental parameters on the characteristics of poly(lactic acid) nanoparticles prepared by a double emulsion method. J Control release. 1998;50:31–40. doi:10.1016/S0168-3659(97)00106-5
69. Üner B, Özdemir S, Taş Ç, et al. Development of solid lipid nanoparticles and nanostructured lipid carriers of loteprednol etabonate: physicochemical characterization and *ex vivo* permeation studies. Res Sq. 2021;1:1–27. doi:10.21203/RS.3.RS-1145116/V1
70. Molska A, Nyman AKG, Sofias AM, et al. *In vitro* and *in vivo* evaluation of organic solvent-free injectable melatonin nanoformulations. Eur J Pharm Biopharm. 2020;152:248–256. doi:10.1016/J.EJPB.2020.05.003
71. Nguyen VH, Thuy VN, Van TV, et al. Nanostructured lipid carriers and their potential applications for versatile drug delivery via oral administration. Open Nano. 2022;8:100064. doi:10.1016/J.ONANO.2022.100064
72. Salvi VR, Pawar P. Nanostructured lipid carriers (NLC) system: a novel drug targeting carrier. J Drug Deliv Sci Technol. 2019;51:255–267. doi:10.1016/J.JDDST.2019.02.017
73. Khan S, Baboota S, Ali J, et al. Nanostructured lipid carriers: an emerging platform for improving oral bioavailability of lipophilic drugs. Int J Pharm Investig. 2015;5:191. doi:10.4103/2230-973X.167661
74. Rodrigues Da Silva GH, David De Moura L, Vieira De Carvalho F, et al. Antineoplastics encapsulated in nanostructured lipid carriers. Molecules. 2021;26:6929. doi:10.3390/MOLECULES26226929
75. Selvamuthukumar S, Velmurugan R. Nanostructured Lipid Carriers: a potential drug carrier for cancer chemotherapy. Lipids Health Dis. 2012;11:1–8. doi:10.1186/1476-511X-11-159
76. Ojo AT, Ma C, Lee PI. Elucidating the effect of crystallization on drug release from amorphous solid dispersions in soluble and insoluble carriers. Int J Pharm. 2020;591:120005. doi:10.1016/J.IJPHARM.2020.120005
77. Li S, Zhao Y. Preparation of melatonin-loaded zein nanoparticles using supercritical CO_2 antisolvent and *in vitro* release evaluation. Int J Food Eng. 2017;13(11):1–11. doi:10.1515/ijfe-2017-0239
78. Noori Siahdasht F, Farhadian N, Karimi M, et al. Enhanced delivery of melatonin loaded nanostructured lipid carriers during *in vitro* fertilization: NLC formulation, optimization and IVF efficacy. RSC Adv. 2020;10:9475. doi:10.1039/C9RA10867J
79. Yener S, Akbulut KG, Karakuş R, et al. Development of melatonin loaded pectin nanoparticles for the treatment of inflammatory bowel disease: *in vitro* and *in vivo* studies. J Drug Deliv Sci Technol. 2022;67:102861. doi:10.1016/J.JDDST.2021.102861
80. Marathe S, Shadambikar G, Mehraj T, et al. Development of α-tocopherol succinate-based nanostructured lipid carriers for delivery of paclitaxel. Pharmaceutics. 2022;14:1034. doi:10.3390/PHARMACEUTICS14051034
81. Czajkowska-Kośnik A, Szymańska E, Czarnomysy R, et al. Nanostructured lipid carriers engineered as topical deliv-

ery of etodolac: optimization and cytotoxicity studies. Materials (Basel). 2021;14:596. doi:10.3390/MA14030596
82. Shafabakhsh R, Mirzaei H, Asemi Z. Melatonin: a promising agent targeting leukemia. J Cell Biochem. 2020;121:2730–2738. doi:10.1002/JCB.29495
83. Lomovsky AI, Baburina YL, Fadeev RS, et al. Melatonin can enhance the effect of drugs used in the treatment of leukemia. Biochem. 2023;88:73–85. doi:10.1134/S0006297923010078
84. Tian T, Li J, Li Y, et al. Melatonin enhances sorafenib-induced cytotoxicity in FLT3-ITD acute myeloid leukemia cells by redox modification. Theranostics. 2019;9:3779. doi:10.7150/THNO.34327
85. Mármol I, Sánchez-De-Diego C, Jiménez-Moreno N, et al. Therapeutic applications of rose hips from different Rosa species. Int J Mol Sci. 2017;18:1137. doi:10.3390/IJMS18061137
• **Evidence of rosehip extract multiple therapeutic activities.**
86. Chao CC, Chen PC, Chiou PC, et al. Melatonin suppresses lung cancer metastasis by inhibition of epithelial-mesenchymal transition through targeting to twist. Clin Sci. 2019;133:709–722. doi:10.1042/CS20180945
87. Gurunathan S, Jeyaraj M, Kang MH, et al. Melatonin enhances palladium-nanoparticle-induced cytotoxicity and apoptosis in human lung epithelial adenocarcinoma cells A549 and H1229. Antioxidants. 2020;9:357. doi:10.3390/ANTIOX9040357
88. Zhou Q, Gui S, Zhou Q, et al. Melatonin inhibits the migration of human lung adenocarcinoma A549 cell lines involving JNK/MAPK pathway. PLOS ONE. 2014;9:e101132. doi:10.1371/JOURNAL.PONE.0101132
89. Trayes KP, Cokenakes SEH. Breast cancer treatment. Am Fam Physician. 2021;104:171–178.
90. Harbeck N, Penault-Llorca F, Cortes J, et al. Breast cancer. Nat Rev Dis Prim. 2019;5:1–31. doi:10.1038/s41572-019-0111-2
91. Kumar P, Aggarwal R. An overview of triple-negative breast cancer. Arch Gynecol Obstet. 2015;293:247–269. doi:10.1007/S00404-015-3859-Y
92. Nooshinfar E, Safaroghli-Azar A, Bashash D, et al. Melatonin, an inhibitory agent in breast cancer. Breast Cancer. 2017;24:42–51. doi:10.1007/S12282-016-0690-7
93. Hill SM, Belancio VP, Dauchy RT, et al. Melatonin: an inhibitor of breast cancer. Endocr Relat Cancer. 2015;22:R183–R204. doi:10.1530/ERC-15-0030
94. Önder GÖ, Sezer G, Özdamar S, et al. Melatonin has an inhibitory effect on MCF-7 and MDA-MB-231 human breast cancer cell lines by inducing autophagy and apoptosis. Fundam Clin Pharmacol. 2022;36:1038–1056. doi:10.1111/FCP.12813
95. Nooshinfar E, Bashash D, Safaroghli-Azar A, et al. Melatonin promotes ATO-induced apoptosis in MCF-7 cells: proposing novel therapeutic potential for breast cancer. Biomed Pharmacother. 2016;83:456–465. doi:10.1016/J.BIOPHA.2016.07.004
96. Gisleine de Oliveira J, Helena de Mora Marques J, Zani Lacerda J, et al. Melatonin down-regulates microRNA-10a and decreases invasion and migration of triple-negative breast cancer cells. Melatonin Res. 2019;2:86–99. doi:10.32794/MR11250023
97. Marques JHM, Mota AL, Oliveira JG, et al. Melatonin restrains angiogenic factors in triple-negative breast cancer by targeting miR-152-3p: *in vivo* and *in vitro* studies. Life Sci. 2018;208:131–138. doi:10.1016/J.LFS.2018.07.012
98. Berkoz M, Ozkan Yılmaz F, Hunt AO, et al. Rosa Canina L. ethanolic extract induces the anti-proliferative and apotosis potential in MCF-7 And MDA-MB-468 cell lines. Fresenius Environ Bull. 2019;28:3718–3723.
99. Zhang W, Liu J, Zhang Q, et al. Enhanced cellular uptake and anti-proliferating effect of chitosan hydrochlorides modified genistein loaded NLC on human lens epithelial cells. Int J Pharm. 2014;471:118–126. doi:10.1016/J.IJPHARM.2014.05.030
100. Buhr CR, Wiesmann N, Tanner RC, et al. The chorioallantoic membrane assay in nanotoxicological research-an alternative for *in vivo* experimentation. Nanomaterials. 2020;10:2328. doi:10.3390/NANO10122328
101. Wierzbicki M, Jaworski S, Sawosz E, et al. Graphene oxide in a composite with silver nanoparticles reduces the fibroblast and endothelial cell cytotoxicity of an antibacterial nanoplatform. Nanoscale Res Lett. 2019;14:1–11. doi:10.1186/S11671-019-3166-9

3.3. Novel nanostructured lipid carriers loading Apigenin for anterior segment ocular pathologies

Lorena Bonilla Vidal, Marta Espina, María Luisa García, Laura Baldomà, Josefa Badia, Luis María Delgado, Anna Gliszczyńska, Eliana B Souto, Elena Sánchez López

International Journal of Pharmaceutics

2024

IF (JCR-2023) 5.3, Pharmacology & Pharmacy 34/354 (Q1)

10.1016/j.ijpharm.2024.124222

International Journal of Pharmaceutics 658 (2024) 124222

Contents lists available at ScienceDirect

International Journal of Pharmaceutics

journal homepage: www.elsevier.com/locate/ijpharm

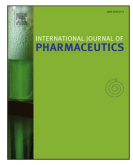

Novel nanostructured lipid carriers loading Apigenin for anterior segment ocular pathologies

L. Bonilla-Vidal [a,b], M. Espina [a,b], M.L. García [a,b], L. Baldomà [c,d], J. Badia [c,d], J.A. González [e], L.M. Delgado [f], A. Gliszczyńska [g], E.B. Souto [h,i], E. Sánchez-López [a,b,j,*]

[a] Department of Pharmacy, Pharmaceutical Technology and Physical Chemistry, University of Barcelona, 08028 Barcelona, Spain
[b] Institute of Nanoscience and Nanotechnology (IN^{2}UB), University of Barcelona, 08028 Barcelona, Spain
[c] Department of Biochemistry and Physiology, University of Barcelona, 08028 Barcelona, Spain
[d] Institute of Biomedicine of the University of Barcelona (IBUB), Institute of Research of Sant Joan de Déu (IRSJD), 08950 Barcelona, Spain
[e] Department of Endodontics, Faculty of Dentistry, International University of Catalonia (UIC), 08195 Barcelona, Spain
[f] Bioengineering Institute of Technology, International University of Catalonia (UIC), 08028 Barcelona, Spain
[g] Department of Food Chemistry and Biocatalysis, Wrocław University of Environmental and Life Sciences, Wrocław, Poland
[h] REQUIMTE/UCIBIO, Laboratory of Pharmaceutical Technology, Department of Drug Sciences, Faculty of Pharmacy, University of Porto, Rua de Jorge Viterbo Ferreira, 228, 4050-313 Porto, Portugal
[i] Associate Laboratory i4HB—Institute for Health and Bioeconomy, Faculty of Pharmacy, University of Porto, 4050-313 Porto, Portugal
[j] Unit of Synthesis and Biomedical Applications of Peptides, IQAC-CSIC, 08034 Barcelona, Spain

ARTICLE INFO

Keywords:
Apigenin
Nanostructured lipid carriers
Rosehip oil
Lipid nanoparticles

ABSTRACT

Dry eye disease (DED) is a chronic multifactorial disorder of the ocular surface caused by tear film dysfunction and constitutes one of the most common ocular conditions worldwide. However, its treatment remains unsatisfactory. While artificial tears are commonly used to moisturize the ocular surface, they do not address the underlying causes of DED. Apigenin (APG) is a natural product with anti-inflammatory properties, but its low solubility and bioavailability limit its efficacy. Therefore, a novel formulation of APG loaded into biodegradable and biocompatible nanoparticles (APG-NLC) was developed to overcome the restricted APG stability, improve its therapeutic efficacy, and prolong its retention time on the ocular surface by extending its release. APG-NLC optimization, characterization, biopharmaceutical properties and therapeutic efficacy were evaluated. The optimized APG-NLC exhibited an average particle size below 200 nm, a positive surface charge, and an encapsulation efficiency over 99 %. APG-NLC exhibited sustained release of APG, and stability studies demonstrated that the formulation retained its integrity for over 25 months. *In vitro* and *in vivo* ocular tolerance studies indicated that APG-NLC did not cause any irritation, rendering them suitable for ocular topical administration. Furthermore, APG-NLC showed non-toxicity in an epithelial corneal cell line and exhibited fast cell internalization. Therapeutic benefits were demonstrated using an *in vivo* model of DED, where APG-NLC effectively reversed DED by reducing ocular surface cellular damage and increasing tear volume. Anti-inflammatory assays *in vivo* also showcased its potential to treat and prevent ocular inflammation, particularly relevant in DED patients. Hence, APG-NLC represent a promising system for the treatment and prevention of DED and its associated inflammation.

1. Introduction

Dry eye disease (DED) or keratoconjunctivitis sicca is one of the most prevalent ocular conditions worldwide and a leading cause of doctor appointments, imposing a significant societal and economic burden (Kumari et al., 2021). Despite its high incidence, its treatment remains unsatisfactory, leading to a diminished quality of life for affected patients. DED is a multifactorial pathology of the ocular surface characterized by the disruption of tear film homeostasis. This disruption is accompanied by ocular symptoms, including tear film instability, hyperosmolarity, ocular surface inflammation and damage, and neurosensory abnormalities, all of which contribute to its etiology (López-

* Corresponding author at: Department of Pharmacy, Pharmaceutical Technology and Physical Chemistry, University of Barcelona, 08028 Barcelona, Spain.
E-mail address: esanchezlopez@ub.edu (E. Sánchez-López).

https://doi.org/10.1016/j.ijpharm.2024.124222
Received 7 March 2024; Received in revised form 23 April 2024; Accepted 9 May 2024
Available online 11 May 2024

Machado et al., 2021; Huang et al., 2021; Craig et al., 2017). Moreover, DED may also be associated with other conditions or medication side effects, and its incidence increases with age (De Paiva, 2017). Topical treatment is the preferred approach for managing DED due to its ease and painlessness of application. Artificial tears, typically administered as eye drops, gels, or ointments, are commonly used to moisturize and lubricate the ocular surface, serving as the first line of treatment. These agents temporarily alleviate symptoms by reducing tear film osmolarity and diluting inflammatory markers. However, they provide only short-term relief, lack anti-inflammatory properties, and do not address the underlying causes of DED (Kelly et al., 2023; Baiula and Spampinato, 2021). For inflammation, conventional marketed drugs, such as corticosteroids and NSAIDs possess anti-inflammatory effects but are associated with serious long-term side effects, such as an increased intraocular pressure and cataract formation (Wei et al., 2023). Cyclosporine, another conventional DED treatment, exhibits immunomodulatory activity, but it can lead to side effects such as ocular burning sensation and itching, among others (Periman et al., 2020; Peng et al., 2022).

In recent years, Apigenin (APG) has emerged as a potential treatment option due to its excellent therapeutic properties. APG has been shown to ameliorate ocular surface lesions and protect the retina from oxidative damage in *in vivo* models (Zhang et al., 2020; Liu et al., 2019). Given the therapeutic potential and safety profile of APG, it represents a promising novel treatment for DED (Liu et al., 2019). However, despite the interest in APG as an ocular treatment, it is hindered by its low solubility and bioavailability (Wang et al., 2019). Due to this fact, novel ocular delivery systems have been developed. One of the most interesting delivery systems are lipid nanoparticles, which offer multiple advantages including decreased toxicity, suitable stability over time, eco-friendly and economical production, easy industrial scale-up, the ability to be autoclaved or sterilized, and increased kinetic stability compared to other drug delivery systems such as liposomes or niosomes (Battaglia et al., 2016). Moreover, the latest generation of lipid nanoparticles, known as nanostructured lipid carriers (NLC), hold promise as an ocular delivery system due to their enhanced stability compared to previous nanoparticles like solid lipid nanoparticles (SLN). This improvement is achieved through the addition of a liquid lipid component. Additionally, the lipids used in NLC formulations can be tailored to provide specific benefits such as hydrating the ocular surface or imparting anti-inflammatory or antioxidant properties (Bonilla et al., 2022).

To increase the stability of APG and enhance its therapeutic efficacy and retention time on the ocular surface, a novel strategy was developed involving encapsulation into biocompatible and biodegradable NLC. This approach aims to achieve prolonged release of APG, thereby minimizing its degradation and maximizing its therapeutic impact on the ocular surface. Furthermore, a liquid lipid with antioxidant, anti-inflammatory, and regenerative properties was chosen: rosehip oil. Extracted from *Rosa canina* seeds, rosehip oil possesses exceptional value due to its rich composition of essential fatty acids, tocopherols, sterols, and phenolic compounds, all of which offer diverse and beneficial functional properties (Kiralan and Yildirim, 2019). Moreover, hyaluronic acid (HA), a naturally occurring anionic polysaccharide with mucomimetic properties, has been incorporated into the formulation. HA ability to prolong precorneal residence time and reduce surface desiccation makes it a valuable viscosity-building agent in ocular delivery devices. It enhances drug retention and alleviates ocular surface dryness (Agarwal et al., 2021). Moreover, to enhance the bioavailability of the formulation upon administration to the ocular mucosa, a cationic lipid has been selected. Cationic lipids promote electrostatic interactions between the positively charged surface of the particles and the negatively charged ocular mucosa, significantly extending drug residence time (Fangueiro et al., 2016). Furthermore, in previous ocular delivery studies, the chosen cationic lipid, dimethyldioctadecylammonium bromide (DDAB), demonstrated no toxicity up to a concentration of 0.5 % (Silva et al., 2019).

As a result, the objective of this research was to develop a novel nanostructured drug delivery system comprising a surface-functionalized cationic HA-coated APG-loaded NLC for the effective treatment of DED. Currently, there is no formulation designed for topical administration containing this composition capable of increase ocular tear volume, reduce inflammation, and improve corneal erosions. Therefore, this work is focused on comprehensive *in vitro* and *in vivo* investigations to evaluate the biocompatibility, therapeutic potential, and anti-inflammatory efficacy of the APG-NLC.

2. Materials and methods

2.1. Materials

APG was acquired from Apollo Scientific (Cheshire, UK). Compritol 888 ATO® (Glyceryl distearate) was gifted by Gattefossé (Madrid, Spain). Tween® 80 (Polysorbate 80), rose Bengal, fluorescein and Nile red (NR) were obtained from Sigma Aldrich (Madrid, Spain). Rosehip oil was acquired from Acofarma Formulas Magistrales (Barcelona, Spain). DDAB was purchased to TCI Europe (Zwijndrecht, Belgium). HA was gifted by Bloomage Freda Biopharm (Jinan, China). All the others reagents used in this research were of analytical grade. Purified water was obtained by a Millipore Milli-Q Plus system.

2.2. APG-NLC preparation and optimization

APG-NLC production was performed using the hot high-pressure homogenization method (Homogenizer FPG 12800, Stansted, United Kingdom). Briefly, an initial emulsion was prepared by mixing the compounds using an Ultraturrax T25 (IKA, Germany) at 8000 rpm for 30 s. The fabrication conditions included a temperature of 85 °C, three homogenization cycles and 900 bars of pressure (Carvajal-Vidal et al., 2019). The formulation was previously optimized (Bonilla-Vidal et al., 2023), and increasing amounts of a cationic lipid were added to obtain surface-functionalized NLC by means of cationic surface charge. Then, 0.01 mg/10 mL of HA was added to the formulation. (Carvajal-Vidal et al., 2019; Sánchez-López et al., 2018).

2.3. Physicochemical parameters

Photon correlation spectroscopy (PCS) was used for measuring zeta average (Z_{av}) and polidispersity index (PI) employing a ZetaSizer Nano ZS (Malvern Instruments, Malvern, UK). Zeta pontetial (ZP) was elucidated by electrophoretic mobility. Prior to measurements, samples were diluted with Milli-Q water 1:10 and analyzed in triplicate at 25 °C. The encapsulation efficiency (EE) was quantified by measuring the non-loaded drug, which was separated from NLC by filtration/centrifugation at 14,000 r.p.m. (Mikro 22 Hettich Zentrifugen, Germany) using an Amicon® Ultra 0.5 centrifugal filter device (Amicon Millipore Corporation, Ireland). Then, the EE was calculated by the difference between the total amount used for the nanoformulation and the free drug, which could be quantified in the filtered fraction, using Eq. (1) (Sánchez-López et al., 2020):

$$EE(\%) = \frac{Total\ amount\ of\ APG - Free\ APG}{Total\ amount\ of\ APG} \times 100 \quad (1)$$

The quantification of APG was performed by a modified reverse-phase high-performance liquid chromatography (RP-HPLC). Briefly, the non-encapsulated drug was quantified using an HPLC Waters 2695 (Waters, Massachusetts, USA) separation module and a Kromasil® C18 column (5 μm, 150 × 4.6 mm), with a mobile phase composed of 2 % acetic acid and methanol, as an aqueous and organic phase respectively. Agradient (from 40 % to 60 % of water phase in 5 min and back in next 5 min) was employed at a flow rate of 0.9 $mL{\cdot}min^{-1}$. A diode array detector Waters® 2996 at a wavelength of 300 nm was used to detect APG

and data were processed with Empower 3® Software (Carvajal-Vidal et al., 2019; Romanová et al., 2000).

2.4. Characterization of optimized APG-NLC

2.4.1. Transmission electron microscopy

In order to confirm the spherical morphology of the nanoparticles, transmission electron microscopy (TEM) was used by means of a JEOL 1010 microscope (JEOL USA, Dearborn Road, Peabody, MA 01960, USA). Copper grids were activated with ultraviolet (UV) light, and samples were diluted (1:10) and placed on the grid surface. Prior to TEM analysis, samples were negatively stained with uranyl acetate (2 %) (Sánchez-López et al., 2020).

2.4.2. Interaction studies

Differential scanning calorimetry (DSC) analysis was employed to characterize the thermal behavior of APG-NLC formulations. A DSC 823e System from Mettler-Toledo (Barcelona, Spain) was utilized for this purpose. A pan containing indium (≥99.95 % purity; Fluka, Switzerland) was employed to verify the calibration of the calorimetric system. Throughout the DSC measurements, an empty pan served as a reference. APG-NLC analysis were conducted employing a heating ramp from 25 to 105 °C at a rate of 10 °C/min in an inert nitrogen atmosphere. Data acquired during DSC was analyzed using Mettler STARe V 9.01 dB software (Mettler-Toledo, Barcelona, Spain) (Carvajal-Vidal et al., 2019; Sánchez-López et al., 2020).

X-ray diffraction (XRD) was employed to determine the crystalline state of the samples using the conditions described elsewhere (Carvajal-Vidal et al., 2019).

Fourier transform infrared (FTIR) was used to identify covalent bonds in the samples. FTIR spectra of APG-NLC were acquired using a Thermo Scientific Nicolet iZ10 spectrometer equipped with an ATR diamond crystal and a DTGS detector (Barcelona, Spain) (Esteruelas et al., 2022).

2.5. Stability studies

APG-NLC samples were stored at three different temperatures (4, 25, and 37 °C) for several months. The stability of the formulations was evaluated by analyzing the light backscattering (BS) profiles using a Turbiscan® Lab instrument. A glass measurement cell containing 10 mL of sample was used for each measurement. The BS profiles were acquired at regular intervals of 30 days. The radiation source employed was a pulsed near-infrared light-emitting diode (LED) operating at a wavelength of 880 nm. The BS signal was detected by a detector positioned at a 45° angle from the incident beam. Simultaneously to the BS measurements, values of Z_{av}, PI, ZP, and EE were determined to assess the stability of the APG-NLC formulations (Sánchez-López et al., 2018).

2.6. Biopharmaceutical behavior

The *in vitro* APG release test for APG-NLC was performed using Franz-type diffusion cells (PermeGear Hellertown, USA) with 0.20 cm^2 diffusion area and cellulose dialysis membranes (MWCO 12 kDa). A solution of PBS with 5 % polysorbate 80 and 20 % ethanol under continuous stirring was used as a receptor medium accomplishing sink conditions (ability of the medium to dissolve the expected amount of drug) (Liu et al., 2013). The formulations were compared with free-APG solution. The assay was performed at 32 ± 0.5 °C along 48 h. 150 μL of each formulation were added to the donor compartment by direct contact with the membrane. The drug content of the samples was analyzed by HPLC using the previously described method. The test was performed three times, and the cumulative amount of APG was calculated (Carvajal-Vidal et al., 2019).

2.7. Ocular tolerance

2.7.1. In vitro study: HET-CAM test and HET-CAM TBS

The *in vitro* ocular tolerance of APG-NLC formulations was assessed using the HET-CAM test to evaluate their potential irritation when administered as eye drops. This assay was conducted following the guidelines established by ICCVAM. For each formulation, 300 μL of the test solution was applied to the chorioallantoic membrane of a fertilized chicken egg. Irritation, coagulation, and hemorrhage were monitored during the first 5 min post-application. Both a positive control (0.1 M NaOH) and a negative control (0.9 % NaCl) were included in the study. The ocular irritation index (OII) was calculated by summing the scores assigned to each injury, as defined by the following expression (Eq (2)) (Sánchez-López et al., 2020):

$$OII = \frac{(301 - H)\cdot 5}{300} + \frac{(301 - V)\cdot 7}{300} + \frac{(301 - C)\cdot 9}{300} \quad (2)$$

where H, V and C indicate the time (s) where hemorrhage (H), vasoconstriction (V) and coagulation (C) start to occur. The formulations were categorized based on the following criteria: OII ≤ 0.9 non-irritating; 0.9 < OII ≤ 4.9 weakly irritating; 4.9 < OII ≤ 8.9 moderately irritating; 8.9 < OII ≤ 21 irritating.

Furthermore, at the end of the HET-CAM experiment, in order to quantify the damage of the membrane, trypan blue staining (TBS) was applied. 1000 μL of 0.1 % trypan blue solution were added to the CAM for 1 min. The excess of TBS was removed and the CAM was dissected and extracted with 5 mL of formamide. The absorbance of the extract was then measured spectrophotometrically at a λ_{595nm}. The amount of TBS absorbed was determined using a calibration curve of TBS in formamide (Lagarto et al., 2006).

2.7.2. In vivo ocular tolerance

All experimental procedures were conducted in accordance with the guidelines of the Ethical Committee for Animal Experimentation of the UB and current legislation (Decree 214/97, Gencat). To validate HEM-CAM test results, ocular tolerance of the formulations was assessed *in vivo*. Male New Zealand white rabbits (2.0–2.5 kg, San Bernardo farm, Navarra, Spain) were used in this experiment. A total of 3 rabbits were assigned to each test group. Each rabbit received 50 μL of the respective formulation instilled into the ocular conjunctival sac. A mild massage was applied to ensure proper distribution of the sample within the eye. The eyes were examined for signs of irritation, including corneal opacity and area of involvement, conjunctival hyperemia, chemosis, ocular discharges, and iris abnormalities, at the time of instillation and after 1 h. The contralateral untreated eye served as a negative control. *In vivo* tolerance test scores were assigned based on the observed changes in the anterior segment of the eye, particularly the cornea (turbidity or opacity), iris, and conjunctiva (congestion, chemosis, swelling, and secretion) (Valadares et al., 2021).

2.8. Cellular experiments

2.8.1. Cell culture

Human corneal epithelial cells (HCE-2) (LGC Standards, Barcelona, Spain) were cultured in keratinocyte serum-free growth medium (SFM; Life Technologies, Invitrogen, GIBCO®, Paisley, UK). It was supplemented with bovine pituitary extract 0.05 $mg{\cdot}mL^{-1}$ and epidermal growth factor 5 $ng{\cdot}mL^{-1}$ containing insulin 0.005 $mg{\cdot}mL^{-1}$ and penicillin 100 $U{\cdot}mL^{-1}$ plus streptomycin 100 $mg{\cdot}mL^{-1}$. Cells were grown on a culture flask up to 80 % confluency in a humidified 10 % CO_2 atmosphere at 37 °C (López-Machado et al., 2021).

2.8.2. Cell viability

Cell viability of APG-NLC was assessed using the MTT assay, which measures the reduction of tetrazolium salt by intracellular

dehydrogenases of viable living cells. For this, 100 μL of a cell suspension containing 2×10^5 cells/mL was seeded in a 96-well plate and incubated for 48 h at 37 °C in the appropriate complete medium before treatment. Cells were then treated with samples at different concentrations (ranging from 1×10^{-3} to 0.1 mg/mL) for 5 or 15 min to simulate real conditions of the cornea. Subsequently, the culture medium was aspirated and replaced with 200 μL of MTT solution (0.25 % w/v in PBS, Sigma-Aldrich Chemical Co., St. Louis, MO, USA). After a 2 h incubation period, the supernatant was replaced with 100 μL of DMSO (99 %, Sigma-Aldrich) to solubilize the formazan product formed by viable cells. Cell viability was determined by measuring the absorbance of the formazan solution at 560 nm using a Modulus® microplate photometer (Turner BioSystems Inc., Sunnyvale, CA, USA). Viability was expressed as a percentage of the untreated control cells (López-Machado et al., 2021; Olivo-Martínez et al., 2023; Folle et al., 2021).

2.8.3. Cellular uptake

To evaluate the internalization of APG-NLC in HCE-2 cells, 1×10^5 cell·mL^{-1} HCE-2 were grown in eight-well chamber slider (ibidi®, Gräfelfing, Germany) until 80 % confluence and subsequently incubated with APG-NLC labelled with the fluorescent dye NR at different times (5, 15 and 30 min) at 37 °C. To remove non-internalized NLC, cells were subjected to three washes with PBS. Subsequently, cells were fixed with 4 % paraformaldehyde for 30 min at 25 °C. After fixation, cells were washed three times with PBS to remove unbound paraformaldehyde. The nuclei were stained with DAPI during 10 min. Afterwards, cells were washed using PBS and Alexa Fluor™ 488 conjugated Wheat Germ Agglutinin (WGA) was used to stain cell membranes for 30 min at 25 °C. Cells were washed and finally, mounting solution (PBS) was added for microscopic analysis. Images were acquired using a Leica Thunder Imager DMI8 (Leica Microsystems GmbH, Wetzlar, Germany) with a 63x oil immersion objective lens (López et al., 2020; Gonzalez-Pizarro et al., 2019).

2.9. In vivo efficacy studies

2.9.1. Induction and treatment of dry eye

Twelve male New Zealand white rabbits weighing between 2.0 and 2.5 kg were used for the study. The rabbits were randomly divided into 4 groups: empty NLC, APG-NLC, free APG solution and a commercial solution based on 0.15 % HA. All rabbits were housed at a room temperature of 23 ± 2 °C with relative humidity 75 % ± 10 % and alternating 12 h light–dark cycles.

Both eyes of each rabbit were treated twice-daily with a topical administration of 0.1 % benzalkonium chloride (BAK) for 2 weeks. On day 14, DED was confirmed using the Schirmer test, fluorescein and rose Bengal staining. Treatment commenced after the confirmation of DED, with one eye of each rabbit randomly chosen for twice-daily topical administration of empty NLC, APG-NLC, free APG solution, or a commercial solution (0.15 % HA). After one week of treatment, the Schirmer test, fluorescein staining, and rose Bengal staining were performed again to evaluate the efficacy of the treatments (López-Machado et al., 2021; Xiong et al., 2008).

2.9.1.1. Measurement of aqueous tear production. Tear production was determined using Schirmer test strips. After instilling anesthetic drops containing 1 mg·mL^{-1} tetracaine hydrochloride and 4 mg·mL^{-1} oxybuprocaine hydrochloride, a Schirmer paper strip was placed on the palpebral conjunctiva, positioned near the junction of the middle and outer thirds of the lower eyelid. After 5 min, the extent of wetted paper was measured in millimeters (López-Machado et al., 2021; Xiong et al., 2008).

2.9.1.2. Fluorescein staining on the ocular surface. Fluorescein staining occurs when fluorescein sodium diffuses through disrupted corneal epithelial cell junctions or damaged corneal epithelial cells (Xiong et al., 2008). Corneal fluorescein staining was performed by instilling 2 μL of 1 % fluorescein sodium into the conjunctival sac and allowing it to remain for 2 min. The ocular surface was then examined under a slit lamp microscope equipped with a cobalt blue filter. Images of the ocular surface were captured using a digital camera and scored according to the stained score with 9 indicating maximum score and 0 indicating the minimum (Holzchuh et al., 2011).

2.9.1.3. Rose Bengal staining on the ocular surface. Rose Bengal stains corneal and conjunctival epithelial cells that are not adequately protected by the ocular tear film. It can stain both live and dead cells if they are not protected by an intact mucin layer (Xiong et al., 2008). To assess ocular surface damage, 2 μL of 0.1 % rose Bengal solution were instilled into the conjunctival sac and allowed to remain for 2 min. The ocular surface was then examined under a slit lamp microscope with white light, and images were captured using a digital camera. The degree of staining was assessed using the Van Bijsterveld grading system, and the scores were recorded after 15 s (9: maximum score; 0: minimum) (Xiong et al., 2008).

2.9.2. Anti-inflammatory efficacy

The *in vivo* anti-inflammatory effectiveness of the formulations was evaluated through two studies encompassing inflammation prevention and treatment. Male New Zealand white rabbits (n = 3/group) were used for these experiments as previously described. The activity of APG-NLC was compared with free APG, empty NLC, and 0.9 % NaCl (control group). For the inflammation prevention, 50 μL of each formulation was topically applied to the right eye. After 30 min, a 0.5 % sodium arachidonate (SA) solution dissolved in PBS (inflammatory stimulus) and instilled into the right eye, (left eye served as a control). In the anti-inflammatory treatment study, the inflammatory stimulus was applied 30 min before the application of each formulation. Inflammation was evaluated from the first application up to 210 min following administration, based on the modified ocular tolerance test scoring system (López-Machado et al., 2021; Sánchez-López et al., 2020).

2.10. Statistical analysis

Two-way ANOVA followed by Tukey post hoc test was performed for multi-group comparison. Student's *t*-test was used for two-group comparisons. All the data are presented as the mean ± S.D. Statistical significance was set at $p < 0.05$ by using GraphPad Prism 9.

3. Results

3.1. APG-NLC preparation and optimization

In previous studies, an optimized formulation was obtained (Bonilla-Vidal et al., 2023). In this work, increasing amounts of the cationic lipid DDAB were added to further optimize the formulation (Table 1). The formulation was constituted by Compritol® 888 ATO as the solid lipid component since it provided suitable APG solubility. Compritol® 888 ATO is a well-known excipient used in various administration routes due to its favorable characteristics, including non-polarity, lower

Table 1
Effect of cationic lipid on the physicochemical parameters.

DDAB (%)	Z_{av} ± SD (nm)	PI ± SD	ZP ± SD (mV)
0.025	301.8 ± 2.0	0.186 ± 0.003	−0.8 ± 0.1
0.05	**146.8 ± 0.8**	**0.253 ± 0.003**	**21.2 ± 0.4**
0.06	144.3 ± 2.4	0.326 ± 0.036	27.3 ± 1.0
0.075	150.0 ± 3.8	0.363 ± 0.040	29.3 ± 0.5
0.1	148.2 ± 1.5	0.427 ± 0.018	35.6 ± 0.8
0.3	153.6 ± 1.9	0.407 ± 0.011	54.8 ± 1.6
0.5	147.7 ± 0.3	0.382 ± 0.009	54.4 ± 0.6

cytotoxicity, and its capacity to increase encapsulation efficiency (Aburahma and Badr-Eldin, 2014). Rosehip oil was included as an active ingredient in the formulation to complement the activity of APG with its wound-healing, antioxidant, and anti-inflammatory characteristics (Belkhelladi and Bougrine, 2024; Bhave et al., 2017). The surfactant, Tween® 80, was selected because it is included in official European Medicines Agency (EMA) documents for ocular use at the concentrations employed in this study (Mazet et al, 2020). Additionally, in some cellular models, it has been found to enhance penetration through tight junctions, which could facilitate crossing the human ocular surface epithelial barrier (Khuda et al., 2022; Mantelli et al., 2013).

The optimized formulation was selected based on the physicochemical parameters, with criteria including values of ZP higher than 20 mV and PI lower than 0.3. As a result, the cationic optimized formulation containing 0.05 % of cationic lipid was chosen. Additionally, a small amount of hyaluronic acid (HA) was added. Subsequently, the optimized APG-NLC formulation was obtained.

3.2. Characterization of optimized APG-NLC

TEM analysis revealed that APG-NLC exhibited a predominantly spherical morphology with particle size below 200 nm (specifically, in Fig. 1A APG-NLC size was 166.5 nm), consistent with the results obtained by PCS. Moreover, no particle aggregation phenomena were observed.

DSC was carried out in order to study the crystallinity and melting point variations of the lipid mixtures and APG-NLC. Thermograms (Fig. 1B) showed endothermal peaks of 70.37 °C for lipid mixture, 69.78 °C for lipid mixture-APG and 69.16 °C APG-NLC. The melting point of APG-NLC was slightly lower due to its small size and surfactant presence (Tween® 80) (Bunjes et al., 1996). The peaks moved to slightly lower temperatures when APG was added and the enthalpy was similar between the lipid mixture and lipid mixture-APG being ΔH Lipid mixture = 82.69 Jg^{-1}, ΔH Lipid mixture-APG = 84.03 Jg^{-1} and a smaller enthalpy for the nanoparticles, being ΔH APG-NLC = 54.11 Jg^{-1}. APG melting transition was characterized by an endothermal peak at 365.5 °C (ΔH = 198.5 Jg^{-1}) followed by decomposition, as other authors had also reported (Shakeel et al., 2017).

XRD patterns (Fig. 1C) demonstrated the physicochemical state of APG incorporated into NLC. The presence of intense and sharp peaks for APG and for the solid mixture of lipids indicated a crystalline structure for these components. Notably, the peaks observed for APG were absent in the APG-NLC profile, suggesting that APG was present in a dissolved state within the NLC, forming a molecular dispersion. The crystallinity of the structure of all the components was studied. The lipid mixture showed three peaks in 19.34 (2θ), i.e. $d = 0.46$ nm indicating the most stable form of triacylglycerols, the β form, 21.28 (2θ) i.e. $d = 0.42$ nm and 23.43 (2θ) i.e. $d = 0.38$ nm, which confirmed the existence of the second stable form of triacylglycerols, known as the β' form. The APG-NLC profile showed also the three peaks, which could indicate a good stability of the formulation (Souto et al., 2006; Freitas and Müller, 1999; Zimmermann et al., 2005).

FTIR spectroscopy was employed to investigate the interactions between the drug, the surfactant, and the lipid matrix (Fig. 1D). The FTIR spectra of APG revealed distinct vibrational bands, including a characteristic peak at 3278 cm^{-1} corresponding to the O–H stretching vibration. The C–H stretching vibration exhibited multiple, smaller peaks at 2800 cm^{-1}. Additionally, the presence of the C-O functional group was indicated by characteristic peaks at 1650 and 1605 cm^{-1}. (Alshehri et al., 2019). There was no evidence of strong bonds between APG and lipid phase and the surfactant. APG peaks were not found in the NLC. These results indicate that APG was encapsulated in the NLC.

3.3. Stability studies

Stability studies were carried out analyzing the BS profiles of each sample at different temperatures. BS provides information of destabilization mechanisms in the media, such as sedimentation, creaming, or aggregation (Bonilla-Vidal et al., 2023). In this way, BS profiles of APG-NLC were studied at 4, 25 and 37 °C (Fig. 2A-C). APG-NLC was stable at 4 °C for a period of 25 months, while at 25 °C the stability was 1 month. The physicochemical parameters were kept constant at 4 °C for all the

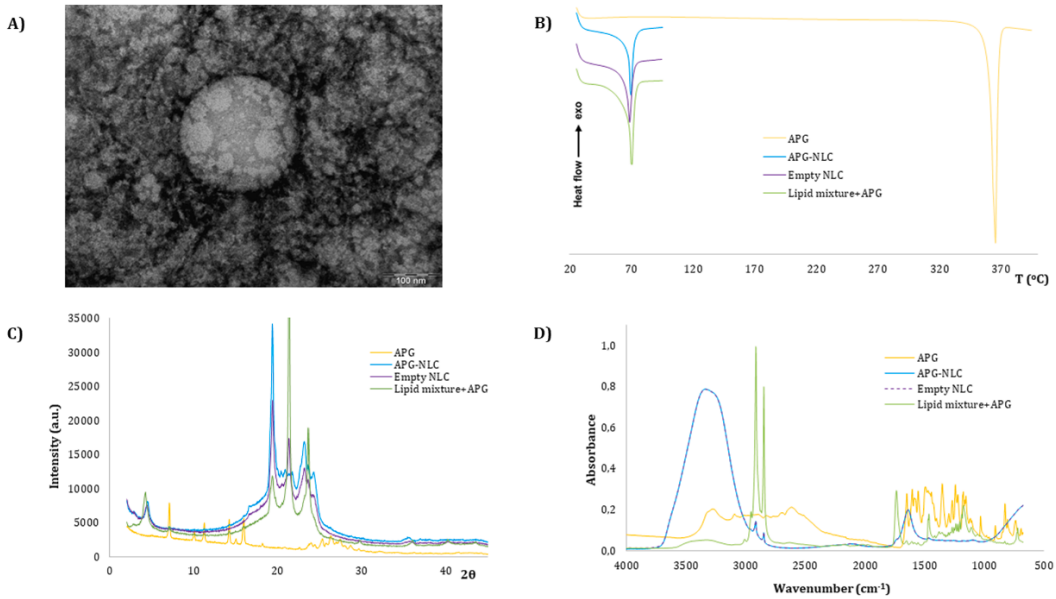

Fig. 1. Characterization of optimized APG-NLC and their components. (A) TEM image (scale bar 100 nm), (B) DSC curves, (C) XRD patterns, (D) FTIR analysis.

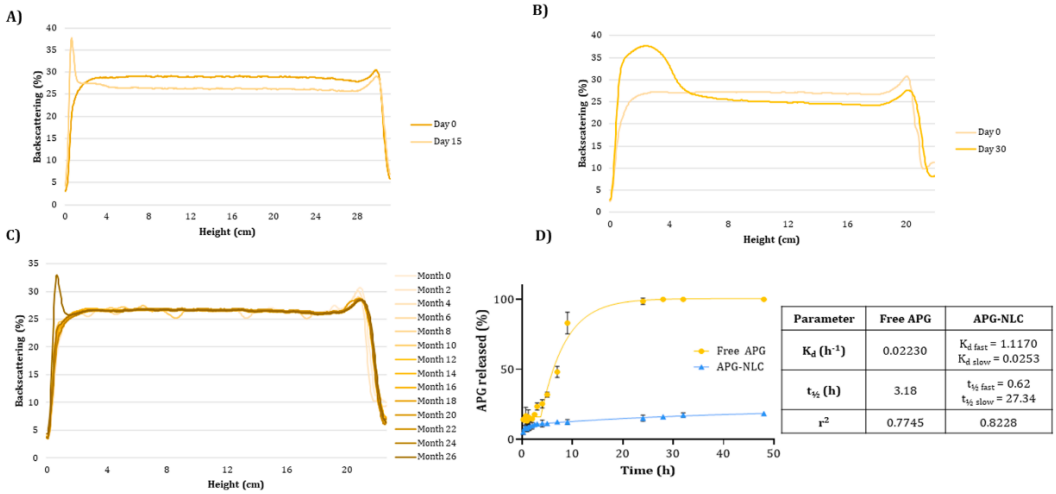

Fig. 2. Characterization of APG-NLC. Backscattering profiles of APG-NLC stored at (A) 37 °C, (B) 25 °C, and (C) 4 °C. (D) *In vitro* release profile of APG-NLC vs free APG carried out for 48 h and adjustment to a two-phase decay and Plateau followed by one phase decay model respectively.

study, being the most suitable storage temperature.

3.4. Biopharmaceutical behavior

The *in vitro* release profile of APG from the NLC exhibited a biphasic drug release pattern, characteristic of prolonged drug delivery systems. A two-phase decay model provided the best fit for APG-NLC release (Fig. 2). An initial burst release of APG was observed during the first 2 h, followed by a sustained release phase that lasted until the end of the experiment. In contrast, free APG exhibited a rapid diffusion, reaching 100 % release within 24 h, while the APG-NLC formulation released only approximately 30 % during the same time period. The dissociation constant (K_d) values for APG-NLC were significantly higher in fast release phase compared to those of free APG (1.1170 vs 0.02230 h), suggesting a rapid initial release, followed by a slower one (Liu et al., 2013). Moreover, half-life results ($t_{1/2}$) showed that initially there was a burst release during the fast phase of the formulation, and then it was followed by a slow phase, in which it had a sustained and lower release, with a $t_{1/2}$ value of 9.14 h.

3.5. Ocular tolerance

Ocular tolerance was studied *in vitro* using the HET-CAM test and *in vivo* using the Draize test (Fig. 3A-D). The HET-CAM test results demonstrated that the positive control (1 M NaOH, 18.75 ± 1.05) induced severe hemorrhage, intensifying over a 5-minute period. This characterization classifies the solution as a severe irritant. In contrast, application of the negative control (0.9 % NaCl, 0.07 ± 0.01) and both the loaded and empty formulations to the chorioallantoic membrane did not elicit any signs of irritation, leading to their classification as non-irritant substances (0.07 ± 0.01 and 0.07 ± 0.01 respectively). Otherwise, free APG caused a fast vasoconstriction, being classified as a severe irritant (14.86 ± 0.30). Moreover, TBS quantitative results supported the results of the HET-CAM test, where APG-NLC were non-irritant while free APG resulted irritant (0.06 ± 0.04 and 0.18 ± 0.01 respectively).

However, as a single *in vitro* test is insufficient to accurately assess ocular tolerance in a living organism, ocular tolerance Draize tests were conducted to further evaluate the formulations. The tests were carried out with free APG, empty NLC, and APG-NLC. In this sense, none of the developed NLC were irritant *in vivo* or *in vitro*, while the free APG

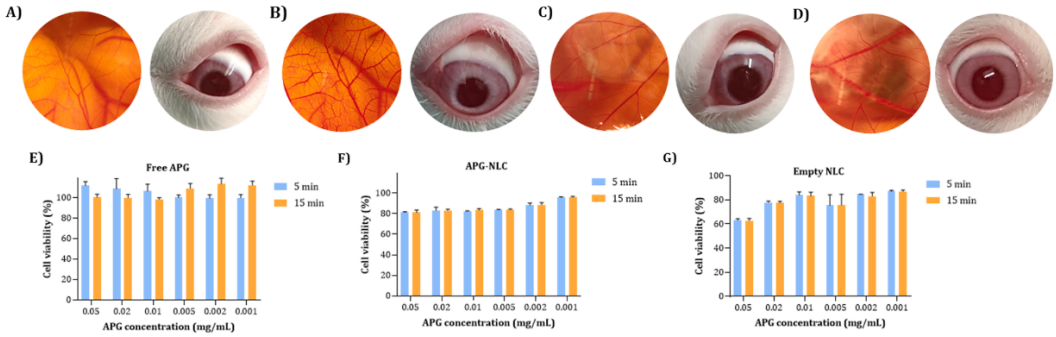

Fig. 3. Ocular tolerance. *In vitro* and *in vivo* irritation assay. (A) Negative control, NaCl 0.9 %, (B) Free APG, (C) APG-NLC, and (D) Empty NLC. (E) Scores obtained on the HET-CAM and *in vivo* ocular tolerance. (F-H) Effect of (F) free APG, (G) APG-NLC and (H) empty NLC on the viability of HCE-2 cells at 5 and 15 min. 100 % cell viability corresponds to the average of MTT reduction values of untreated cells.

resulted irritant *in vitro* (14.86 ± 0.30) and non-irritant *in vivo* (2.00 ± 1.00) but caused an initial discomfort. These results confirmed the non-irritant potential of APG loaded lipid nanoparticles, meanwhile the free APG can induce some discomfort.

3.6. Cellular experiments

3.6.1. Cell viability in corneal cells

Cell viability of several concentrations of free APG, APG-NLC, and empty NLC (without APG) were evaluated on HCE-2 cells. The HCE-2 cell line was selected to analyze the compatibility of the formulations on corneal cells after topical administration. Samples were incubated for various time points to simulate the real conditions of contact between the formulation and the cornea in humans (Mofidfar et al., 2021). For this reason, cell viability was tested incubating for 5 and 15 min. According to ISO 10993–5, percentages of cell viability above 80 % are considered non-cytotoxic; within 80 – 60 % weak; 60 – 40 % moderate and below 40 % strongly cytotoxic, respectively (López-García et al., 2014). Results showed that after 5- and 15-min incubation, free APG did not cause relevant cytotoxic effects (≥80 % viability). Free APG did not show any effects on cell viability at any of the concentrations tested or incubation times (Fig. 3F). APG-NLC after 5- and 15- min incubation showed suitable cell viability in all the assessed concentrations (Fig. 3G). Similarly, empty NLC resulted in suitable cell viability for 5- and 15- min incubation from 0.02 to 0.001 mg·mL^{-1} (Fig. 3H). The most concentrated dilution of empty NLC showed weak toxicity at both times. However, it can be observed that APG-NLC were safe (high cell viability) in all the studied concentrations.

3.6.2. Cellular uptake

Following incubation at different time points, fluorescent NLC were visualized using fluorescence microscopy. The nucleus was stained with DAPI, and the cell membrane was stained with Alexa Fluor™ 488-WGA to facilitate better bio-localization of the NLC. In the merged images, APG-NLC were observed inside the cells, indicating that the particles were able to penetrate without altering the morphology of the corneal

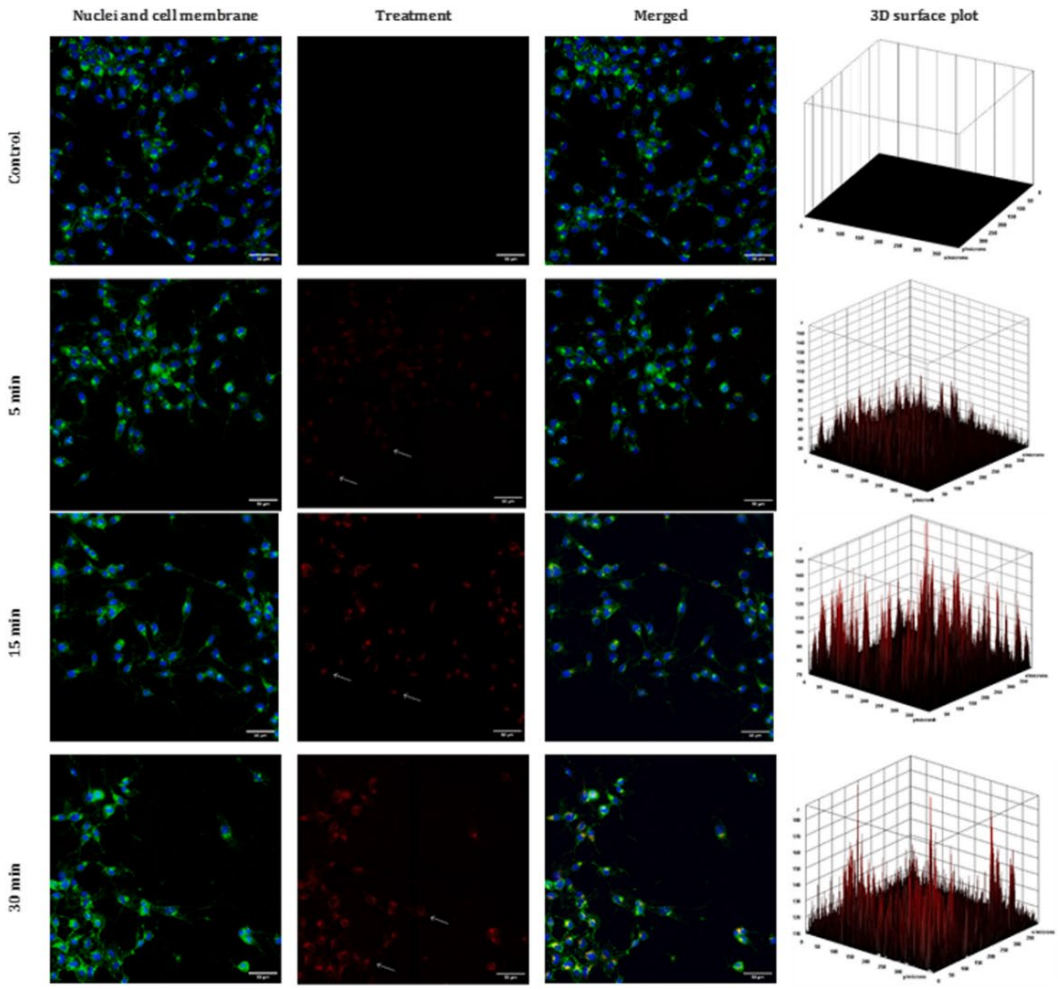

Fig. 4. Cellular uptake of APG-NLC in HCE-2 at different incubation time (5, 15, or 30 min). White arrows highlight samples localization. Surface plot is shown as relative fluorescence intensity per cell in 3D coordinates.

cells (Fig. 4). It is noteworthy that toxic substances, such as benzalkonium chloride, can induce morphological changes in the cell membrane, such as vacuolization of corneal cells Kinnunen et al, 2014. Moreover, the fluorescence signal had increased along with the incubation time. Furthermore, after 30 min incubation of APG-NLC displayed higher intensity than cells incubated 5 or 15 min. No fluorescence was observed in the control cells (Fig. 4).

3.7. Induction and treatment of DED

In order to evaluate the potential to treat DED using APG-NLC, Schirmer test, fluorescein and rose Bengal assessments were performed to measure the effects of empty NLC, free APG and commercial solution based on 0.15 % of HA as a moisturizing agent.

3.7.1. Schirmer test

To evaluate the improvement on tear flow caused by the developed NLC in a DED model, Schirmer's test was employed. A marked decrease in aqueous tear secretion was observed after applying BAK for 2 weeks. Fig. 5A shows the differences between each experimental group. Empty NLC and APG-NLC were able to increase the tear flow obtaining statistically significant differences against DED control, $p < 0.01$ and $p < 0.0001$ respectively. Otherwise, free APG and the 0.15 % HA solution did not improve tear flow. APG-NLC showed statistically significant differences between all the groups: $p < 0.05$ against empty NLC, and $p < 0.0001$ against free APG and 0.15 % HA solution. Empty NLC showed statistically significant differences between free APG group ($p < 0.05$). Interestingly, APG-NLC was the only treatment that showed statistically significant differences compared to 0.15 % HA solution ($p < 0.0001$).

3.7.2. Fluorescein staining on the ocular surface

Fluorescein staining is an effective method for evaluating the state of the ocular surface. It results from fluorescein uptake, which is caused by the disruption of corneal epithelial cell–cell junctions or damaged corneal epithelial cells (Begley et al., 2019; Srinivas and Rao, 2023). Fig. 5B shows the differences between each experimental group. There were statistically significant differences between all the groups against dry eye control. However, the two treatments that provided the best improvement on the ocular corneal surface were empty NLC and APG-NLC ($p < 0.001$, 0.67 ± 0.58 and 1.00 ± 1.00 respectively). Moreover, free APG solution and the 0.15 % HA solution presented higher staining (2.33 ± 0.58 and 3.00 ± 1.15 respectively), indicating a diminished capacity to restore the corneal surface (Fig. 6).

3.7.3. Rose Bengal staining on the ocular surface

Rose Bengal is a valuable tool for assessing tear film integrity. It selectively stains corneal and conjunctival epithelial cells that are exposed due to compromised preocular tear film protection. Its ability to stain both live and dead cells, provided the mucin layer is disrupted, enables it to detect various degrees of tear film dysfunction (Xiong et al., 2008). As can be observed in Fig. 5C, there were statistically significant differences between dry eye control and empty NLC and APG-NLC staining (5.08 ± 1.78, 1.67 ± 1.15 and 1.67 ± 1.15 respectively). The results showed that only NLC were able to restore the disrupted tear film. Moreover, HA 0.15 % solution (4.67 ± 1.15) did not show significant differences against the control, indicating that it did not exert significant tear film restoring capacity (Fig. 7).

3.8. Anti-inflammatory efficacy

Anti-inflammatory efficacy was assessed in New Zealand rabbits to elucidate the capacity of the developed APG-NLC to treat and/or prevent ocular inflammation.

Firstly, the *in vivo* inflammation treatment was assessed. Fig. 8A revealed that the degree of inflammation was significantly reduced after the first 30 min post-administration of APG-NLC. Free APG were able to rapidly treat inflammation. Moreover, empty NLC exerted anti-inflammatory activity after 90 min of instillation. Comparing APG-NLC with empty NLC, it can be observed that APG-NLC had significantly higher anti-inflammatory effects than empty NLC after 2 h post-application, probably due to APG prolonged release.

The *in vivo* inflammation prevention test revealed significant differences in the severity of inflammation between APG formulations and the control at all time points evaluated (Fig. 8B). However, APG-NLC-treated eyes exhibited a more rapid reduction in corneal edema compared to free APG. This finding can be attributed to the rapid tear clearance of free APG and the lipid components of the nanoparticles that may result in a prolonged drug residence time within the cornea. APG-NLC demonstrated superior inflammation-relieving effects compared to the control over time. Otherwise, empty NLC also showed an anti-inflammatory effect *in vivo*. Initially, the effect was similar to the APG-NLC activity, but after 90 min of treatment a significant anti-inflammatory effect produced by APG can be observed since significant differences between empty NLC and APG-NLC were obtained (Strugala et al., 2016).

Thus, APG-NLC exhibited a preventive effect on inflammatory processes caused by the sustained release of APG and the synergic activity of

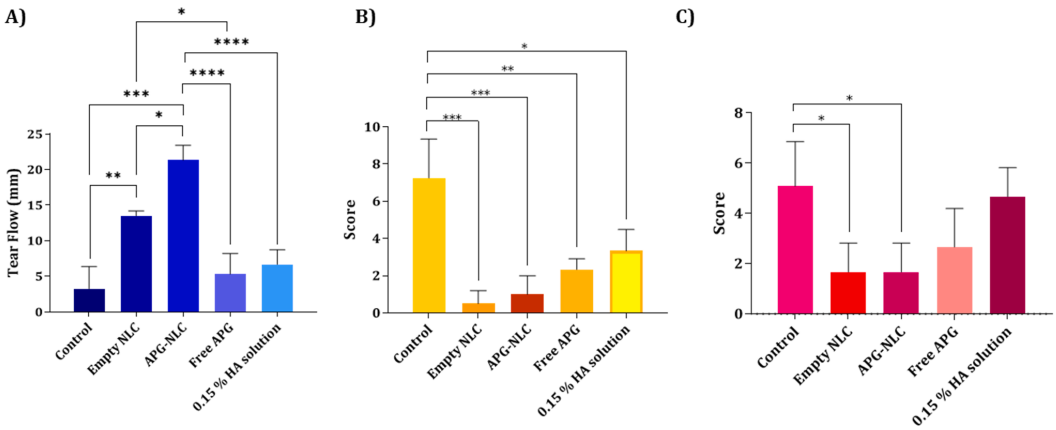

Fig. 5. DED results with statistically significant differences (* $p < 0.05$, ** $p < 0.01$, *** $p < 0.001$; **** $p < 0.0001$). (A) Schirmer test, (B) Fluorescein staining, (C) Rose Bengal staining.

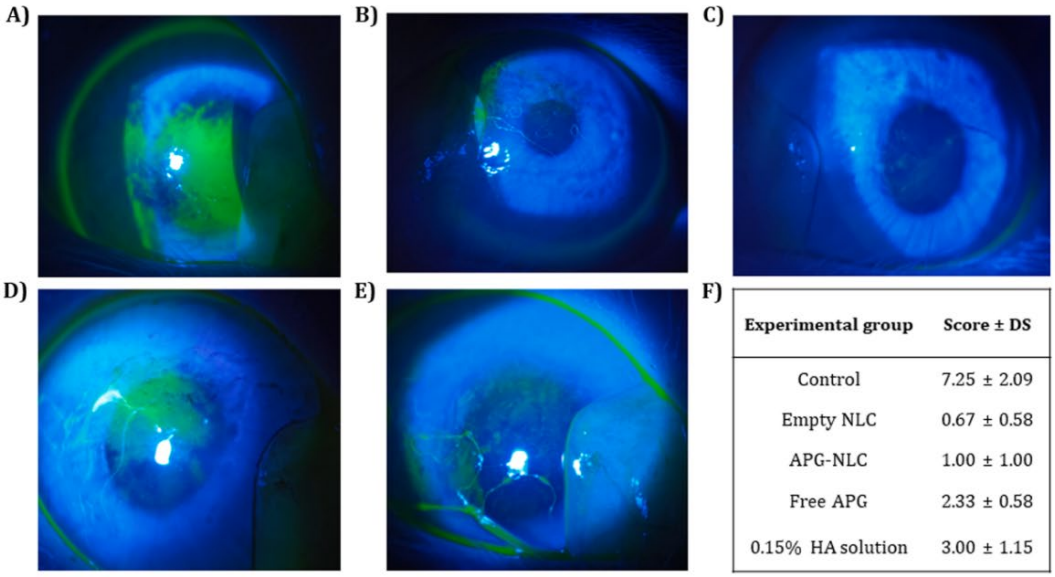

Experimental group	Score ± DS
Control	7.25 ± 2.09
Empty NLC	0.67 ± 0.58
APG-NLC	1.00 ± 1.00
Free APG	2.33 ± 0.58
0.15% HA solution	3.00 ± 1.15

Fig. 6. Fluorescein staining test. (A) Control. (B) Empty NLC (C) APG-NLC. (D) 0.15 HA % solution. (E) Free APG (F) Scores obtained on the fluorescein staining test.

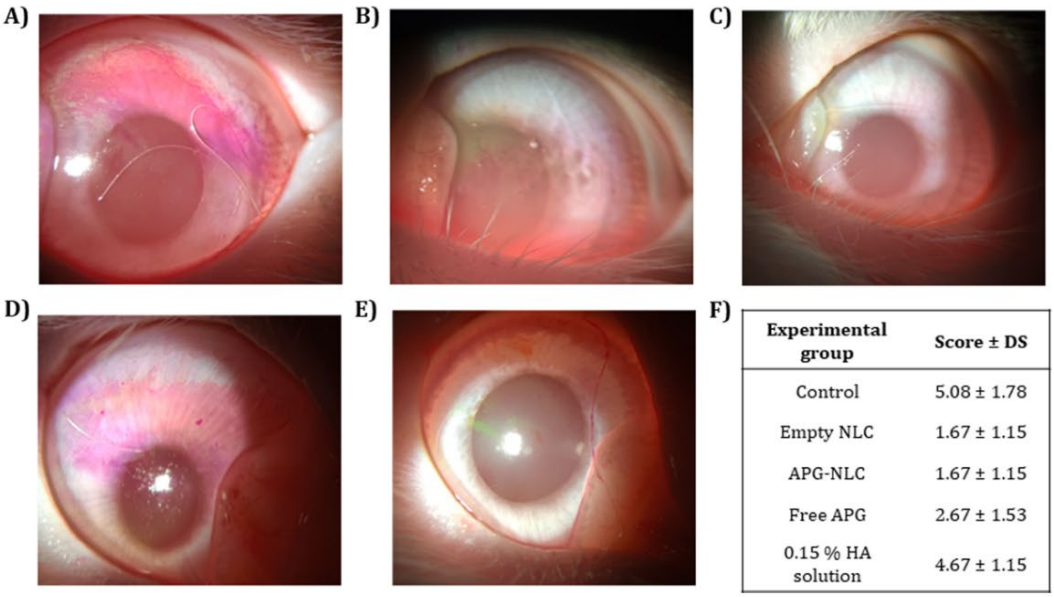

Experimental group	Score ± DS
Control	5.08 ± 1.78
Empty NLC	1.67 ± 1.15
APG-NLC	1.67 ± 1.15
Free APG	2.67 ± 1.53
0.15 % HA solution	4.67 ± 1.15

Fig. 7. Rose Bengal staining test. (A) Control. (B) Empty NLC. (C) APG-NLC. (D) 0.15 % HA solution. (E) Free APG. (F) Scores obtained on the rose Bengal staining test.

the vehicle, which may contribute towards an initial anti-inflammatory effect.

Hence, it can be confirmed that APG-NLC possess ocular anti-inflammatory activity, both for prevention and inflammation treatment. Furthermore, the vehicle also showed anti-inflammatory properties, which could be attributed to the rosehip oil (Winther et al., 2016).

4. Discussion

In this study, a new formulation was developed loading APG into a cationic rosehip-based NLC coated with HA. APG-NLC was prepared using the hot high-pressure homogenization method, which is widely used for lipid nanoparticle fabrication. The high temperature facilitates greater size reduction due to lower inner-phase viscosity. Furthermore,

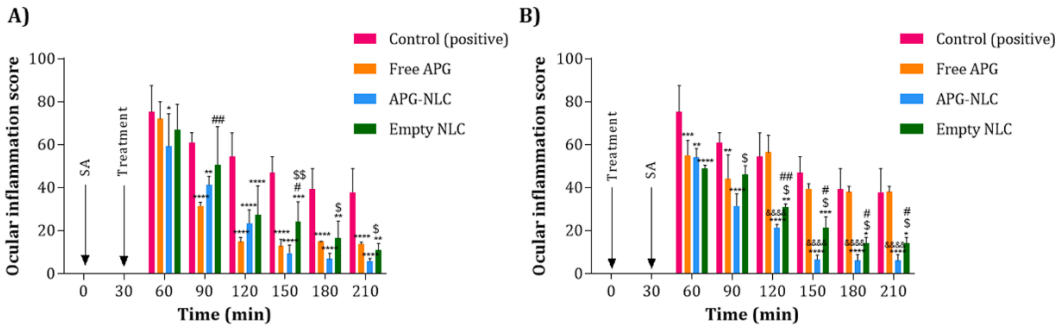

	Experimental groups	60 min	90 min	120 min	150 min	180 min	210 min
Inflammation treatment	Control vs Free APG	ns	****	****	****	****	****
	Control vs APG-NLC	*	**	****	****	****	****
	Control vs Empty NLC	ns	ns	****	***	**	**
	Free APG vs APG-NLC	ns	ns	ns	ns	ns	ns
	Free APG vs Empty NLC	ns	##	ns	#	ns	ns
	APG-NLC vs Empty NLC	ns	ns	ns	$$	$	$
Inflammation prevention	Control vs Free APG	***	**	ns	ns	ns	ns
	Control vs APG-NLC	**	****	****	****	****	****
	Control vs Empty NLC	****	ns	**	***	*	*
	Free APG vs APG-NLC	ns	ns	&&&&	&&&&	&&&&	&&&&
	Free APG vs Empty NLC	ns	ns	##	#	#	#
	APG-NLC vs Empty NLC	ns	$	$	$	$	$

Fig. 8. Comparison of ocular anti-inflammatory efficacy of free APG, APG-NLC, and empty NLC. SA (sodium arachidonate) was used as inflammatory stimuli. (A) Inflammation treatment, (B) inflammation prevention. Values are expressed as mean ± SD; ns: non-significant, *p < 0.05, **p < 0.01, ***p < 0.005, and ****p < 0.001 significantly lower than the inflammatory effect induced by SA; $p < 0.05 and $$p < 0.05 significantly lower effect of APG-NLC than the inflammatory effect induced by empty NLC; &&&&p < 0.0001 significantly lower effect of APG-NLC than the corresponding free drug; #p < 0.05 and ##p < 0.01 significantly lower effect of empty NLC than the corresponding free drug.

this method offers several advantages such as ease of scale-up, absence of organic solvents, and shorter production times (Vinchhi et al., 2021; Khairnar et al., 2022). Sterile fabrication is facilitated by equipment that can be sterilized using steam, and manufacturing can be conducted in an aseptic environment in a laminar airflow unit (Khairnar et al., 2022). Additionally, sterile filtration, autoclaving, ionizing radiation, and non-ionizing radiation can be used in the final formulation for sterilization, with gamma radiation being one of the most commonly used methods (Bernal-Chávez et al., 2021; Youshia et al., 2021).

The cationic lipid DDAB was used in order to increase the ocular retention time on the ocular surface and mucoadhesion due to electrostatic interactions between the negatively charged ocular surface and the nanocarrier. Cationic carriers have shown to effectively penetrate through the negatively charged pores of the corneal epithelium, making them an interesting tool to obtain an efficient drug delivery (Abruzzo et al., 2021; Vedadghavami et al., 2020). Furthermore, the formulation was improved with the addition of HA, which possesses a relatively high viscosity, improving tear film stability and reducing the washout from the ocular surface. Additionally, it promotes epithelial wound healing, which could work in synergy with the liquid lipid (rosehip oil) (Johnson et al., 2006).

In order to optimize the concentration of DDAB, increasing amounts of it were added to the previously optimized formulation (Bonilla-Vidal et al., 2023). The results showed that the Z_{av} was similar from 0.05 to 0.5 %, while the PI and the ZP increased when higher amounts were added. For this reason, the selected concentration was 0.05 %, providing a PI below 0.3, indicating an homogeneous distribution of the nanoparticles, and a ZP around + 20 mV, which contributed to overcome the attractive forces between particles, achieving suitable stability of the colloidal system (Bonilla et al., 2022).

Interaction studies showed that the addition of APG to the lipid matrix resulted in an increase in the amorphous structure of the lipids, suggesting that APG was internalized in the lipid matrix (Ojo et al., 2020). Further analysis using FTIR confirmed that no covalent bonds were formed between APG and the lipid matrix, implying that the interaction between them was primarily mediated by hydrogen bonds and hydrophobic forces. This interaction facilitated the entrapment of APG within the NLC and promoted its release from the particles (Huang et al., 2020). Additionally, XRD studies indicated that APG-NLC exhibited good stability over an extended period due to the presence of the most stable forms of triacylglycerols in Compritol® 888 ATO, namely, the β and β' phases (Souto et al., 2006; Freitas and Müller, 1999; Zimmermann et al., 2005). These findings align with the stability studies, which demonstrated that the formulation remained stable at 4 °C for 25 months. However, at the end of the 25-month period, the electrostatic forces between the APG-NLC may have begun to weaken, leading to aggregation and sedimentation, as observed in the BS profile. In comparison to the previous studies in which the negatively charged formulation (without DDAB nor HA), the stability at 4 °C endured for 11 months (Bonilla-Vidal et al., 2023). The main difference between both formulations was the addition of the cationic lipid, which has a chemical structure and physicochemical properties of a surfactant. The addition of a co-surfactant into the formulation may contribute to stabilize the emulsion droplets during homogenization and upon polymorphic transition during storage, as other studies confirmed (Salminen et al., 2014).

Furthermore, APG-NLC showed a slow *in vitro* release profile, whereas the APG solution exhibited a rapid diffusion. The fitted model for APG-NLC was a two-phase association, due to the fact that the formulation demonstrated a dual release profile, offering an initial fast release followed by a sustained release, where approximately a 20 % of APG was liberated into the receptor medium. This two-phase release pattern could be attributed to the formulation ability to encapsulate APG

within the NLC while also facilitating its gradual diffusion into the medium. Compared to our previous studies, this formulation showed a faster release in the initial phase with a higher rate constant ($K_{d\ fast}$ = 0.2662 vs 1.1170 h^{-1} of the negatively and positively charged formulation respectively), and a more sustained release in the slow phase, with a much lower constant ($K_{d\ slow}$ = 0.0662 vs 0.0253 h^{-1} of the negatively and positively charged formulation respectively) (Bonilla-Vidal et al., 2023). These differences could be related to its modified surface with DDAB and HA. It has been documented that HA surface modification can restrict water diffusion into the carrier matrix which subsequently slows down the drug release process (Huang et al., 2017).

In order to demonstrate the safety of APG-NLC at the ocular level, *in vitro* experiments were carried out. HCE-2 cells were used to evaluate the cytocompatibility of the APG-NLC in a corneal cell line. The results showed that free APG was safe at all the tested concentrations (0.050–0.001 $mg{\cdot}mL^{-1}$) which indicates that APG was non-toxic in this corneal epithelial cell line. Similarly, empty NLC resulted non-toxic in the majority of the assessed concentrations. This may be due to its positive charge, which produces a higher electrostatic attraction between negatively charged cell surfaces, leading to increase in oxidative stress and reactive oxygen species (ROS) (Yang et al., 2021). Furthermore, lipid components of NLC may possess affinity for cell membranes, which facilitates the interaction between them (Zhang et al., 2014). However, APG-NLC was safe in all the tested concentrations (except for the higher ones where it was slightly toxic). This effect could be related with the protective activity of APG on these cells. Some authors reported that APG was able to protect corneal cells from excessive superoxide radicals and hydrogen peroxide (Bigagli et al., 2017). Moreover, in a DED study, APG showed to protect the cells due to its anti-inflammatory activity (Liu et al., 2019). Otherwise, the internalization of the NLC was performed to evaluate their capacity to interact with HCE-2 cells by labelling APG-NLC with the fluorescent NR. In this study, it has been demonstrated that APG-NLC quickly interacted with corneal cells in the first 5 min of incubation. Furthermore, with increasing incubation time, the NLC increased its accumulation inside the cells. No changes in the morphology of the HCE-2 cells were observed, which confirmed its *in vitro* safety in comparison to toxic substances such as BAK (Kinnunen et al., 2014).

To evaluate the ocular safety of the formulation, an *in vitro* HET-CAM test was conducted. The HET-CAM test allows observation of vascular responses due to the acute effects of the test substance on the small blood vessels and soft tissue proteins of the CAM. These responses are similar to those produced by the substance in the rabbit eye, owing to the similar vascular and inflammatory framework of the eye conjunctival tissue (Valadares et al., 2021; Abdelkader et al., 2012). Other methods used to evaluate ocular tolerability, such as the bovine corneal opacity and permeability (BCOP) assay or the isolated chicken eye assay, are employed to study the opacity and permeability of the cornea (Lebrun et al., 2021). Results demonstrated that APG was irritating when directly applied to the CAM. However, both the empty and loaded NLC were non-irritating, indicating that the encapsulation strategy effectively mitigates the irritation potential of APG. These results were also confirmed by the HET-CAM TBS, a quantitative assay based on the ability of trypan blue to stain damaged or dead cells (Vinardell and García, 2000). *In vivo* testing within the eye offers advantages for studying chemical damage due to the presence of physiological response and repair mechanisms in living tissue. However, severe damage from the chemicals themselves can impede these repair processes. While *in vitro* methods are used to assess acute effects from a single application, they fail to consider the reversibility of these lesions (Valadares et al., 2021; Cazedey et al., 2009; Budai et al., 2021). The tolerance ocular test incorporates a post-treatment period to allow for healing, providing a more complete picture. While the tear layer can act as a barrier and influence the absorption of water-soluble chemicals, it can also wash away the test substance, reducing its efficacy. The HET-CAM test, while useful for assessing conjunctival damage due to its similarity to human ocular tissue, may not fully capture corneal irritation, which is a key focus of the *in vivo* tolerance test (Budai et al., 2021). For this reason, to confirm the safety of the formulations, an *in vivo* ocular tolerance assessment was carried out. The results showed that free APG caused an initial discomfort in the rabbits, but it did not cause irritation or redness on the eye. Furthermore, results confirmed that neither APG-NLC nor empty NLC caused any irritation, which demonstrates that the formulations were safe for ocular administration.

The potential activity of APG-NLC against DED was demonstrated through an *in vivo* assay based on the induction of DED by administering BAK twice daily for two weeks, followed by one-week treatment. BAK is a commonly used eye drop preservative with inherent detergent properties that destabilize the tear film's lipid layer. This leads to increased evaporation of the aqueous tear layer and decreased tear film break-up time, leaving the ocular surface vulnerable to dryness and irritation. Additionally, BAK directly targets the corneal epithelium, the outermost layer of the cornea, exhibiting a dose-dependent cytotoxic effect. BAK effects can also trigger an inflammatory response characterized by increased expression of various inflammatory markers such as interleukins and TNF-α, as well as infiltration of immune cells into the conjunctiva (Rosin and Bell, 2013; Lin et al., 2011). Chronic exposure to BAK can lead to a heightened inflammatory state, which promotes the recruitment of fibroblasts and subsequent fibrosis of the subconjunctival tissue (Rosin and Bell, 2013; Clouzeau et al., 2012). The four treatment groups studied in this work were APG-NLC, empty NLC to elucidate the effect of the lipid matrix, free APG to observe its therapeutic potential, and a commercial artificial tear based on HA as a commonly used first line treatment of DED. Three different evaluation assays were conducted to determine both the induction of DED and the efficacy of the treatments: i) Schirmer test, ii) fluorescein staining, iii) rose bengal staining. The Schirmer test constitutes a simple diagnostic procedure used to assess tear production. The test relies on the principle of capillary action, which allows the water content of tears to migrate along the length of a filter paper strip. The rate of migration along the strip corresponds to the tear production rate (Nr and Y, 2020). The results of the Schirmer test showed that APG-NLC were the treatment that attained the best score, followed by the empty NLC, indicating that both were able to restore the tear secretion of the animals. These results reveal the potential of the composition of the nanoformulations to restore tear flow *in vivo*. APG-NLC presented a significantly better score than all the other groups, probably due to APG encapsulation. APG possess anti-inflammatory properties, improving DED associated inflammation (Kashyap et al., 2018). In this study, free APG was not able to restore the tear flow which may be attributed to the high clearance of APG when it was administered as eyedrops (Lanier et al., 2021). Furthermore, regarding tear volume, the commercial solution (0.15 % HA solution) did not show significant differences against the control either due to the short-treatment period (5-days) or to HA short-lifespan at the ocular level (Semp et al., 2023).

In order to evaluate the improvement of the ocular surface, fluorescein and rose bengal staining were used. Fluorescein penetrates poorly into the lipid layer of the corneal epithelium. However, fluorescein readily binds to areas where the cell-to-cell junctions of the corneal epithelium are disrupted. This property makes it an effective tool for detecting corneal abrasions, ulcers, and other injuries (Srinivas and Rao, 2023). In this study, all the tested formulations showed a lower score than dry eye control, which means that all were able to improve the corneal epithelium. Specifically, APG-NLC and empty NLC were the treatments with higher statistical differences between dry eye control (*** $p < 0.001$). It is well known that rosehip oil possesses wound healing properties when applied to the skin, but there is no information about its ocular use (Lei et al., 2019). It has been described that rosehip oil influence on skin wound healing is hypothesized to be mediated by promoting the phenotypic transition of macrophages from the M1 to the M2 state. M1 macrophages are characterized by their pro-inflammatory activity, while M2 macrophages contribute to extracellular matrix

regeneration and the resolution of inflammation (Belkhelladi and Bougrine, 2024). Other actions such as its capacity to increase the collagen III content in wound tissue, and inhibit epithelial-mesenchymal transition during wound healing to improve scarring has been also described in dermal applications (Criollo-Mendoza et al., 2023). In this study, the lipid matrix was able to improve the corneal injuries produced by DED, which could be related to its wound healing, anti-inflammatory and antioxidant properties (Strugaia et al., 2016; Lei et al., 2019). In the same manner, when this active matrix was loaded with APG, an improvement of the corneal injuries was observed, which could be also attributed to APG anti-inflammatory and anti-oxidant properties (Kashyap et al., 2018). On the other hand, rose bengal is a dye that stains any part of the ocular surface that is not adequately covered by tear film, particularly areas lacking mucin (Srinivas and Rao, 2023; Doughty, 2013). In this study, only the nanoformulations were able to restore the tear film. This fact could be related to the lipids that are used to prepare the NLC, which usually had occlusive and moisturizing effects (Bonilla et al., 2022). The 0.15 % HA solution and free APG did not show statistically significant differences, may be due to the fast clearance that artificial tears and small molecules undergo in the ocular surface (Weng et al., 2018). In comparison to other drug delivery systems, NLC exhibit high potential for the treatment of DED. Composed of lipid assemblies, NLC exhibit high mucoadhesive properties towards corneal epithelial cells, which may extend precorneal retention time and sustained release of encapsulated therapeutics. In previous studies it has been described that NLC adhere to the glycocalyx, a protective layer on the corneal epithelium, facilitating gradual release of their lipid components into the tear film (Niamprem et al., 2019). Lipids would then integrate within the tear film lipid layer, enhancing its stability and reducing tear evaporation (Niamprem et al., 2019). Furthermore, other *in vivo* studies demonstrated that NLC exhibited prolonged precorneal film formation, promoting tear film stability under desiccated conditions and protecting corneal epithelial cells from damage. These findings suggest that NLC possess properties similar to a biomimetic tear film, offering potential as a therapeutic strategy for tear replacement and replenishment in DED treatment (Niamprem et al., 2019).

It is well-established that inflammation is part of DED pathology and it is triggered by the activation of innate immune components within ocular surface cells, a decrease in tear film stability, and an elevated tear osmolarity. For this reason, anti-inflammatory eye drops may be used but they possess associated side effects (Perez et al., 2020; Yagci and Gurdal, 2014). Therefore, *in vivo* experiments were carried out to explore the anti-inflammatory activity of APG-NLC, in which treatment and prevention of the inflammation by using SA as an inflammatory stimulus were performed. In the treatment assay, it was observed that free APG had a great anti-inflammatory response 1 h after application. APG is a flavone with a well-known anti-inflammatory activity, which decreases inflammatory markers (Ginwala et al., 2019). To date, there have been no reports indicating that APG acts as an anti-inflammatory molecule when administered ocularly. Only a few studies have demonstrated the *in vitro* capacity of APG to reduce certain inflammatory markers. For instance, it has been described that APG alleviated TNF-α-induced apoptosis in retinal ganglion cells (Fu et al., 2014). Furthermore, one of the plants that contains APG, chamomile, has shown several properties when applied ocularly (Bigagli et al., 2017). Eye drops containing chamomile and Euphrasia, showed to protect corneal epithelial cells exhibiting wound healing activity, strong antioxidant activity, and anti-inflammatory properties by decreasing COX-2, IL-1β, iNOS expression. Otherwise, empty NLC also exerted an anti-inflammatory activity 1.5 h after instillation. As mentioned above, rosehip oil has been reported to possess anti-inflammatory activity, then the reduction of the inflammation exerted by SA could be reduced. APG-NLC resulted very effective in the treatment of inflammation because of their reduction of swelling since the first 30 min of instillation. This effect could be related to the combined effect of all the components in the nanoparticles, in which the release of APG from the NLC possessed an initial burst and a posterior sustained release, increasing its anti-inflammatory properties, and the rosehip oil present in the lipid matrix could also contribute to the activity exerted. On the other hand, the *in vivo* experiment about the prevention of the inflammation highlighted the potential of APG-NLC to prevent the inflammation caused by DED. In this assessment, the free APG showed its properties at the beginning of the experiment, which could be related to its fast clearance from the ocular surface, being not able to exert its full activity. The empty formulation also showed a fast action, mainly related to the presence of rosehip oil. Finally, APG-NLC was the most effective treatment, probably due to the NLC composition. Firstly, its cationic charge and HA improved its mucoadhesion to the ocular surface, followed by the action of the lipid matrix, mainly the rosehip oil, and the initial burst release of APG. Then, it could be observed that when APG was released, the ocular inflammation score was progressively reduced, almost reaching the minimum. Therefore, after topical application, the synergy of all the components in APG-NLC produced a suitable anti-inflammatory response.

These results showed the ability of the lipid nanoparticles to revert the signs of DED. Empty NLC and APG-NLC were able to improve all the studied parameters of DED. These results could be due to the novel composition of the nanoparticles. The addition of the rosehip oil grants anti-inflammatory and antioxidant properties to NLC (Kiralan and Yildirim, 2019; Lin et al., 2017). Because of this fact, empty NLC showed interesting properties against DED. The addition of APG improved the tear secretion on the Schirmer test, probably due to its encapsulation in NLC conferring improved anti-inflammatory properties against DED symptomatology.

5. Conclusions

In summary, a novel nanotechnological approach has been developed for the effective management of DED and its associated ocular complications. This approach involves encapsulating APG within cationic NLC coated with HA, resulting in a nanosystem with suitable physical stability and sustained APG release. Extensive *in vitro* and *in vivo* assessments confirm the biocompatibility of the developed NLC, with no adverse effects on ocular tissues and demonstrated uptake by corneal cells. Additionally, APG-NLC exhibit enhanced therapeutic efficacy in DED and ocular inflammation animal models. Empty NLC also ameliorate DED signs, but the addition of APG to NLC improved tear flow and anti-inflammatory capacity. Hence, APG-NLC may represent a promising system for the treatment and prevention of DED.

CRediT authorship contribution statement

L. Bonilla-Vidal: Writing – original draft, Methodology, Investigation, Formal analysis. **M. Espina:** Writing – review & editing, Methodology, Investigation, Formal analysis. **M.L. García:** Writing – review & editing, Methodology, Funding acquisition, Conceptualization. **L. Baldomà:** Writing – review & editing, Methodology, Investigation, Funding acquisition. **J. Badia:** Writing – review & editing, Methodology, Investigation, Funding acquisition. **J.A. González:** Investigation, Conceptualization. **L.M. Delgado:** Methodology, Investigation. **A. Gliszczyńska:** Writing – review & editing, Supervision, Investigation. **E. B. Souto:** Writing – review & editing, Investigation, Formal analysis. **E. Sánchez-López:** Writing – review & editing, Supervision, Methodology, Investigation, Funding acquisition, Formal analysis.

Declaration of competing interest

Research data and results obtained are protected under patent (PCT/EP2024/052923). LB, ME, MLG and ESL hold the intellectual property of the mentioned patent.

Data availability

No data was used for the research described in the article.

Acknowledgements

This research was supported by the Spanish Ministry of Science and Innovation (PID2021-122187NB-C32) and a Llavors project (LLAV 0004). EBS acknowledges FCT—Fundação para a Ciência e a Tecnologia, I.P., in the scope of the project UIDP/04378/2020 and UIDB/04378/2020 of the Research Unit on Applied Molecular Biosciences—UCIBIO and the project LA/P/0140/ 2020 of the Associate Laboratory Institute for Health and Bioeconomy—i4HB. E.S.-L. acknowledges the support of Grants for the Requalification of the Spanish University System.

References

Abdelkader, H., Ismail, S., Hussein, A., Wu, Z., Al-Kassas, R., Alany, R.G., 2012. Conjunctival and corneal tolerability assessment of ocular naltrexone niosomes and their ingredients on the hen's egg chorioallantoic membrane and excised bovine cornea models. Int. J. Pharm. 432 (1–2), 1–10.

Abruzzo, A., Giordani, B., Miti, A., Vitali, B., Zuccheri, G., Cerchiara, T., et al., 2021. Mucoadhesive and mucopenetrating chitosan nanoparticles for glycopeptide antibiotic administration. Int. J. Pharm. 606, 120874.

Aburahma, M.H., Badr-Eldin, S.M., 2014. Compritol 888 ATO: a multifunctional lipid excipient in drug delivery systems and nanopharmaceuticals. Expert Opin. Drug Deliv. 11 (12), 1865–1883.

Agarwal, P., Craig, J.P., Rupenthal, I.D., 2021. Formulation considerations for the management of dry eye disease. Pharmaceutics. 13 (2), 207.

Alshehri, S.M., Shakeel, F., Ibrahim, M.A., Elzayat, E.M., Altamimi, M., Mohsin, K., et al., 2019. Dissolution and bioavailability improvement of bioactive apigenin using solid dispersions prepared by different techniques. Saudi Pharm J. 27 (2), 264–273.

Baiula, M., Spampinato, S., 2021. Experimental pharmacotherapy for dry eye disease: a review. J. Exp. Pharmacol. 13, 345–358.

Battaglia, L., Serpe, L., Foglietta, F., Muntoni, E., Gallarate, M., Del Pozo, R.A., et al., 2016. Application of lipid nanoparticles to ocular drug delivery. Expert Opin. Drug Deliv. 13 (12), 1743–1757.

Begley, C., Caffery, B., Chalmers, R., Situ, P., Simpson, T., Nelson, J.D., 2019. Review and analysis of grading scales for ocular surface staining. Ocul. Surf. 17 (2), 208–220.

Belkhelladi, M., Bougrine, A., 2024. Rosehip extract and wound healing: A review. J. Cosmet. Dermatol. 23 (1), 62–67.

Bernal-Chávez, S.A., Del Prado-Audelo, M.L., Caballero-Florán, I.H., Giraldo-Gomez, D. M., Figueroa-Gonzalez, G., Reyes-Hernandez, O.D., et al., 2021. Insights into terminal sterilization processes of nanoparticles for biomedical applications. Molecules 26 (7).

Bhave, A., Schulzova, V., Chmelarova, H., Mrnka, L., Hajslova, J., 2017. Assessment of rosehips based on the content of their biologically active compounds. J. Food Drug Anal. 25 (3), 681–690.

Bigagli, E., Cinci, L., D'Ambrosio, M., Luceri, C., 2017. Pharmacological activities of an eye drop containing Matricaria chamomilla and Euphrasia officinalis extracts in UVB-induced oxidative stress and inflammation of human corneal cells. J. Photochem. Photobiol. B Biol. 173, 618–625.

Bonilla, L., Espina, M., Severino, P., Cano, A., Ettcheto, M., Camins, A., et al., 2022. Lipid nanoparticles for the posterior eye segment. Pharmaceutics. 14 (1), 90.

Bonilla-Vidal, L., Świtalska, M., Espina, M., Wietrzyk, J., García, M.L., Souto, E.B., et al., 2023. Dually active apigenin-loaded nanostructured lipid carriers for cancer treatment. Int. J. Nanomed. 18, 6979–6997.

Budai, P., Kormos, É., Buda, I., Somody, G., Lehel, J., 2021. Comparative evaluation of HET-CAM and ICE methods for objective assessment of ocular irritation caused by selected pesticide products. Toxicol Vitr. 74, 105150.

Bunjes, H., Westesen, K., Koch, M.H.J., 1996. Crystallization tendency and polymorphic transitions in triglyceride nanoparticles. Int. J. Pharm. 129 (1–2), 159–173.

Carvajal-Vidal, P., Fábrega, M.J., Espina, M., Calpena, A.C., García, M.L., 2019. Development of Halobetasol-loaded nanostructured lipid carrier for dermal administration: Optimization, physicochemical and biopharmaceutical behavior, and therapeutic efficacy. Nanomedicine Nanotechnology, Biol Med. 20, 102026.

Cazedey, E.C.L., Carvalho, F.C., Fiorentino, F.A.M., Gremião, M.P.D., Salgado, H.R.N., 2009. Corrositex®, BCOP and HET-CAM as alternative methods to animal experimentation. Brazilian J Pharm Sci. 45 (4), 759–766.

Clouzeau, C., Godefroy, D., Riancho, L., Rostène, W., Baudouin, C., Brignole-Baudouin, F., 2012. Hyperosmolarity potentiates toxic effects of benzalkonium chloride on conjunctival epithelial cells in vitro. Mol. Vis. 18, 863.

Craig, J.P., Nichols, K.K., Akpek, E.K., Caffery, B., Dua, H.S., Joo, C.K., et al., 2017. TFOS DEWS II definition and classification report. Ocul. Surf. 15 (3), 276–283.

Criollo-Mendoza, M.S., Contreras-Angulo, L.A., Leyva-López, N., Gutiérrez-Grijalva, E.P., Jiménez-Ortega, L.A., Heredia, J.B., 2023. Wound healing properties of natural products: mechanisms of action. Molecules 28 (2), 598.

De Paiva, C.S., 2017. Effects of aging in dry eye. Int. Ophthalmol. Clin. 57 (2), 64.

Doughty, M.J., 2013. Rose bengal staining as an assessment of ocular surface damage and recovery in dry eye disease—A review. Contact Lens Anterior Eye. 36 (6), 272–280.

Esteruelas, G., Halbaut, L., García-Torra, V., Espina, M., Cano, A., Ettcheto, M., et al., 2022. Development and optimization of Riluzole-loaded biodegradable nanoparticles incorporated in a mucoadhesive in situ gel for the posterior eye segment. Int. J. Pharm. 612, 121379.

Fangueiro, J.F., Calpena, A.C., Clares, B., Andreani, T., Egea, M.A., Veiga, F.J., et al., 2016. Biopharmaceutical evaluation of epigallocatechin gallate-loaded cationic lipid nanoparticles (EGCG-LNs): In vivo, in vitro and ex vivo studies. Int. J. Pharm. 502 (1–2), 161–169.

Folle, C., Marqués, A.M., Díaz-Garrido, N., Espina, M., Sánchez-López, E., Badia, J., et al., 2021. Thymol-loaded PLGA nanoparticles: an efficient approach for acne treatment. J Nanobiotechnology. 19 (1), 359.

Freitas, C., Müller, R.H., 1999. Correlation between long-term stability of solid lipid nanoparticles (SLN) and crystallinity of the lipid phase. Eur. J. Pharm. Biopharm. 47 (2), 125–132.

Fu, M.-S., Zhu, B.-J., Luo, D.-W., 2014. Apigenin prevents TNF-α induced apoptosis of primary rat retinal ganglion cells. Cell. Mol. Biol. 60 (4), 37–42.

Ginwala, R., Bhavsar, R., Chigbu, D.G.I., Jain, P., Khan, Z.K., 2019. Potential role of flavonoids in treating chronic inflammatory diseases with a special focus on the anti-inflammatory activity of apigenin. Antioxidants. 8 (2), 35.

Gonzalez-Pizarro, R., Parrotta, G., Vera, R., Sánchez-López, E., Galindo, R., Kjeldsen, F., et al., 2019. Ocular penetration of fluorometholone-loaded PEG-PLGA nanoparticles functionalized with cell-penetrating peptides. Nanomedicine 14 (23), 3089–3104.

Holzchuh, R., Villa Albers, M.B., Osaki, T.H., Igami, T.Z., Santo, R.M., Kara-Jose, N., et al., 2011. Two-year outcome of partial lacrimal punctal occlusion in the management of dry eye related to Sjögren syndrome. Curr. Eye Res. 36 (6), 507–512.

Huang, D., Chen, Y.S., Rupenthal, I.D., 2017. Hyaluronic acid coated albumin nanoparticles for targeted peptide delivery to the retina. Mol. Pharm. 14 (2), 533–545.

Huang, L., Gao, H., Wang, Z., Zhong, Y., Hao, L., Du, Z., 2021. Combination nanotherapeutics for dry eye disease treatment in a rabbit model. Int. J. Nanomed. 16, 3631.

Huang, Z., Ma, C., Wu, M., Li, X., Lu, C., Zhang, X., et al., 2020. Exploring the drug-lipid interaction of weak-hydrophobic drug loaded solid lipid nanoparticles by isothermal titration calorimetry. J Nanoparticle Res. 22 (1), 1–14.

Johnson, M.E., Murphy, P.J., Boulton, M., 2006. Effectiveness of sodium hyaluronate eyedrops in the treatment of dry eye. Graefe's Arch Clin Exp Ophthalmol. 244 (1), 109–112.

Kashyap, D., Sharma, A., Tuli, H.S., Sak, K., Garg, V.K., Buttar, H.S. et al., 2018. Apigenin: A natural bioactive flavone-type molecule with promising therapeutic function. vol. 48, Journal of Functional Foods. Elsevier Ltd, pp. 457–471.

Kelly, J.D.S., Nichols, K., Sheppard, J.D., Nichols, K.K., 2023. Dry eye disease associated with Meibomian gland dysfunction: focus on tear film characteristics and the therapeutic landscape. Ophthalmol Ther. 12 (3), 1397–1418.

Khairnar, S.V., Pagare, P., Thakre, A., Nambiar, A.R., Junnuthula, V., Abraham, M.C., et al., 2022. Review on the scale-up methods for the preparation of solid lipid nanoparticles. Pharmaceutics. 14 (9), 1886.

Khuda, S.E., Nguyen, A.V., Sharma, G.M., Alam, M.S., Balan, K.V., Williams, K.M., 2022. Effects of emulsifiers on an in vitro model of intestinal epithelial tight junctions and the transport of food allergens. Mol. Nutr. Food Res. 66 (4), e2100576.

Kinnunen, K., Kauppinen, A., Piippo, N., Koistinen, A., Toropainen, E., Kaarniranta, K., 2014. Cationorm shows good tolerability on human HCE-2 corneal epithelial cell cultures. Exp Eye Res. 120, 82–89.

Kiralan, M., Yildirim, G., 2019. Rosehip (Rosa canina L.) Oil. Fruit Oils Chem Funct. 803–814.

Kumari, S., Dandamudi, M., Rani, S., Behaeghel, E., Behl, G., Kent, D., et al., 2021. Dexamethasone-loaded nanostructured lipid carriers for the treatment of dry eye disease. Pharmaceutics. 13 (6), 905.

Lagarto, A., Vega, R., Guerra, I., González, R., 2006. In vitro quantitative determination of ophthalmic irritancy by the chorioallantoic membrane test with trypan blue staining as alternative to eye irritation test. Toxicol. In Vitro 20 (5), 699–702.

Lanier, O.L., Manfre, M.G., Bailey, C., Liu, Z., Sparks, Z., Kulkarni, S., et al., 2021. Review of approaches for increasing ophthalmic bioavailability for eye drop formulations. AAPS PharmSciTech 22 (3), 1–16.

Lebrun, S., Nguyen, L., Chavez, S., Chan, R., Le, D., Nguyen, M., et al., 2021. Same-chemical comparison of nonanimal eye irritation test methods: Bovine corneal opacity and permeability, EpiOcular™, isolated chicken eye, ocular Irritection®, OptiSafe™, and short time exposure. Toxicol Vitr. 72, 105070.

Lei, Z., Cao, Z., Yang, Z., Ao, M., Jin, W., Yu, L., 2019. Rosehip oil promotes excisional wound healing by accelerating the phenotypic transition of macrophages. Planta Med. 85 (7), 563–569.

Lin, Z., Liu, X., Zhou, T., Wang, Y., Bai, L., He, H., et al., 2011. A mouse dry eye model induced by topical administration of benzalkonium chloride. Mol. Vis. 17, 264.

Lin, T.K., Zhong, L., Santiago, J.L., 2017. Anti-inflammatory and skin barrier repair effects of topical application of some plant oils. Int. J. Mol. Sci. 19 (1), 70.

Liu, P., De Wulf, O., Laru, J., Heikkilä, T., Van Veen, B., Kiesvaara, J., et al., 2013. Dissolution studies of poorly soluble drug nanosuspensions in non-sink conditions. AAPS PharmSciTech 14 (2), 748.

Liu, L., Wei, D., Xu, H., Liu, C., 2019. Apigenin ameliorates ocular surface lesions in a rat model of dry eye disease. Eur. J. Inflamm. 17.

López, E.S., Machado, A.L.L., Vidal, L.B., González-Pizarro, R., Silva, A.D., Souto, E.B., 2020. Lipid nanoparticles as carriers for the treatment of neurodegeneration associated with Alzheimer's disease and glaucoma: present and future challenges. Curr. Pharm. Des. 26 (12), 1235–1250.

López-García, J., Lehocký, M., Humpolíček, P., Sáha, P., 2014. HaCaT keratinocytes response on antimicrobial atelocollagen substrates: extent of cytotoxicity, cell viability and proliferation. J Funct Biomater. 5 (2), 57.

López-Machado, A., Díaz-Garrido, N., Cano, A., Espina, M., Badia, J., Baldomà, L., et al., 2021. Development of lactoferrin-loaded liposomes for the management of dry eye disease and ocular inflammation. Pharmaceutics. 13 (10), 1698.
Mantelli, F., Mauris, J., Argüeso, P., 2013. The ocular surface epithelial barrier and other mechanisms of mucosal protection: from allergy to infectious diseases. Curr. Opin. Allergy Clin. Immunol. 13 (5), 563–568.
Mazet, R., Yaméogo, J.B.G., Wouessidjewe, D., Choisnard, L., Gèze, A., 2020. Recent Advances in the Design of Topical Ophthalmic Delivery Systems in the Treatment of Ocular Surface Inflammation and Their Biopharmaceutical Evaluation. Pharmaceutics. 12 (6), 570.
Mofidfar, M., Abdi, B., Ahadian, S., Mostafavi, E., Desai, T.A., Abbasi, F., et al., 2021. Drug delivery to the anterior segment of the eye: A review of current and future treatment strategies. Int. J. Pharm. 607, 120924.
Niamprem, P., Milla, T.J., Schuett, B.S., Srinivas, S.P., Tiyaboonchai, W., 2019. Interaction of nanostructured lipid carriers with human meibum. Int J Appl Pharm. 11 (3), 35–42.
Niamprem, P., Teapavarapruk, P., Srinivas, S.P., Tiyaboonchai, W., 2019. Impact of nanostructured lipid carriers as an artificial tear film in a rabbit evaporative dry eye model. Cornea 38 (4), 485–491.
Nr, B., Y, R., 2020. Schirmer test. Encycl Ophthalmol. 1–2.
Ojo, A.T., Ma, C., Lee, P.I., 2020. Elucidating the effect of crystallization on drug release from amorphous solid dispersions in soluble and insoluble carriers. Int. J. Pharm. 591, 120005.
Olivo-Martínez, Y., Bosch, M., Badia, J., Baldomà, L., 2023. Modulation of the intestinal barrier integrity and repair by microbiota extracellular vesicles through the differential regulation of trefoil factor 3 in LS174T goblet cells. Nutrients 15 (11), 2437.
Peng, W., Jiang, X., Zhu, L., Li, X., Zhou, Q., Wu, Y.J.M., et al., 2022. Cyclosporine A (0.05%) ophthalmic gel in the treatment of dry eye disease: A multicenter, randomized, double-masked, phase III, COSMO trial. Drug Des. Devel. Ther. 16, 3183–3194.
Perez, V.L., Stern, M.E., Pflugfelder, S.C., 2020. Inflammatory basis for dry eye disease flares. Exp. Eye Res. 201, 108294.
Periman, L.M., Mah, F.S., Karpecki, P.M., 2020. A review of the mechanism of action of Cyclosporine A: the role of Cyclosporine A in dry eye disease and recent formulation developments. Clin. Ophthalmol. 14, 4200.
Romanová, D., Grančai, D., Jóžová, B., Božek, P., Vachálková, A., 2000. Determination of apigenin in rat plasma by high-performance liquid chromatography. J. Chromatogr. A 870 (1–2), 463–467.
Rosin, L.M., Bell, N.P., 2013. Preservative toxicity in glaucoma medication: clinical evaluation of benzalkonium chloride-free 0.5% timolol eye drops. Clin. Ophthalmol. 7, 2135.
Salminen, H., Helgason, T., Aulbach, S., Kristinsson, B., Kristbergsson, K., Weiss, J., 2014. Influence of co-surfactants on crystallization and stability of solid lipid nanoparticles. J. Colloid Interface Sci. 426, 256–263.
Sánchez-López, E., Ettcheto, M., Egea, M.A., Espina, M., Cano, A., Calpena, A.C., et al., 2018. Memantine loaded PLGA PEGylated nanoparticles for Alzheimer's disease: In vitro and in vivo characterization. J Nanobiotechnology. 16 (1), 1–16.
Sánchez-López, E., Esteruelas, G., Ortiz, A., Espina, M., Prat, J., Muñoz, M., et al., 2020. Dexibuprofen biodegradable nanoparticles: one step closer towards a better ocular interaction study. Nanomaterials 10 (4).
Semp, D.A., Beeson, D., Sheppard, A.L., Dutta, D., Wolffsohn, J.S., 2023. Artificial tears: a systematic review. Clin. Optom. 15, 27.
Shakeel, F., Alshehri, S., Ibrahim, M.A., Elzayat, E.M., Altamimi, M.A., Mohsin, K., et al., 2017. Solubility and thermodynamic parameters of apigenin in different neat solvents at different temperatures. J. Mol. Liq. 234, 73–80.
Silva, A.M., Martins-Gomes, C., Fangueiro, J.F., Andreani, T., Souto, E.B., 2019. Comparison of antiproliferative effect of epigallocatechin gallate when loaded into cationic solid lipid nanoparticles against different cell lines. Pharm. Dev. Technol. 24 (10), 1243–1249.
Souto, E.B., Mehnert, W., Müller, R.H., 2006. Polymorphic behaviour of Compritol888 ATO as bulk lipid and as SLN and NLC. J. Microencapsul. 23 (4), 417–433.
Srinivas, S.P., Rao, S.K., 2023. Ocular surface staining: Current concepts and techniques. Indian J. Ophthalmol. 71 (4), 1089.
Strugała, P., Gładkowski, W., Kucharska, A.Z., Sokół-Łętowska, A., Gabrielska, J., 2016. Antioxidant activity and anti-inflammatory effect of fruit extracts from blackcurrant, chokeberry, hawthorn, and rosehip, and their mixture with linseed oil on a model lipid membrane. Eur. J. Lipid Sci. Technol. 118 (3), 461–474.
Valadares, M.C., de Oliveira, G.A.R., de Ávila, R.I., da Silva, A.C.G., 2021. Strategy combining nonanimal methods for ocular toxicity evaluation. Methods Mol. Biol. 2240, 175–195.
Vedadghavami, A., Zhang, C., Bajpayee, A.G., 2020. Overcoming negatively charged tissue barriers: Drug delivery using cationic peptides and proteins. Nano Today 34, 100898.
Vinardell, M., García, L., 2000. The quantitive chlorioallantoic membrane test using trypan blue stain to predict the eye irritancy of liquid scintillation cocktails. Toxicol Vitr. 14 (6), 551–555.
Vinchhi, P., Patel, J.K., Patel, M.M., 2021. High-pressure homogenization techniques for nanoparticles. Emerg Technol Nanoparticle Manuf. 263–285.
Wang, M., Firrman, J., Liu, L.S., Yam, K., 2019. A review on flavonoid apigenin: Dietary intake, ADME, antimicrobial effects, and interactions with human gut microbiota. Biomed Res. Int. 7010467.
Wei, J., Mu, J., Tang, Y., Qin, D., Duan, J., Wu, A., 2023. Next-generation nanomaterials: advancing ocular anti-inflammatory drug therapy. J Nanobiotechnology. 21 (1), 1–60.
Weng, Y.-H., Ma, X.-W., Che, J., Li, C., Liu, J., Chen, S.-Z., et al., 2018. Nanomicelle-assisted targeted ocular delivery with enhanced antiinflammatory efficacy in vivo. Adv. Sci. 5 (1), 1700455.
Winther, K., Sophie, A., Hansen, V., Campbell-Tofte, J., 2016. Bioactive ingredients of rose hips (Rosa canina L) with special reference to antioxidative and anti-inflammatory properties: in vitro studies. Bot Targets Ther. 6, 23.
Xiong, C., Chen, D., Liu, J., Liu, B., Li, N., Zhou, Y., et al., 2008. A rabbit dry eye model induced by topical medication of a preservative benzalkonium chloride. Invest. Ophthalmol. Vis. Sci. 49 (5), 1850–1856.
Yagci, A., Gurdal, C., 2014. The role and treatment of inflammation in dry eye disease. Int. Ophthalmol. 34 (6), 1291–1301.
Yang, W., Wang, L., Mettenbrink, E.M., Deangelis, P.L., Wilhelm, S., 2021. Nanoparticle toxicology. Annu. Rev. Pharmacol. Toxicol. 61, 269–289.
Youshia, J., Kamel, A.O., El Shamy, A., Mansour, S., 2021. Gamma sterilization and in vivo evaluation of cationic nanostructured lipid carriers as potential ocular delivery systems for antiglaucoma drugs. Eur. J. Pharm. Sci. 163.
Zhang, W., Li, X., Ye, T., Chen, F., Yu, S., Chen, J., et al., 2014. Nanostructured lipid carrier surface modified with Eudragit RS 100 and its potential ophthalmic functions. Int. J. Nanomed. 9, 4315.
Zhang, Y., Yang, Y., Yu, H., Li, M., Hang, L., Xu, X., 2020. Apigenin protects mouse retina against oxidative damage by regulating the Nrf2 pathway and autophagy. Oxid. Med. Cell. Longev. 2020.
Zimmermann, E., Souto, E.B., Müller, R.H., 2005. Physicochemical investigations on the structure of drug-free and drug-loaded solid lipid nanoparticles (SLN) by means of DSC and 1H NMR. Pharmazie 60 (7), 508–513.

3.4. Melatonin loaded nanostructured lipid carriers for the treatment of uveal melanoma

Lorena Bonilla Vidal, Marta Espina, María Luisa García, Cinzia Cimino, Claudia Carbone, Laura Baldomà, Josefa Badia, Anna Gliszczyńska, Eliana B Souto, Elena Sánchez López.

Journal of Drug Delivery Science and Technology

2024

IF (JCR-2023) 4.5, Pharmacology & Pharmacy 60/354 (Q1)

10.1016/j.jddst.2024.106057

Journal of Drug Delivery Science and Technology 100 (2024) 106057

Contents lists available at ScienceDirect

Journal of Drug Delivery Science and Technology

journal homepage: www.elsevier.com/locate/jddst

Melatonin loaded nanostructured lipid carriers for the treatment of uveal melanoma

Lorena Bonilla-Vidal [a,b], Marta Espina [a,b], María Luisa García [a,b], Cinzia Cimino [c,d,e], Claudia Carbone [d,e], Laura Baldomà [f,g], Josefa Badia [f,g], Anna Gliszczyńska [h], Eliana B. Souto [i], Elena Sánchez-López [a,b,*]

[a] Department of Pharmacy, Pharmaceutical Technology and Physical Chemistry, University of Barcelona, 08028, Barcelona, Spain
[b] Institute of Nanoscience and Nanotechnology (IN^{2}UB), University of Barcelona, 08028, Barcelona, Spain
[c] Department of Biomedical and Biotechnological Sciences, University of Catania, Via Santa Sofia 97, 95123, Catania, Italy
[d] Laboratory of Drug Delivery Technology, Department of Drug and Health Sciences, University of Catania, Viale A. Doria 6, 95124, Catania, Italy
[e] NANOMED, Research Centre for Ocular Nanotechnology, University of Catania, Italy
[f] Department of Biochemistry and Physiology, University of Barcelona, 08028, Barcelona, Spain
[g] Institute of Biomedicine of the University of Barcelona (IBUB), Institute of Research of Sant Joan de Déu (IRSJD), 08950, Barcelona, Spain
[h] Department of Food Chemistry and Biocatalysis, Wrocław University of Environmental and Life Sciences, Norwida 25, 50-375, Wrocław, Poland
[i] UCD School of Chemical and Bioprocess Engineering, University College Dublin, Belfield, Dublin 4 D04 V1W8, Ireland

ARTICLE INFO

Keywords:
Drug delivery
Nanostructured lipid carriers
Melatonin
Uveal melanoma
Anti-inflammatory efficacy
Cytotoxicity studies

ABSTRACT

Uveal melanoma, a highly aggressive intraocular tumor and the second most common form of ocular malignancy, currently lacks effective therapeutic options. Therefore, this study addresses an unmet medical need by developing nanostructured lipid carriers (NLC) as a potential delivery system for melatonin (MEL) to target uveal melanoma. NLC were optimized for ophthalmic administration by the addition of a cationic surfactant to increase mucoadhesivity to the negatively charged ocular surface. MEL-loaded NLC (MEL-NLC) exhibited suitable particle size (<200 nm), good colloidal stability (5 months), and sustained MEL release. *In vitro* cytotoxicity assays demonstrated antiproliferative activity against uveal melanoma cells while maintaining corneal cell viability, further confirmed by *in vitro* HET-CAM test and *in vivo* ocular tolerance studies. Additionally, inflammation studies were performed since inflammation constitutes one of the main hallmarks of cancer development and progression. Consequently, MEL-NLC displayed anti-inflammatory properties. Furthermore, preliminary biodistribution results suggested their ability to reach the posterior segment of the eye, mainly the retina and the ciliary body, positioning them as a promising strategy for uveal melanoma treatment.

1. Introduction

Uveal melanoma (UM) is the second most common type of primary ocular malignancy, with an incidence ranging from 0.1 to 8.6 cases per million individuals. It is particularly prevalent among individuals of Caucasian descent and its incidence also increases with age, with the majority of cases occurring in individuals over 50 years old. Despite its relative rarity, UM is a highly aggressive cancer that poses significant challenges due to the lack of effective therapeutic options [1]. UM originates from melanocytes residing in the uvea, a pigmented layer of the eye comprising the iris (in the front chamber), choroid, and ciliary body. More than 90 % of UM develops in the choroid, while only 6 % occurs in the ciliary body and 4 % involve the iris [2,3]. Ocular treatment primarily aims to preserve vision and the eye itself, encompassing a diverse range of therapies including radiotherapy, phototherapy, and local resection, with enucleation reserved for exceptionally severe cases [4]. Despite extensive research efforts, the overall survival rate of patients with metastatic UM has remained stagnant over the past three decades. Even following successful treatment of the primary tumor, approximately 50 % of UM patients develop a metastatic disease, which typically disseminates in a heterogeneous manner. Currently, there are no effective therapies to prevent metastasis, but a rapid intervention may potentially prevent the development of lethal UM. Metastases from UM exhibit limited responsiveness to chemotherapy or targeted therapy

* Corresponding author. Department of Pharmacy, Pharmaceutical Technology and Physical Chemistry, University of Barcelona, 08028, Barcelona, Spain
E-mail address: esanchezlopez@ub.edu (E. Sánchez-López).

https://doi.org/10.1016/j.jddst.2024.106057
Received 4 June 2024; Received in revised form 2 August 2024; Accepted 8 August 2024
Available online 10 August 2024

and are typically fatal within one year of their appearance [1,3,5].

Melatonin (MEL), a ubiquitously expressed endogenous molecule, is primarily produced by the pineal gland, intestinal tract, immune system, and brain. Beyond its role in regulating circadian rhythms, MEL exhibits a broad spectrum of biological activities, influencing endocrine processes, reproductive cycles, bone metabolism, cell cycle progression, and mitochondrial function regulation [6]. Notably, MEL possesses oncostatic properties, demonstrating promising potential as an anti-cancer therapeutic agent in various malignancies. Studies conducted on UM and normal uveal melanocyte cell lines have suggested MEL selective ability to suppress the growth of UM cells while sparing normal melanocytes. Additionally, cell culture and animal model studies have provided evidence that MEL can inhibit the proliferation of both uveal and cutaneous melanoma cells. In UM patients undergoing plaque brachytherapy, MEL's antioxidant properties may offer additional benefits by counteracting the detrimental ocular side effects associated with radiation exposure [7,8]. Despite its promising properties, MEL is degraded when exposed to air and light. Studies have shown that MEL's half-life is significantly reduced when exposed to these conditions [9]. This degradation can lead to reduced effectiveness of MEL as a therapeutic agent.

In last decades, different nanocarriers with sustained drug delivery capabilities have been developed for ocular applications. These nanoscale delivery systems present few advantages in comparison to traditional drug delivery methods for treating posterior eye diseases, such as their ability to effectively target specific ocular tissues and release medication over an extended period [10,11]. Nanotechnology has the potential to improve oncology by providing innovative approaches for cancer therapy, detection, and diagnosis. This field offers the possibility of directly targeting chemotherapeutic agents to cancerous cells and tumors, guiding surgical resection, and enhancing the therapeutic efficacy of radiation and other existing treatment modalities [12,13]. Among various types of nanoparticles (NP), lipid NP have gained considerable attention owing to their ease of scale-up and low toxicity. Solid lipid nanoparticles (SLN), the first-generation lipid NP, emerged in the early 1990s. While demonstrating promising results, they exhibited limitations such as drug expulsion during storage and limited drug loading capacity. To address these shortcomings, nanostructured lipid carriers (NLC), the second-generation lipid NP, emerged. By incorporating liquid lipids into the formulation, NLC enhanced the cargo capacity of NP and improved storage stability [14–16].

Previous studies have demonstrated the potential of NLC encapsulating MEL using natural compounds as a suitable delivery system to potentially treat several types of tumors [17]. Therefore, we aimed to develop a novel formulation, MEL-NLC, designed to protect MEL from degradation and extend its short half-life, incorporating a cationic surfactant, dimethyldioactadecylammonium bromide (DDAB), in order to enhance the bioavailability of NLC when administered onto the ocular mucosa. Cationic surfactants, due to their positive charge, exhibit electrostatic attraction with the negatively charged ocular mucosa. This interaction leads to prolonged drug residence time on the ocular surface [18]. Furthermore, DDAB has a well-established safety profile in other studies for ocular delivery, demonstrating no toxicity up to a concentration of 0.5 %, in comparison to other cationic surfactants such as cetyltrimethylammonium bromide [19]. Moreover, in our previous studies using DDAB as a cationic surfactant, the formulation showed *in vitro* safety in human corneal cells, and *in vivo* ocular safety when administrated into rabbit eyes [20].

This investigation aimed to optimize a nanostructured drug delivery system utilizing cationic NLC loaded with MEL for the therapeutic management of UM. This study focused on the different *in vitro* and *in vivo* studies to assess their biocompatibility, cytotoxicity against UM cell lines, and anti-inflammatory efficacy to mitigate the inflammation related to cancer [21].

2. Materials and methods

2.1. Materials

MEL was sourced from Thermo Fisher Scientific (Massachusetts, USA). Gattefossé (Madrid, Spain) provided Compritol® 888 ATO (glyceryl distearate). Sigma Aldrich (Madrid, Spain) supplied Tween® 80 (Polysorbate 80) and Nile red (NR). Rosehip oil was obtained from Acofarma Fórmulas Magistrales (Barcelona, Spain), and DDAB from TCI Europe (Zwijndrecht, Belgium). All other reagents were of analytical grade. Water purification was achieved using a Millipore Milli-Q Plus system.

2.2. MEL-NLC preparation and optimization

The preparation of MEL-NLC was performed using the hot high-pressure homogenization technique (Homogenizer FPG 12800, Stansted, United Kingdom). First, an initial emulsion was obtained by mixing the components at 8000 rpm for 30 s using an Ultraturrax® T25 (IKA, Germany). The fabrication conditions were 85 °C, three homogenization cycles, and a pressure of 900 bar. In order to obtain a positive surface charge, increasing amounts of cationic lipid DDAB were incorporated into the optimized formulation derived from previous studies (data not shown).

2.3. Physicochemical characterization

The physicochemical characteristics of mean average size (Z_{av}) and polydispersity index (PI) were assessed using photon correlation spectroscopy (PCS) with a Zetasizer NanoZS instrument (Malvern Instruments, Malvern, UK). Measurements were conducted at 25 °C and a scattering angle of 90°. Samples were diluted 1:10 with Milli-Q water. Zeta potential (ZP) was determined by electrophoretic light scattering using the same instrument. Samples were diluted 1:20 with Milli-Q water to ensure optimal measurement conditions. All measurements were performed in triplicate to ensure data reproducibility [22,23].

Encapsulation efficiency (EE) was indirectly determined by quantifying the free drug content in the MEL-NLC dispersion [23]. Each sample was centrifugated using Amicon® Ultra 0.5 centrifugal filter device (Amicon Millipore Corporation, Ireland) at 14000 rpm for 15 min. The supernatant contained free MEL, which was quantified by high-performance liquid chromatography (HPLC). EE was determined by calculating the difference between the initial drug quantity and the amount of free drug remaining in the supernatant after centrifugation, using Eq. (1) [24]:

$$EE = \frac{Total\ amount\ of\ MEL\ -\ Free\ amount\ of\ MEL}{Total\ amount\ of\ MEL} x\,100 \qquad \text{Equation 1}$$

The quantification of MEL was carried out employing a Kromasil® C18 column (5 μm, 150 × 4.6 mm) with a mobile phase gradient. The gradient consisted of a water phase containing 2 % acetic acid and an organic phase constituted by methanol. The gradient eluted from 40 % to 60 % water phase over 5 min and returned to the initial composition in the following 5 min. The flow rate was set at 0.9 mL/min. Detection of MEL was achieved using a Waters® 2996 diode array detector at 300 nm, and data processing was performed with Empower® 3 Software [25].

2.4. Characterization of optimized MEL-NLC

2.4.1. Transmission electron microscopy

The morphology of the NLC was studied by transmission electron microscopy (TEM) on a JEOL 1010 microscope (Akishima, Japan). To visualize the morphology of MEL-NLC, negative staining was employed. Uranyl acetate (2 %) was applied to copper grids previously activated with UV light [26].

2.4.2. Interaction studies

Differential scanning calorimetry (DSC) was employed to analyse the thermal profile of MEL-NLC. DSC 823e System (Mettler-Toledo, Barcelona, Spain) was utilized. System calibration was verified using an indium pan (purity ≥99.95 %; Fluka, Switzerland), and an empty pan served as reference. Measurements were conducted within a nitrogen atmosphere with a heating ramp from 25 to 105 °C at 10 °C/min. Data analysis was performed using Mettler STARe V 9.01 dB software (Mettler-Toledo, Barcelona, Spain) [27].

The crystallinity of the samples was assessed using X-ray diffraction (XRD). Samples were positioned between 3.6 μm polyester films and irradiated with CuKα radiation (45 kV, 40 mA, λ = 1.5418 Å) in the 2θ range of 2°–60° with a step size of 0.026° and a dwell time of 200 s per step [28].

Fourier-transform infrared (FTIR) analysis of MEL-NLC was performed using a Thermo Scientific Nicolet iZ10 spectrometer equipped with an ATR diamond and a DTGS detector (Barcelona, Spain) [26].

2.5. Stability studies

MEL-NLC samples were stored at 4, 25, and 37 °C for several months. The stability of these samples was evaluated by analysing their light backscattering (BS) profile using a Turbiscan® Lab instrument. A glass cell containing 10 mL of sample was employed. Data were collected at 30-day intervals. The light source employed was a pulsed near-infrared light-emitting diode (λ = 880 nm), and the BS signal was received by a detector placed at an angle of 45° relative to the incident beam. Simultaneously, Z_{av}, PI, ZP, and EE values were determined [24].

2.6. Biopharmaceutical behaviour

To study the *in vitro* release profile of MEL from the NLC in comparison with free MEL, the direct dialysis method under sink conditions for 48 h was performed (n = 3). 9 mL of each formulation were loaded into separated dialysis bags (cellulose membrane, 12–14 kDa MWCO, 3.20/32″ diameter, Iberlabo). The bags were then immersed in phosphate-buffered saline (PBS, 0.1 M) containing 0.1 % sodium dodecyl sulphate at pH 7.4 (release media) at 37 °C (body temperature). At predetermined intervals, 0.3 mL aliquots of the release media were withdrawn and replaced with fresh media. MEL concentration in the collected samples was quantified by HPLC, and the data were subsequently analysed using various kinetic models [22,25].

2.7. Ocular tolerance

2.7.1. In vitro study: HET-CAM test and HET-CAM TBS

The HET-CAM assay was used to evaluate the *in vitro* ocular tolerance of MEL-NLC formulations, ensuring their suitability for ophthalmic administration [29]. Following Interagency Coordinating Committee on the Validation of Alternative Methods (ICCVAM) guidelines, 300 μL of each formulation (free MEL, MEL-NLC, positive control of NaOH 0.1 M, and negative control of NaCl 0.9 %) were applied to the chorioallantoic membrane of fertilized chicken eggs (3 eggs per group). Each egg was monitored for 5 min post-application, noting the onset of irritation, coagulation, and hemorrhage [30]. The ocular irritation index (OII) was calculated using Eq. (2):

$$OII = \frac{(301 - H)\cdot 5}{300} + \frac{(301 - V)\cdot 7}{300} + \frac{(301 - C)\cdot 9}{300} \qquad \text{Equation 2}$$

where H, V, and C represent time (in seconds) until the onset of hemorrhage, vasoconstriction, or coagulation, respectively. Formulations were then classified as: non-irritating (OII ≤0.9), weakly irritating (0.9 < OII ≤4.9), moderately irritating (4.9 < OII ≤8.9), or irritating (8.9 < OII ≤21).

Furthermore, at the end of the HET-CAM experiment, in order to quantify the damage of the membrane, trypan blue staining (TBS) was applied. Following topical exposure, the chorioallantoic membrane (CAM) was incubated with 1 mL of 0.1 % TBS for 1 min. Dye excess was removed by rinsing with distilled water. The stained CAM was then excised and homogenized in 5 mL formamide. The absorbance of the extract was measured spectrophotometrically at 595 nm to quantify the incorporated trypan blue. A calibration curve of TBS in formamide was used to determine the amount of absorbed dye [31].

2.7.2. In vivo study: Draize test

To validate the findings from the HET-CAM assay, the Draize primary eye irritation test was conducted on New Zealand albino rabbits. Firstly, 50 μL of each formulation were instilled into the conjunctival sac of each rabbit (n = 3/group) with a gentle massage to ensure corneal penetration. Signs of irritation (corneal opacity, conjunctival hyperaemia, chemosis, ocular discharge, and iris abnormalities) were monitored immediately, 1 h post-instillation, and at predetermined intervals (24 h, 48 h, 72 h, 7 days, and 21 days). The untreated contralateral eye served as the negative control. Draize scores were assigned based on direct observation of corneal opacity/cloudiness, iris changes, and conjunctival alterations (hyperaemia, chemosis, swelling, and discharge) [27].

2.8. Cellular experiments

2.8.1. Cell culture

Human corneal epithelial (HCE-2) cells were cultured in keratinocyte serum-free growth medium (SFM; Life Technologies, Invitrogen, GIBCO®, Paisley, UK). The medium was supplemented with bovine pituitary extract (0.05 mg/mL), epidermal growth factor (5 ng/mL) containing insulin (0.005 mg/mL), penicillin (100 U/mL), and streptomycin (100 mg/mL). Cells were cultured in flasks at 37 °C in a humidified atmosphere with 10 % CO_2 until reaching 80 % confluency [30].

Human uveal melanoma (UM 92–1) cells were cultured in RPMI-1640 medium (Euroclone, Milan, Italy), added with 10 % fetal bovine serum, 2 mM L-glutamine, 100 U/mL penicillin and 100 μg/mL streptomycin. Cells were incubated on a culture flask up to 80 % confluency at 37 °C and 10 % CO_2 [32].

2.8.2. Cell viability

The cytotoxicity of MEL-NLC was assessed using the MTT (3-(4,5-dimethylthiazol-2-yl)-2,5-diphenyltetrazolium bromide) assay. This assay measures the metabolic activity of viable cells through the reduction of the tetrazolium salt by intracellular dehydrogenases. For this, 100 μL of a cell suspension of 2×10^5 cells/mL for HCE-2, or 1×10^4 cells/mL for UM 92–1 cells, were seeded in a 96-well plate and incubated for 48 h at 37 °C in the appropriate complete medium before treatment. To mimic real corneal conditions, HCE-2 cells were exposed to various sample concentrations (1×10^{-3} - 0.1 mg/mL) for 5, 15, or 30 min, while UM 92–1 cells were incubated for 24 h. Following incubation, the medium was discarded, and a solution of MTT (0.25 % in PBS, Sigma-Aldrich Chemical Co., St. Louis, MO, USA) was added. After a 2-h incubation, the medium was replaced with 100 μL DMSO (99 % dimethyl sulfoxide, Sigma-Aldrich). Cell viability was then quantified by measuring absorbance at 560 nm using a Modulus® Microplate Photometer (Turner BioSystems Inc., Sunnyvale, CA, USA). The results were expressed as the percentage of viable cells compared to untreated control cells [28,30,33].

2.8.3. Cellular uptake

To assess MEL-NLC internalization within HCE-2 cells, 1×10^5 HCE-2 cells/mL were seeded into an eight-well chamber slide (ibidi®, Gräfelfing, Germany) until 80 % confluence. Cells were then incubated with NR labeled MEL-NLC at 37 °C for 5, 15, and 30 min. PBS washes removed non-internalized NLC, followed by fixation with 4 % paraformaldehyde (30 min, 25 °C). After additional PBS washes, nuclei were stained with 4′,6-diamidino-2-phenylindole (DAPI) during 10 min at

25 °C, cell membranes with Alexa Fluor™ 488 conjugated Wheat Germ Agglutinin (WGA, 30 min, 25 °C). Images were captured using a Leica Thunder Imager DMI8 (Leica Microsystems GmbH, Wetzlar, Germany) equipped with a 63x oil immersion objective lens [34,35].

2.9. In vivo studies

2.9.1. Anti-inflammatory efficacy

To evaluate MEL-NLC ability to mitigate ocular inflammation, both preventative and anti-inflammatory efficacy tests were conducted on New Zealand male albino rabbits (n = 3/group). Formulations included MEL-NLC, free MEL, and NaCl 0.9 % (control).

For the prevention study, 50 μL of each formulation was applied to the rabbit's eye. After 30 min, 50 μL of 0.5 % sodium arachidonate (SA) in PBS was instilled to induce inflammation (right eye), with the left eye serving as control. In the anti-inflammatory study, SA was applied 30 min before the formulation. Ocular evaluations were performed from initial application to 210 min following a modified Draize scoring system [29,30].

2.9.2. Ocular in vivo biodistribution

In vivo biodistribution studies were conducted by administering two separate 50 μL doses of either MEL-NLC loaded with NR or NR solution into the conjunctival sac of New Zealand albino rabbits, separated by 5 min of clearance. After 3 h, the animals were euthanized, and the eyes were enucleated. Each eye was then immersed in 4 % paraformaldehyde in PBS for 24 h and then transferred to a solution containing 4 % paraformaldehyde and 30 % sucrose. After another 24 h, the eyes were embedded in O.C.T. compound cryo-embedding medium and frozen at −80 °C. Subsequently, frozen eyes were sliced using a cryostat (Leica CM 3050 S, Leica Microsystems GmbH, Wetzlar, Germany) and the cellular nuclei were stained with DAPI to visualize cell structures. Fluorescence images were acquired using a Leica Thunder Imager DMI8 (Leica Microsystems GmbH, Wetzlar, Germany) and analysed using ImageJ software [36].

2.10. In vivo experimentation

All procedures adhered to the guidelines of the UB Ethical Committee for Animal Experimentation and followed current regulations (Decree 214/97, Gencat) and protocols were approved under the code 326/19. Furthermore, all the *in vivo* procedures comply with the ARRIVE guidelines and were carried out in accordance with the U.K. Animals (Scientific Procedures) Act, 1986 and associated guidelines, EU Directive 2010/63/EU for animal experiments.

New Zealand white male rabbits (2–2.5 kg, San Bernardo farm, Navarra, Spain) were kept in individual cages with free access to food and water in a controlled 12/12 h light/dark cycle under veterinary supervision. Rabbits were anesthetized with intramuscular administration of ketamine HCl (35 mg/kg) and xylazine (5 mg/kg) and euthanized by an overdose of sodium pentobarbital (200 mg/kg).

2.11. Statistical analysis

Statistical analyses were conducted using GraphPad Prism 9. Two-way ANOVA followed by Tukey's post-hoc test was used for multiple group comparisons, while Student's t-test was used for pairwise comparisons. Data are presented as mean ± standard deviation (SD). Statistical significance was set at $p < 0.05$.

3. Results

3.1. MEL-NLC preparation and optimization

The optimized formulation obtained in a previous study was used for the present investigation (7.5 % lipid phase, 5 % surfactant, and 0.05 % MEL). Based on this formulation, increasing amounts of the cationic lipid DDAB were added to study its influence on the physicochemical properties of the nanoparticles (Table 1). The optimized formulation was selected based on the physicochemical parameters, aiming to obtain ZP values greater than +15 mV and PI below 0.3. Following these criteria, the cationic optimized formulation was the one containing 0.07 % of DDAB.

3.2. Characterization of optimized MEL-NLC

TEM analysis revealed that MEL-NLC exhibited almost spherical and soft morphologies (Fig. 1A and B), with particle sizes below 200 nm, corroborating the findings obtained by PCS (Fig. 1C). Moreover, as predicted by the obtained ZP values (+20 mV), no particle aggregation was found (Fig. 1D).

DSC was employed to investigate the melting behavior of the lipid mixtures and MEL-NLC. Thermograms (Fig. 2A) showed an endothermal peak of 72.22 °C for the lipid mixture with MEL, and the lipid mixture without MEL had a melting point of 73.14 °C. Regarding to the formulations, the empty and the loaded NLC presented a melting temperature of 72.89 °C and 72.30 °C respectively. It can be observed that the incorporation of MEL on the bulk lipid or into the particles provoked a decrease in the melting temperature, which could be related to the accommodation of MEL into the lipid crystals, becoming more amorphous [37,38]. The melting enthalpy for the lipid mixture without MEL was 121.29 Jg^{-1}, for the lipid mixture with MEL was 119.44 Jg^{-1}, for the empty NLC was 93.76 Jg^{-1}, and for the MEL-NLC 91.91 Jg^{-1}. It was observed that the samples with a higher crystalline structure possessed the higher values, while the most amorphous sample was MEL-NLC with the lower melting enthalpy [38]. MEL melting transition was characterized by an endothermal peak at 118.52 °C ($\Delta H = 134.70$ Jg^{-1}) followed by decomposition.

FTIR spectroscopy was employed to examine the interactions between the drug, surfactant, and lipid matrix (Fig. 2B). MEL characteristic peaks were located at 3303 cm^{-1} (N-H), 1629 cm^{-1} (C=O), 1555 cm^{-1} (C-O), and 1212 cm^{-1} (C-N). The NLC (empty and loaded) spectra displayed a prominent peak at 1100 cm^{-1}, which corresponds to the surfactant [39]. Discrete MEL peaks were observed in the MEL-NLC spectrum at 1000-1200 cm^{-1}. No evidence of strong bonds between MEL, the lipid phase, and the surfactant were detected.

XRD profiles demonstrated the physical state of MEL encapsulated in NLC (Fig. 2C). MEL and the lipid bulk exhibit a crystalline structure as evidenced by prominent and sharp peaks. Certain characteristic MEL peaks (19.13, 19.94, and 24.27°) exhibited a minor intensity in the MEL-NLC profile, suggesting that the drug exists in a dissolved state within the NLC (molecular dispersion). The crystallinity of the other formulation components was also examined. The physical mixture of the lipids and the physical mixture containing MEL revealed two pronounced peaks at 21.17° (2θ) i.e., $d = 0.42$ nm and 23.09° (2θ) i.e., $d = 0.46$ nm. These peaks indicated the second stable form of triacylglycerols, the β' phase. MEL-NLC had a highly intense peak at 19.36° (2θ) i.e., $d = 0.46$ nm and 21.23° (2θ) i.e., $d = 0.42$ nm, followed by another peak at 23.27° (2θ) i.e., $d = 0.38$ nm, indicating suitable stability of the formulation [37,40,41]. In contrast, two of these peaks, at 19.36° and 23.22°, were observed in the empty NLC with lower intensity.

Table 1
Effect of cationic lipid on the physicochemical parameters.

DDAB (%)	Z_{av} ± SD (nm)	PI ± SD	ZP ± SD (mV)
0.010	293.7 ± 4.2	0.199 ± 0.032	−3.4 ± 0.2
0.025	200.4 ± 2.4	0.219 ± 0.003	0.9 ± 0.3
0.050	179.5 ± 2.6	0.193 ± 0.004	10.2 ± 0.2
0.060	172.1 ± 1.5	0.231 ± 0.013	13.1 ± 0.6
0.070	**164.2 ± 0.6**	**0.212 ± 0.013**	**19.2 ± 0.7**
0.080	135.7 ± 0.8	0.364 ± 0.011	20.6 ± 0.4
0.090	130.4 ± 0.2	0.480 ± 0.009	24.1 ± 0.6

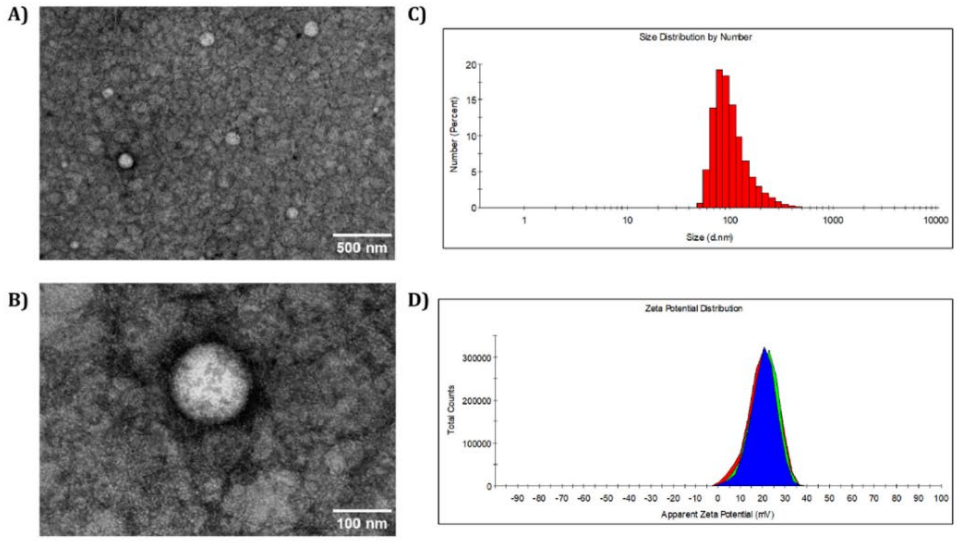

Fig. 1. Physicochemical and morphological characterization. (**A**) TEM images with scale bar 500 nm; (**B**) TEM images with scale bar 100 nm; (**C**) Histogram of average size distribution measured by dynamic light scattering; (D) Zeta potential plot measured by laser-Doppler electrophoresis.

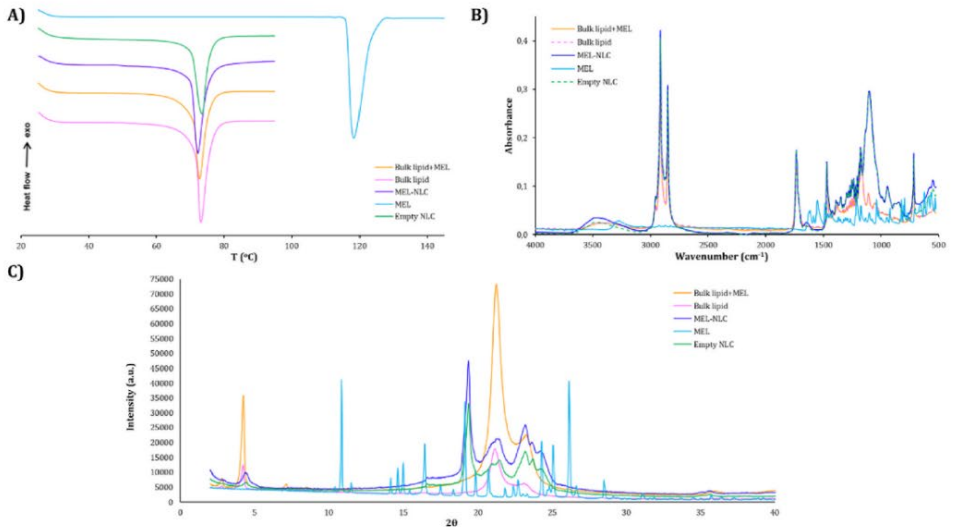

Fig. 2. Interaction studies of MEL-NLC and their components. (A) DSC curves; (B) FTIR analysis; (C) XRD patterns.

3.3. *Stability studies*

Stability studies were conducted using BS profiles of each sample at different temperatures (Fig. 3). BS profiles provide insights into the destabilization mechanisms, including sedimentation, aggregation, and agglomeration. In this context, BS profiles of MEL-NLC were investigated at 4, 25, and 37 °C. MEL-NLC formulation demonstrated stability at 4 °C for a period of 5 months, whilst at 25 °C, stability lasted for 15 days (BS differences >10 %). Physicochemical parameters remained consistent at 4 °C throughout the investigation (Table 2). The optimal storage temperature of 4 °C was consequently chosen.

3.4. *Biopharmaceutical behaviour*

The *in vitro* release profile of MEL from the NLC exhibits a slow and sustained release kinetics, indicative of a prolonged drug delivery formulation (Fig. 4). The best fit model for free MEL was exponential plateau ($r^2 = 0.9873$) and for MEL-NLC was the two-phase association ($r^2 = 0.9845$). The MEL solution achieved the 100 % before the first 7 h following a zero-order kinetic, while MEL-NLC reached the *plateau* after the first 24 h approximately a 77 % adhering to a first-order kinetic. The liberation of MEL from MEL-NLC showed a first fast release, with a higher kinetic constant (K_d) and a shorter half-life time ($t_{1/2}$, the time

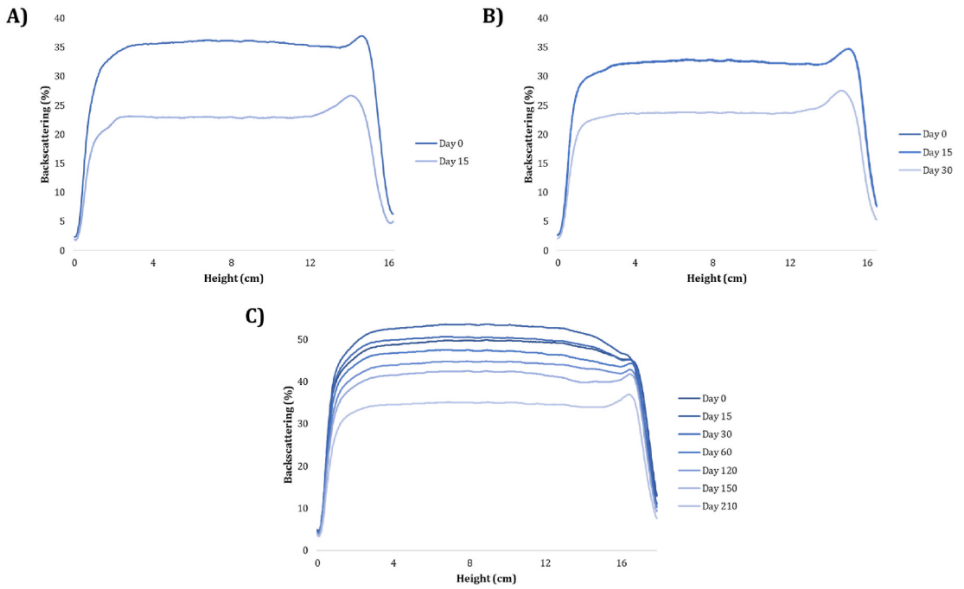

Fig. 3. Backscattering profiles of MEL-NLC stored at (A) 37 °C, (B) 25 °C, and (C) 4 °C.

Table 2
Physicochemical parameters of MEL-NLC stored at different temperatures.

Temperature (°C)	Day	Z_{av} ± SD (nm)	PI ± SD	ZP ± SD (mV)	EE ± SD (%)
	0	168.9 ± 2.4	0.216 ± 0.007	19.1 ± 0.5	79.8 ± 0.2
37	15	193.8 ± 0.3	0.232 ± 0.007	14.4 ± 0.3	75.1 ± 0.5
25	15	170.1 ± 0.7	0.200 ± 0.004	18.0 ± 0.1	78.4 ± 0.1
	30	230.4 ± 3.1	0.224 ± 0.035	11.7 ± 0.5	76.1 ± 0.2
4	15	162.0 ± 1.2	0.218 ± 0.012	20.3 ± 0.9	77.9 ± 0.6
	30	163.1 ± 0.8	0.221 ± 0.007	20.5 ± 0.4	78.4 ± 0.1
	60	167.8 ± 1.5	0.213 ± 0.015	21.2 ± 0.9	76.8 ± 0.8
	120	166.2 ± 1.4	0.218 ± 0.021	19.2 ± 0.4	78.9 ± 0.3
	150	167.1 ± 0.8	0.234 ± 0.007	20.5 ± 0.4	77.1 ± 0.4
	210	179.9 ± 0.1	0.268 ± 0.016	18.7 ± 0.4	77.6 ± 0.1

required for the initial concentration to decrease to one-half). In contrast, the slow and sustained release phase of MEL-NLC had the slowest K_d and the highest $t_{1/2}$.

3.5. Ocular tolerance

Ocular tolerance was assayed *in vitro* and *in vivo* (Fig. 5) examining free MEL and MEL-NLC. Previous to this assay, DDAB ocular tolerance was assessed by HET-CAM at the maximum concentration reported as safe in other studies (0.5 %), confirming that it was non-irritant. Afterwards, the developed NLC resulted non-irritant neither *in vitro* nor *in vivo*, while the free MEL resulted moderately irritating *in vitro* and non-irritant *in vivo*. Although the HET-CAM test is useful for assessing eye irritation from water-soluble and surfactant-based substances, and that it is useful to identify non-irritant compounds, such as MEL-NLC, occasionally it could show a poor correlation with the *in vivo* assays, as it is observed in the case of free MEL, which resulted non-irritant *in vivo* [42].

3.6. Cellular experiments

3.6.1. Cell viability

The cytotoxicity of free MEL and MEL-NLC formulations was determined on HCE-2 cells to assess their compatibility with corneal cells following topical application (Fig. 6A). Samples were incubated for 5, 15, and 30 min to simulate the *in vivo* contact between the formulation and the human cornea. Cell viability was assessed using ISO 10993-5 guidelines, where viability above 80 % indicates non-cytotoxicity, 60–80 % weak cytotoxicity, 40–60 % moderate cytotoxicity, and below 40 % indicates strong cytotoxicity. Results demonstrated that free MEL exhibited minimal cytotoxic effects on HCE-2 cells, with viability remaining above 80 % for all tested concentrations and incubation times. Otherwise, the most concentrated dilutions of MEL-NLC (0.1 mg/mL) resulted moderately toxic at all the incubation times, which could be related to the high electrostatic interaction between the negatively charged surface with the cationic NLC [43]. All the other concentrations resulted weakly toxic for the corneal cells.

The cytotoxic effect exerted on the tumoral cells is shown in Fig. 6B. It can be observed that in most of the studied concentrations, MEL-NLC showed a significantly higher antitumoral effect than the free MEL, probably, because of the slow release of MEL and the increased cell penetration of MEL-NLC, leading to a higher cytotoxic effect. In the diluted concentrations, free MEL did not show toxicity to the UM cells after 24 h.

3.6.2. Cellular uptake

The cellular uptake of MEL-NLC was investigated in the HCE-2 cell line. Following various incubation times, the fluorescent NLC were visualized by fluorescence microscopy. The nucleus was stained with DAPI and the cell membrane with Alexa Fluor™ 488-WGA. The merged

A)

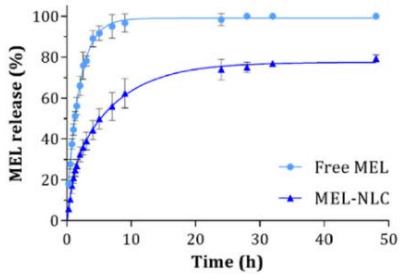

B)

Parameter	Free MEL	MEL-NLC
K_d (h^{-1})	0.520	$K_{d\ fast}$ = 1.146 $K_{d\ slow}$ = 0.140
$t_{1/2}$ (h)	1.134	$t_{1/2\ fast}$ = 0.605 $t_{1/2\ slow}$ = 4.941
Plateau **(%)**	98.97	77.42
r^2	0.9873	0.9845

Fig. 4. *In vitro* release profile of free MEL against MEL-NLC performed by triplicate. (A) Release profile graphical representation of MEL-NLC vs free MEL carried out for 48 h. Results were expressed on drug accumulative release percentage (%) vs sampling time point (h), (B) adjustment to a two-phase association (MEL-NLC) and exponential plateau model (free MEL).

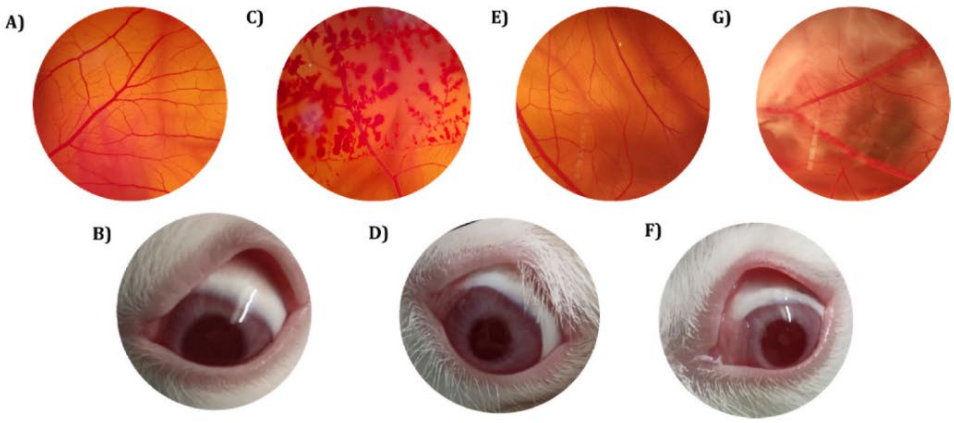

Fig. 5. *In vitro* and *in vivo* irritation assay. (A–B) Negative control, NaCl 0.9 % and untreated contralateral eye respectively, (C) Positive control, NaOH 0.1 M, (D–E) Free MEL and (F–G) MEL-NLC.

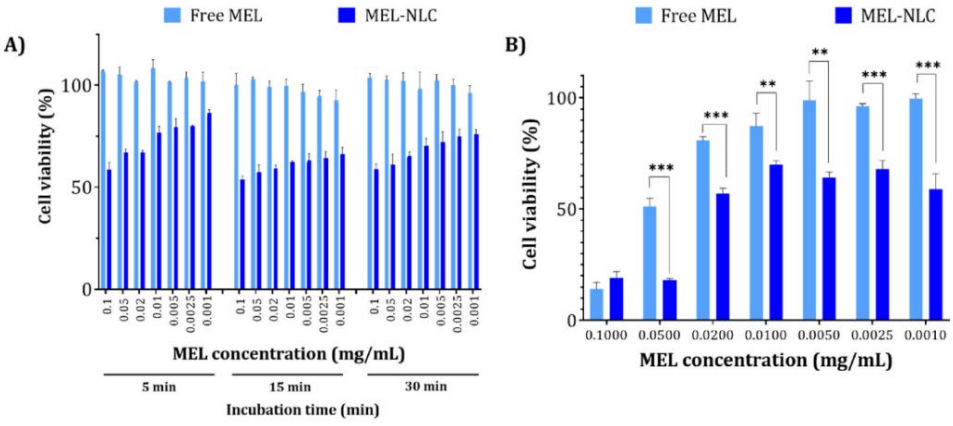

Fig. 6. Cell viability assays on HCE-2 and UV-92-1 cells, experiments were assessed in triplicate, and the experiments were repeated up to 5 times. The results were expressed as the percentage of viable cells compared to untreated control cells. (A) Effect of free MEL and MEL-NLC on the viability of HCE-2 cells at 5, 15 and 30 min, (B) Cytotoxic effects of free MEL and MEL-NLC on UM-92-1 cells at 24 h.

images (Fig. 7) revealed the presence of MEL-NLC inside the cells, mainly in the cytoplasm, indicating that the particles successfully penetrated the corneal cells without disrupting their morphology, such as vacuolization caused by benzalkonium chloride [44]. Additionally, the fluorescence signal intensified with increasing incubation time. Analysis using Interactive 3D Surface Plot in ImageJ confirmed this observation and demonstrated that cells incubated with MEL-NLC for 30 min exhibited higher fluorescence intensity compared to those incubated for 5 or 15 min. No fluorescence was detected in control cells.

3.7. In vivo experiments

3.7.1. Anti-inflammatory efficacy

To evaluate the anti-inflammatory efficacy of MEL-NLC *in vivo*, the capacity to prevent and treat ocular inflammation was investigated.

The efficacy of NLC in preventing inflammation was examined. Treatments were administered 30 min before exposure to SA, and the severity of inflammation was assessed. Fig. 8A demonstrates a significant reduction in inflammation after 30 min exposure to SA. Free MEL exhibited a slower reduction in corneal swelling compared to MEL-NLC. This difference can be attributed to tear clearance, which rapidly removes free MEL from the ocular surface. In contrast, MEL-NLC exhibit enhanced adhesion to the cornea, enabling them to remain in the ocular environment for a longer timepoints, thereby providing sustained anti-inflammatory effects. Furthermore, MEL-NLC demonstrated significant differences compared to the positive control and free MEL over time ($p < 0.001$).

The efficacy of NLC as a treatment for inflammation was further evaluated *in vivo*. Treatments were administered 30 min after SA exposure, and the severity of inflammation was assessed at various time points. Fig. 8B shows a significant reduction in inflammation within 120 min following MEL-NLC administration. This slower but effective anti-inflammatory response can be attributed to the controlled release of NLC. Otherwise, free MEL showed a faster onset of anti-inflammatory activity compared to MEL-NLC. This difference can be attributed to the controlled release of MEL from NLC, which prolongs its therapeutic effect but delays its initial delivery.

3.7.2. In vivo biodistribution

To visualize the distribution of MEL-NLC after topical ophthalmic

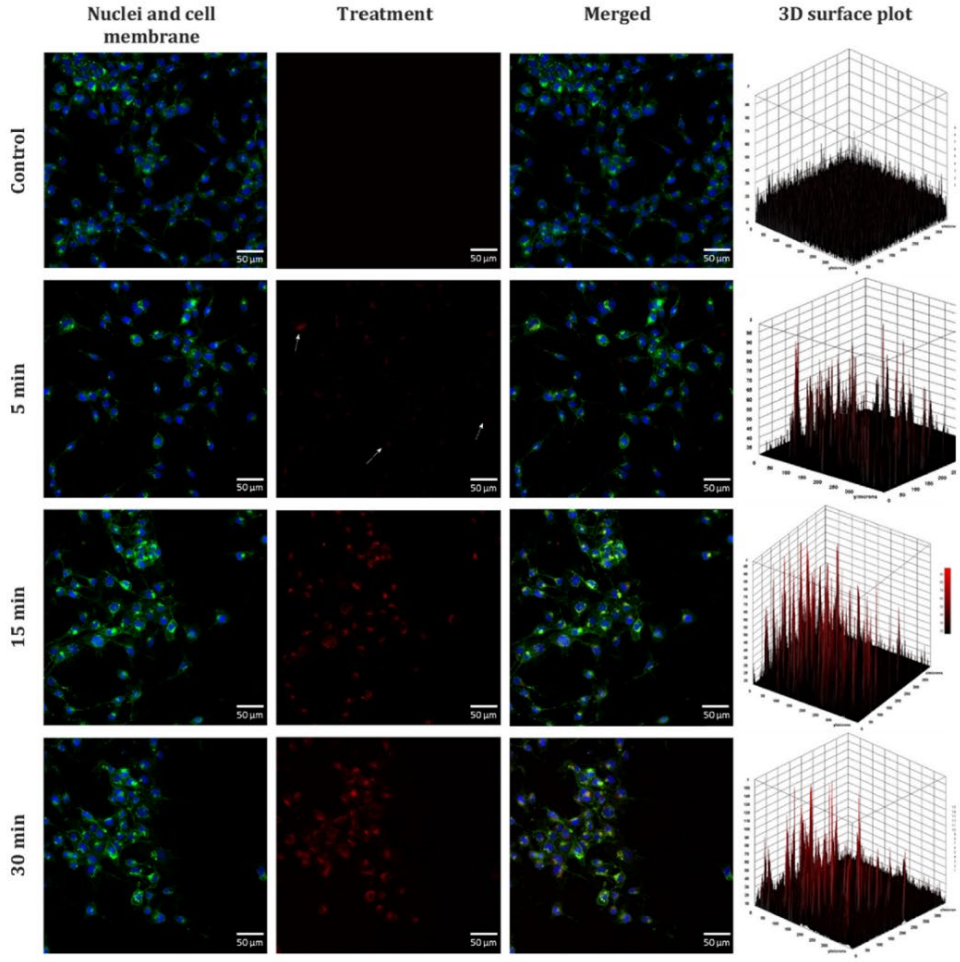

Fig. 7. Cellular uptake of MEL-NLC in HCE-2 at different incubation time (5, 15, or 30 min). White arrows highlight the samples localization, scale bar 50 µm.

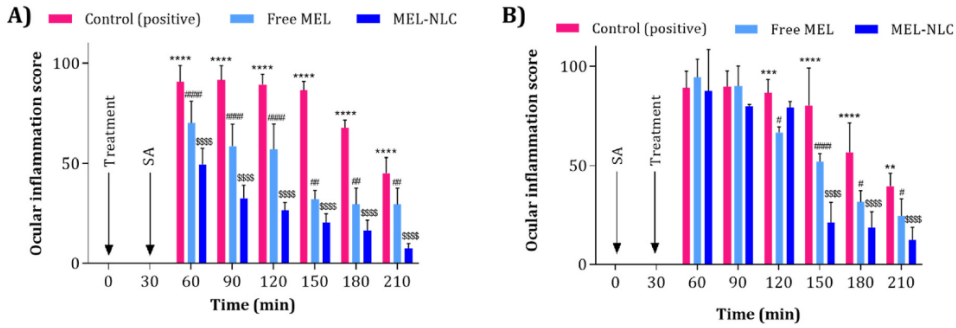

Fig. 8. Comparison of ocular anti-inflammatory efficacy of free MEL an MEL-NLC. (A) Inflammation prevention, (B) inflammation treatment. Values are expressed as mean ± SD; **p < 0.01, ***p < 0.005, and ****p < 0.001 significantly lower effect of free MEL than the inflammatory effect induced by SA; $$$$p < 0.001 significantly lower effect of MEL-NLC than the inflammatory effect induced by SA; #p < 0.05, ##p < 0.01 and ####p < 0.001 significantly lower effect of MEL-NLC than the free MEL.

administration, NR, a lipophilic probe, was encapsulated into NLC, resulting in the formation of MEL-NLC-NR. Topical administration of both MEL-NLC-NR and free NR solution was performed on New Zealand albino rabbits to investigate the *in vivo* biodistribution. After 3 h, animals were sacrificed, and their eyes were collected and subsequently sliced. Whole eye images were analysed, and their fluorescence intensity was quantified in order to stablish the biolocalization of the formulation. Fluorescence microscopy analysis revealed that MEL-NLC-NR appeared to accumulate in the posterior segment of the eye, specifically in the retina. Fig. 9A shows statistical differences between the 3 studied groups. Control eyes showed some retinal autofluorescence, mainly caused by the photoreceptors and retinal pigment epithelium [45]. Moreover, no statistically significant differences in the mean fluorescent intensity (MFI) between NR and the control were found indicating that no NR was able to achieve posterior segment tissues after 3 h. Moreover, MEL-NLC-NR showed significant differences between both control and NR, which indicates that the formulation achieved the inner tissues of the eye, specifically, the retina (Fig. 9B).

4. Discussion

UM is a rare type of ocular cancer, in which approximately a 50 % of patients develop metastases [5]. In the present study, a formulation loading MEL into a cationic rosehip-based NLC has been developed. Based on a prior formulation developed, the incorporation of a cationic surfactant shifted surface charge towards a positive, probably enhancing MEL-NLC adhesion to the ocular mucosa and promoting their bioavailability upon topical administration. This is particularly advantageous due to the negatively charged mucus layer that coats the corneal surface. In this area, cationic surfactants facilitate electrostatic interactions between the positively charged nanoparticle surface and the anionic ocular mucosa, leading to a prolonged drug residence time. Among cationic surfactants, DDAB demonstrated minimal ocular toxicity and reduced irritation potential compared to other cationic surfactants [46,47].

To optimize the concentration of DDAB in the formulation, incremental amounts were incorporated. The preferable amount of DDAB should achieve suitable physicochemical parameters for ocular delivery, such as a small size below 200 nm, PI under 0.3 and a ZP around +20 mV [16]. Increasing amounts of DDAB leaded to smaller particle sizes, which could be related to the reduction of the surface tension [48]. PI was maintained around 0.2 until 0.08 % DDAB, whereas at higher concentrations increased over 0.3. ZP varied from negative to positive surface charge, in which the concentrations up to 0.07 % DDAB produced a ZP around +20 mV. Based on these parameters, the optimal DDAB amount was 0.07 % since it accomplished suitable physicochemical parameters suitable for ocular administration.

Using this formulation, interaction studies demonstrated the successful incorporation of MEL into NLC [49]. DSC analysis revealed that MEL-NLC exhibited the lowest melting point, indicating a highly amorphous state, probably due to the incorporation of the drug inside the amorphous lipid structure. This could prevent expulsion of the drug from the nanoparticles during storage [50]. In comparison to the

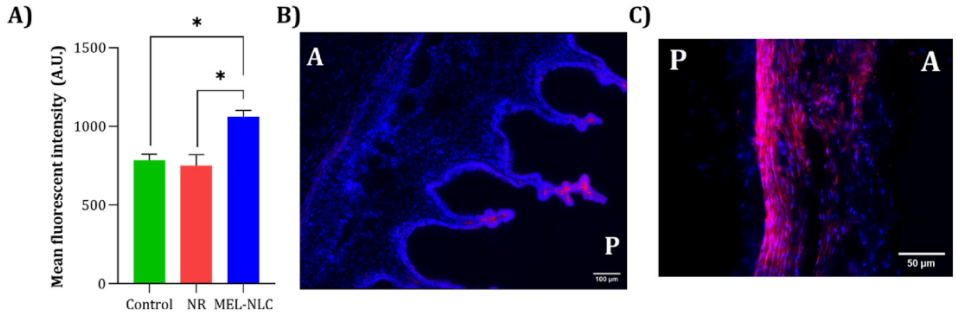

Fig. 9. Biodistribution studies performed in New Zealand rabbits. (A) Comparison of mean fluorescent intensity on the posterior eye part of a control, NR solution and MEL-NLC labeled to NR. (B) Fluorescent image of a rabbit ciliary processes treated with MEL-NLC-NR (in red) showed with a scale bar of 100 µm. (C) Fluorescent image of a rabbit sclera treated with MEL-NLC-NR (in red) showed with a scale bar of 50 µm. (For interpretation of the references to colour in this figure legend, the reader is referred to the Web version of this article.)

negatively charged NLC, the cationic formulation presented higher melting enthalpies for all the mixtures (bulk lipid, empty NLC or loaded NLC). This fact indicates that the positive formulation shifts towards a more crystalline structure, since higher energy was necessary to achieve the melting point, thus leading to a reduced stability in comparison to the prior formulation [17,40]. Further analysis employing FTIR spectroscopy indicated the absence of covalent bonds between MEL and the lipid matrix, suggesting that their interaction was primarily mediated by non-covalent forces, such as hydrogen bonds and hydrophobic interactions [51]. Additionally, XRD studies showed characteristic peaks of the stable forms of triacylglycerols, known as the β and β′ forms [37,40,41]. However, the formulation showed a reduced stability in comparison to the negatively charged NLC from previous studies, which was 16 months at 4 °C, probably due to the increase in the crystallinity degree caused by this DDAB addition [17]. Moreover, the samples at higher temperatures (25 and 37 °C) showed a short stability, which could be related to their Brownian motion, increasing their collision frequency, facilitating their destabilization [52]. Furthermore, MEL-NLC demonstrated sustained *in vitro* release, in contrast to MEL solution, which exhibited a rapid release profile. Release studies revealed that MEL solution achieved its *plateau* rapidly, reaching approximately 100 % drug release within the first few hours. In contrast, MEL-NLC required approximately 24 h to reach its *plateau*, releasing approximately 78 % of the drug into the receptor medium. In comparison to previous studies [17], in which the negatively charged formulation was prepared, the initial burst phase was much faster in the positively formula, with a higher K_d and a lower $t_{1/2}$ (K_d of 1.15 vs 0.32 h^{-1}, and $t_{1/2}$ of 0.60 vs 2.16 h from positive and negative formulation respectively). Furthermore, the prolonged release phase was faster in the positive formula (K_d of 0.14 vs 0.06 h^{-1}, and $t_{1/2}$ of 4.94 vs 11.52 h from positive and negative formulation respectively). Other studies reported differences between the release of different drugs from lipid nanoparticles regarding their composition. Specifically, Zoubari et al. [53] found that the addition of a different lipid into the formulation resulted in a faster drug release due to the less organized lipid matrix, making softer particles. Regarding to the kinetic order, the free drug adhered to a zero-order kinetic, in which the drug is released at a constant rate [54]. Otherwise, MEL-NLC adhered to a first-order kinetic, in which the amount of drug released is proportional to the amount of remaining drug in the matrix. Thus, the amount of active released tends to decrease in function of time, creating a sustained and slow release [55]. This kinetics were also observed by Shafiei et al. [56] in their polymeric film incorporating metronidazole, in which the drug was released slowly during a week, reaching the plateau after 4 days. Our results among to the stability and interaction studies could mean that the addition of the cationic surfactant DDAB could result in a more ordered lipid structure, which decreased its stability, and increased MEL release, which could be favourable in order to achieve higher amounts in a faster manner into the inner tissues of the eye.

To assess ocular safety of the formulated drug, *in vitro* and *in vivo* evaluations were performed. The *in vitro* HET-CAM test revealed that MEL-NLC exhibited no irritation upon direct application to the chorioallantoic membrane. Additionally, the HET-CAM TBS assay, a quantitative method based on trypan blue uptake to assess cell viability, confirmed the lack of significant cellular damage induced by MEL-NLC. Free MEL resulted moderately irritating *in vitro*, fact that other studies have also reported [57]. However, this data could be related to the use of organic solvents or surfactants that are necessary to ensure MEL solubilization [58]. Subsequently, an *in vivo* ocular Draize test was conducted to further evaluate the formulations safety. The results demonstrated that free MEL and MEL-NLC did not cause any ocular irritation or redness in animal eyes, indicating their safety for ocular administration.

Moreover, *in vitro* studies confirmed that free MEL was non-toxic in corneal cells in all the studied concentrations. These findings agreed with the role of MEL into the eye under physiological conditions, in which mainly MEL is a regulator of physiological circadian rhythm processes [59]. Regarding to the formulation, it was found that with 5 min incubation time, the concentrations up to 0.01 mg/mL MEL-NLC resulted non-toxic. These results were significant due to the real residence time of formulations into the ocular surface, which usually is very reduced due to the nasolacrimal clearance [60,61]. Otherwise, when incubation time was increased, the formulation showed a weak toxicity in all the tested concentrations. This effect could be attributed to several factors, including the positive charge of the lipid NLC, which promotes electrostatic interaction with the negatively charged cell surfaces. This interaction could lead to an increase in oxidative stress and reactive oxygen species (ROS) [62]. Additionally, NLC exhibit high affinity for cells, facilitating their interaction [63]. These facts were observed during the internalization study, in which from the first 5 min until 30 min incubation time, MEL-NLC were internalized into the cells, increasing the fluorescence signal at longer timepoints. Furthermore, in despite cell viability assays resulted in a weak toxicity, the morphology of the cells did not change or showed vacuolization, which is related to toxic substances in corneal cells [44].

In order to assess the potential activity of the nanoformulation against UM, cytotoxicity was assessed in UM cells. For free MEL, the most concentrated dilutions caused cytotoxic effects. Previous studies reported that MEL in UM cells was active in a range of 0.1–10 nM [64]. However, in our studies, the concentrations able to achieve cytotoxic effects were higher which may be due to the increased cell density used (3×10^3 vs 1×10^4 cells/well respectively). It has been reported that when higher cell density is used, it could result in lower cytotoxicity [65]. Regarding MEL-NLC, the two most concentrated dilutions resulted in high cytotoxicity (<20 % cell viability), while the other tested dilutions were moderately cytotoxic (40–60 % cell viability). The higher cytotoxicity could be related to the increased release of MEL inside the tumoral cells, improving its bioavailability and therapeutic efficacy. Furthermore, other investigations have reported that UM cells express transmembrane receptors for MEL, and its membrane receptor agonists inhibited the growth of UM cells even at low concentrations [7]. These findings could also contribute to the highest activity of MEL-NLC, as in addition to the high penetration of NLC into cells, non-encapsulated MEL or the initial burst release of MEL could also be effective by reaching the membrane receptors of the UM cells.

Inflammation is a hallmark of cancer development and progression, involving a complex interplay between immune cells, stromal cells, and tumor microenvironment [66]. The cells contributing to cancer-associated inflammation are relatively genetically stable, exhibiting lower rates of drug resistance compared to cancer cells themselves. Therefore, targeting inflammation represents a promising strategy for both cancer prevention and therapy [67]. Despite decades of research, the precise role of inflammation in UM progression remains poorly understood. UM tumors exhibit an inflammatory phenotype characterized by abundance of immune mediators and proinflammatory cytokines in their surrounding microenvironment [68]. For this reason, the potential anti-inflammatory activity of MEL-NLC was performed. In the treatment and prevention assays, it was observed that MEL had a great anti-inflammatory action. It is well known that MEL possesses protective properties against various ocular disorders, including photokeratitis, cataract, retinopathy of prematurity, and ischemic/reperfusion injury [69]. Additionally, MEL has been shown to mitigate retinal damage associated with glaucoma and diabetes [70]. In this area, Meng et al. [71] explored the anti-inflammatory activity of MEL after a corneal alkali injury in mice model. They reported that the infiltration of inflammatory cells and pro-inflammatory cytokines, such as TNF-α, IL-1β and IL-6 were reduced after MEL treatment. In another study, ocular uveitis was induced with an injection of lipopolysaccharide (LPS) and posteriorly treated with MEL. It was observed that the leakage of cells and proteins decreased. Also, MEL treatment protected the retinal structure and decreased NOS activity, lipid peroxidation and TNF-α [70]. Otherwise, MEL-NLC showed greater anti-inflammatory activity, probably because of the increased delivery of MEL into the ocular

tissues, and its prolonged release.

Finally, *in vivo* biodistribution confirmed the ability of MEL-NLC to reach the inner tissues of the eye. Mainly, the formulation showed high affinity for the retina, and also it was retained in the ciliary processes. Its relatively high penetration could be related to the small size of the nanocarrier, its lipid matrix nature, and its improved mucoadhesion properties because of the cationic surface charge. Other studies confirmed that NLC were able to increase drug penetration rate, increasing drug levels into ocular tissues [72]. Moreover, numerous studies have highlighted the enhanced interaction of cationic nanoparticles with the ocular surface [73–76]. For instance, a study investigated the mucoadhesive properties of cationic nanoparticles loaded with an antifungal drug. The results revealed a strong interaction between the negatively charged mucins of the ocular surface and the nanoparticles, demonstrating their potential for targeted drug delivery to ocular tissues [73]. These findings are relevant due to the location of UM tumors, which are the ciliary body and choroids [4]. As MEL-NLC had an increased accumulation on the inner tissues of the eye, the formulation could be able to target these tumors and release MEL, increasing its therapeutic activity.

5. Conclusions

This study introduces a novel formulation of cationic lipid nanoparticles capable of encapsulating MEL for topical ophthalmic administration. MEL-NLC exhibit suitable physicochemical characteristics, including particle size below 200 nm, monomodal size distribution, spherical shape, and suitable stability. Encapsulation of MEL within NLC significantly enhanced its therapeutic efficacy, both *in vitro* and *in vivo*, demonstrating potent preventive and therapeutic anti-inflammatory activities. Furthermore, *in vitro* studies demonstrated selective cytotoxicity in uveal melanoma cells and *in vivo* biodistribution studies using fluorescent-labeled NLC suggested their ability to penetrate to the posterior ocular segment, potentially targeting uveal melanoma.

CRediT authorship contribution statement

Lorena Bonilla-Vidal: Writing – original draft, Methodology, Investigation. **Marta Espina:** Writing – review & editing, Supervision. **María Luisa García:** Methodology, Investigation, Funding acquisition. **Cinzia Cimino:** Writing – review & editing, Methodology. **Claudia Carbone:** Writing – review & editing, Methodology. **Laura Baldomà:** Methodology, Investigation, Funding acquisition. **Josefa Badia:** Methodology, Investigation, Funding acquisition. **Anna Gliszczyńska:** Writing – review & editing, Supervision. **Eliana B. Souto:** Methodology, Investigation, Funding acquisition. **Elena Sánchez-López:** Writing – review & editing, Supervision, Methodology, Investigation, Funding acquisition.

Declaration of competing interest

The authors declare that they have no known competing financial interests or personal relationships that could have appeared to influence the work reported in this paper.

Data availability

No data was used for the research described in the article.

Acknowledgment

This research was supported by the Ministerio de Ciencia, Innovación y Universidades (**MICIU**) under the reference PID2021-122187NB-C32. E.S.-L. acknowledges the support of Grants for the Requalification of the Spanish University System.

References

[1] E.S. Rantala, M.M. Hernberg, S. Piperno-Neumann, H.E. Grossniklaus, T.T. Kivelä, Metastatic uveal melanoma: the final frontier, Prog. Retin. Eye Res. 90 (2022) 101041.
[2] K.N. Smit, M.J. Jager, A. de Klein, E. Kiliç, Uveal melanoma: towards a molecular understanding, Prog. Retin. Eye Res. 75 (2020) 100800.
[3] J. Yang, D.K. Manson, B.P. Marr, R.D. Carvajal, Treatment of uveal melanoma: where are we now? Ther Adv Med Oncol 10 (2018).
[4] M.J. Jager, C.L. Shields, C.M. Cebulla, M.H. Abdel-Rahman, H.E. Grossniklaus, M. H. Stern, et al., Uveal melanoma, Nat. Rev. Dis. Prim. 6 (1) (2020) 24.
[5] R.D. Carvajal, J.J. Sacco, M.J. Jager, D.J. Eschelman, R. Olofsson Bagge, J. W. Harbour, et al., Advances in the clinical management of uveal melanoma, Nat. Rev. Clin. Oncol. 20 (2) (2023) 99–115.
[6] F. Moradkhani, M. Moloudizargari, M. Fallah, N. Asghari, H. Heidari Khoei, M. H. Asghari, Immunoregulatory role of melatonin in cancer, J. Cell. Physiol. 235 (2) (2020) 745–757.
[7] A. Hagström, Omar R. Kal, P.A. Williams, G. Stålhammar, The rationale for treating uveal melanoma with adjuvant melatonin: a review of the literature, BMC Cancer 22 (1) (2022) 1–17.
[8] Omar R. Kal, A. Hagström, G. Stålhammar, Adjuvant melatonin for uveal melanoma (AMUM): protocol for a randomized open-label phase III study, Trials 24 (1) (2023) 1–14.
[9] V. Lopes, J. Assis, T. Ribeiro, G. de Castro, M. Pacheco, L. Borges, et al., Melatonin loaded lecithin-chitosan nanoparticles improved the wound healing in diabetic rats, Int. J. Biol. Macromol. 162 (2020) 1465–1475.
[10] L. Xie, W. Yue, K. Ibrahim, J. Shen, A long-acting curcumin nanoparticle/in situ hydrogel composite for the treatment of uveal melanoma, Pharmaceutics 13 (9) (2021) 1335.
[11] K. Bilmin, K.J. Synoradzki, A.M. Czarnecka, M.J. Spałek, T. Kujawska, M. Solnik, et al., New perspectives for eye-sparing treatment strategies in primary uveal melanoma, Cancers 14 (1) (2022) 134.
[12] A. Narvekar, C. Rich, A. Savinainen, I.K. Kim, Nanoparticles for the treatment of uveal melanoma, Uveal Melanoma Biol Manag. (2021) 135–149.
[13] H. Sabit, M. Abdel-Hakeem, T. Shoala, S. Abdel-Ghany, M.M. Abdel-Latif, J. Almulhim, et al., Nanocarriers: a reliable tool for the delivery of anticancer drugs, Pharmaceutics 14 (8) (2022) 1566.
[14] S. Nasirizadeh, B. Malaekeh-Nikouei, Solid lipid nanoparticles and nanostructured lipid carriers in oral cancer drug delivery, J. Drug Deliv. Sci. Technol. 55 (2020) 101458.
[15] L. Bayón-Cordero, I. Alkorta, L. Arana, Application of Solid Lipid Nanoparticles to improve the efficiency of anticancer drugs, Nanomaterials 9 (3) (2019) 474.
[16] L. Bonilla, M. Espina, P. Severino, A. Cano, M. Ettcheto, A. Camins, et al., Lipid nanoparticles for the posterior eye segment, Pharmaceutics 14 (1) (2022) 90.
[17] L. Bonilla-Vidal, M. Świtalska, M. Espina, J. Wietrzyk, M.L. García, E.B. Souto, A. Gliszczyńska, E. Sánchez-López, Antitumoral melatonin-loaded nanostructured lipid carriers, Nanomedicine (2024) 1–16.
[18] J.F. Fangueiro, A.C. Calpena, B. Clares, T. Andreani, M.A. Egea, F.J. Veiga, et al., Biopharmaceutical evaluation of epigallocatechin gallate-loaded cationic lipid nanoparticles (EGCG-LNs): in vivo, in vitro and ex vivo studies, Int. J. Pharm. 502 (1–2) (2016) 161–169.
[19] A.M. Silva, C. Martins-Gomes, J.F. Fangueiro, T. Andreani, E.B. Souto, Comparison of antiproliferative effect of epigallocatechin gallate when loaded into cationic solid lipid nanoparticles against different cell lines, Pharmaceut. Dev. Technol. 24 (10) (2019) 1243–1249.
[20] L. Bonilla-Vidal, M. Espina, M.L. García, L. Baldomà, J. Badia, J.A. González, et al., Novel nanostructured lipid carriers loading Apigenin for anterior segment ocular pathologies, Int. J. Pharm. 658 (2024) 124222.
[21] J. Hou, M. Karin, B. Sun, Targeting cancer-promoting inflammation — have anti-inflammatory therapies come of age? Nat. Rev. Clin. Oncol. 18 (5) (2021) 261–279.
[22] G. Esteruelas, L. Halbaut, V. García-Torra, M. Espina, A. Cano, M. Ettcheto, et al., Development and optimization of Riluzole-loaded biodegradable nanoparticles incorporated in a mucoadhesive in situ gel for the posterior eye segment, Int. J. Pharm. 612 (2022) 121379.
[23] E. Sánchez-López, G. Esteruelas, A. Ortiz, M. Espina, J. Prat, M. Muñoz, et al., Dexibuprofen biodegradable nanoparticles: one step closer towards a better ocular interaction study, Nanomaterials 10 (4) (2020).
[24] X. Llorente, G. Esteruelas, L. Bonilla, M.G. Agudelo, I. Filgaira, D. Lopez-Ramajo, et al., Riluzole-loaded nanostructured lipid carriers for hyperproliferative skin diseases, Int. J. Mol. Sci. 24 (9) (2023) 8053.
[25] E. Sánchez-López, M. Ettcheto, M.A. Egea, M. Espina, A. Cano, A.C. Calpena, et al., Memantine loaded PLGA PEGylated nanoparticles for Alzheimer's disease: in vitro and in vivo characterization, J. Nanobiotechnol. 16 (1) (2018) 1–16.
[26] F. Elmsmari, J.A. González Sánchez, F. Duran-Sindreu, R. Belkadi, M. Espina, M. L. García, et al., Calcium hydroxide-loaded PLGA biodegradable nanoparticles as an intracanal medicament, Int. Endod. J. 54 (11) (2021) 2086–2098.
[27] R. Galindo, E. Sánchez-López, M.J. Gómara, M. Espina, M. Ettcheto, A. Cano, et al., Development of peptide targeted PLGA-PEGylated nanoparticles loading Licochalcone-A for ocular inflammation, Pharmaceutics 14 (2) (2022) 285.
[28] C. Folle, A.M. Marqués, N. Díaz-Garrido, M. Espina, E. Sánchez-López, J. Badia, et al., Thymol-loaded PLGA nanoparticles: an efficient approach for acne treatment, J. Nanobiotechnol. 19 (1) (2021) 359.
[29] R. Gonzalez-Pizarro, P. Carvajal-Vidal, L. Halbault Bellowa, A.C. Calpena, M. Espina, M.L. García, In-situ forming gels containing fluorometholone-loaded polymeric nanoparticles for ocular inflammatory conditions, Colloids Surf. B Biointerfaces 175 (2019) 365–374.

[30] A. López-Machado, N. Díaz-Garrido, A. Cano, M. Espina, J. Badia, L. Baldomà, et al., Development of lactoferrin-loaded liposomes for the management of dry eye disease and ocular inflammation, Pharmaceutics 13 (10) (2021) 1698.
[31] A. Lagarto, R. Vega, I. Guerra, R. González, In vitro quantitative determination of ophthalmic irritancy by the chorioallantoic membrane test with trypan blue staining as alternative to eye irritation test, Toxicol. Vitro 20 (5) (2006) 699–702.
[32] C. Cimino, E. Sánchez López, A. Bonaccorso, L. Bonilla, T. Musumeci, J. Badia, et al., In vitro and in vivo studies of ocular topically administered NLC for the treatment of uveal melanoma, Int. J. Pharm. 660 (2024) 124300.
[33] Y. Olivo-Martínez, M. Bosch, J. Badia, L. Baldomà, Modulation of the intestinal barrier integrity and repair by microbiota extracellular vesicles through the differential regulation of trefoil factor 3 in LS174T goblet cells, Nutrients 15 (11) (2023) 2437.
[34] E.S. López, A.L.L. Machado, L.B. Vidal, R. González-Pizarro, A.D. Silva, E.B. Souto, Lipid nanoparticles as carriers for the treatment of neurodegeneration associated with Alzheimer's disease and glaucoma: present and future challenges, Curr. Pharmaceut. Des. 26 (12) (2020) 1235–1250.
[35] R. Gonzalez-Pizarro, G. Parrotta, R. Vera, E. Sánchez-López, R. Galindo, F. Kjeldsen, et al., Ocular penetration of fluorometholone-loaded PEG-PLGA nanoparticles functionalized with cell-penetrating peptides, Nanomedicine 14 (23) (2019) 3089–3104.
[36] S. Swetledge, R. Carter, R. Stout, C.E. Astete, J.P. Jung, C.M. Sabliov, Stability and ocular biodistribution of topically administered PLGA nanoparticles, Sci. Rep. 11 (1) (2021) 1–11.
[37] E.B. Souto, W. Mehnert, R.H. Müller, Polymorphic behaviour of Compritol 888 ATO as bulk lipid and as SLN and NLC, J. Microencapsul. 23 (4) (2006) 417–433.
[38] H. Bunjes, K. Westesen, M.H.J. Koch, Crystallization tendency and polymorphic transitions in triglyceride nanoparticles, Int. J. Pharm. 129 (1–2) (1996) 159–173.
[39] X. Fu, W. Kong, Y. Zhang, L. Jiang, J. Wang, J. Lei, Novel solid–solid phase change materials with biodegradable trihydroxy surfactants for thermal energy storage, RSC Adv. 5 (84) (2015) 68881–68889.
[40] C. Freitas, R.H. Müller, Correlation between long-term stability of solid lipid nanoparticles (SLN) and crystallinity of the lipid phase, Eur. J. Pharm. Biopharm. 47 (2) (1999) 125–132.
[41] E. Zimmermann, E.B. Souto, R.H. Müller, Physicochemical investigations on the structure of drug-free and drug-loaded solid lipid nanoparticles (SLN) by means of DSC and 1H NMR, Pharmazie 60 (7) (2005) 508–513.
[42] A.M. da Nóbrega, E.N. Alves, R. de Farias Presgrave, R.N. Costa, I.F. Delgado, Determination of eye irritation potential of low-irritant products: comparison of in vitro results with the in vivo draize rabbit test, Braz. Arch. Biol. Technol. 55 (3) (2012) 381–388.
[43] M. Adabi, M. Naghibzadeh, M. Adabi, M.A. Zarrinfard, S.S. Esnaashari, A. M. Seifalian, et al., Biocompatibility and nanostructured materials: applications in nanomedicine. Artif Cells, Nanomedicine, Biotechnol. 45 (4) (2017) 833–842.
[44] K. Kinnunen, A. Kauppinen, N. Piippo, A. Koistinen, E. Toropainen, K. Kaarniranta, Cationorm shows good tolerability on human HCE-2 corneal epithelial cell cultures, Exp. Eye Res. 120 (2014) 82–89.
[45] C. Pole, H. Ameri, Fundus autofluorescence and clinical applications, J. Ophthalmic Vis. Res. 16 (3) (2021) 432–461.
[46] M. Koutsoviti, A. Siamidi, P. Pavlou, M. Vlachou, Recent advances in the excipients used for modified ocular drug delivery, Mater 14 (15) (2021) 4290.
[47] A. Vedadghavami, C. Zhang, A.G. Bajpayee, Overcoming negatively charged tissue barriers: drug delivery using cationic peptides and proteins, Nano Today 34 (2020) 100898.
[48] N. Sharma, P. Madan, S. Lin, Effect of process and formulation variables on the preparation of parenteral paclitaxel-loaded biodegradable polymeric nanoparticles: a co-surfactant study, Asian J. Pharm. Sci. 11 (3) (2016) 404–416.
[49] A.T. Ojo, C. Ma, P.I. Lee, Elucidating the effect of crystallization on drug release from amorphous solid dispersions in soluble and insoluble carriers, Int. J. Pharm. 591 (2020) 120005.
[50] A. Khosa, S. Reddi, R.N. Saha, Nanostructured lipid carriers for site-specific drug delivery, Biomed. Pharmacother. 103 (2018) 598–613.
[51] Z. Huang, C. Ma, M. Wu, X. Li, C. Lu, X. Zhang, et al., Exploring the drug-lipid interaction of weak-hydrophobic drug loaded solid lipid nanoparticles by isothermal titration calorimetry, J. Nanoparticle Res. 22 (1) (2020) 1–14.
[52] A. Hutin, N. Lima, F. Lopez, M. Carvalho, Stability of silica nanofluids at high salinity and high temperature, Powders 2 (1) (2022) 1–20.
[53] G. Zoubari, S. Staufenbiel, P. Volz, U. Alexiev, R. Bodmeier, Effect of drug solubility and lipid carrier on drug release from lipid nanoparticles for dermal delivery, Eur. J. Pharm. Biopharm. 110 (2017) 39–46.
[54] X. Li, Q. Li, C. Zhao, Zero-order controlled release of water-soluble drugs using a marker pen platform, ACS Omega 6 (21) (2021) 13774–13778.
[55] M. Luciano, Mathematical models of drug release, in: Strategies to Modify the Drug Release from Pharmaceutical Systems, Woodhead Publishing, 2015, pp. 63–86.
[56] F. Shafiei, M. Ghavami-Lahiji, T.S.J. Kashi, F. Najafi, Drug release kinetics and biological properties of a novel local drug carrier system, Dent. Res. J. 18 (2021) 94.
[57] J.H. Ahn, H Do Kim, S.M. Abuzar, J.Y. Lee, S.E. Jin, E.K. Kim, et al., Intracorneal melatonin delivery using 2-hydroxypropyl-β-cyclodextrin ophthalmic solution for granular corneal dystrophy type 2, Int. J. Pharm. 529 (1–2) (2017) 608–616.
[58] V. Andrés-Guerrero, P. Alarma-Estrany, I.T. Molina-Martínez, A. Peral, R. Herrero-Vanrell, J. Pintor, Ophthalmic formulations of the intraocular hypotensive melatonin agent 5-MCA-NAT, Exp. Eye Res. 88 (3) (2009) 504–511.
[59] A. Crooke, F. Huete-Toral, B. Colligris, J. Pintor, The role and therapeutic potential of melatonin in age-related ocular diseases, J. Pineal Res. 63 (2) (2017) e12430.
[60] S.S. Chrai, T.F. Patton, A. Mehta, J.R. Robinson, Lacrimal and instilled fluid dynamics in rabbit eyes, J. Pharmaceut. Sci. 62 (7) (1973) 1112–1121.
[61] A. Subrizi, E.M. del Amo, V. Korzhikov-Vlakh, T. Tennikova, M. Ruponen, A. Urtti, Design principles of ocular drug delivery systems: importance of drug payload, release rate, and material properties, Drug Discov. Today 24 (8) (2019) 1446–1457.
[62] W. Yang, L. Wang, E.M. Mettenbrink, P.L. Deangelis, S. Wilhelm, Nanoparticle toxicology, Annu. Rev. Pharmacol. Toxicol. 61 (2021) 269–289.
[63] W. Zhang, X. Li, T. Ye, F. Chen, S. Yu, J. Chen, et al., Nanostructured lipid carrier surface modified with Eudragit RS 100 and its potential ophthalmic functions, Int. J. Nanomed. 9 (2014) 4315.
[64] D.N. Hu, J.E. Roberts, Melatonin inhibits growth of cultured human uveal melanoma cells, Melanoma Res. 7 (1) (1997) 27–31.
[65] E.A. Carreño, Alberto Avp, C.A.M. de Souza, H.L. de Mello, A. Henriques-Pons, L. A. Alves, Considerations and technical pitfalls in the employment of the MTT assay to evaluate photosensitizers for photodynamic therapy, Appl. Sci. 11 (6) (2021) 2603.
[66] H. Zhao, L. Wu, G. Yan, Y. Chen, M. Zhou, Y. Wu, et al., Inflammation and tumor progression: signaling pathways and targeted intervention, Signal Transduct. Targeted Ther. 6 (1) (2021) 1–46.
[67] N. Singh, D. Baby, J. Rajguru, P. Patil, S. Thakkannavar, V. Pujari, Inflammation and cancer, Ann. Afr. Med. 18 (3) (2019) 126.
[68] S. Liau, J.Z. Wang, E. Zagarella, P. Paulus, N.H.Q.H. Dang, T. Rawling, et al., An update on inflammation in uveal melanoma, Biochimie 212 (2023) 114–122.
[69] J. Blasiak, R.J. Reiter, K. Kaarniranta, Melatonin in retinal physiology and pathology: the case of age-related macular degeneration, Oxid. Med. Cell. Longev. 2016 (2016) 6819736.
[70] P.H. Sande, D. Dorfman, D.C. Fernandez, M. Chianelli, A.P. Domínguez Rubio, A. M. Franchi, et al., Treatment with melatonin after onset of experimental uveitis attenuates ocular inflammation, Br. J. Pharmacol. 171 (24) (2014) 5696–5707.
[71] J. Meng, B. Lin, S. Huang, Y. Li, P. Wu, F. Zhang, et al., Melatonin exerts anti-angiogenic and anti-inflammatory effects in alkali-burned corneas, Ann. Transl. Med. 10 (8) (2022), 432–432.
[72] S.P. Balguri, G.R. Adelli, S. Majumdar, Topical ophthalmic lipid nanoparticle formulations (SLN, NLC) of indomethacin for delivery to the posterior segment ocular tissues, Eur. J. Pharm. Biopharm. 109 (2016) 224–235.
[73] A.M. Mohsen, Cationic polymeric nanoparticles for improved ocular delivery and antimycotic activity of terconazole, J. Pharmaceut. Sci. 111 (2) (2022) 458–468.
[74] A.R. Fernandes, L.B. Vidal, E. Sánchez-López, T. dos Santos, P.L. Granja, A.M. Silva, et al., Customized cationic nanoemulsions loading triamcinolone acetonide for corneal neovascularization secondary to inflammatory processes, Int. J. Pharm. 623 (2022) 121938.
[75] R. Yan, L. Xu, Q. Wang, Z. Wu, H. Zhang, L. Gan, Cyclosporine A nanosuspensions for ophthalmic delivery: a comparative study between cationic nanoparticles and drug-core mucus penetrating nanoparticles, Mol. Pharm. 18 (12) (2021) 4290–4298.
[76] P. Nirbhavane, L. Moksha, G. Sharma, T. Velpandian, B. Singh, O.P. Katare, Cationic nano-lipidic carrier mediated ocular delivery of triamcinolone acetonide: a preclinical investigation in the management of uveitis, Life 13 (4) (2023) 1057.

3.5. Nanostructured lipid carriers co-encapsulating Apigenin and Melatonin: an innovative strategy against cancer

Lorena Bonilla Vidal, Marta Świtalska, Marta Espina, Joanna Wietrzyk, Maria Luisa García, Eliana B Souto, Anna Gliszczyńska, Elena Sánchez López.

Materials & Design

IF (JCR- 2023) 7.6, Materials Science, Multidisciplinary 80/438 (Q1)

Enviado

Nanostructured lipid carriers co-encapsulating Apigenin and Melatonin: an innovative strategy against cancer

Lorena Bonilla-Vidal[1,2]; Marta Świtalska [3]; Marta Espina [1,2]; Joanna Wietrzyk [3]; María Luisa García [1,2]; Eliana B Souto [4]; Anna Gliszczyńska[5*]; Elena Sánchez-López [1,2*]

[1] Department of Pharmacy, Pharmaceutical Technology and Physical Chemistry, University of Barcelona, 08028 Barcelona, Spain
[2] Institute of Nanoscience and Nanotechnology (IN^{2}UB), University of Barcelona, 08028 Barcelona, Spain
[3] Department of Experimental Oncology, Hirszfeld Institute of Immunology and Experimental Therapy, Polish Academy of Sciences, Weigla 12, 53-114 Wrocław, Poland
[4] UCD School of Chemical and Bioprocess Engineering, University College Dublin, Belfield, Dublin 4, D04 C1P1, Ireland
[5] Department of Food Chemistry and Biocatalysis, Wrocław University of Environmental and Life Sciences, Norwida 25, 50-375 Wrocław, Poland

*corresponding authors and equal contribution: esanchezlopez@ub.edu; anna.gliszczynska@upwr.edu.pl

Abstract

Cancer threatens the lives of about 9 million people every year globally, making it one of the biggest causes of death. However, current cancer treatments are frequently associated with significant adverse event profiles and can exhibit limitations in therapeutic efficacy. Therefore, the combination of the pharmaceutical properties of the natural flavone Apigenin (APG) and the neurohormone Melatonin (MEL), could represent a key combination therapy for tumoral processes. However, both possess low aqueous solubility and high light degradation. To overcome these limitations, APG and MEL are here proposed for their dual-loading into nanostructured lipid carriers (NLC) based on rosehip oil, in order to increase the bioavailability and efficacy of these two drugs. Optimization, physicochemical characterization, biopharmaceutical behaviour, and in vitro studies were assessed and compared to the single-loaded NLC. The optimized formulation co-encapsulating APG and MEL owned suitable physicochemical properties, with an appropriate stability. Biopharmaceutical behaviour studies demonstrated that both compounds were released from NLC in a prolonged and sustained manner. Cytotoxicity studies showed great potential and selective cytotoxicity in tumoral cell lines, especially in the leukaemia cell line. This novel and natural treatment could open a new therapeutical window in cancer treatment.

Keywords

Lipid nanoparticles; Apigenin; Melatonin, cancer; natural compounds, co-encapsulation.

1. Introduction

Cancer remains a global health concern, being one of the leading causes of premature death worldwide. In 2020, around 19 million people were diagnosed with cancer, leading to approximately 10 million deaths [1,2]. Conventional cancer therapies, including chemotherapy and radiotherapy, often exhibit adverse effects and suboptimal treatment outcomes. Specifically, chemotherapy is frequently administered to over 50 % of cancer patients, but it can simultaneously impact both healthy and cancerous cells, causing significant side effects. Moreover, these therapies can induce chemoresistance, impeding their effectiveness over time [3,4]. As a result, there is an urgent need for the development of innovative therapeutic strategies to address these limitations.

In previous studies, the natural flavone Apigenin (APG) and the neurohormone Melatonin (MEL), have shown their promising activity against several cancer cell lines [5,6]. APG is a natural flavonoid, with a extremely low toxicity, that has shown a significant potential in the prevention and therapy of tumoral processes [7]. Despite of its anti-cancer activity, the combination of other drugs with APG may concurrently activate multiple cell signalling pathways. Several studies have shown that combination therapy with APG in various types of cancer, not only enhances the effectiveness of chemotherapy, but also reduces its side effects by targeting multiple cell signalling pathways [8]. APG is mainly known for influencing apoptotic pathways, such as TRAIL, MAPK, Akt and JAK-STAT signalling [9]. In this way, MEL is an endogen neurohormone that possesses anticancer and oncostatic properties mediated by different mechanisms of action. Several studies indicated that MEL used in combination with other anticancer therapies, was able to improve the drug sensitivity of tumoral cells, including solid and liquid tumours, and reducing its side effects, protecting non-tumorigenic cells from the toxicity of chemodrugs [10–12]. Furthermore, it possesses several molecular pathways, such as inhibition of apoptosis in healthy cells to protect them, modulation of autophagy, and inhibition of angiogenesis and metastasis [13,14]. For these reasons, the combination of APG and MEL could constitute a new tool for cancer treatment. Despite the great potential of this combination, the main challenge relies on the fact that both molecules suffer from low bioavailability because of the degradation by light, fast clearance and low aqueous solubility in the case of MEL, and a high metabolization and low aqueous solubility in the case of APG [15,16].

In recent years, pharmaceutical research has been focused on the development of nanotechnological systems for several applications, particularly in the field of drug delivery. Nanocarriers are designed to deliver drugs to specific tissues with enhanced therapeutic efficacy and reduced side effects [17]. These nanocarriers overcome the limitations of conventional therapies by improving drug solubility, enhancing pharmacokinetics, and enabling targeted delivery. In particular, lipid nanoparticles have garnered significant attention for cancer therapy due to the possibility of passive targeting, a mechanism wherein tumour cells selectively accumulate nanoparticles due to their enhanced permeability and retention (EPR) properties [18,19]. Among them, nanostructured lipid carriers (NLC) have emerged as promising candidates owing to their ability to encapsulate both lipophilic and hydrophilic drugs, the use of biocompatible lipids, to provide a prolonged drug release profile, and facilitate large-scale production [20]. Furthermore, in previous studies, the use of NLC has shown to offer an efficient encapsulation of individually loaded APG or MEL, with a favourable *in vitro* release, and good stability [5,6].

In order to overcome bioavailability problems and chemical instability of APG and MEL, we developed APG and MEL loaded NLC (APG-MEL-NLC) for the treatment of various types of

tumours. Furthermore, the natural compound rosehip oil, extracted from the seeds of wild roses, served as the liquid lipid choice due to its appealing pharmaceutical properties [21]. Rosehip oil has traditionally been employed in dermal applications as a skin regenerative agent and exhibited anti-inflammatory and antioxidant effects [22,23]. Moreover, previous studies suggested that the incorporation of the rosehip oil to the formulation, increased the antitumoral activity [5,24]. These properties could potentially exert a synergic mechanism with the anticarcinogenic activity of both, APG and MEL to enhance the therapeutic efficacy.

A dual formulation of next-generation lipid nanoparticles was developed and optimized for the simultaneous co-administration of APG and MEL. Physicochemical and morphological characterization, compound interactions, and *in vitro* release profiles were investigated. Furthermore, their cellular internalization was assessed. Additionally, the antiproliferative activity of the NLC was evaluated in different tumour cell lines to determine their potential therapeutic benefits and compared to the previous formulation encapsulating each compound alone.

2. Materials and methods

2.1. Materials

APG was purchased from Apollo Scientific (Cheshire, UK). MEL was obtained from Thermo Fisher Scientific (Massachusetts, USA). Compritol 888 ATO® (glyceryl distearate) as the solid lipid (SL) was kindly gifted from Gattefossé (Madrid, Spain). Tween® 80 (Polysorbate 80) and Nile red (NR) were purchased to Sigma Aldrich (Madrid, Spain). Rosehip oil was purchased to Acofarma Fórmulas Magistrales (Barcelona, Spain). All others chemical reagents and components used in this research were of analytical grade. A Millipore Milli-Q Plus system was used to obtain purified water.

2.2. APG-MEL-NLC preparation and optimization

APG-MEL-NLC were produced using a hot high-pressure homogenization process [25]. Initially, a primary emulsion was prepared employing an Ultraturrax® T10 basic homogenizer at 8,000 rpm for 30 seconds. Subsequently, the primary emulsion was subjected to three homogenization cycles at 900 bar pressure and 85 °C.

The production of APG-MEL-NLC labelled with NR (APG-MEL-NLC-NR) was carried out following the same procedure as APG-MEL-NLC, but with the addition of a 0.025 % of NR to the formulation.

Design of Experiments (DoE) was employed to optimize the formulation parameters due to its ability to gather information efficiently, minimizing the number of experiments required. This was achieved by utilizing a central composite factorial design, encompassing two replicated centre points, sixteen factorial points, and eight axial points, implemented using Statgraphics Centurion® 18 version 18.1.12 software (Virginia, USA). Four independent variables, APG/MEL concentration, surfactant concentration, lipid phase concentration, and solid lipid concentration (SL/lipid phase), were examined to determine their impact on the physicochemical properties of NLC. The dependent variables investigated were Z_{av}, PDI, ZP, and EE [5].

2.3. Characterization of optimized APG-MEL-NLC

The mean average size (Z_{av}) and polydispersity index (PDI) were evaluated using dynamic light scattering (DLS) employing a ZetaSizer Nano ZS instrument (Malvern Instruments, Malvern, UK).

Zeta potential (ZP) was assessed based on electrophoretic mobility measurements. For Z_{av} and PDI analysis, the formulations were diluted 1:10 with Milli-Q water. For ZP measurements, the nanoparticles were diluted 1:20.
Encapsulation efficiency (EE) was indirectly determined by quantifying the non-encapsulated APG and MEL in the APG-MEL-NLC. Prior to analysis, APG-MEL-NLC was diluted 1:40 with a mixture of miliQ water with a 10 % ethanol. The non-encapsulated APG and MEL were separated from the NLC by filtration/centrifugation at 14,000 rpm (Mikro 22 Microliter Centrifuge, Germany) utilizing an Amicon® Ultra-0.5 centrifugal filter device (Amicon Millipore Corporation, Ireland)[26]. The non-encapsulated APG and MEL passed through the filter and was analysed by HPLC. EE was calculated for each drug following Equation 1:

$$EE\ (\%) = \frac{Total\ amount\ of\ APG/MEL - Free\ APG/MEL}{Total\ amount\ of\ APG/MEL}$$

APG and MEL quantification was carried out using reverse-phase high performance liquid chromatography (HPLC) [5]. Briefly, samples were analysed using an HPLC Waters 2695 separation module (Waters, Massachusetts, USA) equipped with a Kromasil® C18 column (5 µm, 150 × 4.6 mm). The mobile phase consisted of a mixture of a water phase containing 2 % acetic acid and an organic phase composed of methanol. A gradient elution was employed, starting with 40 % water phase, and increasing to 60 % water phase over 5 minutes, followed by a reverse gradient back to 40 % water phase over the next 5 minutes. The flow rate was maintained at 0.9 mL/min. Quantification of APG was achieved using a Waters® 2996 diode array detector at 300 nm, and the data were processed using Empower® 3 Software.

2.4. Interaction studies

Differential scanning calorimetry (DSC) analysis was conducted using a DSC 823e system (Mettler-Toledo, Barcelona, Spain). Thermograms of APG-MEL-NLC and their individual components were obtained under a nitrogen atmosphere, employing a heating ramp from 25 to 105 °C at 10 °C/min. The acquired data was evaluated using the Mettler STARe V 9.01 dB software (Mettler-Toledo, Barcelona, Spain)[27].

Fourier-transform infrared (FTIR) spectra of APG-MEL-NLC, and their components were determined utilizing a Thermo Scientific Nicolet iZ10 spectrometer equipped with a diamond attenuated total reflectance crystal and a DTGS detector (Barcelona, Spain) [28].

X-ray diffraction (XRD) patterns of APG-NLC and their components were also evaluated by placing the samples between two polyester films of 3.6 µm thickness and exposing them to CuKα radiation (45 kV, 40 mA, λ = 1.5418 Å). The measurements were conducted within a working range (2θ) of 2° to 60°, using a step size of 0.026° and an exposure time of 200 seconds for each step [29].

2.5. Morphology studies

Transmission electronic microscopy (TEM) was utilized to examine the morphology of APG-MEL-NLC using a JEOL 1010 instrument (JEOL USA, Massachusetts, USA). Initially, copper grids were activated using UV light, and the APG-MEL-NLC (previously diluted 1:10) were negatively stained with 2 % uranyl acetate [30].

2.6. Stability studies

APG-MEL-NLC were subjected to long-term storage at three distinct temperatures (4, 25, and 37 °C) for several months. The stability of the nanoparticles was evaluated by analysing their light backscattering (BS) profiles using a Turbiscan® Lab instrument (Formulation Inc, Worthington, USA). To this end, 10 mL of each sample was placed in a glass measurement cell, and BS measurements were acquired every 15-30 days. Simultaneously, the physicochemical properties of the APG-NLCs, including Z_{av}, PDI, ZP, and EE, were monitored at 15-day intervals or monthly until any signs of degradation or instability appeared [31].

2.7. Biopharmaceutical behaviour

The *in vitro* release of APG and MEL from the NLC formulations was investigated employing Franz-type diffusion cells (Permegear, Germany) equipped with a diffusion area of 0.20 cm^2 and cellulose dialysis membranes (MWCO 12 kDa). The conditions of the experiment were described previously [5]. Briefly, a receptor medium simulating physiological conditions (a solution of PBS with 5 % Tween® 80 and 20 % ethanol at pH 7.4) was employed to ensure sink conditions. The formulations were compared to solution of APG and MEL as a reference. The release study was conducted at 37 ± 0.5 °C for 48 h. An initial volume of 300 µL of each formulation were placed on the donor compartment, and sample aliquots (150 µL) were withdrawn at predetermined time intervals. The withdrawn volume was replaced with fresh receptor solution to maintain sink conditions. The APG and MEL content of the receptor medium was determined using HPLC. Each sample was analysed in triplicate, and the cumulative amount of APG and MEL released over time was calculated.

2.8. Biological studies

2.8.1. Cell lines

Human biphenotypic B myelomonocytic leukemia MV4-11, human normal breast MCF-10A cells were obtained from American Type Culture Collection (USA), human lung carcinoma A549, human breast cancer MCF-7 were obtained from European Collection of Authenticated Cell Cultures (UK). Human breast cancer MDA-MB-468 cells were obtained from Leibniz Institute DSMZ-German Collection of Microorganisms and Cell Cultures (Germany). All the cell lines are being maintained at the Hirszfeld Institute of Immunology and Experimental Therapy, PAS, Wroclaw, Poland.

MV4-11 and MDA-MB-468 cells were cultured in RPMI 1640 medium (IIET PAS, Poland) with 1.0 mM sodium pyruvate (only MV4-11) and 10 % (MV4-11) or 20 % (MDA-MB-468) foetal bovine serum (FBS) (all from Merck, Germany). A549 cells were cultured in RPMI 1640+Opti-MEM (1:1) ((IIET PAS, Poland and Gibco, UK) supplemented with 5 % FBS (Merck, Germany). The MCF-7 cells were cultured in Eagle medium (IIET PAS, Poland) supplemented with 10% FBS, 8 µg/mL of insulin and 1 % of MEM NON-Essential amino acid (all Merck, Germany). Normal breast epithelial MCF-10A cells were cultured in the HAM'S F-12 medium (Corning), which was supplemented with 10 % Hors Serum (Gibco), 20 ng/mL EGFh, 10 µg/mL insulin, 0.5 µg/mL Hydrocortisone and 0.05 mg/mL Cholera Toxin from Vibrio cholerae (all from Merck, Germany).

All culture media were supplemented with 2 mM L-glutamine (Merck, Germany), 100 units/mL penicillin, (Polfa Tarchomin S.A., Poland) and 100 µg/mL streptomycin (Merck, Germany). All cell lines were grown at 37 °C with 5 % CO_2 humidified atmosphere.

2.8.2. Determination of antiproliferative activity

The solutions of nanoformulation of APG (APG-NLC) (1 mg/mL), MEL (MEL-NLC) (0.5 mg/mL) and both APG and MEL (APG-MEL-NLC with a concentration of 0.67 mg/mL of APG and 0.33 mg/mL of MEL) were prepared by dissolving the samples in water. Then the tested samples were diluted in culture medium to reach the final concentrations. Before adding the tested compounds (24 h prior), cells were plated in 96-well plates (Sarstedt, Germany) at a density of 1×10^4 or 0.5×10^4 (A549) cells per well. The assay was performed after 24 h and 72 h of exposure to 33.5, 3.35, 1.68, 0.34 μg/mL concentration of the APG-NLC and 16.5, 1.65, 0.83 and 0.17 μg/mL of the MEL-NLC. The concentration of APG-MEL-NLC was prepared to obtain the same concentrations of APG and MEL as in APG-NLC and MEL-NLC. The *in vitro* cytotoxic effect of all agents was examined using the MTT (MV4-11) or SRB assay, described previously [32]. The results were calculated as an IC_{50} (inhibitory concentration 50 %) the concentration of tested agent, which is cytotoxic for 50 % of the cancer cells. IC values were calculated for each experiment separately using Prolab-3 system based on Cheburator 0.4 software [33]. Each compound in each concentration was tested in triplicate in a single experiment, which was repeated 3–5 times. Statistical analysis of cell growth inhibition was performed by Kruskall-Walis test, GraphPad Prism 7. A statically significant difference was considered at $p \leq 0.05$.

2.8.3. Determination of compounds accumulation in cells by flow cytometry

The APG-NLC, MEL-NLC and APG-MEL-NLC were fluorescently labelled with NR to determine its accumulation in cells. The leukemia MV4-11 cells were incubated by 5, 15, 30 min and 1, 2, 4 h with APG-MEL-NLC-NR (in concentration 1.675 μg/mL and 0.335 μg/mL). After incubation the cells were collected and washed with PBS. The mean fluorescence of cells incubated with tested compounds labelled with NR was analysed by flow cytometry using BD LSRFortessa cytometer (BD Bioscience, San Jose, USA). The untreated cells were used as an unlabelled control. Obtained results were analysed using Flowing software 2 (Cell Imaging Core, Turku Centre for Biotechnology, University of Turku Åbo Akademi University) [5].

3. Results

3.1. APG-MEL-NLC preparation and optimization

The optimization process was implemented using a DoE approach. A full composite factorial design with four levels and four factors was developed to systematically evaluate the influence of the independent variables, namely, the APG/MEL content, the lipid phase (mixture of solid and liquid lipid), the percentage of SL in the lipid phase, and the surfactant concentration, on the dependent variables, the Z_{av}, PDI, ZP, and EE of APG and MEL. Moreover, APG/MEL ratio was fixed at 2/1 respectively, based on previously optimized formulations [5,6].

As illustrated in Table 1, the particle average size of the formulations were approximately 250 nm and the PDI was approximately 0.2, indicating a well-dispersed distribution of nanoparticles [34]. Moreover, the formulations exhibited a negative ZP below −20 mV, suggesting a suitable stability of the nanoparticles [31]. The negative charge could be attributed to the ionization of glyceryl behenate, a fatty acid component of Compritol® 888 ATO [35]. All formulations achieved EE exceeding 95 % for APG, confirming the complete encapsulation of APG within the APG-MEL-NLC. However, MEL showed a lower EE into the APG-MEL-NLC. It could be attributed to its higher solubility in the aqueous phase containing Tween® 80 [15,36].

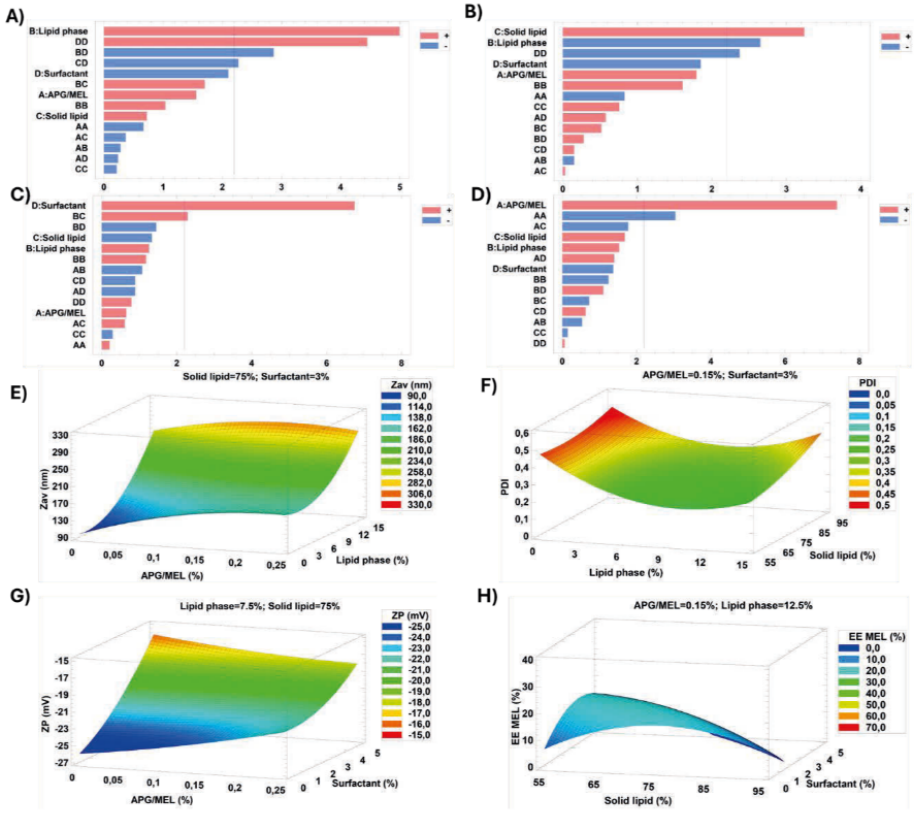

Figure 1. DoE optimization of APG-MEL-NLC. (A-D) Pareto's chart of the influence of the independent variables for each dependent variable. (A) Z_{av}; (B) PDI; (C) ZP; (D) EE APG. (E-H) DoE surface response of APG-MEL-NLC; (E) Concentration of APG/MEL regarding to the lipid phase influence on Z_{av}; (F) Concentration of Lipid phase regarding to the lipid phase influence on PDI; (G) Concentration of Surfactant regarding to the SL influence on ZP; (H) Concentration of Solid lipid regarding to the Surfactant influence on EE MEL.

In Figure 1 Pareto's diagram with significant effects on the formulation parameters are shown. The lipid phase highly influenced the Z_{av} of the NLC, in which a higher amount of the mixture of lipids increased the size of the formulation ($p < 0.001$). PDI was significantly influenced by the lipid composition, in which a higher amount of lipid phase ($p < 0.05$) but low SL proportion ($p < 0.01$), decreased the PDI. Moreover, the surface charge was significantly influenced by the surfactant ($p < 0.0001$), and the APG EE was significantly influenced by the amount of APG/MEL in the particle ($p < 0.0001$).

As illustrated in Figure 1, increasing the lipid phase concentration resulted in larger NLC with reduced size dispersion. Surface response analysis (Figure 1E) suggested that employing less than 10 % lipid phase generated APG-MEL-NLC with diameters below 200 nm. The smallest particles were obtained using mixtures containing less than 0.1 % of APG/MEL. However, to achieve PDI below 0.2, high lipid phase concentrations were needed containing low SL concentration (Figure 1F). Regarding to the ZP, a more negative surface charge was obtained when a lower concentration of surfactant was added (Figure 1G). MEL EE was influenced by the SL concentration, in which the central values around 75 % obtained the highest EE (Figure 1H).

Considering all the evaluated parameters and their subsequent trends, a formulation containing 0.67 mg/mL of APG and 0.33 mg/mL of MEL, 5 % of lipid phase formed by a 75 % of SL, and 4 % of surfactant has been optimized to carry out further experiments.

Table 1. Design of experiments and characterization of the different formulations developed.

	Independent variables								Dependent variables				
	APG/MEL (%)		Lipid phase (%)		SL (%)		Surfactant (%)		Z_{av} ± SD (nm)	PDI ± SD	ZP ± SD (mV)	EE APG ± SD (%)	EE MEL ± SD (%)
Factorial points													
D1	-1	0.1	1	10	1	85	-1	2	270.4 ± 3.6	0.245 ± 0.004	-21.0 ± 0.4	98.2 ± 0.2	5.3 ± 0.3
D2	1	0.2	-1	5	1	85	1	4	150.3 ± 3.2	0.283 ± 0.008	-21.0 ± 0.2	99.1 ± 0.1	22.8 ± 1.3
D3	1	0.2	1	10	1	85	-1	2	279.6 ± 2.8	0.275 ± 0.006	-21.6 ± 0.1	98.8 ± 0.5	23.2 ± 0.5
D4	-1	0.1	1	10	-1	65	-1	2	220.2 ± 1.4	0.189 ± 0.021	-21.2 ± 0.1	97.3 ± 0.3	20.2 ± 0.1
D5	1	0.2	1	10	1	85	1	4	200.5 ± 1.5	0.264 ± 0.023	-19.3 ± 0.5	98.7 ± 0.1	10.0 ± 1.2
D6	1	0.2	-1	5	-1	65	-1	2	172.5 ± 1.4	0.230 ± 0.005	-21.6 ± 0.3	99.1 ± 0.2	4.2 ± 0.1
D7	-1	0.1	-1	5	-1	65	-1	2	153.9 ± 0.9	0.223 ± 0.006	-23.1 ± 0.6	97.7 ± 0.1	13.4 ± 1.9
D8	-1	0.1	-1	5	1	85	1	4	151.7 ± 0.9	0.216 ± 0.001	-21.2 ± 0.3	97.7 ± 1.1	14.3 ± 0.7
D9	-1	0.1	1	10	-1	65	1	4	190.9 ± 0.7	0.157 ± 0.015	-19.9 ± 0.6	97.6 ± 0.3	14.6 ± 2.0
D10	1	0.2	-1	5	-1	65	1	4	209.5 ± 2.5	0.229 ± 0.018	-18.4 ± 0.3	98.5 ± 0.1	19.8 ± 1.1
D11	-1	0.1	-1	5	-1	65	1	4	176.2 ± 2.9	0.182 ± 0.015	-17.4 ± 0.5	95.9 ± 0.9	25.8 ± 0.6
D12	1	0.2	-1	5	1	85	-1	2	187.0 ± 1.8	0.284 ± 0.020	-22.8 ± 0.3	98.4 ± 0.1	19.1 ± 0.1
D13	-1	0.1	-1	5	1	85	-1	2	164.2 ± 0.8	0.273 ± 0.004	-23.2 ± 0.6	98.2 ± 0.1	17.3 ± 0.1
D14	1	0.2	1	10	-1	65	1	4	195.2 ± 2.3	0.197 ± 0.008	-21.4 ± 0.4	99.1 ± 0.1	23.4 ± 1.9
D15	-1	0.1	1	10	1	85	1	4	185.7 ± 1.1	0.250 ± 0.013	-19.4 ± 0.1	97.7 ± 0.6	12.0 ± 1.0
D16	1	0.2	1	10	-1	65	-1	2	241.1 ± 1.7	0.212 ± 0.015	-21.8 ± 0.1	98.7 ± 0.7	14.3 ± 0.1
Axial points													
D17	-2	0.05	0	7.5	0	75	0	3	170.9 ± 1.3	0.206 ± 0.009	-22.5 ± 1.3	94.8 ± 1.2	10.9 ± 0.2
D18	2	0.25	0	7.5	0	75	0	3	192.4 ± 0.4	0.272 ± 0.003	-19.6 ± 0.9	99.2 ± 0.6	19.3 ± 0.6
D19	0	0.15	-2	2.5	0	75	0	3	188.7 ± 3.3	0.442 ± 0.012	-20.7 ± 0.4	97.3 ± 0.7	13.3 ± 0.1
D20	0	0.15	2	12.5	0	75	0	3	245.4 ± 2.9	0.233 ± 0.009	-19.4 ± 0.1	98.5 ± 0.1	17.1 ± 0.1
D21	0	0.15	0	10	-2	55	0	3	174.8 ± 3.4	0.174 ± 0.025	-21.2 ± 0.3	98.1 ± 0.3	26.0 ± 0.8
D22	0	0.15	0	10	2	95	0	3	202.8 ± 3.4	0.353 ± 0.012	-21.9 ± 0.2	98.8 ± 0.1	6.8 ± 1.0
D23	0	0.15	0	10	0	75	-2	1	176.3 ± 0.1	0.245 ± 0.008	-19.3 ± 0.5	98.9 ± 0.1	31.7 ± 0.4
D24	0	0.15	0	10	0	75	2	5	289.4 ± 3.5	0.119 ± 0.016	-16.4 ± 0.2	98.2 ± 0.8	15.5 ± 0.6
Central points													
D25	0	0.15	0	7.5	0	75	0	3	179.3 ± 1.4	0.253 ± 0.012	-21.0 ± 0.1	98.4 ± 0.1	29.9 ± 0.1
D26	0	0.15	0	7.5	0	75	0	3	175.5 ± 2.3	0.239 ± 0.010	-21.6 ± 0.7	98.9 ± 0.1	32.1 ± 1.3

3.2. Interaction studies of APG-MEL-NLC

The interactions between both drugs and the lipid matrix carried out by DSC, FTIR, and XRD are shown in Figure 2. DSC was used to investigate the variations in the crystallinity and melting point of the lipid mixtures in comparison with APG-MEL-NLC (Figure 2A). The results showed that the melting temperature (T_m) of the lipid mixture was slightly higher than that of the lipid mixture with drugs (67.06 °C and 66.24 °C, respectively). Additionally, the T_m of APG-MEL-NLC was slightly lower than both physical lipid mixture (65.60 °C), which could be attributed to the small size and surfactant incorporation into the APG-MEL-NLC [37]. The enthalpy values (ΔH) were similar between the lipid mixture and lipid mixture-APG/MEL (77.55 Jg^{-1} and 80.00 Jg^{-1}, respectively), and

the ΔH of APG-MEL-NLC was lower (56.98 Jg^{-1}). APG alone was also assessed, showing a T_m of 365.50 °C and ΔH = 198.50 Jg^{-1}, and MEL had a T_m of 118.52 °C and ΔH = 134.70 Jg^{-1}, indicating their higher crystallinity and melting point when compared to the lipid mixtures.

FTIR analysis was used to study the interactions between the drugs, surfactant, and the lipid matrix (Figure 2B). FTIR spectra of APG presented vibrational bands at approximately 3278 cm^{-1}, characteristic of the O-H group, multiple small peaks at 2800 cm^{-1} from C-H groups, and additional peaks at 1650 and 1605 cm^{-1} from the C-O groups [38]. Otherwise, MEL presented characteristic peaks at 3303 cm^{-1} from the N–H group, at 1629 cm^{-1} from the C=O groups, at 1555 cm^{-1} from the C–O groups, and at 1212 cm^{-1} from the C–N group. The spectra of the APG-MEL-NLC showed a pronounced peak at 1100 cm^{-1} which corresponds to the surfactant [39]. Furthermore, there was no evidence of new strong bonds formed in the formulation, and APG and MEL peaks were not observed, or the peaks were too small, thus confirming drug encapsulation in the lipid matrix.

The XRD patterns in Figure 2C provide evidence of the physical state of the drugs incorporated into the NLC. APG, MEL and the solid mixture of lipids exhibit a crystalline structure, as indicated by the strong and sharp peaks observed in the XRD spectra. Some of the characteristic MEL peaks (19.83°, 22.67°, and 24.30°) showed a lower intensity in the APG-MEL-NLC profile and APG peaks were not visible, indicating that both drugs were present in a dissolved state, corroborating the EE data. The crystallinity of other formulation components was also studied. The physical mixture of lipids (bulk lipid) and the mixture with both drugs (bulk lipid + APG/MEL) showed 3 pronounced peaks at 19.36° (2θ) i.e. *d*=0.46 nm, indicating the most stable form of triacylglycerols, the β form, and two pronounced peaks at 21.36° (2θ) i.e. *d*=0.42 nm), and 23.59° (2θ) i.e. *d*=0.38 nm, indicating the second stable form of triacylglycerols, the β′ form [40,41]. APG-MEL-NLC showed a peak at 19.36° (2θ) i.e. *d*=0.46 nm, attributed to the β form [40].

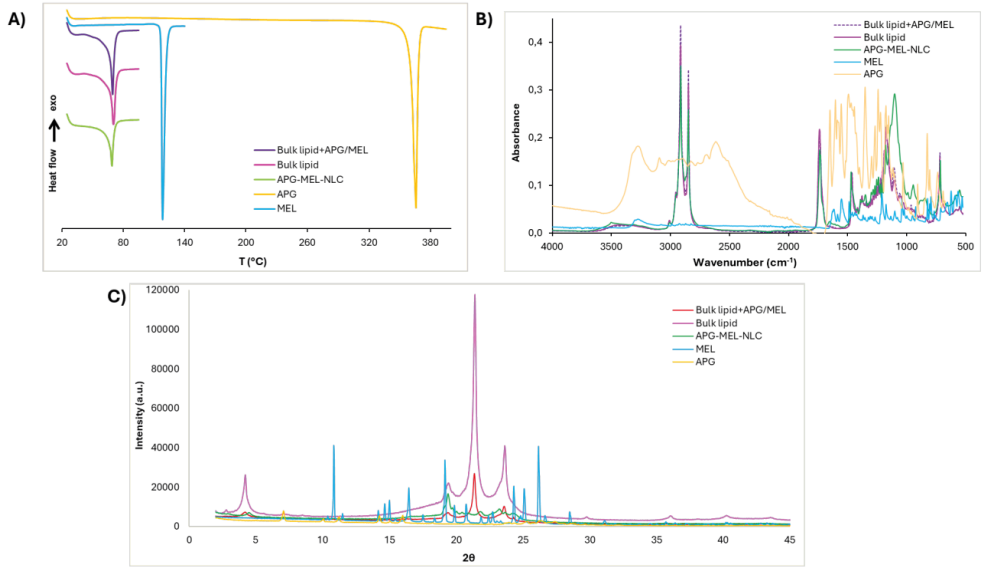

Figure 2. Interaction studies of APG-MEL-NLC and their components. (A) DSC curves; (B) FTIR analysis; (C) X-ray diffraction patterns.

3.3. Morphological studies

The morphology of the APG-MEL-NLC was evaluated by TEM and DLS to ensure a comprehensive characterization. TEM images revealed almost spherical and soft round shapes of the NLC (Figure 3). DLS measurements confirmed the TEM findings, showing Z_{av} below 200 nm. These results were consistent with the negative ZP values (-20 mV), indicating stable colloidal dispersions without aggregation. In comparison to the formulations containing APG or MEL, they shared a similar round and soft shape morphology.

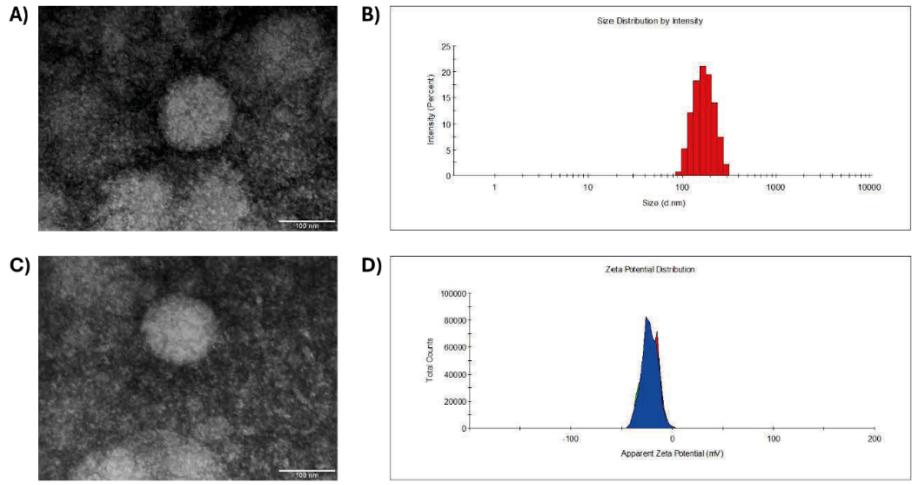

Figure 3. Physicochemical and morphological characterization. (A) TEM images with scale bar 100 nm; (B) Histogram of average size distribution measured by DLS; (C) TEM images with scale bar 100 nm; (D) ZP plot measured by laser-Doppler electrophoresis.

3.4. Stability of APG-MEL-NLC

Stability assessments were performed by evaluating Z_{av}, PDI, ZP, and EE of APG-MEL-NLC along with analysing BS profiles at different temperatures. BS specifically provides insights into destabilization mechanisms like sedimentation, agglomeration, or aggregation, which can be discerned upon detecting differences exceeding 10 % [28]. BS profiles of APG-MEL-NLC were evaluated at 4, 25, and 37 °C (Figure 4). The APG-MEL-NLC formulation demonstrated stability at 4 °C for 4 months, preserving its physicochemical parameters, while at 25 °C, stability lasted 3 months, and at 37 °C, stability was limited to 15 days.

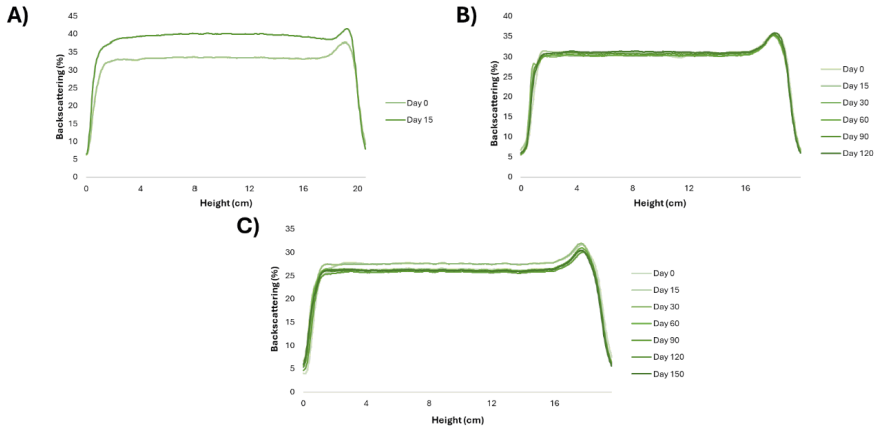

Figure 4. Backscattering profiles of APG-MEL-NLC stored at (A) 37 °C; (B) 25 °C; and (C) 4 °C.

Furthermore, higher temperatures accelerated particle destabilisation by increasing the ZP to neutral. As it can be seen in table 2, the formulations maintained their physicochemical parameters until ZP decreased in the case of 25 and 37 °C or increased PDI at 4 °C. These phenomena can be easily observed in the BS results at 37 °C in which the profile increased because of the decrease in ZP, promoting aggregation phenomena. In the case of 4 and 25 °C, the BS changes were not visible, probably because it was in an early stage of destabilisation in which the BS changes were not patent. Considering these results into account, APG-MEL-NLC stored at 4 °C showed suitable stability up to 4 months.

Table 2. Physicochemical parameters of APG-MEL-NLC stored at different temperatures.

Temperature (°C)	Day	Z_{av} ± SD (nm)	PDI ± SD	ZP ± SD (mV)	EE APG ± SD (%)	EE MEL ± SD (%)
	0	147.4 ± 0.4	0.125 ± 0.018	-22.1 ± 1.6	99.9 ± 0.1	52.2 ± 0.2
37	15	151.4 ± 0.6	0.140 ± 0.003	-12.7 ± 2.0	99.9 ± 0.1	50.1 ± 1.2
25	30	152.9 ± 1.0	0.142 ± 0.013	-19.7 ± 0.4	98.9 ± 0.2	52.2 ± 0.2
	60	155.2 ± 1.9	0.121 ± 0.015	-14.9 ± 0.7	99.5 ± 0.3	51.9 ± 0.5
	120	158.9 ± 2.0	0.130 ± 0.024	-9.2 ± 1.0	99.9 ± 0.1	52.9 ± 0.1
4	30	151.4 ± 0.6	0.140 ± 0.003	-19.9 ± 0.1	99.8 ± 0.1	52.1 ± 0.2
	60	155.6 ± 2.0	0.164 ± 0.012	-21.1 ± 0.4	98.5 ± 0.9	50.5 ± 1.9
	120	144.9 ± 0.4	0.143 ± 0.023	-24.4 ± 1.0	99.7 ± 0.1	51.7 ± 0.3
	160	131.2 ± 0.4	0.221 ± 0.011	-24.3 ± 1.4	99.9 ± 0.1	52.2 ± 0.2

3.5. Biopharmaceutical behaviour

The *in vitro* release profile of APG and MEL from NLC against its respective free counterparts demonstrated that the formulation had a kinetic profile characteristic of prolonged drug release formulations. As shown in Figure 5, APG release from APG-MEL-NLC best fit was a two-phase association. An initial burst release of APG was observed during the first two hours, probably due to the rapid diffusion of APG molecules from the outer lipid shell of the NLC. Subsequently, a slower release phase occurred, possibly reflecting the release of APG encapsulated within the inner lipid core of the NLC. In contrast, free APG exhibited a rapid and complete release within 24

hours, reaching 100 % release, while APG from APG-MEL-NLC released only approximately 35 % of its APG content under the same conditions. APG release from APG-MEL-NLC was adjusted to two phase association equation, and its kinetic constant (K_d) demonstrated that after the fast initial release of APG from the NLC, showed a slow release due to its smaller K_d in comparison to free APG. This fact was also corroborated by the higher half-time life ($t_{1/2}$, the time required for the initial concentration to decrease to half) of the slow-release phase respect to the free APG, 5.259 vs 4.5934 h respectively. Otherwise, MEL from APG-MEL-NLC was fitted to one-phase association (r^2=0.9787). In this case, both the free MEL and MEL from the NLC showed a slow initial release, followed by a complete faster release. Free MEL achieved 100 % during the first 24 h, while the encapsulated MEL reached a 75 % approximately, demonstrating a slower prolonged release. The kinetic parameters highlighted this fact, in which the K_d was the half of the value of free MEL, and the $t_{1/2}$ was the double for MEL from APG-MEL-NLC.

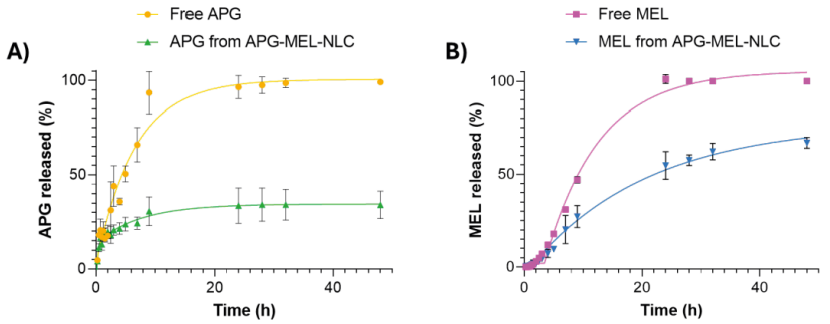

	K_d (h^{-1})	$t_{1/2}$ (h)	*Plateau* (%)	r^2
Free APG	0.151	4.5934	100.4	0.9382
APG from APG-MEL-NLC	$K_{d\ fast}$=4.651 $K_{d\ slow}$=0.132	$t_{1/2\ fast}$=0.1490 $t_{1/2\ slow}$=5.259	34.5	0.7844
Free MEL	0.109	6.372	105.5	0.9940
MEL from APG-MEL-NLC	0.051	13.720	76.6	0.9787

Figure 5. *In vitro* release profile of APG and MEL from APG-MEL-NLC vs free APG and MEL carried out for 48 h and adjustment to a two-phase association, one-phase association, exponential Plateau, and Plateau followed by one phase decay model respectively. (A) APG release profile from APG-MEL-NLC; (B) MEL release profile from APG-MEL-NLC.

3.6. Cytotoxicity towards selected cancer cell lines

The antiproliferative activity of APG-NLC, MEL-NLC and APG-MEL-NLC, towards leukemia (MV4-11), lung (A549) and two breast MCF-7 (ER+) and MDA-MB-468 (triple-negative breast cancer, TNBC) cancer cell lines were evaluated after 24 and 72 h. The toxicity of these compounds was also tested towards the human normal breast epithelial MCF-10A cells. The results were obtained by cellular viability assessment MTT (MV4-11) or SRB colorimetric assay. The data for the *in vitro* anticancer activity are reported in Table 3, expressed as the IC_{50} concentration of the individually loaded NLC (based on either APG or MEL concentration) or the sum of compounds (APG + MEL

concentration) that inhibits proliferation of the cells by 50 % compared to the untreated control cells.

Table 3. IC_{50} of APG-NLC, MEL-NLC and APG-MEL-NLC against selected cancer cell lines and non-tumorigenic human breast epithelial cell line (MCF-10A).

Compound	Cell lines IC_{50} [μg/mL]									
	MV4-11		A549		MDA-MB-468		MCF-7		MCF-10A	
	24 h	72 h	24 h	72 h	24 h	72 h	24 h	72 h	24 h	72 h
APG-NLC	0.9 ± 0.4	0.7 ± 0.2	2.1 ± 0.9	1.1 ± 0.7	7.3 ± 1.7	2.1 ± 0.5	18.9 ± 4.4	2.9 ± 1.3	17.4 ± 6.6	12.1 ± 0.6
MEL-NLC	n.a.	1.0 ± 0.5	12.3 ± 2.6	2.9 ± 0.4	8.7 ± 1.9	5.3 ± 0.5	13.2 ± 0.8	2.1 ± 0.6	8.8 ± 3.7	5.2 ± 0.2
APG-MEL-NLC	0.7 ± 0.1	0.6 ± 0.1	14.9 ± 3.8	3.0 ± 0.8	10.5 ± 0.3	7.9 ± 1.5	13.9 ± 4.7	2.9 ± 1.2	12.2 ± 1.9	10.1 ± 0.5

Moreover, detailed results at three different concentrations of MEL and APG are detailed in Figure 6. Specifically, in Figure 6A, the highest effect for all the samples was found on the leukemia cell line MV4-11, in which after 72 h, the tested formulations caused a potent cytotoxic effect. Statistically significant ($p < 0.05$) higher cell growth inhibition was observed for APG-MEL-NLC in comparison to MEL-NLC after 24h and 72h (Figure 6A). APG-MEL-NLC showed the highest effectiveness and having into account the drug ratio and their release, probably the first and faster MEL release from the NLC exerted a sensibilizing effect on the cells, allowing to APG to provoke a higher cytotoxic effect, by using a lower concentration than the APG-NLC or MEL-NLC. On A549 cells, APG-NLC showed higher effects than APG-MEL-NLC and MEL-NLC (statistically significant, $p < 0.05$); Figure 6B), specially at high doses which is also correlated with high IC_{50} values obtained with the latter formulations. Moreover, in MCF-7 cells the antiproliferative effect of APG-MEL-NLC was similar to effect of APG-NLC and MEL-NLC individually loaded. In addition, for MDA-MB-468 cells (triple negative breast cancer, TNBC), similar effects than A549 cells were found showing superior properties with APG-NLC after 72 h of incubation (which correlates with APG slowed release).

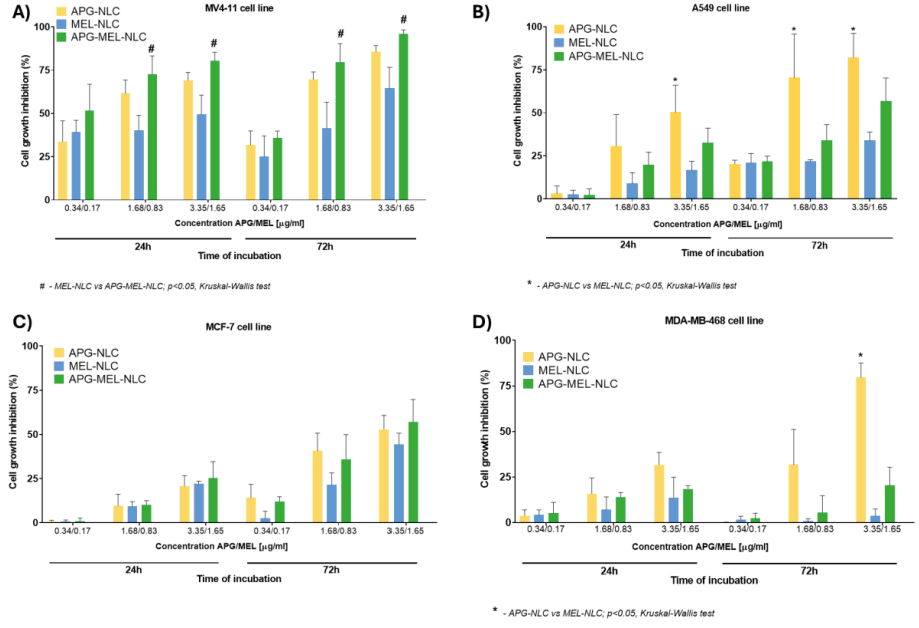

Figure 6. Cell growth inhibition of the formulations in each cancer cell line at different concentrations and incubation times. (A) Cell growth inhibition in the MV4-11 cell line; (B) Cell growth inhibition in A549 cell line; (C) Cell growth inhibition in the MCF-7 cell line; (D) Cell growth inhibition in the MDA-MB-468 cell line. Statistical analysis: Kruskal-Wallis test (GraphPad Prism 7); * significant statistically ($p < 0.05$) differences between APG-NLC and MEL-NLC; # significant statistically ($p < 0.05$) differences between MEL-NLC and APG+MEL-NLC.

3.7. Accumulation of APG-MEL-NLC in tumoral cells

To evaluate the ability of APG-MEL-NLC to accumulate in leukemia cells, a cytometric approach with the fluorescent dye NR was employed. NR selectively binds to neutral fats and phospholipids, and the amount of bound dye is directly proportional to the cellular neutral fat content. MV4-11 leukemia cells were incubated with fluorescently labelled APG-MEL-NLC-NR formulation (in a concentration of 0.335 µg/mL). Cell fluorescence was assessed using flow cytometry at various time points, and the findings are presented in Supp. 1. The results corroborate NLC could serve as an effective transport for delivering biologically active compounds into cells. The mean fluorescence intensity (MFI) of cells treated with APG-MEL-NLC-NR was compared to that of the control (unlabelled cells). As shown in Suppl. 1A, after 5 minutes of incubation with APG-MEL-NLC-NR, significant fluorescence was observed. At all-time points, the MFI was significantly higher than that of the control ($p < 0.05$). Notably, the accumulation of APG-MEL-NLC in cells was fast and stable. MFI values remained stable after 4 h of incubation. The graph in Supp. 1B further confirms APG-MEL-NLC-NR accumulation in cancer cells, demonstrating a change towards higher fluorescence intensity (A.U.) in histograms for cells treated with labelled formulations compared to control, unlabelled leukemia cells.

4. Discussion

In the present study, a novel formulation involving the incorporation of APG and MEL into rosehip-based NLC was used. In previous studies, both drugs encapsulated into NLC showed a potential antiproliferative activity in different cancer cell lines, which could lead to a highest therapeutic activity when they were combined [5,8,11]. A full factorial design was employed to optimize this formulation through an experimental approach. The analysis showed that the lipid phase had a statistically significant effect on Z_{av} ($p < 0.001$), when the amount of the mixture of lipids increased, the mean size of the particle also increased. Other authors also reported similar results, obtaining larger nanoparticles when increasing amounts of lipids were added [42]. Moreover, it was observed on the surface response plot that the lowest amount of APG/MEL, leaded to the smallest sizes. That fact has been also reported for other authors that increasing amounts of drug, produced larger SLN and NLC [42]. Otherwise, the lipid phase also affected significantly to the PDI, lowering it when increasing amounts were added. Furthermore, when the proportion of SL in the lipid matrix was higher, a more polydisperse formulation was obtained, as other studies also reported [43]. Regarding to the ZP, in this study was found to become more neutral with increasing Tween® 80 concentration, which could be attributed to the adsorption of the surfactant onto the nanoparticles surface and neutralizing its charge [44]. Lastly, the encapsulation of both drugs followed different trends. APG encapsulation was high in all the formulations (> 95 %), probably due to its high lipophilic character, possessing a highest affinity for the internal lipid matrix than the aqueous phase [45]. Otherwise, MEL presented a lower EE, which could be attributed to its slightly greater aqueous solubility [36]. There are no studies that co-encapsulate

APG and MEL, and there are very few studies that combine APG or MEL with other drugs in nanocarriers. In this area, APG has been combined and co-encapsulated with the anticancer drug 5-fluorouracil [46]. The authors prepared liposomes that resulted smaller than our formulation (105.2 nm vs 155.3 nm respectively), with a similar PDI. However, the ZP was practically neutral, which could result in an unstable formulation. Regarding to the EE of both drugs, the results were similar than those obtained in this study, in which APG was mostly encapsulated (about 90 %), but the 5-fluorouracil had a 35 % EE, which could be related to its higher aqueous solubility [47]. MEL has been also co-encapsulated with another drug, tretinoin, into chitosan nanocarriers [48]. In this study, the nanoparticles obtained were higher than the obtained NLC (199.0 nm vs 155.6 nm respectively), with a lower PDI. Their particles obtained a positive ZP due to chitosan [49], and the obtained EE was of 99 %, without specifying the amount of encapsulated drug.

Interaction studies carried out showed that the lipid bulk became more amorphous when both drugs were incorporated, indicating the great solubility of APG and MEL into the matrix. This fact could be observed by the ΔH and T_m reduction when more amorphous was the sample, in this case, the most amorphous was the APG-MEL-NLC [40,41,50]. FTIR studies confirmed that no covalent bonds were formed between the drugs and the lipid matrix. This suggests that hydrogen bonds and hydrophobic forces may be the main forces responsible for the encapsulation and release of both drugs from NLC [51]. Furthermore, XRD results showed that the formulation had the characteristic peak of the most stable form of triacylglycerols, the β form, which could be attributed to a long-term stability. These results agree with the stability studies, in which the formulation was stable at 4 °C for 4 months. In comparison to the formulations containing APG or MEL alone, the XRD spectra showed only one of the characteristic peak of stables forms of triacylglycerols with less intensity, which could be related to its reduced stability (APG-NLC endured 12 moths, MEL-NLC 17 months, and APG-MEL-NLC 4 months). Furthermore, the APG-MEL-NLC formulation contained less lipid matrix (5 % in APG-MEL-NLC vs 7.5 % in APG-NLC and MEL-NLC), which probably could contribute to present a lower stability.

Biopharmaceutical behaviour studies showed a sustained *in vitro* release profile compared to free drugs. The release of APG from APG-MEL-NLC fitted the two-phase association model, in which the formulation provided a first fast release followed by a slower liberation, in which APG reached approximately 35 %. In comparison to previous studies with APG-NLC, the APG-MEL-NLC was able to liberate into the medium APG in a faster manner, achieving a higher amount of APG in the medium. Comparing the kinetic parameters of the prolonged release phase, the $t_{1/2\ slow}$ was lower for APG-MEL-NLC (160.5 h vs 5.3 h), and the kinetic constant was also lower (0.0662 h^{-1} vs 0.1318 h^{-1}), thus indicating that APG-MEL-NLC released slightly faster APG than APG was alone encapsulated. Otherwise, the release of MEL from APG-MEL-NLC fitted the one-phase association model, in which MEL was released slowly during all the experiment (48 h), achieving approximately a 75 %. As mentioned above, MEL probably had a higher EE, that agrees with the *in vitro* release study, in which more of a 50 % of MEL had been released into the receptor medium. In comparison to the previous studies with MEL-NLC, the release of MEL from APG-MEL NLC had a similar kinetic behaviour, owning similar K_d and $t_{1/2}$ values. The main difference between both studies was the release medium, in which the actual ones contained the surfactant Tween® 80 (5 %), which has been described that could cause a slower release of drugs [26], and the previous one for MEL-NLC, was formed by 0.1 % sodium dodecyl sulphate (SDS). The medium containing SDS was not used because of the insolubility of APG in it. In this way, free MEL showed a slower release in comparison to the previous study, which could be attributed to the high concentration of the surfactant.

The antiproliferative activity of APG-MEL-NLC towards five different cell lines was evaluated after 24 and 72 h and compared with APG-NLC and MEL-NLC. In the leukemia cell line MV4-11 it was observed a high cytotoxic effect which was maintained up to 72h. Furthermore, in comparison with individually loaded formulations, they exhibited an equal or slightly higher activity. APG and MEL have been investigated using different leukemia cell lines by other authors. In this area, APG is advocated to induce leukemia cell-cycle arrest, being a potential chemopreventive [52]. MEL is also reported to exhibit anti-proliferation, apoptosis induction, and immunomodulation activities against leukemia during *in vitro* and *in vivo* experiments [53]. These mechanisms led us to the hypothesis of a possible additive effects between them which may be highlighted by NLC entrapment. In this sense, our screening confirms this fact for leukemia cells but it was not found in the other cell lines analyzed. Specifically, for lung cancer cell line A549, APG-MEL-NLC effects were similar to MEL-NLC and APG-NLC showed higher cytotoxic effects. In other studies, it has been reported that APG showed an inhibitory effect on growth, migration and invasion through the downstream of several protein expression, such as Akt and pro-inflammatory cytokines [54–56]. MEL upregulates the expression of occluding, suppressed cell proliferation through Akt pathway and downregulated several pro-inflammatory cytokines [57–60]. These mechanisms could be related to APG-MEL-NLC lower activity against A549 in comparison to APG-NLC [61]. However, further studies in this area may be necessary. Otherwise, TNBC is a subtype of breast cancer that lacks expression of estrogen receptors (ER), progesterone receptors (PR), and human epidermal growth factor receptor 2 (HER2). These causes TNBC cells to be less responsive to traditional hormone therapy and targeted HER2 therapies, and as a result, these tumors show poor prognosis compared to other breast cancer subtypes [62]. Results obtained showed that APG-MEL-NLC were toxic to TNBC cells but similarly to A549 cells, APG-NLC showed higher therapeutic efficacy. APG has been reported to target different signal transduction pathways, reducing the proliferation of MDA-MB-468 cell line through inhibiting interferon-γ-induced PD-L1 upregulation, G_2/M phase cell cycle arrest, production of reactive oxygen species, and reducing phosphorylation of Akt [63–65]. Otherwise, other authors in the recent years found out that MEL reduced cell viability, migration, and/or proliferation in a time- and concentration-dependent manner, decreasing protein expression of IGF-1R, HIF-1α, VEGF and TRPC6 expression [66–68]. Interestingly, in the breast cancer cell line MCF-7, APG-MEL-NLC showed high antitumoral properties, with similar IC_{50} values in comparison to APG-NLC, which had a higher effect than MEL-NLC. In comparison to MDA-MB-468 cell line, MCF-7 cells present a hormone sensitivity through expression of ER and PR, leaking of HER2. These cell line also form tightly cohesive structures displaying strong cell-cell adhesions, while TNBC cell line form a loosely cohesive grape-like or stellate structures [69]. It has been described that APG increased intracellular ROS levels, leading to G_2/M cell cycle arrest and activation of the p53 and caspase-cascade signaling pathway, and also caused significant damage to lipids and DNA. This results in changes in cell morphology, decreased viability, and ultimately apoptosis [70–72]. Otherwise, MEL has been shown to exert antiproliferative and anti-invasive effects on MCF-7 breast cancer cells. It achieves this by modulating cell cycle progression through the control of the p53–p21 pathway, as well as by reducing cell attachment and motility, likely through its impact on estrogen-regulated mechanisms. In addition, MEL antiestrogenic properties and the reduction of aromatase activity, contributed to its inhibitory effects on MCF-7 cell growth and invasion [73–75]. The different molecular mechanisms of both drugs seemed to have a significant effect in this breast cell line, while on the TNBC their pathways did not increase its therapeutic activity.

On the other hand, the lipid matrix used for the preparation of APG-MEL-NLC contained rosehip oil, which demonstrated remarkable antitumor activity against the studied cancer cell lines in our previous research. Furthermore, the formulation contained Tween 80®, this non-ionic surfactant

is known to effectively inhibit P-gp and play a crucial role in opening tight junctions, enhancing the paracellular uptake of NLC and increasing their permeability [76]. Rosehip oil, traditionally used for skin care, has recently shown novel pharmacological features. This oil, derived from the seeds of *Rosa canina* sp., is rich in polyunsaturated fatty acids, linoleic acid, linolenic acid, and phytosterols, particularly β-sitosterol [77]. Studies have assessed the efficacy of rosehip extract against various cancer cell lines, including colon, lung, prostate, cervix, liver, brain, and breast, suggesting its potential use in chemotherapy. Treatment with rosehip extract or its purified fractions resulted in a significant reduction in cell viability, due to its antioxidant properties. However, its activity may not only be attributed to its antioxidant nature, as it also exhibited antiproliferative effects. Additionally, in combination with conventional chemotherapeutic agents, rosehip extract effectively reduced cell proliferation and migration in tissue cultures, indicating its potential as a valuable addition to cancer treatment regimens [22,78–80]. The combination of APG and MEL loading of NLC containing rosehip oil demonstrated promising therapeutic potential for the treatment of leukemia.

The cellular uptake of APG-MEL-NLC was investigated using flow cytometry by encapsulating the fluorescent dye NR. Leukemic cells were selected for this study due to their high cytotoxic activity. APG-MEL-NLC-NR demonstrated rapid uptake within the first 5 minutes, and the fluorescence intensity remained stable throughout all experiments (4 hours). These results suggest that APG-MEL-NLC were able to effectively penetrate and remain within the leukemic cells, providing a possible explanation for their high cytotoxic activity against these cells. It is widely recognized that lipid nanoparticles possess the capacity to quickly penetrate lipid membranes due to their lipidic composition [81]. These findings could potentially explain the observed high efficacy against these cells, as the NLC were able to effectively infiltrate and persist within the cell membranes.

5. Conclusions

APG and MEL were effectively encapsulated into NLC containing rosehip oil, resulting in particles with a mean size below 200 nm, with a PDI lower than 0.2 indicating the uniform size. The EE of APG was high, reaching nearly 100 %, and for MEL was lower because its higher aqueous solubility. The APG-MEL-NLC formulation demonstrated excellent stability over a four-month period, with a sustained release profile for both active compounds. In vitro studies across various cancer cell lines underscored the therapeutic potential of this novel combination, particularly in leukemia cells, where the dual natural drugs exhibited an additive effect. This synergy amplified their pharmacological impact, resulting in heightened cytotoxic activity.

These findings constitute a promising step towards the exploration of combining natural active ingredients like APG and MEL with bioactive matrices as rosehip oil NLC. By leveraging the diverse pharmacological mechanisms of these compounds, this approach could pioneer a new avenue in cancer treatment—potentially outperforming conventional therapies by targeting multiple pathways simultaneously.

6. Additional statements

Competing interests: the authors have no relevant financial or non-financial interests to disclose.

Funding: This research was supported by the Spanish Ministry of Science and Innovation (PID2021-122187NB-C32) and by Wrocław University of Environmental and Life Sciences (Poland) under the Leading Research Groups support project.

Authors' contributions: L.B. has carried out the experimental work and investigation as well written the original manuscript draft. M.S. has contributed to the investigation and methodology and data visualization. M.E. has investigated, supervised and reviewed the manuscript. J.W. has carried out the investigation and formal analysis. M.L.G. has funded and contributed with the methodology and investigation. E.B.S has contributed with the formal analysis and investigation. A.G. has contributed to the methodology, investigation, supervision, review, and funding. E.S.L. has contributed to the methodology, investigation, supervision, funding, and review and editing of the manuscript. All authors read and approved the final manuscript.

Acknowledgements: E.S.-L. wants to acknowledge the support of the Grants for the Requalification of the Spanish University System.

Data Availability Statement: generated data has been included in the manuscript and no additional data was generated.

7. References

[1] S. Hyuna, J. Ferlay, R.L. Siegel, M. Laversanne, I.S.A. Jemal, F. Bray, Global cancer statistics 2020: GLOBOCAN estimates of incidence and mortality worldwide for 36 cancers in 185 countries, CA. Cancer J. Clin. 71 (2021) 209–249. https://doi.org/10.3322/CAAC.21660.

[2] J. Ferlay, M. Colombet, I. Soerjomataram, D.M. Parkin, M. Piñeros, A. Znaor, F. Bray, Cancer statistics for the year 2020: An overview, Int. J. Cancer 149 (2021) 778–789. https://doi.org/10.1002/IJC.33588.

[3] G.-H. Nam, Y. Choi, G. Beom Kim, S. Kim, S.A. Kim, I.-S. Kim, G.H. Nam, Y. Choi, G.B. Kim, S. Kim, S.A. Kim, I.S. Kim, Emerging prospects of exosomes for cancer treatment: from conventional therapy to immunotherapy, Adv. Mater. 32 (2020) 2002440. https://doi.org/10.1002/ADMA.202002440.

[4] S. Kannampuzha, A.V. Gopalakrishnan, Cancer chemoresistance and its mechanisms: Associated molecular factors and its regulatory role, Med. Oncol. 40 (2023) 1–14. https://doi.org/10.1007/S12032-023-02138-Y.

[5] L. Bonilla-Vidal, M. Świtalska, M. Espina, J. Wietrzyk, M.L. García, E.B. Souto, A. Gliszczyńska, E.S. López, Dually active apigenin-loaded nanostructured lipid carriers for cancer treatment, Int. J. Nanomedicine 18 (2023) 6979–6997. https://doi.org/10.2147/IJN.S429565.

[6] L. Bonilla-Vidal, M. Świtalska, M. Espina, J. Wietrzyk, M.L. García, E.B. Souto, A. Gliszczyńska, E. Sánchez-López, Antitumoral melatonin-loaded nanostructured lipid carriers, Nanomedicine (2024) 1–16. https://doi.org/10.1080/17435889.2024.2379757.

[7] S.A. Ahmed, D. Parama, E. Daimari, S. Girisa, K. Banik, C. Harsha, U. Dutta, A.B. Kunnumakkara, Rationalizing the therapeutic potential of apigenin against cancer, Life Sci. 267 (2021) 118814. https://doi.org/10.1016/J.LFS.2020.118814.

[8] Z. Nozhat, S. Heydarzadeh, Z. Memariani, A. Ahmadi, Chemoprotective and chemosensitizing effects of apigenin on cancer therapy, Cancer Cell Int. 21 (2021) 1–26.

https://doi.org/10.1186/S12935-021-02282-3.

[9] Z. Javed, H. Sadia, M.J. Iqbal, S. Shamas, K. Malik, R. Ahmed, S. Raza, M. Butnariu, N. Cruz-Martins, J. Sharifi-Rad, Apigenin role as cell-signaling pathways modulator: implications in cancer prevention and treatment, Cancer Cell Int. 21 (2021) 1–11. https://doi.org/10.1186/S12935-021-01888-X/FIGURES/1.

[10] W.H. Talib, A.R. Alsayed, A. Abuawad, S. Daoud, A.I. Mahmod, Melatonin in cancer treatment: current knowledge and future opportunities, Mol. 2021, Vol. 26, Page 2506 26 (2021) 2506. https://doi.org/10.3390/MOLECULES26092506.

[11] L. Wang, C. Wang, W.S. Choi, Use of melatonin in cancer treatment: where are we?, Int. J. Mol. Sci. 23 (2022) 3779. https://doi.org/10.3390/IJMS23073779.

[12] S. Gurunathan, M. Qasim, M.H. Kang, J.H. Kim, Role and therapeutic potential of melatonin in various type of cancers, Onco. Targets. Ther. 14 (2021) 2019–2052. https://doi.org/10.2147/OTT.S298512.

[13] S. Pan, Y. Guo, F. Hong, P. Xu, Y. Zhai, Therapeutic potential of melatonin in colorectal cancer: Focus on lipid metabolism and gut microbiota, Biochim. Biophys. Acta - Mol. Basis Dis. 1868 (2022) 166281. https://doi.org/10.1016/J.BBADIS.2021.166281.

[14] S. Mehrzadi, M.H. Pourhanifeh, A. Mirzaei, F. Moradian, A. Hosseinzadeh, An updated review of mechanistic potentials of melatonin against cancer: pivotal roles in angiogenesis, apoptosis, autophagy, endoplasmic reticulum stress and oxidative stress, Cancer Cell Int. 21 (2021) 1–28. https://doi.org/10.1186/S12935-021-01892-1.

[15] J. Zhang, D. Liu, Y. Huang, Y. Gao, S. Qian, Biopharmaceutics classification and intestinal absorption study of apigenin, Int. J. Pharm. 436 (2012) 311–317. https://doi.org/10.1016/J.IJPHARM.2012.07.002.

[16] V. Lopes, J. Assis, T. Ribeiro, G. de Castro, M. Pacheco, L. Borges, A. Correa, Melatonin loaded lecithin-chitosan nanoparticles improved the wound healing in diabetic rats, Int. J. Biol. Macromol. 162 (2020) 1465–1475. https://doi.org/10.1016/J.IJBIOMAC.2020.08.027.

[17] K. Elumalai, S. Srinivasan, A. Shanmugam, Review of the efficacy of nanoparticle-based drug delivery systems for cancer treatment, Biomed. Technol. 5 (2024) 109–122. https://doi.org/10.1016/J.BMT.2023.09.001.

[18] H. Sabit, M. Abdel-Hakeem, T. Shoala, S. Abdel-Ghany, M.M. Abdel-Latif, J. Almulhim, M. Mansy, Nanocarriers: a reliable tool for the delivery of anticancer drugs, Pharmaceutics 14 (2022) 1566. https://doi.org/10.3390/PHARMACEUTICS14081566.

[19] F.U. Din, W. Aman, I. Ullah, O.S. Qureshi, O. Mustapha, S. Shafique, A. Zeb, Effective use of nanocarriers as drug delivery systems for the treatment of selected tumors, Int. J. Nanomedicine 12 (2017) 7309. https://doi.org/10.2147/IJN.S146315.

[20] L. Bonilla, M. Espina, P. Severino, A. Cano, M. Ettcheto, A. Camins, M.L. García, E.B. Souto, E. Sánchez-López, Lipid nanoparticles for the posterior eye segment, Pharmaceutics 14 (2021) 90. https://doi.org/10.3390/pharmaceutics14010090.

[21] M. Kiralan, G. Yildirim, Rosehip (Rosa canina L.) Oil, Fruit Oils Chem. Funct. (2019) 803–814. https://doi.org/10.1007/978-3-030-12473-1_43.

[22] A. Bhave, V. Schulzova, H. Chmelarova, L. Mrnka, J. Hajslova, Assessment of rosehips based on the content of their biologically active compounds, J. Food Drug Anal. 25 (2017) 681–690. https://doi.org/10.1016/J.JFDA.2016.12.019.

[23] P. Strugała, W. Gładkowski, A.Z. Kucharska, A. Sokół-Łetowska, J. Gabrielska, Antioxidant activity and anti-inflammatory effect of fruit extracts from blackcurrant, chokeberry, hawthorn, and rosehip, and their mixture with linseed oil on a model lipid membrane, Eur. J. Lipid Sci. Technol. 118 (2016) 461–474. https://doi.org/10.1002/EJLT.201500001.

[24] M. Gehrcke, L.M. Giuliani, L.M. Ferreira, A.V. Barbieri, M.H.M. Sari, E.F. da Silveira, J.H. Azambuja, C.W. Nogueira, E. Braganhol, L. Cruz, Enhanced photostability, radical scavenging and antitumor activity of indole-3-carbinol-loaded rose hip oil nanocapsules, Mater. Sci. Eng. C 74 (2017) 279–286. https://doi.org/10.1016/J.MSEC.2016.12.006.

[25] L. Bonilla-Vidal, M. Espina, M.L. García, C. Cimino, C. Carbone, L. Baldomà, J. Badia, A. Gliszczyńska, E.B. Souto, E. Sánchez-López, Melatonin loaded nanostructured lipid carriers for the treatment of uveal melanoma, J. Drug Deliv. Sci. Technol. (2024) 106057. https://doi.org/10.1016/J.JDDST.2024.106057.

[26] G. Esteruelas, L. Halbaut, V. García-Torra, M. Espina, A. Cano, M. Ettcheto, A. Camins, E.B. Souto, M. Luisa García, E. Sánchez-López, Development and optimization of Riluzole-loaded biodegradable nanoparticles incorporated in a mucoadhesive in situ gel for the posterior eye segment, Int. J. Pharm. 612 (2022) 121379. https://doi.org/10.1016/j.ijpharm.2021.121379.

[27] X. Llorente, G. Esteruelas, L. Bonilla, M.G. Agudelo, I. Filgaira, D. Lopez-Ramajo, R.C. Gong, C. Soler, M. Espina, M.L. García, J. Manils, M. Pujol, E. Sánchez-López, Riluzole-loaded nanostructured lipid carriers for hyperproliferative skin diseases, Int. J. Mol. Sci. 24 (2023) 8053. https://doi.org/10.3390/IJMS24098053/S1.

[28] R. Galindo, E. Sánchez-López, M.J. Gómara, M. Espina, M. Ettcheto, A. Cano, I. Haro, A. Camins, M.L. García, Development of peptide targeted PLGA-PEGylated nanoparticles loading Licochalcone-A for ocular inflammation, Pharmaceutics 14 (2022) 285. https://doi.org/10.3390/PHARMACEUTICS14020285.

[29] V. Thiruchenthooran, M. Świtalska, L. Bonilla, M. Espina, M.L. García, J. Wietrzyk, E. Sánchez-López, A. Gliszczyńska, Novel strategies against cancer: dexibuprofen-loaded nanostructured lipid carriers, Int. J. Mol. Sci. 23 (2022) 11310. https://doi.org/10.3390/IJMS231911310.

[30] F. Elmsmari, J.A. González Sánchez, F. Duran-Sindreu, R. Belkadi, M. Espina, M.L. García, E. Sánchez-López, Calcium hydroxide-loaded PLGA biodegradable nanoparticles as an intracanal medicament, Int. Endod. J. 54 (2021) 2086–2098. https://doi.org/10.1111/IEJ.13603.

[31] C. Folle, A.M. Marqués, N. Díaz-Garrido, M. Espina, E. Sánchez-López, J. Badia, L. Baldoma, A.C. Calpena, M.L. García, Thymol-loaded PLGA nanoparticles: an efficient approach for acne treatment, J. Nanobiotechnology 19 (2021) 359. https://doi.org/10.1186/S12951-021-01092-Z.

[32] A. Gliszczyńska, N. Niezgoda, W. Gładkowski, M. Czarnecka, M. Świtalska, J. Wietrzyk, Synthesis and Biological Evaluation of Novel Phosphatidylcholine Analogues Containing Monoterpene Acids as Potent Antiproliferative Agents, PLoS One 11 (2016). https://doi.org/10.1371/JOURNAL.PONE.0157278.

[33] D. Nevozhay, Cheburator software for automatically calculating drug inhibitory concentrations from in vitro screening assays, PLoS One 9 (2014) e106186. https://doi.org/10.1371/JOURNAL.PONE.0106186.

[34] A. Zeb, O.S. Qureshi, H.S. Kim, M.S. Kim, J.H. Kang, J.S. Park, J.K. Kim, High payload

itraconazole-incorporated lipid nanoparticles with modulated release property for oral and parenteral administration, J. Pharm. Pharmacol. 69 (2017) 955–966. https://doi.org/10.1111/JPHP.12727.

[35] A.A. Khan, I.M. Abdulbaqi, R. Abou Assi, V. Murugaiyah, Y. Darwis, Lyophilized hybrid nanostructured lipid carriers to enhance the cellular uptake of verapamil: statistical optimization and in vitro evaluation, Nanoscale Res. Lett. 13 (2018) 323. https://doi.org/10.1186/S11671-018-2744-6.

[36] M. Vlachou, A. Eikosipentaki, V. Xenogiorgis, Pineal hormone melatonin: solubilization studies in model aqueous gastrointestinal environments, Curr. Drug Deliv. 3 (2006) 255–265. https://doi.org/10.2174/156720106777731073.

[37] H. Bunjes, K. Westesen, M.H.J. Koch, Crystallization tendency and polymorphic transitions in triglyceride nanoparticles, Int. J. Pharm. 129 (1996) 159–173. https://doi.org/10.1016/0378-5173(95)04286-5.

[38] S.M. Alshehri, F. Shakeel, M.A. Ibrahim, E.M. Elzayat, M. Altamimi, K. Mohsin, O.T. Almeanazel, M. Alkholief, A. Alshetaili, B. Alsulays, F.K. Alanazi, I.A. Alsarra, Dissolution and bioavailability improvement of bioactive apigenin using solid dispersions prepared by different techniques, Saudi Pharm. J. 27 (2019) 264–273. https://doi.org/10.1016/J.JSPS.2018.11.008.

[39] X. Fu, W. Kong, Y. Zhang, L. Jiang, J. Wang, J. Lei, Novel solid–solid phase change materials with biodegradable trihydroxy surfactants for thermal energy storage, RSC Adv. 5 (2015) 68881–68889. https://doi.org/10.1039/C5RA11842E.

[40] E.B. Souto, W. Mehnert, R.H. Müller, Polymorphic behaviour of Compritol 888 ATO as bulk lipid and as SLN and NLC, J. Microencapsul. 23 (2006) 417–433. https://doi.org/10.1080/02652040600612439.

[41] C. Freitas, R.H. Müller, Correlation between long-term stability of solid lipid nanoparticles (SLN) and crystallinity of the lipid phase, Eur. J. Pharm. Biopharm. 47 (1999) 125–132. https://doi.org/10.1016/S0939-6411(98)00074-5.

[42] L.A.S. Bahari, H. Hamishehkar, The impact of variables on particle size of solid lipid nanoparticles and nanostructured lipid carriers; a comparative literature review, Adv. Pharm. Bull. 6 (2016) 151. https://doi.org/10.15171/APB.2016.021.

[43] S.H. Suhaimi, R.H. Hisam, N.A. Rosli, Effects of dormulation parameters on particle size and polydispersity index of Orthosiphon stamineus loaded nanostructured lipid carrier, J. Adv. Res. Appl. Sci. Eng. Technol. 1 (2015) 36–39.

[44] K.S. Oh, R.S. Kim, J. Lee, D. Kim, S.H. Cho, S.H. Yuk, Gold/chitosan/pluronic composite nanoparticles for drug delivery, J. Appl. Polym. Sci. 108 (2008) 3239–3244. https://doi.org/10.1002/APP.27767.

[45] Y. Seo, H. Lim, H. Park, J. Yu, J. An, H.Y. Yoo, T. Lee, Recent progress of lipid nanoparticles-based lipophilic drug delivery: focus on surface modifications, Pharmaceutics 15 (2023) 772. https://doi.org/10.3390/PHARMACEUTICS15030772.

[46] K. Sen, S. Banerjee, M. Mandal, Dual drug loaded liposome bearing apigenin and 5-Fluorouracil for synergistic therapeutic efficacy in colorectal cancer, Colloids Surfaces B Biointerfaces 180 (2019) 9–22. https://doi.org/10.1016/J.COLSURFB.2019.04.035.

[47] S. Akay, B. Kayan, Y. Yang, Solubility and chromatographic separation of 5-Fluorouracil under subcritical water conditions, J. Chem. Eng. Data 62 (2017) 1538–1543.

https://doi.org/10.1021/ACS.JCED.7B00015/ASSET/IMAGES/MEDIUM/JE-2017-00015J_0004.GIF.

[48] F. Aghaz, A. Vaisi-Raygani, M. Khazaei, E. Arkan, S. Kashanian, Enhanced synergistic-antioxidant activity of melatonin and tretinoin by co-encapsulation into amphiphilic chitosan nanocarriers: during mice in vitro matured oocyte/morula-compact stage embryo culture model, Reprod. Sci. 28 (2021) 3361–3379. https://doi.org/10.1007/S43032-021-00670-8/TABLES/5.

[49] L. Ding, Y. Huang, X.X. Cai, S. Wang, Impact of pH, ionic strength and chitosan charge density on chitosan/casein complexation and phase behavior, Carbohydr. Polym. 208 (2019) 133–141. https://doi.org/10.1016/J.CARBPOL.2018.12.015.

[50] A.T. Ojo, C. Ma, P.I. Lee, Elucidating the effect of crystallization on drug release from amorphous solid dispersions in soluble and insoluble carriers, Int. J. Pharm. 591 (2020) 120005. https://doi.org/10.1016/J.IJPHARM.2020.120005.

[51] Z. Huang, C. Ma, M. Wu, X. Li, C. Lu, X. Zhang, X. Ma, Y. Yang, Y. Huang, X. Pan, C. Wu, Exploring the drug-lipid interaction of weak-hydrophobic drug loaded solid lipid nanoparticles by isothermal titration calorimetry, J. Nanoparticle Res. 22 (2020) 1–14. https://doi.org/10.1007/S11051-019-4671-6/METRICS.

[52] R.R. Ruela-De-Sousa, G.M. Fuhler, N. Blom, C. V. Ferreira, H. Aoyama, M.P. Peppelenbosch, Cytotoxicity of apigenin on leukemia cell lines: implications for prevention and therapy, Cell Death Dis. 1 (2010). https://doi.org/10.1038/cddis.2009.18.

[53] M.G. Ng, K.Y. Ng, R.Y. Koh, S.M. Chye, Potential role of melatonin in prevention and treatment of leukaemia, Horm. Mol. Biol. Clin. Investig. 42 (2021) 445–461. https://doi.org/10.1515/HMBCI-2021-0009/ASSET/GRAPHIC/J_HMBCI-2021-0009_FIG_001.JPG.

[54] S. Das, J. Das, A. Samadder, N. Boujedaini, A.R. Khuda-Bukhsh, Apigenin-induced apoptosis in A375 and A549 cells through selective action and dysfunction of mitochondria, Exp. Biol. Med. 237 (2012) 1433–1448. https://doi.org/10.1258/EBM.2012.012148.

[55] R.H. Patil, R.L. Babu, M. Naveen Kumar, K.M. Kiran Kumar, S.M. Hegde, G.T. Ramesh, S. Chidananda Sharma, Apigenin inhibits PMA-induced expression of pro-inflammatory cytokines and AP-1 factors in A549 cells, Mol. Cell. Biochem. 403 (2015) 95–106. https://doi.org/10.1007/S11010-015-2340-3/METRICS.

[56] Z. Zhou, M. Tang, Y. Liu, Z. Zhang, R. Lu, J. Lu, Apigenin inhibits cell proliferation, migration, and invasion by targeting Akt in the A549 human lung cancer cell line, Anticancer. Drugs 28 (2017) 446–456. https://doi.org/10.1097/CAD.0000000000000479.

[57] M.H. Kahkesh, Z. Salehi, M. Najafi, A. Ghobadi, M. Izad, A. Shirazi, The inhibitory effect of melatonin on the proliferation of irradiated A549 cell line, J. Cancer Res. Ther. 16 (2020) 1500–1505. https://doi.org/10.4103/JCRT.JCRT_682_19.

[58] Q. Zhou, S. Gui, Q. Zhou, Y. Wang, Melatonin inhibits the migration of human lung adenocarcinoma A549 cell lines involving JNK/MAPK pathway, PLoS One 9 (2014) e101132. https://doi.org/10.1371/JOURNAL.PONE.0101132.

[59] J.J. Lu, L. Fu, Z. Tang, C. Zhang, L. Qin, J. Wang, Z. Yu, D. Shi, X. Xiao, F. Xie, W. Huang, W. Deng, Melatonin inhibits AP-2β/hTERT, NF-κB/COX-2 and Akt/ERK and activates caspase/Cyto C signaling to enhance the antitumor activity of berberine in lung cancer cells, Oncotarget 7 (2016) 3001. https://doi.org/10.18632/ONCOTARGET.6407.

[60] P.P. Phiboonchaiyanan, P. Puthongking, V. Chawjarean, S. Harikarnpakdee, M. Sukprasansap, P. Chanvorachote, A. Priprem, P. Govitrapong, Melatonin and its derivative disrupt cancer stem-like phenotypes of lung cancer cells via AKT downregulation, Clin. Exp. Pharmacol. Physiol. 48 (2021) 1712–1723. https://doi.org/10.1111/1440-1681.13572.

[61] T.C. Chou, Theoretical basis, experimental design, and computerized simulation of synergism and antagonism in drug combination studies, Pharmacol. Rev. 58 (2006) 621–681. https://doi.org/10.1124/PR.58.3.10.

[62] P. Zagami, L.A. Carey, Triple negative breast cancer: Pitfalls and progress, Npj Breast Cancer 8 (2022) 1–10. https://doi.org/10.1038/s41523-022-00468-0.

[63] M.R.P. Coombs, M.E. Harrison, D.W. Hoskin, Apigenin inhibits the inducible expression of programmed death ligand 1 by human and mouse mammary carcinoma cells, Cancer Lett. 380 (2016) 424–433. https://doi.org/10.1016/J.CANLET.2016.06.023.

[64] D. Bauer, E. Mazzio, A. Hilliard, E.T. Oriaku, K.F.A. Soliman, Effect of apigenin on whole transcriptome profile of TNFα–activated MDA–MB–468 triple negative breast cancer cells, Oncol. Lett. 19 (2020) 2123–2132. https://doi.org/10.3892/OL.2020.11327/HTML.

[65] M.E. Harrison, M.R. Power Coombs, L.M. Delaney, D.W. Hoskin, Exposure of breast cancer cells to a subcytotoxic dose of apigenin causes growth inhibition, oxidative stress, and hypophosphorylation of Akt, Exp. Mol. Pathol. 97 (2014) 211–217. https://doi.org/10.1016/J.YEXMP.2014.07.006.

[66] J.H.M. Marques, A.L. Mota, J.G. Oliveira, J.Z. Lacerda, J.P. Stefani, L.C. Ferreira, T.B. Castro, A.F. Aristizábal-Pachón, D.A.P.C. Zuccari, Melatonin restrains angiogenic factors in triple-negative breast cancer by targeting miR-152-3p: In vivo and in vitro studies, Life Sci. 208 (2018) 131–138. https://doi.org/10.1016/J.LFS.2018.07.012.

[67] B.L.V. de Godoy, M.G. Moschetta-Pinheiro, L.G. de A. Chuffa, N.F. Pondé, R.J. Reiter, J. Colombo, D.A.P. de C. Zuccari, Synergistic actions of Alpelisib and Melatonin in breast cancer cell lines with PIK3CA gene mutation, Life Sci. 324 (2023). https://doi.org/10.1016/J.LFS.2023.121708.

[68] I. Jardin, R. Diez-Bello, D. Falcon, S. Alvarado, S. Regodon, G.M. Salido, T. Smani, J.A. Rosado, Melatonin downregulates TRPC6, impairing store-operated calcium entry in triple-negative breast cancer cells, J. Biol. Chem. 296 (2021) 100254. https://doi.org/10.1074/JBC.RA120.015769.

[69] D.L. Holliday, V. Speirs, Choosing the right cell line for breast cancer research, Breast Cancer Res. 13 (2011) 215. https://doi.org/10.1186/BCR2889.

[70] H.S. Seo, H.S. Choi, S.R. Kim, Y.K. Choi, S.M. Woo, I. Shin, J.K. Woo, S.Y. Park, Y.C. Shin, S.K. Ko, Apigenin induces apoptosis via extrinsic pathway, inducing p53 and inhibiting STAT3 and NFκB signaling in HER2-overexpressing breast cancer cells, Mol. Cell. Biochem. 366 (2012) 319–334. https://doi.org/10.1007/S11010-012-1310-2/FIGURES/7.

[71] I. Vrhovac Madunić, J. Madunić, M. Antunović, M. Paradžik, V. Garaj-Vrhovac, D. Breljak, I. Marijanović, G. Gajski, Apigenin, a dietary flavonoid, induces apoptosis, DNA damage, and oxidative stress in human breast cancer MCF-7 and MDA MB-231 cells, Naunyn. Schmiedebergs. Arch. Pharmacol. 391 (2018) 537–550. https://doi.org/10.1007/S00210-018-1486-4/FIGURES/6.

[72] A.K. Shendge, D. Chaudhuri, T. Basu, N. Mandal, A natural flavonoid, apigenin isolated from Clerodendrum viscosum leaves, induces G2/M phase cell cycle arrest and apoptosis in

MCF-7 cells through the regulation of p53 and caspase-cascade pathway, Clin. Transl. Oncol. 23 (2021) 718–730. https://doi.org/10.1007/S12094-020-02461-0/FIGURES/9.

[73] S. Cos, M.D. Mediavilla, R. Fernández, D. González-Lamuño, E.J. Sánchez-Barceló, Does melatonin induce apoptosis in MCF-7 human breast cancer cells in vitro?, J. Pineal Res. 32 (2002) 90–96. https://doi.org/10.1034/J.1600-079X.2002.1821.X.

[74] A. Cucina, S. Proietti, F. D'Anselmi, P. Coluccia, S. Dinicola, L. Frati, M. Bizzarri, Evidence for a biphasic apoptotic pathway induced by melatonin in MCF-7 breast cancer cells, J. Pineal Res. 46 (2009) 172–180. https://doi.org/10.1111/J.1600-079X.2008.00645.X.

[75] S. Cos, C. Martínez-Campa, M.D. Mediavilla, E.J. Sánchez-Barceló, Melatonin modulates aromatase activity in MCF-7 human breast cancer cells, J. Pineal Res. 38 (2005) 136–142. https://doi.org/10.1111/J.1600-079X.2004.00186.X.

[76] S.E. Khuda, A. V. Nguyen, G.M. Sharma, M.S. Alam, K. V. Balan, K.M. Williams, Effects of emulsifiers on an in vitro model of intestinal epithelial tight junctions and the transport of food allergens, Mol. Nutr. Food Res. 66 (2022) e2100576. https://doi.org/10.1002/MNFR.202100576.

[77] H. Ilyasoğlu, H. Ilyaso, Characterization of rosehip (Rosa canina L.) seed and seed oil, Int. J. Food Prop. 17 (2014) 1591–1598. https://doi.org/10.1080/10942912.2013.777075.

[78] I. Mármol, N. Jiménez-Moreno, C. Ancín-Azpilicueta, J. Osada, E. Cerrada, M.J. Rodríguez-Yoldi, A combination of Rosa Canina extracts and gold complex favors apoptosis of Caco-2 cells by increasing oxidative stress and mitochondrial dysfunction, Antioxidants 9 (2019) 17. https://doi.org/10.3390/ANTIOX9010017.

[79] P. Cagle, O. Idassi, J. Carpenter, R. Minor, I. Goktepe, P. Martin, Effect of rosehip (Rosa Canina) extracts on human brain tumor cell proliferation and apoptosis, J. Cancer Ther. 2012 (2012) 534–545. https://doi.org/10.4236/JCT.2012.35069.

[80] Z. Ayati, M.S. Amiri, M. Ramezani, E. Delshad, A. Sahebkar, S.A. Emami, Phytochemistry, traditional uses and pharmacological profile of rose hip: a review, Curr. Pharm. Des. 24 (2018) 4101–4124. https://doi.org/10.2174/1381612824666181010151849.

[81] J.B. Strachan, B.P. Dyett, Z. Nasa, C. Valery, C.E. Conn, Toxicity and cellular uptake of lipid nanoparticles of different structure and composition, J. Colloid Interface Sci. 576 (2020) 241–251. https://doi.org/10.1016/J.JCIS.2020.05.002.

3.6. Combination of Apigenin and Melatonin loaded nanostructured lipid carriers as a natural ocular inflammation treatment

Lorena Bonilla Vidal, Marta Espina, Maria Luisa García, Laura Baldomà, Josefa Badia, Anna Gliszczyńska, Eliana B Souto, Elena Sánchez López

Colloids and Surfaces B: Biointerfaces

IF (JCR- 2023) 5.4, Biophysics 8/77 (Q1)

Enviado

Combination of Apigenin and Melatonin with nanostructured lipid carriers as anti-inflammatory ocular treatment

Lorena Bonilla-Vidal[1,2]; Marta Espina[1,2]; María Luisa García[1,2]; Laura Baldomà[3,4]; Josefa Badia[3,4]; Anna Gliszczyńska[5], Eliana B. Souto[6]; Elena Sánchez-López[1,2*]

[1] Department of Pharmacy, Pharmaceutical Technology and Physical Chemistry, University of Barcelona, 08028 Barcelona, Spain
[2] Institute of Nanoscience and Nanotechnology (IN^{2}UB), University of Barcelona, 08028 Barcelona, Spain
[3] Department of Biochemistry and Physiology, University of Barcelona, 08028 Barcelona, Spain
[4] Institute of Biomedicine of the University of Barcelona (IBUB), Institute of Research of Sant Joan de Déu (IRSJD), 08950 Barcelona, Spain
[5] Department of Food Chemistry and Biocatalysis, Wrocław University of Environmental and Life Sciences, Norwida 25, 50-375 Wrocław, Poland
[6] UCD School of Chemical and Bioprocess Engineering, University College Dublin, Belfield, Ireland

*corresponding author: esanchezlopez@ub.edu

Abstract

Ocular inflammation is a complex pathology with limited treatment options. While traditional therapies have side effects, novel approaches, such as natural compounds like Apigenin (APG) and Melatonin (MEL) offer promising solutions. APG and MEL, in combination with nanostructured lipid carriers (NLC), may provide a synergistic effect in treating ocular inflammation, potentially improving patient outcomes and reducing adverse effects. NLC could provide a chemical protection of these compounds, while offering a sustained release into the ocular surface. Optimized NLC exhibited suitable physicochemical parameters, physical stability, sustained release of APG and MEL, and were biocompatible *in vitro* in a corneal cell line, and *in ovo* by using HET-CAM test. *In vitro* and *in vivo* studies confirmed the NLCs' ability to attenuate inflammation by reducing IL-6, IL-8 and MCP-1 cytokine levels and decreasing inflammation in a rabbit model. These findings suggest that the co-encapsulation of APG and MEL into NLC could represent a promising strategy for managing ocular inflammatory conditions.

Keywords

Lipid nanoparticles, Apigenin, Melatonin, co-encapsulation, ocular inflammation, in vitro.

1. Introduction

Ocular inflammation constitutes a significant and multifaceted challenge in ophthalmology. Encompassing a spectrum of disorders affecting several ocular structures, from the orbit to the optic nerve, ocular inflammation treatment requires a comprehensive

approach involving multiple medical disciplines (1). The etiology of ocular inflammation is diverse, ranging from infectious and autoimmune processes to vascular and degenerative conditions (2). While often considered a secondary manifestation of systemic diseases, such as rheumatoid arthritis or lupus, ocular inflammation can also be a primary disorder with potentially severe consequences, including vision loss (3,4).

The management of ocular inflammation involves substantial therapeutic challenges. Traditionally, corticosteroids and nonsteroidal anti-inflammatory drugs (NSAIDs) have constituted the first-line treatment (5,6), but these agents are associated with significant adverse effects, both locally and systemically (7). The emergence of novel therapeutic strategies, including immunomodulatory and biologic agents, offers promising avenues for improved patient outcomes (8). In this area, a better understanding of the underlying pathophysiology of ocular inflammatory diseases is crucial in order to develop targeted and effective therapies (9). Recent research has highlighted the role of inflammatory mediators in conditions previously considered non-inflammatory, such as age-related macular degeneration (AMD) and diabetic retinopathy, emphasizing the need for a re-evaluation of treatment paradigms (10,11).

Among anti-inflammatory molecules, natural compounds constitute an emerging novel therapeutic field. In this area, two compounds stand out: Apigenin (APG), the main flavone of chamomile, and Melatonin (MEL), a neurohormone. APG exhibits potent anti-inflammatory properties primarily by inhibiting the expression of inducible nitric oxide synthase (iNOS) and cyclooxygenase-2 (COX-2), key enzymes in inflammatory pathways (12,13). This reduction in pro-inflammatory mediators is attributed to APG ability to suppress the activation of transcription factors, such as NF-κB, responsible for regulating inflammatory gene expression. Additionally, APG antioxidant properties contribute to its anti-inflammatory effects (14). On the other hand, MEL, an indoleamine synthesized primarily in the pineal gland, exhibits also potent anti-inflammatory properties. Its antioxidant activity, including direct radical scavenging and induction of antioxidant enzymes, mitigates oxidative stress, a key driver of inflammation (15). MEL also modulates inflammatory responses by inhibiting the nuclear translocation of NF-κB, a transcription factor pivotal in regulating pro-inflammatory gene expression (16). Consequently, MEL suppresses the production of cytokines, such as TNF-α and IL-6, and adhesion molecules, thereby attenuating inflammatory processes (17). Furthermore, it is well-known that MEL is able to decrease intraocular pressure (IOP), which could counteract the side effects of NSAIDs and corticosteroids (18). In this way, the combination of PAG and MEL via complementary therapeutic pathways to inhibit inflammation, could represent a disruptive therapeutic strategy to treat ocular inflammatory pathologies also avoiding common adverse effects of conventional treatments. Despite the promising synergistic potential of this combination, a primary limitation is the low bioavailability of both components. MEL exhibits poor aqueous solubility, rapid clearance, and susceptibility to photodegradation, while APG suffers from extensive metabolism and low aqueous solubility (19,20).

The ocular surface presents a barrier to drug delivery, characterized by rapid tear turnover, anatomical corneal barrier, enzymatic degradation, and efficient drug efflux. These physiological challenges, coupled with the delicate nature of ocular tissues, significantly hinder the development of effective ophthalmic formulations (21). Conventional dosage forms, such as solutions and suspensions, often exhibit poor bioavailability due to rapid drainage and precorneal loss. Consequently, frequent administration is required, increasing patient burden and potentially inducing ocular irritation. To address these limitations, nanotechnology-based drug delivery systems have emerged as promising alternatives (22,23). Lipid nanoparticles offer several advantages including enhanced drug solubility, prolonged ocular residence time, and protection from enzymatic degradation.

This approach holds the potential to improve therapeutic efficacy, reduce dosing frequency, and minimize adverse effects, ultimately enhancing patient compliance and treatment outcomes (22). Furthermore, last generation of lipid nanoparticles, the nanostructured lipid carriers (NLC), also incorporate a liquid lipid which, in this case is rosehip oil, since it also may reinforce the intrinsic anti-inflammatory and anti-oxidant properties of APG and MEL (24,25).

Previous studies have demonstrated the potential of NLC encapsulating APG for dry eye disease (26), or MEL for the potential treatment of uveal melanoma (27). In order to combine the potential of both compounds, a novel cationic NLC formulation co-encapsulating APG and MEL was developed. The incorporation of dimethyldioctadecylammonium bromide (DDAB) as a cationic surfactant aimed to improve the ocular bioavailability of the NLC by promoting electrostatic interactions with the negatively charged ocular mucosa (28). This approach was supported by previous studies demonstrating DDAB's safety and efficacy in ocular drug delivery (29). The present investigation sought to optimize this cationic NLC formulation for the treatment of ocular inflammation through comprehensive *in vitro* and *in vivo* evaluation of biocompatibility, cytotoxicity, and anti-inflammatory properties *in vitro* and *in vivo*.

2. Materials and methods

2.1. Materials

APG was procured from Apollo Scientific (Cheshire, UK). MEL was obtained from Thermo Fisher Scientific (Massachusetts, USA). Compritol® 888 ATO (glyceryl distearate) was supplied by Gattefossé (Madrid, Spain). Tween® 80 (Polysorbate 80) and Nile red (NR) were purchased from Sigma-Aldrich (Madrid, Spain). Rosehip oil was acquired from Acofarma Fórmulas Magistrales (Barcelona, Spain), and DDAB was obtained from TCI Europe (Zwijndrecht, Belgium). All additional reagents employed were of analytical grade purity. Ultrapure water was generated using a Millipore Milli-Q Plus system.

2.2. APG-MEL-NLC preparation and optimization

APG-MEL-NLC were fabricated by the hot high-pressure homogenization using a Homogenizer FPG 12800 (Stansted, UK) previously optimized (30). Briefly, a pre-emulsion was initially formed by subjecting the components to 8000 rpm agitation for 30 seconds using an Ultraturrax® T25 (IKA, Germany). Subsequent homogenization was conducted under controlled conditions of 85 °C, with three cycles at a pressure of 900 bar. In order to produce a positive surface charge NLC, incremental amounts of the cationic lipid DDAB were integrated into APG-MEL-NLC obtained in previous investigations (data not shown).

2.3. Physicochemical characterization

The physicochemical properties average size (Z_{av}) and polydispersity index (PI) were characterized by photon correlation spectroscopy (PCS), using a Zetasizer NanoZS (Malvern Instruments, UK) at 25 °C. Samples were diluted 1:10 in Milli-Q water. Zeta potential (ZP) was assessed using the same instrument, by laser-Doppler electrophoresis, with samples diluted 1:20 in Milli-Q water. All measurements were conducted in triplicate (31).

Encapsulation efficiency (EE) was determined indirectly by quantifying the free APG and MEL in the supernatant after centrifugation of the APG-MEL-NLC dispersion through an Amicon® Ultra 0.5 centrifugal filter device. The free drug concentrations were determined

by high performance liquid chromatography (HPLC), and EE was calculated based on the difference between the initial drug amount and the free drug content using Eq. 1 (32).

$$EE = \frac{Total\ amount\ of\ APG{+}MEL - Free\ amount\ of\ APG{+}MEL}{Total\ amount\ of\ APG{+}MEL} x\ 100 \quad \text{Equation 1}$$

APG and MEL concentrations were quantified via reverse-phase HPLC. An HPLC Waters 2695 separation module (Waters, Massachusetts, USA) equipped with a Kromasil® C18 column (5 µm, 150 × 4.6 mm) was used for analysis. The mobile phase comprised a water phase containing 2 % acetic acid and an organic phase composed of methanol. A gradient elution was implemented, initiating with 40 % water phase, progressing to 60 % water phase over 5 min, followed by a reverse gradient returning to 40 % water phase in the subsequent 5 min. The flow rate was maintained at 0.9 mL/min. Drug quantifications were achieved using a Waters® 2996 diode array detector at 300 nm, with data processed using Empower® 3 Software (30).

2.4. Characterization of optimized APG-MEL-NLC

2.4.1. Transmission electron microscopy

The morphology of the NLC was examined using transmission electron microscopy (TEM) on a JEOL 1010 microscope (Akishima, Japan). Negative staining with 2 % uranyl acetate was performed on UV-activated copper grids to visualize the morphology of APG-MEL-NLC (33).

2.4.2. Interaction studies

Thermal properties of APG-MEL-NLC were characterized using differential scanning calorimetry (DSC) on a DSC 823e System (Mettler-Toledo, Barcelona, Spain). The system was calibrated with an indium pan and an empty pan as reference. Samples were heated from 25 to 105 °C at 10 °C/min under nitrogen atmosphere. Data were analyzed using Mettler STARe V 9.01 dB software. The crystallinity of the samples was evaluated using X-ray diffraction (XRD) with CuKα radiation in the 2θ range of 2° to 60°. Fourier transformed-infrared (FTIR) analysis of APG-MEL-NLC was conducted using a Thermo Scientific Nicolet iZ10 spectrometer equipped with an ATR diamond and a DTGS detector (34).

2.5. Stability studies

APG-MEL-NLC samples were subjected to storage at 4, 25, and 37 °C for several days. Stability was assessed by monitoring light backscattering (BS) profiles using a Turbiscan® Lab instrument at 30-day intervals. A glass cell containing 10 mL of sample was utilized, with measurements conducted using a pulsed near-infrared light-emitting diode (λ = 880 nm) and a detector positioned at a 45° angle. Simultaneously, Z_{av}, PI, ZP, and EE values were determined (35).

2.6. Biopharmaceutical behavior

In vitro release of APG and MEL from NLC formulations was evaluated using Franz-type diffusion cells with a diffusion area of 0.20 cm^2 and cellulose dialysis membranes (MWCO 12 kDa). Experiments were conducted under previously described conditions (30), using a PBS solution containing 5 % Tween® 80 and 20 % ethanol (pH 7.4) as the receptor medium. NLC formulations were compared to APG and MEL solutions as controls. Release studies were performed at 37.0 ± 0.5 °C for 48 h. Formulations (300 µL) were applied to the donor compartment, and samples (150 µL) were collected at specific time intervals, replaced with fresh receptor solution. APG and MEL concentrations in the receptor medium were

determined by HPLC, and cumulative release amounts were calculated. Each sample was analyzed in triplicate.

2.7. Ocular tolerance

2.7.1. *In vitro* study: HET-CAM test and HET-CAM TBS

The HET-CAM assay was employed to assess the *in vitro* ocular tolerance of APG-MEL-NLC formulations for ophthalmic suitability. Adhering to ICCVAM guidelines, 300 µL of each formulation (free APG/MEL, APG-MEL-NLC, NaOH 0.1 M, and NaCl 0.9 %) were applied to the choriolantoic membrane (CAM) of fertilized chicken eggs (n=3/group) for 5 min. Signs of irritation, coagulation, and hemorrhage were monitored and the ocular irritation index (OII) was calculated using Eq. 2, where H, V, and C represent time (seconds) to hemorrhage, vasoconstriction, or coagulation, respectively. Formulations were categorized as non-irritating (OII ≤ 0.9), weakly irritating (0.9 < OII ≤ 4.9), moderately irritating (4.9 < OII ≤ 8.9), or irritating (8.9 < OII ≤ 21) (36).

$$OII = \frac{(301-H)\cdot 5}{300} + \frac{(301-V)\cdot 7}{300} + \frac{(301-C)\cdot 9}{300}$$ Equation 2

To quantify membrane damage, trypan blue (TBS) was applied to the CAM following the HET-CAM assay. The CAM was incubated with 1 mL of 0.1 % TBS for 1 min, then rinsed with distilled water to remove excess dye. Subsequently, the stained CAM was excised, homogenized in 5 mL formamide, and the absorbance of the extract measured spectrophotometrically at 595 nm to determine trypan blue incorporation. A calibration curve of TBS in formamide was used to quantify the absorbed dye (26).

2.7.2. *In vivo* study: Draize test

All experimental procedures were conducted in accordance with the guidelines of the UB Ethical Committee for Animal Experimentation and prevailing regulations (Decree 214/97, Gencat). To corroborate HET-CAM results, the Draize primary eye irritation test was performed on male New Zealand albino rabbits (2.0-2.5 kg, San Bernardo farm, Spain). Fifty microliters of each formulation were instilled into the conjunctival sac of each rabbit (n=3/group), followed by gentle massage for corneal penetration. Irritation signs (corneal opacity, conjunctival hyperaemia, chemosis, ocular discharge, iris abnormalities) were monitored immediately, at 1 h, and at 24 h, 48 h, 72 h, 7 days, and 21 days post-instillation. The contralateral untreated eye served as a negative control. Draize scores were assigned based on corneal opacity/cloudiness, iris changes, and conjunctival alterations (hyperaemia, chemosis, swelling, discharge) (37).

2.8. Cellular experiments

2.8.1. Cell culture

Human corneal epithelial (HCE-2) cells were maintained in keratinocyte serum-free growth medium (SFM; Life Technologies, Invitrogen, GIBCO®, Paisley, UK) supplemented with bovine pituitary extract (0.05 mg/mL), epidermal growth factor (5 ng/mL), insulin (0.005 mg/mL), penicillin (100 U/mL), and streptomycin (100 mg/mL). Cells were incubated in flasks at 37 °C with 10 % CO_2 in a humidified environment until reaching 80 % confluence (26).

2.8.2. Cell viability

The cytotoxicity of APG-MEL-NLC was evaluated using the MTT assay, which quantifies metabolic activity of viable cells via tetrazolium salt reduction by intracellular dehydrogenases. HCE-2 cells (100 µL, 2×10^5 cells/mL) were seeded in a 96-well plate and incubated for 48 h at 37 °C. To simulate corneal conditions, cells were exposed to several sample concentrations (6.67×10^{-4} – 5.00×10^{-2} mg/mL of drugs combination) for 5, 15, or 30 min. Following incubation, MTT solution (0.25 % in PBS) was added, and after 2 h, replaced with DMSO. Cell viability was determined by measuring absorbance at 560 nm using a Modulus® Microplate Photometer, expressed as a percentage of untreated control cells (26,38).

2.8.3. Determination of proinflammatory cytokines

To assess the anti-inflammatory activity APG-NLC and free drug combination, HCE-2 cells were seeded at a density of 2×10^5 cells/mL in 12-well plates and cultured until reaching 90 % confluence. Samples were administered for 30 min incubation at a concentration of 0.02 mg drugs combination/mL, and inflammation was induced with lipopolysaccharide (LPS) at 10 µg/mL. LPS-stimulated cells served as a positive control, and untreated cells as a negative control. For the inflammation prevention, treatments were incubated for 30 min, washed with PBS, and incubated with LPS for 24 h. Following 24 h incubation, supernatants were collected, centrifuged at 16,000 g for 10 min at 4 °C, and stored at –80 °C. For the inflammation treatment, LPS was administered for 24 h, and then the treatments were applied for 30 min. Afterwards, supernatants were processed in the same manner.

The levels of pro-inflammatory cytokines interleukin 6 (IL-6), IL-8 and monocyte chemoattractant protein 1 (MCP-1) were quantified in the supernatants using Custom ProcartaPlex Multiplex immunoassays (Labclinics, Barcelona, Spain) according to the manufacturer's protocol, with results expressed as pg/mL.

2.9. *In vivo* anti-inflammatory efficacy

All experimental procedures adhered to the guidelines of the UB Ethical Committee for Animal Experimentation, complying with current regulations (Decree 214/97, Gencat), and were approved under protocol code 326/19. To assess the preventive and anti-inflammatory efficacy of APG-MEL-NLC against ocular inflammation, New Zealand male albino rabbits (n=3/group) were used. Formulations included APG-MEL-NLC, free APG/MEL, and NaCl 0.9 % (control). For the prevention study, 50 µL of each formulation was topically administered, followed by 50 µL of 0.5 % sodium arachidonate (SA) in PBS to induce inflammation in the right eye after 30 min (left eye as control). Conversely, in the anti-inflammatory study, SA was applied 30 min prior to formulation administration. Ocular evaluations were conducted from initial application to 210 min using a modified Draize scoring system (26,39).

2.10. Statistical analysis

Data analysis was performed using GraphPad Prism 9. Two-way ANOVA followed by Tukey's post-hoc test was applied for multiple group comparisons, while Student's t-test was used for pairwise comparisons. Data are presented as mean ± standard deviation (SD), with statistical significance set at $p < 0.05$.

3. Results

3.1. APG-MEL-NLC preparation and optimization

The present study used a previously optimized formulation (lipid phase 5.0 % containing 3.25 % of lipid solid, surfactant 4.0 %, APG 0.067 % and MEL 0.033 %) as a starting point. To investigate the influence of the cationic surfactant on nanoparticle physicochemical properties, increasing concentrations of DDAB were added to APG-MEL-NLC (Table 1). The selection of the optimal cationic formulation was based on achieving a ZP exceeding + 15 mV and a PI below 0.3. In accordance with these parameters, the formulation containing 0.06 % DDAB was determined to be optimal.

Table 1. Effect of cationic lipid on the physicochemical parameters.

DDAB (%)	Z_{av} ± SD (nm)	PI ± SD	ZP ± SD (mV)	EE APG ± SD (%)	EE MEL ± SD (%)
0.05	187.5 ± 0.5	0.211 ± 0.008	11.4 ± 0.2	99.9 ± 0.1	54.9 ± 0.4
0.06	166.2 ± 2.4	0.265 ± 0.007	16.8 ± 0.7	99.9 ± 0.1	54.5 ± 0.2
0.07	148.3 ± 1.3	0.299 ± 0.016	15.3 ± 0.5	99.8 ± 0.1	55.1± 1.0

3.2. Characterization of optimized APG-MEL-NLC

TEM analysis revealed that APG-MEL-NLC particles exhibited a predominantly spherical morphology with a mean hydrodynamic diameter below 200 nm, as confirmed by PCS (Figure 1A). No evidence of particle aggregation was observed.

FTIR spectroscopy was used to investigate molecular interactions among the drugs, surfactant, and lipid matrix (Figure 1B). The FTIR spectrum of APG exhibited characteristic peaks at approximately 3278, 2800, 1650 and 1605 cm^{-1}, attributed to O-H, C-H, and C-O functional groups, respectively (29). MEL displayed distinct peaks at 3303, 1629, 1555, and 1212 cm^{-1}, corresponding to N-H, C=O, C-O, and C-N groups. FTIR spectra obtained from the APG-MEL-NLC system exhibited a prominent absorption band centered at 1100 cm^{-1}, indicative of the presence of the surfactant (40). Notably, no new intense bands were observed in the formulation, suggesting the absence of significant covalent bond formation. Additionally, the diminished or absent peaks of APG and MEL support the encapsulation of both drugs within the lipid matrix.

DSC analysis was employed to evaluate alterations in the crystallinity and melting behavior of the lipid mixtures relative to APG-MEL-NLC (Figure 1C). The melting temperature (T_m) of the lipid mixture was equal than that of the drug-loaded lipid mixture (69.50 °C). Otherwise, T_m of APG-MEL-NLC was lower than that of the physical lipid mixture (67.59 °C), potentially attributed to its reduced particle size and surfactant incorporation (41). Enthalpy values (ΔH) were comparable for the lipid mixture and drug + lipid mixture (74.1 Jg^{-1} vs. 79.2 Jg^{-1}), whereas APG-MEL-NLC exhibited a lower ΔH (55.4 Jg^{-1}). Thermograms of APG and MEL revealed significantly higher T_m and ΔH values (365.50 °C, 198.50 Jg^{-1} and 118.52 °C, 134.70 Jg^{-1}, respectively), suggesting greater crystallinity and melting points compared to the lipid mixtures.

XRD patterns (Figure 1D) provided insights into the physical state of the drugs within the NLC. APG, MEL, and the solid lipid mixture exhibited crystalline characteristics, as evidenced by the presence of sharp, intense peaks in their respective XRD spectra. A reduction in peak intensity for some characteristic MEL diffraction angles (16.34, 20.44 and 26.14°) within the APG-MEL-NLC profile, coupled with small APG peaks (7.02, 11.25 and

15.95°), suggested that both drugs were solubilized within the lipid matrix, consistent with EE data. The crystallinity of other formulation components was also evaluated. The bulk lipid and drug-loaded lipid mixture displayed prominent peaks at 19.36° (2θ) i.e. *d* = 0.46 nm, indicative of the stable β-form of triacylglycerols. Additionally, two distinct peaks at 21.36° (2θ) i.e. *d* = 0.42 nm and 23.59° (2θ) i.e. *d* = 0.38 nm were attributed to the β'-form of triacylglycerols. APG-MEL-NLC also exhibited these characteristic signals, corresponding to the most common triacylglycerol crystallin forms (42,43).

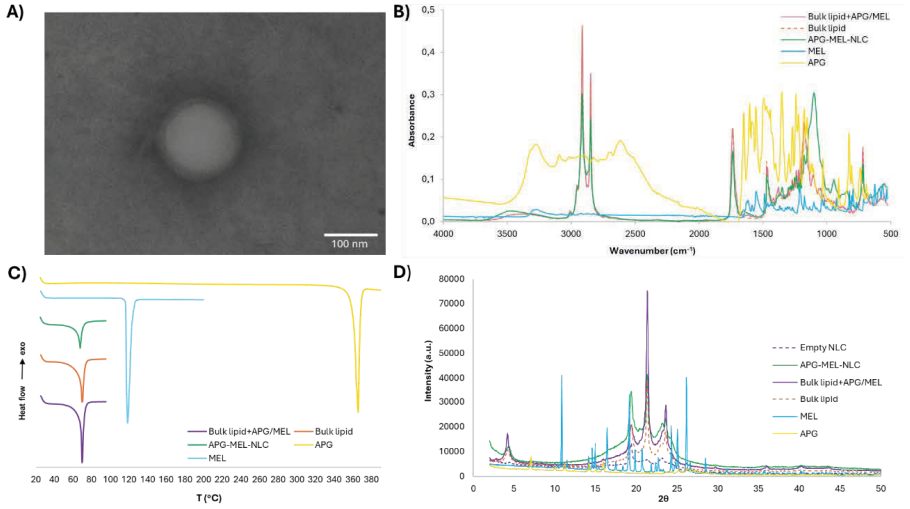

Figure 1. Characterization of optimized APG-MEL-NLC and their components. (A) TEM image (scale bar 100 nm), (B) FTIR analysis, (C) DSC curves, (D) XRD patterns.

3.3. Stability studies

Stability of APG-MEL-NLC was assessed by monitoring changes in Z_{av}, PI, ZP, and EE over time. Additionally, BS profiles were acquired at 4, 25, and 37 °C to detect potential destabilization processes, such as sedimentation, agglomeration, or aggregation, indicated by BS variations exceeding 10 %. The APG-MEL-NLC formulation exhibited stability for 3 months at 4 °C, maintaining consistent physicochemical properties. At 25 °C, stability was observed for 1 months, whereas at 37 °C, the formulation demonstrated stability for only 15 days.

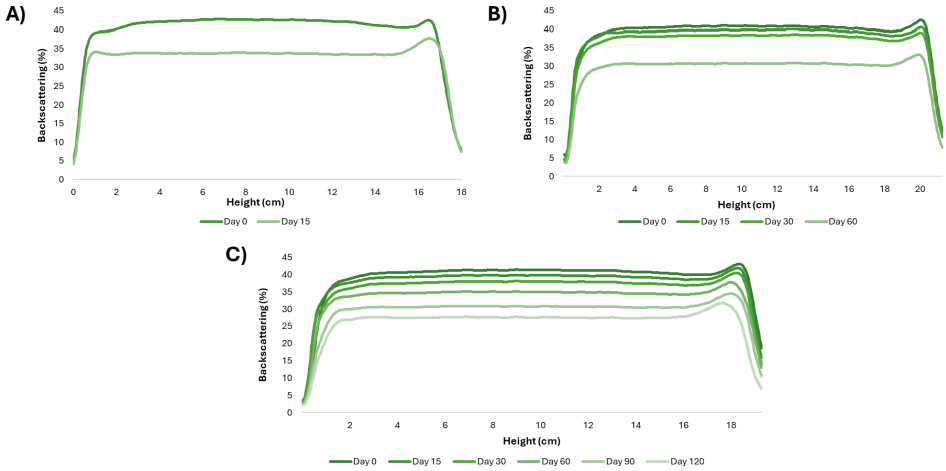

Figure 2. Backscattering profiles of APG-MEL-NLC stored at (A) 37 °C; (B) 25 °C; and (C) 4 °C.

Higher temperatures were associated with accelerated particle destabilization, characterized by a neutralization of ZP. As indicated in Table 2, the formulations maintained their physicochemical properties until a decrease in ZP was observed at 25 and 37 °C, or a decrease in Z_{av} at 4 °C. These alterations were visually observed in the BS profiles, in which a decrease in BS due to the mean size difference regarding to the original formulation occurred. In all the cases, the destabilization was observed because of the 10 % BS difference on the profiles, where the data collectively suggest that APG-MEL-NLC stored at 4 °C exhibited higher stability for up to 3 months.

Table 2. Physicochemical parameters of APG-MEL-NLC stored at different temperatures.

Temperature (°C)	Day	Z_{av} ± SD (nm)	PI ± SD	ZP ± SD (mV)	EE APG ± SD (%)	EE MEL ± SD (%)
	0	160.4 ± 1.6	0.217 ± 0.018	16.1 ± 0.5	99.9 ± 0.1	55.9 ± 0.5
37	15	135.1 ± 1.9	0.201 ± 0.002	11.4 ± 0.4	99.7 ± 0.3	54.2 ± 0.8
25	15	156.0 ± 1.2	0.175 ± 0.014	15.7 ± 0.3	99.9 ± 0.1	53.8 ± 0.4
	30	157.8 ± 2.3	0.189 ± 0.006	13.7 ± 0.3	99.3 ± 0.3	54.1 ± 0.2
	60	147.9 ± 1.0	0.189 ± 0.011	13.1 ± 1.1	99.9 ±0.1	55.1 ± 0.2
4	15	159.6 ± 1.1	0.199 ± 0.007	15.8 ± 0.8	99.9 ± 0.1	55.7 ± 0.4
	30	160.2 ± 5.0	0.173 ± 0.003	15.0 ± 1.3	99.9 ± 0.1	54.9 ± 0.7
	60	157.8 ± 2.1	0.185 ± 0.019	15.9 ± 0.6	99.8 ± 0.2	55.0 ± 0.3
	120	139.1 ± 0.6	0.200 ± 0.010	15.0 ± 0.8	99.9 ± 0.1	54.1 ± 0.9

3.4. Biopharmaceutical behaviour

In vitro release profiles of APG and MEL from NLC were compared to their respective free drug counterparts to characterize the drug release kinetics of the formulation.

As depicted in Figure 5, APG release from APG-MEL-NLC exhibited a biphasic pattern adjusted to a two-phase association model. An initial rapid release phase, likely attributed to APG diffusion from the NLC outer lipid layer, was followed by a sustained release phase associated with APG liberation from the inner lipid core. In contrast, free APG demonstrated

a complete release within 24 h, adjusted to an exponential plateau model. APG-MEL-NLC released approximately 30 % of its APG content over the same period. Kinetic analysis revealed a smaller rate constant (K_d) and a longer half-life ($t_{1/2}$) for the sustained release phase of APG from NLC compared to free APG, confirming the prolonged release profile of the formulation.

MEL release from APG-MEL-NLC followed a biphasic pattern with an initial faster release compared to free MEL, followed by a slower one. While free MEL was completely released within 24 h, approximately 75 % of encapsulated MEL was released. Kinetic parameters demonstrated a lower K_d and a higher $t_{1/2}$ for MEL from NLC, indicating a sustained release profile.

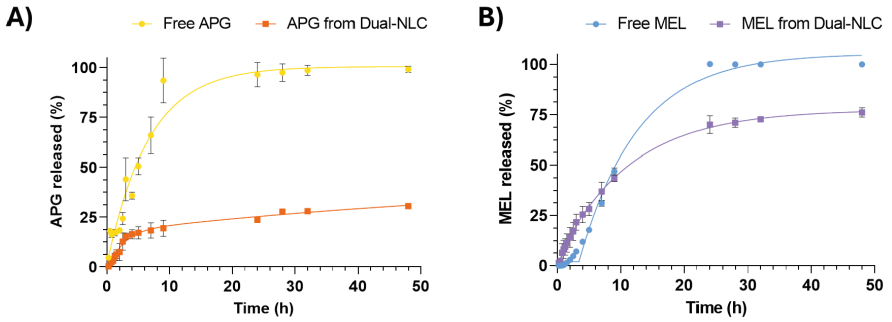

	K_d (h^{-1})	$t_{1/2}$ (h)	*Plateau* (%)	r^2
Free APG	0.1507	4.965	100.5	0.9486
APG from APG-MEL-NLC	$K_{d\,fast}$=0.4340 $K_{d\,slow}$=0.0134	$t_{1/2\,fast}$=1.597 $t_{1/2\,slow}$=51.740	45.9	0.9450
Free MEL	0.1080	6.418	105.4	0.9945
MEL from APG-MEL-NLC	$K_{d\,fast}$=1.2920 $K_{d\,slow}$=0.0885	$t_{1/2\,fast}$=0.537 $t_{1/2\,slow}$=7.836	77.5	0.9863

Figure 3. *In vitro* release profile of APG and MEL from APG-MEL-NLC vs free APG and MEL carried out for 48 h and adjustment to a two-phase association, two-phase association, exponential Plateau, and Plateau followed by one phase decay model respectively. (A) APG release profile from APG-MEL-NLC. (B) MEL release profile from APG-MEL-NLC.

3.5. Ocular tolerance

Ocular tolerance was evaluated both *in vitro* using the HET-CAM assay and *in vivo* using the Draize test (Figure 3). The HET-CAM test demonstrated that 1 M NaOH, as a positive control, induced severe hemorrhage with increasing intensity over a 5 min observation period, indicative of a severe irritant. In contrast, the negative control (0.9 % NaCl) and both loaded and empty formulations, and the free drugs did not elicit any irritant responses on the choriolantoic membrane, classifying them as non-irritant. These findings were corroborated by quantitative TBS analysis, which confirmed the non-irritant nature of APG-MEL-NLC. Because of the limitations of *in vitro* models in predicting *in vivo* ocular tolerance, Draize tests were conducted on free compounds, empty NLC, and APG-MEL-NLC formulations. Results indicated that neither formulation induced ocular irritation *in vivo*. Collectively, these data support the conclusion that APG-MEL-NLC possess a favorable ocular tolerance profile being suitable for further anti-inflammatory studies.

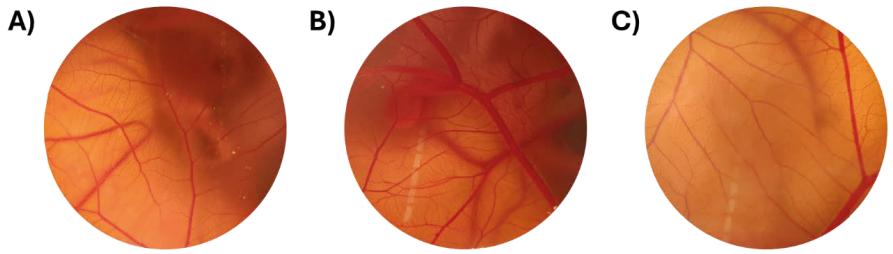

Figure 4. *In vitro* and *in vivo* irritation assay. (A) Negative control, NaCl 0.9 %, (B) Free APG+MEL and (C) APG-MEL-NLC.

3.6. Cellular experiments

3.6.1. Cell viability

The cytotoxicity of various concentrations of free APG/MEL, APG-MEL-NLC, and empty NLC was assessed on HCE-2 corneal epithelial cells. This cell line was selected to simulate the *in vivo* contact between the formulations and the cornea following topical administration (44). Cell viability was evaluated after 5, 15, and 30 min of incubation to mimic real exposure conditions. According to ISO 10993-5, cell viability exceeding 80 % indicates non-cytotoxicity, while values between 60 % and 80 %, 40 % and 60 %, and below 40 % correspond to weak, moderate, and strong cytotoxicity, respectively (45). Results demonstrated that free drug solution (MEL+APG) did not induce significant cytotoxic effects (≥80 % viability) at any concentration or incubation timepoint. Otherwise, both formulations showed a moderate toxicity in the higher tested concentration (0.05 mg/mL of total drug concentration). When increasing the dilution, the formulations became less toxic for the cells, but with higher incubation time, the formulations were slightly more toxic. However, it can be observed that APG-MEL-NLC were safer (higher cell viability) in all the studied concentrations than empty NLC.

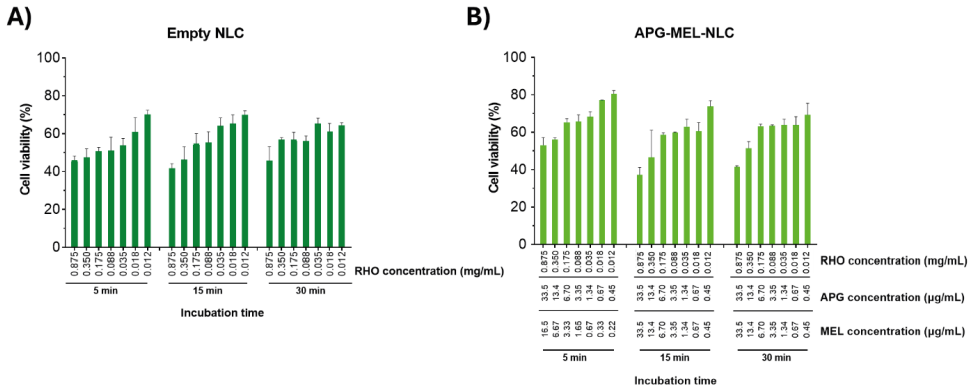

Figure 5. Cell viability assays. Effect APG-MEL-NLC and empty NLC on the viability of HCE-2 cells at 5, 15 and 30 min. Free drug solution did not induce cytotoxicity at any concentration (≥ 80 % viability).

3.6.2. Anti-inflammatory activity of nanoparticles in HCE-2 cells

The anti-inflammatory potential of the NLC was assessed *in vitro* by evaluating their ability to inhibit LPS-induced cytokine secretion in HCE-2 cells in a prevention and treatment model. IL-6, IL-8 and MCP-1 were selected as inflammatory markers. LPS stimulation

resulted in significantly elevated levels of cytokines. In the treatment of inflammation, when the tested formulations were applied after LPS stimulus, free drug solution was not able to reduce the inflammatory response, but APG-MEL-NLC was able to inhibit significantly the secretion of the cytokines. Otherwise, in the prevention of the inflammation, in which the formulation was applied for 30 min incubation before LPS stimulation, the free drugs and the formulation were not able to reduce IL-6 and IL-8 cytokines, but they decreased significatively the MCP-1 levels (****$p < 0.001$).

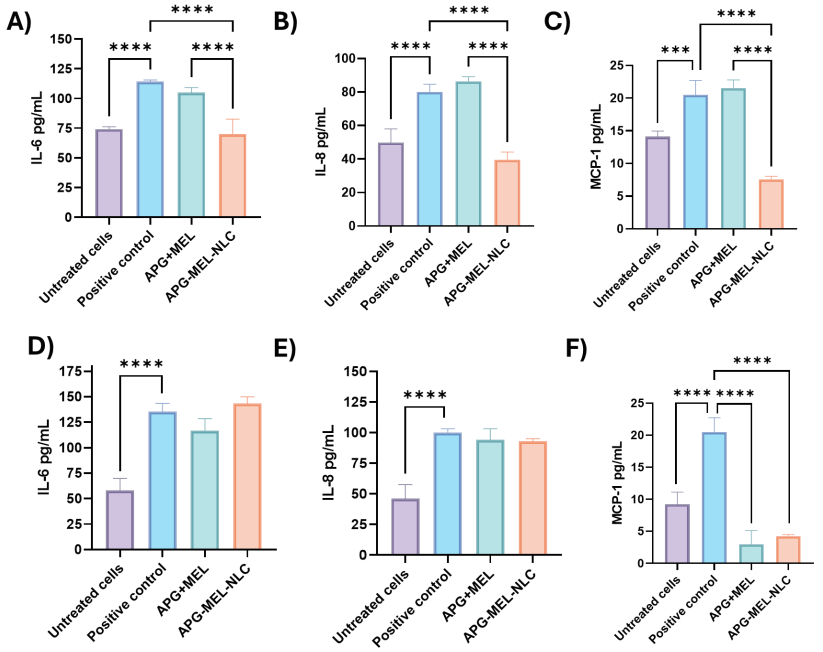

Figure 6. (A) Quantification of secreted IL-6 proinflammatory cytokine in LPS-stimulated HCE-2 cells in inflammation treatment; (B) Quantification of secreted IL-8 inflammation treatment. (C) Quantification of secreted MCP-1 inflammation treatment; (D) Quantification of secreted IL-6 proinflammatory cytokine in LPS-stimulated HCE-2 cells in inflammation prevention; (B) Quantification of secreted IL-8 inflammation prevention. (C) Quantification of secreted MCP-1 inflammation prevention. Negative control: no treatment; Positive control: LPS. Results are expressed as the mean ± SD with statistically significant differences (***$p < 0.005$ and ****$p < 0.001$).

3.7. Anti-inflammatory efficacy

To assess the in vivo anti-inflammatory potential of APG-MEL-NLC, its prophylactic and therapeutic efficacy in an ocular inflammation model was evaluated.

The therapeutic efficacy of APG-MEL-NLC was determined by administering treatment 30 min post-inflammatory stimuli. Inflammation severity was monitored over time. Figure 6A demonstrates a significant reduction in inflammation within 30 min post APG-MEL-NLC administration. Furthermore, the combination of both drugs was demonstrated also a significant reduction of inflammation in the first 30 min. In all the monitored times, the formulation showed a significant anti-inflammatory effect.

The preventive capacity of NLC against inflammation was also investigated. Treatment with APG-MEL-NLC or free drugs was administered 30 min prior to induction of ocular inflammation. Subsequent inflammation severity was evaluated. Figure 6B illustrates a significant reduction in inflammation following exposure to the inflammatory stimulus compared to untreated control. In this study, also both treatments showed a significant anti-inflammatory effect, in which APG-MEL-NLC showed a higher activity.

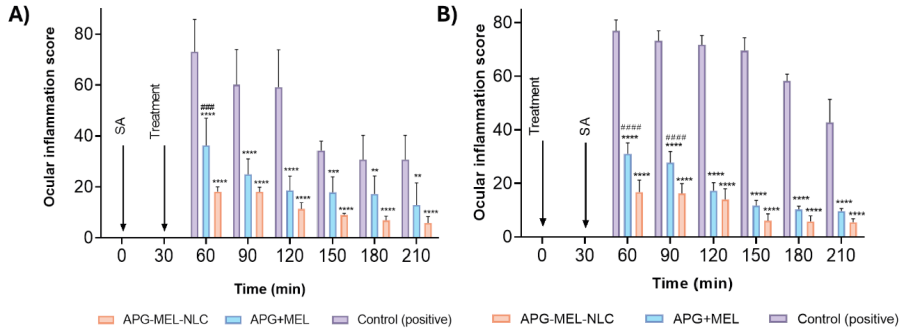

Figure 7. Comparison of ocular anti-inflammatory efficacy of free APG/MEL and APG-MEL-NLC. (A) Inflammation treatment, (B) inflammation prevention. Values are expressed as mean ± SD; **p < 0.01, ***p < 0.005, and ****p < 0.001 significantly lower effect of the tested formulation than the inflammatory effect induced by SA; ###p < 0.005 and ####p < 0.001 significantly lower effect of APG-MEL-NLC than the free drugs.

4. Discussion

A cationic NLC derived containing rosehip oil was formulated to co-encapsulate APG and MEL. The negatively charged corneal mucus layer presents a barrier for drug delivery (46). For this reason, this study aimed to modify a previous formulation by incorporating a cationic surfactant to revert surface charge, potentially enhancing mucoadhesion to the ocular mucosa and subsequently improving bioavailability following topical administration (47). Besides the cationic charge of the NLC, it is expected to obtain an enhanced and synergistic effect with the rosehip oil contained in the lipid matrix, which has been described as an anti-inflammatory active (25,26,48).

To optimize DDAB concentration, the surfactant was incrementally added to a previously optimized formulation (data not shown). Z_{av} remained relatively below 200 nm, whereas the PI increased at higher DDAB concentrations. Otherwise, ZP did not increase from 0.06 to 0.07 %, remaining at ≈16 mV, and EE was stable in all the tested concentrations. In this way, a DDAB concentration of 0.06 % was selected, yielding a PI below 0.3 and a ZP of approximately 17 mV, achieving a suitable physicochemical parameters (21).

Interaction studies revealed an enhancement of lipid matrix amorphism upon APG and MEL incorporation, suggesting its integration within the lipid structure (49). FTIR analysis confirmed the absence of covalent bonds between both drugs and the lipid matrix, indicating that non-covalent interactions, commonly hydrogen bonding and hydrophobic forces, were predominantly responsible for APG and MEL entrapment within the NLC system. This interaction facilitated the sustained release profile of APG and MEL from the particles (50). DSC analysis of APG-MEL-NLC revealed a significantly lower melting point compared to the bulk lipid samples. This suggests a highly amorphous state, possibly attributed to the incorporation of the drug within the amorphous lipid matrix (51). In

comparison to the negatively charged formulation, the T_m values were slightly higher with a similar ΔH, which could be attributed to a greater crystallinity of the present formulation. This fact was also observed in previous studies encapsulating MEL, in which the positively charged formulation showed a higher degree of crystallinity, and consequently, a lower stability (27). XRD patterns exhibited characteristic diffraction peaks corresponding to the β and β' polymorphic forms of triacylglycerols (42,52). In comparison to the negatively charged formulation, the present formulation showed the two main forms of triacylglycerols, the stable (β) and the metastable (β') ones, which could be related to its slightly lower stability of the formulation at 4 and 25 °C. Moreover, the formulations encapsulating each compound showed higher stability, which could be mainly attributed to the more neutral ZP of the APG-MEL-NLC (+21 mV for APG-NLC and +20 mV for MEL-NLC), but also could be related to its lower concentration of lipid phase (5 % in APG-MEL-NLC vs 7.5 % in APG-NLC and MEL-NLC). In the case of the formulation containing only MEL (27), it was also observed that the stability of the positively charged formulation presented a reduced stability in comparison to the negatively one, which could be related to the increased crystallinity of the NLC when DDAB was incorporated.

Regarding to the biopharmaceutical behaviour of APG-MEL-NLC, it has been demonstrated a slow-release profile compared to a rapid diffusion observed for the drugs solution. The release kinetics of APG-MEL-NLC were best described by a two-phase association model, indicative of a biphasic release pattern. This pattern was characterized by an initial burst release phase followed by a sustained release period, during which approximately 30 and 75 % of the encapsulated APG and MEL respectively were liberated into the receptor medium. The observed biphasic behavior suggests that the NLC formulation effectively encapsulates APG and MEL while simultaneously permitting its gradual diffusion through the carrier matrix. In comparison to the dually negatively charged formulation release studies performed (data not shown), the positively charged APG-MEL-NLC showed a slower APG release but a faster MEL diffusion, the latter probably due to the modification of the release media. Otherwise, both actives were able to achieve a higher *plateau* (34.5 and 76.6 % for APG and MEL respectively in the negatively charged formulation vs 45.9 and 77.5 % for APG and MEL respectively in the positively charged formulation). In the case of APG, this slower release from the positive formulation has been described by other authors (53,54). Wang et al. (53) related this effect to the long carbon chains of the cationic surfactant, which could form an ordered close packing and strengthening the interfacial layer in the particles. In the case of MEL, other authors also found a faster release from a positively charged formulation in comparison to a negatively and neutral charged lipid nanoparticle (55). In contrast, in comparison to the formulations containing each compound by itself, the co-encapsulation of APG and MEL resulted in a slower release of both compounds. This difference could be related to the lower concentration of each compound in the dually loaded NLC or the lowest concentration of lipids (26,27).

To evaluate the ocular safety profile of the formulation, a combination of *in vitro* and *in vivo* assessments was conducted. The *in vitro* HET-CAM assay demonstrated no irritation phenomena following direct application of APG-MEL-NLC. Posterior quantitative analysis of trypan blue uptake corroborated these findings, indicating no toxicity. Subsequently, an *in vivo* ocular irritation study using the Draize test was performed. Results revealed no clinically significant ocular irritation or hyperemia in animals treated with either free APG/MEL or APG-MEL-NLC, suggesting suitable ocular tolerability for the formulation.

Furthermore, *in vitro* cytotoxicity assays demonstrated that a solution of APG and MEL exhibited no toxic effects on corneal cells across the tested concentration range. Otherwise, empty NLC showed moderately toxicity the majority of the assessed concentrations. The cationic nature of the particles may contribute to enhanced

electrostatic interactions with the negatively charged cell membrane, potentially inducing oxidative stress and subsequent reactive oxygen species (ROS) generation (56). Additionally, the lipid constituents of the NLC might exhibit affinity for cellular membranes, promoting strong interactions (21,57). Nevertheless, APG-MEL-NLC demonstrated a favorable safety profile across a range of concentrations, except for moderate toxicity observed at the highest tested dose. This protective effect could be related to the drugs properties. Jung (58) demonstrated that APG attenuated H_2O_2-induced downregulation of PI3K, AKT2, and ERK2, essential components of cell survival signaling. Concurrently, APG stimulated the expression of antioxidant enzymes SOD1, SOD2, and GPx1. These findings suggested that APG exerts its protective effects by counteracting oxidative stress and restoring cellular redox balance. Cavelier et al. (59) showed that APG can suppress inflammation-related gene and protein expression. Otherwise, it has been widely described that MEL exerts its antioxidant effects by stimulating enzymatic defenses within cells, safeguarding mitochondrial membrane phospholipids from oxidative damage, thereby preserving membrane integrity. Additionally, this indolamine influences mitochondrial membrane potential, contributing to its overall protective role in cellular homeostasis, and regulates inflammation processes (60–62). In this way, the initial burst that both drugs possessed, could contribute to their fast protective effects in HCE-2 cells.

IL-6, IL-8, and MCP-1 are key inflammatory mediators implicated in ocular diseases. IL-8 primarily recruits neutrophils and eosinophils, while MCP-1 attracts monocytes and lymphocytes. Both chemokines are upregulated in various ocular inflammatory conditions and contribute to monocyte infiltration (63). IL-6, a pleiotropic cytokine involved in inflammation and hematopoiesis, is also upregulated in these settings. These cytokines exhibit synergistic effects, with IL-8 and MCP-1 promoting inflammation and angiogenesis, while IL-6 amplifies inflammatory responses (64). Collectively, they play pivotal roles in the pathogenesis of ocular disorders characterized by chronic inflammation and neovascularization. In this way, the *in vitro* anti-inflammatory potential was evaluated by analyzing these three pro-inflammatory cytokines. In the treatment assay, the results showed that in 30 min exposition to inflamed human corneal cells, APG-MEL-NLC were able to revert inflammation levels of LPS in comparison to the free combination drugs. Probably, this strong anti-inflammatory activity of the NLC was related to the interactions of the lipid matrix with the cellular membrane, enhancing the uptake of the formulation in comparison to the free drugs, facilitating its therapeutical action (65). Other authors found that APG was able to reduce IL-6, IL-8 and MCP-1 cytokine levels in different cell lines (66,67). In the case of MEL, it has been also described that the neurohormone was able to reduce the levels of the same cytokines (15,68). However, the prevention results showed that both, APG-MEL-NLC and the combination of free drugs were not able to decrease IL-6 and IL-8 levels. This fact could be related with the exposure of the treatments to the cells, in which during the treatment when the cells were already inflamed, their membrane could be more permeable, promoting a higher uptake of NLC facilitating its action (69).

Finally, to corroborate *in vitro* experiments, an *in vivo* inflammation assay was performed to evaluate both, inflammation prevention and treatment. The results showed that APG-MEL-NLC possessed a faster and more effective anti-inflammatory properties than the free combination drugs. In the inflammation treatment, during the first 30 min post-instillation, APG-MEL-NLC were able to reduce significantly ocular inflammation, which correlated with the *in vitro* results. Furthermore, in the inflammation prevention, APG-MEL-NLC also showed promising results, decreasing the ocular inflammation score after 30 min. As *in vivo* processes are more complex than *in vitro* ones, both experiments are needed to corroborate the possible therapeutical properties of a formulation. Each NLC containing each drug by itself were also tested in previous studies (26,27). Free APG showed a faster and higher anti-

inflammatory effect on the inflammation prevention, while free MEL showed the same effect in the inflammation treatment. In the present study, the combination of both drugs acted in a faster way, which could be related to the faster release of MEL in the burst initial phase, and the higher amount of each drug released in each timepoint. It is well-documented that both compounds possess a promising anti-inflammatory activity *in vivo*. Benedeto et al. (70) demonstrated that in an *in vivo* model, MEL prevented an LPS-induced increase in pro-inflammatory cytokines TNF-α and IL-6 and NF-κB levels. Moreover, APG was able to reduce NF-κB and STAT3 activity, inhibiting the inflammation process (71).

5. Conclusions

NLC encapsulating APG and MEL demonstrated promising activity as a potential therapeutic for ocular inflammation. The formulation exhibited physical stability and sustained release of both encapsulated drugs, enhancing their biopharmaceutical profiles. *In vitro* and *in vivo* assessments confirmed the biocompatibility of the NLC, with no evidence of ocular irritation or cytotoxicity. Moreover, NLC-mediated delivery of APG and MEL effectively attenuated inflammation *in vitro* by reducing IL-6, IL-8 and MCP-1 cytokine levels and *in vivo* by decreasing the SA inflammation in a rabbit model. These findings collectively suggest that the developed NLC formulation represents a promising strategy for the management and prevention of ocular inflammatory conditions.

6. References

1. Xu H, Rao NA. Grand challenges in ocular inflammatory diseases. Front Ophthalmol. 2022;2:756689.
2. Egwuagu CE, Sun L, Kim S-H, Dambuza IM. Ocular inflammatory diseases: molecular pathogenesis and immunotherapy. Curr Mol Med. 2015;15(6):517–28.
3. Musa M, Chukwuyem E, Ojo OM, Topah EK, Spadea L, Salati C, et al. Unveiling ocular manifestations in systemic lupus erythematosus. J Clin Med. 2024;13(4):1047.
4. Artifoni M, Rothschild PR, Brézin A, Guillevin L, Puéchal X. Ocular inflammatory diseases associated with rheumatoid arthritis. Nat Rev Rheumatol. 2013;10(2):108–16.
5. Colin J. The role of NSAIDs in the management of postoperative ophthalmic inflammation. Drugs. 2007;67(9):1291–308.
6. Schalnus R. Topical nonsteroidal anti-inflammatory therapy in ophthalmology. Ophthalmologica. 2003;217(2):89–98.
7. Rigas B, Huang W, Honkanen R. NSAID-induced corneal melt: Clinical importance, pathogenesis, and risk mitigation. Surv Ophthalmol. 2020;65(1):1–11.
8. Mazet R, Yaméogo JBG, Wouessidjewe D, Choisnard L, Gèze A. Recent advances in the design of topical ophthalmic delivery systems in the treatment of ocular surface inflammation and their biopharmaceutical evaluation. Pharmaceutics. 2020;12(6):570.
9. Lee RWJ, Dick AD. Current concepts and future directions in the pathogenesis and treatment of non-infectious intraocular inflammation. Eye. 2011;26(1):17–28.

10. Starace V, Battista M, Brambati M, Cavalleri M, Bertuzzi F, Amato A, et al. The role of inflammation and neurodegeneration in diabetic macular edema. Ther Adv Ophthalmol. 2021;13:25158414211055964.

11. Yue T, Shi Y, Luo S, Weng J, Wu Y, Zheng X. The role of inflammation in immune system of diabetic retinopathy: Molecular mechanisms, pathogenetic role and therapeutic implications. Front Immunol. 2022;13:1055087.

12. Mushtaq Z, Sadeer NB, Hussain M, Mahwish, Alsagaby SA, Imran M, et al. Therapeutical properties of apigenin: a review on the experimental evidence and basic mechanisms. Int J Food Prop. 2023;26(1):1914–39.

13. Yoon JH, Kim MY, Cho JY. Apigenin: a therapeutic agent for treatment of skin inflammatory diseases and cancer. Int J Mol Sci . 2023;24(2):1498.

14. Ali F, Rahul, Naz F, Jyoti S, Siddique YH. Health functionality of apigenin: A review. Int J Food Prop. 2016;20(6):1197–238.

15. Cho JH, Bhutani S, Kim CH, Irwin MR. Anti-inflammatory effects of melatonin: A systematic review and meta-analysis of clinical trials. Brain Behav Immun. 2021;93:245–53.

16. Bantounou M, Plascevic J, Galley HF. Melatonin and related compounds: antioxidant and anti-inflammatory actions. Antioxidants . 2022;11(3):532.

17. Zarezadeh M, Khorshidi M, Emami M, Janmohammadi P, Kord-varkaneh H, Mousavi SM, et al. Melatonin supplementation and pro-inflammatory mediators: a systematic review and meta-analysis of clinical trials. Eur J Nutr. 2020;59(5):1803–13.

18. Alkozi HA, Navarro G, Franco R, Pintor J. Melatonin and the control of intraocular pressure. Prog Retin Eye Res. 2020;75:100798.

19. Zhang J, Liu D, Huang Y, Gao Y, Qian S. Biopharmaceutics classification and intestinal absorption study of apigenin. Int J Pharm. 2012;436(1–2):311–7.

20. Lopes V, Assis J, Ribeiro T, de Castro G, Pacheco M, Borges L, et al. Melatonin loaded lecithin-chitosan nanoparticles improved the wound healing in diabetic rats. Int J Biol Macromol. 2020;162:1465–75.

21. Bonilla L, Espina M, Severino P, Cano A, Ettcheto M, Camins A, et al. Lipid nanoparticles for the posterior eye segment. Pharmaceutics. 2022;14(1):90.

22. Souto EB, Doktorovova S, Gonzalez-Mira E, Egea MA, Garcia ML. Feasibility of lipid nanoparticles for ocular delivery of anti-inflammatory drugs. Curr Eye Res. 2010;35(7):537–52.

23. Wong CW, Wong TT. Posterior segment drug delivery for the treatment of exudative age-related macular degeneration and diabetic macular oedema. Br J Ophthalmol. 2019;103(10):1356–60.

24. Mármol I, Sánchez-De-Diego C, Jiménez-Moreno N, Ancín-Azpilicueta C, Rodríguez-Yoldi M. Therapeutic applications of rose hips from different Rosa species. Int J Mol Sci. 2017;18(6):1137.

25. Belkhelladi M, Bougrine A. Rosehip extract and wound healing: A review. J Cosmet Dermatol. 2024;23(1):62–7.

26. Bonilla-Vidal L, Espina M, García ML, Baldomà L, Badia J, González JA, et al. Novel nanostructured lipid carriers loading Apigenin for anterior segment ocular pathologies. Int J Pharm. 2024;658:124222.

27. Bonilla-Vidal L, Espina M, García ML, Cimino C, Carbone C, Baldomà L, et al. Melatonin loaded nanostructured lipid carriers for the treatment of uveal melanoma. J Drug Deliv Sci Technol. 2024;106057.

28. Fangueiro JF, Calpena AC, Clares B, Andreani T, Egea MA, Veiga FJ, et al. Biopharmaceutical evaluation of epigallocatechin gallate-loaded cationic lipid nanoparticles (EGCG-LNs): In vivo, in vitro and ex vivo studies. Int J Pharm. 2016;502(1–2):161–9.

29. Silva AM, Martins-Gomes C, Fangueiro JF, Andreani T, Souto EB. Comparison of antiproliferative effect of epigallocatechin gallate when loaded into cationic solid lipid nanoparticles against different cell lines. Pharm Dev Technol. 2019;24(10):1243–9.

30. Bonilla-Vidal L, Świtalska M, Espina M, Wietrzyk J, García ML, Souto EB, et al. Dually active apigenin-loaded nanostructured lipid carriers for cancer treatment. Int J Nanomedicine. 2023;18:6979–97.

31. Esteruelas G, Halbaut L, García-Torra V, Espina M, Cano A, Ettcheto M, et al. Development and optimization of Riluzole-loaded biodegradable nanoparticles incorporated in a mucoadhesive in situ gel for the posterior eye segment. Int J Pharm. 2022;612:121379.

32. Llorente X, Esteruelas G, Bonilla L, Agudelo MG, Filgaira I, Lopez-Ramajo D, et al. Riluzole-loaded nanostructured lipid carriers for hyperproliferative skin diseases. Int J Mol Sci. 2023;24(9):8053.

33. Galindo R, Sánchez-López E, Gómara MJ, Espina M, Ettcheto M, Cano A, et al. Development of peptide targeted PLGA-PEGylated nanoparticles loading Licochalcone-A for ocular inflammation. Pharmaceutics. 2022;14(2):285.

34. Thiruchenthooran V, Świtalska M, Bonilla L, Espina M, García ML, Wietrzyk J, et al. Novel strategies against cancer: dexibuprofen-loaded nanostructured lipid carriers. Int J Mol Sci. 2022;23(19):11310.

35. Thiruchenthooran V, Espina M, Świtalska M, Bonilla-Vidal L, Wietrzyk J, Garcia ML, et al. Combination of indomethacin with nanostructured lipid carriers for effective anticancer therapy. Int J Nanomedicine. 2024;19:7033–48.

36. Sánchez-López E, Esteruelas G, Ortiz A, Espina M, Prat J, Muñoz M, et al. Dexibuprofen biodegradable nanoparticles: one step closer towards a better ocular interaction study. Nanomaterials. 2020;10(4).

37. Fernandes AR, Vidal LB, Sánchez-López E, dos Santos T, Granja PL, Silva AM, et al. Customized cationic nanoemulsions loading triamcinolone acetonide for corneal neovascularization secondary to inflammatory processes. Int J Pharm. 2022;623:121938.

38. López-Machado A, Díaz-Garrido N, Cano A, Espina M, Badia J, Baldomà L, et al. Development of lactoferrin-loaded liposomes for the management of dry eye disease and ocular inflammation. Pharmaceutics. 2021;13(10):1698.

39. López-Machado A, Díaz N, Cano A, Espina M, Badía J, Baldomà L, et al. Development

of topical eye-drops of lactoferrin-loaded biodegradable nanoparticles for the treatment of anterior segment inflammatory processes. Int J Pharm. 2021;609:121188.

40. Fu X, Kong W, Zhang Y, Jiang L, Wang J, Lei J. Novel solid–solid phase change materials with biodegradable trihydroxy surfactants for thermal energy storage. RSC Adv. 2015;5(84):68881–9.

41. Bunjes H, Westesen K, Koch MHJ. Crystallization tendency and polymorphic transitions in triglyceride nanoparticles. Int J Pharm. 1996;129(1–2):159–73.

42. Souto EB, Mehnert W, Müller RH. Polymorphic behaviour of Compritol 888 ATO as bulk lipid and as SLN and NLC. J Microencapsul. 2006;23(4):417–33.

43. Freitas C, Müller RH. Correlation between long-term stability of solid lipid nanoparticles (SLN) and crystallinity of the lipid phase. Eur J Pharm Biopharm. 1999;47(2):125–32.

44. Mofidfar M, Abdi B, Ahadian S, Mostafavi E, Desai TA, Abbasi F, et al. Drug delivery to the anterior segment of the eye: A review of current and future treatment strategies. Int J Pharm. 2021;607:120924.

45. López-García J, Lehocký M, Humpolíček P, Sáha P. HaCaT keratinocytes response on antimicrobial atelocollagen substrates: extent of cytotoxicity, cell viability and proliferation. J Funct Biomater. 2014;5(2):57.

46. Vedadghavami A, Zhang C, Bajpayee AG. Overcoming negatively charged tissue barriers: Drug delivery using cationic peptides and proteins. Nano Today. 2020;34.

47. Abruzzo A, Giordani B, Miti A, Vitali B, Zuccheri G, Cerchiara T, et al. Mucoadhesive and mucopenetrating chitosan nanoparticles for glycopeptide antibiotic administration. Int J Pharm. 2021;606:120874.

48. Strugała P, Gładkowski W, Kucharska AZ, Sokół-Łetowska A, Gabrielska J. Antioxidant activity and anti-inflammatory effect of fruit extracts from blackcurrant, chokeberry, hawthorn, and rosehip, and their mixture with linseed oil on a model lipid membrane. Eur J Lipid Sci Technol. 2016;118(3):461–74.

49. Ojo AT, Ma C, Lee PI. Elucidating the effect of crystallization on drug release from amorphous solid dispersions in soluble and insoluble carriers. Int J Pharm. 2020;591:120005.

50. Huang Z, Ma C, Wu M, Li X, Lu C, Zhang X, et al. Exploring the drug-lipid interaction of weak-hydrophobic drug loaded solid lipid nanoparticles by isothermal titration calorimetry. J Nanoparticle Res. 2020;22(1):1–14.

51. Khosa A, Reddi S, Saha RN. Nanostructured lipid carriers for site-specific drug delivery. Biomed Pharmacother. 2018;103:598–613.

52. Zimmermann E, Souto EB, Müller RH. Physicochemical investigations on the structure of drug-free and drug-loaded solid lipid nanoparticles (SLN) by means of DSC and 1H NMR. Pharmazie. 2005;60(7):508–13.

53. Wang JJ, Sung KC, Hu OYP, Yeh CH, Fang JY. Submicron lipid emulsion as a drug delivery system for nalbuphine and its prodrugs. J Control Release. 2006;115(2):140–9.

54. Baspinar Y, Borchert HH. Penetration and release studies of positively and

negatively charged nanoemulsions—Is there a benefit of the positive charge? Int J Pharm. 2012;430(1–2):247–52.

55. Landh E, Moir LM, Traini D, Young PM, Ong HX. Properties of rapamycin solid lipid nanoparticles for lymphatic access through the lungs & part II: the effect of nanoparticle charge. Nanomedicine . 2020;15(20):1947–63.

56. Yang W, Wang L, Mettenbrink EM, Deangelis PL, Wilhelm S. Nanoparticle toxicology. Annu Rev Pharmacol Toxicol. 2021;61:269–89.

57. Zhang W, Li X, Ye T, Chen F, Yu S, Chen J, et al. Nanostructured lipid carrier surface modified with Eudragit RS 100 and its potential ophthalmic functions. Int J Nanomedicine. 2014;9:4315.

58. Jung WW. Protective effect of apigenin against oxidative stress-induced damage in osteoblastic cells. Int J Mol Med. 2014;33(5):1327–34.

59. Cavalier AN, Clayton ZS, Wahl D, Hutton DA, McEntee CM, Seals DR, et al. Protective effects of apigenin on the brain transcriptome with aging. Mech Ageing Dev. 2024;217:111889.

60. Gu W, Wu M, Cui S, Bo J, Wu H. Melatonin's protective effects on neurons in an in vitro cell injury model. Discov Med. 2024;36(182):509–17.

61. Tarocco A, Caroccia N, Morciano G, Wieckowski MR, Ancora G, Garani G, et al. Melatonin as a master regulator of cell death and inflammation: molecular mechanisms and clinical implications for newborn care. Cell Death Dis. 2019;10(4):1–12.

62. Kopustinskiene DM, Bernatoniene J. Molecular mechanisms of melatonin-mediated cell protection and signaling in health and disease. Pharmaceutics. 2021;13(2):129.

63. Ghasemi H, Ghazanfari T, Yaraee R, Faghihzadeh S, Hassan ZM. Roles of IL-8 in ocular inflammations: a review. Ocul Immunol Inflamm. 2011;19(6):401–12.

64. Da Cunha AP, Zhang Q, Prentiss M, Wu XQ, Kainz V, Xu YY, et al. The hierarchy of proinflammatory cytokines in ocular inflammation. Curr Eye Res. 2018;43(4):553–65.

65. Mahor AK, Singh PP, Gupta R, Bhardwaj P, Rathore P, Kishore A, et al. Nanostructured lipid carriers for improved delivery of therapeutics via the oral route. J Nanotechnol. 2023;2023(1):4687959.

66. Wang J, Liao Y, Fan J, Ye T, Sun X, Dong S. Apigenin inhibits the expression of IL-6, IL-8, and ICAM-1 in DEHP-Stimulated human umbilical vein endothelial cells and in vivo. Inflammation. 2012;35(4):1466–76.

67. Funakoshi-Tago M, Nakamura K, Tago K, Mashino T, Kasahara T. Anti-inflammatory activity of structurally related flavonoids, Apigenin, Luteolin and Fisetin. Int Immunopharmacol. 2011;11(9):1150–9.

68. Deng SL, Zhang BL, Reiter RJ, Liu YX. Melatonin ameliorates inflammation and oxidative stress by suppressing the p38MAPK signaling pathway in LPS-induced sheep orchitis. Antioxidants. 2020;9(12):1–17.

69. Aguilar-Briseño JA, Moser J, Rodenhuis-Zybert IA. Permeability of endothelium. Curr Opin Virol. 2020;43:41–9.

70. Benedeto-Stojanov D, Ničković VP, Petrović G, Rancić A, Grgov I, Nikolić GR, et al. Melatonin as a promising anti-inflammatory agent in an in vivo animal model of sepsis-induced rat liver damage. Int J Mol Sci. 2024;25(1):455.

71. Ai XY, Qin Y, Liu HJ, Cui ZH, Li M, Yang JH, et al. Apigenin inhibits colonic inflammation and tumorigenesis by suppressing STAT3-NF-κB signaling. Oncotarget. 2017;8(59):100216.

4

Discusión

4. Discusión

Los NLC son unos sistemas nanoestructurados capaces tanto de transportar activos y liberarlos de manera sostenida de manera dirigida, como de ejercer una acción local al ser administrado tópicamente. En esta tesis doctoral se exploraron ambas características de estos sistemas, encapsulando APG, MEL o ambos activos para el tratamiento de procesos tumorales, o su administración en forma de colirio para el tratamiento de enfermedades oculares.

Los procesos tumorales y las enfermedades oculares representan dos desafíos para la salud pública a nivel mundial. Ambas afecciones tienen como características comunes a diferente nivel su impacto significativo en la calidad de vida de los pacientes, la complejidad de sus mecanismos patogénicos, el incremento de la incidencia anual y la necesidad de estrategias terapéuticas innovadoras.

4.1. NLC para el tratamiento de enfermedades proliferativas

El método de fabricación seleccionado para la preparación de las NPs fue la homogeneización de alta presión en caliente, debido a sus múltiples ventajas, tales como la capacidad de producción a gran escala, la ausencia de solventes orgánicos y su bajo coste [12,156]. La optimización de los parámetros de la técnica mediante un diseño de experimentos (DoE) permite obtener un espacio de diseño asociado a un elevado grado de información sobre las tendencias que siguen estos sistemas, realizando un número mínimo de experimentos [157]. Este se llevó a cabo analizando el efecto de las variables independientes seleccionadas (presión, número de ciclos de homogeneización y tiempo de emulsión primaria) sobre las variables dependientes (tamaño promedio de partícula (Z_{av}) y el índice de polidispersión (PI)). Utilizando una formulación sin fármaco encapsulado, la optimización del método mostró que, a mayor presión y mayor número de ciclos de homogenización, se producían NLC más

pequeños y homogéneos. Un comportamiento similar fue reportado por Ding *et al*. [158], analizando los cambios de Z_{av} a medida que modificaban la concentración de lípido líquido, tensioactivo y la presión de trabajo. También observaron una tendencia en la presión, cuyo incremento disminuía el tamaño de las NPs, mientras que la proporción de los demás componentes únicamente disminuía el tamaño en rangos intermedios del estudio. El efecto de la presión fue atribuido a que las colisiones entre gotas, que aceleran su ruptura, se intensificaron al aumentar la presión. Los experimentos llevados a cabo por Nekkanti *et al*. [159] pusieron en relieve que al aumentar el número de ciclos de homogenización de 5 a 60, las NPs obtenidas eran cada vez más pequeñas.

La concentración de los componentes se optimizó mediante un diseño de experimentos compuesto de cuatro niveles y cuatro factores para cada fármaco y uno para la combinación de estos, seleccionando como variables independientes la concentración de fármaco, la concentración de fase lipídica, la proporción de lípido sólido en ésta y la concentración de tensioactivo. Para las tres formulaciones, se observó la misma tendencia respecto al Z_{av}, donde los incrementos de la concentración de fase lipídica, aumentaba el tamaño. Este hecho ya ha sido reportado por otros autores [160]. Por otra parte, en el PI se obtuvieron tendencias opuestas y la variable independiente que influía significativamente en el DoE fue la concentración de lípido sólido. En el caso de los APG-NLC, a menor concentración de lípido sólido aumentaba el PI, y de manera opuesta en los MEL-NLC y los APG-MEL-NLC. Se observó que, en las formulaciones cargadas con los fármacos individuales, el efecto de esta tendencia era mayor que en la formulación dual, por lo que se atribuyó esta tendencia a la diferencia estructural química de los fármacos, que podría estar relacionada con sus diferentes solubilidades. Por otro lado, el ZP mostró la misma tendencia en todas las formulaciones, donde a mayor concentración del tensioactivo no iónico Tween® 80, el ZP se volvía más neutral. Este comportamiento, descrito también por otros autores, puede atribuirse a que el carácter negativo de las NPs, (en este caso debido principalmente a la ionización del lípido sólido Compritol® 888 ATO [161]), se ve disminuido por la adsorción del tensioactivo en la superficie de la partícula [162]. El último parámetro estudiado, la EE, no se vio afectado significativamente por ninguna variable independiente en el caso de las formulaciones cargadas con cada

fármaco individualmente, donde la EE fue elevada en ambos casos (superior al 80 % en prácticamente todas las formulaciones del DoE), pero sí en las co-encapsuladas, donde a mayor proporción de fármacos, aumentaba la EE. Esta tendencia ya fue observada por otros autores [163], que atribuyeron este efecto a la capacidad de los NLC a tener una mayor carga de activos debido a la incorporación del lípido líquido a la matriz y a la naturaleza lipofílica del fármaco utilizado. Colectivamente, se obtuvieron NLC con un tamaño promedio inferior a 200 nm, un PI menor a 0,2, una carga superficial de alrededor de −20 mV y una elevada EE para ambos fármacos.

Los estudios de interacción fármaco-matriz mostraron un incremento en el carácter amorfo de la matriz lipídica tras la incorporación de los fármacos, sugiriendo su solubilización en la fase lipídica [164]. Los termogramas obtenidos mostraron que las mezclas de lípidos fueron en todos los casos más cristalinas, debido a que tenían una temperatura de fusión (T_m) y una entalpía de fusión (ΔH) mayores que los NLC estudiados, indicando que necesitaban más energía para conseguir su fusión [165]. En cambio, las formulaciones de NLC en todos los casos mostraron valores menores, indicando que eran estructuras más amorfas. Comparando todas las formulaciones cargadas negativamente, la estructura más cristalina fue la de los MEL-NLC, probablemente debido a que éstos estaban compuestos por un alto porcentaje de lípido sólido en comparación a los APG-NLC y los APG-MEL-NLC. Por otro lado, la formulación más amorfa que mostró valores menores de T_m y ΔH fueron los APG-MEL-NLC, que podría estar atribuido a su porcentaje menor de fase lipídica, con una alta proporción de lípido líquido. La espectroscopia de infrarrojos de transformada de Fourier (FTIR) confirmó la ausencia de enlaces covalentes entre cualquiera de los dos fármacos y los componentes lipídicos de la matriz, sugiriendo que los enlaces de hidrógeno y las fuerzas hidrófobas eran las fuerzas predominantes que median la asociación fármaco-lípido, permitiendo así la acomodación tanto de la APG como de la MEL dentro de la NLC y facilitando la posterior liberación de los fármacos [166]. El análisis de difracción de rayos X (XRD) puso de relieve que la presencia de las formas polimórficas estables β y β' de los triacilglicéridos contribuye a una mejor estabilidad de los NLC [24,167]. Concretamente, todas las formulaciones

mostraron uno de los picos característicos de la forma más estable de los lípidos, la forma β, pero con diferentes intensidades, lo cual se correlacionó con su estabilidad, siendo las intensidades de mayor a menor el de MEL-NLC, seguida de APG-NLC y el de menor intensidad la combinación de fármacos APG-MEL-NLC [165].

Los resultados de los estudios de estabilidad revelaron que todas las formulaciones fueron más estables almacenadas a temperatura de 4 °C, donde la formulación MEL-NLC presentó la mayor estabilidad durante un periodo de 16 meses, seguida por APG-NLC que mantuvo sus parámetros fisicoquímicos y perfil de BS durante 10 meses, y finalmente APG-MEL-NLC, que tuvo una estabilidad de 4 meses. La mayor estabilidad de MEL-NLC podría ser atribuida a la formación de una estructura cristalina más estable, que protege a la formulación contra la agregación y sedimentación [24]. Por otro lado, la menor estabilidad de los APG-MEL-NLC podría estar relacionada con su menor contenido de matriz lipídica y la posible disminución de las fuerzas electrostáticas entre las partículas [168]. Estos hallazgos sugirieron que la composición lipídica y la estructura cristalina fueron los factores cruciales que influyeron en la estabilidad a largo plazo de estas formulaciones.

Los estudios de liberación *in vitro* realizados demostraron perfiles de liberación sostenida para ambos activos en comparación con sus soluciones o fármacos libres. En las tres formulaciones se observó una liberación inicial rápida (“*burst release”*) seguida de una liberación lenta y prolongada. La liberación inicial rápida podría corresponder a la liberación del fármaco adsorbido en la superficie de la nanopartícula, mientras que la liberación lenta y prolongada podría estar relacionada con la liberación del fármaco encapsulado en el núcleo lipídico interno. En cuanto a los parámetros farmacocinéticos, se observaron diferencias en la liberación entre los diferentes fármacos dependiendo de la formulación. La liberación de la APG desde los APG-NLC fue más lenta que la MEL desde los MEL-NLC, lo que podría estar relacionado con la mayor solubilidad de APG en la matriz lipídica [169,170]. La incorporación de ambos fármacos en una única nanopartícula lipídica afectó la liberación de APG en comparación con los APG-NLC. Los APG-MEL-NLC liberaron APG a una velocidad ligeramente superior y alcanzaron una mayor cantidad de fármaco

liberado en el medio. En cambio, la MEL se liberó de una manera más lenta desde la formulación dual, lo cual podría estar relacionado con la diferente composición del medio de liberación, formado por el tensioactivo Tween® 80 a una elevada concentración, el cual está descrito que produce una liberación más lenta en comparación al medio de liberación del estudio previo, formado por dodecilsulfato sódico a una concentración menor [171]. La adición del Tween® 80 fue necesaria para asegurar la completa disolución de la APG.

Se realizaron estudios *in ovo* para investigar un posible mecanismo de acción de los APG-NLC y para demostrar la biocompatibilidad de los MEL-NLC. Los resultados de los ensayos de angiogénesis *in ovo* corroboraron la actividad antiangiogénica de las NPs lipídicas cargadas con APG. Como controles se emplearon una solución salina fisiológica como control negativo y para el estudio de la actividad angiogénica, el factor de crecimiento fibroblástico básico (bFGF) como control positivo de angiogénesis, que es un potente inductor de la formación de nuevos vasos sanguíneos, y su implicación en la angiogénesis patológica es ampliamente reconocida debido a su capacidad para estimular la proliferación de células endoteliales vasculares [172]. Por un lado, se evaluó el efecto del APG libre a la misma concentración que la utilizada en los APG-NLC. Los resultados indicaron una reducción no significativa en el número de microvasos de la membrana corioalantoidea (CAM) tras el tratamiento con APG. En otros estudios se ha demostrado que concentraciones de APG superiores a las empleadas en este trabajo pueden inhibir la angiogénesis en la CAM. En cambio, los APG-NLC fueron capaces de reducir significativamente la angiogénesis en el embrión. Los resultados obtenidos sugirieron que la encapsulación de la APG incrementó tanto su biodisponibilidad como su bioactividad [173]. Dado que la APG es un inhibidor de diversos factores de crecimiento, como el factor de crecimiento endotelial vascular y el bFGF [174,175], y considerando que las NLC vacías no ejercieron ningún efecto modulador sobre la angiogénesis, se concluyó que las NPs desarrolladas favorecieron la penetración de la APG potenciando así su actividad antiangiogénica. Por otra parte, debido a que la CAM es una membrana extraembrionaria altamente vascularizada que carece de inervación y es funcionalmente análoga a la placenta de los mamíferos, ofrece un método de cribado inicial, que podría complementar a los estudios

posteriores convencionales en roedores [176]. Por ese motivo, para confirmar la compatibilidad de los MEL-NLC se realizó el mismo estudio analizando la CAM en la búsqueda de daños en ésta. Los resultados mostraron que tanto la MEL libre como los MEL-NLC no causaron ningún efecto letal en el embrión de gallina ni dañaron o provocaron cambios morfológicos en la CAM, confirmando así su seguridad y biocompatibilidad. Tanto el fármaco libre como la formulación tampoco indujeron cambios en la angiogénesis del embrión. Esto puede ser debido a que la MEL en tejidos sanos contribuye a regular la angiogénesis. Su actividad reguladora está bien documentada, donde el triptófano, la serotonina y la MEL participan en procesos clave durante la gestación, incluyendo el desarrollo fetal y la función placentaria [177]. La placenta humana presenta capacidad para sintetizar MEL y estudios experimentales sugieren un papel beneficioso de esta hormona en el crecimiento fetal [177,178].

La actividad antiproliferativa de las formulaciones se evaluó frente a cinco líneas celulares diferentes después de 24 y 72 horas. Las líneas celulares seleccionadas fueron de pulmón A549 y dos de mama, uno que expresa receptores de estrógeno (MCF-7) y el triple negativo MDA-MB-468, que no tiene los receptores hormonales más comunes. Estas líneas representan dos de los tipos de tumores sólidos que más muertes causan mundialmente [74]. También se escogió una línea celular de leucemia (MV4-11), debido a que es la neoplasia maligna infantil más común en todo el mundo [179,180]. Los resultados mostraron que las soluciones de fármacos libres no tuvieron efecto sobre la proliferación celular a las 24 horas, excepto en el caso de la APG sobre la línea celular de leucemia. En cambio, las NLC tuvieron efecto antiproliferativo desde las 24 horas, excepto en el caso de MEL-NLC en la línea celular de leucemia. Este efecto se atribuyó a la capacidad de los NLC para penetrar en las células, resultando un aumento de la concentración intracelular del fármaco [181]. A las 72 horas, los fármacos libres mostraron cierta actividad antiproliferativa contra todas las líneas tumorales utilizadas. En cambio, los NLC mostraron una gran actividad citotóxica en todas las líneas celulares a las 72 horas, probablemente relacionado con su capacidad de liberar lenta y sostenidamente el fármaco de su interior [182]. Comparando todas las formulaciones, los resultados demostraron una marcada actividad

antiproliferativa de APG-MEL-NLC en la línea celular de leucemia MV4-11, superior a las formulaciones individuales. Esta sinergia potencialmente se atribuye a la combinación de los mecanismos de acción de APG y MEL, favorecida por la encapsulación en NLC. Sin embargo, en la línea celular de cáncer de pulmón A549, la actividad de APG-MEL-NLC fue similar a la de MEL-NLC, sugiriendo una posible interacción entre ambos compuestos que impide un efecto sinérgico. En el contexto del cáncer de mama se observó un contraste interesante. Mientras que APG-MEL-NLC mostró una alta citotoxicidad en la línea celular MCF-7, su efecto fue menos pronunciado en la línea celular triple negativa MDA-MB-468. Estos resultados sugieren que la estructura celular y el microambiente tumoral pueden influir en la eficacia terapéutica proveniente de la co-encapsulación de APG y MEL. Por otro lado, los NLC vacíos mostraron una notable actividad antitumoral debido principalmente al RHO y también su combinación con el tensioactivo Tween® 80. El tensioactivo mejora la penetración celular de los NLC [183], mientras que el RHO presenta propiedades antioxidantes y antiproliferativas. Estudios previos han demostrado la eficacia del RHO en diferentes tipos de cáncer, incluyendo su capacidad para reducir la migración celular e inhibir el crecimiento tumoral [90,113]. Por lo tanto, la combinación de APG con NLC que contienen RHO podría ser una estrategia terapéutica prometedora.

Los resultados de la internalización celular a través de citometría de flujo demostraron que los NLC son rápidamente absorbidos por las células leucémicas y permanecen en su interior durante un período prolongado. Esta capacidad de penetración celular podría explicar su alta eficacia antitumoral. La composición lipídica de los NLC, especialmente la presencia de lípidos líquidos, favorece su absorción y retención intracelular, lo que los convierte en un sistema de liberación prometedor para fármacos [184,185].

4.2. NLC para el tratamiento de enfermedades oculares

A partir de cada formulación con carga superficial negativa se prepararon 3 nuevas formulaciones conteniendo un co-tensioactivo que le aportó un ZP positivo. Este cambio de carga superficial, de negativa a positiva, se realizó con el objetivo de aumentar la biodisponibilidad ocular de la formulación, favoreciendo la adhesión de las partículas a la mucosa ocular negativa gracias a las interacciones electrostáticas, aumentando así el tiempo de residencia de la formulación en la superficie ocular [186]. Además, a la formulación conteniendo APG se le incorporó HA, un polisacárido aniónico de origen natural con propiedades muco-miméticas, formando así HA-APG-NLC. El HA permite prolongar el tiempo de residencia precorneal y reducir la desecación de la superficie ocular, y además aumenta la viscosidad en dispositivos de liberación ocular [187].

La concentración del bromuro de dimetildioctadecilamonio (DDAB) se escogió en base a obtener un Z_{av} inferior a 200 nm, un PDI lo menor posible y un ZP cercano a +20 mV. La adición de cantidades crecientes del co-tensioactivo catiónico DDAB afectó de manera similar a todas las formulaciones. A mayor concentración de éste, el Z_{av} disminuía, lo cual podría estar relacionado con la disminución de la tensión superficial [188], el PDI aumentaba y el ZP se volvía más positivo. Basándose en estos parámetros, las concentraciones escogidas fueron 0,05 % para HA-APG-NLC, 0,07 % para la formulación de MEL cargada positivamente (MEL-NLC+) y 0,06 % para la formulación dual positiva (APG-MEL-NLC+), concentraciones muy similares que afectaron de diferente manera a cada formulación.

Los estudios de interacción demostraron que la adición de cada uno de los activos a la matriz lipídica dio lugar a un aumento de la estructura amorfa de los lípidos, sugiriendo que estos fueron internalizados en la matriz lipídica. En el caso de la APG, tanto la T_m como la ΔH fueron menores en la formulación cargada positivamente (HA-APG-NLC), sugiriendo que estos sistemas tenían una estructura más amorfa, ya que necesitaban menos energía para conseguir su completa fusión [165]. En cambio, los MEL-NLC presentaron un

comportamiento diferente, siendo la formulación cargada negativamente la que mostró menores valores de ΔH, sugiriendo así que la estructura de los MEL-NLC+ era más cristalina. La formulación dual también mostró un comportamiento similar, en este caso con unos valores de ΔH similares en la formulación positiva y negativa, pero mayor T_m en la formulación positiva, lo cual podría estar relacionado con una mayor cristalinidad de las partículas cargadas positivamente [189]. Generalmente, la disminución del T_m y ΔH también es resultado del tamaño de partícula en el rango nanométrico, la elevada área superficial específica y la presencia de tensioactivo [190]. En cuanto al análisis mediante espectroscopia FTIR, para todas las formulaciones indicó la ausencia de enlaces covalentes entre los activos y la matriz lipídica, respaldando la hipótesis de que su interacción está principalmente mediada por fuerzas no covalentes, como enlaces de hidrógeno e interacciones hidrofóbicas [166]. En los estudios de XRD se pudieron observar las formas β y β' en las formulaciones. En todas las formulaciones se pudo observar que, en la mezcla de lípidos había principalmente la forma β', pero las formulaciones de NLC en cambio, aparecía o aumentaba la señal de la forma β, la forma más estable físicamente de las estructuras cristalinas de los lípidos [191]. Además, la cristalinidad de las muestras observadas en los estudios de interacción se correlaciona con su estabilidad, de forma que las formulaciones más amorfas resultaron formulaciones más estables. Este efecto también podría estar relacionado con la concentración de fase lipídica que contienen estos sistemas [165].

Los estudios de liberación *in vitro* pusieron de manifiesto que, en todos los casos, los fármacos fueron liberados lenta y sostenidamente de los NLC en comparación con las soluciones de fármaco libre. Todas las formulaciones mostraron en común una liberación bifásica, iniciada con una primera etapa de liberación rápida del fármaco depositado en la superficie, seguido del encapsulado en el interior de la matriz lipídica. Por un lado, los HA-APG-NLC y MEL-NLC+ mostraron una liberación más rápida en comparación con sus respectivas formulaciones cargadas negativamente. Sin embargo, la co-encapsulación de APG y MEL en NLC dio lugar a en una liberación más lenta de ambos compuestos en comparación con sus formulaciones individuales. Esta discrepancia podría deberse a la menor concentración individual de cada

compuesto en los NLC de carga dual o a una menor concentración total de lípidos.

Con el objetivo de evaluar la biocompatibilidad ocular de las formulaciones, se llevaron a cabo ensayos *in vitro* utilizando células HCE-2 como modelo celular corneal. En todas las concentraciones estudiadas, ni APG ni MEL mostraron toxicidad celular. Por otro lado, los resultados demostraron que los NLC con un tiempo de incubación de 5 minutos no presentaron toxicidad, lo cual es significativo considerando el breve tiempo de residencia en la superficie ocular debido al drenaje nasolacrimal [192]. Sin embargo, un aumento en el tiempo de incubación condujo a una toxicidad leve en la mayoría de las concentraciones evaluadas. Este hecho se atribuyó a la carga positiva de los NLC, que facilita la interacción electrostática con las células cargadas negativamente. Esta interacción puede incrementar el estrés oxidativo y la producción de ROS [193]. Además, la alta afinidad de los NLC por las células favorece su internalización, como se observó en los estudios de fluorescencia [194]. A pesar de la toxicidad leve detectada en los ensayos de viabilidad celular, la morfología celular no se alteró, lo que sugiere que las formulaciones no causan daño estructural significativo [195]. Además, las formulaciones encapsulando los fármacos, mostraron menor toxicidad que las formulaciones vacías. Esto podría ser debido a que APG y MEL podrían ejercer efectos protectores en las células HCE-2 al contrarrestar el estrés oxidativo y restaurar el equilibrio redox celular. La APG ha demostrado atenuar la disminución de proteínas clave en la señalización de supervivencia celular y estimular la expresión de enzimas antioxidantes [196]. Además, la MEL ha sido descrita por sus propiedades antioxidantes y su capacidad para proteger la membrana mitocondrial y regular los procesos inflamatorios [197]. Estos efectos combinados podrían contribuir a la rápida protección que ambos fármacos brindan a las células HCE-2.

Con el fin de evaluar la seguridad ocular de las diferentes formulaciones se llevaron a cabo estudios *in vitro* e *in vivo*. El ensayo *in vitro* HET-CAM permite la evaluación de respuestas vasculares inducidas por la exposición aguda de la sustancia de prueba a la CAM. Estas respuestas son comparables a las observadas en el ojo de conejo debido a la similitud estructural y funcional entre los tejidos vasculares e inflamatorios de la conjuntiva ocular y la CAM

[198]. Los resultados de la prueba HET-CAM *in vitro* indicaron que las formulaciones no produjeron ningún signo de irritación en la CAM. Asimismo, el ensayo cuantitativo HET-CAM TBS confirmó la ausencia de daño celular significativo. Tanto las soluciones de APG como de MEL causaron cierta irritación *in vitro*, lo cual podría atribuirse al uso de pequeñas cantidades de solventes orgánicos para disolver los activos. A nivel *in vivo*, ninguna formulación causó ningún signo de irritación ocular, únicamente la solución de APG causó una ligera molestia al ser aplicada, sin causar posteriormente enrojecimiento o inflamación.

En cuanto a los estudios de eficacia terapéutica *in vivo*, los APG-NLC mostraron ser una opción terapéutica prometedora para el tratamiento del DED, debido a la combinación de las propiedades antioxidantes y antiinflamatorias del APG con la capacidad de los NLC para proporcionar una liberación sostenida y mejorar la biodisponibilidad [199,200]. En el test de Schirmer, donde se evaluó la cantidad de lágrimas, los APG-NLC mostraron diferencias significativas ($p < 0,0001$) en comparación a una solución comercial basada en HA. Además, en la tinción con fluoresceína, que evalúa el estado de la córnea [201], tanto los APG-NLC como los NLC vacíos mostraron diferencias significativas ($p < 0,001$) respecto al control tratado con suero fisiológico. Finalmente, se realizó la tinción de rosa de Bengala, que se utiliza para evaluar la integridad de la película lagrimal [202]. En esta tinción, se pudo observar que los únicos tratamientos capaces de restaurar la película fueron los APG-NLC y los NLC vacíos ($p < 0,05$). La eficacia de los NLC vacíos fue principalmente atribuido al RHO contenido en la matriz lipídica, que podría aportar propiedades adicionales, como favorecer la cicatrización de heridas y la regeneración tisular, ya que contiene ácidos grasos esenciales que desempeñan un papel crucial en la reparación de tejidos y en la reducción de la inflamación [203].

Los MEL-NLC fueron aplicados en estudios *in vitro* para estudiar su potencial contra el UM. Los resultados obtenidos sugirieron que los MEL-NLC presentaron una mayor citotoxicidad contra las células de UM en comparación con la solución de MEL. Esta mayor efectividad podría atribuirse a una mejor penetración de los NLC en las células tumorales, lo que aumenta la concentración intracelular de MEL. Además, se ha descrito que las células de

UM expresan receptores de MEL [204]. Esto podría ser de relevante importancia, debido a que los MEL-NLC presentaron una liberación rápida *in vitro,* lo cual podría ayudar a un primer efecto antiproliferativo de la formulación cuando se comienza a liberar MEL de los NLC. Los estudios *in vivo* con los MEL-NLC marcados fluorescentemente demostraron que penetraban y distribuían por los tejidos internos del ojo, acumulándose en la retina y los procesos ciliares. Su elevada penetración se atribuyó a su tamaño nanométrico, a su naturaleza lipídica y a sus propiedades mucoadhesivas [205,206]. Estos hallazgos son relevantes debido a la ubicación de los tumores de UM en el cuerpo ciliar y la coroides [207]. La acumulación de MEL-NLC en estos tejidos podría permitir una liberación dirigida de MEL, aumentando su actividad terapéutica en este tipo de tumor ocular.

Debido a que la inflamación ocular es un problema de salud importante que puede causar pérdida de visión, comprender mejor la fisiopatología de la inflamación ocular es esencial para desarrollar tratamientos más efectivos [208]. Investigaciones recientes han demostrado la importancia de los mediadores inflamatorios en enfermedades oculares como la AMD y la retinopatía diabética, lo que sugiere la necesidad de reevaluar los enfoques terapéuticos actuales [209]. La evaluación del mecanismo de acción de los NLC conteniendo APG y MEL puso de relieve de los sistemas duales (APG-MEL-NLC) fueron capaces de modular la respuesta inflamatoria a través de la inhibición de las citoquinas IL-6 y IL-8, y la molécula de adhesión MCP-1, sugiriendo un mecanismo de acción multifactorial.

La inflamación es un proceso común en diferentes enfermedades oculares, como en el DED, el glaucoma, la AMD y el UM [210]. Particularmente, en el DED, la inflamación desencadena una respuesta inmune que daña la superficie ocular [211], y en el UM crea un microambiente que favorece el crecimiento tumoral [212]. La evidencia sugiere que la modulación de la inflamación podría ser una estrategia prometedora para tratar muchas de las enfermedades oculares actuales [213]. Debido al potencial de los activos encapsulados, se estudió la capacidad de las formulaciones desarrolladas para prevenir y tratar la inflamación *in vivo* en un modelo de conejo New Zeland. En cuanto a la prevención de la inflamación se administraron las formulaciones, los fármacos

libres, o el suero fisiológico (control positivo de inflamación) y 30 minutos después de aplicó araquidonato sódico. Las soluciones de APG, MEL y su combinación ejercieron efecto antinflamatorio inicial, pero mucho menor que cuando se administraron encapsuladas en NPs, lo cual podría estar relacionado con una posible eliminación rápida de la superficie ocular ya que, generalmente, menos de un 5 % de la dosis administrada entra en la cámara anterior del ojo [214]. Los NLC en cambio, desde los primeros tiempos analizados, mostraron un mayor efecto antinflamatorio, lo cual podría estar relacionado con su capacidad de mucoadhesión inducida por su carga positiva, que facilita la interacción con las mucinas cargadas negativas de la superficie ocular [215] y su liberación bifásica, iniciándose rápidamente por el fármaco depositado en la superficie y posteriormente más lento. En el tratamiento de la inflamación se instiló inicialmente el estímulo inflamatorio y 30 minutos después se administraron cada uno de los tratamientos. En este caso las soluciones de fármacos mostraron un efecto generalmente más rápido que la formulación, pero las formulaciones mostraron un mayor efecto antinflamatorio en los tiempos posteriores. Comparando el efecto de las 3 formulaciones, los sistemas duales (APG-MEL-NLC) mostraron un efecto antinflamatorio más rápido y potente en la etapa inicial. Esto podría ser resultado de mecanismos de acción complementarios y un efecto sinérgico en su liberación, ya que la MEL se libera más más rápido que la APG en la formulación dual y la APG liberada más lentamente posee un potente efecto antinflamatorio. Ha sido reportado que tanto la MEL como la APG presentan propiedades antiinflamatorias [200,216] que podrían actuar de forma sinérgica. La MEL, además de ser un potente antioxidante, inhibe la activación del factor de transcripción NF-κB, reduciendo así la producción de citocinas proinflamatorias [217]. Por su parte, la APG también inhibe NF-κB y otros factores de transcripción como AP-1 y STAT, disminuyendo la expresión de genes proinflamatorios [218]. Esta acción combinada sobre NF-κB amplifica el efecto antiinflamatorio, ya que este factor es un regulador clave de la respuesta inflamatoria [219]. Además, la MEL posee propiedades inmunomoduladoras y la APG reduce la producción de moléculas de adhesión, lo que contribuye a disminuir la inflamación de forma complementaria [220,221]. En conjunto,

estas moléculas ofrecen una estrategia terapéutica prometedora para el tratamiento de enfermedades inflamatorias.

5

Conclusiones

5. Conclusions

Six formulations of lipid NPs encapsulating APG, MEL, or both have been developed for the treatment of proliferative diseases, or ocular pathologies by functionalizing them with a positive charge. In this context and based on the obtained results, the conclusions of the present doctoral thesis are:

1. APG-NLC, MEL-NLC, and APG-MEL-NLC prepared with an optimized hot high-pressure homogenization method exhibit suitable physicochemical properties, being able to be administered for proliferative diseases or ocular pathologies as eye drops.
2. All the NLC formulations have been characterized by spectroscopic (FTIR and XRD) and thermal analysis (DSC), showing the NLC amorphous structure and their lipid conformation, which posteriorly have been related to their physical stability.
3. All the formulations have a sustained release, characterized with a biphasic behaviour, in which they show an initial burst release followed by a slow and sustained phase.
4. Anti-angiogenic studies performed *in ovo* with the APG-NLC demonstrate that these NPs release APG in an efficient manner, enhancing the APG therapeutic properties.
5. *In vitro* assays carried out with 4 different cancer cell lines at two different incubation times have showed that all the negatively charged NLC possess anti-proliferative activity, which increases along the incubation time.
6. *In vitro* cytotoxicity and *in vivo* ocular tolerance demonstrate that the positively charged formulations are safe and well-tolerated at cellular and histological level.

7. APG-NLC demonstrate excellent efficacy in the treatment of dry eye disease, restoring both tear flow and damaged corneal surface after five days of treatment. Moreover, empty NLC also has great properties against dry eye disease, mainly attributed to the rosehip oil contained in the lipid matrix.
8. MEL-NLC demonstrate anti-proliferative activity against uveal melanoma cells, with a higher cytotoxic effect in comparison to the free MEL solution. Furthermore, *in vivo* biodistribution studies show that the MEL-NLC are able to reach and accumulate at the ciliary processes and the retina in three hours post-instillation.
9. APG-MEL-NLC exhibit *in vitro* anti-inflammatory activity in a treatment model by using LPS as an inflammatory stimulus, decreasing the levels of the cytokines IL-6 and IL-8 and the adhesion protein MCP-1.
10. *In vivo* anti-inflammatory efficacy studies show that the three positively charged formulations are effective in the prevention and treatment of inflammatory disorders at ocular level.

In summary, the nanostructured lipid systems encapsulating APG, MEL, or both, offer a promising approach for treating proliferative and ocular diseases. These bioactive compounds, known for their antioxidant and anti-inflammatory properties, can be effectively delivered to target tissues using a nanotechnological tool. The combination of these agents may enhance their therapeutic efficacy, providing a potential tool for innovative and effective treatments.

6

Bibliografía

6. Bibliografía

[1] Carissimi M, Fuster M, Víllora G. Nanoparticles as drug delivery systems. In: Pham P, editor. 21st Century nanostructured Mater. - physics, Chem. Classif. Emerg. Appl. Ind. Biomed. Agric., IntechOpen; 2022, p. 227–42. https://doi.org/10.5772/intechopen.94802.

[2] Boulaiz H, Alvarez PJ, Ramirez A, Marchal JA, Prados J, Rodríguez-Serrano F, et al. Nanomedicine: application areas and development prospects. Int J Mol Sci 2011;12:3303–21. https://doi.org/10.3390/IJMS12053303.

[3] Tenchov R, Bird R, Curtze AE, Zhou Q. Lipid nanoparticles from liposomes to mRNA vaccine delivery, a landscape of research diversity and advancement. ACS Nano 2021;15:16982–7015. https://doi.org/10.1021/ACSNANO.1C04996.

[4] Zhang C, Yan L, Wang X, Zhu S, Chen C, Gu Z, et al. Progress, challenges, and future of nanomedicine. Nano Today 2020;35:101008. https://doi.org/10.1016/J.NANTOD.2020.101008.

[5] Germain M, Caputo F, Metcalfe S, Tosi G, Spring K, Åslund AKO, et al. Delivering the power of nanomedicine to patients today. J Control Release 2020;326:164–71. https://doi.org/10.1016/J.JCONREL.2020.07.007.

[6] Farokhzad OC, Langer R. Impact of nanotechnology on drug delivery. ACS Nano 2009;3:16–20. https://doi.org/10.1021/nn900002m.

[7] McClements DJ, Xiao H. Is nano safe in foods? Establishing the factors impacting the gastrointestinal fate and toxicity of organic and inorganic food-grade nanoparticles. Npj Sci Food 2017;1:1–13. https://doi.org/10.1038/s41538-017-0005-1.

[8] Khalid M, Abdollahi M. Toxicity of inorganic nanoparticles. Compr Anal Chem 2022;99:25–85. https://doi.org/10.1016/BS.COAC.2021.12.001.

[9] Joudeh N, Linke D. Nanoparticle classification, physicochemical properties, characterization, and applications: a comprehensive review for biologists. J Nanobiotechnology 2022;20:1–29. https://doi.org/10.1186/S12951-022-01477-8.

[10] Kaur M, Sodhi RK, Sainaga Jyothi VGS, Sree VH, Shubhra, Singh PK, et al. Brain targeting drug delivery systems for the management of brain

disorders: molecular targets and nanotechnological strategies. Multifunct Nanocarriers 2022:289–345. https://doi.org/10.1016/B978-0-323-85041-4.00012-3.

[11] Müller RH, Mäder K, Gohla S. Solid lipid nanoparticles (SLN) for controlled drug delivery - A review of the state of the art. Eur J Pharm Biopharm 2000;50:161–77. https://doi.org/10.1016/S0939-6411(00)00087-4.

[12] Bonilla L, Espina M, Severino P, Cano A, Ettcheto M, Camins A, et al. Lipid nanoparticles for the posterior eye segment. Pharmaceutics 2022;14:90. https://doi.org/10.3390/pharmaceutics14010090.

[13] Pilkington EH, Suys EJA, Trevaskis NL, Wheatley AK, Zukancic D, Algarni A, et al. From influenza to COVID-19: Lipid nanoparticle mRNA vaccines at the frontiers of infectious diseases. Acta Biomater 2021;131:16–40. https://doi.org/10.1016/J.ACTBIO.2021.06.023.

[14] Scioli Montoto S, Muraca G, Ruiz ME. Solid lipid nanoparticles for drug delivery: pharmacological and biopharmaceutical aspects. Front Mol Biosci 2020;7:319. https://doi.org/10.3389/FMOLB.2020.587997.

[15] Zhu Y, Inada H, Hartschuh A, Shi L, Della Pia A, Costantini G, et al. Solid lipid nanoparticles - SLN. Encycl Nanotechnol 2012:2471–87. https://doi.org/10.1007/978-90-481-9751-4_249.

[16] Ghasemiyeh P, Mohammadi-Samani S. Solid lipid nanoparticles and nanostructured lipid carriers as novel drug delivery systems: applications, advantages and disadvantages. Res Pharm Sci 2018;13:303. https://doi.org/10.4103/1735-5362.235156.

[17] Subroto E, Andoyo R, Indiarto R. Solid lipid nanoparticles: review of the current research on encapsulation and delivery systems for active and antioxidant compounds. Antioxidants 2023;12:633. https://doi.org/10.3390/ANTIOX12030633.

[18] Naseri N, Valizadeh H, Zakeri-Milani P. Solid lipid nanoparticles and nanostructured lipid carriers: structure,preparation and application. Adv Pharm Bull 2015;5:313. https://doi.org/10.15171/APB.2015.043.

[19] H. Muller R, Shegokar R, M. Keck C. 20 years of lipid nanoparticles (SLN & NLC): present state of development & industrial applications. Curr Drug Discov Technol 2011;8:207–27. https://doi.org/10.2174/157016311796799062.

[20] Müller RH, Radtke M, Wissing SA. Nanostructured lipid matrices for

improved microencapsulation of drugs. Int J Pharm 2002;242:121–8. https://doi.org/10.1016/S0378-5173(02)00180-1.

[21] Duan Y, Dhar A, Patel C, Khimani M, Neogi S, Sharma P, et al. A brief review on solid lipid nanoparticles: part and parcel of contemporary drug delivery systems. RSC Adv 2020;10:26791. https://doi.org/10.1039/D0RA03491F.

[22] Aguilera JM, Lillford PJ, Barbosa-Cánovas G V. Food materials science: Principles and practice. 2008. https://doi.org/10.1007/978-0-387-71947-4.

[23] Severino P, Pinho SC, Souto EB, Santana MHA. Polymorphism, crystallinity and hydrophilic–lipophilic balance of stearic acid and stearic acid–capric/caprylic triglyceride matrices for production of stable nanoparticles. Colloids Surfaces B Biointerfaces 2011;86:125–30. https://doi.org/10.1016/J.COLSURFB.2011.03.029.

[24] Souto EB, Mehnert W, Müller RH. Polymorphic behaviour of Compritol 888 ATO as bulk lipid and as SLN and NLC. J Microencapsul 2006;23:417–33. https://doi.org/10.1080/02652040600612439.

[25] Salvi VR, Pawar P. Nanostructured lipid carriers (NLC) system: A novel drug targeting carrier. J Drug Deliv Sci Technol 2019;51:255–67. https://doi.org/10.1016/J.JDDST.2019.02.017.

[26] Elmowafy M, Al-Sanea MM. Nanostructured lipid carriers (NLCs) as drug delivery platform: Advances in formulation and delivery strategies. Saudi Pharm J 2021;29:999–1012. https://doi.org/10.1016/J.JSPS.2021.07.015.

[27] Heo S, Lee G, Na HE, Park JH, Kim T, Oh SE, et al. Current status of the novel food ingredient safety evaluation system. Food Sci Biotechnol 2024;33:1–11. https://doi.org/10.1007/S10068-023-01396-W.

[28] Hemmrich E, McNeil S. Active ingredient vs excipient debate for nanomedicines. Nat Nanotechnol 2023;18:692–5. https://doi.org/10.1038/s41565-023-01371-w.

[29] Khan S, Sharma A, Jain V. An overview of nanostructured lipid carriers and its application in drug delivery through different routes. Adv Pharm Bull 2023;13:460. https://doi.org/10.34172/APB.2023.056.

[30] Chauhan I, Yasir M, Verma M, Singh AP. Nanostructured lipid carriers: a groundbreaking approach for transdermal drug delivery. Adv Pharm Bull 2020;10:165. https://doi.org/10.34172/APB.2020.021.

[31] Aburahma MH, Badr-Eldin SM. Compritol 888 ATO: a multifunctional lipid excipient in drug delivery systems and nanopharmaceuticals. Expert Opin Drug Deliv 2014;11:1865–83. https://doi.org/10.1517/17425247.2014.935335.

[32] Averina ES, Müller RH, Popov D V., Radnaeva LD. Physical and chemical stability of nanostructured lipid drug carriers (NLC) based on natural lipids from Baikal region (Siberia, Russia). Pharmazie 2011;66:348–56. https://doi.org/10.1691/PH.2011.0326.

[33] Ahmad N, Anwar F, Gilani A ul H. Rose hip (Rosa canina L.) oils. Essent Oils Food Preserv Flavor Saf 2016:667–75. https://doi.org/10.1016/B978-0-12-416641-7.00076-6.

[34] Saini A, Kaur R, Kumar S, Saini RK, Kashyap B, Kumar V. New horizon of rosehip seed oil: Extraction, characterization for its potential applications as a functional ingredient. Food Chem 2024;437:137568. https://doi.org/10.1016/J.FOODCHEM.2023.137568.

[35] Qadir R, Anwar F. Cold pressed rosehip seed oil. Cold Press Oils Green Technol Bioact Compd Funct Appl 2020:315–22. https://doi.org/10.1016/B978-0-12-818188-1.00028-1.

[36] Muralidharan J, Papandreou C, Sala-Vila A, Rosique-Esteban N, Fitó M, Estruch R, et al. Fatty acids composition of blood cell membranes and peripheral inflammation in the PREDIMED study: A cross-sectional analysis . Nutrients 2019;11:576. https://doi.org/10.3390/NU11030576.

[37] Grajzer M, Prescha A, Korzonek K, Wojakowska A, Dziadas M, Kulma A, et al. Characteristics of rose hip (Rosa canina L.) cold-pressed oil and its oxidative stability studied by the differential scanning calorimetry method. Food Chem 2015;188:459–66. https://doi.org/10.1016/J.FOODCHEM.2015.05.034.

[38] Ambavade SD, Misar A V., Ambavade PD. Pharmacological, nutritional, and analytical aspects of β-sitosterol: A review. Orient Pharm Exp Med 2014;14:193–211. https://doi.org/10.1007/S13596-014-0151-9.

[39] Napoli JL. Physiological insights into all-trans-retinoic acid biosynthesis. Biochim Biophys Acta - Mol Cell Biol Lipids 2012;1821:152–67. https://doi.org/10.1016/J.BBALIP.2011.05.004.

[40] Valerón-Almazán P, Gómez-Duaso AJ, Santana-Molina N, García-Bello MA, Carretero G, Valerón-Almazán P, et al. evolution of post-surgical scars treated with pure rosehip seed oil. J Cosmet Dermatological Sci Appl 2015;5:161–7. https://doi.org/10.4236/JCDSA.2015.52019.

[41] Concha J, Soto C, Chamy R, Zúñiga ME. Effect of rosehip extraction process on oil and defatted meal physicochemical properties. JAOCS, J Am Oil Chem Soc 2006;83:771–5. https://doi.org/10.1007/S11746-006-5013-2/METRICS.

[42] Kiralan M, Yildirim G. Rosehip (Rosa canina L.) oil. Fruit Oils Chem Funct 2019:803–14. https://doi.org/10.1007/978-3-030-12473-1_43.

[43] Javed S, Mangla B, Almoshari Y, Sultan MH, Ahsan W. Nanostructured lipid carrier system: A compendium of their formulation development approaches, optimization strategies by quality by design, and recent applications in drug delivery. Nanotechnol Rev 2022;11:1744–77. https://doi.org/10.1515/ntrev-2022-0109.

[44] Sun W, Xie C, Wang H, Hu Y. Specific role of polysorbate 80 coating on the targeting of nanoparticles to the brain. Biomaterials 2004;25:3065–71. https://doi.org/10.1016/J.BIOMATERIALS.2003.09.087.

[45] Salminen H, Helgason T, Aulbach S, Kristinsson B, Kristbergsson K, Weiss J. Influence of co-surfactants on crystallization and stability of solid lipid nanoparticles. J Colloid Interface Sci 2014;426:256–63. https://doi.org/10.1016/J.JCIS.2014.04.009.

[46] Vedadghavami A, Zhang C, Bajpayee AG. Overcoming negatively charged tissue barriers: Drug delivery using cationic peptides and proteins. Nano Today 2020;34. https://doi.org/10.1016/J.NANTOD.2020.100898.

[47] Augustine R, Hasan A, Primavera R, Wilson RJ, Thakor AS, Kevadiya BD. Cellular uptake and retention of nanoparticles: Insights on particle properties and interaction with cellular components. Mater Today Commun 2020;25:101692. https://doi.org/10.1016/J.MTCOMM.2020.101692.

[48] Raval N, Maheshwari R, Kalyane D, Youngren-Ortiz SR, Chougule MB, Tekade RK. Importance of physicochemical characterization of nanoparticles in pharmaceutical product development. Basic Fundam Drug Deliv 2019:369–400. https://doi.org/10.1016/B978-0-12-817909-3.00010-8.

[49] Yagublu V, Karimova A, Hajibabazadeh J, Reissfelder C, Muradov M, Bellucci S, et al. Overview of physicochemical properties of nanoparticles as drug carriers for targeted cancer therapy. J Funct Biomater 2022;13:196. https://doi.org/10.3390/JFB13040196.

[50] Foroozandeh P, Aziz AA. Insight into cellular uptake and intracellular trafficking of nanoparticles. Nanoscale Res Lett 2018;13:1–12.

https://doi.org/10.1186/S11671-018-2728-6.

[51] Lu Y, Qi J, Wu W. Lipid nanoparticles: In vitro and in vivo approaches in drug delivery and targeting. Drug Target Stimuli Sensitive Drug Deliv Syst 2018:749–83. https://doi.org/10.1016/B978-0-12-813689-8.00020-3.

[52] Li Y, Chen X, Gu N. Computational investigation of interaction between nanoparticles and membranes: Hydrophobic/hydrophilic effect. J Phys Chem B 2008;112:16647–53. https://doi.org/10.1021/JP8051906.

[53] Sukhanova A, Bozrova S, Sokolov P, Berestovoy M, Karaulov A, Nabiev I. Dependence of nanoparticle toxicity on their physical and chemical properties. Nanoscale Res Lett 2018;13:1–21. https://doi.org/10.1186/S11671-018-2457-X.

[54] Gatoo MA, Naseem S, Arfat MY, Mahmood Dar A, Qasim K, Zubair S. Physicochemical properties of nanomaterials: implication in associated toxic manifestations. Biomed Res Int 2014;2014:498420. https://doi.org/10.1155/2014/498420.

[55] Bueno Barbezan AA; ;, Daruich De Souza C;, Chuery M, Rostelato ME, Domb A, Alexander W, et al. Review of advances in coating and functionalization of gold nanoparticles: from theory to biomedical application. Pharmaceutics 2024;16:255. https://doi.org/10.3390/PHARMACEUTICS16020255.

[56] De Rosa E, Fernandez-Moure J, Tasciotti E. Polymer coatings. Encycl Nanotechnol 2015:1–8. https://doi.org/10.1007/978-94-007-6178-0_105-2.

[57] Brown MB, Jones SA. Hyaluronic acid: a unique topical vehicle for the localized delivery of drugs to the skin. J Eur Acad Dermatology Venereol 2005;19:308–18. https://doi.org/10.1111/J.1468-3083.2004.01180.X.

[58] Huynh A, Priefer R. Hyaluronic acid applications in ophthalmology, rheumatology, and dermatology. Carbohydr Res 2020;489:107950. https://doi.org/10.1016/J.CARRES.2020.107950.

[59] Marques AC, Costa PC, Velho S, Amaral MH. Lipid nanoparticles functionalized with antibodies for anticancer drug therapy. Pharmaceutics 2023;15:216. https://doi.org/10.3390/PHARMACEUTICS15010216.

[60] Menon I, Zaroudi M, Zhang Y, Aisenbrey E, Hui L. Fabrication of active targeting lipid nanoparticles: Challenges and perspectives. Mater Today Adv 2022;16:100299. https://doi.org/10.1016/J.MTADV.2022.100299.

[61] Khosa A, Reddi S, Saha RN. Nanostructured lipid carriers for site-specific drug delivery. Biomed Pharmacother 2018;103:598–613. https://doi.org/10.1016/J.BIOPHA.2018.04.055.

[62] Assali M, Zaid AN. Features, applications, and sustainability of lipid nanoparticles in cosmeceuticals. Saudi Pharm J 2022;30:65. https://doi.org/10.1016/J.JSPS.2021.12.018.

[63] Haider M, Abdin SM, Kamal L, Orive G. Nanostructured lipid carriers for delivery of chemotherapeutics: a review. Pharmaceutics 2020;12:288. https://doi.org/10.3390/pharmaceutics12030288.

[64] Liu M, Wen J, Sharma M. Solid lipid nanoparticles for topical drug delivery: mechanisms, dosage form perspectives, and translational status. Curr Pharm Des 2020;26:3203–17. https://doi.org/10.2174/1381612826666200526145706.

[65] Santonocito D, Puglia C. Applications of lipid-based nanocarriers for parenteral drug delivery. Curr Med Chem 2022;29:4152–69. https://doi.org/10.2174/0929867329666220104111949.

[66] Salah E, Abouelfetouh MM, Pan Y, Chen D, Xie S. Solid lipid nanoparticles for enhanced oral absorption: A review. Colloids Surfaces B Biointerfaces 2020;196:111305. https://doi.org/10.1016/J.COLSURFB.2020.111305.

[67] Li L, Xu ZP, Leong EWX, Ge R. Lipid nanoparticles as delivery vehicles for inhaled therapeutics. Biomedicines 2022;10:2179. https://doi.org/10.3390/BIOMEDICINES10092179.

[68] Formica ML, Real DA, Picchio ML, Catlin E, Donnelly RF, Paredes AJ. On a highway to the brain: A review on nose-to-brain drug delivery using nanoparticles. Appl Mater Today 2022;29:101631. https://doi.org/10.1016/J.APMT.2022.101631.

[69] Pardeike J, Hommoss A, Müller RH. Lipid nanoparticles (SLN, NLC) in cosmetic and pharmaceutical dermal products. Int J Pharm 2009;366:170–84. https://doi.org/10.1016/j.ijpharm.2008.10.003.

[70] Loo CH, Basri M, Ismail R, Lau HLN, Tejo BA, Kanthimathi MS, et al. Effect of compositions in nanostructured lipid carriers (NLC) on skin hydration and occlusion. Int J Nanomedicine 2013;8:13–22. https://doi.org/10.2147/IJN.S35648.

[71] Brown JS, Amend SR, Austin RH, Gatenby RA, Hammarlund EU, Pienta KJ. Updating the Definition of Cancer. Mol Cancer Res 2023;21:1147.

https://doi.org/10.1158/1541-7786.MCR-23-0411.

[72] Upadhyay A. Cancer: An unknown territory; rethinking before going ahead. Genes Dis 2021;8:661. https://doi.org/10.1016/J.GENDIS.2020.09.002.

[73] Bray F, Laversanne M, Cao B, Varghese C, Mikkelsen B, Weiderpass E, et al. Comparing cancer and cardiovascular disease trends in 20 middle- or high-income countries 2000–19: A pointer to national trajectories towards achieving Sustainable Development goal target 3.4. Cancer Treat Rev 2021;100. https://doi.org/10.1016/J.CTRV.2021.102290.

[74] Global Cancer Observatory n.d. https://gco.iarc.fr/en (accessed February 16, 2024).

[75] Ma X, Yu H. Cancer issue: global burden of cancer. Yale J Biol Med 2006;79:94. https://doi.org/10.1007/978-3-030-45009-0_26.

[76] Gaidai O, Yan P, Xing Y. Future world cancer death rate prediction. Sci Rep 2023;13:1–9. https://doi.org/10.1038/s41598-023-27547-x.

[77] Baranwal J, Barse B, Di Petrillo A, Gatto G, Pilia L, Kumar A. Nanoparticles in cancer diagnosis and treatment. Materials (Basel) 2023;16:5354. https://doi.org/10.3390/MA16155354.

[78] Vu SH, Vetrivel P, Kim J, Lee MS. Cancer resistance to immunotherapy: molecular mechanisms and tackling strategies. Int J Mol Sci 2022;23:10906. https://doi.org/10.3390/IJMS231810906.

[79] Chhabra N, Kennedy J. A review of cancer immunotherapy toxicity: immune checkpoint inhibitors. J Med Toxicol 2021;17:411–24. https://doi.org/10.1007/S13181-021-00833-8.

[80] Hoeben A, Joosten EAJ, van den Beuken-Van Everdingen MHJ. Personalized medicine: recent progress in cancer therapy. Cancers (Basel) 2021;13:242. https://doi.org/10.3390/CANCERS13020242.

[81] Dey A, Mitra A, Pathak S, Prasad S, Zhang AS, Zhang H, et al. Recent advancements, limitations, and future perspectives of the use of personalized medicine in treatment of colon cancer. Technol Cancer Res Treat 2023;22. https://doi.org/10.1177/15330338231178403.

[82] Sabit H, Abdel-Hakeem M, Shoala T, Abdel-Ghany S, Abdel-Latif MM, Almulhim J, et al. Nanocarriers: a reliable tool for the delivery of anticancer drugs. Pharmaceutics 2022;14:1566. https://doi.org/10.3390/PHARMACEUTICS14081566.

[83] Gavas S, Quazi S, Karpiński TM. Nanoparticles for cancer therapy: current progress and challenges. Nanoscale Res Lett 2021;16:1–21. https://doi.org/10.1186/S11671-021-03628-6.

[84] Rizwanullah M, Ahmad MZ, Garg A, Ahmad J. Advancement in design of nanostructured lipid carriers for cancer targeting and theranostic application. Biochim Biophys Acta - Gen Subj 2021;1865:129936. https://doi.org/10.1016/J.BBAGEN.2021.129936.

[85] Nguyen VH, Thuy VN, Van TV, Dao AH, Lee BJ. Nanostructured lipid carriers and their potential applications for versatile drug delivery via oral administration. OpenNano 2022;8:100064. https://doi.org/10.1016/J.ONANO.2022.100064.

[86] Rodrigues da Silva GH, de Moura LD, de Carvalho FV, Geronimo G, Mendonça TC, de Lima FF, et al. Antineoplastics encapsulated in nanostructured lipid carriers. Molecules 2021;26:6929. https://doi.org/10.3390/MOLECULES26226929.

[87] de la Puente P, Azab AK. Nanoparticle delivery systems, general approaches and their implementation in multiple myeloma. Eur J Haematol 2017;98:541. https://doi.org/10.1111/EJH.12870.

[88] Kashyap D, Tuli HS, Yerer MB, Sharma A, Sak K, Srivastava S, et al. Natural product-based nanoformulations for cancer therapy: Opportunities and challenges. Semin Cancer Biol 2021;69:5–23. https://doi.org/10.1016/J.SEMCANCER.2019.08.014.

[89] Yap KM, Sekar M, Fuloria S, Wu YS, Gan SH, Rani NNIM, et al. Drug delivery of natural products through nanocarriers for effective breast cancer therapy: a comprehensive review of literature. Int J Nanomedicine 2021;16:7891–941. https://doi.org/10.2147/IJN.S328135.

[90] Gehrcke M, Giuliani LM, Ferreira LM, Barbieri AV, Sari MHM, da Silveira EF, et al. Enhanced photostability, radical scavenging and antitumor activity of indole-3-carbinol-loaded rose hip oil nanocapsules. Mater Sci Eng C 2017;74:279–86. https://doi.org/10.1016/J.MSEC.2016.12.006.

[91] Berkoz M, Ozkan Yılmaz F, Hunt AO, Yildirim M. Rosa Canina L. ethanolic extract induces the anti-proliferative and apotosis potential in MCF-7 And MDA-MB-468 cell lines. Fresenius Environ Bull 2019;28:3718–23.

[92] Jiménez S, Gascón S, Luquin A, Laguna M, Ancin-Azpilicueta C, Rodríguez-Yoldi MJ. Rosa canina extracts have antiproliferative and antioxidant efects on Caco-2 human colon cancer. PLoS One

2016;11:e0159136. https://doi.org/10.1371/JOURNAL.PONE.0159136.

[93] Acar ÇA, Pehlivanoğlu S. Biosynthesis of silver nanoparticles using Rosa canina extract and its anti-cancer and anti-metastatic activity on human colon adenocarcinoma cell line HT29. Mehmet Akif Ersoy Univ J Heal Sci Inst 2019;7:124–31. https://doi.org/10.24998/MAEUSABED.653206.

[94] Cagle P, Idassi O, Carpenter J, Minor R, Goktepe I, Martin P. Effect of rosehip (Rosa Canina) extracts on human brain tumor cell proliferation and apoptosis. J Cancer Ther 2012;2012:534–45. https://doi.org/10.4236/JCT.2012.35069.

[95] Mármol I, Jiménez-Moreno N, Ancín-Azpilicueta C, Osada J, Cerrada E, Rodríguez-Yoldi MJ. A combination of Rosa Canina extracts and gold complex favors apoptosis of Caco-2 cells by increasing oxidative stress and mitochondrial dysfunction. Antioxidants 2019;9:17. https://doi.org/10.3390/ANTIOX9010017.

[96] Tumbas VT, Čanadanović-Brunet JM, Četojević-Simin DD, Ćetković GS, Dilas SM, Gille L. Effect of rosehip (Rosa canina L.) phytochemicals on stable free radicals and human cancer cells. J Sci Food Agric 2012;92:1273–81. https://doi.org/10.1002/JSFA.4695.

[97] Mármol I, Sánchez-De-Diego C, Jiménez-Moreno N, Ancín-Azpilicueta C, Rodríguez-Yoldi M. Therapeutic applications of rose hips from different Rosa species. Int J Mol Sci 2017;18:1137. https://doi.org/10.3390/IJMS18061137.

[98] Campagnoli LIM, Varesi A, Barbieri A, Marchesi N, Pascale A. Targeting the gut–eye axis: an emerging strategy to face ocular diseases. Int J Mol Sci 2023;24:24. https://doi.org/10.3390/IJMS241713338.

[99] Onugwu AL, Nwagwu CS, Onugwu OS, Echezona AC, Agbo CP, Ihim SA, et al. Nanotechnology based drug delivery systems for the treatment of anterior segment eye diseases. J Control Release 2023;354:465–88. https://doi.org/10.1016/J.JCONREL.2023.01.018.

[100] Shah shalin S, Denham LV, Elison JR, Bhattacharjee PS, Huq T, Clement C, et al. Drug delivery to the posterior segment of the eye for pharmacologic therapy. Expert Rev Ophthalmol 2010;5:93. https://doi.org/10.1586/EOP.09.70.

[101] Bachu RD, Chowdhury P, Al-Saedi ZHF, Karla PK, Boddu SHS. Ocular drug delivery barriers—role of nanocarriers in the treatment of anterior segment ocular diseases. Pharmaceutics 2018;10. https://doi.org/10.3390/pharmaceutics10010028.

[102] Bonilla L, Espina M, Severino P, Cano A, Ettcheto M, Camins A, et al. Lipid nanoparticles for the posterior eye segment. Pharmaceutics 2021;14:90. https://doi.org/10.3390/pharmaceutics14010090.

[103] Agarwal P, Rupenthal ID. Non-aqueous formulations in topical ocular drug delivery – A paradigm shift? Adv Drug Deliv Rev 2023;198:114867. https://doi.org/10.1016/J.ADDR.2023.114867.

[104] Reimondez-Troitiño S, Csaba N, Alonso MJ, De La Fuente M. Nanotherapies for the treatment of ocular diseases. Eur J Pharm Biopharm 2015;95:279–93. https://doi.org/10.1016/J.EJPB.2015.02.019.

[105] Wang R, Gao Y, Liu A, Zhai G. A review of nanocarrier-mediated drug delivery systems for posterior segment eye disease: challenges analysis and recent advances. J Drug Target 2021;29:687–702. https://doi.org/10.1080/1061186X.2021.1878366.

[106] Sánchez-López E, Espina M, Doktorovova S, Souto EB, García ML. Lipid nanoparticles (SLN, NLC): Overcoming the anatomical and physiological barriers of the eye – Part I – Barriers and determining factors in ocular delivery. Eur J Pharm Biopharm 2017;110:70–5. https://doi.org/10.1016/j.ejpb.2016.10.009.

[107] Niamprem P, Milla TJ, Schuett BS, Srinivas SP, Tiyaboonchai W. Interatcion of nanostructured lipid carriers with human meibum. Int J Appl Pharm 2019;11:35–42. https://doi.org/10.22159/IJAP.2019V11I3.29158.

[108] Sun GF, Qu XH, Jiang LP, Chen ZP, Wang T, Han XJ. The mechanisms of natural products for eye disorders by targeting mitochondrial dysfunction. Front Pharmacol 2024;15:1270073. https://doi.org/10.3389/FPHAR.2024.1270073/BIBTEX.

[109] Ikonne EU, Ikpeazu VO, Ugbogu EA. The potential health benefits of dietary natural plant products in age related eye diseases. Heliyon 2020;6:e04408. https://doi.org/10.1016/J.HELIYON.2020.E04408.

[110] Lei Z, Cao Z, Yang Z, Ao M, Jin W, Yu L. Rosehip oil promotes excisional wound healing by accelerating the phenotypic transition of macrophages. Planta Med 2019;85:563–9. https://doi.org/10.1055/A-0725-8456/BIB.

[111] Strugała P, Gładkowski W, Kucharska AZ, Sokół-Łetowska A, Gabrielska J. Antioxidant activity and anti-inflammatory effect of fruit extracts from blackcurrant, chokeberry, hawthorn, and rosehip, and their mixture with linseed oil on a model lipid membrane. Eur J Lipid Sci Technol

2016;118:461–74. https://doi.org/10.1002/EJLT.201500001.

[112] Ayati Z, Amiri MS, Ramezani M, Delshad E, Sahebkar A, Emami SA. Phytochemistry, traditional uses and pharmacological profile of rose hip: a review. Curr Pharm Des 2018;24:4101–24. https://doi.org/10.2174/1381612824666181010151849.

[113] Gruenwald J, Uebelhack R, Moré MI. Rosa canina – Rose hip pharmacological ingredients and molecular mechanics counteracting osteoarthritis – A systematic review. Phytomedicine 2019;60:152958. https://doi.org/10.1016/J.PHYMED.2019.152958.

[114] Huerva V, Ascaso FJ, Grzybowski A. Ocular inflammation. Mediators Inflamm 2015;2015. https://doi.org/10.1155/2015/398076.

[115] Lalu L, Tambe V, Pradhan D, Nayak K, Bagchi S, Maheshwari R, et al. Novel nanosystems for the treatment of ocular inflammation: Current paradigms and future research directions. J Control Release 2017;268:19–39. https://doi.org/10.1016/J.JCONREL.2017.07.035.

[116] Iwamoto S, Koga T, Ohba M, Okuno T, Koike M, Murakami A, et al. Non-steroidal anti-inflammatory drug delays corneal wound healing by reducing production of 12-hydroxyheptadecatrienoic acid, a ligand for leukotriene B4 receptor 2. Sci Rep 2017;7:1–10. https://doi.org/10.1038/s41598-017-13122-8.

[117] McGhee CNJ, Dean S, Danesh-Meyer H. Locally administered ocular corticosteroids. Drug Saf 2012;25:33–55. https://doi.org/10.2165/00002018-200225010-00004.

[118] Souto EB, Doktorovova S, Gonzalez-Mira E, Egea MA, Garcia ML. Feasibility of lipid nanoparticles for ocular delivery of anti-inflammatory drugs. Curr Eye Res 2010;35:537–52. https://doi.org/10.3109/02713681003760168.

[119] Lemp MA, Baudouin C, Baum J, Dogru M, Foulks GN, Kinoshita S, et al. The definition and classification of dry eye disease: report of the definition and classification subcommittee of the international dry eye workShop (2007). Ocul Surf 2007;5:75–92. https://doi.org/10.1016/S1542-0124(12)70081-2.

[120] Ling J, Chan BCL, Tsang MSM, Gao X, Leung PC, Lam CWK, et al. Current advances in mechanisms and treatment of dry eye disease: toward anti-inflammatory and immunomodulatory therapy and traditional chinese medicine. Front Med 2022;8:815075. https://doi.org/10.3389/FMED.2021.815075.

[121] O'Neil EC, Henderson M, Massaro-Giordano M, Bunya VY. Advances in dry eye disease treatment. Curr Opin Ophthalmol 2019;30:166. https://doi.org/10.1097/ICU.0000000000000569.

[122] Semp DA, Beeson D, Sheppard AL, Dutta D, Wolffsohn JS. Artificial tears: a systematic review. Clin Optom 2023;15:27. https://doi.org/10.2147/OPTO.S350185.

[123] Yeu E, Silverstein S, Guillon M, Schulze MM, Galarreta D, Srinivasan S, et al. Efficacy and safety of phospholipid nanoemulsion-based ocular lubricant for the management of various subtypes of dry eye disease: a phase IV, multicenter trial. Clin Ophthalmol 2020;14:2570. https://doi.org/10.2147/OPTH.S261318.

[124] Zhang MG, Lee JY, Gallo RA, Tao W, Tse D, Doddapaneni R, et al. Therapeutic targeting of oncogenic transcription factors by natural products in eye cancer. Pharmacol Res 2018;129:374. https://doi.org/10.1016/J.PHRS.2017.11.033.

[125] Onugwu AL, Ugorji OL, Ufondu CA, Ihim SA, Echezona AC, Nwagwu CS, et al. Nanoparticle-based delivery systems as emerging therapy in retinoblastoma: recent advances, challenges and prospects. Nanoscale Adv 2023;5:4628–48. https://doi.org/10.1039/D3NA00462G.

[126] Madunić J, Madunić IV, Gajski G, Popić J, Garaj-Vrhovac V. Apigenin: a dietary flavonoid with diverse anticancer properties. Cancer Lett 2018;413:11–22. https://doi.org/10.1016/J.CANLET.2017.10.041.

[127] Yan X, Qi M, Li P, Zhan Y, Shao H. Apigenin in cancer therapy: anti-cancer effects and mechanisms of action. Cell Biosci 2017;7:50. https://doi.org/10.1186/S13578-017-0179-X.

[128] Wang M, Firrman J, Liu LS, Yam K. A review on flavonoid apigenin: Dietary intake, ADME, antimicrobial effects, and interactions with human gut microbiota. Biomed Res Int 2019;7010467. https://doi.org/10.1155/2019/7010467.

[129] Rahmani AH;, Alsahli MA;, Almatroudi A;, Almogbel MA;, Khan AA;, Anwar S;, et al. The potential role of apigenin in cancer prevention and treatment. Molecules 2022;27:6051. https://doi.org/10.3390/MOLECULES27186051.

[130] Singh D, Gupta M, Sarwat M, Siddique HR. Apigenin in cancer prevention and therapy: A systematic review and meta-analysis of animal models. Crit Rev Oncol Hematol 2022;176:103751. https://doi.org/10.1016/J.CRITREVONC.2022.103751.

[131] Srivastava JK, Shankar E, Gupta S. Chamomile: A herbal medicine of the past with a bright future (review). Mol Med Rep 2010;3:895–901. https://doi.org/10.3892/MMR.2010.377.

[132] Salehi B, Venditti A, Sharifi-Rad M, Kręgiel D, Sharifi-Rad J, Durazzo A, et al. The therapeutic potential of apigenin. Int J Mol Sci 2019;20:1305. https://doi.org/10.3390/IJMS20061305.

[133] Liu L, Wei D, Xu H, Liu C. Apigenin ameliorates ocular surface lesions in a rat model of dry eye disease. Eur J Inflamm 2019;17:205873921881868. https://doi.org/10.1177/2058739218818681.

[134] Zhang Y, Yang Y, Yu H, Li M, Hang L, Xu X. Apigenin protects mouse retina against oxidative damage by regulating the Nrf2 pathway and autophagy. Oxid Med Cell Longev 2020;2020. https://doi.org/10.1155/2020/9420704.

[135] Fu M-S, Zhu B-J, Luo D-W. Apigenin prevents TNF-α induced apoptosis of primary rat retinal ganglion cells. Cell Mol Biol 2014;60:37–42. https://doi.org/10.14715/cmb/2014.60.4.6.

[136] Jiang W, Chen H, Tai Z, Li T, Luo L, Tong Z, et al. Apigenin and Ethaverine hydrochloride enhance retinal vascular barrier in vitro and in vivo. Transl Vis Sci Technol 2020;9:8. https://doi.org/10.1167/TVST.9.6.8.

[137] Wu J, zhang D, Liu H, Li J, Li T, Wu J, et al. Neuroprotective effects of apigenin on retinal ganglion cells in ischemia/reperfusion: modulating mitochondrial dynamics in in vivo and in vitro models. J Transl Med 2024;22:447. https://doi.org/10.1186/S12967-024-05260-1.

[138] Chumsakul O, Wakayama K, Tsuhako A, Baba Y, Takai Y, Kurose T, et al. Apigenin regulates activation of microglia and counteracts retinal degeneration. J Ocul Pharmacol Ther 2020;36:311–9. https://doi.org/10.1089/jop.2019.0163.

[139] Shu N, Zhang Z, Wang X, Li R, Li W, Liu X, et al. Apigenin alleviates autoimmune uveitis by inhibiting microglia M1 pro-inflammatory polarization. Invest Ophthalmol Vis Sci 2023;64:21. https://doi.org/10.1167/IOVS.64.5.21.

[140] Sarigul Sezenoz A, Akkoyun I, Helvacioglu F, Haberal N, Dagdeviren A, Bacanli Di, et al. Antiproliferative and mitochondrial protective effects of Apigenin in an oxygen-induced retinopathy in vivo mouse model. J Ocul Pharmacol Ther Off J Assoc Ocul Pharmacol Ther 2021;37:580–90. https://doi.org/10.1089/JOP.2021.0046.

[141] Zou Y, Chiou GCY. Apigenin inhibits laser-induced choroidal neovascularization and regulates endothelial cell function. J Ocul Pharmacol Ther Off J Assoc Ocul Pharmacol Ther 2006;22:425–30. https://doi.org/10.1089/JOP.2006.22.425.

[142] Xu X, Li M, Chen W, Yu H, Yang Y, Hang L. Apigenin attenuates oxidative injury in ARPE-19 cells thorough activation of Nrf2 pathway. Oxid Med Cell Longev 2016;2016:4378461. https://doi.org/10.1155/2016/4378461.

[143] Srinivasan V, R. Pandi-Perumal S, Brzezinski A, P. Bhatnagar K, P. Cardinali D. Melatonin, immune function and cancer. Recent Pat Endocr Metab Immune Drug Discov 2011;5:109–23. https://doi.org/10.2174/187221411799015408.

[144] Li Y, Li S, Zhou Y, Meng X, Zhang JJ, Xu DP, et al. Melatonin for the prevention and treatment of cancer. Oncotarget 2017;8:39921. https://doi.org/10.18632/ONCOTARGET.16379.

[145] Pranil T, Moongngarm A, Loypimai P. Influence of pH, temperature, and light on the stability of melatonin in aqueous solutions and fruit juices. Heliyon 2020;6:e03648. https://doi.org/10.1016/J.HELIYON.2020.E03648.

[146] Reiter RJ, Rosales-Corral SA, Tan DX, Acuna-Castroviejo D, Qin L, Yang SF, et al. Melatonin, a full service anti-cancer agent: inhibition of initiation, progression and metastasis. Int J Mol Sci 2017;18. https://doi.org/10.3390/IJMS18040843.

[147] Wang L, Wang C, Choi WS. Use of melatonin in cancer treatment: where are we? Int J Mol Sci 2022;23:3779. https://doi.org/10.3390/IJMS23073779.

[148] Talib WH, Alsayed AR, Abuawad A, Daoud S, Mahmod AI. Melatonin in cancer treatment: current knowledge and future opportunities. Mol 2021, Vol 26, Page 2506 2021;26:2506. https://doi.org/10.3390/MOLECULES26092506.

[149] Schernhammer ES, Schulmeister K. Melatonin and cancer risk: does light at night compromise physiologic cancer protection by lowering serum melatonin levels? Br J Cancer 2004;90:941–3. https://doi.org/10.1038/sj.bjc.6601626.

[150] Alarma-Estrany P, Pintor J. Melatonin receptors in the eye: Location, second messengers and role in ocular physiology. Pharmacol Ther 2007;113:507–22. https://doi.org/10.1016/j.pharmthera.2006.11.003.

[151] Alkozi HA, Navarro G, Franco R, Pintor J. Melatonin and the control of intraocular pressure. Prog Retin Eye Res 2020;75:100798. https://doi.org/10.1016/J.PRETEYERES.2019.100798.

[152] Karslioğlu I, Ertekin MV, Taysi S, Koçer I, Sezen O, Gepdiremen A, et al. Radioprotective effects of melatonin on radiation-induced cataract. J Radiat Res 2005;46:277–82. https://doi.org/10.1269/JRR.46.277.

[153] Ku LC, Sheu ML, Cheng HH, Lee CY, Tsai YC, Tsai CY, et al. Melatonin protects retinal integrity through mediated immune homeostasis in the sodium iodate-induced mouse model of age-related macular degeneration. Biomed Pharmacother 2023;161:114476. https://doi.org/10.1016/J.BIOPHA.2023.114476.

[154] Wiechmann AF, Summers JA. Circadian rhythms in the eye: The physiological significance of melatonin receptors in ocular tissues. Prog Retin Eye Res 2008;27:137–60. https://doi.org/10.1016/J.PRETEYERES.2007.10.001.

[155] Kal Omar R, Hagström A, Stålhammar G. Adjuvant melatonin for uveal melanoma (AMUM): protocol for a randomized open-label phase III study. Trials 2023;24:1–14. https://doi.org/10.1186/S13063-023-07245-9.

[156] Mehnert W, Mäder K. Solid lipid nanoparticles: Production, characterization and applications. Adv Drug Deliv Rev 2012;64:83–101. https://doi.org/10.1016/j.addr.2012.09.021.

[157] Elmsmari F, González Sánchez JA, Duran-Sindreu F, Belkadi R, Espina M, García ML, et al. Calcium hydroxide-loaded PLGA biodegradable nanoparticles as an intracanal medicament. Int Endod J 2021;54:2086–98. https://doi.org/10.1111/IEJ.13603.

[158] Ding Y, Kan J. Optimization and characterization of high pressure homogenization produced chemically modified starch nanoparticles. J Food Sci Technol 2017;54:4509. https://doi.org/10.1007/S13197-017-2934-8.

[159] Nekkanti V, Vabalaboina V, Pillai R, Nekkanti V, Vabalaboina V, Pillai R. Drug nanoparticles - An overview. Deliv Nanoparticles 2012. https://doi.org/10.5772/34680.

[160] Bahari LAS, Hamishehkar H. The impact of variables on particle size of solid lipid nanoparticles and nanostructured lipid carriers; a comparative literature review. Adv Pharm Bull 2016;6:151. https://doi.org/10.15171/APB.2016.021.

[161] Khan AA, Abdulbaqi IM, Abou Assi R, Murugaiyah V, Darwis Y. Lyophilized hybrid nanostructured lipid carriers to enhance the cellular uptake of verapamil: statistical optimization and in vitro evaluation. Nanoscale Res Lett 2018;13:323. https://doi.org/10.1186/S11671-018-2744-6.

[162] Oh KS, Kim RS, Lee J, Kim D, Cho SH, Yuk SH. Gold/chitosan/pluronic composite nanoparticles for drug delivery. J Appl Polym Sci 2008;108:3239–44. https://doi.org/10.1002/APP.27767.

[163] Llorente X, Esteruelas G, Bonilla L, Agudelo MG, Filgaira I, Lopez-Ramajo D, et al. Riluzole-loaded nanostructured lipid carriers for hyperproliferative skin diseases. Int J Mol Sci 2023;24:8053. https://doi.org/10.3390/IJMS24098053/S1.

[164] Ojo AT, Ma C, Lee PI. Elucidating the effect of crystallization on drug release from amorphous solid dispersions in soluble and insoluble carriers. Int J Pharm 2020;591:120005. https://doi.org/10.1016/J.IJPHARM.2020.120005.

[165] Freitas C, Müller RH. Correlation between long-term stability of solid lipid nanoparticles (SLN) and crystallinity of the lipid phase. Eur J Pharm Biopharm 1999;47:125–32. https://doi.org/10.1016/S0939-6411(98)00074-5.

[166] Huang Z, Ma C, Wu M, Li X, Lu C, Zhang X, et al. Exploring the drug-lipid interaction of weak-hydrophobic drug loaded solid lipid nanoparticles by isothermal titration calorimetry. J Nanoparticle Res 2020;22:1–14. https://doi.org/10.1007/S11051-019-4671-6/.

[167] Zimmermann E, Souto EB, Müller RH. Physicochemical investigations on the structure of drug-free and drug-loaded solid lipid nanoparticles (SLN) by means of DSC and 1H NMR. Pharmazie 2005;60:508–13.

[168] Pochapski DJ, Carvalho Dos Santos C, Leite GW, Pulcinelli SH, Santilli CV. Zeta Potential and colloidal stability predictions for inorganic nanoparticle dispersions: effects of experimental conditions and electrokinetic models on the interpretation of results. Langmuir 2021;37:13379–89. https://doi.org/10.1021/ACS.LANGMUIR.1C02056.

[169] Zoubari G, Staufenbiel S, Volz P, Alexiev U, Bodmeier R. Effect of drug solubility and lipid carrier on drug release from lipid nanoparticles for dermal delivery. Eur J Pharm Biopharm 2017;110:39–46. https://doi.org/10.1016/J.EJPB.2016.10.021.

[170] Alfaleh MA, Hashem AM, Abujamel TS, Alhakamy NA, Kalam MA, Riadi Y, et al. Apigenin loaded Lipoid–PLGA–TPGS nanoparticles for colon cancer

therapy: characterization, sustained release, cytotoxicity, and apoptosis pathways. Polymers (Basel) 2022;14:3577. https://doi.org/10.3390/POLYM14173577/S1.

[171] Esteruelas G, Halbaut L, García-Torra V, Espina M, Cano A, Ettcheto M, et al. Development and optimization of Riluzole-loaded biodegradable nanoparticles incorporated in a mucoadhesive in situ gel for the posterior eye segment. Int J Pharm 2022;612:121379. https://doi.org/10.1016/j.ijpharm.2021.121379.

[172] Sun D, Liu Y, Yu Q, Zhou Y, Zhang R, Chen X, et al. The effects of luminescent ruthenium(II) polypyridyl functionalized selenium nanoparticles on bFGF-induced angiogenesis and AKT/ERK signaling. Biomaterials 2013;34:171–80. https://doi.org/10.1016/J.BIOMATERIALS.2012.09.031.

[173] Gunasekaran T, Haile T, Nigusse T, Dhanaraju MD. Nanotechnology: an effective tool for enhancing bioavailability and bioactivity of phytomedicine. Asian Pac J Trop Biomed 2014;4:S7. https://doi.org/10.12980/APJTB.4.2014C980.

[174] Kim TJ, Zhang YH, Kim Y, Lee CK, Lee MK, Hong JT, et al. Effects of apigenin on the serum- and platelet derived growth factor-BB-induced proliferation of rat aortic vascular smooth muscle cells. Planta Med 2002;68:605–9. https://doi.org/10.1055/S-2002-32901.

[175] Fang J, Xia C, Cao Z, Zheng JZ, Reed E, Jiang B-H. Apigenin inhibits VEGF and HIF-1 expression via PI3K/AKT/p70S6K1 and HDM2/p53 pathways. FASEB J 2005;19:342–53. https://doi.org/10.1096/FJ.04-2175COM.

[176] Buhr CR, Wiesmann N, Tanner RC, Brieger J, Eckrich J. The chorioallantoic membrane assay in nanotoxicological research—an alternative for in vivo experimentation. Nanomaterials 2020;10:2328. https://doi.org/10.3390/NANO10122328.

[177] Huang Z, Huang S, Song T, Yin Y, Tan C. Placental angiogenesis in mammals: a review of the regulatory effects of signaling pathways and functional nutrients. Adv Nutr 2021;12:2434. https://doi.org/10.1093/ADVANCES/NMAB070.

[178] Wang L, Han Q, Yan L, Ma X, Li G, Wu H, et al. Mtnr1b deletion disrupts placental angiogenesis through the VEGF signaling pathway leading to fetal growth restriction. Pharmacol Res 2024;206:107290. https://doi.org/10.1016/J.PHRS.2024.107290.

[179] Mohammadian-Hafshejani A, Farber IM, Kheiri S. Global incidence and

mortality of childhood leukemia and its relationship with the Human Development Index. PLoS One 2024;19:e0304354. https://doi.org/10.1371/JOURNAL.PONE.0304354.

[180] Namayandeh SM, Khazaei Z, Najafi ML, Goodarzi E, Moslem A. GLOBAL leukemia in children 0-14 statistics 2018, incidence and mortality and human development index (HDI): GLOBOCAN sources and methods. Asian Pacific J Cancer Prev 2020;21:1494. https://doi.org/10.31557/APJCP.2020.21.5.1487.

[181] Behzadi S, Serpooshan V, Tao W, Hamaly MA, Alkawareek MY, Dreaden EC, et al. Cellular uptake of nanoparticles: journey inside the cell. Chem Soc Rev 2017;46:4244. https://doi.org/10.1039/C6CS00636A.

[182] Bai X, Smith ZL, Wang Y, Butterworth S, Tirella A. Sustained drug release from smart nanoparticles in cancer therapy: a comprehensive review. Micromachines 2022;13:1623. https://doi.org/10.3390/MI13101623.

[183] Badr-Eldin SM, Aldawsari HM, Ahmed OAA, Alhakamy NA, Neamatallah T, Okbazghi SZ, et al. Optimized semisolid self-nanoemulsifying system based on glyceryl behenate: A potential nanoplatform for enhancing antitumor activity of raloxifene hydrochloride in MCF-7 human breast cancer cells. Int J Pharm 2021;600:120493. https://doi.org/10.1016/J.IJPHARM.2021.120493.

[184] Neves AR, Queiroz JF, Costa Lima SA, Figueiredo F, Fernandes R, Reis S. Cellular uptake and transcytosis of lipid-based nanoparticles across the intestinal barrier: Relevance for oral drug delivery. J Colloid Interface Sci 2016;463:258–65. https://doi.org/10.1016/J.JCIS.2015.10.057.

[185] Zhang W, Liu J, Zhang Q, Li X, Yu S, Yang X, et al. Enhanced cellular uptake and anti-proliferating effect of chitosan hydrochlorides modified genistein loaded NLC on human lens epithelial cells. Int J Pharm 2014;471:118–26. https://doi.org/10.1016/J.IJPHARM.2014.05.030.

[186] Fangueiro JF, Calpena AC, Clares B, Andreani T, Egea MA, Veiga FJ, et al. Biopharmaceutical evaluation of epigallocatechin gallate-loaded cationic lipid nanoparticles (EGCG-LNs): In vivo, in vitro and ex vivo studies. Int J Pharm 2016;502:161–9. https://doi.org/10.1016/J.IJPHARM.2016.02.039.

[187] Agarwal P, Craig JP, Rupenthal ID. Formulation considerations for the management of dry eye disease. Pharmaceutics 2021;13:207. https://doi.org/10.3390/PHARMACEUTICS13020207.

[188] Sharma N, Madan P, Lin S. Effect of process and formulation variables

on the preparation of parenteral paclitaxel-loaded biodegradable polymeric nanoparticles: A co-surfactant study. Asian J Pharm Sci 2016;11:404–16. https://doi.org/10.1016/J.AJPS.2015.09.004.

[189] Ronkay F, Molnár B, Nagy D, Szarka G, Iván B, Kristály F, et al. Melting temperature versus crystallinity: new way for identification and analysis of multiple endotherms of poly(ethylene terephthalate). J Polym Res 2020;27:1–17. https://doi.org/10.1007/S10965-020-02327-7.

[190] Teeranachaideekul V, Morakul B, Boonme P, Pornputtapitak W, Junyaprasert V. Effect of lipid and oil compositions on physicochemical properties and photoprotection of octyl methoxycinnamate-loaded nanostructured lipid carriers (Nlc). J Oleo Sci 2020;69:1627–39. https://doi.org/10.5650/jos.ess20093.

[191] Teeranachaideekul V, Morakul B, Boonme P, Pornputtapitak W, Junyaprasert V. Effect of lipid and oil compositions on physicochemical properties and photoprotection of octyl methoxycinnamate-loaded nanostructured lipid carriers (NLC). J Oleo Sci 2020;69:1627–39. https://doi.org/10.5650/jos.ess20093.

[192] Chrai SS, Patton TF, Mehta A, Robinson JR. Lacrimal and instilled fluid dynamics in rabbit eyes. J Pharm Sci 1973;62:1112–21. https://doi.org/10.1002/JPS.2600620712.

[193] Yang W, Wang L, Mettenbrink EM, Deangelis PL, Wilhelm S. Nanoparticle toxicology. Annu Rev Pharmacol Toxicol 2021;61:269–89. https://doi.org/10.1146/ANNUREV-PHARMTOX-032320-110338.

[194] Zhang W, Li X, Ye T, Chen F, Yu S, Chen J, et al. Nanostructured lipid carrier surface modified with Eudragit RS 100 and its potential ophthalmic functions. Int J Nanomedicine 2014;9:4315. https://doi.org/10.2147/IJN.S63414.

[195] Kinnunen K, Kauppinen A, Piippo N, Koistinen A, Toropainen E, Kaarniranta K. Cationorm shows good tolerability on human HCE-2 corneal epithelial cell cultures. Exp Eye Res 2014;120:82–9. https://doi.org/10.1016/J.EXER.2014.01.006.

[196] Jung WW. Protective effect of apigenin against oxidative stress-induced damage in osteoblastic cells. Int J Mol Med 2014;33:1327–34. https://doi.org/10.3892/IJMM.2014.1666.

[197] Tarocco A, Caroccia N, Morciano G, Wieckowski MR, Ancora G, Garani G, et al. Melatonin as a master regulator of cell death and inflammation: molecular mechanisms and clinical implications for newborn care. Cell

Death Dis 2019;10:1–12. https://doi.org/10.1038/s41419-019-1556-7.

[198] Valadares MC, de Oliveira GAR, de Ávila RI, da Silva ACG. Strategy combining nonanimal methods for ocular toxicity evaluation. Methods Mol Biol 2021;2240:175–95. https://doi.org/10.1007/978-1-0716-1091-6_13.

[199] Tsai C-H, Wang P-Y, Lin I-C, Huang H, Liu G-S, Tseng C-L. Ocular drug delivery: role of degradable polymeric nanocarriers for ophthalmic application. Int J Mol Sci 2018;19:2830. https://doi.org/10.3390/ijms19092830.

[200] Mushtaq Z, Sadeer NB, Hussain M, Mahwish, Alsagaby SA, Imran M, et al. Therapeutical properties of apigenin: a review on the experimental evidence and basic mechanisms. Int J Food Prop 2023;26:1914–39. https://doi.org/10.1080/10942912.2023.2236329.

[201] Srinivas SP, Rao SK. Ocular surface staining: Current concepts and techniques. Indian J Ophthalmol 2023;71:1089. https://doi.org/10.4103/IJO.IJO_2137_22.

[202] Xiong C, Chen D, Liu J, Liu B, Li N, Zhou Y, et al. A rabbit dry eye model induced by topical medication of a preservative benzalkonium chloride. Invest Ophthalmol Vis Sci 2008;49:1850–6. https://doi.org/10.1167/IOVS.07-0720.

[203] Belkhelladi M, Bougrine A. Rosehip extract and wound healing: A review. J Cosmet Dermatol 2024;23:62–7. https://doi.org/10.1111/JOCD.15971.

[204] Hagström A, Kal Omar R, Williams PA, Stålhammar G. The rationale for treating uveal melanoma with adjuvant melatonin: a review of the literature. BMC Cancer 2022;22:1–17. https://doi.org/10.1186/S12885-022-09464-W.

[205] Balguri SP, Adelli GR, Majumdar S. Topical ophthalmic lipid nanoparticle formulations (SLN, NLC) of indomethacin for delivery to the posterior segment ocular tissues. Eur J Pharm Biopharm 2016;109:224–35. https://doi.org/10.1016/J.EJPB.2016.10.015.

[206] Fernandes AR, Vidal LB, Sánchez-López E, dos Santos T, Granja PL, Silva AM, et al. Customized cationic nanoemulsions loading triamcinolone acetonide for corneal neovascularization secondary to inflammatory processes. Int J Pharm 2022;623:121938. https://doi.org/10.1016/J.IJPHARM.2022.121938.

[207] Jager MJ, Shields CL, Cebulla CM, Abdel-Rahman MH, Grossniklaus HE,

Stern MH, et al. Uveal melanoma. Nat Rev Dis Prim 2020;6:24. https://doi.org/10.1038/S41572-020-0158-0.

[208] Xu H, Rao NA. Grand challenges in ocular inflammatory diseases. Front Ophthalmol 2022;2:756689. https://doi.org/10.3389/FOPHT.2022.756689.

[209] Lee RWJ, Dick AD. Current concepts and future directions in the pathogenesis and treatment of non-infectious intraocular inflammation. Eye 2011;26:17–28. https://doi.org/10.1038/eye.2011.255.

[210] Rosa JGS, Disner GR, Pinto FJ, Lima C, Lopes-Ferreira M. Revisiting retinal degeneration hallmarks: insights from molecular markers and therapy perspectives. Int J Mol Sci 2023;24:13079. https://doi.org/10.3390/IJMS241713079.

[211] Yagci A, Gurdal C. The role and treatment of inflammation in dry eye disease. Int Ophthalmol 2014;34:1291–301. https://doi.org/10.1007/S10792-014-9969-X.

[212] Liau S, Wang JZ, Zagarella E, Paulus P, Dang NHQH, Rawling T, et al. An update on inflammation in uveal melanoma. Biochimie 2023;212:114–22. https://doi.org/10.1016/J.BIOCHI.2023.04.013.

[213] Ahmad A, Ahsan H. Biomarkers of inflammation and oxidative stress in ophthalmic disorders. J Immunoass Immunochem 2020;41:257–71. https://doi.org/10.1080/15321819.2020.1726774.

[214] del Amo EM. Topical ophthalmic administration: Can a drug instilled onto the ocular surface exert an effect at the back of the eye? Front Drug Deliv 2022;2:954771. https://doi.org/10.3389/FDDEV.2022.954771.

[215] Popov A. Mucus-penetrating particles and the role of ocular mucus as a barrier to micro- and nanosuspensions. J Ocul Pharmacol Ther 2020;36:366–75. https://doi.org/10.1089/JOP.2020.0022.

[216] Benedeto-Stojanov D, Ničković VP, Petrović G, Rancić A, Grgov I, Nikolić GR, et al. Melatonin as a promising anti-inflammatory agent in an in vivo animal model of sepsis-induced rat liver damage. Int J Mol Sci 2024;25:455. https://doi.org/10.3390/IJMS25010455.

[217] Cho JH, Bhutani S, Kim CH, Irwin MR. Anti-inflammatory effects of melatonin: A systematic review and meta-analysis of clinical trials. Brain Behav Immun 2021;93:245–53. https://doi.org/10.1016/J.BBI.2021.01.034.

[218] Yoon JH, Kim MY, Cho JY. Apigenin: a therapeutic agent for treatment of

skin inflammatory diseases and cancer. Int J Mol Sci 2023;24:1498. https://doi.org/10.3390/IJMS24021498.

[219] Liu T, Zhang L, Joo D, Sun SC. NF-κB signaling in inflammation. Signal Transduct Target Ther 2017;2:1–9. https://doi.org/10.1038/sigtrans.2017.23.

[220] Carrascal L, Nunez-Abades P, Ayala A, Cano M. Role of melatonin in the inflammatory process and its therapeutic potential. Curr Pharm Des 2018;24:1563–88. https://doi.org/10.2174/1381612824666180426112832.

[221] Lee JH, Zhou HY, Cho SY, Kim YS, Lee YS, Jeong CS. Anti-inflammatory mechanisms of apigenin: Inhibition of cyclooxygenase-2 expression, adhesion of monocytes to human umbilical vein endothelial cells, and expression of cellular adhesion molecules. Arch Pharm Res 2007;30:1318–27. https://doi.org/10.1007/BF02980273/.

Anexo

Patent: Lipid nanoparticles for the treatment of ocular diseases

EP 4 410 281 A1

Inventors: Lorena Bonilla Vidal, Elena Sánchez López, Marta Espina, Maria Luisa García.

Publication date: 07-08-2024

(19) Europäisches Patentamt
European Patent Office
Office européen des brevets

(11) EP 4 410 281 A1

(12) EUROPEAN PATENT APPLICATION

(43) Date of publication:
07.08.2024 Bulletin 2024/32

(21) Application number: **23382105.7**

(22) Date of filing: **06.02.2023**

(51) International Patent Classification (IPC):
A61K 9/51 *(2006.01)* ***A61K 9/00*** *(2006.01)*
A61K 36/738 *(2006.01)* ***A61K 31/352*** *(2006.01)*
A61P 27/00 *(2006.01)* ***A61P 27/06*** *(2006.01)*
A61P 27/12 *(2006.01)* ***A61P 31/04*** *(2006.01)*
A61P 31/12 *(2006.01)* ***A61P 35/00*** *(2006.01)*

(52) Cooperative Patent Classification (CPC):
(C-Sets available)
A61K 9/0048; A61K 9/5123; A61K 31/352; A61K 36/738; A61P 27/00; A61P 27/06; A61P 27/12; A61P 31/04; A61P 31/12; A61P 35/00

(Cont.)

(84) Designated Contracting States:
AL AT BE BG CH CY CZ DE DK EE ES FI FR GB GR HR HU IE IS IT LI LT LU LV MC ME MK MT NL NO PL PT RO RS SE SI SK SM TR
Designated Extension States:
BA
Designated Validation States:
KH MA MD TN

(71) Applicant: **Universitat de Barcelona**
08028 Barcelona (ES)

(72) Inventors:
- **SÁNCHEZ LÓPEZ, Elena**
  08028 Barcelona (ES)
- **GARCÍA LÓPEZ, María Luisa**
  08028 Barcelona (ES)
- **BONILLA VIDAL, Lorena**
  08028 Barcelona (ES)
- **ESPINA GARCÍA, Marta**
  08028 Barcelona (ES)

(74) Representative: **Hoffmann Eitle**
Hoffmann Eitle S.L.U.
Paseo de la Castellana 140, 3a planta
Edificio LIMA
28046 Madrid (ES)

(54) LIPID NANOPARTICLES FOR THE TREATMENT OF OCULAR DISEASES

(57) The present invention relates to a composition comprising lipid nanoparticles comprising at least one liquid lipid with anti-inflammatory properties, such as for example rosehip oil, at least one solid lipid, at least one cationic surfactant, optionally at least one non-cationic surfactant and optionally at least one active ingredient, as well as their use in a method of treating ocular diseases, such as for example dry eye disease.

FIG.7

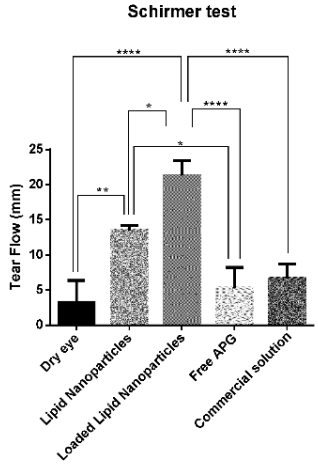

Processed by Luminess, 75001 PARIS (FR)

(Cont. next page)

(52) Cooperative Patent Classification (CPC): (Cont.)

C-Sets
A61K 31/352, **A61K 2300/00**;
A61K 36/738, **A61K 2300/00**

Description

TECHNICAL FIELD

[0001] The present invention relates to a composition comprising lipid nanoparticles comprising at least one liquid lipid with anti-inflammatory properties, such as for example rosehip oil, at least one solid lipid, at least one cationic surfactant and optionally, at least a non-cationic surfactant, and optionally at least one active ingredient, as well as their use in a method of treating ocular diseases, such as for example dry eye disease.

BACKGROUND OF THE INVENTION

[0002] Dry eye disease (DED) is a condition frequently encountered in ophthalmology practice worldwide. DED is a multifactorial disease of the ocular surface characterized by a loss of homeostasis of the tear film, and accompanied by ocular symptoms, in which tear film instability and hyperosmolarity, ocular surface inflammation and damage, and neurosensory abnormalities play etiological roles. The prevalence of DED in the population ranges from 5 - 34 % depending on the country [1]. Topical administration is the preferred route to treat DED because it is painless and easy to handle. Artificial tears in the form of eyedrops, gel or ointment are used to lubricate dry eyes maintaining moisture of the eye's surface and often constitute the first line of therapy. They instantly relieve symptoms by lowering osmolarity and diluting inflammatory markers. However, artificial tears have no anti-inflammatory properties and do not deal with the fundamental pathogenesis of the disease. Moreover, usual treatments for ocular inflammation comprise corticosteroids and non-steroidal anti-inflammatory drugs (NSAIDs), but its prolonged use involves severe side effects, such as increasing ocular pressure and cataract formation [2,3].

[0003] Plant oils have been used for a variety of purposes with their integration into foods, cosmetics, and pharmaceutical products. Specifically, the use of plant oils for topical skin applications as well as the therapeutic benefits of these plant oils according to their anti-inflammatory and antioxidant effects on the skin have been described. One of the plant oils used for such applications is rosehip oil (*R.canina*).

[0004] Apigenin (APG) is a natural flavonoid that has been used in the form of plant extract for the treatment of several disorders and inflammatory conditions. Of all the flavonoids, APG is one of the most widely distributed in plants, and one of the most studied phenolics. APG is present in significant amount in its glycosylated form in vegetables, fruits, herbs and plant-based beverages. Based on preclinical and clinical data, it has been suggested that APG is a potent therapeutic agent to overcome diseases, such as inflammatory diseases, bacterial, viral, and parasitic infections, autoimmune disorders, diabetes, hypertension, hypercholesterolemia, and various types of cancers [4,5].Several clinical trials have been carried out for the use of APG as a dietary supplement. In clinical trial NCT04114916, the reduction of cardiovascular risk in healthy subjects has been evaluated [6]. In clinical trial NCT01286324 APG, as a natural part of a chamomile extract, was studied as a dietary supplement for the treatment of chronic primary insomnia. It was concluded that the extract could provide modest benefits of daytime functioning and mixed benefits on sleep diary measures relative to placebo in adults with chronic primary insomnia [7]. Furthermore, APG itself is currently commercialized as a dietary supplement in Spain in the form of capsules containing 50 mg APG for improving prostate health, decrease glucose levels, and maintain the function of the nervous system [8,9].

[0005] Whilst commercialized eye drops containing chamomile extract for the enhancement of ocular discomfort, such as irritation, tired eyes, and itchiness are on the market [10,11], APG itself has to date not been suggested or approved as a therapy for ocular diseases, such as for example DED. This may partially be due to the disadvantages of APG for topical treatments caused among other by its low solubility and low bioavailability [12].

[0006] In the recent years new delivery systems, such as lipid nanoparticles, have been developed which provide multiple advantages, such as low in vivo toxicity, good long-term stability, economic and solvent-free production techniques, easy production at large scale, possibility to be autoclaved or sterilized, increased kinetic stability compared to liposomes and niosomes [13]. Moreover, the last generation of lipid nanoparticles, nanostructured lipid carriers (NLC), represent a topical delivery system with improved stability in comparison to the solid lipid nanoparticles (SLN).

[0007] As mentioned above topical administration is a preferred route to treat DED. The currently available remedies using artificial tears have no anti-inflammatory properties and do not deal with the fundamental pathogenesis of the disease. Available treatment options for ocular inflammation in general include corticosteroids and NSAIDs which after prolonged use can be the cause of severe side effects. Another drawback of currently available topical applications is the generally fast release of the active ingredient(s). Furthermore, topical applications into the eye require that the active ingredient is able to permeate through the corneal barrier to reach its destination.

[0008] To date, no lipid nanoparticles containing liquid lipids have been described that are suitable for topical use in the ocular system and that can provide for benefits/treatment for ocular inflammatory diseases, such as DED. The inventors have therefore set out to develop lipid nanoparticles with intrinsic activity that are suitable for such applications and that provide biocompatibility, capability to reverse disease symptoms as well as anti-inflammatory efficacy.

[0009] In addition, the inventors have set out to provide a topical delivery system that is suitable for the application of APG overcoming its low solubility and low bioavailability, and that furthermore provides for sustained drug release and corneal permeability which is essential for improving the pharmacokinetic and pharmacodynamic profile of APG.

BRIEF DESCRIPTION OF THE FIGURES

[0010]

Fig.1: Scheme of the evaluation of the fluorescein staining on the ocular surface. 9: maximum score; 0: minimum score.

Fig.2: Scheme of the evaluation of bengal rose staining on the ocular surface. 9: maximum score; 0: minimum score.

Fig.3: Design of Experiments (DoE) surface response of Loaded Lipid Nanoparticles. (A) Concentration of APG (%) and glyceryl dibehenate + rosehip oil (%) influence on Z_{av} (nm). (B) Concentration of Polysorbate 80 (%) and glyceryl dibehenate + rosehip oil (%) influence on PDI. (C) Concentration of Polysorbate 80 (%) and glyceryl dibehenate + rosehip oil (%) influence on ZP (mV). (D) Concentration of APG (%) and glyceryl dibehenate + rosehip oil (%) influence on EE (%).

Fig.4: Physicochemical characterization of optimized Loaded Lipid Nanoparticles, empty lipid nanoparticles and apigenin. (A) Transmission electron microscopy (TEM) image of loaded lipid nanoparticles (scale bar 100 nm). (B) Differential scanning calorimetry (DSC) curves. (C) X-ray diffraction (XRD) patterns. (D) Fourier-transformed infrared (FTIR) analysis.

Fig.5: Backscattering profiles of Loaded Lipid Nanoparticles stored at: (A) 4 °C and, (B) 25 °C.

Fig.6: Biopharmaceutical behavior. In vitro APG release from Loaded Lipid nanoparticles against free-APG (adjusted to two phase decay and plateau followed by one phase decay respectively) and pharmacokinetic parameters Loaded Lipid Nanoparticles applied to a one-phase association.

Fig.7: Results of the Schirmer test on New Zealand rabbits after dry eye disease induction with statistically significant differences (* $p < 0.05$, ** $p < 0.01$, *** $p < 0.001$; **** $p < 0.0001$).

Fig.8: Fluorescein staining of the ocular surface of New Zealand rabbits after dry eye disease induction. Results of the fluorescein staining with statistically significant differences (* $p < 0.05$, ** $p < 0.01$, and *** $p < 0.001$) of: Dry eye, Lipid Nanoparticles, Loaded Lipid Nanoparticles, Free APG, Commercial solution.

Fig.9: Bengal rose staining of the ocular surface of New Zealand rabbits after dry eye disease induction. Results of the Bengal rose staining with statistically significant (* $p < 0.05$) of: Dry eye, Lipid Nanoparticles, Loaded Lipid Nanoparticles, Free APG, Commercial solution.

Fig.10: Ocular inflammation prevention results on New Zealand rabbits. Values are expressed as mean ± SD; * $p < 0.05$, ** $p < 0.01$ and *** $p < 0.001$ and **** $p < 0.0001$ significantly different ocular inflammation score.

Fig.11: Ocular inflammation treatment results on New Zealand rabbits. Values are expressed as mean ± SD; * $p < 0.05$, ** $p < 0.01$ and *** $p < 0.001$ and **** $p < 0.0001$ significantly different ocular inflammation score.

BRIEF DESCRIPTION OF THE INVENTION

[0011] The problem addressed by the present invention is to provide a topical ocular nanoparticulated lipid system that provides biocompatibility, the capability to treat ocular disease or reverse their symptoms, treat and/or prevent ocular inflammation and the capacity to act as drug delivery carrier. A further problem addressed is the provision of a topical delivery system for APG that overcomes its disadvantages, such as its low solubility and bioavailability and that provides for sustained drug release and corneal permeability and thus improved pharmacokinetic and pharmacodynamic profiles of APG.

SUMMARY OF THE INVENTION

[0012] In one aspect the present invention relates to a composition comprising lipid nanoparticles, said lipid nanoparticles comprising

a. at least one liquid lipid with anti-inflammatory properties;
b. at least one solid lipid;
c. at least one cationic surfactant
d. optionally, at least one non-cationic surfactant;
e. optionally, at least one active ingredient.

[0013] In one embodiment of the composition of present invention the said liquid lipid with anti-inflammatory properties

is selected from the group consisting of rosehip oil, tea tree oil, lavender oil, linoleic acid, stearic acid, palmitic acid, castor oil, safflower oil, melon seed oil, salicornia oil, evening primrose oil, poppyseed oil, grape seed oil, prickly pear oil, artichoke oil, hemp oil, wheat germ oil, cottonseed oil, corn oil, walnut oil, soybean oil, sesame oil, rice bran oil, argan oil, pistachio oil, peach oil, almond oil, canola oil, avocado oil, flaxseed oil, sunflower oil, peanut oil, palm oil, olive oil, macadamia oil, coconut oil, rosemary oil, lavender oil, origanum vulgare oil, thyme oil, mint oil, eucalyptus oil, ginger oil, cuminum cyminum l. oil, turmeric oil, clove oil, oleic acid, oregano oil, rose oil, fennel oil, bergamot oil, chamomile oil, helichrysum oil, patchouli oil, frankincense oil, copaiba oil, peppermint oil, black pepper oil, sweet marjoram oil, basil oil, clove oil, clary sage oil, lemongrass oil, geranium oil, wintergreen oil, cannabis oil, cannabidiol, spruce oil, niaouli oil, cardamom oil, pine tree oil, fir tree oil, juniper tree oil, verbena oil, marjoram oil, katafray oil, bitter orange oil, hypericum oil, arnica oil, coriander oil, mustard oil, perilla seed oil, centella asiatica oil, calendula oil, laurel oil, camphor oil, cinnamon oil, oatmeal oil, docosahexaenoic acid, eicosapentaenoic acid, dandelion oil, krill oil, electrophorus electricus oil, potamotrygon motoro oil, boa constrictor oil, chelonoidis denticulate oil, melanosuchus niger oil, inia geoffrensis oil, horse oil, anchovy oil, prunus seed oil, tropidurus hispidus oil, emu oil, maqian fruits essential oil, fructus alpinia oil, cinnamomum cassia essential oil, angelica sinensis oil, gynura procumbens oil, spirulina oil, citrus limetta oil, citrus aurantium oil, atractylodes macrocephala oil, artemisia argyi oil, gynura procumbens oil, acorus gramineusand oil, algal oil, fish oil, zanthoxylum coreanum nakai oil, cod liver oil, perna canaliculus oil, chia seed oil, or combinations thereof.

[0014] In one embodiment of present invention the said liquid lipid with anti-inflammatory properties is selected from derivatives of the above listed liquid lipids.

[0015] In a preferred embodiment the said liquid lipid with anti-inflammatory properties is rosehip oil.

[0016] In one embodiment of the composition of the present invention the solid lipid is selected from monoglycerides, diglycerides, triglycerides, cholesterols, steroids, fatty alcohols, glycerol esters glyceryl tridecanoate, glycerol trilaurate, glyceryl trimyristate, glyceryl tripalmitate, glyceryl tristearate, hydrogenated coco-glycerides, hard fat types, mixtures of triglycerides and/or diglycerides and/or monoglycerides and/or glycerol, acyl glycerols, glyceryl monostearate, glyceryl distearate, glyceryl monooleate, glyceryl dibehenate, glyceryl palmitostearate, waxes, cetyl palmitate, fatty acids, stearic acid, palmitic acid, decanoic acid, behenic acid, glycerol stearate citrate, polyethylene glycol monostearate, cyclic complexes, cyclodextrin para-acyl-calix-arenes, or mixtures thereof.

[0017] In a preferred embodiment said solid lipid is glyceryl dibehenate.

[0018] In one embodiment of the composition comprising lipid nanoparticles of present invention the cationic surfactant is selected from the group consisting of dimethyl-dioctadecyl-ammonium bromide (DDAB), dioleoyl phosphatidylethanolamine, 1,2-distearyloxy-N,N-dimethyl-3-aminopropane, 1,2 dioleyloxy-N,N-dimethyl-3-aminopropane,1,2-dilinoleyloxy-N,N-dimethyl-3-aminopropane, 1,2-dilinolenyloxy-N,N-dimethyl-3-aminopropane, cetyltrimethylammonium bromide, 3β-[N(N',N'-dimethylaminoethane)-carbamoyl]cholesterol, 1,2-dioleoyl-3-trimethylammonium-propane, 1,2-dimyristoyl-3-trimethylammonium-propane, 1,2-stearoyl-3-trimethylammonium-propane, N-(4-carboxybenzyl)-N,N-dimethyl-2,3-bis(oleoyl-oxy)propan-1-aminium, 1-Palmitoyl-2-oleoyl-sn-glycero-3-phosphoethanolamine, N,N-di-(β-stearoylethyl)-N,N-dimethyl-ammonium chloride, benzalkonium chloride, cetylpyridinium chloride, cetrimide, *N*-[1-(2,3-dioleoyloxy)propyl]-*N,N,N*-trimethylammonium chloride, 1,2-dilineoyl-3-dimethylammonium-propane, 1,2-dilinoleyloxy-3-*N,N*-dimethylaminopropane, 1,2-dilinoleyloxy- keto-N,N-dimethyl-3-aminopropane, 1,2-dilinoleyl-4-(2- dimethylaminoethyl)-[1,3]-dioxolane(3-o-[2''-(meth oxypolyethyleneglycol 2000) succinoyl]-1,2-dimyristoyl-sn-glycol, R-3-[(ω-methoxy-poly(ethyleneglycol)2000)carbamoyl]-1,2-dimyristyloxlpropyl-3-amine, cetyltrimethylammo-nium bromide, octadecylamine, 1-oleoyl-rac-glycerol, octadecyl quaternized carboxymethyl chitosan, hexadecyl trimethyl ammonium bromide.

[0019] In a preferred embodiment of the composition of present invention the cationic surfactant is dimethyldioctadecylammonium bromide (DDAB).

[0020] In a further embodiment of the composition of present invention the non-cationic surfactant is selected from the group consisting of polysorbate 80, soya lecithin, sodium dodecyl sulphate, polysorbate 20, polysorbate 40, polysorbate 60, PEG-30 glyceryl stearate, cholic acid, phosphatidyl choline, phospholipids with phosphatidylcholine, egg lecithin, poloxamer 188, poloxamer407, poloxamer 184, poloxamer 338, poloxamine 908, tyloxopol, taurocholate sodium salt, taurodeoxycholicacid sodium salt, sodium glycocholate, sodium oleate, cholesteryl hemisuccinate, butanol, sodium cholate, nonionic polyoxyethylene, non-ionic amphiphilic surfactant with an alkyl moiety and an ethylene oxide chain, palmitic acid, stearic acid, mixtures of palmitic and stearic acid, lecithin, polyglycerol 6-distearate, caprylyl/capryl glucoside, coco-glucoside, sucrose palmitate, sucrose stearate, sucrose distearate, tyloxapol, lecithin, cetylpyridinium chloride, sorbitan laurate, polyethylene glycol ether of cetyl or stearyl alcohol, castor oil polyoxyethylene ether, macrogolglycerol ricinoleate, dioctyl sodium sulfosuccinate, monooctylphosphoric acid sodium, hexadecyl trimethyl ammonium bromide, polyvinyl alcohol, polyoxyethylene (40) stearate, polyethylene glycol-polypropylene glycol-polyethylene glycol triblock copolymer, olyoxyethylene nonylphenyl ether, hexadecyltrimethylammonium bromide, sodium dodecyl sulfate, sodium cholate, stearate sodium hydrolysed polyvinyl alcohol 9000-10000 MW, dioctyl sulfosuccinate, taurocholate, 4-dodecylbenzenesulfonic acid, long chain carboxylic acid, alkyldiphenyloxide disulfonate, or mixtures thereof.

[0021] In a preferred embodiment the non-cationic surfactant is polysorbate 80.

[0022] In one embodiment the at least one active ingredient is apigenin (APG).

[0023] In one embodiment the at least one active ingredient, preferably apigenin, is encapsulated in the lipid nanoparticles.

[0024] In a further embodiment said lipid nanoparticles further comprise a coating, preferably wherein said coating comprises hyaluronic acid.

[0025] In one preferred embodiment of the composition of present invention said lipid nanoparticles comprise

a. 0.01 - 30 % (w/v) lipid liquid with anti-inflammatory properties, preferably rosehip oil;
b. 1 - 50 % (w/v) solid lipid, preferably glyceryl dibehenate;
c. 0.001 - 10 % (w/v) cationic surfactant, preferably DDAB;
d. optionally 0.00 - 10 % (w/v) non-cationic surfactant, preferably polysorbate 80;
e. optionally 0.00 - 10 % (w/v) active ingredient, preferably apigenin.

[0026] In one preferred embodiment of the composition of present invention said lipid nanoparticles comprise

a. 2.5 - 12.5% (w/v) lipid liquid with anti-inflammatory properties, preferably rosehip oil;
b. 1 - 30 % (w/v) solid lipid, preferably glyceryl dibehenate;
c. 0.025 - 0.5 % (w/v) cationic surfactant, preferably DDAB;
d. 1.0 - 5.0% (w/v) non-cationic surfactant, preferably polysorbate 80;
e. optionally 0.1 - 2.5% (w/v) active ingredient, preferably apigenin.

[0027] In one preferred embodiment of the composition of present invention said lipid nanoparticles comprise

a. 3.0% (w/v) rosehip oil,
b. 4.5 % (w/v) glyceryl dibehenate,
c. 0.05% (w/v) DDAB,
d. 3.5% (w/v) polysorbate 80,
e. optionally 0.1% (w/v) apigenin.

[0028] In one embodiment the lipid nanoparticles further comprise from 0.00001 % - 0.001 % (w/v), preferably 0.0001 % (w/v) hyaluronic acid, more preferably wherein said hyaluronic acid coats the lipid nanoparticles.

[0029] In another aspect the present invention relates to a composition comprising lipid nanoparticles as described herein for use in the treatment, amelioration or prevention of ocular diseases, such as ocular inflammation, glaucoma, ocular tumors, bacterial and viral infections of the eye, age-related macular degeneration, cataracts, diabetic retinopathy, or dry eye disease (DED).

[0030] In one embodiment the composition is administered topically into the eye.

DETAILED DESCRIPTION OF THE INVENTION

DEFINITIONS

[0031] The use of the word "a" or "an" may mean "one," but it is also consistent with the meaning of "one or more," "at least one," and "one or more than one". The use of the term "another" may also refer to one or more. The use of the term "or" in the claims is used to mean "and/or" unless explicitly indicated to refer to alternatives only or the alternatives are mutually exclusive.

[0032] As used in this specification and claim(s), the words "comprising" (and any form of comprising, such as "comprise" and "comprises"), "having" (and any form of having, such as "have" and "has"), "including" (and any form of including, such as "includes" and "include") or "containing" (and any form of containing, such as "contains" and "contain") are inclusive or open-ended and do not exclude additional, unrecited elements or method steps. The term "comprises" also encompasses and expressly discloses the terms "consists of" and "consists essentially of". As used herein, the phrase "consisting essentially of" limits the scope of a claim to the specified materials or steps and those that do not materially affect the basic and novel characteristic(s) of the claimed invention. As used herein, the phrase "consisting of" excludes any element, step, or ingredient not specified in the claim except for, e.g., impurities ordinarily associated with the element or limitation.

[0033] As used herein, words of approximation such as, without limitation, "about", "around", "approximately" refers to a condition that when so modified is understood to not necessarily be absolute or perfect but would be considered close enough to those of ordinary skill in the art to warrant designating the condition as being present. The extent to which the description may vary will depend on how great a change can be instituted and still have one of ordinary skilled in the art recognize the modified feature as still having the required characteristics and capabilities of the unmodified

feature. In general, but subject to the preceding discussion, a numerical value herein that is modified by a word of approximation such as "about" may vary from the stated value by ±1, 2, 3, 4, 5, 6, 7, 8, 9, or 10%. Accordingly, the term "about" may mean the indicated value ± 5% of its value, preferably the indicated value ± 2% of its value, most preferably the term "about" means exactly the indicated value (+ 0%).

[0034] The terms "comprise" and "comprising" are used in the inclusive, open sense, meaning that additional elements may be included. The term "comprises" also encompasses and may be used interchangeably with the terms "consists of" and "consists essentially of".

DETAILED DESCRIPTION

[0035] Dry eye disease (DED) is a condition frequently encountered in ophthalmology practice worldwide. Topical administration is a preferred route to treat DED, but currently available artificial tears have no anti-inflammatory properties and do not deal with the fundamental pathogenesis of the disease. Usual treatments for ocular inflammation include corticosteroids and non-steroidal anti-inflammatory drugs (NSAIDs) which after prolonged use led to severe side effects. Another drawback of topical applications is the generally fast release of the active ingredient(s). Furthermore, for topical applications into the eye, it needs to be assured that the active ingredient can permeate through the corneal barrier to reach its destination.

[0036] The inventors have therefore set out to develop a drug delivery system that can overcome these drawbacks and that provides biocompatibility, anti-inflammatory efficacy as well as capability to reverse ocular disease symptoms, such as DED. A further aim of the invention is to provide an ocular topical delivery system for APG that overcomes its low solubility and bioavailability and that provides for sustained drug release as well as corneal permeability thus improving the pharmacokinetic and pharmacodynamic profile of APG.

[0037] To achieve this the inventors have developed lipid nanoparticles comprising rosehip oil extracted from Rosa canina seeds as a liquid lipid having antioxidant, anti-inflammatory and regenerative properties. Rosehip oil contains essential fatty acids, tocopherols, sterols and phenolics with functional properties (15). The inventors could show that the lipid nanoparticles according to present invention comprising rosehip oil and no further active ingredient, herein named "lipid nanoparticles", already provide for an improved tear flow, could restore the corneal surface and were able to restore the tear film (see Example 7, Figures 7-9).

[0038] In one aspect the present invention relates to a composition comprising lipid nanoparticles, said lipid nanoparticles comprising

a. at least one liquid lipid with anti-inflammatory properties;
b. at least one solid lipid;
c. at least one cationic surfactant
d. optionally, at least a non-cationic surfactant;
e. optionally, at least one active ingredient.

[0039] In one embodiment the at least one said liquid lipid with anti-inflammatory properties is selected from the group consisting of rosehip oil, tea tree oil, lavender oil, linoleic acid, stearic acid, palmitic acid, castor oil, safflower oil, melon seed oil, salicornia oil, evening primrose oil, poppyseed oil, grape seed oil, prickly pear oil, artichoke oil, hemp oil, wheat germ oil, cottonseed oil, corn oil, walnut oil, soybean oil, sesame oil, rice bran oil, argan oil, pistachio oil, peach oil, almond oil, canola oil, avocado oil, flaxseed oil, sunflower oil, peanut oil, palm oil, olive oil, macadamia oil, coconut oil, rosemary oil, lavender oil, origanum vulgare oil, thyme oil, mint oil, eucalyptus oil, ginger oil, cuminum cyminum l. oil, turmeric oil, clove oil, oleic acid, oregano oil, rose oil, fennel oil, bergamot oil, chamomile oil, helichrysum oil, patchouli oil, frankincense oil, copaiba oil, peppermint oil, black pepper oil, sweet marjoram oil, basil oil, clove oil, clary sage oil, lemongrass oil, geranium oil, wintergreen oil, cannabis oil, cannabidiol, spruce oil, niaouli oil, cardamom oil, pine tree oil, fir tree oil, juniper tree oil, verbena oil, marjoram oil, katafray oil, bitter orange oil, hypericum oil, arnica oil, coriander oil, mustard oil, perilla seed oil, centella asiatica oil, calendula oil, laurel oil, camphor oil, cinnamon oil, oatmeal oil, docosahexaenoic acid, eicosapentaenoic acid, dandelion oil, krill oil, electrophorus electricus oil, potamotrygon motoro oil, boa constrictor oil, chelonoidis denticulate oil, melanosuchus niger oil, inia geoffrensis oil, horse oil, anchovy oil, prunus seed oil, tropidurus hispidus oil, emu oil, maqian fruits essential oil, fructus alpinia oil, cinnamomum cassia essential oil, angelica sinensis oil, gynura procumbens oil, spirulina oil, citrus limetta oil, citrus aurantium oil, atractylodes macrocephala oil, artemisia argyi oil, gynura procumbens oil, acorus gramineusand oil, algal oil, fish oil, zanthoxylum coreanum nakai oil, cod liver oil, perna canaliculus oil, chia seed oil, or combinations thereof.

[0040] The above listed liquid lipids are known to contain anti-inflammatory properties and are thus suitable for use in the compositions of present invention. Anti-inflammatory properties herein refer to the ability of the liquid lipid to reduce inflammation and/or redness, and/or pain and/or swelling of a tissue.

[0041] The preferred liquid lipid is rosehip oil. The lipid nanoparticles of present invention can comprise from 0.01 -

30.0% (w/v), from 0.1 - 30.0% (w/v), from 0.5 - 25.0% (w/v), from 1.0 - 20.0% (w/v), from 1.5 - 15.0% (w/v), from 2.0 - 14.0% (w/v), from 2.5 - 12.5% (w/v), from 2.5 - 10.0% (w/v), from 2.5 - 9.0% (w/v), from 2.5 - 8.0% (w/v), from 2.5 - 7.0% (w/v), from 2.7 - 6.0% (w/v), from 2.8 - 5.0% (w/v), from 2.9 - 4.0% (w/v) rosehip oil. Preferred is an amount of from 2.5 - 12.5% (w/v), more preferred an amount from 2.9 - 4.0% (w/v), most preferred 3.0% (w/v).

[0042] In one embodiment of the composition of the present invention the solid lipid is selected from monoglycerides, diglycerides, triglycerides, cholesterols, steroids, fatty alcohols, glycerol esters glyceryl tridecanoate, glycerol trilaurate, glyceryl trimyristate, glyceryl tripalmitate, glyceryl tristearate, hydrogenated coco-glycerides, hard fat types, mixtures of triglycerides and/or diglycerides and/or monoglycerides and/or glycerol, acyl glycerols, glyceryl monostearate, glyceryl distearate, glyceryl monooleate, glyceryl dibehenate, glyceryl palmitostearate, waxes, cetyl palmitate, fatty acids, stearic acid, palmitic acid, decanoic acid, behenic acid, glycerol stearate citrate, polyethylene glycol monostearate, cyclic complexes, cyclodextrin para-acyl-calix-arenes, or mixtures thereof.

[0043] The solid lipid can be present in the lipid nanoparticles of present invention from 1.0 - 50 % (w/v), from 1.0 - 40 % (w/v), from 1.0 - 30 % (w/v), from 1.0 - 20 % (w/v), from 1.0 - 15 % (w/v), from 1.0 - 10 % (w/v), from 1.5 - 9.5 % (w/v), from 2.0 - 9.0 % (w/v), from 2.5 - 8.5 % (w/v), from 3.0 - 8.0 % (w/v), from 3.2 - 7.5 % (w/v), from 3.5 - 7.0 % (w/v), from 3.7 - 6.5 % (w/v), from 4.0 - 6.0% (w/v), from 4.1 - 5.5 % (w/v), from 4.2 - 5.0 % (w/v), from 4.3 - 4.9 % (w/v), from 4.4 - 4.8 % (w/v).

[0044] The lipid nanoparticles comprise at least at least one cationic surfactant. The cationic surfactant provides an increased bioavailability of the formulation when administered onto the ocular mucosa. Cationic surfactants promote electrostatic interactions between the surface of the cationic particles and the anionic ocular mucosa, with a considerable improvement of the drug residence time [14].

[0045] In one embodiment of the composition of present invention the cationic surfactant is selected from the group consisting of dimethyldioctadecylammonium bromide (DDAB), dioleoyl phosphatidylethanolamine, 1,2-distearyloxy-N,N-dimethyl-3-aminopropane, 1,2 dioleyl-oxy-*N,N*-dimethyl-3-aminopropane,1,2-dilinoleyloxy-N,N-dimethyl-3-aminopropane, 1,2 - dilinolen-yloxy-N,N-dimethyl-3- aminopropane, cetyltri-methylammonium bromide, 3R-[N(N',N'-dimethylaminoethane)-carbamoyl]cholesterol, 1,2-dioleoyl-3-trimethylammo-nium-propane, 1,2-dimyristoyl-3-trimethylammonium-propane, 1,2-stearoyl-3-tri-methylammonium-propane, N-(4-carboxybenzyl)-N,N-dimethyl-2,3-bis(oleoyloxy) propan-1-aminium, 1-Palmitoyl-2-oleoyl-sn-glycero-3-phosphoethanolamine, N,N-di-(β-stearoylethyl)-N,N-dimethyl-ammonium chloride, benzalkonium chloride, cetylpyridinium chloride, cetrimide, N-[1-(2,3-dioleoyloxy)propyl]-N,N,N-trimethylammonium chloride, 1,2-dilineoyl-3-dimethylammonium-propane, 1,2-dilinoleyloxy-3-N,N-dimethylaminopropane, 1,2-dilinoleyloxy- keto-N,N-dimethyl-3-aminopropane, 1,2-dilinoleyl-4-(2- dimethylaminoethyl)-[1,3]-dioxolane(3-o-[2''-(methoxypolyethyleneglycol 2000) succinoyl]-1,2-dimyristoyl-sn-glycol, R-3-[(ω-methoxy-poly(ethyleneglycol)2000) carbamoyl]-1,2-dimyristyloxlpropyl-3-amine, cetyltri-methylammonium bromide, octadecylamine, 1-oleoyl-rac-glycerol, octadecyl quaternized carboxymethyl chitosan, hexadecyl trimethyl ammonium bromide.

[0046] A preferred cationic surfactant according to present invention is dimethyl-dioctadecyl-ammonium bromide (DDAB). DDAB is a commercially available double chain cationic surfactant that is for example used in the prior art for preparation of lipid bilayer-protected gold nanoparticles (AuNPs) or for delivery systems into mammalian cells, such as RNAi delivery.

[0047] The lipid nanoparticles of present invention can comprise from 0.001 - 10 % (w/v), from 0.0015 - 5 % (w/v), from 0.010 - 4 % (w/v), from 0.015 - 2 % (w/v), from 0.020 - 1 % (w/v), from 0.021 - 0.9 % (w/v), from 0.022 - 0.8 % (w/v), from 0.023 - 0.7 % (w/v), from 0.024 - 0.6 % (w/v), from 0.025 - 0.5 % (w/v), from 0.030 - 0.4 % (w/v), from 0.035 - 0.3 % (w/v), from 0.040 - 0.2 % (w/v), from 0.045 - 0.1 % (w/v) of a cationic surfactant.

[0048] In previous studies for ocular delivery DDAB had not shown any toxicity at a concentration of 0.5% (18). As such, in one preferred embodiment the lipid nanoparticles of present invention comprise 0.05% (w/v) of DDAB.

[0049] The lipid nanoparticles further comprise at least one further surfactant that is not a cationic surfactant, herein referred to also as "non-cationic surfactant". Surfactant type and concentration play an important role in designing lipid nanoparticles. Lipid nanoparticles are stabilized by different types of surfactants which are efficiently adsorbed onto particles' surfaces reducing the interfacial tension. Either a sole surfactant or a mixture of hydrophilic and lipophilic surfactants can be used for the preparation. A blend can provide improved physical stability and functional properties to the lipid nanoparticles.

[0050] In one embodiment of the composition of present invention the non-cationic surfactant is selected from the group consisting of polysorbate 80, soya lecithin, sodium dodecyl sulphate, polysorbate 20, polysorbate 40, polysorbate 60, PEG-30 glyceryl stearate, cholic acid, phosphatidyl choline, phospholipids with phosphatidycholine, egg lecithin, poloxamer 188, poloxamer407, poloxamer 184, poloxamer 338, poloxamine 908, tyloxopol, taurocholate sodium salt, taurodeoxycholicacid sodium salt, sodium glycocholate, sodium oleate, cholesteryl hemisuccinate, butanol, sodium cholate, nonionic polyoxyethylene, non-ionic amphiphilic surfactant with an alkyl moiety and an ethylene oxide chain, palmitic acid, stearic acid, mixtures of palmitic and stearic acid, lecithin, polyglycerol 6-distearate, caprylyl/capryl glucoside, coco-glucoside, sucrose palmitate, sucrose stearate, sucrose distearate, tyloxapol, lecithin, cetylpyridinium chloride, sorbitan laurate, polyethylene glycol ether of cetyl or stearyl alcohol, castor oil polyoxyethylene ether, macrogolglycerol

ricinoleate, dioctyl sodium sulfosuccinate, monooctylphosphoric acid sodium, hexadecyl trimethyl ammonium bromide, polyvinyl alcohol, polyoxyethylene (40) stearate, polyethylene glycol-polypropylene glycol-polyethylene glycol triblock copolymer, olyoxyethylene nonylphenyl ether, hexadecyltrimethylammonium bromide, sodium dodecyl sulfate, sodium cholate, stearate sodium hydrolysed polyvinyl alcohol 9000-10000 MW, dioctyl sulfosuccinate, taurocholate, 4-dodecylbenzenesulfonic acid, long chain carboxylic acid, alkyldiphenyloxide disulfonate, or mixtures thereof.

[0051] The concentration of the non-cationic surfactant particularly influences the particle size of the lipid nanoparticles. Generally, the higher the non-cationic surfactant concentration, the smaller the particle sizes will be. The non-cationic surfactant can be present in the lipid nanoparticles from 0.01 - 10% (w/v), from 0.1 - 9.5% (w/v), from 0.2 - 9.0% (w/v), from 0.3 - 8.5% (w/v), from 0.4 - 8.0% (w/v), from 0.5 - 7.5% (w/v), from 0.6 - 7.0% (w/v), from 0.7 - 6.5% (w/v), from 0.8 - 6.0% (w/v), from 0.9 - 5.5% (w/v), from 1.0 - 5.0% (w/v), from 1.5 - 4.5% (w/v), from 2.0 - 4.0% (w/v), from 2.5 - 3.5% (w/v). For clarity, the ranges disclosed refer to the amount of non-cationic surfactant in the lipid nanoparticles, thus not including the amount of cationic surfactant. The amount of cationic surfactant is specified further above.

[0052] The lipid nanoparticles of present invention can further comprise at least one active ingredient. In one embodiment the at least one active ingredient is selected from the group consisting of flavonoids, resveratrol (3,5,4'-trihydroxy-trans-stilbene) and curcumin. Preferred active ingredients are flavonoids due to their antioxidant and anti-inflammatory properties.

[0053] A preferred active ingredient of present invention is apigenin. APG is a natural flavonoid that is contained in various plant extracts, among others chamomile extracts, and has been used as plant extract for the treatment of several disorders and inflammatory conditions. Based on preclinical and clinical data, it has been suggested that APG is a potent therapeutic agent to overcome diseases, such as inflammatory diseases, bacterial, viral, and parasitic infections, autoimmune disorders, diabetes, hypertension, hypercholesterolemia, and various types of cancers [4,5]. Furthermore, APG itself is currently commercialized as a dietary supplement in Spain in the form of capsules containing 50 mg APG for improving prostate health, decrease glucose levels, and maintain the function of the nervous system [8,9].

[0054] Whilst commercialized eye drops containing chamomile extract for the enhancement of ocular discomfort, such as irritation, tired eyes, and itchiness are on the market [10,11], APG itself has to date not been suggested or approved as a therapy for ocular diseases, such as for example DED. This may partially be due to the disadvantages of APG for topical treatments caused among other by its low solubility and low bioavailability [12]. The same problem occurs with other flavonoids. To overcome these disadvantages the inventors have encapsulated APG into the lipid nanoparticles as described above. APG encapsulation into biocompatible and biodegradable lipid nanoparticles has been carried out to overcome its compromised stability and increase therapeutic activity and half-life on the ocular surface, granting its prolonged release.

[0055] In a further embodiment said lipid nanoparticles further comprise a coating. The coating can comprise carbomers, such as CMC (carboxymethyl cellulose), chitosan or hyaluronic acid. In a preferred embodiment said coating comprises hyaluronic acid. Hyaluronic acid (HA) is one of the most utilised viscosity-building macromolecules in ocular delivery devices. This anionic polysaccharide with ocular mucomimetic properties exhibits the capacity of prolonging the precorneal residence time and reducing surface desiccation [15]. In addition, hyaluronic acid can act as a lubricant and provide for an additional moisturizing effect.

[0056] This nanosystem has been proven to be physically stable with a prolonged APG release as well as high corneal permeability, thus improving biopharmaceutical APG behavior. In addition, in vitro and in vivo tests corroborate that the developed formulation is biocompatible without any sign of ocular irritation. As already described above, empty lipid nanoparticles showed an ability to revert DED symptoms due to its composition. When the lipid nanoparticles were loaded with APG ("Loaded Lipid Nanoparticles"), tear secretion improved due to the therapeutic properties of APG. In addition, a complementary anti-inflammatory effect of such Loaded Lipid Nanoparticles is also confirmed (see Example 7, Figures 7-9). Hence, Loaded Lipid Nanoparticles constitute a suitable system for the treatment, amelioration and prevention of ocular inflammatory diseases, such as DED.

[0057] In one preferred embodiment of the composition of present invention said lipid nanoparticles comprise

a. 0.01 - 30 % (w/v) lipid liquid with anti-inflammatory properties, preferably rosehip oil;
b. 1 - 50 % (w/v) solid lipid, preferably glyceryl dibehenate;
c. 0.001 - 10 % (w/v) cationic surfactant, preferably DDAB;
d. optionally 0.00 - 10 % (w/v) non cationic surfactant, preferably polysorbate 80;
e. optionally 0.00 - 10 % (w/v) active ingredient, preferably apigenin.

[0058] In one preferred embodiment of the composition of present invention said lipid nanoparticles comprise

a. 0.01 - 30 % (w/v) lipid liquid with anti-inflammatory properties, preferably rosehip oil;
b. 1 - 50 % (w/v) solid lipid, preferably glyceryl dibehenate;
c. 0.005 - 10 % (w/v) cationic surfactant, preferably DDAB;

d. 0.01 - 10 % (w/v) non cationic surfactant, preferably polysorbate 80;
e. optionally 0.01 - 10 % (w/v) active ingredient, preferably apigenin.

[0059] In one preferred embodiment of the composition of present invention said lipid nanoparticles comprise

a. 0.1 - 10 % (w/v) lipid liquid with anti-inflammatory properties, preferably rosehip oil;
b. 1 - 30 % (w/v) solid lipid, preferably glyceryl dibehenate;
c. 0.01 - 5 % (w/v) cationic surfactant, preferably DDAB;
d. 0.5 - 7 % (w/v) non cationic surfactant, preferably polysorbate 80;
e. optionally 0.01 - 10 % (w/v) active ingredient, preferably apigenin.

[0060] In one preferred embodiment of the composition of present invention said lipid nanoparticles comprise

a. 2.5 - 12.5% (w/v) lipid liquid with anti-inflammatory properties, preferably rosehip oil;
b. 1 - 30 % (w/v) solid lipid, preferably glyceryl dibehenate;
c. 0.025 - 0.5 % (w/v) cationic surfactant, preferably DDAB;
d. 1.0 - 5.0% (w/v) non cationic surfactant, preferably polysorbate 80;
e. optionally 0.1 - 2.5% (w/v) active ingredient, preferably apigenin.

[0061] In one preferred embodiment of the composition of present invention said lipid nanoparticles comprise

a. 3.0% (w/v) rosehip oil,
b. 4.5 % (w/v) glyceryl dibehenate,
c. 0.05% (w/v) DDAB,
d. 3.5% (w/v) polysorbate 80,
e. optionally 0.1% (w/v) apigenin.

[0062] In one embodiment the lipid nanoparticles further comprise from 0.00001 % - 0.001 % (w/v), preferably 0.0001 % (w/v) hyaluronic acid, more preferably wherein said hyaluronic acid coats the lipid nanoparticles.

[0063] In another aspect the present invention relates to a composition comprising lipid nanoparticles as described herein for use in the treatment, amelioration or prevention of ocular diseases, such as ocular inflammation, glaucoma, ocular tumors, bacterial and viral infections of the eye, age-related macular degeneration, cataracts or diabetic retinopathy, Dry Eye Disease. In a preferred embodiment the treatment of, amelioration or prevention of DED is envisaged.

[0064] It is finally contemplated that any features described herein can optionally be combined with any of the embodiments of any product, method or medical use of the invention; and any embodiment discussed in this specification can be implemented with respect to any of these. It will be understood that particular embodiments described herein are shown by way of illustration and not as limitations of the invention.

[0065] All publications and patent applications are herein incorporated by reference to the same extent as if each individual publication or patent application was specifically and individually indicated to be incorporated by reference.

[0066] The following examples serve to illustrate the present invention and should not be construed as limiting the scope thereof.

EXAMPLES

Materials

[0067] APG was obtained from Apollo Scientific (Cheshire, UK). Compritol® 888 ATO (Glyceryl dibehenate) was kindly gifted from Gattefossé (Madrid, Spain). Tween® 80 (Polysorbate 80), Bengal Rose and Fluorescein were purchased to Sigma Aldrich (Madrid, Spain). Rosehip oil was purchased to Acofarma Fórmulas Magistrales (Barcelona, Spain). Dimethyldioctadecylammonium bromide (DDAB) was purchased to TCI Europe (Zwijndrecht, Belgium). Sodium hyaluronate was kindly donated by Bloomage Freda Biopharm (Jinan, China). All others chemical reagents and components used in this research were of analytical grade. A Millipore Milli-Q Plus system was used to obtain purified water.

Example 1: LOADED LIPID NANOPARTICLES PREPARATION AND OPTIMIZATION

[0068] The production of Loaded Lipid Nanoparticles was carried out by high-pressure homogenization method (Homogenizer FPG 12800, Stansted, United Kingdom) after generating a primary emulsion with the mixture of components with an Ultraturrax T25 (IKA, Germany) at 8000 rpm for 30 s. The production conditions were 85 °C, three homogenization

cycles and 900 bars of pressure [16]. A design of experiments approach (DoE) used in order to optimize formulation parameters. A central composite factorial design (containing 2 replicated centre points, 16 factorial points and 8 axial points) was developed using statistical program Statgraphics Centurion 18® version 18.1.12 software (Virginia, USA). Four independent variables: APG concentration (%), surfactant concentration (%), glyceryl dibehenate + rosehip oil concentration (%) and glyceryl dibehenate concentration contained in the mixture glyceryl dibehenate + rosehip oil (%) were evaluated to determine their influence on the NLC properties. Mean particle diameter size (Z_{av}), polydispersity index (PDI), entrapment efficiency (EE) and Zeta potential (ZP) were designated as the dependent variables. Once the optimized formulation was obtained, increasing amounts of a cationic surfactant were added in order to obtain a cationic surface charge. Then, sodium hyaluronate was added to the formulation [16,17].

1.1 PHYSICOCHEMICAL PARAMETERS

[0069] Z_{av} and PDI were assessed by photon correlation spectroscopy (PCS) with a ZetaSizer Nano ZS (Malvern Instruments, Malvern, UK). ZP was estimated by electrophoretic mobility. For these measurements, samples were diluted with Milli-Q water 1:10 and analysed by triplicate at 25 °C. EE was determined indirectly. Previously to the analysis, the non-loaded drug was separated from NPs by filtration/centrifugation at 14,000 r.p.m. (Mikro 22 Hettich Zentrifugen, Germany) using an Amicon® Ultra 0.5 centrifugal filter device (Amicon Millipore Corporation, Ireland). The encapsulation efficiency (EE) was calculated by the difference between the total amount of drug and the free drug, present in the filtered fraction, using Eq. 1 [18]:

$$EE\ (\%) = \frac{Total\ amount\ of\ APG - Free\ APG}{Total\ amount\ of\ APG} \qquad \text{Eq. 1}$$

[0070] The quantification of APG was performed by a modified reverse-phase high-performance liquid chromatography (RP-HPLC). Briefly, samples were quantified using HPLC Waters 2695 (Waters, Massachusetts, USA) separation module and a Kromasil® C18 column (5 μm, 150 × 4.6 mm) with a mobile phase formed by a water phase of 2 % acetic acid and an organic phase of methanol, in a gradient (from 40 % to 60 % of water phase in 5 min and back in next 5 min) at a flow rate of 0.9 mL/min. A diode array detector Waters® 2996 at a wavelength of 300 nm was used to detect the APG and data were processed using Empower 3® Software [16,19].

1.2 CHARACTERIZATION OF OPTIMIZED LOADED LIPID NANOPARTICLES

1.2.1 Transmission electron microscopy

[0071] Transmission electron microscopy (TEM) was used to investigate the morphology of the Loaded Lipid Nanoparticles on a Jeol 1010 (Jeol USA, Dearborn Road, Peabody, MA 01960, USA). Copper grids were activated with UV light and samples were diluted (1:10) and placed on the grid surface to visualize the particles. Samples were previously subjected to negative staining with uranyl acetate (2%) [18].

1.2.2 Interaction studies

Interaction studies were carried out with the formulation without HA.

[0072] Differential scanning calorimetry (DSC) analysis was performed using a DSC 823e System Mettler-Toledo, Barcelona, Spain. A pan with indium (purity ≥99.95%; Fluka, Switzerland) was used to check the calibration of the calorimetric system. An empty pan served as a reference. The DSC measurements were carried out in the Loaded Lipid Nanoparticles formulations using a heating ramp from 25 to 105 °C at 10 °C/min in a nitrogen atmosphere. Data was evaluated using the Mettler STARe V 9.01 dB software (Mettler-Toledo, Barcelona, Spain) [16,18].

[0073] X-ray spectroscopy (XRD) was used to analyse the amorphous or crystalline state of the samples. Samples were sandwiched between 3.6 μm polyester films and exposed to CuKα radiation (45 kV, 40 mA, λ = 1.5418 Å) in the range (2θ) of 2-60° with a step size of 0.026° and a measuring time of 200 s per step [16].

[0074] Fourier transform infrared (FTIR) spectra of Loaded Lipid Nanoparticles were obtained using a Thermo Scientific Nicolet iZ10 with an ATR diamond and DTGS detector (Barcelona, Spain).

RESULTS:

a) LOADED LIPID NANOPARTICLES PREPARATION AND OPTIMIZATION

[0075] Table 1 shows the effect of independent variables used on dependent variables analysed and the values obtained. Z_{av} values are mostly around 200 nm. The developed Loaded Lipid Nanoparticles exhibit a negative surface charge ZP < -20 mV. In all cases EE was higher than 95 %, thus meaning that APG was completely encapsulated. Most of the formulations have PDI values below 0.3, indicating a homogeneous distribution of nanoparticles [20].

Table 1. Design of experiments and characterization of the different formulations developed.

	Independent variables								Dependent variables			
	APG (%)		Liquid Lipid (%)		Solid Lipid (%)		Polysorbate 80 (%)		Z_{av} – SD (nm)	PDI ± SD	ZP ± SD (mV)	EE ± SD (%)
Factorial points												
A1	-1	1	-1	0.75	1	4.25	-1	2	176.1 ± 2.3	0.278 ± 0.009	-21.7 ± 0.7	99.9 ± 0.1
A2	1	2	-1	1.75	-1	3.25	1	4	221.5 ± 2.5	0.313 ± 0.012	-21.4 ± 0.5	96.7 ± 0.1
A3	1	2	1	3.50	-1	6.50	-1	2	253.9 ± 4.4	0.246 ± 0.012	-22.6 ± 0.3	99.9 ± 0.1
A4	-1	1	1	1.50	1	8.50	-1	2	271.4 ± 5.5	0.273 ± 0.008	-23.0 ± 0.8	99.9 ± 0.1
A5	-1	1	1	3.50	-1	6.50	-1	2	243.7 ± 0.7	0.236 ± 0.014	-24.6 ± 0.5	99.7 ± 0.3
A6	-1	1	1	3.50	-1	6.50	1	4	214.7 ± 1.6	0.181 ± 0.010	-18.2 ± 0.9	99.9 ± 0.1
A7	-1	1	-1	0.75	1	4.25	1	4	165.9 ± 1.2	0.265 ± 0.012	-17.6 ± 0.2	99.9 ± 0.1
A8	-1	1	-1	1.75	-1	3.25	-1	2	161.2 ± 2.3	0.255 ± 0.023	-22.3 ± 0.4	95.1 ± 0.2
A9	1	2	1	4.50	-1	6.50	1	4	212.2 ±1.8	0.217 ± 0.019	-19.6 ± 0.2	99.9 ± 0.1
A10	-1	1	1	1.50	1	8.50	1	4	236.8 ± 2.0	0.244 ± 0.017	-18.4 ± 0.5	99.9 ± 0.1
A11	1	2	-1	0.75	1	4.25	1	4	191.9 ± 2.7	0.318 ± 0.058	-19.2 ± 0.6	99.9 ± 0.1
A12	-1	1	-1	1.75	-1	3.25	1	4	202.7 ± 2.4	0.203 ± 0.002	-18.7 ± 0.2	97.7 ± 0.1
A13	1	2	1	1.50	1	8.50	-1	2	304.6 ± 5.7	0.276 ± 0.007	-20.1 ± 0.4	99.1 ± 0.1
A14	1	2	-1	1.75	-1	3.25	-1	2	188.7 ± 2.3	0.374 ± 0.008	-22.2 ± 0.4	99.9 ± 0.1
A15	1	2	1	1.50	1	8.50	1	4	240.5 ± 2.5	0.277 ± 0.015	-18.0 ± 0.4	99.6 ± 0.1
A16	1	2	-1	0.75	1	4.25	-1	2	200.5 ± 2.8	0.425 ± 0.015	-22.4 ± 0.6	99.9 ± 0.1
Axial points												
A17	-2	0.5	0	1.857	0	5.625	0	3	181.2 ± 1.4	0.221 ± 0.029	-19.5 ± 0.3	99.9 ± 0.1
A18	2	2.5	0	1.875	0	5.625	0	3	230.3 ± 2.7	0.327 ± 0.007	-20.2 ± 0.2	99.9 ± 0.1
A19	0	1.5	-2	0.625	0	1.875	0	3	202.0 ± 3.9	0.556 ± 0.015	-22.3 ± 0.3	99.9 ± 0.1

(continued)

Axial points												
A20	0	1.5	2	3.125	0	9.375	0	3	280.9 ± 5.7	0.259 ± 0.009	-20.7 ± 0.4	99.9 ± 0.1
A21	0	1.5	0	4.50	-2	5.50	0	3	187.3 ± 1.3	0.195 ± 0.012	-20.4 ± 0.5	99.9 ± 0.1
A22	0	1.5	0	0.50	2	9.50	0	3	202.5 ± 3.3	0.331 ± 0.026	-20.7 ± 0.2	99.9 ± 0.1
A23	0	1.5	0	2.50	0	7.50	-2	1	271.0 ± 4.3	0.231 ± 0.020	-24.1 ± 0.7	99.9 ± 0.1
A24	0	1.5	0	2.50	0	7.50	2	5	239.1 ± 1.6	0.182 ± 0.027	-17.2 ± 0.8	98.1 ± 0.3
Central points												
A25	0	1.5	0	1.875	0	5.625	0	3	202.0 ± 0.8	0.267 ± 0.012	-20.3 ± 0.4	99.9 ± 0.1
A26	0	1.5	0	1.875	0	5.625	0	3	199.3 ± 0.7	0.292 ± 0.038	-19.6 ± 0.1	99.9 ± 0.1

[0076] As it can be appreciated in Figure 3, the four variables studied had a significant effect on the formulation of the NLC. Average size and PDI of Loaded Lipid Nanoparticles are directly influenced by the concentration of glyceryl dibehenate + rosehip oil. Higher concentrations of glyceryl dibehenate + rosehip oil provide bigger Loaded Lipid Nanoparticles but lower PDI (Figure 3A, 3B). ZP is influenced by the amount of surfactant, a higher concentration of surfactant, less superficial charge is obtained (Figure 3C). EE is highly influenced by the proportion of glyceryl dibehenate added to the formulation. At higher glyceryl dibehenate concentrations, lower encapsulation of APG is obtained (Figure 3D). With these trends, the optimized formulation contains 0.1% of APG, 4.5% glyceryl dibehenate, 3.0% rosehip oil, and 3.5% of non-cationic surfactant.

[0077] To the optimized formulation, increasing amounts of the cationic surfactant were added (Table 2). The optimized formulation was chosen based on the physicochemical parameters, where values of ZP higher than 20 mV and PDI lower than 0.3 were selected. Because of that fact, the cationic optimized formulation was 0.05% of cationic surfactant.

Table 2. Effect of cationic surfactant on the physicochemical parameters.

DDAB (%)	Z_{av} ± SD (nm)	PDI ± SD	ZP ± SD (mV)
0.025	301.8 ± 2.0	0.186 ± 0.003	-0.8 ± 0.1
0.05	**146.8 ± 0.8**	**0.253 ± 0.003**	**21.2 ± 0.4**
0.06	144.3 ± 2.4	0.326 ± 0.036	27.3 ± 1.0
0.075	150.0 ± 3.8	0.363 ± 0.040	29.3 ± 0.5
0.1	148.2 ± 1.5	0.427 ± 0.018	35.6 ± 0.8
0.3	156.6 ± 1.9	0.407 ± 0.011	54.8 ± 1.6
0.5	147.7 ± 0.3	0.382 ± 0.009	54.4 ± 0.6

[0078] To this, 0.0001 % of HA was added and then, the optimized Loaded Lipid Nanoparticles were obtained (Table 3).

Table 3. Composition and physicochemical parameters of optimized formulation, Loaded Lipid Nanoparticles

Composition of Loaded Lipid Nanoparticles	
APG	0.1 % (w/v)
Glyceryl dibehenate	4.5 % (w/v)
Rosehip oil	3.0 % (w/v)
Polysorbate 80	3.5 % (w/v)
DDAB	0.05 % (w/v)
HA	0.0001 % (w/v)

Physycochemical parameters of Loaded Lipid Nanoparticles			
Z_{av} ± SD (nm)	PI ± SD	ZP ± SD (mV)	EE ± SD (%)
143.6 ± 1.3	0.254 ± 0.009	21.8 ± 0.6	99.9 ± 0.1

b) CHARACTERIZATION OF OPTIMIZED LOADED LIPID NANOPARTICLES

[0079] The morphology of Loaded Lipid Nanoparticles obtained by TEM shows almost spherical and soft shapes and the size below 200 nm is consistent with the results found by PCS. Particle aggregation phenomena is not observed (Figure 4A).

[0080] DSC was carried out in order to study the crystallinity and the melting point variations of the lipid mixtures and Loaded Lipid Nanoparticles. Thermogram (Figure 4B) shows endothermal peaks, of 70.37 °C for lipid mixture, 69.78 °C for lipid mixture-APG and 69.16 °C Loaded Lipid Nanoparticles. Melting point of Loaded Lipid Nanoparticles is slightly lower because of its small size and the addition of a surfactant (Polysorbate 80) in the formulation (28). The peaks move to slightly lower temperatures when APG is added and the enthalpy is similar between the lipid mixture and lipid mixture-APG being ΔH Lipid mixture = 82.69 Jg^{-1}, ΔH Lipid mixture-APG = 84.03 Jg^{-1} and a smaller enthalpy for the nanoparticles, being ΔH Loaded Lipid Nanoparticles = 54.11 Jg^{-1}. APG melting transition is characterized by an endothermal peak at 365.5°C (ΔH = 198.5 Jg^{-1}) followed by decomposition [21].

[0081] XRD profiles in Figure 4C show the physical state of APG incorporated in NLC. Intense and sharp peaks for APG and for the solid mixture of lipids are shown, indicating that these components have a crystalline structure. The peaks found for APG are not detected in Loaded Lipid Nanoparticles profile, which could mean that the drug is present in a dissolved state in the NLC (molecular dispersion). The crystallinity of the structure of all the components was studied. The lipid mixture shows three peaks in 19.34 (2θ), i.e. d=0,46 nm indicating the most stable form of triacylglycerols, the β form, 21,28 (2θ) i.e. d=0,42 nm and 23,43 (2θ) i.e. d=0,38 nm, indicating the second stable form of triacylglycerols, the β' form. The Loaded Lipid Nanoparticles profile shows also the three peaks, which could indicate a good stability of the formulation [21-23].

[0082] FTIR analysis was used to study the interactions between the drug, the surfactant and lipid mixture (Figure 4D). The FTIR spectra of pure APG presented vibrational bands with characteristic peak at the wave number of 3278 cm^{-1} for O-H group. However, C-H group presented multiple small peaks at 2800 cm^{-1}. The characteristic peaks at 1650 and 1605 cm^{-1} were obtained for the C-O functional group [24]. There was no evidence of strong bonds between APG and lipid mixture and the surfactant. APG peaks were not found in the NLC. These results meaning that APG was encapsulated in the NLC.

Example 4: STABILITY STUDIES

[0083] Loaded Lipid Nanoparticles were stored at 4 and 25 °C during several months. The study was assessed analysing light backscattering (BS) profiles by a Turbiscan® Lab equipment. A glass measurement cell containing 20 ml of sample was used. Data were acquired every 30 days. The radiation source used was pulsed near-infrared light-

emitting diode LED (λ = 880 nm), the signal was detected by a BS detector at an angle of 45° from the incident beam. At the same time interval, values of Z_{av}, PDI, ZP and EE were measured (20). The study is still running.

[0084] Stability studies were carried out by the backscattering (BS) profiles of each sample at different temperatures. BS profiles provides information of destabilization mechanisms in the media, such as sedimentation, agglomeration, or aggregation [25]. In this way, BS profiles of Loaded Lipid Nanoparticles were studied at 4 °C and 25 °C. The Loaded Lipid Nanoparticles formulation is stable at 4 °C for a period of 19 months, while at 25 °C the stability endures 2 months. The physicochemical parameters kept constant at 4 °C for all the study. The best storage temperature is at 4 °C.

Example 5: BIOPHARMACEUTICAL BEHAVIOUR

[0085] The in vitro APG release test for Loaded Lipid Nanoparticles was performed using Franz-type diffusion cells (Crown Glass, NY, USA) with a diffusion area of 0.20 cm^2 and dialysis membranes of cellulose (MWCO 12 kDa). A solution of PBS with 5% polysorbate 80 and 20% ethanol under continuous stirring was used as a receptor medium assuring sink conditions (ability of the medium to dissolve the expected amount of drug) [26]. The formulations were compared with free-APG solution. The assay was carried out at 32 ± 0.5 °C along 48h. 300 µl of each formulation were added to the donor compartment by direct contact with the membrane. At a certain timepoints, 150 µl of sample were collected with a syringe and the volume withdrawn was replaced with receptor solution. Drug content of the samples was analysed with HPLC. The test was performed by triplicate, and the cumulative amount of APG was calculated [16].

[0086] The in vitro release profile of APG from the NLC demonstrates that the formulation has a kinetic profile that is characteristic of prolonged drug release formulations. The release best fit for NLC was two phase decay. Figure 6 shows a faster release of APG from the NLC during the first 8h, after that the speed was decreased. The free APG had a faster release, achieving a 100% at 24h while the Loaded Lipid Nanoparticles released less than 20%. It has been reported that modifying the surface of nanocarriers with hyaluronic acid can restrict water diffusion into the carrier matrix which subsequently slows down the drug release process [27]. These results indicated the formulation had a prolonged release of APG.

Example 6: OCULAR TORELANCE

6.1 In vitro study: HET-CAM test and TBS

[0087] In vitro ocular tolerance was assessed using the HET-CAM test to ensure that the formulations of Loaded Lipid Nanoparticles were non-irritating when administered as eye-drops. Irritation, coagulation, and haemorrhage phenomena were measured by applying 300 µL of the formulation studied on chorioallantoic membrane of a fertilized chicken egg and monitoring it during the first 5 min after the application. This assay was conducted according to the guidelines of ICCVAM (The Interagency Coordinating Committee on the Validation of Alternative Methods). The development of the test was carried out using 3 eggs for each group (free APG, Loaded Lipid Nanoparticles, positive control (NaOH 0.1 M) and negative control (0.9 % NaCl)). The ocular irritation index (OII) was calculated by the sum of the scores of each injury according to the following expression (Eq 3) [18]:

$$OII = \frac{(301-H)\cdot 5}{300} + \frac{(301-V)\cdot 7}{300} + \frac{(301-C)\cdot 9}{300} \qquad \text{Eq. 3}$$

where H, V and C are times (s) until the start of haemorrhage (H), vasoconstriction (V) and coagulation (C), respectively. The formulations were classified according to the following: OII ≤ 0.9 non-irritating; 0.9 < OII ≤ 4.9 weakly irritating; 4.9 < OII ≤ 8.9 moderately irritating; 8.9 < OII ≤ 21 irritating.

[0088] Furthermore, at the end of the HET-CAM experiment, in order to quantify the damage of the membrane, trypan blue staining (TBS) was applied. The CAM was treated with 1000 µL of 0.1% trypan blue solution for 1 min. Excess dye was rinsed off with distilled water. The dyed CAM was excised and extracted with 5 mL formamide, and the absorbance of the extract was measured spectrophotometrically at 595 nm. The absorbed trypan blue was determined from a calibration curve of trypan blue in formamide [28].

[0089] HET-CAM test was applied showing that the positive controls (NaOH 1 M) resulted in severe haemorrhage, which increased over five minutes grading this solution as a severe irritant. On the other hand, application of the formulations to the chorioallantoic membrane did not cause irritation and therefore, the formulations were classified as non-irritant. Moreover, TBS quantitative results supported the results of the HET-CAM test, where Loaded Lipid Nanoparticles were non-irritant while free APG resulted irritant.

6.2 In vivo study: Draize test

[0090] All of the procedures were approved by the Ethical Committee for Animal Experimentation of the UB and current legislation (Decree 214/97, Gencat). The formulations were evaluated using primary eye irritation test of Draize to ensure the results obtained from the HEM-CAM test. For this experiment, New Zealand male albino rabbits (2.0-2.5 kg, San Bernardo farm, Navarra, Spain) were used. 50 μL of each sample were instilled in the ocular conjunctival sac (n = 3/group) and a mild massage was applied to guarantee the passage of the sample through the eyeball. The possible appearance of irritation signs (corneal opacity and area of corneal involvement, conjunctival hyperemia, chemosis, ocular discharges, and iris abnormalities) was observed at the time of instillation and after 1 h from its application and if necessary, at predefined intervals: 24 h, 48 h, 72 h, 7 days, and 21 days after administration. The opposite untreated eye was used as a negative control. Draize test score was determined directly by observing the anterior segment of the eye and changes in the structures of the cornea (turbidity or opacity), iris and conjunctiva (congestion, chemosis, swelling and secretion) [2].

[0091] The tests were carried out with free APG, Lipid Nanoparticles, Loaded Lipid Nanoparticles. In this sense, none of the developed NLC were irritant in vivo or in vitro, while the free APG resulted irritant in vitro and non-irritant in vivo but caused an initial discomfort. These results confirmed the non-irritant potential of APG loaded lipid nanoparticles, meanwhile the free APG can induce some discomfort.

Example 7: IN VIVO EFFICACY STUDIES

[0092] In order to evaluate the potential to treat dry eye of Loaded Lipid Nanoparticles, Schirmer test, fluorescein and rose Bengal assessments were performed against Lipid Nanoparticles, free APG and 0.15% hyaluronic acid (commercial solution Hyabak®).

7.1 Induction and treatment of dry eye

[0093] Twelve male New Zealand white rabbits (purchased from Livestock Research Institute, Council of Agriculture, Executive Yuan, Taiwan) weighing between 2.0 and 2.5 kg were used for the study. The rabbits were randomly divided into 4 groups: Lipid Nanoparticles, Loaded Lipid Nanoparticles, free APG solution and 0.15% hyaluronic acid (commercial solution (Hyabak®). All rabbits were housed at a room temperature of 23° ± 2 °C with relative humidity 75% ± 10% and alternating 12-hour light-dark cycles (8 a.m. to 8 p.m.). Both eyes of each rabbit were treated twice-daily by a topical administration of 0.1% benzalkonium chloride (BAC) drops for 2 weeks. On day 14, DES was confirmed by Schirmer test, fluorescein and rose Bengal staining. The treatment began after the confirmation of DES, where on eye of each rabbit was chosen randomly for twice-daily topical administration of Lipid Nanoparticles, Loaded Lipid Nanoparticles, free APG solution and a commercial solution. After one week of treatment, Schirmer test, fluorescein and rose Bengal staining were performed [2,29].

7.1.1. Measurement of aqueous tear production

[0094] Tear production was measured using Schirmer test strips. After the topical application of anaesthetic drops (1 mg/ml tetracaine hydrochloride/4 mg/ml oxybuprocaine hydrochloride), the lower eyelid was pulled down, and a Schirmer paper strip was placed on the palpebral conjunctiva near the junction of the middle and outer thirds of the lower eyelid. After 5 min, the wetted length (mm) of the paper strips was recorded [2,29].

[0095] A severe decrease in the aqueous tear secretion was achieved after the application of benzalkonium chloride for 2 weeks. Figure 7 shows the differences between each group of treatment. Lipid Nanoparticles and Loaded Lipid Nanoparticles were able to increase the tear flow in the animals, with statistically significant differences against dry eye group, $p < 0.01$ and $p < 0.0001$ respectively. Otherwise, free APG and the commercial solution did not improve the tear flow. Loaded Lipid Nanoparticles showed statically significant differences between all the groups: $p < 0.01$ against Lipid Nanoparticles, and $p < 0.0001$ against free APG and commercial solution. Lipid Nanoparticles showed statistically significant differences between free APG group ($p < 0.01$). Loaded Lipid Nanoparticles were the treatment that attained the best score in the Schirmer test, followed by the Lipid Nanoparticles, meaning that both were able to restore the tear secretion of the animals. These results reveal the potential of the composition of the nanoformulations because of the restoring of the tear flow in the animals. Loaded Lipid Nanoparticles presented a better score due to the encapsulation of APG, which it has anti-inflammatory properties, leading to a better improvement of one of the symptoms of DED.

7.1.2. Fluorescein staining on the ocular surface

[0096] Fluorescein staining is an effective method for ocular surface evaluation. Fluorescein staining is the result of

uptake caused by the disruption of corneal epithelial cell-cell junctions or damaged corneal epithelial cells [29]. Corneal fluorescein staining was performed after 2 μL of 1 % fluorescein sodium were dropped into the conjunctival sac for 2 min. The ocular surface was examined under a slit lamp microscope with a cobalt blue filter. The images were collected by a digital camera (Figure 1) and punctuated according to the stained score (9: maximum score; 0: minimum)[30]. Figure 8 shows the differences between each group of treatment. There were statistically significant differences between all the groups against dry eye control. However, the two treatments that had a better improvement of the ocular corneal surface were Lipid Nanoparticles and Loaded Lipid Nanoparticles ($p < 0.001$). Moreover, free APG solution and the commercial solution presented worse punctuation in the staining, meaning that both did not have the ability to restore the corneal surface as Lipid Nanoparticles and Loaded Lipid Nanoparticles.

7.1.3. Bengal rose staining on the ocular surface

[0097] Bengal rose is an effective method to evaluate the tear film integrity. Bengal rose has been demonstrated to stain corneal and conjunctival epithelial cells that are not adequately protected by the preocular tear film. It can stain live and dead cells if they are not protected by an intact mucin layer [29]. Ocular fluorescein staining was performed after 2 μL of 0.1% Bengal rose were dropped into the conjunctival sac for 2 min. The ocular surface was examined under a slit lamp microscope with a white light. The images were collected by a digital camera. Using the Van Bijsterveld grading system, the scores were graded after 15 seconds (Figure 2) (9: maximum score; 0: minimum) [29].

[0098] There were statistically significant differences between dry eye and Lipid Nanoparticles and Loaded Lipid Nanoparticles intensity (Figure 9). The results showed that only NLC were able to restore tear film in the animals. The worst punctuation for the rose Bengal staining was the commercial solution. Thus, indicating that Loaded Lipid Nanoparticles were able to restore the tear film.

[0099] These results showed the ability of the lipid nanoparticles to revert the symptoms of the DED. Lipid Nanoparticles and Loaded Lipid Nanoparticles were able to improve all the studied parameters of DED. These results could be due to the novel composition of the lipid nanoparticles. The addition of the rosehip oil provides anti-inflammatory and antioxidant properties to the Lipid Nanoparticles [31,32]. Because of this fact, Lipid Nanoparticles improves the score of both different staining of the ocular surface, showing interesting properties against DED. The addition of the APG had improved the tear secretion on the Schirmer test, which could mean that NLC protects APG to be released and enhance the anti-inflammatory properties of the formulation, improving the DED symptomatology.

7.1.4 Anti-inflammatory efficacy

[0100] In vivo anti-inflammatory efficacy was assayed to explore the capacity of the NLC to prevent and treat ocular inflammation through two different tests. The assays were carried out throughout the evaluation test for the inflammation prevention ability and the anti-inflammatory efficacy using New Zealand male albino rabbits (n = 3/group), described previously. The activity of Loaded Lipid Nanoparticles in comparison with free APG and NaCl 0.9% (control group) was measured. The inflammation prevention study consisted of the ocular application of 50 μL of each formulation.

[0101] After 30 min of exposure, an inflammatory stimulus, 50 μL of 0.5% sodium arachidonate (SA) dissolved in PBS, was instilled in the right eye and the left eye was used as a control. In the anti-inflammatory treatment study, the inflammatory stimulus was applied 30 min before than the application of each formulation tested. The evaluation of prevention and treatment of each formulation were carried out from the first application up to 210 min, according to the Draize modified test scoring system [2,18].

[0102] In vivo inflammatory prevention test showed significant differences between the degree of inflammation of APG formulations or physiological serum during all the timepoints tested (Figure 10). Nevertheless, eyes treated with Loaded Lipid Nanoparticles presented a faster swelling reduction rather than free APG, mainly owing to tear clearance in case of free APG and the improved ocular surface adherence of lipid nanoparticles, thus presenting longer residence time in the cornea. Loaded Lipid Nanoparticles exhibited significant differences regarding positive control over the time. Thus, Loaded Lipid Nanoparticles exhibited a preventive effect of inflammation caused by the sustained release of APG to the corneal cells.

[0103] In addition, the in vivo inflammation treatment was assessed. Loaded Lipid Nanoparticles and free APG were applied after 30 min of SA exposure, and the degree of inflammation was quantified. Figure 11 revealed that the degree of inflammation was significantly reduced after the first 90 minutes post-administration of Loaded Lipid Nanoparticles. Free APG were able to treat faster inflammation due to the NLC had a controlled release. After 90 min of contact, both APG formulations were effective in treating inflammation symptoms. Hence, it can be concluded that the controlled release system based on Loaded Lipid Nanoparticles has ocular anti-inflammatory activity, both for prevention level and inflammation treatment.

7.1.5 STATISTICAL ANALYSIS

[0104] Two-way ANOVA followed by Tukey post hoc test was performed for multi-group comparison. Student's t-test was used for two-group comparisons. All the data are presented as the mean + S.D. Statistical significance was set at $p < 0.05$ by using GraphPad Prism 6.0.1.

REFERENCES

[0105]

[1] Hantera MM. Trends in Dry Eye Disease Management Worldwide. Clin Ophthalmol 2021;15:173.

[2] López-Machado A, Díaz-Garrido N, Cano A, Espina M, Badia J, Baldomà L, et al. Development of Lactoferrin-Loaded Liposomes for the Management of Dry Eye Disease and Ocular Inflammation. Pharmaceutics 2021;13 (10):1698.

[3] Huang L, Gao H, Wang Z, Zhong Y, Hao L, Du Z. Combination Nanotherapeutics for Dry Eye Disease Treatment in a Rabbit Model. Int J Nanomedicine 2021;16:3631.

[4] Salehi B, Venditti A, Sharifi-Rad M, Kregiel D, Sharifi-Rad J, Durazzo A, et al. The Therapeutic Potential of Apigenin. Int J Mol Sci 2019;20 (6):1305.

[5] Ali F, Rahul, Naz F, Jyoti S, Siddique YH. Health functionality of apigenin: A review. Int J Food Prop 2016;20 (6):1197-238.

[6] Clinical Trial to Evaluate the Reduction of Cardiovascular Risk - ClinicalTrials.gov n.d. https://clinicaltrials.gov/ct2/show/NCT04114916?term=apigenin&draw=4&rank=3 (accessed November 19, 2021).

[7] Zick SM, Wright BD, Sen A, Arnedt JT. Preliminary examination of the efficacy and safety of a standardized chamomile extract for chronic primary insomnia: a randomized placebo-controlled pilot study. BMC Complement Altern Med 2011;11:78.

[8] Apigenbell 60 cápsulas Jellybell | Naturitas n.d. https://www.naturitas.es/p/suplementos/fitoterapia/compuestos-herbarios/apigenbell-60-capsulas-jelly-bell?gclid=CjwKCAiAs92MBhAXEiwAXTi25z_Q5qx2aeNYvzbrUCyGRG6PfdA91wTKXvtWHr461rXXYtFP_cDcZxoCkrAQAvD_BwE (accessed November 19, 2021).

[9] Apigenina 90 cápsulas de 50mg Swanson | Naturitas n.d. https://www.naturitas.es/p/suplementos/suplementos-compuestos/apigenina-90-capsulas-de-50mg-swanson (accessed November 19, 2021).

[10] Optrex Colirio para el Picor de Ojos n.d. https://www.optrex.es/gama-optrex/colirio/optrex-colirio-calmante-para-el-picor-de-ojos/optrex-colirio-calmante-para-el-picor-de-ojos/ (accessed November 19, 2021).

[11] Optiben - Irritación ocular n.d. https://optiben.cmfa.com/Producto/7/alivio-natural-de-la-irritacin-ocular (accessed November 19, 2021).

[12] Wang M, Firrman J, Liu LS, Yam K. A review on flavonoid apigenin: Dietary intake, ADME, antimicrobial effects, and interactions with human gut microbiota. Biomed Res Int 2019;7010467.

[13] Battaglia L, Serpe L, Foglietta F, Muntoni E, Gallarate M, Del Pozo Rodriguez A, et al. Application of lipid nanoparticles to ocular drug delivery. Expert Opin Drug Deliv 2016;13 (12):1743-57.

[14] Fangueiro JF, Calpena AC, Clares B, Andreani T, Egea MA, Veiga FJ, et al. Biopharmaceutical evaluation of epigallocatechin gallate-loaded cationic lipid nanoparticles (EGCG-LNs): In vivo, in vitro and ex vivo studies. Int J Pharm 2016;502 (1-2):161-9.

[15] Agarwal P, Craig JP, Rupenthal ID. Formulation Considerations for the Management of Dry Eye Disease. Pharmaceutics 2021;13 (2):207.

[16] Carvajal-Vidal P, Fábrega MJ, Espina M, Calpena AC, Garcia ML. Development of Halobetasol-loaded nanostructured lipid carrier for dermal administration: Optimization, physicochemical and biopharmaceutical behavior, and therapeutic efficacy. Nanomedicine Nanotechnology, Biol Med 2019;20:102026.

[17] Sánchez-López E, Ettcheto M, Egea MA, Espina M, Cano A, Calpena AC, et al. Memantine loaded PLGA PEGylated nanoparticles for Alzheimer's disease: In vitro and in vivo characterization. J Nanobiotechnology 2018;16 (1):1-16.

[18] Sánchez-López E, Esteruelas G, Ortiz A, Espina M, Prat J, Muñoz M, et al. Dexibuprofen Biodegradable Nanoparticles: One Step Closer towards a Better Ocular Interaction Study. Nanomaterials 2020;10 (4).

[19] Romanová D, Grancai D, Jozová B, Bozek P, Vachálková A. Determination of apigenin in rat plasma by high-performance liquid chromatography. J Chromatogr A 2000;870 (1-2):463-7.

[20] Zeb A, Qureshi OS, Kim HS, Kim MS, Kang JH, Park JS, et al. High payload itraconazole-incorporated lipid nanoparticles with modulated release property for oral and parenteral administration. J Pharm Pharmacol 2017;69 (8):955-66.

[21] Souto EB, Mehnert W, Müller RH. Polymorphic behaviour of Compritol888 ATO as bulk lipid and as SLN and

NLC. J Microencapsul 2006;23 (4):417-33.
[22] Freitas C, Müller RH. Correlation between long-term stability of solid lipid nanoparticles (SLN) and crystallinity of the lipid phase. Eur J Pharm Biopharm 1999;47 (2):125-32.
[23] Zimmermann E, Souto EB, Müller RH. Physicochemical investigations on the structure of drug-free and drug-loaded solid lipid nanoparticles (SLN) by means of DSC and 1H NMR. Pharmazie 2005;60 (7):508-13.
[24] Alshehri SM, Shakeel F, Ibrahim MA, Elzayat EM, Altamimi M, Mohsin K, et al. Dissolution and bioavailability improvement of bioactive apigenin using solid dispersions prepared by different techniques. Saudi Pharm J 2019;27 (2):264-73.
[25] Stability of Dispersions | 3P Instruments n.d. https://www.3p-instruments.com/measurement-methods/stability-turbiscan/ (accessed November 22, 2021).
[26] Liu P, De Wulf O, Laru J, Heikkilä T, Van Veen B, Kiesvaara J, et al. Dissolution Studies of Poorly Soluble Drug Nanosuspensions in Non-sink Conditions. AAPS PharmSciTech 2013;14 (2):748.
[27] Huang D, Chen YS, Rupenthal ID. Hyaluronic Acid Coated Albumin Nanoparticles for Targeted Peptide Delivery to the Retina. Mol Pharm 2017;14 (2):533-45.
[28] Lagarto A, Vega R, Guerra I, González R. In vitro quantitative determination of ophthalmic irritancy by the chorioallantoic membrane test with trypan blue staining as alternative to eye irritation test. Toxicol In Vitro 2006;20 (5):699-702.
[29] Xiong C, Chen D, Liu J, Liu B, Li N, Zhou Y, et al. A rabbit dry eye model induced by topical medication of a preservative benzalkonium chloride. Invest Ophthalmol Vis Sci 2008;49 (5):1850-6.
[30] Holzchuh R, Villa Albers MB, Osaki TH, Igami TZ, Santo RM, Kara-Jose N, et al. Two-year outcome of partial lacrimal punctal occlusion in the management of dry eye related to Sjögren syndrome. Curr Eye Res 2011;36 (6):507-12.
[31] Lin TK, Zhong L, Santiago JL. Anti-Inflammatory and Skin Barrier Repair Effects of Topical Application of Some Plant Oils. Int J Mol Sci 2017;19 (1):70.
[32] Kiralan M, Yildirim G. Rosehip (Rosa canina L.) Oil. Fruit Oils Chem Funct 2019:803-14.

Claims

1. A composition comprising lipid nanoparticles, said lipid nanoparticles comprising

   a. at least one liquid lipid with anti-inflammatory properties;
   b. at least one solid lipid;
   c. at least one cationic surfactant;
   d. optionally, at least one non-cationic surfactant;
   e. optionally, at least one active ingredient.

2. The composition of claim 1, wherein the said liquid lipid with anti-inflammatory properties is selected from the group consisting of rosehip oil, tea tree oil, lavender oil, linoleic acid, stearic acid, palmitic acid, castor oil, safflower oil, melon seed oil, salicornia oil, evening primrose oil, poppyseed oil, grape seed oil, prickly pear oil, artichoke oil, hemp oil, wheat germ oil, cottonseed oil, corn oil, walnut oil, soybean oil, sesame oil, rice bran oil, argan oil, pistachio oil, peach oil, almond oil, canola oil, avocado oil, flaxseed oil, sunflower oil, peanut oil, palm oil, olive oil, macadamia oil, coconut oil, rosemary oil, lavender oil, origanum vulgare oil, thyme oil, mint oil, eucalyptus oil, ginger oil, cuminum cyminum l. oil, turmeric oil, clove oil, oleic acid, oregano oil, rose oil, fennel oil, bergamot oil, chamomile oil, helichrysum oil, patchouli oil, frankincense oil, copaiba oil, peppermint oil, black pepper oil, sweet marjoram oil, basil oil, clove oil, clary sage oil, lemongrass oil, geranium oil, wintergreen oil, cannabis oil, cannabidiol, spruce oil, niaouli oil, cardamom oil, pine tree oil, fir tree oil, juniper tree oil, verbena oil, marjoram oil, katafray oil, bitter orange oil, hypericum oil, arnica oil, coriander oil, mustard oil, perilla seed oil, centella asiatica oil, calendula oil, laurel oil, camphor oil, cinnamon oil, oatmeal oil, docosahexaenoic acid, eicosapentaenoic acid, dandelion oil, krill oil, electrophorus electricus oil, potamotrygon motoro oil, boa constrictor oil, cheloncidis denticulate oil, melanosuchus niger oil, inia geoffrensis oil, horse oil, anchovy oil, prunus seed oil, tropidurus hispidus oil, emu oil, maqian fruits essential oil, fructus alpinia oil, cinnamomum cassia essential oil, angelica sinensis oil, gynura procumbens oil, spirulina oil, citrus limetta oil, citrus aurantium oil, atractylodes macrocephala oil, artemisia argyi oil, gynura procumbens oil, acorus gramineusand oil, algal oil, fish oil, zanthoxylum coreanum nakai oil, cod liver oil, perna canaliculus oil, chia seed oil, or combinations thereof.

3. The composition of claim 1, wherein the liquid lipid with anti-inflammatory properties is rosehip oil.

4. The composition of any one of the preceding claims, wherein the solid lipid is selected from monoglycerides, diglycerides, triglycerides, cholesterols, steroids, fatty alcohols, glycerol esters glyceryl tridecanoate, glycerol trilaurate, glyceryl trimyristate, glyceryl tripalmitate, glyceryl tristearate, Hydrogenated coco-glycerides, Hard fat types, mixtures of triglycerides and/or diglycerides and/or monoglycerides and/or glycerol, acyl glycerols, glyceryl monostearate, glyceryl distearate, glyceryl monooleate, glyceryl dibehenate, glyceryl palmitostearate, waxes, cetyl palmitate, fatty acids, stearic acid, palmitic acid, decanoic acid, behenic acid, glycerol stearate citrate, polyethylene glycol monostearate, cyclic complexes, cyclodextrin para-acyl-calix-arenes, or mixtures thereof.

5. The composition of any one of the preceding claims, wherein the cationic surfactant is selected from the group consisting of dimethyldioctadecylammonium bromide (DDAB), dioleoyl phosphatidylethanolamine, 1,2-distearyloxy-N,N-dimethyl-3-aminopropane, 1,2 dioleyl-oxy-N,N-dimethyl-3-aminopropane,1,2-dilinoleyloxy-N,N-dimethyl-3-aminopropane, 1,2 - dilinolenyloxy-N,N-dimethyl-3- aminopropane, cetyltri-methylammonium bromide, 3β-[N(N',N'-dimethylaminoethane)-carbamoyl]cholesterol, 1,2-dioleoyl-3-trimethylammo-nium-propane, 1,2-dimyristoyl-3-trimethylammonium-propane, 1,2-stearoyl-3-tri-methylammonium-propane, N-(4-carboxybenzyl)-N,N-dimethyl-2,3-bis(oleoyloxy) propan-1-aminium, 1-Palmitoyl-2-oleoyl-sn-glycero-3-phosphoethanol-amine, N,N-di-(β-stearoylethyl)-N,N-dimethyl-ammonium chloride, benzalkonium chloride, cetylpyridinium chloride, cetrimide, N-[1-(2,3-dioleoyloxy)propyl]-N,N,N-trimethylammonium chloride, 1,2-dilineoyl-3-dimethylammonium-propane, 1,2-dilinoleyloxy-3-N,N-dimethylaminopropane, 1,2-dilinoleyloxy- keto-N,N-dimethyl-3-aminopropane, 1,2-dilinoleyl-4-(2- dimethylaminoethyl)-[1,3]-dioxolane(3-o-[2''-(meth oxypolyethyleneglycol 2000) succinoyl]-1,2-dimyristoyl-sn-glycol, R-3-[(ω-methoxy-poly(ethyleneglycol)2000) carbamoyl]-1,2-dimyristyloxlpropyl-3-amine, cetyltrimethylammonium bromide, octadecylamine, 1-oleoyl-rac-glycerol, octadecyl quaternized carboxymethyl chitosan, hexadecyl trimethyl ammonium bromide.

6. The composition of any one of the preceding claims, wherein the cationic surfactant is dimethyl-dioctadecyl-ammonium bromide (DDAB).

7. The composition of any one of the preceding claims, wherein the non-cationic surfactant is selected from the group consisting of polysorbate 80, soya lecithin, sodium dodecyl sulphate, polysorbate 20, polysorbate 40, polysorbate 60, PEG-30 glyceryl stearate, cholic acid, phosphatidyl choline, phospholipids with phosphatidycholine, egg lecithin, poloxamer 188, poloxamer 407, poloxamer 184, poloxamer 338, poloxamine 908, tyloxopol, taurocholate sodium salt, taurodeoxycholicacid sodium salt, sodium glycocholate, sodium oleate, cholesteryl hemisuccinate, butanol, sodium cholate, nonionic polyoxyethylene, non-ionic am-phiphilic surfactant with an alkyl moiety and an ethylene oxide chain, palmitic acid, stearic acid, mixtures of palmitic and stearic acid, lecithin, polyglycerol 6-distearate, caprylyl/capryl glucoside, coco-glucoside, sucrose palmitate, sucrose stearate, sucrose distearate, tyloxapol, lecithin, cetylpyridinium chloride, sorbitan laurate, polyethylene glycol ether of cetyl or stearyl alcohol, castor oil polyoxyethylene ether, macrogolglycerol ricinoleate, dioctyl sodium sulfosuccinate, monooctylphosphoric acid sodium, hexadecyl trimethyl ammonium bromide, polyvinyl alcohol, polyoxyethylene (40) stearate, polyethylene glycol-polypropylene glycol-polyethylene glycol triblock copolymer, olyoxyethylene nonylphenyl ether, hexadecyltrimethylammonium bromide, sodium dodecyl sulfate, sodium cholate, stearate sodium hydrolysed polyvinyl alcohol 9000-10000 MW, dioctyl sulfosuccinate, taurocholate, 4-dodecylbenzenesulfonic acid, long chain carboxylic acid, alkyldiphenyloxide disulfonate, or mixtures thereof, preferably polysorbate 80.

8. The composition of any one of the preceding claims, wherein the at least one active ingredient is apigenin.

9. The composition of any one of the preceding claims, wherein the at least one active ingredient is encapsulated in the lipid nanoparticles.

10. The composition of any one of the preceding claims, wherein said lipid nanoparticles further comprise a coating, preferably wherein said coating comprises hyaluronic acid.

11. The composition of any one of the preceding claims, wherein said lipid nanoparticles comprise

a. 0.01 - 30 % (w/v) liquid lipid with inflammatory properties, preferably rosehip oil
b. 1 - 50 % (w/v) solid lipid, preferably glyceryl dibehenate;
c. 0.001 - 10 % (w/v) cationic surfactant, preferably DDAB;
d. optionally 0.00 - 10 % (w/v) non-cationic surfactant, preferably polysorbate 80;
e. optionally 0.00 - 10 % (w/v) active ingredient, preferably apigenin.

12. The composition of any one of the preceding claims, wherein said lipid nanoparticles comprise

    a. 2.5 - 12.5% (w/v) liquid lipid with inflammatory properties, preferably rosehip oil
    b. 1 - 30 % (w/v) solid lipid, preferably glyceryl dibehenate;
    c. 0.025 - 0.5 % (w/v) cationic surfactant, preferably DDAB;
    d. 1.0 - 5.0% (w/v) non-cationic surfactant, preferably polysorbate 80;
    e. optionally 0.1 - 2.5% (w/v) active ingredient, preferably apigenin.

13. The composition of any one of the preceding claims, wherein said lipid nanoparticles comprise

    a. 3.0% (w/v) rosehip oil,
    b. 4.5 % (w/v) glyceryl dibehenate,
    c. 0.05% (w/v) DDAB,
    d. 3.5% (w/v) polysorbate 80,
    e. optionally 0.1% (w/v) apigenin.

14. The composition of any one of the preceding claims, wherein the lipid nanoparticles further comprise from 0.00001 % - 0.001 % (w/v), preferably 0.0001 % (w/v) hyaluronic acid, more preferably wherein said hyaluronic acid coats the lipid nanoparticles.

15. A composition comprising lipid nanoparticles according to any one of the preceding claims for use in the treatment, amelioration or prevention of ocular diseases, such as ocular inflammation, glaucoma, ocular tumors, bacterial and viral infections of the eye, age-related macular degeneration, cataracts, diabetic retinopathy, or Dry Eye Disease (DED).

FIG.1

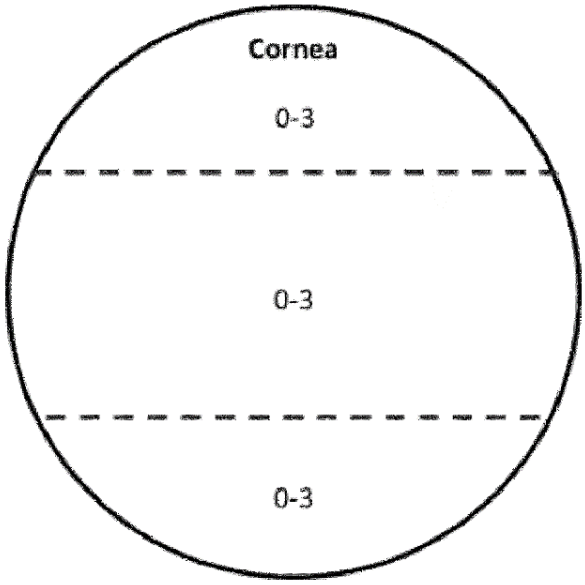

FIG.2

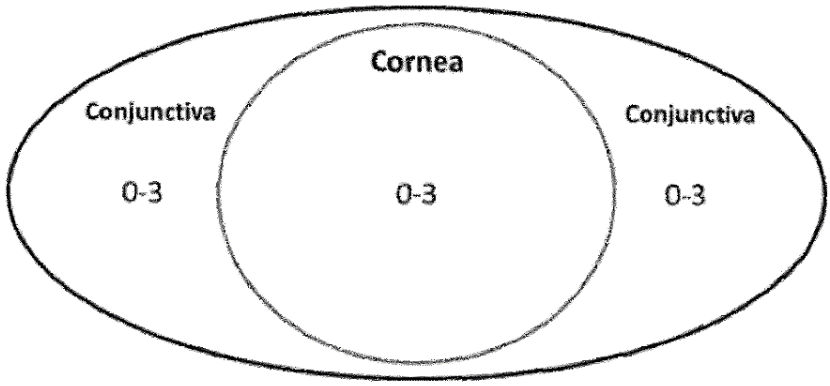

FIG.3

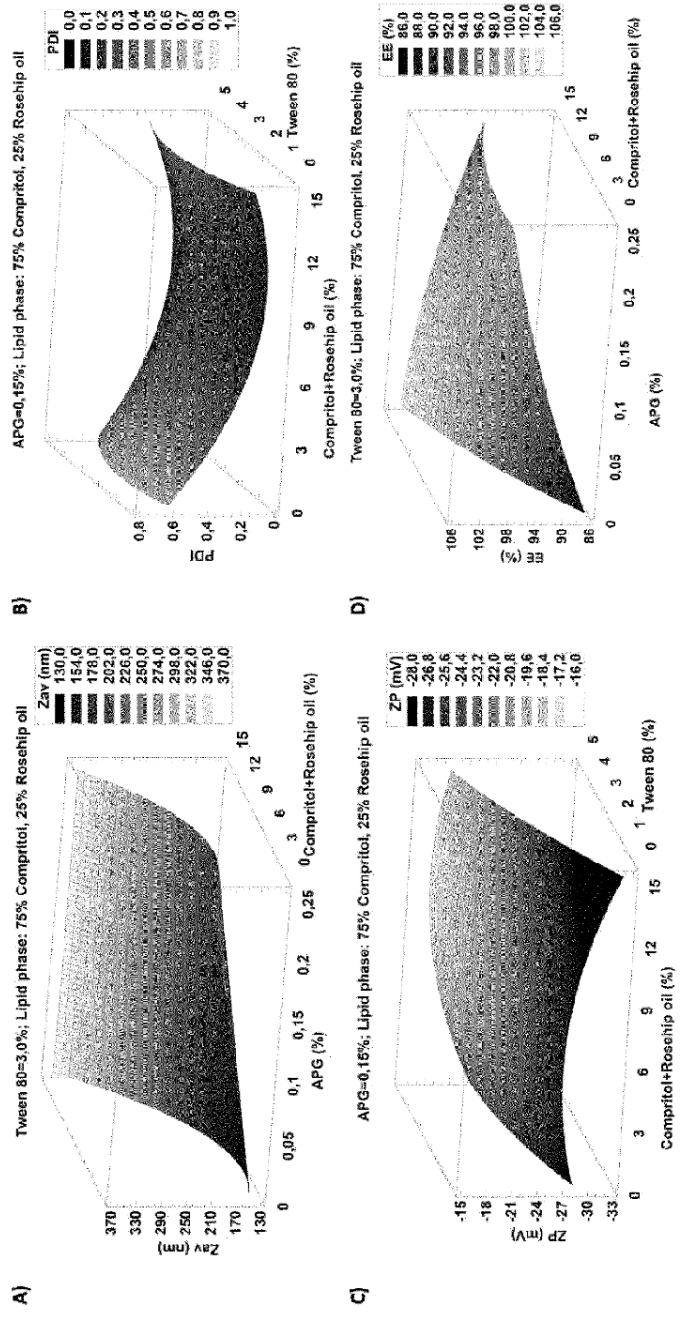
A)
Tween 80=3,0%; Lipid phase: 75% Compritol, 25% Rosehip oil
Zav (nm)
130,0
154,0
178,0
202,0
226,0
250,0
274,0
298,0
322,0
346,0
370,0
Zav (nm)
APG (%)
Compritol+Rosehip oil (%)
B)
APG=0,15%; Lipid phase: 75% Compritol, 25% Rosehip oil
PDI
0,0
0,1
0,2
0,3
0,4
0,5
0,6
0,7
0,8
0,9
1,0
PDI
Compritol+Rosehip oil (%)
Tween 80 (%)
C)
APG=0,15%; Lipid phase: 75% Compritol, 25% Rosehip oil
ZP (mV)
-28,0
-26,8
-25,6
-24,4
-23,2
-22,0
-20,8
-19,6
-18,4
-17,2
-16,0
ZP (mV)
Compritol+Rosehip oil (%)
Tween 80 (%)
D)
Tween 80=3,0%; Lipid phase: 75% Compritol, 25% Rosehip oil
EE (%)
86,0
88,0
90,0
92,0
94,0
96,0
98,0
100,0
102,0
104,0
106,0
EE (%)
APG (%)
Compritol+Rosehip oil (%)

FIG.4

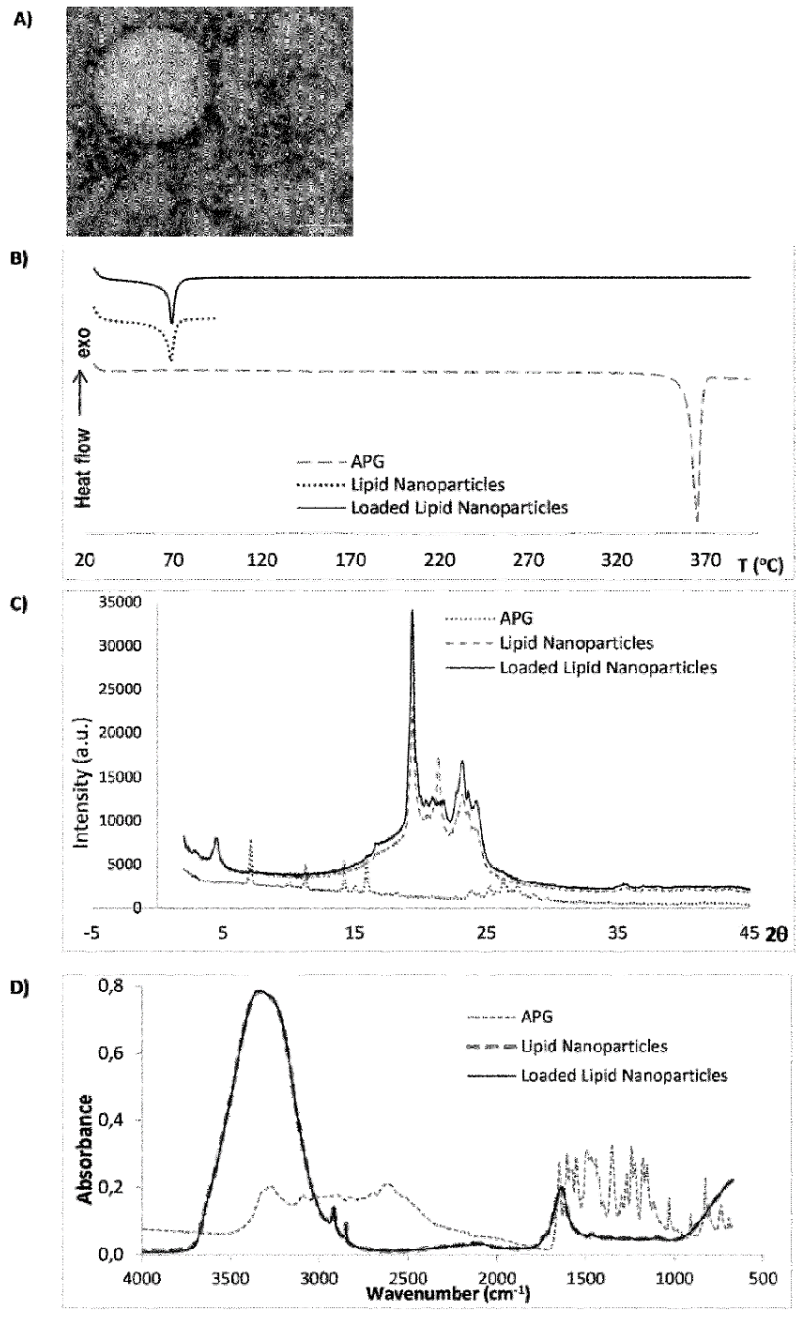
A)
B)
exo
Heat flow
APG
Lipid Nanoparticles
Loaded Lipid Nanoparticles
20
70
120
170
220
270
320
370
T (°C)
C)
35000
30000
25000
20000
15000
10000
5000
0
Intensity (a.u.)
APG
Lipid Nanoparticles
Loaded Lipid Nanoparticles
-5
5
15
25
35
45
2θ
D)
0,8
0,6
0,4
0,2
0,0
Absorbance
APG
Lipid Nanoparticles
Loaded Lipid Nanoparticles
4000
3500
3000
2500
2000
1500
1000
500
Wavenumber (cm-1)

FIG.5

A)

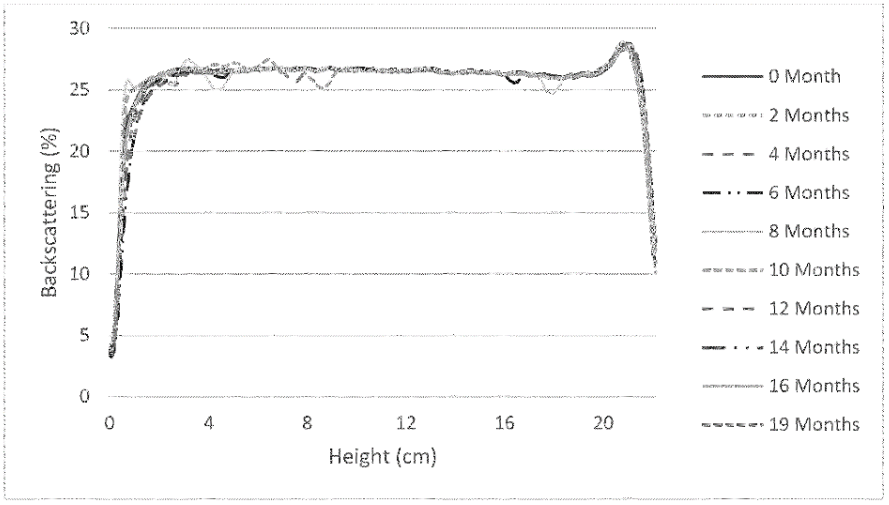
30
25
20
15
10
5
0
Backscattering (%)
0
4
8
12
16
20
Height (cm)
0 Month
2 Months
4 Months
6 Months
8 Months
10 Months
12 Months
14 Months
16 Months
19 Months

B)

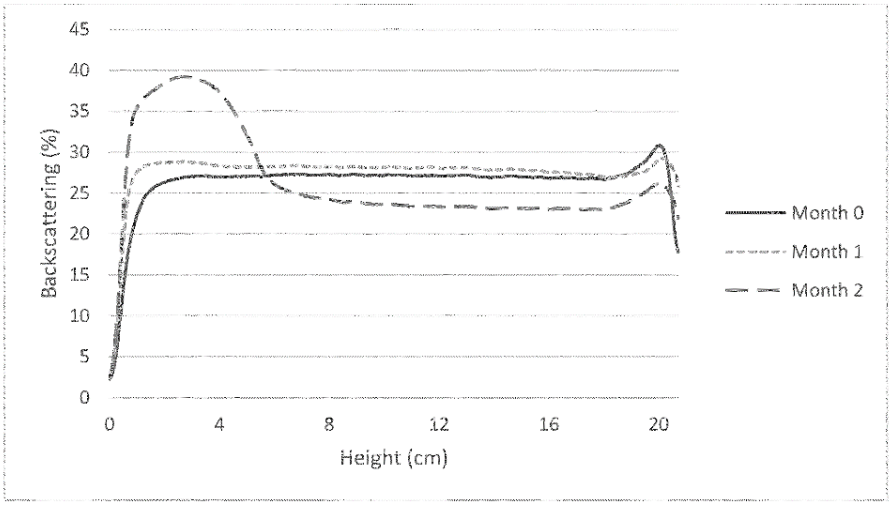
45
40
35
30
25
20
15
10
5
0
Backscattering (%)
0
4
8
12
16
20
Height (cm)
Month 0
Month 1
Month 2

FIG.6

Parameter	Loaded Lipid Nanoparticles	Free APG
B_{max} ± SD (%)	22.06 ± 6.75	100.6 ± 1.6
K ± SD (h^{-1})	K_{fast} 1.117 ± 0.612	0.2078 ± 0.0207
	K_{slow} 0.02536 ± 0.02508	
r^2	0.8228	0.9797

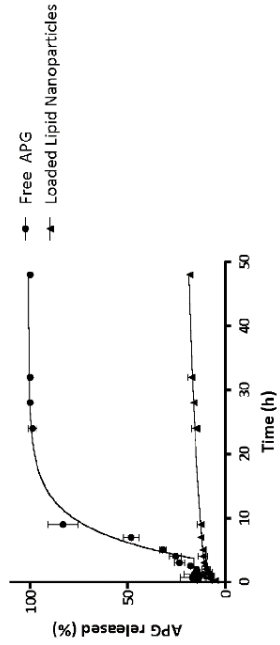

FIG.7

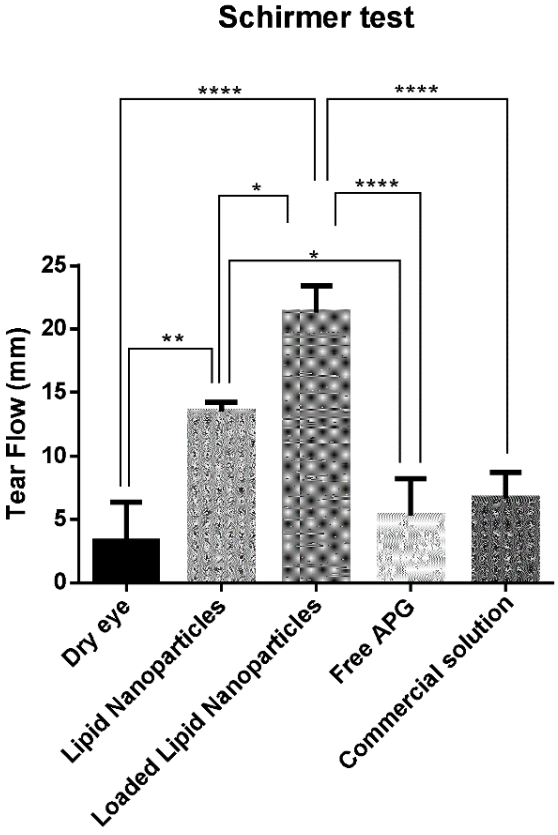
Schirmer test
Tear Flow (mm)
0
5
10
15
20
25
****
****
*
****
*
**
Dry eye
Lipid Nanoparticles
Loaded Lipid Nanoparticles
Free APG
Commercial solution

FIG.8

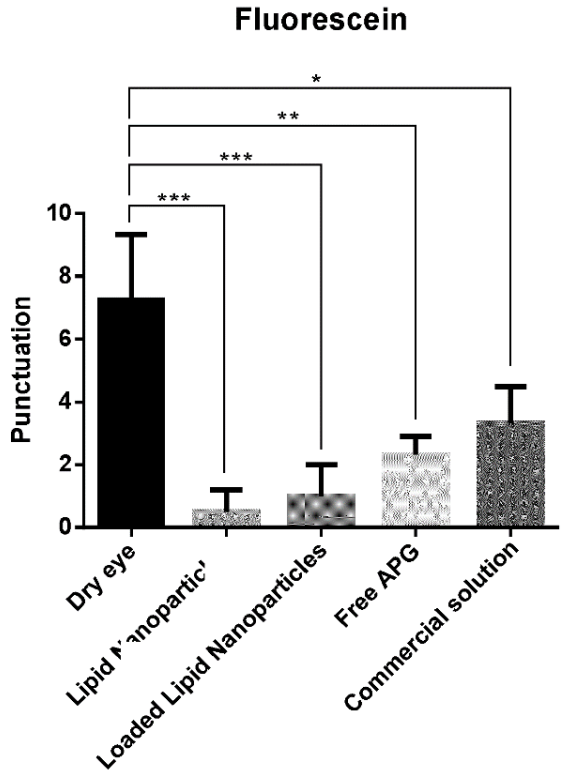
Fluorescein
*
**
***
***
Punctuation
10
8
6
4
2
0
Dry eye
Lipid Nanoparticles
Loaded Lipid Nanoparticles
Free APG
Commercial solution

FIG.9

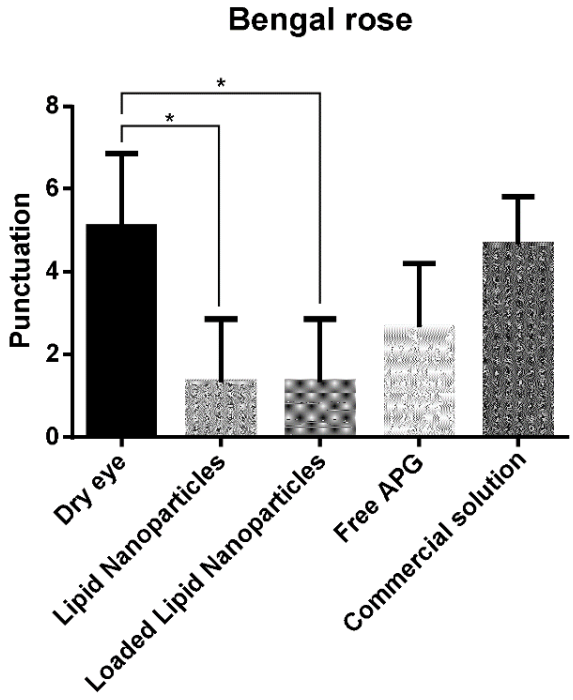
Bengal rose
Punctuation
0
2
4
6
8
*
*
Dry eye
Lipid Nanoparticles
Loaded Lipid Nanoparticles
Free APG
Commercial solution

FIG.10

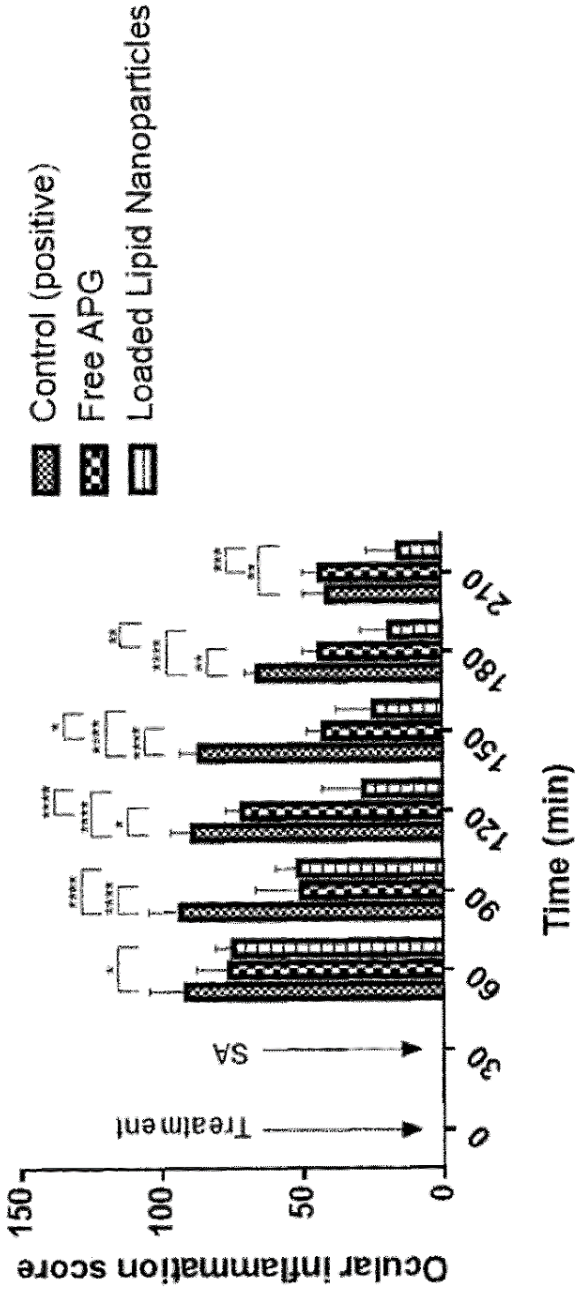
Control (positive)
Free APG
Loaded Lipid Nanoparticles
Ocular inflammation score
150
100
50
0
Treatment
SA
0
30
60
90
120
150
180
210
Time (min)

FIG.11

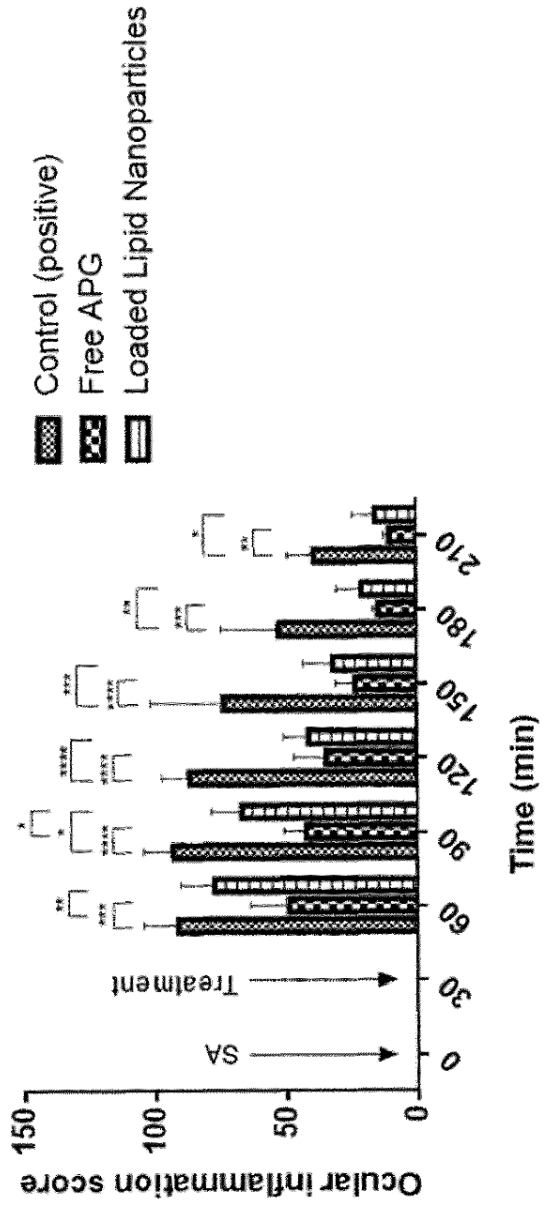
Control (positive)
Free APG
Loaded Lipid Nanoparticles
Ocular inflammation score
150
100
50
0
SA
Treatment
0
30
60
90
120
150
180
210
Time (min)

244

Europäisches Patentamt
European Patent Office
Office européen des brevets

EUROPEAN SEARCH REPORT

Application Number
EP 23 38 2105

DOCUMENTS CONSIDERED TO BE RELEVANT

Category	Citation of document with indication, where appropriate, of relevant passages	Relevant to claim	CLASSIFICATION OF THE APPLICATION (IPC)
X	ALMEIDA HUGO ET AL: "Preparation, characterization and biocompatibility studies of thermoresponsive eyedrops based on the combination of nanostructured lipid carriers (NLC) and the polymer Pluronic F-127 for controlled delivery of ibuprofen", PHARMACEUTICAL DEVELOPMENT AND TECHNOLOGY, vol. 22, no. 3, 3 April 2017 (2017-04-03), pages 336-349, XP093066262, US ISSN: 1083-7450, DOI: 10.3109/10837450.2015.1125922 Retrieved from the Internet: URL:http://dx.doi.org/10.3109/10837450.2015.1125922>	1,2,4,5, 7,9,11, 12,15	INV. A61K9/51 A61K9/00 A61K36/738 A61K31/352 A61P27/00 A61P27/06 A61P27/12 A61P31/04 A61P31/12 A61P35/00
Y	* abstract * * page 338, right-hand column, paragraph - page 339, left-hand column, paragraph 1; table 1 * * page 336, right-hand column, paragraph 2 * * page 338, left-hand column, paragraph Materials *	8,10,13, 14	TECHNICAL FIELDS SEARCHED (IPC) A61K
X	WO 2022/235238 A2 (DR SEYDA ATABAY SAGLIK VE KOZMETIK UERUENLERI A S [TR]) 10 November 2022 (2022-11-10)	1-5,7, 9-12	
Y	* page 10, line 7 - page 13, line 4; claims 1-18 *	10,13,14	
X	WO 2011/116963 A2 (LIPOTEC SA [ES]; VILADOT PETIT JOSEP LLUIS [ES] ET AL.) 29 September 2011 (2011-09-29) * examples 3-4-5,7 *	1,2,4, 7-12,14	

-/--

The present search report has been drawn up for all claims

Place of search	Date of completion of the search	Examiner
Munich	24 July 2023	Madalinska, K

CATEGORY OF CITED DOCUMENTS

X : particularly relevant if taken alone
Y : particularly relevant if combined with another document of the same category
A : technological background
O : non-written disclosure
P : intermediate document

T : theory or principle underlying the invention
E : earlier patent document, but published on, or after the filing date
D : document cited in the application
L : document cited for other reasons

& : member of the same patent family, corresponding document

EPO FORM 1503 03.82 (P04C01)

Europäisches Patentamt
European Patent Office
Office européen des brevets

EUROPEAN SEARCH REPORT

Application Number
EP 23 38 2105

DOCUMENTS CONSIDERED TO BE RELEVANT

Category	Citation of document with indication, where appropriate, of relevant passages	Relevant to claim	CLASSIFICATION OF THE APPLICATION (IPC)
X	WO 02/41765 A2 (SALVONA LLC [US]) 30 May 2002 (2002-05-30) * examples I-V *	1,4,5,7, 9,11	
X Y A	WO 2018/054077 A1 (REYOUNG SUZHOU BIOLOGY SCIENCE & TECH CO LTD [CN]) 29 March 2018 (2018-03-29) * examples 3-5; table 1 *	1,4,5,7, 9,11,12, 15 8 13	
X	SHARMA P ET AL: "Formulation and pharmacokinetics of lipid nanoparticles of a chemically sensitive nitrogen mustard derivative: Chlorambucil", INTERNATIONAL JOURNAL OF PHARMACEUTICS, ELSEVIER, NL, vol. 367, no. 1-2, 9 February 2009 (2009-02-09), pages 187-194, XP025879827, ISSN: 0378-5173, DOI: 10.1016/J.IJPHARM.2008.09.032 [retrieved on 2008-09-26] * table 1 * * page 188, left-hand column, paragraph materials, *	1,2,4-7, 9,11	TECHNICAL FIELDS SEARCHED (IPC)
Y	IT MI20 080 516 A1 (PHARMAVAL SRL) 28 September 2009 (2009-09-28) * abstract; claims 1-10 *	8	

The present search report has been drawn up for all claims

Place of search	Date of completion of the search	Examiner
Munich	24 July 2023	Madalinska, K

CATEGORY OF CITED DOCUMENTS
X : particularly relevant if taken alone
Y : particularly relevant if combined with another document of the same category
A : technological background
O : non-written disclosure
P : intermediate document

T : theory or principle underlying the invention
E : earlier patent document, but published on, or after the filing date
D : document cited in the application
L : document cited for other reasons
& : member of the same patent family, corresponding document

EPO FORM 1503 03.82 (P04C01)

ANNEX TO THE EUROPEAN SEARCH REPORT ON EUROPEAN PATENT APPLICATION NO. EP 23 38 2105

This annex lists the patent family members relating to the patent documents cited in the above-mentioned European search report. The members are as contained in the European Patent Office EDP file on
The European Patent Office is in no way liable for these particulars which are merely given for the purpose of information.

24-07-2023

Patent document cited in search report	Publication date	Patent family member(s)	Publication date
WO 2022235238 A2	10-11-2022	TR 202107577 A2	21-06-2021
		WO 2022235238 A2	10-11-2022
WO 2011116963 A2	29-09-2011	BR 112012023638 A2	03-10-2017
		EP 2549977 A2	30-01-2013
		EP 3272398 A1	24-01-2018
		ES 2384060 A1	29-06-2012
		US 2013017239 A1	17-01-2013
		WO 2011116963 A2	29-09-2011
WO 0241765 A2	30-05-2002	AU 3977602 A	03-06-2002
		EP 1328257 A2	23-07-2003
		US 6565873 B1	20-05-2003
		US 2003147956 A1	07-08-2003
		WO 0241765 A2	30-05-2002
WO 2018054077 A1	29-03-2018	CN 107865821 A	03-04-2018
		EP 3515444 A1	31-07-2019
		JP 7018939 B2	14-02-2022
		JP 2019534870 A	05-12-2019
		US 2019224194 A1	25-07-2019
		WO 2018054077 A1	29-03-2018
IT MI20080516 A1	28-09-2009	----------	----------

EPO FORM P0459

For more details about this annex : see Official Journal of the European Patent Office, No. 12/82

REFERENCES CITED IN THE DESCRIPTION

This list of references cited by the applicant is for the reader's convenience only. It does not form part of the European patent document. Even though great care has been taken in compiling the references, errors or omissions cannot be excluded and the EPO disclaims all liability in this regard.

Non-patent literature cited in the description

- **HANTERA MM.** Trends in Dry Eye Disease Management Worldwide. *Clin Ophthalmol*, 2021, vol. 15, 173 **[0105]**
- **LÓPEZ-MACHADO A ; DÍAZ-GARRIDO N ; CANO A ; ESPINA M ; BADIA J ; BALDOMÀ L et al.** Development of Lactoferrin-Loaded Liposomes for the Management of Dry Eye Disease and Ocular Inflammation. *Pharmaceutics*, 2021, vol. 13 (10), 1698 **[0105]**
- **HUANG L ; GAO H ; WANG Z ; ZHONG Y ; HAO L ; DU Z.** Combination Nanotherapeutics for Dry Eye Disease Treatment in a Rabbit Model. *Int J Nanomedicine*, 2021, vol. 16, 3631 **[0105]**
- **ALI F ; RAHUL ; NAZ F ; JYOTI S ; SIDDIQUE YH.** Health functionality of apigenin: A review. *Int J Food Prop*, 2016, vol. 20 (6), 1197-238 **[0105]**
- *Clinical Trial to Evaluate the Reduction of Cardiovascular Risk - ClinicalTrials.gov n.d.*, 19 November 2021, https://clinicaltrials.gov/ct2/show/NCT04114916?term=apigenin&draw=4&rank=3 **[0105]**
- **ZICK SM ; WRIGHT BD ; SEN A ; ARNEDT JT.** Preliminary examination of the efficacy and safety of a standardized chamomile extract for chronic primary insomnia: a randomized placebo-controlled pilot study. *BMC Complement Altern Med*, 2011, vol. 11, 78 **[0105]**
- *Apigenbell 60 cápsulas Jellybell | Naturitas n.d.*, 19 November 2021, https://www.naturitas.es/p/suplementos/fitoterapia/compuestos-herbarios/apigenbell-60-capsulas-jelly-bell?gclid=CjwKCAiAs92MBhAXEiwAXTi25z_Q5qx2aeNYvzbrUCyGRG6PfdA91wTKXvtWHr461rXXYtFP_cDcZxoCkrAQAvD_BwE **[0105]**
- *Apigenina 90 cápsulas de 50mg Swanson | Naturitas n.d.*, 19 November 2021, https://www.naturitas.es/p/suplementos/suplementos-compuestos/apigenina-90-capsulas-de-50mg-swanson **[0105]**
- *Optrex Colirio para el Picor de Ojos n.d.*, 19 November 2021, https://www.optrex.es/gama-optrex/colirio/optrex-colirio-calmante-para-el-picor-de-ojos/optrex-colirio-calmante-para-el-picor-de-ojos **[0105]**
- *Optiben - Irritación ocular n.d.*, 19 November 2021, https://optiben.cmfa.com/Producto/7/alivio-natural-de-la-irritacin-ocular **[0105]**
- **WANG M ; FIRRMAN J ; LIU LS ; YAM K.** A review on flavonoid apigenin: Dietary intake, ADME, antimicrobial effects, and interactions with human gut microbiota. *Biomed Res Int*, 2019, 7010467 **[0105]**
- **BATTAGLIA L ; SERPE L ; FOGLIETTA F ; MUNTONI E ; GALLARATE M ; DEL POZO RODRIGUEZ A et al.** Application of lipid nanoparticles to ocular drug delivery. *Expert Opin Drug Deliv*, 2016, vol. 13 (12), 1743-57 **[0105]**
- **FANGUEIRO JF ; CALPENA AC ; CLARES B ; ANDREANI T ; EGEA MA ; VEIGA FJ et al.** Biopharmaceutical evaluation of epigallocatechin gallate-loaded cationic lipid nanoparticles (EGCG-LNs): In vivo, in vitro and ex vivo studies. *Int J Pharm*, 2016, vol. 502 (1-2), 161-9 **[0105]**
- **AGARWAL P ; CRAIG JP ; RUPENTHAL ID.** Formulation Considerations for the Management of Dry Eye Disease. *Pharmaceutics*, 2021, vol. 13 (2), 207 **[0105]**
- **CARVAJAL-VIDAL P ; FÁBREGA MJ ; ESPINA M ; CALPENA AC ; GARCIA ML.** Development of Halobetasol-loaded nanostructured lipid carrier for dermal administration: Optimization, physicochemical and biopharmaceutical behavior, and therapeutic efficacy. *Nanomedicine Nanotechnology, Biol Med*, 2019, vol. 20, 102026 **[0105]**
- **SÁNCHEZ-LÓPEZ E ; ETTCHETO M ; EGEA MA ; ESPINA M ; CANO A ; CALPENA AC et al.** Memantine loaded PLGA PEGylated nanoparticles for Alzheimer's disease: In vitro and in vivo characterization. *J Nanobiotechnology*, 2018, vol. 16 (1), 1-16 **[0105]**
- **SÁNCHEZ-LÓPEZ E ; ESTERUELAS G ; ORTIZ A ; ESPINA M ; PRAT J ; MUÑOZ M et al.** Dexibuprofen Biodegradable Nanoparticles: One Step Closer towards a Better Ocular Interaction Study. *Nanomaterials*, 2020, vol. 10 (4 **[0105]**
- **ZEB A ; QURESHI OS ; KIM HS ; KIM MS ; KANG JH ; PARK JS et al.** High payload itraconazole-incorporated lipid nanoparticles with modulated release property for oral and parenteral administration. *J Pharm Pharmacol*, 2017, vol. 69 (8), 955-66 **[0105]**
- **SOUTO EB ; MEHNERT W ; MÜLLER RH.** Polymorphic behaviour of Compritol888 ATO as bulk lipid and as SLN and NLC. *J Microencapsul*, 2006, vol. 23 (4), 417-33 **[0105]**
- **FREITAS C ; MÜLLER RH.** Correlation between long-term stability of solid lipid nanoparticles (SLN) and crystallinity of the lipid phase. *Eur J Pharm Biopharm*, 1999, vol. 47 (2), 125-32 **[0105]**

- **ZIMMERMANN E ; SOUTO EB ; MÜLLER RH.** Physicochemical investigations on the structure of drug-free and drug-loaded solid lipid nanoparticles (SLN) by means of DSC and 1H NMR. *Pharmazie,* 2005, vol. 60 (7), 508-13 **[0105]**
- **ALSHEHRI SM ; SHAKEEL F ; IBRAHIM MA ; EL-ZAYAT EM ; ALTAMIMI M ; MOHSIN K et al.** Dissolution and bioavailability improvement of bioactive apigenin using solid dispersions prepared by different techniques. *Saudi Pharm J,* 2019, vol. 27 (2), 264-73 **[0105]**
- *tability of Dispersions | 3P Instruments n.d.,* 22 November 2021, https://www.3p-instruments.com/measurement-methods/stability-turbiscan **[0105]**
- **LIU P ; DE WULF O ; LARU J ; HEIKKILÄ T ; VAN VEEN B ; KIESVAARA J et al.** Dissolution Studies of Poorly Soluble Drug Nanosuspensions in Non-sink Conditions. *AAPS PharmSciTech,* 2013, vol. 14 (2), 748 **[0105]**
- **HUANG D ; CHEN YS ; RUPENTHAL ID.** Hyaluronic Acid Coated Albumin Nanoparticles for Targeted Peptide Delivery to the Retina. *Mol Pharm,* 2017, vol. 14 (2), 533-45 **[0105]**
- **LAGARTO A ; VEGA R ; GUERRA I ; GONZÁLEZ R.** In vitro quantitative determination of ophthalmic irritancy by the chorioallantoic membrane test with trypan blue staining as alternative to eye irritation test. *Toxicol In Vitro,* 2006, vol. 20 (5), 699-702 **[0105]**
- **XIONG C ; CHEN D ; LIU J ; LIU B ; LI N ; ZHOU Y et al.** A rabbit dry eye model induced by topical medication of a preservative benzalkonium chloride. *Invest Ophthalmol Vis Sci,* 2008, vol. 49 (5), 1850-6 **[0105]**
- **HOLZCHUH R ; VILLA ALBERS MB ; OSAKI TH ; IGAMI TZ ; SANTO RM ; KARA-JOSE N et al.** Two-year outcome of partial lacrimal punctal occlusion in the management of dry eye related to Sjögren syndrome. *Curr Eye Res,* 2011, vol. 36 (6), 507-12 **[0105]**
- **LIN TK ; ZHONG L ; SANTIAGO JL.** Anti-Inflammatory and Skin Barrier Repair Effects of Topical Application of Some Plant Oils. *Int J Mol Sci,* 2017, vol. 19 (1), 70 **[0105]**
- **KIRALAN M ; YILDIRIM G.** Rosehip (Rosa canina L.) Oil. *Fruit Oils Chem Funct,* 2019, 803-14 **[0105]**